UNIVERSITY OF LIVERPOOL

Ion channel gene changes with inflammageing

Thesis submitted in accordance with the requirements of the University of Liverpool for the degree of Doctor in Philosophy

By

Omar Mohammad B Haidar

February 2020

Doctor of Philosophy Declaration

I hereby declare that this dissertation is a record of work carried out at the Department of Musculoskeletal Biology II at Institute of Ageing and Chronic Disease at the University of Liverpool from September 2016 to August 2019. This work has not been previously submitted to the University or any other institution in an application for admission to a degree or other qualification except where otherwise indicated as help which is appropriately acknowledged.

February 2020

……

Omar Haidar BSc, MSc

Abstract

Background: Ageing is a major risk factor for chronic diseases of the nervous, cardiovascular and musculoskeletal systems. Since ion channels are key regulatory proteins in all body systems, I investigated whether there were tissue independent changes in ion channel gene expression with age. I hypothesised that the expression of a common set of ion channel genes would change in different tissues with age.

Methods: One theory of ageing states that ageing is associated with a chronic low-grade inflammatory status (”inflammageing”) and, in line with this, cytokines levels are typically increased by 2-3-fold in the elderly. I thus used two models to test my hypothesis (i) real ageing of Wistar Kyoto rats and (ii) cytokine treatment of cells *in vitro*. For the real ageing models; fibroblast-like synoviocytes (FLS) from joints, aortae, and paraventricular nuclei (PVN) from the hypothalamus were dissected from young and old rats and subjected to deep RNA-sequencing (Next Generation Sequencing, NGS). For the inflammatory model, I used FLS, chondrocytes, and aortic vascular smooth muscle cells (VSMC) from young rats and exposed them to 10ng/ml Interleukin-1β+Tumor Necrosis Factor α (IL-1β+TNFα) for 72hrs before NGS RNA-sequencing. Where possible I followed this with patch-clamp electrophysiology to establish functional changes in channel expression.

Results: Our gene expression data from our *in vitro* inflammatory model of ageing showed some similarities with naturally aged (old) rat tissue, in particular, Gene Ontology (GO) clusters were enriched for proteins involved in the extracellular matrix. In general, ion channel gene changes were different between the models and between tissues. An exception to this was the differential expression of *Gja1,* the gene encoding gap junction protein connexin 43. Statistically significant changes in *Gja1* were detected in VSMCs and aged aorta.

Conclusions: Our study suggests that the expression of a common set of ion channel proteins is not linked with age. However, the finding of common patterns of Gja1 expression is interesting particularly in light of recent evidence that knockdown of gap junctions extends lifespan in worms. This family of communicating junctions warrants additional investigation in terms of its contribution to the ageing process. All our data will be publicly shared and together with our novel analysis pipeline, this work will be a valuable resource for ageing research.

Acknowledgement

In the name of Allah, the Most Merciful and Most Gracious.

I am very grateful to the Almighty Allah not only in this journey until the end, but for being with me throughout my life and prayers go to his beloved messenger and prophet Mohammad (PBUH).

I would like to thank my government Saudi Arabia, the Saudi Arabian Cultural Bureau in London, and King Abdulaziz University in Jeddah for sourcing the funds for these studies and providing all kinds of supports I needed to finish my studies and earn this Ph.D. degree.

Then, I would like to thank my supervisors Prof. Richard Barrett-Jolley, Prof. Caroline Dart and Dr. Simon Tew who have supported and encouraged me throughout. Prof. Richard Barrett-Jolley was kind enough to supervise my work and provide invaluable support, time, encouragement and expertise. He has been a brilliant mentor and this work would not have been possible without his limitless support and patience.

A special thank you goes to all my fellow laboratory members and everyone who has helped and guided me throughout my studies, in particular Dr. Caroline Staunton, Dr. Fiona O'Brien, Dr. Rhiannon Morgan, Dr. Numan Celik, and Miss Lina Abdul Kadir. Their help was limitless and took it upon themselves to support me and keep me smiling.

Another very special and biggest thank you goes to Mom; Halima yar, and my uncle Mohammad Taleb Habib Tukar for their valuable help, support and prayers all my life. Also, I would like to thank my ex-wife for her support in my first two years of this Ph.D.

Finally, I am hugely grateful to siblings and friends for endless support and prayers over the years. I would like to dedicate this thesis to my dad; Mohammad B Haidar, who passed away in my first year of this Ph.D. and whom I know would have been incredibly proud.

Contents

List of Figures

List of Tables

Chapter 1 Introduction

1.1 Ageing Theories

There is a growing interest in the field of ageing biology; what exactly is ageing, how and why does it happen (Gavrilov and Gavrilova, 2002)**?** There have been several proposed theories to explain what is happening in the ageing process, and the underlying mechanisms (Medvedev, 1990, Weinert and Timiras, 2003). With more important discoveries at the molecular and cellular levels, new families of ageing theories have been proposed although most of them have old origins. Ageing is more complex than just a single factor cause (i.e. a single gene mutation or a decline of a key body system) (Weinert and Timiras, 2003). Among the factors that make it difficult to study ageing in humans are (a) inadequate models, (b) the long periods involved, and (c) the cost. Also, longevity studies are controversial and the inability to differentiate cause from effects adds to the difficulty. Therefore, no consensus exists over the causes of ageing, the rate of ageing or what changes that occur, leading to the well-established increased chances of death between age 30-70 (Reddy and Kar, 2019).

When talking about evolutionary theories of ageing, it is quite interesting to mention that the scientists thought about the idea that the force of selection declines with ageing. This means that the selection shadow (also known as evolutionary shadow) cannot see the harmful mutations that appear late in life and have negative effects on the organism. Also, these negative effects have been passed to the offspring of the individual who has it. Therefore, the selection is unable to remove such mutations from the population. Although, as mentioned above, there are several evolutionary theories of ageing, I will discuss the major three ones; (i) the theory of programmed death (by August Weismann), (ii) the mutation accumulation theory of ageing (by peter Medawar), and (iii) the antagonistic pleiotropy theory of ageing (by George Williams) (Gavrilov and Gavrilova, 2002).

The theory of programmed death

The theory of programmed death was developed by August Weismann as described here (Gavrilov and Gavrilova, 2002, Moskalev et al., 2014). It states that a specific-death mechanism created by natural selection to remove old members of the population (worn-out) (Gavrilov and Gavrilova, 2002). This occurs to clean up the living space and save resources for the younger generations (Gavrilov and Gavrilova, 2002). Ironically, when he got old he corrected his version of the theory "that ageing is not an adaptive trait but rather simply a neutral trait" which did not receive much attention as his early version of the programmed death theory (Gavrilov and Gavrilova, 2002). One of the ways to test his programmed death theory is to compare two groups of animals. One in the wild (natural) and the other one in a protective environment (i.e. laboratory). It is expected that both will have the same age and there is not much difference. However, the results showed the opposite where the group in the protective environment lived longer (Shock, 1964) compared to those in the wild (Gavrilov and Gavrilova, 2002).

The mutation accumulation theory

The theory of mutation accumulation was suggested by Peter Medawar as described here (Weinert and Timiras, 2003). Briefly, he considered ageing as a by-product of natural selection. This means that ageing is a nonadaptive trait simply because natural selection ignores any events that happen in long-lived animals that offer a slight contribution to offspring numbers. In other words, mutations that are harmful and only-act late in life may accumulate in populations resulting in diseases and senescence (Weinert and Timiras, 2003).

Reproduction depends on an age where it is zero at birth, peaks at young adults and decreases as we age due to increased link to death. The reasons for death can be internal (within the body, i.e. senescence) or external (i.e. accidents, illness, etc). Therefore, harmful mutations expressed at a young age are strongly selected against because of their negative effects on reproduction while harmful mutations expressed later in life are considered

neutral to selection because the one who has it has already passed his/her genes to the offspring (Gavrilov and Gavrilova, 2002). Therefore, according to this theory, the chances that a person can reproduce are really small if he/she were loaded with deleterious mutations that are expressed early in life. For example, a person with deleterious mutations affecting reproduction that appear early in life will not be passed on since the individual cannot reproduce (Ahmed et al., 2017) while the harmful mutations that appear later in the life of a person will not affect reproduction because the person has already passed his genes to the offspring (Gavrilov and Gavrilova, 2002). This theory has survived so far compared to others, but it is still pending further validation.

The antagonistic pleiotropy theory of ageing

The theory of antagonistic pleiotropy of ageing was proposed by George Williams as an evolutionary explanation for senescence. It was built on two assumptions; (i) a gene can influence multiple traits (pleiotropic) of an organism rather than just one trait, and (ii) these pleiotropic effects can affect the individual's fitness in opposite (antagonistic) ways. In other words, this theory applies when one gene control for more than one trait where at least one trait is beneficial, and one is harmful (detrimental) to the organism's fitness.

The disposable soma theory can be considered a special case of the antagonistic pleiotropy theory of ageing that was developed by Tom Kirkwood and Robin Holliday (Kirkwood, 1977, Kirkwood and Holliday, 1979). It was an effort of renaming the antagonistic pleiotropy theory proposed by Kirkwood *et al* (described here (Gavrilov and Gavrilova, 2002, Ackermann et al., 2007)) to explain how the same gene can have both effects (positive and negative). Simply, a special class of gene mutations would end up with saving energy for reproduction (positive effect) by reducing error regulation in somatic cells (negative effect). In other words, reduced investment of resources in the somatic cells for development and reproduction. Eventually, deterioration and death are inevitable (Kirkwood and Holliday, 1979).

It is noteworthy mentioning that Kirkwood's disposable soma theory (above) was primarily proposed to prove the Orgel's theory of error catastrophe that considered ageing as a product of a breakdown in the accuracy of protein synthesis in the somatic cells (Gavrilov and Gavrilova, 2002). Although error catastrophe theory failed, the disposable soma theory remains a narrow definition of the antagonistic pleiotropy theory of ageing and the authors of this disposable soma theory themselves admitted it (Gavrilov and Gavrilova, 2002, Kirkwood and Holliday, 1979).

There are several examples of the antagonistic pleiotropy theory including cytokines such as IL-6 which can play two opposite roles; pro- and anti-inflammatory cytokine (Scheller et al., 2011). The balance between the cytokines (pro-inflammatory and anti-inflammatory) is tightly regulated. When this balance is disturbed, the pro-inflammatory cytokine levels increase leading to several diseases or conditions such as "Inflammageing".

Inflammageing

The word "inflammageing" is composed of two parts; inflammation and ageing relating the perceived association between chronic low-grade inflammation and the ageing process (Franceschi et al., 2007a, Day, 2010). Inflammation is caused by pro-inflammatory cytokines. This process has to be resolved as soon as the threat is cleared. However, with ageing, the level of pro-inflammatory cytokines that initiated the immune defence stays high leading to a state of chronic low-grade systemic inflammation which is also known as the pro-inflammatory phenotype or "inflammageing". There is no clear understanding of the causes of inflammageing that is behind the major age-related diseases such as diabetes, CVD, neurodegenerative diseases, and musculoskeletal diseases although it can affect almost all tissues of the body.

1.2 Tissues

Although all our body tissues can be the target of inflammageing, tissues of the major age-related diseases will be discussed here.

Musculoskeletal system (FLS)

Three systems known to be dysfunctional with age were chosen to be examined in this thesis. As an example of musculoskeletal tissue, synoviocytes that are involved with the development of osteoarthritis were chosen. Fibroblast-like synoviocytes (FLS) are one of the key cells in particular joints. It forms a lining layer in the articular joint.

Structure and functions

The intimal lining layer of the synovium produces lubricious synovial fluid and is composed of two cell types in relatively equal proportions: Type A or macrophage-like synovial cells and Type B or FLS. The synovium is the major barrier between the joint and the systemic circulation (Berenbaum, 2013, Sutton et al., 2009).

It plays a role in maintaining healthy cartilage of the articular joint (Berenbaum, 2013, Sutton et al., 2009). FLS cells contribute to the protection and maintaining (Hui et al., 2012) the structural integrity of the joints by controlling the composition of the (a) synovial fluid and extracellular matrix (ECM) of the joint (Burmester et al., 1983, Iwanaga et al., 2000). The synovial fluid is produced using the FLS cellular components and the two main important molecules secreted by the intimal lining layer of the FLS cells in the fluid are lubricins and hyaluronic acid (HA) that can lubricate the articular surfaces (Hui et al., 2012, Scanzello and Goldring, 2012). Lubricin and HA are high molecular weight molecules that are not permeable through the synovium unlike other molecules such as cytokines. This is vital to maintain the viscosity of the synovial fluid by maintaining the average concentration and molecular weight of these main components. Also, the synovium prevents depositing of other high molecular

weight proteins or plasma components in the articular joint which will eventually reduce viscosity and causes damage to the joint tissues (Scanzello and Goldring, 2012).

FLS can also provide nutrients for chondrocytes within the avascular cartilage. It has also been suggested that catabolic enzymes such as matrix metalloproteinase (MMPs) are produced by synovial cells and diffuse into the cartilage (Sutton et al., 2009). Thus, modulating the activities of the chondrocytes (Hui et al., 2012). Synovium must remain healthy as increased production of MMPs can lead to degradation of the articular matrix (Scanzello and Goldring, 2012).

FLS in diseases and age

The synovial environment changes physically, chemically and physiologically with injury or the onset of disease and is thought to be a mediator in arthritis pain (Grubb, 2004, Kumahashi et al., 2011, Sellam and Berenbaum, 2010). In diseases like inflammation, hyperplasia or arthritis, the permeability of the synovium is changed leading to higher concentrations of hyaluronic acid (HA) detected in the blood (Scanzello and Goldring, 2012). Also, FLS cells have been implicated in arthritis as they exhibit a transformed phenotype with increased invasiveness and production of various pro-inflammatory mediators that perpetuate inflammation and proteases that contribute to cartilage destruction as seen with ageing (Bartok and Firestein, 2010, Noss and Brenner, 2008).

Ion channels in FLS

Like many other cells, FLS cells have several different ion channels that play roles in a multitude of cell regulating processes by modulating the membrane potential and cellular function (Abdul Kadir et al., 2018). Examples of such channels include aquaporins (i.e. AQP0-AQP12), K^+ channels (i.e. Ca^{2+} activated potassium channels Kca1.1, also known as BK channels), acid-sensing ion channels (i.e. ASIC3), and TRP channels ((TRPC1 & TRPC5), TRPV1, TRPV2 & TRPV4), TRPM-Melastatin or -7 & TRPM8) and TRPA1) (Ji and Hong, 2019).

Aquaporins are channels that transport water or small molecules across cell membranes of different cell types. The BK channel is a member of the Ca^{2+}-activated potassium channel family and a very important channel in the FLS plasma membrane (Ji and Hong, 2019). Experimental pieces of evidence including but not limited to wound healing and proliferation assays have shown that BK drives invasiveness of the synoviocyte and progression of arthritis on many species by increasing production of inflammatory mediators and catabolic enzymes (Friebel et al., 2015, Hu et al., 2012b, Tanner et al., 2015a). Acid-sensing channels control tissue acidosis via pH changes. They are associated with inflammatory pain (i.e. musculoskeletal pain). They are also known as voltage-insensitive ligand-gated cation channels with protons (Ji and Hong, 2019). TRP channels have been known as non-selective cation channels and play roles in inflammatory mediated arthritis (Ji and Hong, 2019).

Understanding the biology and regulation of FLS may provide insight into the pathogenesis of inflammatory arthritis. FLS cells could potentially be targeted, pharmacologically, to produce increased volumes of synovial fluid as an alternative to intra-articular hyaluronan (Anon, 2000) or synthetic fluid injection (Dane and Grinstaff, 2012) therapies. They are also a plausible analgesic target because they may interact with sensory neurons (von Banchet et al., 2007) and have been described as “amplifiers” of neuropeptide mediated inflammation and pain (Niissalo et al., 2002).

Cardiovascular system

The second system in this thesis to address is the vasculature which is well known to dysfunction with age (Laina et al., 2018). This project will cover the aorta and vascular smooth muscle cells (VSMC) harvested from the aorta. Smooth muscle cells are part of many hollow organs including but not limited to blood vessels, gastrointestinal tract, airways, reproductive tract (including the uterus), bladder, and urethra. The main and significant roles of smooth muscle cells are (i) to shape and alter the shape of organs and (ii) to resist the force

of internal load that the organ is facing (Cowled and Fitridge, 2011). One example of this is vascular smooth muscle cells which are found in blood vessels, especially thick in arteries.

Structure and functions of VSMC in the artery

The wall of the aorta is composed of three layers: i) Tunica intima which is the innermost layer, ii) Tunica media which is the thick middle layer), and iii) Tunica adventitia which is the outermost layer (Karimi and Milewicz, 2016). Also, the aortic wall contains elastic fibres which are elastin surrounded by microfibrils (Karimi and Milewicz, 2016).

Figure 1 shows the structure of the aortic wall. The tunica intima which is a single layer of endothelial cells is supported by the internal elastic lamina while the tunica media consists of 50 alternating layers of VSMCs and elastic fibres. Microfibrils of the elastic fibres are linked to focal adhesions (on the VSMC surface) which are linked to the contractile units inside the VSMCs.

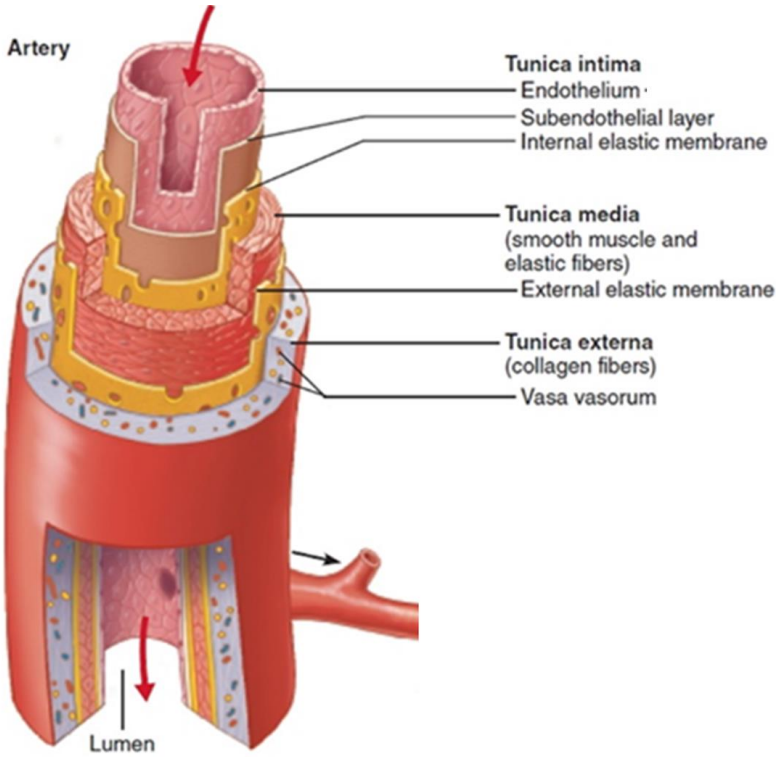

Figure 1: Structure of the aortic wall.
The three layers of the aortic wall are shown above which are (1) Tunica intima, (2) Tunica media and (3) Tunica externa. Also, internal and external elastic membranes that surround the thick middle layer (tunica media) are shown as well. Source: https://healthjade.com/blood-vessels/

Finally, tunica adventitia which is the outermost layer of the aortic wall is composed of collagen and vasa vasorum (which are small arteries that supply the middle layer with nutrients) and autonomic nerves.

This project will focus on the VSMC which are classified as fusiform cells with 200 microns long and 5 microns in diameter and large central nucleus surrounded by an abundant array of ER and Golgi apparatus. Their cytosol and plasma membrane are decreasing toward the poles (Cowled and Fitridge, 2011).

It is thought that aorta has a unique role in blood flow as about 50% of the left ventricular stroke volume during systole is stored there (and with some other proximal large vessels). With the help of the aortic elastic wall forces, this as well as other blood in the left ventricle is pushed forward and circulated to the peripheral circulation which assures continuous blood flow to the peripheral circulation. Interestingly enough, this unique role of the aorta is known as elastic buffering chamber and termed the Windkessel function and it is due to elastin in the aortic wall not the contraction of the VSMC as the elastic recoil of the aorta does not change if the VSMC's contraction is pharmacologically inhibited (Karimi and Milewicz, 2016).

Roles of important ion channels in regulating VSMC function

Ionic balance and VSMC membrane potential are important in regulating VSMC function and electrogenic ion channels are among the best-known ones as well as other potassium channels.

Regulation of cellular Ca^{2+}

Several ion channels play roles in regulating cellular Ca^{2+} including $3Na^{+}/2K^{+}$ ATPase and voltage-gated L-Type Ca^{2+} channels (Martinsen et al., 2014). Different ion channels have different roles in regulating cellular Ca^{2+}. For examples, (a) Na^{+}/Ca^{2+} exchangers (Lytton, 2007)and plasma membrane Ca^{2+} ATPases (PMCA)) play roles in removing Ca^{2+} from cytosol to the extracellular space, (b) Sarcoplasmic Reticulum (SR) Ca^{2+} ATPases (SERCA) channels

have been shown to remove Ca^{2+} from the cytosol to the SR, (c) Stromal Interacting Molecule 1 (STIM1); translocates Ca^{2+} from extracellular space to the SR once SR's Ca^{2+} depletion is sensed by Ca^{2+} sensor proteins in the SR and once Ca^{2+} in the cytosol another channels (Orai1) are activated to facilitate the entry to SR, (d) non-selective cation channels of the transmembrane receptor potential canonical (TRPC) family are thought to regulate Na^{+} and Ca^{2+} entry and (e) a series of potassium channels are involved in re- or hyperpolarization of the VSMC membrane. The latter can be therapeutically targeted to limit Ca^{2+} entry and thereby limiting vasoconstriction (Cowled and Fitridge, 2011). An example of a calcium ion channel that changes with ageing is the voltage-gated L-Type Ca^{2+} channels (Albarwani et al., 2016).

In the cytosol, the Ca^{2+} level is maintained by either Ca^{2+} entry from extracellular space or by release from intracellular Ca^{2+} stores (Zhu et al., 2019b)(Endoplasmic Reticulum (ER) or Sarcoplasmic Reticulum (SR) in muscle cells). Also, in muscle cell agents that activate the ryanodine receptor such as caffeine or phospholipase C (PLC) which releases IP3 that binds to IP3 receptors on the SR resulting in Ca^{2+} release into the cytosol. Ca^{2+} entry into the cytosol of the muscle cell from extracellular space occurs through non-selective cation channels or selective Ca^{2+} channels which could be voltage-gated or non-voltage gated. Additionally, membrane depolarization or stretch/pressure-dependent route of Ca^{2+} entry into the cell has been recognized (Cowled and Fitridge, 2011).

The most important Ca^{2+} entry into VSMC is mediated by the voltage-dependant Ca^{2+} Channels (VDCC) especially the L-type or $Ca_v1.2$. Another VDCC is the T-type Ca^{2+} channels which are known as the Cav3 family which is thought to mediate Ca^{2+} entry into microvasculature (reviewed here (Catterall, 2011)). Depolarization of the plasma membrane activates VDCC which increases the open probability as well as overall Ca^{2+} conductance into the cell. Other ways of Ca^{2+} entry into the VSMC are non-selective cation channels that can allow a variety of ions such as Ca^{2+} and Na^{+} to enter the cell (Cowled and Fitridge, 2011).

Given the importance of the Ca^{2+} channels, they change with age and an example of that is provided by Mansour et al (Mansour et al., 2016).

Potassium channels

Like many other cells, VSMC expresses potassium channels. Different types of K^+ channels have different roles. For example, the insulin-dependent electrogenic $3N^+/2K^+$ ATPase is crucial in establishing the resting membrane potential (E_M) of the VSMC (Mansour et al., 2016). Depolarization (contraction) and hyperpolarization (relaxation/vasodilation) of VSMC are more than just a single ion channel that can exert such effects. Also, when the VSMC gets hyperpolarized the inward rectifier K_{IR} channels get activated resulting in the transportation of more K^+ from extracellular space into the cell to neutralise or offset the hyperpolarization stimulus. Additionally, K_{IR} channels play roles in the equilibrium potential for potassium (Cowled and Fitridge, 2011). In rare conditions where membrane potential ($M_{E)}$ is more negative than equilibrium potential for potassium (E_K), K_{IR} conducts small outward rectifying K^+ current that regulates VSMC tone by combinational effects of K_{IR} and $3Na^+/2K^+$ ATPase channels (Cowled and Fitridge, 2011).

On the other hand, the K_v family are activated by depolarization, and can, therefore, be targeted to hyperpolarize the VSMC to counterbalance any neural or hormonal-mediated depolarization (Cowled and Fitridge, 2011). Also, K_v channels in coronary arteries can be blocked using histamine which acts through H1 receptor while other blocking options (such as venom peptides, antibodies and small molecules) can be used, as well (reviewed here (Wulff et al., 2009, Cowled and Fitridge, 2011).

Physiologically, many K^+ channels (i.e. K_{ATP}, BK, GPCRs) have been shown to play different roles in VSMC functions. K_{ATP} channels are activated or inhibited by different ways. For example, many agents or K^+ openers such as adenosine, calcitonin gene regulated peptide (CGRP), vasoactive intestinal peptide (VIP), pinacidil, minoxidil can activate K_{ATP} channels. Activation of K_{ATP} results in hyperpolarization and vasodilation. Mechanism of activation of

K_{ATP} involves activation of adenylyl cyclase that activates cAMP that activates protein kinase A (PKA). Also, the PCK-dependant pathway activation of K_{ATP} has been recognized. Another different way of K_{ATP} regulation involves high cytosolic ATP: ADP (control the open and close states of the channels) ratio as found in ischemic tissues resulting in attempts to throw K^+ to hyperpolarize the membrane to create vasodilation. Some drugs that are used to treat certain conditions can affect K_{ATP} channels activity. For example, sulfonylurea which is used to treat type II diabetes can inhibit K_{ATP} channels resulting in membrane depolarization and consequently activation of Voltage operated Ca^{2+} Channels (VOCC) in pancreatic cells resulting in insulin release. Overuse of sulfonylurea can result in vasoconstriction as it will interfere with the effectiveness of the vascular K^+ openers (Nichols et al., 2013, Cowled and Fitridge, 2011).

BK channels are among the most studied channels. BK stands for big or large-conductance Ca^{2+} activated potassium (BK) channels. Although BK is mainly activated by Ca^{2+} they are also voltage sensitive, unlike the small conductance smK_{Ca} channels. As the name suggests, these types of K^+ channels are activated by increased cytosolic Ca^{2+} (reviewed here (Yang et al., 2015)).

Potassium channels and especially BK are very important channels in the normal function of the VSMC. Age-related changes in these channels are expected to have serious consequences. Abnormal expression and function of the BK have been observed in animals which indicate that these channels may play significant roles in the abnormalities of aged blood vessels (reviewed here (Carvalho-de-Souza et al., 2013)).

Regulation of VSMC relaxation by endothelial cells

Nitric oxide (NO) is a very potent vasodilator. It is produced within the endothelial cells and has a variety of effects on the blood vessels structure and function including platelet aggregation and adhesion, and acts as a vasoconstrictor. In the endothelial cells, NO can activate both guanylyl cyclase (GC) and cyclooxygenase (CO). Once GC is activated, it can form

cyclic GMP (cGMP) which activates protein kinase G (PKG) leading to activation of K^+ channels affecting removal of intracellular K^+ which leads to membrane hyperpolarization, inactivation of VDCC that leads to low intracellular Ca^{2+} level resulting in vasorelaxation. Additionally, the activation of CO leads to vasoconstriction (Cowled and Fitridge, 2011, Pecanha et al., 2010). VSMC also changes with age that affects its normal contraction relaxation functions. The effects of ageing on VSMC behaviour is reviewed here (Monk and George, 2015).

Brain (PVN)

The paraventricular nucleus (PVN) of the hypothalamus is one of the most important hypothalamic autonomic control centres (Ferguson et al., 2008, Coote, 2005).

Structure and functions of PVN

The PVN has a complicated structure. Briefly, the PVN is composed of magnocellular and parvocellular neurons that can be seen with their subdivisions in (Figure 2-**Error! Reference source not found.**A). The PVN can be simply or 'loosely' separated (as seen in Figure 2**Error! Reference source not found.**B and C) into the posterior magnocellular lateral area, parvocellular area and intermediocellular region (dorsal and caudal PVN). Most of the pre-autonomic neurons are abundant in the intermediocellular (Me) area (Feetham et al., 2018).

'Spinally-projecting PVN neurons project from the parvocellular PVN to the intermediolateral cell column of the thoracolumbar spinal cord (IML) and can control cardiovascular function such as blood pressure and heart rate. There is an additional role for the PVN, often called a "premotor nucleus", where sympathetic premotor neurons play a role in body fluid homeostasis (Shih et al., 2003). Direct projections arise from PVN and innervate the pressor region of the rostral ventrolateral medulla (RVLM) which enables the PVN to control cardiovascular function via sympathetic tone (Shih et al., 2003, Sawchenko and Swanson, 1982).

With the projections mentioned above, the PVN can influence sympathetic nerve activity directly (via PVN–IML connections), indirectly (via PVN–RVLM connections) or by both mechanisms (via neurons with collaterals to the IML and RVLM). It is suggested that with these connections, the PVN can affect the reflex changes in the sympathetic nerve activity involved in the blood volume regulation (Shih et al., 2003).

The PVN has additional physiological roles. Among these are its vital neuroendocrine roles in controlling (Ferguson et al., 2008) (a) the hypothalamo-pituitary-adrenal (HPA) axis (corticotropin-releasing hormone (CRH) neurons projecting to the median eminence), (b) the thyroid axis (thyrotropin-releasing hormone (TRH) neurons projecting to the median eminence), (c) the reproductive axis (dopamine and oxytocin neurons projecting to the median eminence or posterior pituitary), (d) the regulation of body fluid balance (vasopressin and oxytocin neurosecretory cells projecting to the posterior pituitary), (e) cardiovascular function through traditional autonomic outputs (neurons projecting to caudal medullary and spinal autonomic control centres), (f) growth and development (somatostatin neurons projecting to the median eminence), and (g) gastrointestinal (Ferguson et al., 2008).

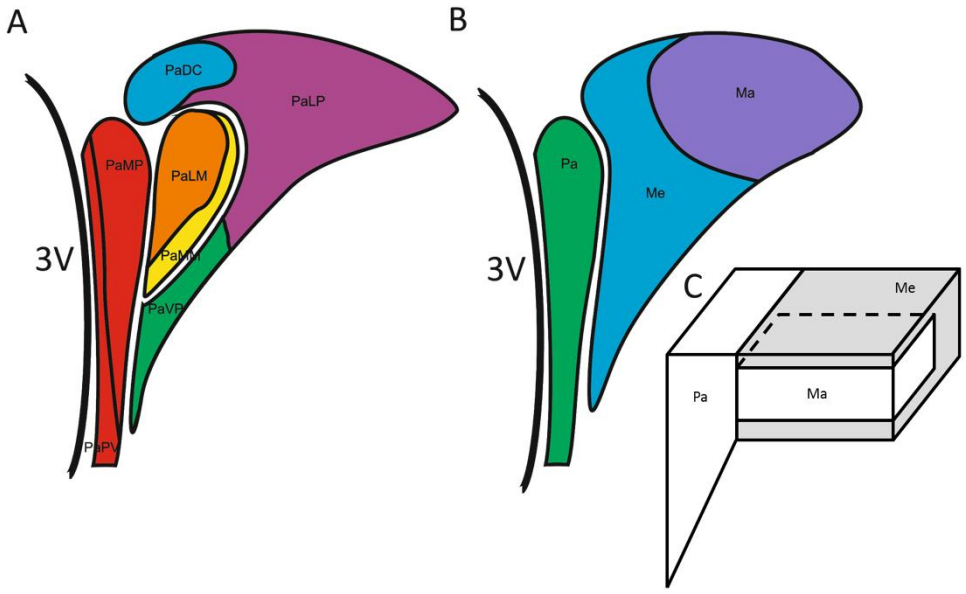

Figure 2:Hypothalamic PVN structure.
The subdivisions of PVN are close to the third ventricle (3V). (A) The major parts of the PVN are the parvocellular and magnocellular. These can be further subdivided into the following: medial parvocellular (PaMP), medial ventral parvocellular (PaVP), lateral parvocellular (PaLP), periventricular subnucleus (PaPV), lateral magnocellular (PaLM), *medial magnocellular (PaMM), and dorsal cap (PaDC). (B, C) the PVN can be divided into major areas; parvocellular (Pa), posterior magnocellular lateral (Ma), and the intermediocellular regions (Me) (Feetham et al., 2018).*

PVN in diseases and ageing

Dysfunction of sympathetic pre-autonomic neurons (usually hyperactivity) has been linked to several serious diseases such as hypertension and heart failure (Patel et al., 2000, Li and Patel, 2002, Li et al., 2003). Additionally, there is some evidence that direct ion channel dysfunction in the PVN is responsible for diseases. Examples include hormonal changes associated with depression, hypertension (i.e. decreased small Ca^{2+} sensitive potassium channels (SK)), heart failure (i.e. inhibition of GABA-ergic neurotransmission), and diabetes (i.e. increased TRPC) (Feetham et al., 2018).

Also importantly, in regards to ageing, the PVN can influence the sympathetic nervous system, control of cardiovascular function (i.e. regulation of blood volume, circadian regulation of blood pressure, cardiovascular response to stress), regulatory functions for hepatic glucose control (liver-related PVN neurons express corticotrophin-releasing hormone and oxytocin), circadian pacemaker in mammals, role in osmoregulation and

thermoregulation (Feetham et al., 2018, Nunn et al., 2011). Not only this but also ageing affects the arginine vasopressin that is synthesized in the magnocellular neurons of the supraoptic nucleus and PVN of the hypothalamus (Greenwood et al., 2018).

Ion channels in the PVN

Due to its multiple and diverse functions, ion channels in PVN are also abundant and variable (Feetham et al., 2018). These channels include the major ones such as amino acid receptor channels, transient receptor potential channels (TRP), potassium channels, sodium channels, voltage-gated Ca^{2+} channels, and other channels like purinergic membrane receptor family, acid-sensing channels (ASICs), and proton-gated voltage insensitive cation channels (Feetham et al., 2018).

Electrophysiologically, in PVN the main difference between neurones types depends on the nature of the principle voltage-gated (voltage-gated potassium and calcium) ion channels expressed. (i) Type I neurosecretory magnocellular neurons that express a rapidly inactivated or "A-type" potassium conductance, and (ii) Type II parvocellular neurons expressing a slowly inactivating delayed rectifier potassium conductance (Feetham et al., 2018).

Role of PVN in the cardiovascular regulation

PVN has a powerful influence on the cardiovascular system (Coote, 2007). GABAergic inhibitory synapses tonically inhibit the PVN's cardiovascular activity (Martin et al., 1991, Martin and Haywood, 1993). PVN has projections to ILM and RVLM that act on the sympathetic neural outflow (Feetham et al., 2018, Nunn et al., 2011). With the decreased activity of the GABAergic inhibitory synapsis and increased excitatory signals to the PVN (as in chronic heart failure), the sympathetic neuronal activity increases and its outflow into the blood increases as well (Li et al., 2003, Li and Patel, 2003, Li et al., 2006b, Li et al., 2006a). This will influence the cardiovascular regulation, kidney and splanchnic beds as seen in

hypertensive models. Therefore, GABAergic influence on the PVN can be considered as a limiting step in the creation of sympathetic overactivity and its consequences.

Catecholamines are other factors affecting the PVN's activity. PVN neurons express α- and β-adrenergic receptors that can be activated by noradrenaline (NE) coming from the brainstem (Flak et al., 2009, Flak et al., 2014). The shift in the sympathetic basal tone that is observed in heart failure could be attributed to NE effects on the PVN. Therefore, Modulation of the activity of the PVN neurons through GABAergic and adrenergic mechanisms can control cardiac function (i.e. blood pressure and heart rate) (Mendonca et al., 2018).

With ageing, dysregulation of the GABAergic system is associated with an imbalance in autonomic nervous activities. Not only this but also the resting blood pressure and heart rate are altered (Li et al., 2017).

Role of PVN in plasma volume control

Data indicates that parvocellular spinal projections are responsible for plasma volume regulation as lesioning of the PVN and destroying a substantial portion of the PVN-spinal neurons leads to a decrease in the renal response to plasma volume expansion (Lovick and Coote, 1988, Lovick and Coote, 1989, Lovick et al., 1993). Many factors can activate or inhibit the PVN-spinal neurons including stimulation of cardiac afferents, arterial baroreceptors or the circulating atrial natriuretic factor. Also, the PVN-spinal neurons can be excited by injection of hyperosmotic solutions into the blood or through brain supply via the internal carotid artery. Not only this but also stimulation of the volume receptors via distending the right atrial-caval junction with a balloon catheter or expanding the plasma volume will activate the c-Fos in the parvocellular neurone of the PVN (Coote, 2007).

Plasma volume is changed with ageing due to several factors including the inappropriate release of arginine vasopressin; which is released by the PVN, affecting the body's water and salt contents which may lead to serious diseases such as hypertension

(Greenwood et al., 2018). Due to its important roles in several body functions and has been associated with age-related diseases, it is interesting to study ion channel changes in PVN with inflammageing.

Inflammageing is one of the events that take place in the body which affect the overall function of different tissues. Inflammaging is largely related to the increased abundance of cytokines.

Cytokines

It is thought that increased levels of cytokines is the key aspect of inflammageing (Ferrucci and Fabbri, 2018). Cytokines are small proteins of less than 80kDa. They are signalling proteins as they regulate a wide range of cellular functions including immune response (innate and acquired), inflammation and repair, haematopoiesis, and proliferation. Several different cells can secrete cytokines at local high concentrations. Cytokines are also involved in cell-to-cell communications. They can apply their effects through autocrine, paracrine or endocrine (systemic) fashions. Individual cytokine cannot exert its effect without activating other cytokines and proteins (Chung, 2009). With ageing, Cytokine levels increase by 2-3 folds (Pedersen, 2006b).

Cytokines are produced and secreted dynamically. Therefore, the immune response must be tightly regulated as lifestyles and some external (i.e. environment) factors can change the cytokine concentrations that initiate inflammatory defence response by fighting infections (i.e. bacterial or viral) through the pro-inflammatory pathway/cytokines (Rea et al., 2018). The initiation of this pathway must be regulated and turned off as soon as the pathogen is cleared. There are two types of inflammatory cytokines/pathways; pro- and anti-inflammatory (Rea et al., 2018).

Rather than just clinical signs and symptoms, more biomarkers and biochemical indices are used in medicine to improve diagnosis and treatment of diseases. For example, a

biomarker for inflammation that circulates in the blood called C-reactive protein. Modest elevation in its level has been associated with large numbers of age-related conditions. Such conditions represent minor metabolic stressors. Different cytokines are also used in the clinical diagnosis of diseases. More investigations are carried to find out their roles in terms of molecular processes and pathways leading to inflammation at all ages in general and in ageing specifically (Rea et al., 2018). Inflammageing is a common finding in ageing and age-related diseases. Pro-inflammatory cytokines play an important role in immune system remodelling with age as shown in Figure 3.

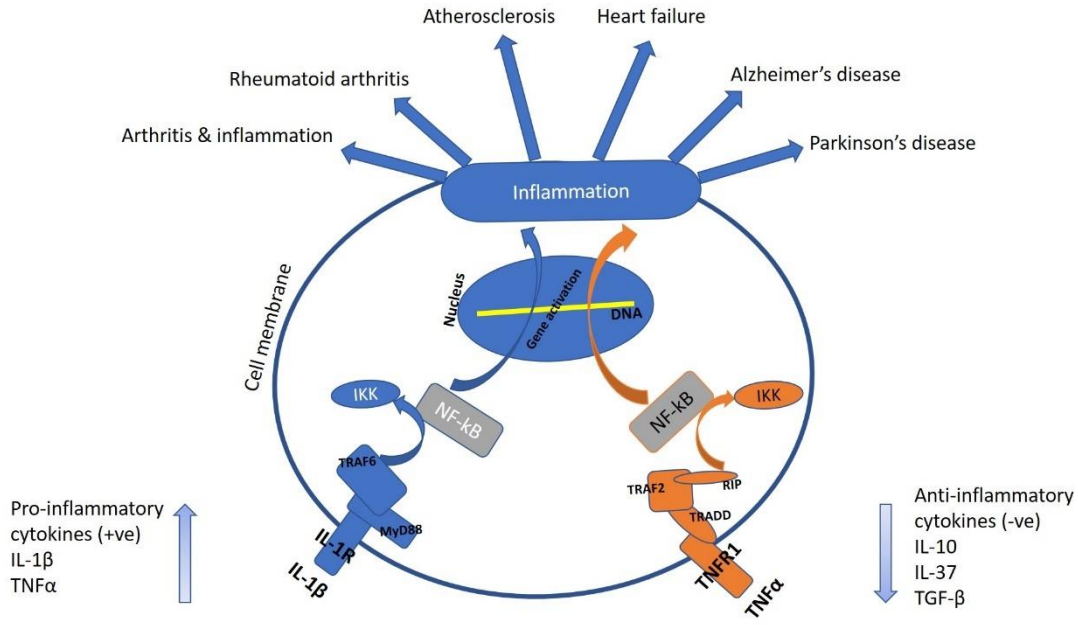

Figure 3: Dysregulation of cytokines and NF-kB signalling in ageing and age-related diseases.
A reshaping of cytokines expression with a tendency towards increased pro-inflammatory and decreased anti-inflammatory cytokines. This tendency called pro-inflammatory phenotype or "Inflammageing". In this figure, IL-1β binds its receptor IL-1R which activates signalling cascades that are mediated through MyD88 and TRAF6 which activates NF-kB. The later is inhibited by IKK. Activated IL-1β-IL-1R leads to phosphorylation of IKK and labels it for proteasomal degradation. Activated NF-kB then translocates into the nucleus and activates gene transcription including the production of cytokines and other enzymes that induce inflammation. Additionally, TNFα binds its receptor TNFR1. Then, a complex is formed containing TRADD, TRAF2 and RIP which activates NF-kB by phosphorylation of IKK. Phosphorylated IKK is degraded by proteasomes. Activated NF-kB is translocated into the nucleus and activates genes involved in inflammation. Inflammation can cause different diseases including arthritis, rheumatoid arthritis, atherosclerosis, heart failure, Alzheimer's disease and Parkinson's diseases. Abbreviations; IL-1β: Interleukin-1 beta, IL-1R: Interleukin-1 Receptor, IL-10: interleukin 10, IL-37: interleukin 37, TGF-β: Tumor growth factor-beta, MyD88, myeloid differentiation factor 88, TRAF6: TNFR-associated factor 6 (TRAF6), NF-κB: nuclear factor κB, IKK: IκB kinase, RIP: Receptor-interacting serine/threonine-protein kinase, TNFα: Tumor necrosis factor-alpha, TNFR1: Tumor necrosis factor receptor 1, TRADD: Tumor necrosis factor receptor type 1-associated DEATH domain protein.

Mechanism of action of cytokines

Cytokines bind to their receptors (soluble or membrane-bound), induce conformational changes, activate proteins that start downstream signalling cascade through second messengers (Figure 4). This may end up with activation of gene transcription and protein synthesis that activate other proteins or cytokines. There can variable final effects including cell survival, activation of other cells, gene activation, apoptosis or cytoskeletal changes.

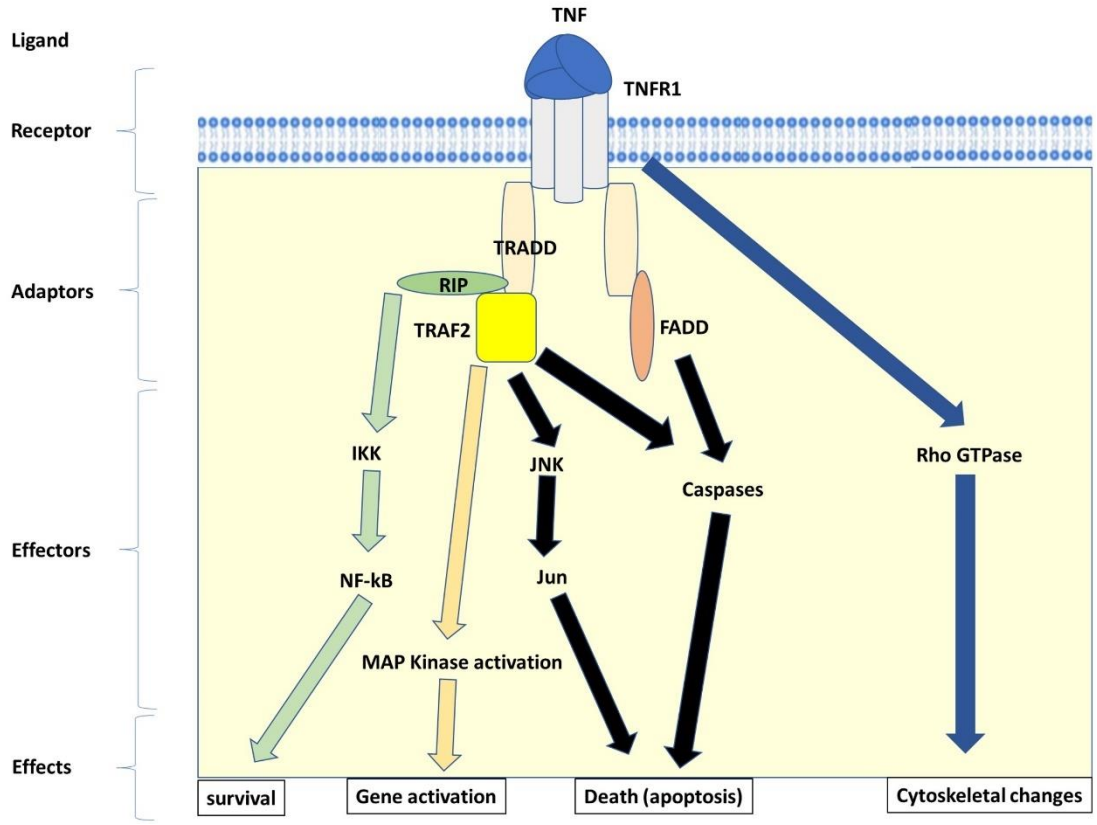

Figure 4: Schematic diagram of how cytokines work in general.
*Cytokines usually bind to their cell surface receptor although some cytokines bind to their intracellular receptor. In this schematic diagram, I show a general mechanism of action of cytokines. Normally, a ligand (cytokine) binds to its receptor activating second messengers (adaptors) which work on effectors leading to a cellular function (effects). The second messenger behaviour of each cytokine is complex and can be quite different. As an example, I show here Tumor necrosis factor-alpha (TNFα) cytokine. Once the TNFα binds its receptor TNFR1, a protein complex containing TRADD protein, TRAF2 and RIP are recruited. TRADD, TRAF2 and RIP and the inhibitor of kB (IKK) can function together to activate NF-kB which **activates** gene transcription leading to cell survival. Gene activation can also occur through the MAP kinase pathway. Apoptosis (cell death) can occur through the interaction of TRADD with FADD protein and caspase-8 leading to activation of caspase-3 and apoptosis. Besides, TNF-mediated recruitment of TRAF2 can activate JNK which in turn activates Jun leading to apoptosis as well. Cytoskeletal changes occur through activation of Rho family GTPases. TRADD: Tumor necrosis factor receptor type 1-associated DEATH domain protein, TRAF2: TNF receptor-associated factors, RIP: Receptor-interacting serine/threonine-protein kinase, MAP: mitogen-activated protein, JNK: c-Jun N-terminal kinase, Jun: Jun Proto-Oncogene, AP-1 Transcription Factor Subunit, FADD: Fas-associated protein with death domain.*

Pro-inflammatory cytokines in ageing and age-related diseases

Pro-inflammatory cytokines are produced and secreted mainly by activated macrophages (Zhang and An, 2007). The major pro-inflammatory cytokines that contribute significantly to the phenomenon of inflammageing, as well as many other age-related diseases in healthy elderly people, are IL-6, TNF α, and IL-1α. To achieve healthy ageing, the balance between pro- and anti-inflammatory cytokines must be retained. This means the ability to respond to immune messengers and integrated return to inflammation resolution and finally restore immune homeostasis (Rea et al., 2018). Next, examples of the important pro-inflammatory cytokines (IL-1β and TNFα) that were used in this study will be covered.

Interleukin-1 (IL-1)

IL-1 is the central mediator of the innate immunity and inflammation in the body. IL-1 binds its receptor and initiate signalling cascades leading to inflammation that can cause several diseases as shown in (Figure 3). Both IL-1 and IL-18 initiate stress-induced inflammatory cascade (Sims and Smith, 2010). Such association has also been linked to ageing. A study involved young, elderly and Centenarians included three different polymorphisms of IL-1α to evaluate whether IL-1 cluster alleles could be differently characterized in people selected for longevity, no significant differences detected in the genotype and allele frequency distribution. However, an increase in the IL-1Ra (antagonist) level was detected while IL-1β showed no age-related trend. The increase in IL-1Ra seemed not to be related to the genotype but to the age-related increased inflammation and as a protection measure (Cavallone et al., 2003). Another study showed an association between increased serum level of IL-1β and congestive heart failure, angina and dyslipidaemia without any associations with age [8]. IL-1β could be related to the cardiomyocyte function alterations rather than ageing itself or age-related diseases (Di Iorio et al., 2003). Only IL-1Ra showed a significant predictor of mortality and a powerful prognostic marker in elderly people (Jylha et al., 2007).

A polymorphism (- 889C > T) IL-1α was found to be strongly associated with increased risk of Alzheimer's disease (Mun et al., 2016). Since inflammation is thought to play a significant role in cognitive decline and dementia with ageing, Trompet et al (Trompet et al., 2008) found that certain IL-1 haplotype in elderly people produced lower levels of IL-1β-converting enzyme that decreased IL-1β levels resulting in improved memory function compared to the other polymorphisms. Therefore, lower levels of IL-1β at old age can be considered as a defensive mechanism against memory loss and learning deficit.

Tumour Necrosis Factor-α (TNF-α)

TNF-α is a pro-inflammatory cytokine and is one of the major players in the immune system. Once this cytokine binds its receptor, the complex initiates signalling cascades that change cellular functions (Figure 3 and Figure 4). It has been reported to increase with ageing and age-related diseases (Ferrucci et al., 2005). A study reported increased levels in ageing in elder people (octogenarians and centenarians) with atherosclerosis and associated with mortality (McNerlan et al., 2002, O'Mahony et al., 1998, Armstrong et al., 2001, Bruunsgaard et al., 2000, Bruunsgaard et al., 2003b, Bruunsgaard et al., 2003a). It has been associated with an increased risk of recurrent cardiac events in post-MI as its levels increased. Additionally, renal patients with TNF-α receptors predicted cardiovascular disease (Ridker et al., 2000, Nilsson et al., 2013, Bae et al., 2017). It is more beneficial when it acts locally and harmful systematically. TNF-α has also been reported to be associated with risk for MI and Alzheimer's diseases. It can affect cellular metabolism, increased in type II diabetes, lower muscle mass and strength in older people (Zhang et al., 2017, Wang, 2015, McCusker et al., 2001, Collins et al., 2000, Zheng et al., 2016). The available TNF-α inhibitors may have possible prophylactic or ameliorating roles in cardiovascular and Alzheimer's disease in animal models (Ruparelia et al., 2017, Shamim and Laskowski, 2017).

There are also other pro-inflammatory cytokines including IL-6, IL-18, IL-2, IL-7, IL-8, IL-12 and IL-17. To ensure the balanced response of the pro-inflammatory cytokines, an anti-inflammatory mechanism must be effective and respond appropriately.

Anti-inflammatory cytokines in ageing and age-related diseases

Anti-inflammatory cytokines play a role in balancing the immune response initiated by the pro-inflammatory cytokines. This role is very important to avoid the transition of the immune response into chronic resulting in a disease-inducing state or even pro-inflammatory phenotype "inflammageing". Anti-inflammatory cytokines act on the pro-inflammatory cytokines such as IL-1α, TNF, and other major pro-inflammatory cytokines to block or modulate their levels to restore immune homeostasis (Rea et al., 2018). There are specific receptors for cytokines such as IL-1, TNFα, IL-18, soluble receptor antagonists/blocker, chemokines, siRNAs and/or microRNA can all play roles as inhibitors of the pro-inflammatory cytokines. The anti-inflammatory cytokines along with soluble receptor antagonists work in a complex network to achieve or restore immune homeostasis. Therefore, enhanced anti-inflammatory phenotype rather than pro-inflammatory phenotype can be a significant contributor to longevity which is highly affected by the pro-inflammatory phenotype (Franceschi et al., 2007b, Franceschi and Campisi, 2014, Westendorp et al., 1997).

The major anti-inflammatory cytokines players are IL-10, IL-37 and TGF-β (Rea et al., 2018).

1.3 Ion channels

A key objective of this project was to identify any common changes in ion channel genes (channelome) across different models of ageing. Ion channels are transmembrane proteins that are located on membranes of all cells and some subcellular organelles. They provide ion fluxes (gating; opening "activation" or closing "deactivation or inactivation" of the ion

channels) following electrochemical ingredients of different ions including K^+, Na^+, Ca^{2+} and Cl^-. The electrochemical ingredients mean that there are different concentrations of these ions across the membrane. Not only this but also different charges as well. When changes in the membrane potential take place, the cell tends to restore its equilibrium potential. To do this, the open channels allow their specific ions to pass through and this moves the membrane potential towards the ion's specific equilibrium potential. Since there are many ions, the final equilibrium potential will be somewhere closer to the major contributor to the membrane potential of the cell. Mostly, the membrane potential is closer to the K^+ equilibrium potential which is around -70mV.

The activity of ion channels depends on several factors such as changes in membrane voltage, binding of ligands (i.e. neurotransmitter and hormone), second messengers, temperature, chemical and/or physical stimuli. Ion channel-dependent cellular functions such as cell excitability, neurotransmitter and hormone release, gene expression, contraction, ion and water/fluid homeostasis are all dependent on ion channel isoforms as well as their tissue-type and age-dependent expression. Ion channels are extensively distributed among all cells in all tissues. They exist in open, inactivated closed, and closed states (de Hooge et al., 2005) as shown in (Figure 5).

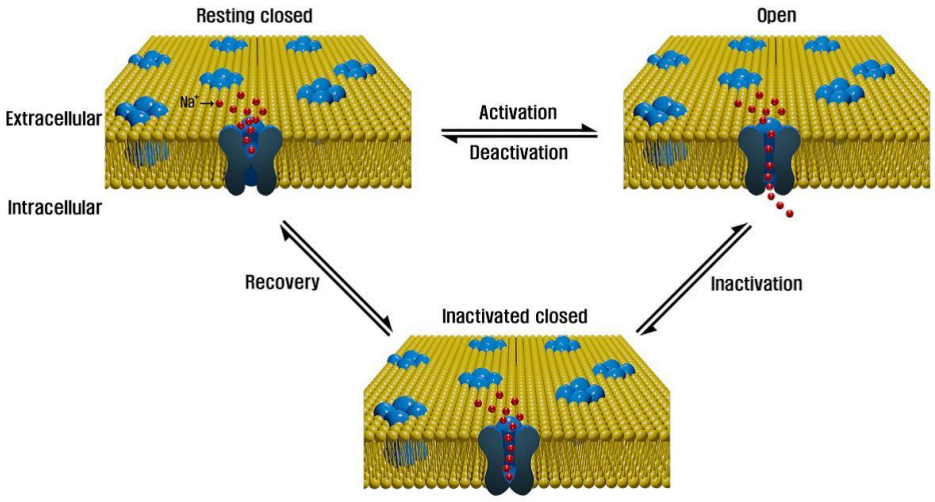

Figure 5: Ion channels states.
Ion channels exist in three forms; resting closed, open or inactivated closed. Cited from(Kim, 2014).

Structurally, a single protein can form an ion channel, but also ion channels often exist in a more complicated form composing of several subunits with each subunit encoded by a different gene (heteromultimers) (Bruunsgaard, 2002, Kang et al., 2009). There are more than 400 genes that encode for ion channels (Bruunsgaard, 2002, Kang et al., 2009).

Ion channels implicated in inflammageing

As described above, there are several ion channels and related porin genes. Many of these could be involved with inflammageing. The best known are described below.

K^+ channels

Potassium cation channels are a diverse family of membrane proteins in excitable and non-excitable cells. In human, there are more than 90 genes coding for α-subunits potassium channels. These channels have been studied for more than 20 years for their structures, gating mechanism, diseases and therapeutic drugs (Tian et al., 2014). Recently, the focus on these channels has increased that led to a deep understanding of their molecular mechanisms including ion selectivity, conduction/gating and related functional domains contributing to gating (Weingarth et al., 2013).

They are often made up of two main subunits; an α-subunit or principal subunit that determines the structure of the channel and a β- or auxiliary subunits that modify the properties of that channel. The α-subunits express in heterologous expression systems as functional homo-multimeric channel complexes and can co-assemble with β-subunits to form functional channels. According to structural and functional similarities, it is predicted that these principal subunits are at least eight families (Wei et al., 1996). Three of them (a) Kv, (b) ether-a-go-go-related gene (EAG), and (c) KQT, share a common motif of six transmembrane domains (TM) and are voltage-gated. Another two families (d) CNG (gated by cyclic nucleotide) and (e) SK/IK (gated by calcium) and the last three families of these α-subunits of the potassium channels are (f) Slo family (BK) channels with seven TM domains and gated by voltage and calcium or pH (Meera et al., 1997, Schreiber, 1998), (g) Kir channels contain two TM domains, and the last functionally diverse family is (h) K2p channels with two tandem repeats of the inward-rectifier motif (Tian et al., 2014).

The above-mentioned families are used to categorize potassium channels into three groups as (i) voltage-gated 6 TM potassium channels (Kv channels), (ii) calcium-activated 6/7 TM potassium channels (Kca channels) and (iii) 2 TM potassium channels.

One example of the K channels is the Big-conductance K channels (BK). It belongs to the calcium-activated 6/7 TM potassium channels (Kca channels) group with the ability to get activated by both Ca^{2+} and voltage (Meera et al., 1997). A unique feature of the BK structure is that it has a unique TM helix known as S0 (segment 0) at the N-terminus which is absent in other potassium channels (Figure 6). Through this S0, the N-terminus of the BK channel ends up in the outside region of the cell. The pore region of K^+ ion pass through the channel is located between S5 and S6 (Tian et al., 2014). The voltage sensors of the BK are like the other potassium channels in which they are comprised of S1-S4 membrane-spanning segments with 4 positively charged arginine residues in the S4 helix (Long et al., 2005a, Long et al., 2005b). The C-terminus of the BK is located inside the cell with two regulators of K^+

conductance (RCK) domains (RCK1 and RCK2) with a binding site for Ca^{2+} ions (referred to as the Ca^{2+} bowl) in an RCK2 domain (Jiang et al., 2001, Latorre and Brauchi, 2006).

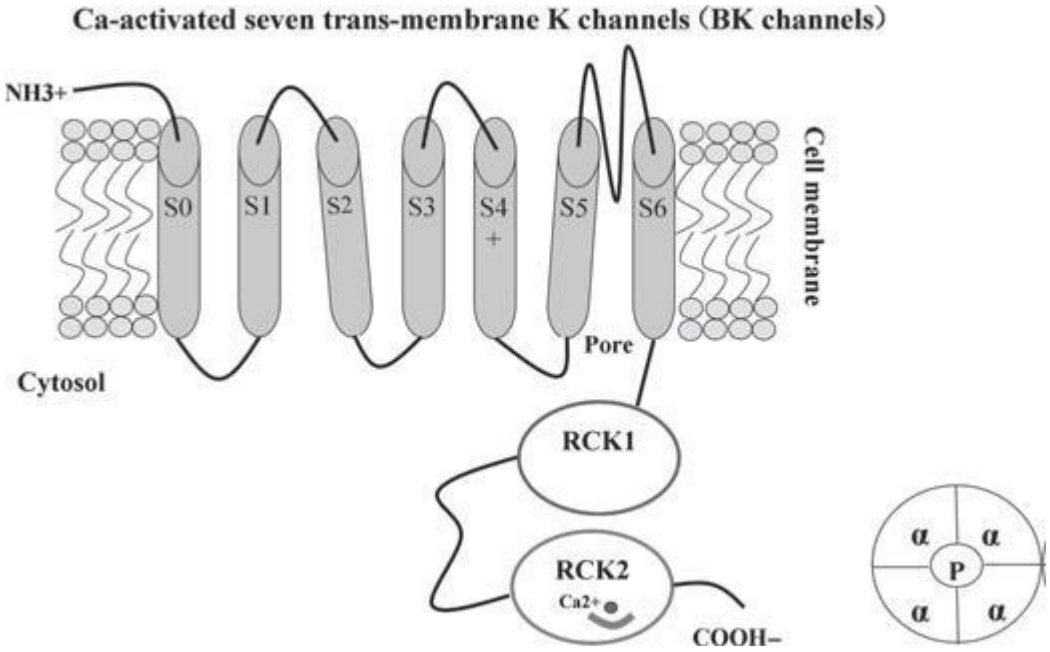

Figure 6: A schematic representation of the topology of the BK channel.
(A) The big conductance K channel (BK) subunits are composed of seven TM segments. The pore region is formed by S5 and S6 segments while the two regulators of the BK channels; RCK 1&2 with the Ca^{2+} bowl are shown in the intracellular (cytoplasmic) side of the cell. Also, the S0 segment that is unique to the BK channel is shown as well as the N-terminus of the channel in the extracellular side. (B) Structure of the tetrameric assembly of the BK channel. Cited here (Tian et al., 2014).

When a mutation(s) in genes coding potassium channels occurs, this can lead to dysfunction of the potassium channels and results in diseases in systems where these channels are broadly distributed (i.e. neuronal or cardiac) or other systems including nervous, musculoskeletal, and circulatory systems (Tian et al., 2014). Table 1 shows examples of diseases and related potassium channels.

Table 1: Diseases with their related potassium channels.

Diseases	Systems	Organs	Potassium channels	References
Alzheimer's disease	Nervous system	Brain	KCNC, KCNC2, KCNC3, KCNC4, KCNN4	(Etcheberrigaray et al., 1993, Angulo et al., 2004, Boda et al., 2012, Maezawa et al., 2012)
Parkinson's disease	Nervous system	Brain	KCNJ2, KCNJ4, KCNJ12, KCNJ14	(Gui et al., 2011, Deutch and Winder, 2006, Wang et al., 2005, Wu et al., 2010, Sander et al., 2012)
Short QT syndrome	Cardiovascular system	Heart	KCNH2, KCNQ1, KCNJ2	(Bellocq et al., 2004)
Rheumatoid arthritis	Musculoskeletal system	Articular joint	KCa1.1	(Beeton, 2017, Okamoto et al., 2010, He et al., 2011, Okamoto et al., 2012)

As more data has become available about potassium channels, researchers have started to test some modulators of these channels to obtain more and deep understanding of the structure, function and possible therapeutic targets. These modulators can be divided into peptide toxins and small molecules (Moczydlowski et al., 1988, Robertson and Steinberg, 1990). Peptide toxins can affect potassium channels from the extracellular side by either (i)

binding to the outer vestibule of potassium channels and mostly they insert a lysine side chain into the channel pore and block it (MacKinnon and Miller, 1989, MacKinnon et al., 1990) or by (ii) interaction with the voltage sensor domain of the potassium channels and keep them stably closed (Swartz and Mackinnon, 1997, Swartz, 2007). On the other hand, the small molecules bind to the inner side of the pore, the gating hinge, or the interface between the channels' subunits (α- and β-). These small molecules can be categorized into blockers and openers or specific vs multitarget (Robertson and Steinberg, 1990, MacKinnon and Miller, 1989, MacKinnon et al., 1990, Swartz and Mackinnon, 1997, Swartz, 2007).

BK channels have been reported to change with ageing in different cells including but not limited to VSMC and suprachiasmatic nucleus (Carvalho-de-Souza et al., 2013, Farajnia et al., 2015). The later is important for normal sleep and rest in the night as it is one of the circadian related genes. Additionally, other potassium channels such as voltage-gated K^+ channels are altered with ageing, as well. Such alterations can occur through oxidation of the potassium channels leading to age-related diseases such as neurodegeneration (Sesti, 2016).

Ca^{2+} channels

There are multiple types of calcium channels, physiologically distinguishable based on their sensitivities to voltage; they can be categorized into high and low voltage-activated Ca^{2+} channels.

Ca^{2+} ion channels are critical channels and they carry out important functions at the cellular and tissue levels including the activation of calcium-dependent enzymes, muscle contraction, secretion of neurotransmitters and hormones, and gene transcription (Zamponi, 2016, Simms and Zamponi, 2014, Zamponi et al., 2015).

Ca^{2+} channels have distinct functions depending on the tissue they are expressed in. For example, Cav2.2 channels are expressed in neurons and trigger the release of neurotransmitters (Zamponi et al., 2015). Additionally, Cav1.1 channels; the sole Ca^{2+} channels expressed in skeletal muscles, are very important in muscle contraction, triggering

excitation-contraction coupling. Skeletal muscle is one of the best-studied tissues in the context of ageing since skeletal muscle loss; sarcopenia is one of the major causes of frailty in the elderly (Vasilaki et al., 2010, Walston, 2012).

Usually, the behaviour of Ca^{2+} channels is regulated by a wide range of second messenger pathway with accessory proteins such as calmodulin. This depends on the isoform of the channel offering cell specificity in fine-tuning cell signalling through these calcium channels (Simms and Zamponi, 2014).

Mutations in genes coding for Ca^{2+} channels subunits can have serious consequences. For example, mutations in different Cav-α1 subunits have been reported in patients with congenital stationary blindness (Cav1.4) and in patients with familial hemiplegic migraine (Cav2.1) (Zamponi et al., 2015, Zamponi, 2016).

Other factors that can lead to dysregulation of calcium channels are abnormal channel expression and function (Zamponi, 2016). There are many examples for this including dysregulation of L-type channels that are involved in the age-related conditions, Parkinson's disease and drug addiction, and upregulation of N- and T-type calcium channels during different age-related conditions, chronic pain (Zamponi, 2016).

Many therapeutic Ca^{2+} channel modulators are available and so these could potentially help to treat age-related conditions involving Ca^{2+} channels. For example, isradipine (for Parkinson's disease), N-type channel blocker (for chronic pain), T-type channel blocker (for absence epilepsy), and dihydropyridine (DHPs, for hypertension) (Zamponi et al., 2015, Zamponi, 2016).

However, the side effects or less efficiency of the above mentioned Ca^{2+} channel modulators have been reported which can be attributed to the lack of specificity because there are different isoforms of the Ca^{2+} channels. (Zamponi, 2017, Zamponi et al., 2015). .

Na^+ channels

Sodium channels largely occur in two families; (a) voltage-gated sodium channels (VGSC) family which are distributed in various cell types throughout the body and (b) the epithelial sodium channels (ESC) that is expressed primarily in the skin and kidneys (Hernandez and Richards, 2019).

Voltage-gated sodium channels are transmembrane proteins. They are made up of two subunits. The first subunit is the one-pore forming α-subunit that allows the ions to pass through. This α-subunit consists of four transmembrane domains with six segments per domain and has the voltage sensor on the fourth segment of each domain (Yu and Catterall, 2003). The second subunit of the VGSC is the one to two β-subunits that regulate cells' excitability through modulating localization, gating and kinetics of the pore formed by the adjacent α-subunit (Hernandez and Richards, 2019). Because of their large and extracellular V-set immunoglobulin domain of the β-subunits, they are part of the Ig superfamily of cell adhesion molecules. The β-subunits are encoded by *SCN1B-SCN4B* genes (Yu et al., 2005, O'Malley and Isom, 2015).

These channels open when the membrane potential in their surrounding area become depolarized. This allows the flow of sodium ions following their concentration gradients. Once the membrane potential altered, these sodium channels are the first to open which leads to the accumulation of positively charged sodium ions inside the cell (Grider and Glaubensklee, 2019). The ability of excitable cells (neurons or muscle cells) to depolarize is vital as it results in the generation of an action potential leading to a formation of cellular response/function such as contraction (Grider and Glaubensklee, 2019). There is two gates for voltage-gated sodium channels; (a) activation gate that allows the flow of sodium ions into the cell and depolarization and (b) inactivation gate that stops the flow of sodium ions regardless of the status of the activation gate. These together maintain the membrane depolarization in balance. This also means that once the activation gate opens, they will

remain like this for a few milliseconds before they close and will never open again unless cell repolarization takes place to a certain voltage threshold even if there is a continuous stimulus. This mechanism is important to prevent cells from prolonged or continuous depolarization (Wang et al., 2017). To achieve such balances, voltage-gated sodium channels must be targeted to specific cellular domains and interact with several proteins (extracellular matrix, membrane and cytoskeletal proteins) to form a multiprotein complex (Wang et al., 2017).

Sodium channels are important clinically in ageing because any impairment or dysfunction can lead to some neurological (i.e. epilepsy) or cardiac (i.e. myopathies or cardiac arrhythmias) diseases. Dysfunction can be genetic or acquired. Many pharmacological compounds target sodium channels such as lidocaine (anaesthetics), phenytoin and lamotrigine (antiepileptics), and flecainide and mexiletine as antiarrhythmics (Kotipoyina and Warrington, 2019, Hernandez and Richards, 2019, Iorga and Horowitz, 2019). With sodium channel blockers, care must be taken as inappropriate use may have negative consequences such as seizures and arrhythmias (Torp and Simon, 2019).

Cl^- channels

Chloride channels are expressed in every cell types with different cellular functions (Jentsch et al., 2002, Jentsch and Gunther, 1997). These channels are involved in the control of transepithelial transport, membrane excitability, the regulation of cell volume, and repolarization after contraction (Jentsch et al., 2002, Planells-Cases and Jentsch, 2009, Vaishali and Satya, 2016). They are also involved in the regulation of the intracellular and intraorganelle pH. The major chloride channels that are involved in these functions are voltage-gated, the cystic fibrosis transmembrane conductance regulator (CFTR) and its related channels, and the ligand-gated chloride channels that are activated by gamma-aminobutyric acid (GABA) and glycine (Planells-Cases and Jentsch, 2009, Vaishali and Satya, 2016).

The importance of chloride channels appears more in cases where there are mutations in the genes encoding these channels resulting in diseases such as osteoporosis, inherited kidney stone disease, some forms of myotonia, epilepsy diseases (GABA and glycine receptor), and the most popular one is the cystic fibrosis (Planells-Cases and Jentsch, 2009).

Although Chloride channels have been targeted for medications ((Tang and Chen, 2011)), they have been less extensively studied at the molecular levels as other channels which resulted in a relative lack of information of their structure, function leading to less utilization of these channels as treatment targets (Martinez and Mohiuddin, 2019).

TRP channels

Transient Receptor Potential Channels (TRPs) are one of the largest families of ion channels. They are involved in the detection of chemical, thermal, mechanical stimuli as well as the transduction of pain in the form of inward current (Wang and Woolf, 2005).

There are many types of TRP channels. Six subfamilies have been identified in mammals. Also, an additional subfamily found in invertebrates and nonmammalian vertebrate animals. TRP channels are members of the voltage-gated ion channels (Rosasco and Gordon, 2017) and they are predominantly non-selective cation channels. They play roles in several physiological functions such as store-operated Ca^{2+} entry, axonal guidance, Mg^{2+} uptake, and thermal/mechano/chemical-sensation (Song and Yuan, 2010, Ramsey et al., 2006, Levine and Alessandri-Haber, 2007). Although heterotetramers of TRP channel subunits have been identified (Cheng et al., 2010), they form tetramers of identical subunits.

Structurally, as other voltage-gated superfamilies, each subunit of the TRP channels consists of six membrane-spanning helices with a re-entrant pole loop between the 5^{th} and 6^{th} transmembrane helices. Also, TRP channels have their amino- and carboxy-terminal in the intracellular compartment. The voltage-sensing or voltage-sensing-like domains are the first

four segments while the ion-conducting pore is formed by the remaining two segments and the re-entrant pole loop (Rosasco and Gordon, 2017).

There are seven subfamilies of TRP channels that are (a) TRPA, (b) TRPC, (c) TRPM, (d) TRPML, (e) TRPN, (f) TRPP, and (g) TRPV. The individual subunits of all subfamilies' members are thought to contain six transmembrane segments assembling in tetrameters to form a functional TRP channel (Rosasco and Gordon, 2017). These subfamilies are not distributed equally in all tissues, species and even their functions are not the same (Rosasco and Gordon, 2017). TRP channels also change with ageing. For example, TRPV4 has been reported to change in terms of its distribution with ageing (Lee and Choe, 2014). Additionally, decreased RyR expression in atrial cells could be attributed to the age-related reduction in the intrinsic heart rate (reviewed here (Rao, 2016).

General roles and functions of ion channels

Resting membrane potential (RMP)

One of the clearest general roles of ion channels is the control of RMP. RMP of a given cell is the electrical potential (voltage) difference across the cell membrane when it is at a non-excitable state. Typically, cells have their RMP in the range of -70 to -80 mV. This means that the potential inside the cell is 70 to 80mV lower than that of the outside when the cell is at rest (Morth et al., 2007, Wright, 2004).

Although many ions contribute to the RMP, the most common candidates are the K^+ channels. Additionally, there are other intracellularly negative proteins and organic phosphates that cannot cross the cell membrane and contribute to the RMP (Morth et al., 2007). Furthermore, Lewis et al (Lewis et al., 2011a) showed that in chondrocytes TRPV5 channels have partially participated in the control of RMP in chondrocytes that eventually controlled cell volume. Different cell types in the body have different and characteristic RMP. The most important ones are those of the nervous and muscular (smooth, skeletal and cardiac cells) systems (Chrysafides and Sharma, 2019).

The importance of RMP is that it allows cells to perform a specific role via a rapid change in the membrane potential when gets excited. For example, in neurons the change in RMP allows the cell to communicate with other cells by releasing neurotransmitters while in muscle cells such changes of RMP can lead to muscle contraction (Chrysafides and Sharma, 2019).

Physiologically, ions that contribute to RMP rarely reach equilibrium potential because they cannot freely move across the cell membrane which is not permeable to most ions. This is because most key K^+ ion channels are closed at rest. One exception here is the K^+ ions that has a "leak" channel that allows it to diffuse out of the cell down its electrochemical gradient which means that the K^+ is close to its equilibrium potential and the cell membrane potential is close to the equilibrium potential of the K^+ ions that is approximately around -90mV (Chrysafides and Sharma, 2019, Wright, 2004).

The ionic distribution necessary to maintain the RMP is created by the ATP-driven pump (Na/K-ATPase). Although both ions do not completely reach their equilibrium potentials, small amounts of Na^+ ions can find their way into the cell and some K^+ ion leaves it through the leak channels. Therefore, Na/K-ATPase removes three Na^+ ions from the intracellular space to outside and brings two K^+ ions into the cell in exchange (Enyedi and Czirjak, 2010).

Clinically, it is vital to maintain the RMP because any abnormal changes in it can affect the normal functions of the cells. In this thesis, there will be a particular focus on any changes of ion channels that might change with age and affect the RMP. An example, clinically where RMP does change is, for example, hypokalaemia (lower concentration of K^+ ions in the blood). This triggers the flux of K^+ ions out of the cell leading to hyperpolarization of the cell. This means that a higher trigger is required to achieve an action potential leading to a more negative potential in the cardiac muscle from the more complete recovery of Na^+ channel

inactivation. Consequently, hypokalaemia leads to delayed ventricular repolarization leading to re-entrant arrhythmias (Castro and Sharma, 2019) and other physiological dysfunctions. On the other hand, hyperkalaemia results in depolarization of the cell membrane that inactivates Na^+ channels leading to major arrhythmias (Simon et al., 2019). In short, due to the fundamental importance of the RMP, any major electrolyte abnormalities with age would have serious consequences.

Action potential

An action potential is defined as the fast sequence of voltage changes across a membrane that transmits information along a neuron or muscle fibre. Although action potential is mainly discussed in the context of neurons, it also occurs in all excitable cells such as cardiac muscle and some cells of the endocrine system (Wei and Richards, 2019, Stojilkovic et al., 2010). This membrane voltage or potential is determined by the relative ratio of ions (extracellular to intracellular) and the membrane's permeability of each ion (i.e. Ca^{2+}, Na^{2+}, K+, Cl-, etc). the initial rapid rise in potential (from the RMP to less negative levels) of cells; is known as depolarization, and mediated by the opening of voltage-gated sodium channels in the cell membrane. This is an all or none event. Once channels open, they would tend to go back to their normal state and in this case, the repolarization is triggered by the opening of potassium ion channels. In turn, the normal resting state, the RMP, as described above is then maintained by the Na/K-ATPase. This pump ensuring that appropriate amounts of these ions are maintained in each side of the membrane (Grider and Glaubensklee, 2019).

There are three main stages of each action potential; depolarization, repolarization and hyperpolarization (Ulbricht, 2005). Depolarization is determined by a cell's threshold voltage at which voltage-gated sodium channels (Nav) open allowing an influx of the positively charged Na ions into the cell leading to further depolarization of the membrane and opening more Na channels. This process lasts up to 1ms. After that, Nav becomes inactivated and can no longer be able to flux ions (Ulbricht, 2005). As a cellular response to

restore its resting state, voltage-gated potassium (Kv) channels open starting the repolarization state. The kinetics of these channels are slower than Nav although both have nearly the same threshold voltage. So, after 1 ms the slow Kv opens while the faster Nav gets inactivated leading to the move of K^+ ions out of the cell and decreasing the membrane potential towards the cell's resting voltage. Once the membrane potential falls below the threshold (repolarization), Nav channels close and the slow Kv starts to close but it remains longer in order to return the cell to resting membrane voltage (Ulbricht, 2005, Grider et al., 2019).

In neurons, action potentials spread a signal along the length of an axon differently in myelinated versus unmyelinated axons based on the lipid contents that acts as an insulator of ion flow (Grider et al., 2019). Therefore, even if ion channels themselves turn-out not to change with age, changes in the control of myelin production could have similar effects.

Deficits in action potentials can be determined by conduction velocity tests especially in the peripheral nerves, but this requires identification of specific mechanism(s) that block the conduction or decrease its velocity (Burke et al., 2001). Some conditions that can affect the conduction velocity by decreasing or even blocking the speed of electrical signal conduction include injured axons and nerve construction as seen in carpal tunnel syndrome while diseases that decrease the conduction velocity involve diabetic neuropathy, and multiple sclerosis (Grider et al., 2019, Burke et al., 2001, Nguyen and Taylor, 2019, Bodman and Varacallo, 2019). Additionally, some genetic disorders that lead to channelopathies can also decrease the conduction velocity in the peripheral nervous system. Examples of such channelopathies include neuromyotonia, epileptic seizures or migraines (Grider and Glaubensklee, 2019).

Clinically, it is important to know how action potential work. For example, local anaesthetics usually work via blocking voltage-gated sodium channels that prevent signal

transmission in pain. This occurs when the anaesthetics pass through the cell membrane and block the open Na channels (Scholz, 2002). To summarize, the action potential is very important to normal cellular functions and any age-related abnormal changes would have global serious consequences on the cell or tissue functions.

Cell volume

The RMP, and thus ion channels, are crucial to cell volume control. A cell needs to maintain its volume for survival (Abdul Kadir et al., 2018). When changes occur in the environment around the cell such as constantly changing osmolality and compressive loads, the cell volume changes (i.e. shrinkage) as well (Abdul Kadir et al., 2018). This requires the cell's response that can either regulate this change or go through the apoptotic pathway (Wibberley et al., 2015). Such changes are called (i) regulatory volume increase (RVI), which is involved in adaptation to hypertonic media and cell survival, and (ii) apoptotic volume decrease (AVD) mechanism which is mainly involved in cell death (Orlov et al., 2013, Lang and Hoffmann, 2013).

Naturally, the osmolarity of the blood must be maintained precisely to allow cell volume to be maintained. At the systemic level, osmolality is affected by several periventricular osmosensing structures in the brain. The response usually involves neurons that act in a way like that of the cell (Wibberley et al., 2015, Feetham et al., 2018).

At the cellular level, one of the key regulators of maintaining cell volume is the membrane potential and has been shown in a few cells such as cardiomyocyte, chondrocyte and retinal Muller cells (Abdul Kadir et al., 2018). Membrane potentials contribute to cell volume control by changes in ion fluxes. For example, ion channels selective for KC behave like osmolyte channels rather than just maintaining the RMP (Abdul Kadir et al., 2018). Additionally, Lewis et al, have shown that TRP channels are significant players of the RMP in chondrocytes (Lewis et al., 2011a) and suggested that these channels may facilitate the control of cell volume (Lewis et al., 2011b). Also, TRPV4 have been suggested as central to

the regulatory volume decrease and that chondrocytes decrease in number but increase in cellular volume with age (Lewis et al., 2011b).

Channelopathies

Diseases resulting from deficits of ion channels are termed channelopathies. To date, there are few channelopathies specifically linked to ageing, but this may be because they have not yet been discovered. Channelopathies can be (a) acquired (i.e by acquired disorders, toxins, drugs, etc) or (b) inherited through genetic mutations in genes encoding ion channels or its associated/accessory proteins (inherited ion channelopathies) (Imbrici et al., 2016). Mutations may include small deletions/insertions, frame-shifts, stop codons, missense, splice-site mutations and deletions or duplications of exons. Consequently, ion channel biophysical properties are altered which include voltage-dependent gating, single-channel conductance, kinetics, ion selectivity and change of signalling pathways. Also, ion channel expression may be decreased. Hyperexcitability disorders may result from mutations that lead to loss-of-function in K^+ or Cl^- channels and gain-of-function mutations in Na^+ and Ca^{2+} channels. An example of this can be seen in epilepsy or myotonia. Oppositely, the excitability of inhibitory neurons can lead to epilepsy through loss-of-function mutation in Na^+ channels and gain-of-function mutations in neuronal K^+ channels. Therefore, the phenotype or the final effect of a mutation in ion channel gene depends on the functional role of the ion channel itself, and the specific expression pattern (Imbrici et al., 2016, Kim, 2014).

Channelopathies can be life-threatening diseases such as sudden cardiac death (Fernandez-Falgueras et al., 2017) and cause rare diseases (Imbrici et al., 2016). Also, the involvement of ion channel dysfunction in some diseases with abnormal movement, epilepsy, and migraine and/or ataxia as seen in Paroxysmal Dyskinesias in which mutations in genes encoding for calcium-activated potassium channel subunit alpha-1 (KCNMA1) and voltage-

gated sodium channel type 8 (SCN8A) affecting ion channel function and neuronal excitability are detected (Erro et al., 2017).

Channelopathies can be detected in any organ. However, some tissues/organs may show symptoms of channelopathies while the same ion channel expressed in other tissues do not. For example, AQP4 (Aquaporin4) is involved in NMO (an autoimmune disease called neuromyelitis optica) with symptoms such as blindness, sensory defects and paralysis but does not manifest any pathological phenotypes when expressed in kidneys. Another example is TRPC6 (Transient Receptor Potential canonical 6) which is expressed in the kidneys. It is involved in Focal and segmental glomerulosclerosis (FSGS type 2) disease with symptoms such as proteinuria and rapid renal function decline but has not been associated with any pathological phenotypes in smooth muscle (Kim, 2014).

Since the major age-related diseases are musculoskeletal, cardiovascular, and brain, disorders, examples of ion channelopathies in these tissues will be covered.

Channelopathies in the Musculoskeletal system

In this section, examples of channelopathies in the musculoskeletal system will be covered. Also, a link to a common age-related disease such as OA will be made.

Genetic mutations of genes coding for musculoskeletal ion channels result in gain/loss of function that can affect muscle relaxation. Generally, most mutations occur in the chloride channel (ClC^{-1}), calcium channel ($Ca_{V1.1}$), sodium channel ($Na_v1.4$) and several potassium channels ($K_{ir2.1}$, $K_{ir2.6}$, and $K_{ir3.4}$) (Cannon, 2015). There are several examples of musculoskeletal ion channelopathies including but not limited to myotonia and periodic paralysis. Myotonia is characterized by impaired muscle relaxation after contraction and periodic paralysis (PP) is characterized by transient loss of muscle excitation. Several diseases are belonging to the same group of Non-dystrophic myotonias such as (a) myotonia congenital (MC) which is caused by loss-of-function mutations in the CLCN1 gene coding for the skeletal muscle

chloride channel ClC^{-1} while (b) paramyotonia congenital (PMC) and (c) sodium channel myotonia (SCM) are caused by missense mutations in the SCN4A gene coding for voltage-gated sodium channel NAv1.4 in the skeletal muscle. On the other hand, periodic paralysis is characterized by transient loss of muscle excitability that leads to flabby paralysis with weakness (Imbrici et al., 2016). PP can be classified into:

a) Hyperkalemic PP caused by gain of function mutations in Nav1.4 that show impaired inactivation leading to continuous Na influx and cell depolarization that inactivates the Nav1.4 channel. The depolarization increases K^+ efflux from the muscle to the serum in which its level increases up to 6 mEq/L leading to paralysis (Imbrici et al., 2016). Hyperkalemia is also observed in elderly people due to several factors including age-related physiological changes and has been associated with increased morbidity and mortality (Turgutalp et al., 2016).

b) Hypokalemic PP is caused by SCN4A (20%) and CACNA1S (60%) mutations of positively charged residues in the voltage sensors of the channel. This produces an abnormal infusion pathway for Na^+ and H^+ ions leading to depolarizing cation leak currents which are known as gating pore currents (*I*gp) (Imbrici et al., 2016). Such fibre depolarization results from the unbalance between the depolarizing *I*gp and repolarizing K_{ir} and sarcoplasmic K_{ATP} channel currents. Marked serum hypokalemia that decreases gene expression of the K_{ir} channels is produced by activation of 3Na+/2K+-ATPase upon administration of insulin/glucose (as a treatment) (Imbrici et al., 2016). Together, these factors contribute to the fibre depolarization which inactivates ion channels; Nav1.4 and Cav1.1 that are associated with paralysis (Imbrici et al., 2016). Hypokalemia has also been reported in elderly people (Bardak et al., 2017). The third classification of the PP is:

c) Andersen-Tawil Syndrome (ATS) which is a multi-organ syndrome. It is associated with PP, cardiac arrhythmias, and dysmorphic features (skeletal malformation). Can occur with both hyper- or hypo-kalemia that is associated with paralysis as well as various

heart manifestations including long QT syndrome. So far, the KCNJ2 gene on chromosome 17 has been found to play a significant role in ATS. About two-thirds of the ATS patients have mutations in this gene. Such mutations can have several consequences including but not limited to (a) suppressing $K_{ir2.1}$ currents and/or enhancing the inward currents because of the dominant-negative effects, (b) decreasing the PIP2 sensitivity, (c) exaggerating the inhibitory effects of intracellular Mg^{2+} or H^{+}. Patients with ATS, the Kir2.1 channel in their heart and skeletal muscle is influenced by the dominant-negative effects exerted by KCNJ5 (Imbrici et al., 2016, Statland et al., 2014).

Osteoarthritis is one of the age-related diseases of the musculoskeletal system. Skeletal muscle wasting has been linked to OA as such muscle waste affects the stability of a joint leading to the development and/or progression of OA (Shorter et al., 2019). Several membrane proteins, ion channels and receptors change in OA models and/or A patients (Lewis and Barrett-Jolley, 2015). Ion channels have been used/suggested as biomarkers for several diseases (Lewis and Barrett-Jolley, 2015, Daniil et al., 2016, Javier Camacho et al., 2016). In Osteoarthritis (OA), Lewis et al (Lewis and Barrett-Jolley, 2015) showed that several membrane ion channels are differentially expressed in OA as illustrated in Figure 7.

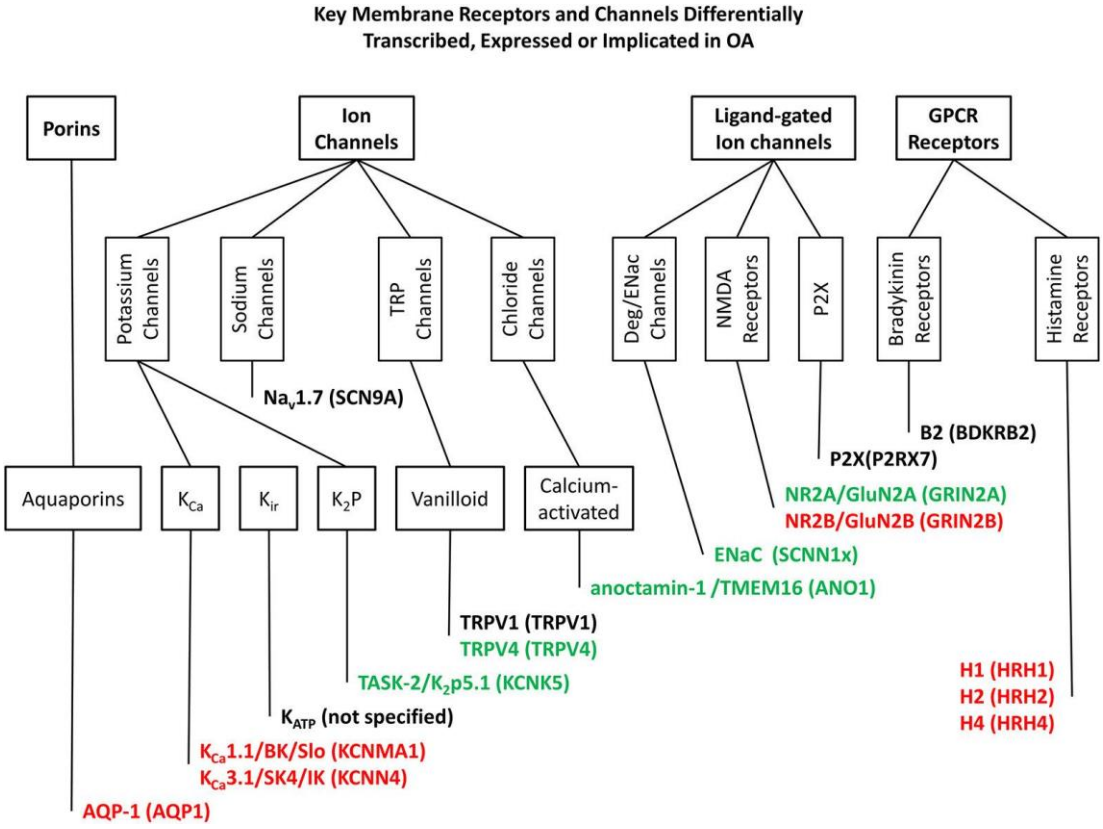

Figure 7: Key membrane ion channels and receptors differentially expressed in OA.
Genes/proteins labelled in red are overexpressed, in green downregulated and in black not changed although linked to OA. The written format is as following: common names/alternative names (human gene or equivalent). Cited from *(Lewis and Barrett-Jolley, 2015)*.

Although there are several drugs targeting ion channels such as Nav channels blockers (which has been successfully employed as anticonvulsants and antiarrhythmics), still several other drugs that target ion channels such as ion channel modulators are not able to distinguish different isoforms of specific ion channels which expose patients to the side effects of the drug that can be very serious (Imbrici et al., 2016). The second example of channelopathies in this thesis will be on the cardiovascular system.

Channelopathies in the Cardiovascular system

Balanced ionic currents generate cardiac action potential which contributes to normal cardiac function (Amin et al., 2010). When such balance is disturbed due to ion channel dysfunction, cardiac arrhythmias may occur which can be life-threatening (Kim, 2014). About 50% of sudden arrhythmic death syndrome (Behr et al., 2008) and around 20% of sudden infant death syndrome (Wilders, 2012) are caused by cardiac ion channel

dysfunction (cardiac channelopathies). Cardiac arrhythmic disorders occur due to mutations in genes encoding for Ca^{2+}, Na^{+}, K^{+} and TRP (Transient Receptor Potential) genes. For example, ATP-sensitive K^{+} channel in mitochondria (mitoK_{ATP}) of the cardiomyocyte plays a significant role in cardiomyocyte protection and this channel is altered with aging. However, the reasons for this age-related dysfunction of the mitoK_{ATP} are not known and could be due to; (a) change of channel density, (b) responsiveness to stress stimuli, or (c) defective communication to respiratory electron transport chain (Pi et al., 2007). Regarding endothelial and vascular smooth muscle cells, several ion channels are expressed including but not limited to chloride, calcium (voltage-gated and store-operated), and stretch-activated cation channels. All those channels can be involved in vascular tone regulation. For instance, BK opening leads to efflux of K^{+} that results in membrane hyperpolarization followed by the closure of a Ca^{2+} channel (voltage-dependent) and decreased Ca+ entry to cell leading to vasodilation. Also, vasodilation can occur through nitric oxide which is regulated by BK as well (Carvalho-de-Souza et al., 2013). With ageing, this channel has its expression, structure and function changed (Carvalho-de-Souza et al., 2013). Since increases in blood pressure (Pinto, 2007) are one of the most common conditions associated with age, and this is dependent, in part, on vascular tone, it will be particularly interesting to discover whether these ion channels involved with vascular tone are altered in age. Next, ion channel dysfunction in the nervous system is also an interesting topic to look at and will be covered in the following section.

Channelopathies in the Brain

Ion channels that are associated with ion disturbance in neurological disorders are of two types; either ligand-gated or voltage-gated ion channels. Epilepsy, seizures and the highly age-related conditions of Alzheimer's and Parkinson's diseases have been associated with mutated or dysfunction of ligand-gated channels such as mutated nAChRs, ionotropic glutamate receptors, GABA receptors (an inhibitory neurotransmitter), and P2X receptors. Besides, ataxia, epilepsy, and periodic paralysis are caused by defects in sodium channels;

SCN2A, SCN8A, and SCN9A. Potassium channel mutations have been linked to diseases such as epilepsy, ataxia, and seizures. Also, ataxia, paralysis, migraine and Alzheimer's disease have been associated with abnormalities in calcium channels, reviewed here (Behr et al., 2008). As an example, Ca^{2+} channels play significant roles in different tissues. Generally, Ca^{2+} ion channelopathies in any excitable tissues result in a periodic disruption of rhythmic activity that leads to a specific function impairment. For instance, mutations in the CACNA1A gene that encode for ion-pore and voltage sensor-containing α1 subunit of the P/Q-type voltage-gated calcium channels lead to several distinct diseases including but not limited to migraine, episodic ataxia type 2 and spinocerebellar ataxia type 6. Among the most common neurological disorders in the elderly are Alzheimer's disease (N-methyl-D-aspartic acid/NMDA receptor, ryanodine receptor and calcium-sensing receptor) and Parkinson's disease (Cav1.3 L-type calcium channel). In the related Huntington's disease, there are mutations in the IP3 receptor and store-operated calcium channel. For instance, in Alzheimer's disease, more evidence points toward changes in the cellular Ca^{2+} homeostasis at very early stages of the disease pathogenesis. Most studied Ca^{2+} ion channels in this disease are the ryanodine and IP3 receptors that have been highly expressed in the brain (cortical and hippocampal) regions. Those regions are associated with learning and memory functions (Chakroborty and Stutzmann, 2014).

So ion channels are involved in a range of disorders of joints, blood vessels, and brain and in this thesis, any changes appear to occur due to age or inflammation will be examined.

1.4 Aims

In the light of the above evidence, I hypothesised that expression of a common set of inflammatory and/or ion channel genes may alter with age across tissues. To address this aim, transcriptomics; RNA deep-sequencing, of a number of different ageing models, were used. These models included both genuine ageing (tissue from young and old rat blood vessels, synovial joints and brain) and an inflammageing model (addition of IL-1ß/TNFα). These large datasets were bioinformatically analysed and validation of ion channels took place where practical.

Specifically, the main aims were to:

1) Identify changes in a) the whole transcriptome and b) ion channel gene transcription in young and old rat aorta, FLS and PVN tissue.

2) Identify changes in a) the whole transcriptome and b) ion channel gene transcription of control and cytokine (IL-1ß/TNFα) treated aortic smooth muscle cells and FLS.

In the future, it may be possible to identify markers of early ageing that may be risk factors for disease.

Chapter 2: Materials and Methods

2.1 Tissues and Cell culture

Tissues and cells were obtained from male Wistar Kyoto skeletally mature young rats (approximately 2 to 3 months unless otherwise stated), culled for associated projects. It is known that rats develop quickly and it has been estimated that every month of rats' life approximately equals 2.5 years of human life. This means that the rats used for the ageing study, aged of 24 months+, were equivalent to a human age of 60-65 years (Van Gulick et al., 2019).

FLS

Culture protocol

FLS cells culture was prepared from synovial tissues of normal rat knee joints from the synovial membrane. Tissues were cultured in low-glucose DMEM X1 with 4mM Glutamine and pyruvate (gibco, life technologies) containing 20% Heat inactivated Fetal Bovine Serum (Gibco, Life technologies cat#: 10500-064), 100U/ml penicillin and 100µg/ml streptomycin (Sigma life science cat#: P4333), and 2.5 µg/ml Amphotericin B (Gibco, life technologies, cat#: 15290-029). For days 1-7, DMEM X1 medium was replaced daily. After day 7, the synovial tissues were discarded, and cells were allowed to grow for two more days. To detach cells from the plates, cells were washed with DMEM X1 (as above but without FBS), pre-warmed 1X trypsin (sigma life science, cat#: T4174) was used to detach cells, incubated at 37°C in 5%CO2 for 2-5 minutes, trypsin was quenched with DMEM X1 containing FBS (as above), centrifuged at 1500 rpm for 5 minutes, and the pellet was resuspended in DMEM X1 containing FBS and sub-cultured. Thereafter, cells were seeded according to the experiments to be carried out. Cells between passage 3 to 6 were used for all experiments.

VSMC

Culture protocol

The thoracic aorta is dissected from rat, cleaned and snipped into branches on ice-cold dissection solution containing (in mM) 134 NaCl (Sigma Cat#: S7653), 6 KCl (Sigma Cat#:

P-4504), 0.42 Na_2HPO4 (Sigma Cat#: S-0876), 1 $MgCl_2$ (BDH VWR International Ltd., Cat#: 22093 3M). 2 $CaCl_2$ (Fluka Analytical Cat#: 21114-1L), 10 HEPES (Sigma Cat#: H3375-500G), and 10 glucose (Sigma Cat#: G-4500), adjusted with NaOH to pH 7.4. Then, these branches were transferred into another dissection solution in which $CaCl_2$ is reduced to 0.1 mM (low-Ca^{2+} solution) and warmed to 35-37^{O}C for 10 min. After that, branches were removed to a digestion buffer containing low-Ca^{2+} solution with papain (1.4mg/ml, Sigma Cat#: 76220-25G), 4-dithioerythritol (0.9 mg/ml, Sigma Cat#: D8255-5G) and bovine serum albumin (BSA) (0.9 mg/ml, Sigma Cat#: A9647-10G) for 25-30 min at 37^{O}C. Branches were then washed 3x in a pre-warmed low-Ca^{2+} solution containing 1 mg/ml BSA. Because branches are very fragile now, they were carefully transferred into a fresh low-Ca^{2+} solution containing 1 mg/ml BSA for cell dispersion by gentle trituration through a sterile plastic Pasteur pipette. Then, connective tissues were discarded, the solution containing VSMCs was split over 2 wells of the 12-well plate and fresh pre-warmed high glucose 1x DMEM complete media (containing 15% Fetal Bovine Serum, 50U/ml Penicillin, 50µg/ml Streptomycin and 2.5µg Amphotericin B (Fungizone), these components were from the same company) added to each well. Cells were allowed to adhere for up to 6 hours in 37^{O}C in a humidified atmosphere (10% CO_2) before the media changed. After 24 hours, the media was changed again and every day afterwards. Once cells grew and became 80-90% confluent, they were washed with PBS or serum free-medium, 1x trypsin/EDTA added, incubated at 37^{O}C for 15 min, trypsin then quenched with complete medium and split into new culture flask/plate as per experiment requirement. Cells between passage 3 to 6 were used for the experiments.

2.2 Electrophysiology

Fire-polished pipettes, fabricated from thick-walled 1.5 mm o.d. borosilicate glass capillary tubes (Sutter Instrument, Novato CA, USA supplied by Intracel, UK) were used. These were prepared using a two-stage vertical pipette puller (Narishige, Japan) and then filled with the intracellular solution. When filled, they had pipette resistance of

approximately 8 MΩ. Recordings were made with a Cairn Optopatch amplifier is largely in voltage-clamp mode (Cairn Research, UK), command potentials controlled with a window PC running WinWCP V5.3.4 (John Dempster, University of Strathclyde). Currents were low-pass filtered (1 kHz) and digitized at 5 kHz with CED1401 interface.

Intracellular solution was 115 mM Gluconic acid/Potassium salt (Sigma Cat#: G-4500), 26 mM KCl, 1 mM $MgCl_2$ (BDH, VWR International Ltd), 5 mM Ethylene glycol tetra-acetic acid (EGTA) (Sigma Cat#: E-0396), 10 mM HEPES, pH 7.2. Extracellular (bath) solution was 140 mM NaCl, 5 mM KCl, 2 mM $CaCl_2$ (Fluka Analytical cat#: 21114), 1 mM $MgCl_2$, 10 mM HEPES, and 5 mM Glucose, pH of 7.4. The bath (extracellular) solution is continuously changed through a flow-system in order to maintain the pH of the bath solution. All drugs were mixed well with the extracellular solution depending on their required final concentration that depends on the nature of the experiment. Then, perfused into the bath at a flow rate of ~3ml/min, left there to exert effects before recordings started. Cells, intracellular and extracellular solutions, and the microscope are all contained within a Faraday cage to minimize the noise signals and for earthing. All recordings were made at RT. All components of intracellular and extracellular solutions were from Sigma unless otherwise stated.

There are different recording configurations, in this project the whole-cell voltage-clamp configuration was used to look at the effects of different potentials and drugs on all cellular channels. Whole-cell current-clamp was used to record membrane potentials.

1.3 Next-generation sequencing (NGS)

This is one of the ways to look at the expression of the cellular genes in response to variable signals. I used whole transcriptomic profile. To be able to establish such experiments, RNA samples must be extracted from cells/tissues. Next, I will cover the RNA extraction from different tissues before and after optimization of the protocol.

RNA extraction

FLS

Cells were washed with serum-free media, 1x trypsin/EDTA added, incubated at 37^{O}C for up to 5 min, quenched with complete medium and centrifuged (1500rpm) for 5 min. RNA extraction kit (RNeasy plus micro kit, cat# 74034) was used to extract RNA from FLS cells. The manufacturer protocol was followed with some additional modifications to increase RNA yields. FLS cells pellet was resuspended in 350 µl of RLT buffer containing 2β-Mercaptoethanol (Sigma Cat#M6250-100ML) (1ml:10µl ratio, respectively), syringed (>30x) using a sterile RNase-free 1ml syringe connected to an RNase-free 19" G needle with 40mm length and stored at -80^{O}C for at least 2 hours to make crystals that would increase cell lysis resulting in increased RNA yields. Cell lysates were then defrosted on ice, briefly spun at full speed for 40-50 seconds to bring down everything, transferred cell lysates into gDNA eliminator spin column, closed the lid and spun at full speed for 30sec. An equal volume of 70% Ethanol added to the flow-through, mixed well by up and down pipetting, transferred into MinElute spin column, closed the lid and spun at full speed for 30 seconds to trap RNA. The flow-through was discarded and the column was placed in a new 2ml collection tube. 700 µl of RW1 buffer added to the column, closed the lid and spun at full speed for 30 seconds. Flow-through was discarded and the column was placed in a new 2ml collection tube. 500µl of RPE buffer added to the column closed the lid and spun at full speed for 30 seconds. Flow-through was discarded and the column was transferred into a new 2 ml collection tube. 500 µl of 80% ethanol added to the column, closed the lid and spun at full speed for 2 minutes. Flow-through was discarded and the column was placed in a new 2ml collection tube. The column was then centrifuged at full speed for 5 minutes with the lid open to dry the membrane of the column. The MinElute spin column was transferred into a new 1.5ml collection tube. 14µl of RNase-free water added to the column closed the lid and spun at full speed for 1 minute. The last step was repeated in order to elute more RNA. RNA

quantity and purity were measured by NanoDrop 2000 spectrophotometer (Thermo Scientific). The replicate number used in this study with FLS for the next-generation sequencing was 4 for control, 4 for cytokine treatment, 4 for young and 4 for old rat samples.

Vascular smooth muscle cells (VSMC)

RNA extraction Protocol

Cells were washed with PBS and completely removed. RNA extraction kit (RNeasy plus micro kit, cat# 74034) was used to extract RNA from FLS cells. The manufacturer protocol was followed with some additional modifications to increase RNA yields. About 500 µl of lysis buffer (RLT buffer + 2β mercaptoethanol, 1ml:10µl ratio, respectively) and distributed evenly. Using cell scraper, cells were scrapped, gathered at the lower edge of the flask and transferred to labelled 15ml tubes. About 450-500µl of lysis buffer added to wash, collect anything left behind, gathered at the lower edge and transferred to the same tubes. Tubes were placed on ice until all cells were collected from all samples. Tubes opening closed with parafilm, RNase-free 1ml syringe connected to RNase-free (~40-50mm) 19" gauge is inserted into the tubes through parafilm, syringed (20-30x), placed on ice and repeated for all samples. Stored at -80 deg for 30-60min or -20 deg overnight to freeze down cell lysates in order to form crystals to lyse un-lysed cells and increase the RNA yields. Cell lysates were defrosted on ice, briefly spun at full speed for 30-40sec to bring everything to the bottom, transferred cell lysates into labelled gDNA Eliminator spin columns closed the lids and spun at full speed for 30sec. Discarded the column and mixed the flow-through with equal volumes of 70% Ethanol, transferred into labelled MinElute spin columns, closed the lids and spun at full speed for 30 sec. The last step was repeated as the sample volume exceeded 700µl which is the maximum volume the column can take. Discarded flow-through and placed MinElute spin columns into new 2ml collection tubes, added 700µl of RW1 buffer, closed the lids and spun at full speed for 30 seconds. Discarded flow-through and placed MinElute spin columns into new 2ml collection tubes, added 500µl of RPE buffer, closed the lids and spun at full speed

for 30 seconds. Discarded flow-through and placed MinElute spin columns into new 2ml collection tubes, added 500µl 80% EtOH, closed the lids and spun at full speed for 2min. Discarded flow-through and placed MinElute spin columns into new 2ml collection tubes and spun with open lids at full speed for 5min to dry membranes of MinElute spin columns. Discarded flow-through and placed MinElute spin columns into new labelled 1.5ml collection tubes, added 14µl of RNase-free water, closed lids and spun at full speed for 1min. Repeated the last step one more time to elute more RNA. Finally, measured RNA quantity and purity by NanoDrop 2000 Spectrophotometer. The replicate number used in this study with VSMC for the next-generation sequencing was 4 for control, and 4 for cytokine treatment samples.

AORTA

RNA extraction Protocol

AORTA tissues were extracted from rats, placed in RNALater, and stored at -80^{O}C. Later on, the tissue was defrosted on ice, taken into a mortar containing liquid nitrogen and powdered by a pistol. 500µl of Trizol (Ambion Ref#: 15596018) added to the mortar to collect the powder, then collected in 1.5ml RNAse-free tube. Another 500µl was added to the mortar to collect anything left behind and poured into the same 1.5ml tube. Because of the effects of liquid nitrogen, the Trizol added turned into a frozen state where I had to scrap to collect it. Trizol helps in tissue lysis. After that, samples were syringed for more than 30x for more lysis, vortexed and left at RT inside fume hood for 10min. 200µl of Chloroform (Sigma Cat#: C0549-1PT) was added to separate RNA from the rest of the sample components, mixed and centrifuged at full speed for 10min at 4^{0}C. RNA in the aqueous (clear) phase was removed into a new 1.5ml RNAse-free tube. 500µl of Iso-propanol (Sigma Cat#: I-9516) added (to precipitate RNA), left at RT inside fume hood for 10min, centrifuged for 15min at full speed at 4ºC. Then, Isopropanol discarded and 200µl of 80% Ethanol added (to wash RNA and help in drying it in the next step), centrifuged at full speed for 2min at 4ºC. Ethanol was discarded and the pellet was left to dry at RT inside the fume hood. RNA was eluted in RNAse free water

(15-20µl). finally, the concentration of RNA was measured by NanoDrop 2000 Spectrophotometer. The replicate number used in this study with Aorta for the next-generation sequencing was 3 for young, and 3 for old samples.

PVN

RNA extraction Protocol

PVN was defrosted on ice. Then, transferred into a cover of a small dish containing about 500µl of Trizol. The tissue was cut into as small pieces as possible and then moved to a 1.5ml tube. Another 500µl of Trizol added to the small dish's cover to wash, collect any pieces left behind and transferred into same 1.5ml tube. Tissues were gently syringed for complete homogenization followed by harsh syringing to lyse cells and release RNA. Cells were then vortexed and left at room temperature (RT) inside fume hood for 10-15 min. 200µl of Chloroform added, mixed by up and down pipetting and centrifuged for 10 min at full speed at 4^{O}C. The aqueous phase (top transparent) containing RNA was removed into a new 15ml tube. 500µl of Iso-propanol added, mixed by up and down pipetting and let to precipitate RNA at RT inside fume hood for 10 min followed by centrifugation at full speed for 15 min at 4^{O}C. The supernatant containing Isopropanol was discarded, 200µl of 80% Ethanol added to the RNA pellet and centrifuged at full speed for 2min at 4^{O}C. Ethanol was discarded and the RNA pellet was let to dry at RT inside the fume hood. RNA was resuspended in 20µl of RNase-free water and the concentration was measured by NanoDrop 2000 Spectrophotometer. The replicate number used in this study with PVN for the next-generation sequencing was 3 for young, and 3 for old samples.

RNA-Seq data analysis steps

RNA samples were extracted as described above. Sequencing of large (>200 nucleotides) messenger RNA (mRNA) enriched with polyA-tail was outsourced with >30M sequencing depth Figure 8. A 50-150bp paired-end read sequencing was carried out on illumine platform. High-quality raw data was delivered as FASTQ files containing sequences

and quality scores. Reads were aligned/mapped with the reference-based assembly tool, Hisat2 (Kim et al., 2015) that covers the splice junctions (Reference Genome: Rat Jul. 2014 (RGSC 6.0/rn6) database). The resulting BAM (a compressed binary version of SAM (Sequence Alignment Map)) was then passed to either StringTie (Pertea et al., 2015) and CuffDiff (Trapnell et al., 2010) or the newer DESeq2 (Trapnell et al., 2010) tools/packages to generate gene abundance estimates (Coverage, FPKM and TPM) or differentially expressed genes, respectively.

Quantification of gene expression took place using StringTie transcript assembly and quantification tool/package. This tool uses BAM and an annotation (GFF3) files as input to generates these files; assembled transcripts, gene abundance estimates [normalised FPKM (Fragments per kilobase exon per million reads mapped) and normalised TPM (Transcripts per kilobase million)], coverage data, transcript counts and gene counts. As state above, differentially expressed genes were detected using the older CuffDiff or newer DESeq2 packages. These assess group differences. They input BAM and GFF3 files as output a Gene Differential Expression Testing file that provides information such as fold change, p-values and adjusted q-values (False Discovery Rate (FDR)). For library normalisation, a geometric method was used. The FDR was less 0.05. Ion channel genes were identified and analysed separately for their gene/transcript abundance and differential expression using several reference servers such as Genenames.org, HUGO Gene Nomenclature Committee and locally edited scripts in MATLAB, Python and or R-studio. Ingenuity pathway analysis (IPA) was used to predict the upstream ligands/affectors, downstream targets and cell functions that were affected by the predicted effectors.

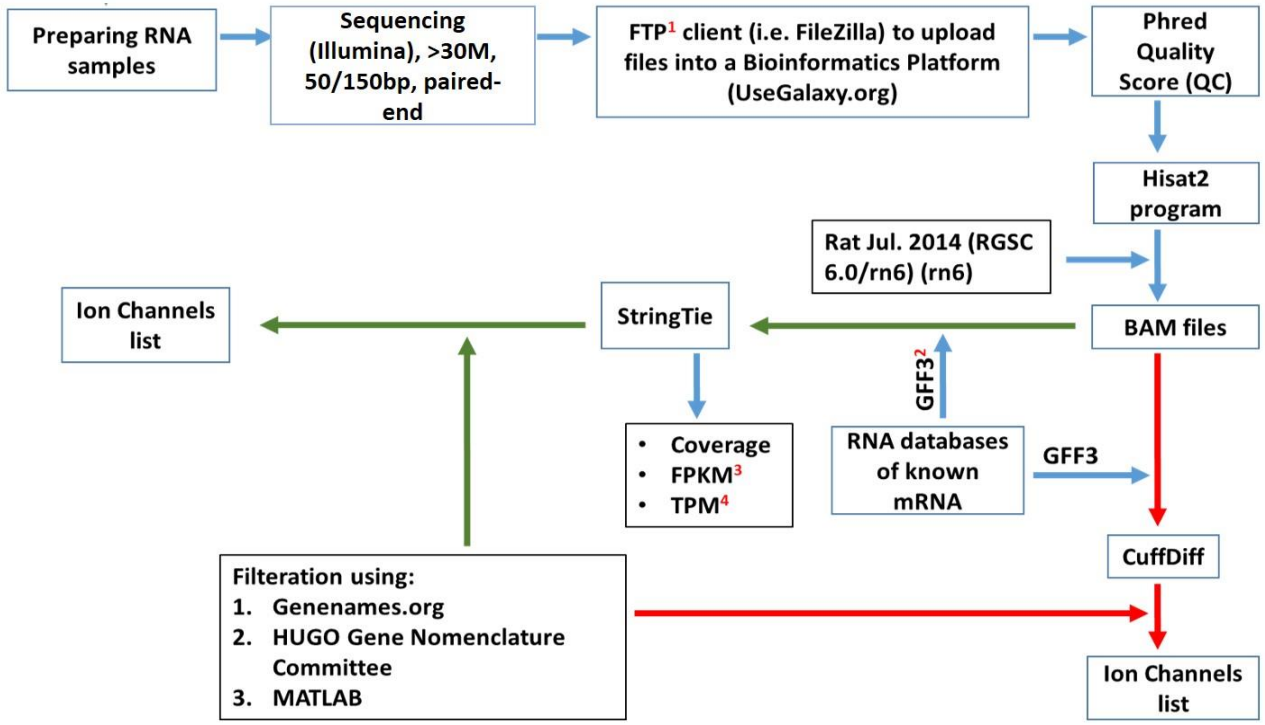

Figure 8: NGS data analysis pipeline.
Cells/tissues were obtained from animals as described in the text. Cells were subjected to ±72hrs of 10ng/ml of IL-1β+TNFα. Cells were then used for experiments; Next-Generation sequencing (NGS), Electrophysiology, quantitative polymerase chain reaction (qPCR), western blot (WB) and/or tissue typing through Immunocytochemistry (ICC). For NGS, RNA samples were extracted, sequenced with illumina and raw data files which had their adaptors trimmed were uploaded using a FTP client to a bioinformatics platform or in home servers for analysis. Within the bioinformatics platform, phred quality score was measured for all samples which was found to be around 37 or greater. Reads were then aligned/mapped with Hisat2 package using the reference genome Rat Jul. 2014 (RGSC 6.0/rn6) (rn6). The resulting BAM files along with an annotation file (Rat GFF3) were used to assemble mapped reads and quantify gene expression. Such assembly and quantification took place to generate gene abundance estimates and gene/transcript counts (StringTie package) and differentially expressed genes (CuffDiff/DESeq2 packages). After that, using several servers and a local custom-script in MATLAB software allowed us to hunt ion channel genes for further analysis. [1] File Transfer Protocol, [2] General Feature Format, [3] Fragments per kilobase exon per million reads mapped and [4] Transcripts per kilobase million.

1.4 Immunocytochemistry (ICC)

FLS

Detection of FLS cell marker; CD248 also known as TEM1, took place through immunocytochemistry. First, cells were prepared onto 100% Ethanol sterilised coverslips in 24-well plate and allowed to dry. 1 ml of cell suspension at a density of $2.5x10^4$ cell/ml was transferred into each well and incubated overnight. Next day, the medium was removed, cells were fixed with ~3 ml fixative (2% paraformaldehyde in PBS X1, pH 7.4), and incubated at room temperature (RT) for 10 minutes. Then, the medium was removed and fixative was quenched by 10 minutes incubation with ~ 3 ml of glycine solution (100mM, pH 7.4), at RT. After that, the medium was discarded and ~ 3ml of permeabilization solution (for each 100ml, 10 ml of PBS X10 and 0.1 ml of Triton-X100 were used, pH adjusted for 7.4) was used and allowed to incubate at RT for 10 minutes. The medium was then discarded and cells were washed with PBS X1, three times, 5 minutes/each. After that, non-specific binding was blocked by incubating cells in each well with 200 µl of antibody (Ab) diluting solution [for each 10 ml of pH 7.2; 0.5 ml of Sodium/Sodium Citrate SSC X20 (150 mM NaCl and 15 mM Na_3Citrate), 0.2 ml of donkey serum, 1% bovine serum albumin (0.1 g), and 0.05% Triton-X100 (5 µl)] for 30 minutes at RT. Ab diluting solution was discarded and cells were incubated in the fridge with primary antibody solution (RAT Ab, 1 in 200 Ab diluting solution), overnight. Next day, primary antibody (Ab) solution was removed and cells were washed three times with Ab wash solution (for every 100 ml of pH 7.2, 5 ml of SSC X20 and 0.05 ml of Triton-X100) for 10 minutes each time. After that, secondary antibody (Anti-RAT Ab, 1 in 500 Ab diluting solution) was added and incubated in dark at RT for 1-2 hrs. Next, cells were washed with Ab wash solution three times for 10 minutes each time in the dark. Then, slides were dipped into two separate universals of distilled water, air-dried in the dark, mounted with mounting media, and left in the dark overnight until visualised under a microscope.

1.5 qPCR

The same RNA samples used for NGS experiments were used for qPCR experiments for confirmation purposes of the expression of ANO1 channel gene. The amount 500ng/sample of RNA (shown in Table 2) was used for cDNA synthesis.

Table 2: amounts of RNA samples used for qPCR experiment.

Samples	Amount per µL (ng)	Volume for 500 ng (µL)	RNase - free water (µL)
VSMC_17C	2433.00	0.21	9.79
VSMC_17T	1506.00	0.33	9.67
VSMC_18C	150.00	3.33	6.67
VSMC_18T	324.00	1.54	8.46
VSMC_13C	203.40	2.46	7.54
VSMC_13T	367.20	1.36	8.64
VSMC_12C	300.00	1.67	8.33
VSMC_12T	486.00	1.03	8.97

The cDNA synthesis materials were RT buffer (5X First-strand Buffer, P/N y02321 from Invitrogen), DTT (0.1M, 500µl, P/N Y00147 from Invitrogen), dNTP (), SuperScript ®II Reverse Transcriptase (P/N 100004925, 10000U "200U/µl"), RiboLock RNAse inhibitor (Ref#EO0381, 2500U, 40U/µl, from Thermo Scientific), RNAse-free Water (Mat. No. 1012888, from Qiagen), and as per the manufacturer's instructions, the 1st step was mixing RNA (500 ng) + H2O (Sigma) + 1 µl random hexamers, and incubated for 10 min at 65˚C. the second step starts with the preparation of the reaction mixture (Total reaction mix = (9 µL x No. of samples) + 1 (for pipetting error)) as follows: 4 µl RT buffer (5x First-Strand Buffer), 2 µl DTT, 1 µl dNTP (10 mM), 1 µl Superscript II, 1 µl RNase Inhibitor (Ribolock), and incubate for 60 minutes at 42˚C. Then, the cDNA was diluted 10 times (+180 µl Sigma water = 200 µl).

Then, the qPCR master mix was prepared. The components of this master mix are the SYBER GREEN (FastStart Essential DNA Green Master, REF#06402712001), β-Actin primers Forward and Reverse (from Sigma). For F, (Cat#1158, SY170426580-084, F sequence 5'-TCCTTCCTGGGTATGGAAT-CCT at 100µM, O.D= 6.7, 225.4µg, 33.7nmol, 0µm, Tm=66.6ºC, 33.6 µg/OD, MW=6692, 0µL) while R, (Cat#1158, SY170426580-085, R sequence 5'-AGCTCAGTAACAGTCCGCCT at 100µM, O.D= 8.2, 262.9µg, 43.4nmol, 0µM, Tm=63ºC, 32.1 µg/OD, MW=6062, 0µL). HRPT1 primers Forward and Reverse (from Sigma). For F, (Cat#1158, SY170426580-088, F sequence 5'-TCCTCCTCAGACCGCTTTTC at 100µM, O.D= 6.7, 238.1µg, 40.0nmol, 0µM, Tm=65.7^{O}C, 35.5 µg/OD, MW=5955, 0µL) while R, (Cat#1158, SY170426580-089, R sequence 5'-ATCACTAATCACGACGCTG-GG at 100µM, O.D= 7.8, 245.3µg, 38.2nmol, 0µM, Tm=66.1^{O}C, 31.4 µg/OD, MW=6415, 0µL). the amounts prepared were:

For the ANO1 gene, a primer (1µl *30= 30µl) was mixed with RNAse free H2O (4µl *30= 120µl), and SYBER green (10µl *30=300µl). For housekeepers (β-actin and HPRT1) genes,

of primer (2µl *30=60µl), RNAse free H2O (3 µl *30= 90 µl), and SYBER green (10µl *30=300 µl). After that, 15 µl of each mix from above aliquoted into its appropriately assigned well (Table 3) followed by the addition of 5 µl of diluted cDNA.

Table 3: qPCR samples/plate layout. Each sample (C=control and T=treatment "IL-1β+TNFα") was run in triplicate.

		1	2	3	4	5	6	7	8	9	10	11	12
ANO-1	A	17C	17C	17C	18C	18C	18C	13C	13C	13C	12C	12C	12C
ANO-1	B	17T	17T	17T	18T	18T	18T	13T	13T	13T	12T	12T	12T
ACTB	C	17C	17C	17C	18C	18C	18C	13C	13C	13C	12C	12C	12C
ACTB	D	17T	17T	17T	18T	18T	18T	13T	13T	13T	12T	12T	12T
HPRT1	E	17C	17C	17C	18C	18C	18C	13C	13C	13C	12C	12C	12C
HPRT1	F	17T	17T	17T	18T	18T	18T	13T	13T	13T	12T	12T	12T
-ve	G	ANO-1 -ve	ANO-1 -ve	ANO-1 -ve	actb -ve	actb -ve	actb -ve	hprt1 -ve	hprt1 -ve	hprt1 -ve			
	H												

The loading/negative controls were actb=β-actin (), hprt1= Hypoxanthine Phosphoribosyltransferase 1 () and PCR reaction for a sample without the target (ANO1 = Anoctamin1) primers (Cat#63914 from PRIMER DESIGN).

the plate was sealed, briefly centrifuged and then placed in the qPCR machine (Biorad). The running protocol started with pre-incubation at 95ºC for 600sec. Then, 3 steps of amplification (95ºC for 10sec, 60ºC for 10sec, and 72ºC for 10sec). This was followed by another 3 steps of amplification (95ºC for 10sec, 65ºC for 10sec, and 97ºC for 1sec (5 reading/continuous ºC)).

2.6 Chemicals and materials

Media (DMEM 1X with Ref#31885-023, DMEM (1X) GlutaMax with Ref#61965-026), Heat Inactivated FBS (Fetal Bovine Serum, Ref# 10500-064, from gibco by life technologies), Penicillin/Streptomycin (Cat# P4333-100ML, from Sigma), Amphotericin B (Ref#15290-026 from gibco by life technologies), Trypsin-EDTA (Cat# T4174-100ML from Sigma), IL-1β (Cat#501-RL/CF, from R&D), TNFα recombinant protein (Cat#PRC3014 from gibco), Calcium Chloride solution (cat# 21114-1L from Fluka Analytical), Ethylene glycol-bis(β-

aminoethyleneether)-N,N,N',N'-tetraacetic acid (EGTA) (Cat#E-0396 from Sigma), D-Gluconic Acid (cat#G-4500 from Sigma), HEPES (Cat#H3375-500G from Sigma), Sodium Chloride (Cat#S7653-1KG from Sigma-Aldrich), Trizma® hydrochloride (Cat#T3253-1KG), Sodium Phosphate (Dibasic Anhydrous, Cat#S-0876), Sodium Phosphate (Monobasic Anhydrous, Cat#S-2554), Tween-20 (Code#233362500 from ACROS ORGANICS), Papain from Canica papaya (Cat#76220-25G), Bovine Serum Albumin (Cat#A9647-10G from Sigma), 1,4-Dithioerythritol (DTT) (Cat#D8255-5G),

RNA extraction kit (RNeasy plus micro kit, cat# 74034), Trizol reagent (cat#15596018 from Ambion by life technologies), Chloroform: Isoamyl alcohol 24:1 (cat#C0549-1PT from Sigma), Isopropanol (cat# I-9516 from Sigma),

Paxiline (Cat#2006 from TOCRIS bioscience), ANO-1 inhibitor (CaCCinh-AO1, Cat#0916-5MG, from Sigma), Magnesium Chloride Solution (Cat# 220931.0M stock, from BDH), Triton X-100 (Cat#30632 from BDH Chemicals Ltd Poole England), D-(+)-Glucose (Cat#G7528-250G from Sigma), POTASSIUM CHLORIDE (Cat# P-4504 from Sigma)

Donkey Serum (Cat#D-9663 from Sigma), VECTASHIELD (hard set, mounting medium, H-1500 from Vector laboratories Inc.), Antibody for CD248 also known as TEM1 (Abcam, cat#: ab67273), Fluorescein (FITC) conjugated AffinintyPure Donkey Anti-Rabbit IgG (Cat#711-095-152 from Jackson immune Research),

These chemicals and materials were used in different techniques and methods in my project.

Statistics are described in the test and were performed in R-studio, Excel or Minitab as appropriate.

2.7 Methods Troubleshooting

Protocols described above were optimized. However, the issues encountered while carrying out the experiments are described in this section either for tissue culture or RNA extraction for NGS experiments.

Tissue cultures

Issues with VSMC culture

After dispersing and culturing VSMC cells in a plate, they grew fast and became confluent. However, after the first passage, they stopped proliferation. Changing medium daily and trying a different fetal calf serum did not solve the problem. Changing DMEM high glucose (with 4500 mg/L glucose and Sodium Bicarbonate but without L-glutamine and Sodium Pyruvate, Sigma D5671 -500ml) medium to a DEME (1X) + GlutaMax (with 4.5g/L D-Glucose and without Pyruvate) solved the problem. Because GlutaMax has a dipeptide Alanine and Glutamine that requires an enzyme to be produced by the cells to breakdown the peptide bond between these two amino acids and consume each one individually, this had guaranteed enough energy supply for the cells for a long time and less ammonia accumulation in the media which is toxic to cells. Of course, the proliferation rate of VSMC is now slower but cells grew eventually.

RNA extraction

Issues with low RNA yields from VSMC

Once cells are ready for RNA extraction, they were washed with PBS and completely removed, 1x trypsin/EDTA added, incubated at 37ºC for up to 30 min and cells still adhered. After that, cells were scrapped, and the flask left in a vertical position to bring everything down. Then, transferred into 15ml tube, spun at 1500 rpm for 5 min to make cells' pellet. However, no observed pellet was seen. This eventually resulted in very low RNA concentrations. The possible reason was that cells were lost either in the transfer from flask

to 15ml tubes or during the centrifugation step as some might have lysed and discarded with the supernatant.

AORTA

Sometimes, the separation of RNA with chloroform did not go well because of the AORTA tissue size. In these cases, the tissue was cut into 2 pieces and each one was run individually and combined after elution step. Trying a different method to improve homogenization, I used a fastmini-prep method where tissues pieces are loaded into a 1.5ml tube containing small beads that run in a controllable speed for seconds to minutes to make sure tissue pieces are completely homogenized. This improved the homogenization but not the quantity or purity.

Additionally, to improve purity, the trizol method with the RNA extraction kit (RNeasy plus micro kit, cat# 74034) were combined. First, the trizol method was followed until RNA was separated in the aqueous phase and removed into a gDNA eliminator column of the RNA extraction kit. Then, the manual's instructions of the kit were followed. However, the purity slightly improved but the quantity dropped. Therefore, the trizol method alone was used as it proved to be the best method for RNA extraction from rat AORTA tissues stored in RNALater at -80^{o}C.

Issues with RNA extraction from PVN

PVN in RNALater stored at -80^{O}C was defrosted on ice. Tissue was then snipped into small pieces either in RNALater or lysis buffer (RLT buffer from Qiagen kit + 2β-Mercaptoethanol), moved to a new 15ml tube and syringed. Then, frozen down at -80^{O}C for 30min to make crystals to lyse the possibly un-lysed cells to increase RNA yields. After that, cell lysate was briefly centrifuged to bring everything to the bottom, then transfer into gDNA Eliminator spin column and follow the kit's protocol. With this, I used to get low RNA yields with mice or rats tissues that were used for optimization purposes only. Eventually, I tried a different RNA extraction method (Trizol method) that worked better.

Chapter 3 – Changes of ion channels in Fibroblast-like Synoviocytes (FLS)

3.1 Introduction

As discussed in Chapter 1, FLS cells are key cells in maintaining healthy articular joint and will be treated, in this thesis, as an example of a musculoskeletal tissue that may change its phenotype with age. FLS work as a barrier between the articular joint and the blood circulation. These cells provide nutrients to the joint tissues (i.e. chondrocytes), synovial fluid to lubricate surfaces and help in removing cellular by-products from the joint. When these cells are inflamed, pro-inflammatory cytokines signalling become activated which can affect the whole joint through increased production of these cytokines and these cells lose their significant feature as a barrier which increases the permeability for high molecular weight proteins and molecules across the joint. Thus, the main components of the synovial fluid (i.e., HA and lubricin) can escape the joint and the levels in plasma increase. Consequently, the viscosity of the affected joints decreases and level of friction between the surfaces increases which can be very painful and can impair with normal functions of the joint as seen in the elderly. These cells may interact with sensory neurons and have been described as "amplifiers" of neuropeptide mediated inflammation and pain. Roles of ion channels of FLS in osteoarthritis (OA) have not been extensively studied.

The synovium is an obvious target for the development of novel interventions in both RA and OA. The role of synovitis, low-grade inflammation of the synovial lining of the joint, in OA progression is gradually emerging. Therefore, in this work, the pathophysiology of cytokine-induced synovitis in cultured synovial cells is investigated.

Aims

Investigation includes:

- Which global FLS transcripts change with natural ageing in rats (transcriptome).
- Which FLS *ion channel* genes change with natural ageing in rats (channelome).

Then, the inflammageing model is used to investigate:

- Which global FLS transcripts change with TNFα and IL1β cytokines treatment *in vitro* (transcriptome).
- Which FLS *ion channel* transcripts change with TNFα and IL1β cytokines treatment *in vitro* (channelome).
- Whether there are detectable electrophysiological changes with TNFα and IL1β cytokines treatment.

Finally, the investigation will cover

- Similarities and differences between the FLS natural ageing and cytokine inflammageing models.

A combination of Next-Generation RNA Sequencing (NGS), qPCR and patch-clamp electrophysiology is used to uncover several changes in potassium channel gene expression together with changes in cellular phenotype which can be explained as a phenotypic switch in response to inflammation.

3.2 Materials and methods

Tissue culture

FLS cells were isolated, cultured, passaged and used for experiments as described in the materials and methods in chapter 2.

RNA extraction

RNA extraction methods were described in the materials and methods of chapter 2 in details. RNA concentrations of FLS cells are shown in Appendix 1.

Next-generation sequencing (NGS)

First, it is vital to determine the integrity of the starting material of RNA when performing gene expression analysis. One of the methods used these days is the measurement of RNA Integrity Number (RIN) using Agilent Bioanalyzer systems which became standard in RNA quality and quantity analysis. RNA samples are electrophoretically separated on microfabricated chips and detected by a laser that induces fluorescence. The output of this machine includes electropherogram, gel-like image, provide information on sample concentration and ribosomal ratio. The electropherogram offers a visualized assessment of the RNA quality. The ribosomal ratio used to be useful in determining the RNA intactness although it does not provide accurate information about the integrity of the RNA. Therefore, researchers mostly rely on the electropherogram more than the ribosomal ratio to see a detailed picture of the distribution of different sizes of RNA fragments (Mueller).

Although RNA degradation is slow, once starts more fragments (Appendix 2-A) can be seen and a band ratio between 18S and 28S will decrease while the baseline signal between the two ribosomal peaks and the lower marker will increase (Mueller).

The introduction of RIN has solved the issue by taking the entire electrophoretic trace into account and using an algorithm for classification that generates a number from 1 to 10 with 1 being most degraded and 10 most intact. This ensures good interpretation, comparison between samples, and repeatability of the experiments.

Appendix 2-B was generated after testing around 1300 RNA samples from different species and using algorithms. The experts who found this, identified the most important information from RNA samples and they came up with this figure showing Pre-Region, Marker, 5S region, Fast region, 18S region, Inter region, 28S region, Precursor region and Post region. These are the regions of the electropherogram. The RIN number takes into account the values of all of these regions. With that, if an unexpected spike appears in the Fast region the software will not compute the RIN. On the other hand, if a spike appeared in the Post region the RIN will be computed.

The height of the 18S and 28S peaks is positively correlated to the RNA concentrations. The higher the RIN number the larger the 28S compared to 18S while others are much smaller to non-visible. The X-axis represents the nucleotides (nt) and the Y-axis represents Fluorescence Unit (FU).

Appendix 3 shows electropherogram, gel-like image, RNA Integrity number and rRNA ratio of 28S/18S for each sample (FLS young and old).

A Phred quality score is used as a measurement of the quality of the identification of nucleobases that are generated by the automated DNA sequencing. The score is assigned to each nucleotide base call in automated sequencer traces (Ewing et al., 1998, Ewing and Green, 1998). Phred quality score has become popular and widely accepted as a measure of the quality of DNA sequences as well as to compare different sequencing methods. As shown in the figures, the graph is divided into different colours with bases fall into the red colour have higher error rates (1 in 10). Error rates decrease as I go to yellow and green with error rates of 1 in 100 and 1 in 1000 for yellow and green, respectively. As the error rates decrease the accuracy increases (Ewing et al., 1998, Ewing and Green, 1998).

After RNA-Seq experiments took place, raw data files were received, the quality check (Phred quality score) of the raw data files “Fastq” was carried out using FASTQC software as

shown in Appendix 4. Then, different tools were used to align/map (HiSAT2), assemble and quantify (StringTie), and detect differentially expressed genes (CuffDiff or Deseq2) as described in the materials and methods chapter 2.

Immunocytochemistry (ICC)

Tissue typing using ICC for FLS cells with CD248 took place as described in the materials and methods in chapter 2.

Electrophysiology

FLS cells were patch clamped using a borosilicate fire-polished glass pipette filled with intracellular solution, a seal was made with a target healthy cell in a bath solution and current recording took place with Cairn Optopatch amplifier after challenging the cell with a series of different potentials ranging from -120 to 120mV. More details can be found in the materials and methods in chapter 2.

Resting membrane potential was read directly from the CAIRN Optopatch amplifier by switching to current clamp protocol (I=0) and recorded in millivolts (mV).

For the drugs used to activate (NS1619) or block (Paxilline) BK channels, the extracellular solution that filled the bath was replaced by an extracellular solution containing the drug (either NS1619 or Paxilline) at a flow rate of 3ml/min. Then, cells were challenged with the same voltage step protocol (-120 to +120 mV at 10mV increment) and whole-cell currents were recorded within the first 5-10 min of solution replacement.

3.3 Results

NGS data analysis

Only those reads that passed FastQC with Phred tests, with quality scores of greater than 30 were retained. The data analyses steps; mapping, assembly and quantification, and detection of differentially expressed genes are described in the materials and methods chapter 2.

Ageing FLS NGS data analysis

This project started with ageing FLS cells by carrying out NGS experiments for young and old FLS samples. FLS cells from young and old rats were dissected, cultured and RNA samples were extracted as described in the methods. Then, RNA samples were sequenced at 150bp, >30M sequencing depth as paired-end (Illumina platform). The quantity of RNA in FLS samples are shown in (Appendix 1). The first 4 samples (FLS_Y1C1, FLS_Y3C, FLS_Y6C, and FLS_Y4C1) are the young samples while the last 4 (FLS_O1C2, FLS_O2C2, FLS_O5C1 and FLS_O4C1) are the old FLS samples. The quality of these RNA samples was also checked and electropherograms were generated. A representative example of such electropherograms and the gel-like image is shown in (Appendix 2-A and -B) and the actual figures of the RNA samples are shown in the (Appendix 3-A and -B).

Ageing FLS Differentially expressed Genes

NGS detected approximately 22038 genes per group. Differential expression testing of *all* genes identified 242 genes with *p-val* for differential <0.05 (Table 4 shows top 10) and 1 gene (Eml1; Echinoderm microtubule-associated protein-like 1) with Benjamini Hochberg corrected expression FDR <0.05.

Table 4: Top 10 differentially expressed (p-value<0.05) genes in young and old FLS cells.

ID	log2 F.C.	p-value	p-adj	Gene Name	Gene symbol
ENSRNOG00000043143	-1.93896	4.70E-07	0.006	Echinoderm microtubule-associated protein-like 1	Eml1
ENSRNOG00000016346	-1.51981	4.90E-05	0.224	Protein kinase C delta type	Prkcd
ENSRNOG00000009329	1.540407	7.12E-05	0.244	Nuclear receptor subfamily 1 group D member 1	Nr1d1
ENSRNOG00000061814	-1.45418	9.18E-05	0.252	DiGeorge syndrome critical region gene 2	Dgcr2
ENSRNOG00000027124	0.880773	0.000168	0.384	Thymine-DNA glycosylase	Tdg
ENSRNOG00000055281	1.085596	0.000244	0.479	Discoidin, CUB and LCCL domain-containing protein 2	Dcbld2
ENSRNOG00000018582	-1.34473	0.000323	0.548	Exosome component 6	Exosc6
ENSRNOG00000054118	1.292525	0.000372	0.548	Tubulin polyglutamylase complex subunit 2	Tpgs2
ENSRNOG00000047447	0.53261	0.000398	0.548	Uncharacterized protein	
ENSRNOG00000020044	1.272062	0.000453	0.551	MOB kinase activator 2	Mob2

Data obtained from the DESeq2 tool.

Ageing FLS Differentially expressed ion channel Genes

Filtering gene lists for ion channels grepping the word “channel” in the official Ensemble gene description (excluding channel “interacting proteins”, “potassium tetramerization domain” and “intracellular” channels) returned 95 genes with greater than zero RNA abundance. Table 5 shows the most abundant 10 channel genes. Of these 95 channel genes, 2 were differentially expressed (pval<0.05) and these are (1) Potassium channel subfamily K member 4 (Kcnk4) (log2 fold change= 0.70, p-value=0.03) and (2) Potassium channel subfamily K member 2 (outward rectifying potassium channel protein TREK-1) (Kcnk2) (log2 fold change= 0.73, p-value=0.04). Both were upregulated.

Table 5: Top 10 differentially expressed channel genes in young and old FLS samples.

No.	ID	Gene Name	Gene symbol
1	ENSRNOG00000021140	Potassium channel subfamily K member 4	Kcnk4
2	ENSRNOG00000002653	Potassium channel subfamily K member 2 (Outward rectifying potassium channel protein TREK-1)	Kcnk2
3	ENSRNOG00000003104	Transient receptor potential cation channel subfamily V member 2	Trpv2
4	ENSRNOG00000019985	Acid-sensing ion channel 4	Asic4
5	ENSRNOG00000007705	ATP-sensitive inward rectifier potassium channel 10	Kcnj10
6	ENSRNOG00000019368	Amiloride sensitive sodium channel alpha1 subunit	Scnn1a
7	ENSRNOG00000021102	Sodium channel subunit beta-1	Scn1b
8	ENSRNOG00000020360	Chloride channel CLIC-like 1	Clcc1
9	ENSRNOG00000014714	Transient receptor potential cation channel subfamily V member 6	Trpv6
10	ENSRNOG00000051621	Catsper channel auxiliary subunit zeta	Catsperz

Ageing FLS Multivariate analysis of all Genes

To investigate whether there were changes in clusters of genes rather than individual genes, PCA with 7 PCs was used. Figure 9-A shows the scree plot of these PCs and the percentages of explained variance by each one. The contribution of each sample to the PCs is shown in Figure 9-B where the first sample (O1; old-1) contributes most to the variability. A comparison of PCs took place via comparing PC1 with PC2 (Figure 10-A), PC1 with PC3 (Figure 10-B) and PC2 with PC3 (Figure 10-C). A clear separation was found with PC1 vs PC3 and PC2 vs PC3, and when the data are considered in 3 dimensions simultaneously with a 3D plot (Figure 10-D). The contributing genes to the separation between PC1 and 3 in Figure 10-B are presented in Table 6.

Table 6: Example of Gene contribution to the separation between PC1 and PC3 of young and old FLS samples.

PC	Gene stable ID	Gene name	Gene description	Contribution value
1	ENSRNOG00000016220	Rpl12	ribosomal protein L12	0.0376
1	ENSRNOG00000019525	Hspa9	heat shock protein family A (Hsp70) member 9	0.0372
1	ENSRNOG00000020266	Eef2	eukaryotic translation elongation factor 2	0.0372
1	ENSRNOG00000020595	Rps11	ribosomal protein S11	0.0372
1	ENSRNOG00000051885	LOC100360413	eukaryotic translation elongation factor 1 alpha 1-like	0.0368
3	ENSRNOG00000008843	Eci1	enoyl-CoA delta isomerase 1	0.0518
3	ENSRNOG00000011167	Wdhd1	WD repeat and HMG-box DNA binding protein 1	0.0511
3	ENSRNOG00000015741	Slc2a13	solute carrier family 2 member 13	0.0497
3	ENSRNOG00000016630	Tln1	talin 1	0.0491
3	ENSRNOG00000051623	Exosc8	exosome component 8	0.0491

Data obtained from the PCA package.

Functional annotation of PC1 and PC3 on David Bioinformatics Resources 6.8 revealed no pathway statistically significantly enriched on the KEGG (Kyoto Encyclopedia of Genes and Genomes) pathway. There were several enriched GOs such as “focal adhesion” (GO:0005925, p=7.4x10-4), “extracellular exosome” (GO:0070062, p=0.005), and “extracellular matrix” (GO:0031012, p=0.006).

Table 7 shows the top contributing genes to the separation between PC2 and 3.

Table 7: Gene contribution to the separation between PC2 and 3 of young and old FLS samples.

PC	Gene stable ID	Gene name	Gene description	Contribution value
2	ENSRNOG00000003174	Tapt1	transmembrane anterior posterior transformation 1	0.0512
2	ENSRNOG00000007060	Plin2	perilipin 2	0.0498
2	ENSRNOG00000025497	Fbxl6	F-box and leucine-rich repeat protein 6	0.0495
2	ENSRNOG00000049785	Ranbp3	RAN binding protein 3	0.0493
2	ENSRNOG00000054896	Pex13	peroxisomal biogenesis factor 13	0.0493
3	ENSRNOG00000008843	Eci1	enoyl-CoA delta isomerase 1	0.0518
3	ENSRNOG00000011167	Wdhd1	WD repeat and HMG-box DNA binding protein 1	0.0511
3	ENSRNOG00000015741	Slc2a13	solute carrier family 2 member 13	0.0497
3	ENSRNOG00000016630	Tln1	talin 1	0.0491
3	ENSRNOG00000051623	Exosc8	exosome component 8	0.0491

Data obtained from the PCA package.

This list of genes (PC2 and PC3) were enriched with only one GO which is “RNA processing” (GO:0006396, p=0.019) and no enrichment with any KEGG pathways or InterPro.

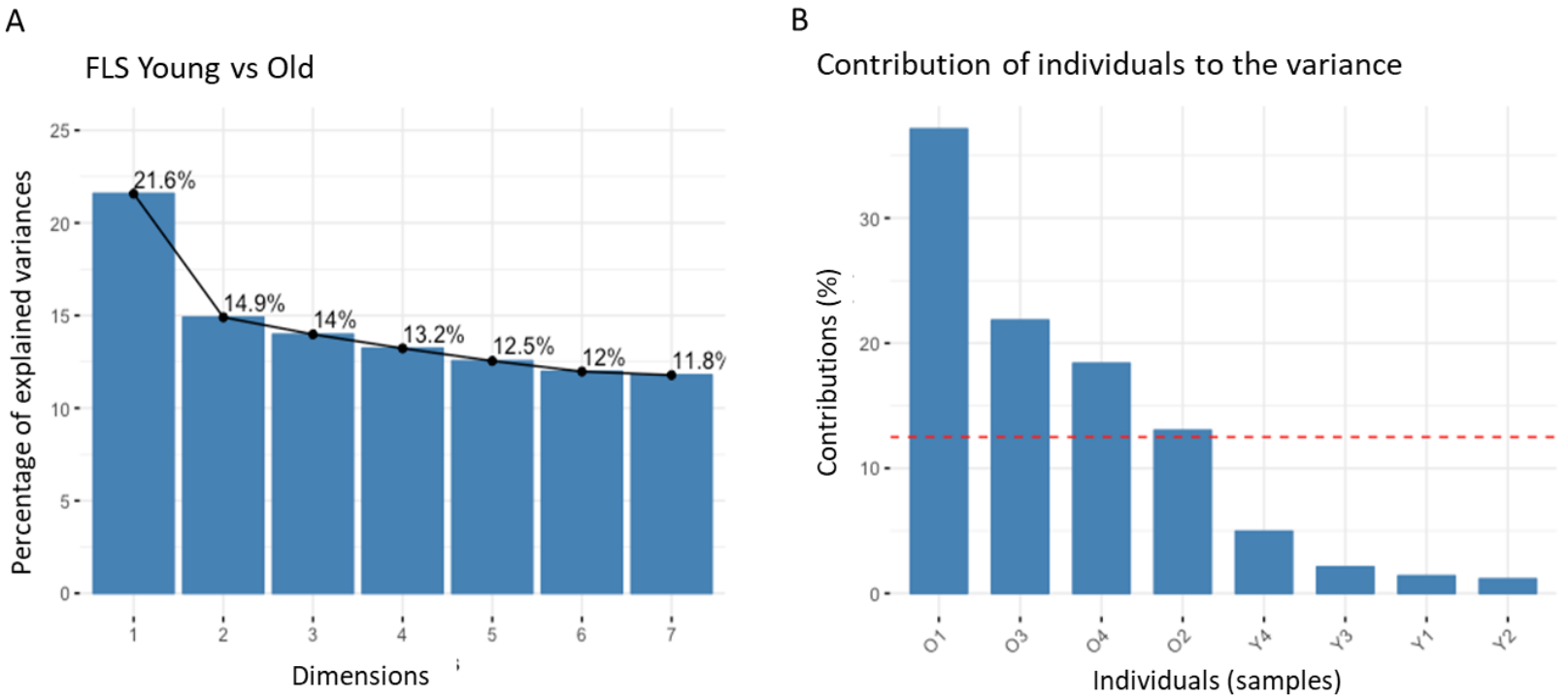

Figure 9: Scree and contribution plots for PCA for Young and Old adult rat FLS.
A. *shows the scree plot for the 7 principle components used to reduce the dimensionality of the FLS Control and Cytokine (IL-1β+TNFα) treated datasets, approximately 22038 variables (genes) reduced to 7 variables (PCs) with 8 subjects; 4 young and 4 old male rats. PCA Component 1 alone accounts for approximately 21% of the variance in the data.* ***B.*** *Contribution plot showing the relative contributions of each of the eight subjects to the variance. The first 3 principal components (O1, 3, and 4 are old FLS). The red dotted line indicates the mean contribution. The first subject contributes most to the variability and the second two contribute least. Individuals are O1, 2, 3, and 4 are old while Y1, 2, 3, and 4 are Young FLS samples.*

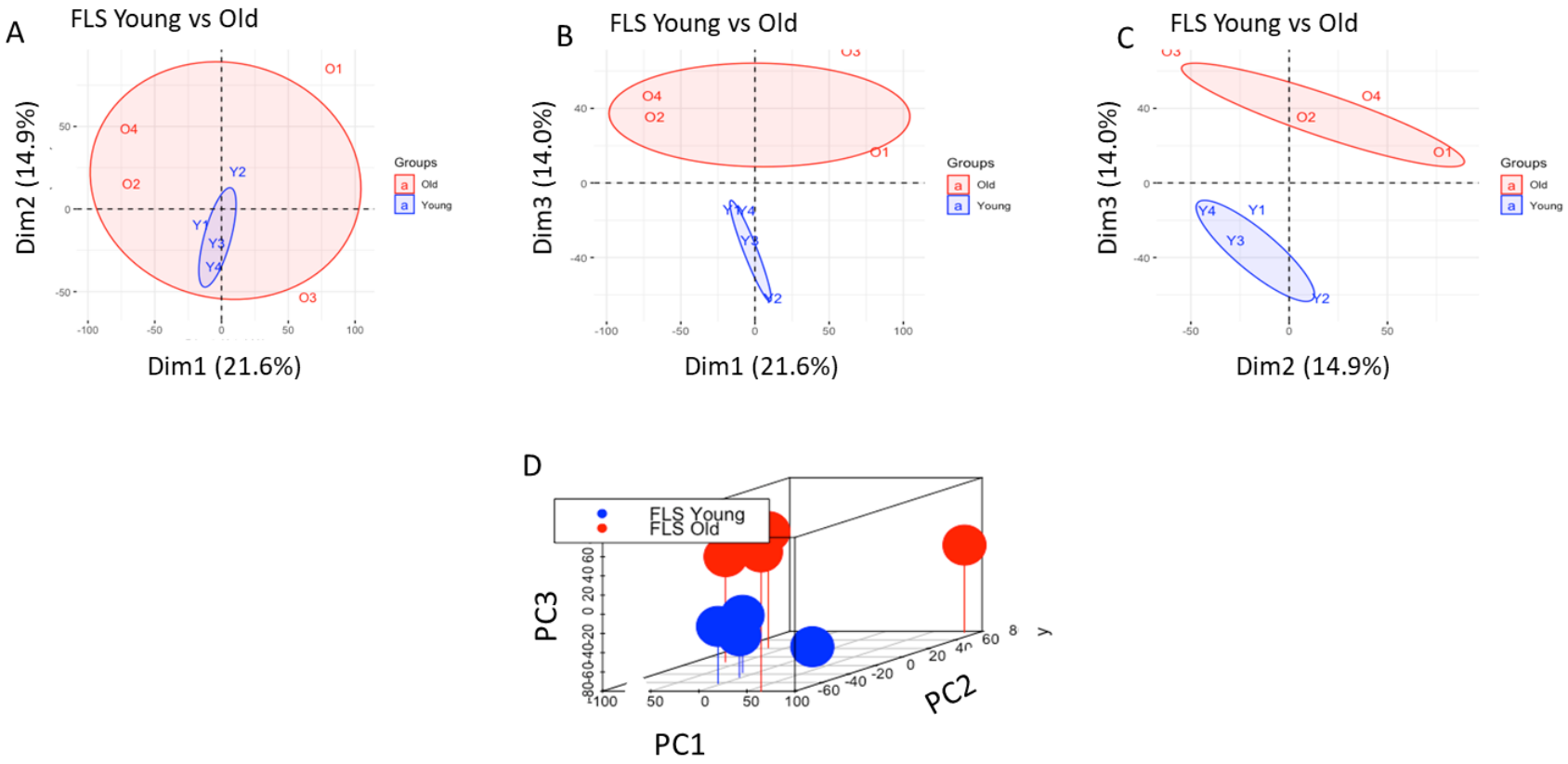

Figure 10: Principle component, k-mean clustering and combined scatter plot.
***A, B** and **C** show plots of PC1 vs PC2, PC1 vs PC2 and PC2 vs PC3 (Dim=PC). The shaded circles show the unsupervised k mean cluster 95% confidence intervals thus there is a clear statistical separation between young and old when combining PC1 and PC3, or PC2 and 3. **D.** 3D plot showing all three principal components plotted against each other.*

For Control and cytokine treated FLS

Then, the work proceeded to the young control and cytokine treated FLS samples. The raw data were analysed as described above in the materials and methods section NGS.

Next-generation sequencing data analysis of gene expression of control and cytokine treated FLS

RNA-seq detected 33251 transcripts and the **full data are available on the EBI Array Express database with Accession Number: E-MTAB-7798.** The top (highest FPKM) expressed 10 genes were similar between control and cytokine treated cells, but with distinct differences (Table 8 and Table 9).

Table 8: Genes with the highest expression levels in control of FLS cells.

Rank	**Gene symbol (rank in cytokine)**	**Official name***	**FPKM/1000 (CI)****
1	Col3a1 (18)	collagen type III alpha 1 chain	5138 (3314-7965)
2	Sparc (5)	secreted protein acidic and cysteine-rich	4519 (3355-6085)
3	Eef2 (1)	eukaryotic translation elongation factor 2	3993 (2951-5404)
4	Serpine1 (2)	serpin family E member 1	3721 (2295-6035)
5	Bgn (3)	biglycan	3455 (3050-3914)
6	Actb (4)	β-actin	2898 (2099-4003)
7	Thbs1 (48)	thrombospondin 1	2388 (1031-5532)
8	Rplp0 (8)	Large ribosomal protein, P0	2668 (2256-3155)
9	Thbs2 (14)	thrombospondin 2	2218 (1483-3316)
10	Gja1 (24)	gap junction protein α1	2265 (1678-3057)

Ordering from Cuffdiff (see methods). *Supplied by the Rat Genome Project https://rgd.mcw.edu/nomen/nomen.shtml. **Geometric mean and 95% CI *n*=4.

Table 9: Genes with the highest expression levels in cytokine (10ng/ml TNFα and IL-1β) treated FLS cells.

Rank	Gene symbol (rank in control)	Official name*	FPKM/1000 (CI)**
1	Eef2 (3)	eukaryotic translation elongation factor 2	4705 (3644-6076)
2	Serpine1 (4)	serpin family E member 1	2801 (1427-5497)
3	Bgn (5)	biglycan	3177 (2635-3831)
4	Dcn (35)	decorin	2486 (1100-5617)
5	Sparc (2)	secreted protein acidic and cysteine-rich	2609 (1509-4511)
6	Lrp1 (11)	LDL receptor related protein 1	2305 (1147-4630)
7	Ctsb (13)	cathepsin B	2495 (2027-3071)
8	Rplp0 (8)	Large ribosomal protein, P0	2487 (1906-3245)
9	Actb (6)	β-actin	2401 (2028-2844)
10	Grem1 (16)	gremlin 1, DAN family BMP antagonist	1985 (967-4076)

Ordering from Cuffdiff (see methods). *Supplied by the Rat Genome Project https://rgd.mcw.edu/nomen/nomen.shtml. **Geometric mean and 95% CI *n*=4.

Next-generation sequencing data analysis of ion channel gene expression of control and cytokine treated FLS

RNA-seq experiments were intended to give a transcriptome-wide, unbiased, assessment of ion channel changes in cytokine treated FLS. 190 channel genes were identified, including porins, connexins and ion-channel isoform genes (including α- to ε-subunits), but excluded interacting proteins, other regulatory proteins and the so-called potassium tetramerization domain proteins. The top 50 genes, in terms of FPKM are given for control and cytokine treated datasets in Table 10 and Table 11 respectively.

Table 10: Channel genes with the highest RNA expression levels in control of FLS cells.

Rank in Control	**Gene (rank in cytokine)**	**Official name***	**FPKM/1000 (CI)****
1	Gja1 (1)	Gap junction channels	2265 (1678-3057)
2	aqp1 (6)	aquaporin 1 (Colton blood group)	369 (223-609)
3	piezo1 (2)	piezo type mechanosensitive ion channel component 1	289 (236-355)
4	vdac2 (4)	voltage dependent anion channel 2	175 (157-195)
5	vdac1 (5)	voltage dependent anion channel 1	192 (142-258)
6	clic1 (10)	chloride intracellular channel 1	150 (117-191)
7	trpv2 (9)	transient receptor potential cation channel subfamily v member 2	130 (85-199)
8	p2rx4 (11)	purinergic receptor p2x 4	89 (67-117)
9	clic4 (14)	chloride intracellular channel 4	90 (77-105)
10	trpm7 (12)	transient receptor potential cation channel subfamily m member 7	77 (72-82)
11	clcn7 (15)	chloride voltage-gated channel 7	62 (55-70)
12	cacnb3 (13)	calcium voltage-gated channel auxiliary subunit beta 3	44 (28-71)
13	kcnk2 (21)	potassium two pore domain channel subfamily k member 2	47 (37-58)
14	tpcn1 (17)	two pore segment channel 1	49 (40-61)
15	clcc1 (16)	chloride channel clic like 1	44 (40-49)
16	scn1b (22)	sodium voltage-gated channel beta subunit 1	41 (31-55)
17	clns1a (19)	chloride nucleotide-sensitive channel 1a	40 (29-54)
18	clcn6 (20)	chloride voltage-gated channel 6	32 (25-40)
19	kcnq5 (18)	potassium voltage-gated channel subfamily q member 5	27 (18-39)
20	cacfd1 (24)	calcium channel flower domain containing 1	24 (21-28)
21	trpm4 (25)	transient receptor potential cation channel subfamily m member 4	20 (17-24)
22	clcn5 (26)	chloride voltage-gated channel 5	20 (17-23)
23	Gjb2 (42)	Gap junction channels	16 (10-26)
24	kcnd1 (32)	potassium voltage-gated channel subfamily d member 1	14 (12-17)

25	kcnk12 (35)	potassium two pore domain channel subfamily k member 12	10 (3-29)
26	clcn3 (27)	chloride voltage-gated channel 3	10 (7-14)
27	Gjc1 (33)	Gap junction channels	10 (7-13)
28	kcnd3 (38)	potassium voltage-gated channel subfamily d member 3	7 (3-16)
29	clic2 (45)	chloride intracellular channel 2	8 (6-12)
30	cacna1g (43)	calcium voltage-gated channel subunit alpha1 g	8 (6-11)
31	cacna1a (34)	calcium voltage-gated channel subunit alpha1 a	7 (5-10)
32	cacna1c (36)	calcium voltage-gated channel subunit alpha1 c	7 (4-11)
33	scnm1 (40)	sodium channel modifier 1	7 (6-8)
34	hvcn1 (23)	hydrogen voltage-gated channel 1	7 (6-8)
35	p2rx5 (37)	purinergic receptor p2x 5	5 (2-13)
36	kcna4 (31)	potassium voltage-gated channel subfamily a member 4	4 (1-14)
37	tpcn2 (39)	two pore segment channel 2	6 (5-8)
38	Gja5 (28)	Gap junction channels	2 (0-11)
39	cacna1b (44)	calcium voltage-gated channel subunit alpha1 b	4 (3-6)
40	trpm3 (47)	transient receptor potential cation channel subfamily m member 3	3 (1-6)
41	trpm1 (53)	transient receptor potential cation channel subfamily m member 1	2 (1-7)
42	kcnn4 (52)	potassium calcium-activated channel subfamily n member 4	3 (2-5)
43	kcnma1 (41)	potassium calcium-activated channel subfamily m alpha 1	2 (1-6)
44	trpv4 (50)	transient receptor potential cation channel subfamily v member 4	3 (2-4)
45	kcne4 (49)	potassium voltage-gated channel subfamily e regulatory subunit 4	2 (1-6)
46	catsper2 (55)	cation channel sperm associated 2	3 (2-3)
47	scn2a (58)	sodium voltage-gated channel alpha subunit 2	2 (2-3)
48	kcnj2 (60)	potassium inward rectifier j member 2	2 (1-3)

49	clic3 (57)	chloride intracellular channel 3	2 (2-2)
50	ano1 (75)	anoctamin 1	0 (0-1)

Ordering from Cuffdiff (see methods). *Supplied by the Rat Genome Project https://rgd.mcw.edu/nomen/nomen.shtml. **Geometric mean and 95% CI *n*=4.

Table 11: Channel genes with the highest RNA expression levels in cytokine (10ng/ml TNFα and IL-1β) treated FLS cells.

Rank	**Gene (control rank)**	**Official name***	**FPKM/1000 (CI)****
1	Gja1 (1)	Gap junction channels	1489 (930-2385)
2	piezo1 (3)	piezo type mechanosensitive ion channel component 1	276 (247-308)
3	vdac2 (5)	voltage dependent anion channel 2	181 (142-233)
4	vdac1 (6)	voltage dependent anion channel 1	227 (169-306)
5	aqp1 (2)	aquaporin 1 (colton blood group)	144 (86-242)
6	vdac3 (7)	voltage dependent anion channel 1 pseudogene 5	155 (121-200)
7	trpv2 (9)	transient receptor potential cation channel subfamily v member 2	115 (77-172)
8	clic1 (8)	chloride intracellular channel 1	125 (108-146)
9	p2rx4 (10)	purinergic receptor p2x 4	85 (52-140)
10	trpm7 (13)	transient receptor potential cation channel subfamily m member 7	85 (75-97)
11	clic4 (11)	chloride intracellular channel 4	79 (68-93)
12	clcn7 (14)	chloride voltage-gated channel 7	64 (52-79)
13	clcc1 (18)	chloride channel clic like 1	52 (42-65)
14	tpcn1 (17)	two pore segment channel 1	56 (48-66)
15	kcnq5 (22)	potassium voltage-gated channel subfamily q member 5	34 (17-68)
16	clns1a (20)	chloride nucleotide-sensitive channel 1a	36 (34-38)
17	clcn6 (21)	chloride voltage-gated channel 6	34 (27-44)
18	kcnk2 (16)	potassium two pore domain channel subfamily k member 2	25 (12-49)
19	scn1b (19)	sodium voltage-gated channel beta subunit 1	28 (19-42)

20	hvcn1 (39)	hydrogen voltage gated channel 1	22 (9-55)
21	cacfd1 (23)	calcium channel flower domain containing 1	27 (24-30)
22	trpm4 (24)	transient receptor potential cation channel subfamily m member 4	19 (13-27)
23	clcn5 (25)	chloride voltage-gated channel 5	19 (16-23)
24	clcn3 (31)	chloride voltage-gated channel 3	15 (9-27)
25	Gja5 (43)	Gap junction channels	2 (0-20)
26	kcna4 (41)	potassium voltage-gated channel subfamily a member 4	4 (0-32)
27	kcnd1 (27)	potassium voltage-gated channel subfamily d member 1	12 (9-15)
28	Gjc1 (32)	Gap junction channels	11 (9-13)
29	cacna1a (36)	calcium voltage-gated channel subunit alpha1 a	11 (9-13)
30	kcnk12 (28)	potassium two pore domain channel subfamily k member 12	8 (3-20)
31	cacna1c (37)	calcium voltage-gated channel subunit alpha1 c	7 (3-19)
32	p2rx5 (40)	purinergic receptor p2x 5	6 (2-18)
33	kcnd3 (33)	potassium voltage-gated channel subfamily d member 3	2 (0-12)
34	tpcn2 (42)	two pore segment channel 2	7 (5-10)
35	scnm1 (38)	sodium channel modifier 1	6 (6-8)
36	kcnma1 (49)	potassium calcium-activated channel subfamily m alpha 1	2 (0-13)
37	Gjb2 (26)	Gap junction channels	4 (1-12)
38	cacna1g (35)	calcium voltage-gated channel subunit alpha1 g	5 (4-6)
39	cacna1b (44)	calcium voltage-gated channel subunit alpha1 b	5 (3-6)
40	clic2 (34)	chloride intracellular channel 2	3 (1-8)
41	trpm3 (46)	transient receptor potential cation channel subfamily m member 3	3 (1-6)
42	kcne4 (51)	potassium voltage-gated channel subfamily e regulatory subunit 4	2 (1-7)

43	trpv4 (50)	transient receptor potential cation channel subfamily v member 4	3 (1-6)
44	kcnn3 (72)	potassium calcium-activated channel subfamily n member 3	1 (0-7)
45	kcnn4 (48)	potassium calcium-activated channel subfamily n member 4	2 (1-6)
46	trpm1 (47)	transient receptor potential cation channel subfamily m member 1	2 (1-5)
47	noct (57)	anoctamin 1	3 (2-3)
48	catsper2 (52)	cation channel sperm associated 2	2 (2-3)
49	kcnn1 (61)	potassium calcium-activated channel subfamily n member 1	2 (2-2)
50	clic3 (56)	chloride intracellular channel 3	2 (1-2)

Ordering from Cuffdiff (see methods). *Supplied by the Rat Genome Project https://rgd.mcw.edu/nomen/nomen.shtml. **Geometric mean and 95% CI *n*=4.

Next-generation sequencing data analysis of ion channel Differential expression

20 ion channel genes, undetectable in control conditions became detectable or 'appeared' after cytokine treatment Table 12), of which, the top expressed of these was trpc3. Conversely, 7 ion channel genes became undetectable or "disappeared" following cytokine treatment (Table 13). Following cytokine treatment, an additional 15 genes to be down by -1.5 (log_2) or more and 21 genes 1.5 (log_2) greater than control (Table 14 and Table 15 respectively) were also found. I used tissue from 4 animals for the NGS study each animal tissue split into test and control groups; the "*n*" presented in the legends refers to the number of biological replicates (= animals).

Table 12: All channel genes "appearing" in cytokine (10ng/ml TNFα and IL-1β) treated FLS cells (undetectable in controls).

Gene	**Official Name**	**FPKM (95% CI)**
kcnip2	potassium voltage-gated channel interacting protein 2	166.5 (110.9-249.9)
trpc3	transient receptor potential cation channel subfamily c member 3	8.3 (0.7-98.2)

kcng3	potassium voltage-gated channel modifier subfamily g member 3	7 (0.7-71.7)
scnn1g	sodium channel epithelial 1 gamma subunit	5.9 (0.7-46.8)
kcnmb3	potassium calcium-activated channel subfamily m regulatory beta subunit 3	5.1 (0.8-33.1)
Gja3	Gap junction type a3	4.6 (0.8-27.3)
kcnj11	potassium inward rectifier j member 11 (Kir6.2)	3.3 (0.3-37.4)
asic5	acid-sensing ion channel subunit family member 5	2.9 (0.3-24.9)
clca1	chloride channel accessory 1	2.6 (0.4-18.4)
kcnc2	potassium voltage-gated channel subfamily c member 2	2.6 (0.4-18.4)
kcnj5	potassium voltage-gated channel subfamily j member 5	2.6 (0.4-18.4)
trpm2	transient receptor potential cation channel subfamily m member 2	2.6 (0.4-18.4)
cacna2d4	calcium voltage-gated channel auxiliary subunit alpha2delta 4	2.5 (0.4-15.3)
kcnk13	potassium two pore domain channel subfamily k member 13	2.5 (0.4-15.3)
trpc4	transient receptor potential cation channel subfamily c member 4	2.2 (0.4-11.2)
p2rx1	purinergic receptor p2x 1	2.2 (0.5-10.9)
scn11a	sodium voltage-gated channel alpha subunit 11	2.2 (0.5-10.9)
Gja8	Gap junction type a8	2.1 (0.5-9.1)
kcnj13	potassium voltage-gated channel subfamily j member 13	1 (1-1)

Data are presented in rank order; top FPKM genes in the presence of cytokine first. None had any expression in control (i.e., non-cytokine treated = 0±0 FPKM *n*=4). Overall, n=4 treated and 4 control animals.

Table 13: Channel genes "disappearing" in cytokine (10ng/ml TNFα and IL-1β) treated FLS cells (undetectable in cytokine).

Gene	Official Name	FPKM (95% CI)
ano2	anoctamin 2	6 (0.8-48.5)
kcnv2	potassium voltage-gated channel subfamily a member 2	5.3 (0.8-36.3)
kcna2	potassium voltage-gated channel modifier subfamily v member 2	2.8 (0.4-21)
kcnmb2	potassium calcium-activated channel subfamily m regulatory beta subunit 2	2.6 (0.4-18.2)
trpm5	transient receptor potential cation channel subfamily m member 5	2.3 (0.4-12.5)
kcne5	potassium voltage-gated channel subfamily e regulatory subunit 5	2.3 (0.4-11.9)
cacna1e	calcium voltage-gated channel subunit alpha1 e	2.2 (0.5-10.4)

Data are presented in rank order; top FPKM genes in the presence of cytokine first. None had any expression in cytokine treated animals (i.e., cytokine treated = 0±0 FPKM *n*=4). Overall, n=4 treated and 4 control animals.

Table 14:FLS channel gene RNA expression lower after cytokine (10ng/ml TNFα and IL1β) treatment.

Gene	Official Name	Log2 (95% CI)
kcnj15	potassium inward-rectified channel subfamily j member 15	-5.51 (-9.57 to -2.48)
ano2	anoctamin 2	-2.59 (-5.5 to 0)
kcnb1	potassium voltage-gated channel subfamily b member 1	-2.44 (-1.85 to -1)
kcnv2	potassium voltage-gated channel modifier subfamily v member 2	-2.4 (-4.85 to 0)
kcnip1	potassium voltage-gated channel interacting protein 1	-2.36 (-3.88 to -0.88)
kcnmb1	potassium calcium-activated channel subfamily m regulatory beta subunit 1	-1.98 (-3.28 to 0.69)
kcns1	potassium voltage-gated channel modifier subfamily s member 1	-1.88 (-6.84 to -0.42)
kcnj8	potassium inward rectifier j member 8 (Kir6.1)	-1.79 (-4.71 to 2.17)

kcnd3	potassium voltage-gated channel subfamily d member 3	-1.78 (-2.63 to 0.29)
nalcn	sodium leak channel, non-selective	-1.77 (-3.43 to -0.85)
clca2	chloride channel accessory 2	-1.76 (-6.72 to 0.65)
kcne3	potassium voltage-gated channel subfamily e regulatory subunit 3	-1.67 (-1.84 to -0.15)
asic1	acid sensing ion channel subunit 1	-1.64 (-6.44 to 0)
clcn4	chloride voltage-gated channel 4	-1.61 (-2.61 to -0.95)
trpm8	trpm8 channel associated factor 1	-1.61 (-2.09 to -0.99)

Qualification cytokine log2 (geometric mean) <-1.5 of control (=approx. 33%), n=4 control and 4 cytokine treated samples (from 4 animals).

Table 15: FLS channel gene RNA expression increased after cytokine (10ng/ml TNFα and IL1β) treatment.

Gene ID	**Official Name**	**Log2 (95% CI)**
kcnc1	potassium voltage-gated channel subfamily c member 1	4.32 (0.68 to 5.93)
kcnc3	potassium voltage-gated channel subfamily c member 3	3.46 (0.76 to 5.94)
trpc3	transient receptor potential cation channel subfamily c member 3	3.06 (3.73 to 6.5)
catsper3	cation channel sperm associated 3	2.83 (0.14 to 5.75)
kcng3	potassium voltage-gated channel modifier subfamily g member 3	2.81 (2.77 to 6.65)
tmc7	transmembrane channel-like 7	2.77 (1.99 to 5.53)
gjc3	gap junction protein gamma 3	2.75 (0.03 to 4.35)
scnn1g	sodium channel epithelial 1 gamma subunit	2.56 (2.77 to 5.45)

asic2	acid-sensing ion channel subunit 2	2.52 (0.66 to 4.65)
kcnmb3	potassium calcium-activated channel subfamily m regulatory beta subunit 3	2.34 (0 to 4.73)
cracr2a	calcium release activated channel regulator 2a	2.32 (0.01 to 1.96)
kcnn3	potassium calcium-activated channel subfamily n member 3	2.07 (0.57 to 4.09)
tmc4	transmembrane channel like 4	1.94 (0.27 to 2.47)
asic4	acid-sensing ion channel subunit family member 4	1.75 (0.52 to 2.76)
kcnj11	potassium inward rectifier j member 11 (Kir6.2)	1.74 (0 to 6.56)
trpv6	transient receptor potential cation channel subfamily v member 6	1.7 (0.01 to 5.43)
hvcn1	hydrogen voltage gated channel 1	1.69 (0.98 to 2.84)
trpv1	transient receptor potential cation channel subfamily v member 1	1.61 (0.98 to 2.07)
kcnk7	potassium two pore domain channel subfamily k member 7	1.6 (-1.85 to 1.03)
cacna1d	calcium voltage-gated channel subunit alpha1 d	1.57 (0.32 to 2.09)
asic5	acid-sensing ion channel subunit family member 5	1.55 (0 to 5.78)

Qualification cytokine log2 (geometric mean) >1.5 of control (=approx. 300%), n=4 control and 4 cytokine treated samples (from 4 animals).

Cytokines treated FLS Multivariate analysis of all genes

To investigate whether there were changes in clusters of genes rather than individual genes, the start was with 7 PCs in PCA. Figure 11-A shows the percentages of explained variance for each PC in which approximately 37% of the variance is explained by the first component. Figure 11-B shows the contribution of each sample to the difference and T1 (cytokine treated sample 1) contributes most to this variance. Figure 12 (A, B, C and C), shows that there is no clear separation between the control and cytokine treated groups. Therefore, DA-PCA was used. Little population difference was detectable until 5 PCs were used (Figure 13), and so the rest of this section models expression changes with 5 principle components. Since there are only two groups (control and cytokine treated FLS) there is only one discriminant function (LD1). DA-PCA (5 PCs) discriminated the control and cytokine treated gene populations well as shown by the kernel density plot (Figure 13-A) using RStudio. The heatmap (Figure 13-B) shows that the 3 control and 2 groups are successfully separated and the prediction of each sample to their group belonging. Next, loading values for the discriminant function were drawn-out, which quantifies the relative contribution of all genes to the differences in control and cytokine treated gene populations. Only the top 50 genes were filtered and the top 15 were displayed in (Figure 13-C) which are considered the most contributing genes to the multivariate population difference.

Enriched pathway in FLS cells

The genes primarily discriminating the treatment and control populations are largely those well established to be important for joint function, including several collagens and a Matrix metallopeptidase (MMP2). Ingenuity Pathway (IPA) Analysis (Qiagen, UK) was then used to identify the upstream regulators of the global differential expression pattern. This analysis predicted the top two regulators to be TNFα and IL1β (p-values 3e-17 and 6e-13 respectively), this is unsurprising since this was indeed the treatment regimen.

Figure 14 shows the canonical calcium signalling pathway (p<0.5e-7), which was enriched following cytokine treatment. Also, the rheumatoid (p<5e-13) and osteoarthritis (p<1e-9) pathways and cellular movement and proliferation canonical pathways (predicted *activation*, p<1e-13 in both cases) were also enriched following cytokine treatment (data not shown). In all cases, TNFα was determined to be the top *causal* agent, but four ion channels were also significant causal regulators (adjusted p<0.05) of the transcript-wide treatment changes; CLCN5, TRPV4, TRPV1, KCNN4.

qPCR

To add further support to the unbiased RNA-seq ion channel analysis, my group colleagues performed qPCR by on sets of control and IL1β/TNFα treated FLS with panels of Ca^{2+}-potassium channels (Kcnma1, Kcnn1, Kcnn2, Kcnn3) and other genes, I have performed the analyses of these data. Not all primers for all the potassium channel genes identified by next-generation sequencing were available. Three potassium genes were differentially expressed; Two voltage-gated potassium channels kcna6 and kcnc2-significantly decreased (p<0.05, *n*=4,4), whereas the large calcium potassium channel kcnma1 was upregulated (p<0.05, *n*=4,4). A correlation analysis between qPCR and NGS data for those genes analysed in both techniques is shown in Figure 15.

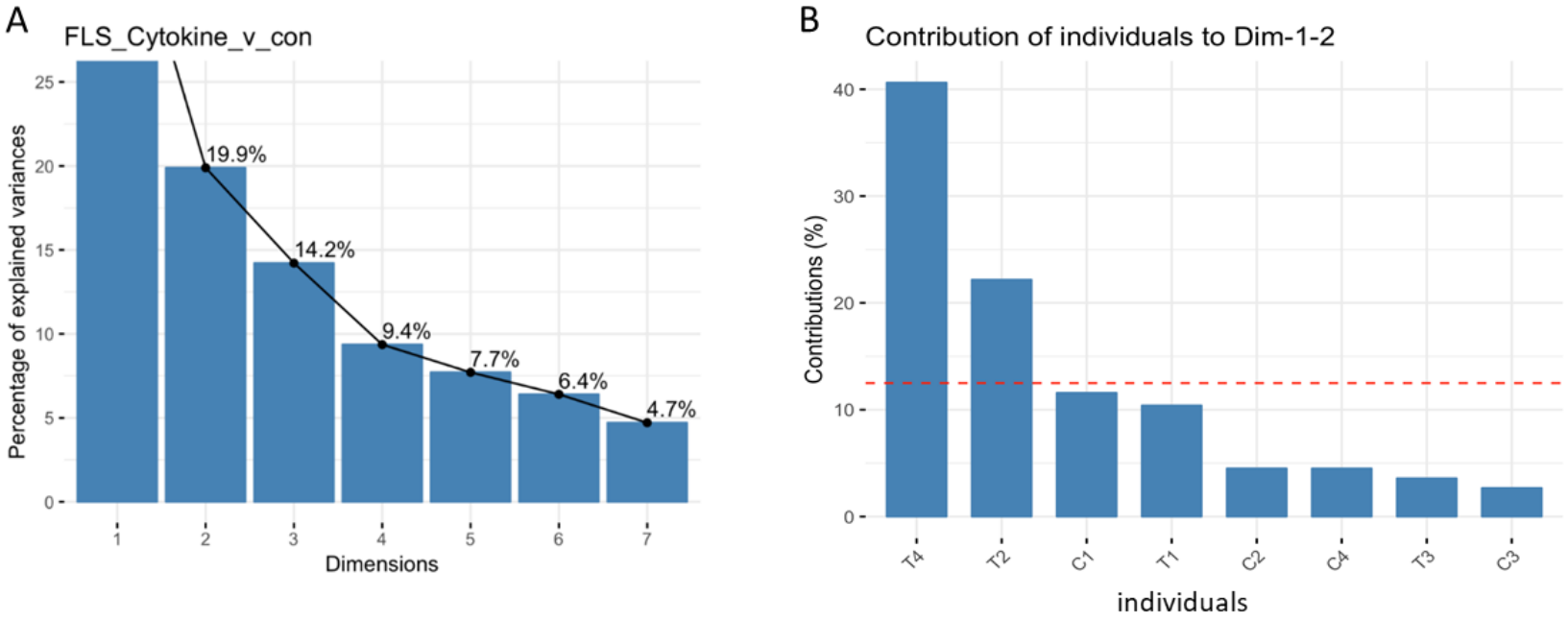

Figure 11: Scree and contribution plots for PCA for Control and Cytokine (IL-1β+TNFα) treated adult rat FLS.
A. *shows the scree plot for the 7 principle components used to reduce dimensionality of the, FLS Control and Cytokine (IL-1β+TNFα) treated datasets, approximately 22038 variables (genes) reduced to 7 variables (PC) with 8 subjects; 4 control and 4 cytokine treated male rats. PCA Component 1 alone accounts for approximately 37% of the variance in the data.* ***B.*** *Contribution plot showing the relative contributions of each of the seven subjects to the variance. The first 2 principle components (T4 and T2 are cytokine treated FLS). The red dotted line indicates the mean contribution. The first subject contributes most to the variability and the second contributes least. Individuals are T1, 2, 3, and 4 are cytokine treated while C1, 2, 3, and 4 are Control FLS samples.*

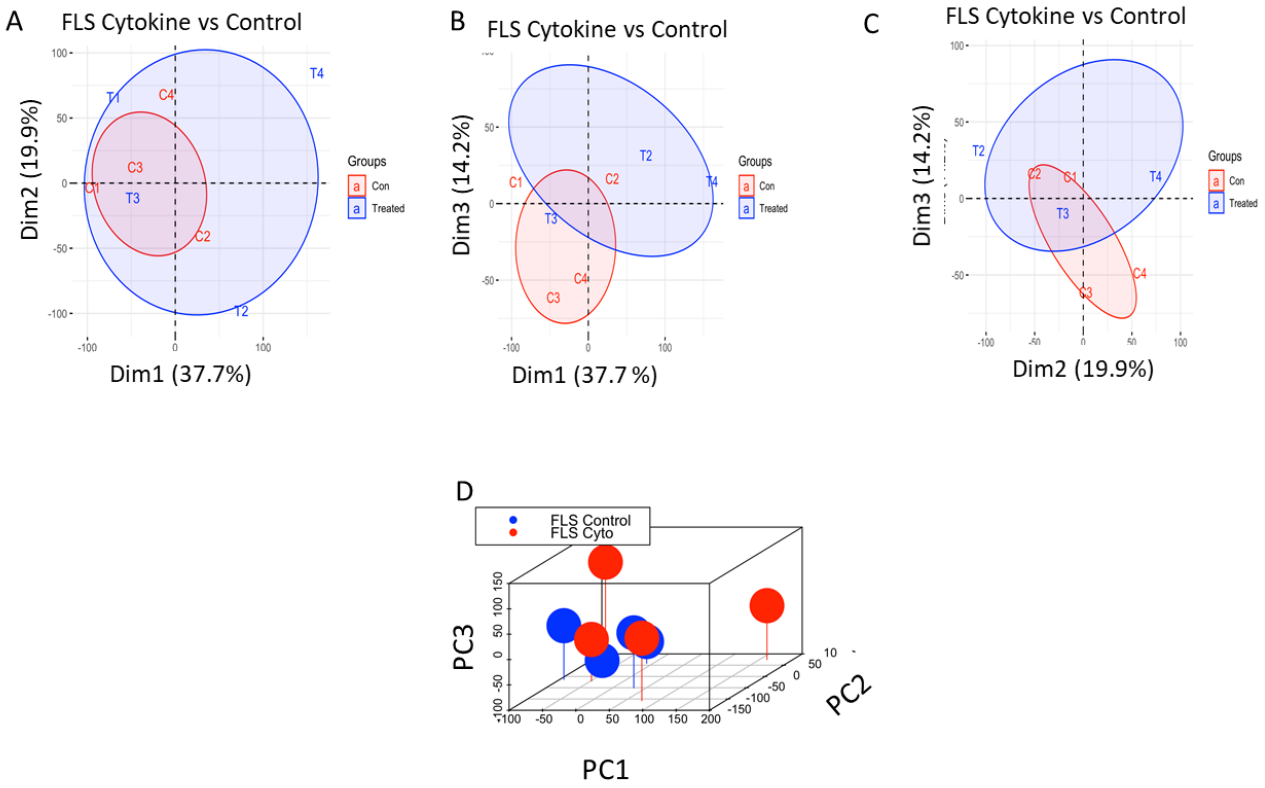

Figure 12: Principle component, k-mean clustering and combined scatter plot.
A, B and C show plots of PC1 vs PC2, PC1 vs PC2 and PC2 vs PC3 (Dim=PC). The shaded circles show the unsupervised k mean cluster 95% confidence intervals thus there is no clear statistical separation between control and cytokine treated samples when combining PC1 and PC2, or PC2 and 3. D. 3D plot showing all three principal components plotted against each other.

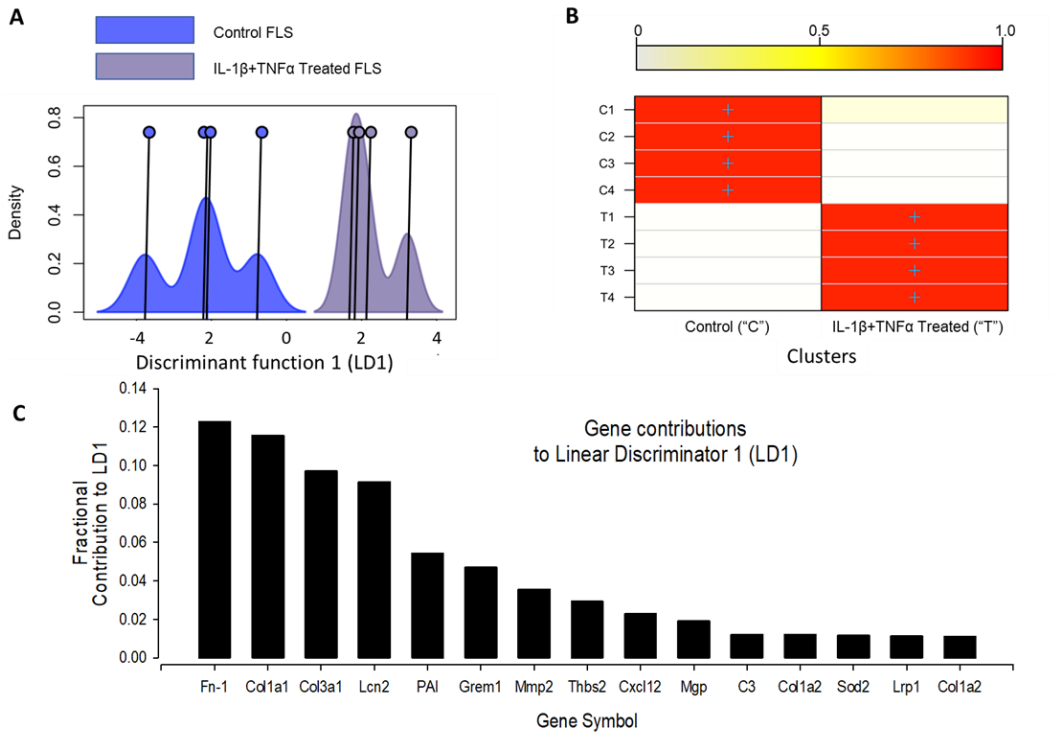

Figure 13: Discriminant Analyses of Global IL-1β TNFα Treatment Effects
A. Shows the kernel density plots of the discriminant component co-ordinates for the control and IL-1β /TNFα treatment groups; co-ordinates on the x-axis and density on the y-axis; Individual co-ordinate centre points are illustrated by the vertical line and circle. There is clear separation between control and cytokine treated FLS samples. B. A graphical confusion matrix showing the actual group membership (y-axis) and predicted cluster membership (on the y-axis). All groups are correctly clustered with greater than 0.9 probability. C. The top 15 contributors to the linear discriminator function; Fn-1=fibronectin 1, Col1a1=collagen type I alpha 1 chain, Col3a1=collagen type III alpha 1 chain, Lcn2=lipocalin 2, PAI=Serpine1, Grem1=Gremlin 1, Mmp2=Matrix metallopeptidase 2, Thbs2=Thrombospondin 2, Cxcl12=C-X-C motif chemokine ligand 12, Mgp=Matrix Gla protein, C3=Complement C3, Col1a2=Collagen type I alpha 2 chain, Sod2=Superoxide dismutase 2 , Lrp1=LDL receptor related protein 1, Col1a2=collagen, type I, alpha 2.

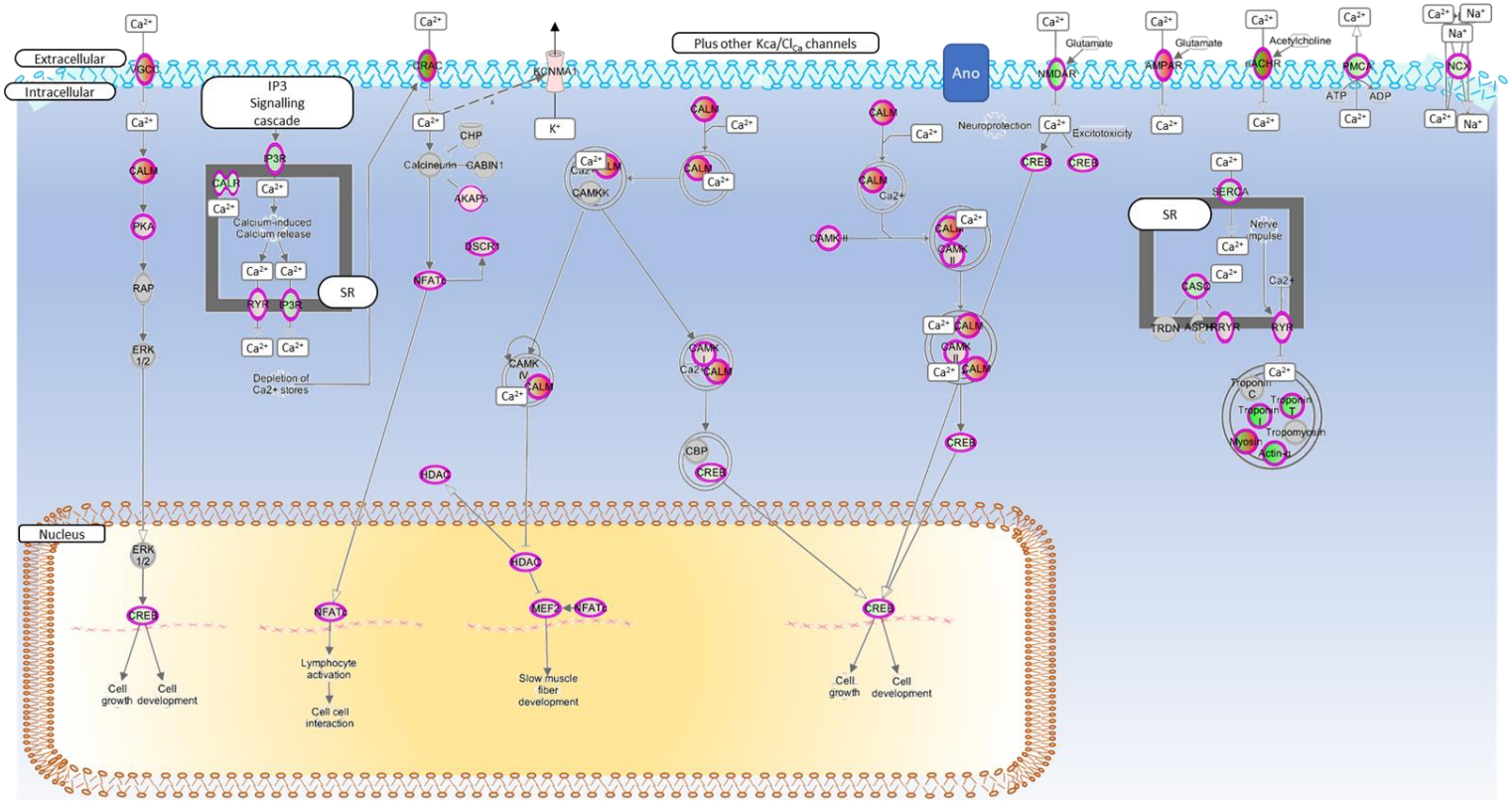

Figure 14: Enriched Calcium regulation pathway.
The nodes differentially expressed within the calcium signalling canonical pathway, identified with IPA. Many Ca2+ activated channels, cytoplasmic proteins and gene activation processes are shown. Calcium pathways have several effects on the cellular functions including activation of cell growth, development, cell-cell interaction, and slow muscle fibre development. Red coloured circles mean increased expression and green coloured circles are decreased expression.

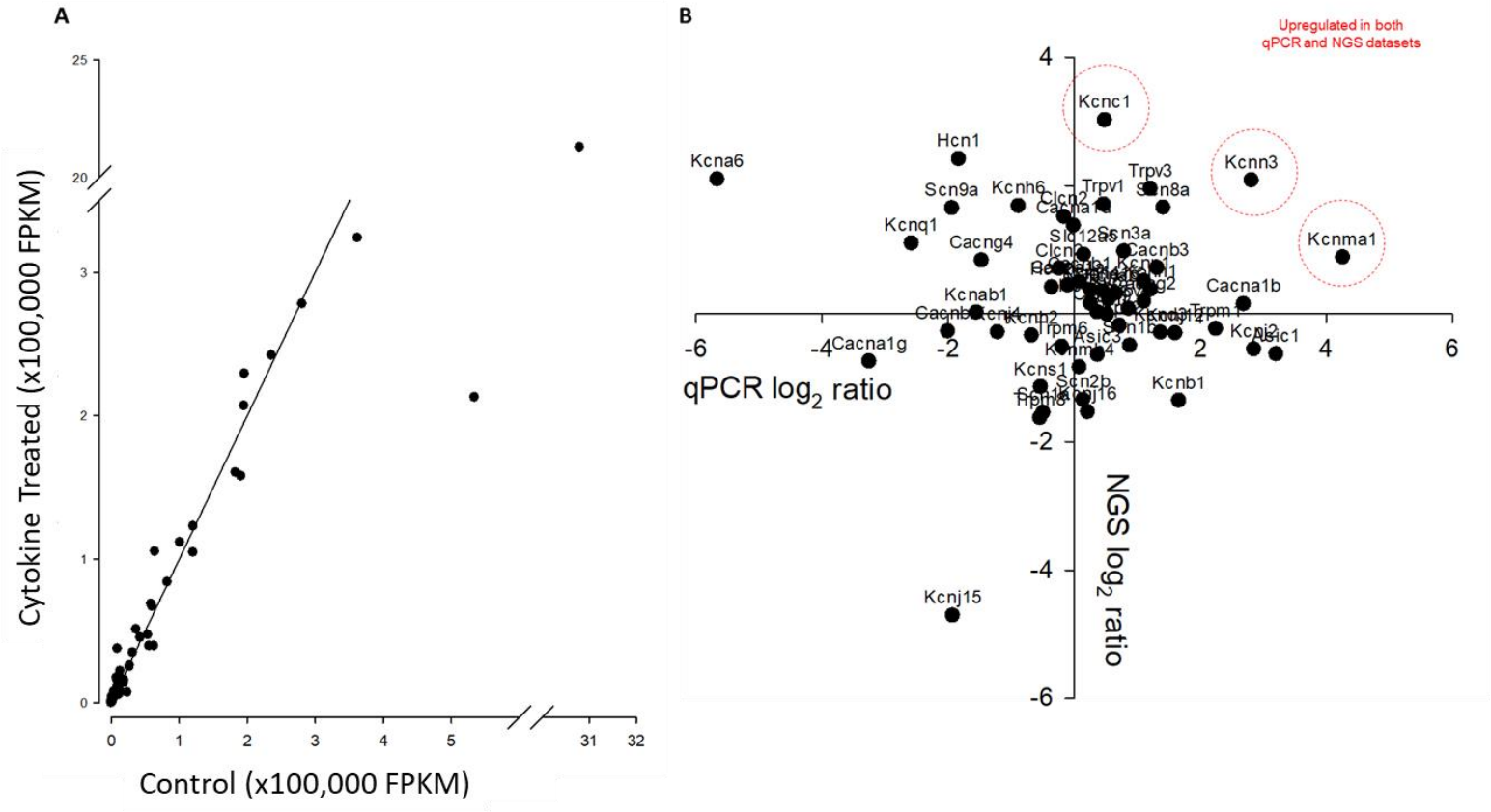

Figure 15: Correlation test between different conditions and techniques of FLS genes.
A. shows the correlation between Control and cytokine in NGS expression data. A strong correlation was found between control and cytokine treated (72 hrs of IL-1β+TNFα) channel expression data. Each point represents the intersection of 4 control and 4 test values. In B, the correlation between qPCR (ΔΔCts) and NGS ratio (FPKM values) are shown. Data suggest that there only a weak linear correlation between qPCR and NGS. P-value=0.3. R=0.29. n=14. Genes that were upregulated in both datasets are indicated in red. Outliers (lower in Cyto) are AQP1 and the gap-junction channel GJa1.

Immunocytochemistry (ICC)

This type of experiments usually confirms the right type of cells were used for experiments especially when working with primary cells because purity is questionable. Therefore, one common marker for FLS cells is the CD248 and this was used in this project. CD248 is a membrane protein, expressed in stromal fibroblast and thought to play a role in tumorigenesis. FLS expressed this marker as shown in (Figure 16-A).

Electrophysiology

Neither RNA nor protein expression studies can confirm changes in functional ion channel expression or, functional changes resulting from post-translational changes. Furthermore, several different potassium channel isoforms were identified, of which some upregulated and some downregulated. Therefore, to investigate the effect of cytokine treatment on electrophysiological fingerprint, functional assays of ion channel expression with patch-clamp electrophysiology were conducted. The primary changes observed in the more limited qRT-PCR data would predict overall *loss of* voltage-gated potassium ion channel activity and increase in the less voltage-dependent calcium-activated potassium channels.

Resting membrane potential (RMP)

Following cytokine treatment, the resting membrane potential of FLS cells was measured by the CAIRN Optopatch amplifier by flicking the dial into the current clamp (I=0) mode and read it directly from the digital screen of the amplifier. The RMP was found to be decreased (depolarized) from -48.6±1.7 to -38.6±2.8 mV (Figure 16-B), junction potential corrected ($p \leq 0.05$, unpaired t-test).

Current-voltage curves

As seen in Figure 17-A, some cells exhibited clear transient and sustained components whereas others exhibited only the sustained component of the current.

Therefore, analysis of both the transient and sustained components of the current took place separately in all cases.

No overall change in the maximum amplitude of the transient (Figure 17-B) or sustained (Figure 17-C) current responses following cytokine treatment was found, although the current-voltage curve of the sustained current appeared shifted to the right. To investigate this systematically sustained current-voltage curves transformed into voltage-conductance curves and fitted these with the Boltzmann equation, which allows the derivation of voltage gating parameters. This analysis shows large shifts in the shape of the currents: Whilst the maximum conductance ("*gmax*") was not significantly changed (Control: 1.20±0.28nS, n=30. Treated: 1.10±0.23nS, n=26 p=0.8), the mid-point for current activation was shifted significantly to the right (Control: 38.64±5.38mV, n=30. Treated: 75.7±7.9mV, n=26 p<0.0005) and the slope of this activation was flattened (Control: 20.86±2.12 mV, n=30. Treated: 31.49±2.29 mV, n=26 p<0.005). To characterise the nature of the conductance apparently *inhibited* by cytokine treatment I calculated the difference current for cytokine treatment (Figure 17-D). This revealed a strongly voltage-gated current with mid-point for activation 40±1.2 mV and slope 17.6±1.2 mV, *n*=25.

Even within the sustained current phase, currents from this population of cells was quite variable and so I performed unbiased K-means clustering analysis on our Boltzmann data. I fit data with 2, 3, 4 and 5 K-means 3 dimensional clusters and used silhouette analysis to determine that fitting with 2 clusters was optimal for our data. Cluster 1 had a centroid of Gmax=1.19±0.26nS, $V_{1/2}$ =31.65±3.45mV, *k*=22.44±1.75 and cluster 2 had centroid of Gmax=1.67±0.43nS, $V_{1/2}$ =107.76±5.97mV, *k*=33.43±2.39. For this sustained data, a significant association between a cluster and cytokine treatment (Fisher Exact test p<0.05, odds ratio 4.5; 95 %CI: 1.98-10.13, *n*=35), (Figure 18), was found.

This was repeated for the transient current and found there was no significance in any of the Boltzmann parameters for the transient currents and it was not associated with cytokine treatment. Boltzmann parameters for these conductances (transient current) were; Control: Gmax =1.28±0.49 nS, $V_{1/2}$ =5.49 ±6.28mV, *k* =8.88 ±3.24mV and cytokine treated: Gmax=1.76±0.65nS, $V_{1/2}$ =1.09±5.62mV, *k*=14.50±2.56mV ($p>0.05$, *n*=4,4).

Pharmacological Interaction with KCNMA1 (BK)

To investigate relative constitutive BK channel activity in control and cytokine treated cells, standard voltage protocol (see *methods section*) in the presence of 1µM of the BK channel inhibitor paxilline was performed. No significant effect of cytokines was found on the size of currents in the present of paxilline (Figure 19); control 1.72± 0.62nS vs cytokine 1.80±0.43nS *n*=20, 25) or the $V_{1/2}$ values (control 53.2± 3.8mV v cytokine 48.4±5.7mV *n*=20,25). However, I found that the slope of the Boltzmann was shallower in cytokine treated paxilline (i.e., BK free) currents (control 24.6±4.5 v cytokine 36.7±11.6, *n*=20,25 $p \leq 0.01$ students t-test).

To investigate if the maximum possible BK current is altered in cytokine treatment, voltage protocol was repeated in the presence of 1µM of the BK channel opener NS1619 (Figure 19-B) and found a large NS1619 activated current in control cells, but significantly less in cytokine treated (Difference current at +70mV was 66.18±19.82pA compared to only 2.94±5.01 with cytokine treated cells, $p \leq 0.05$ Students t-test, *n*=9,6).

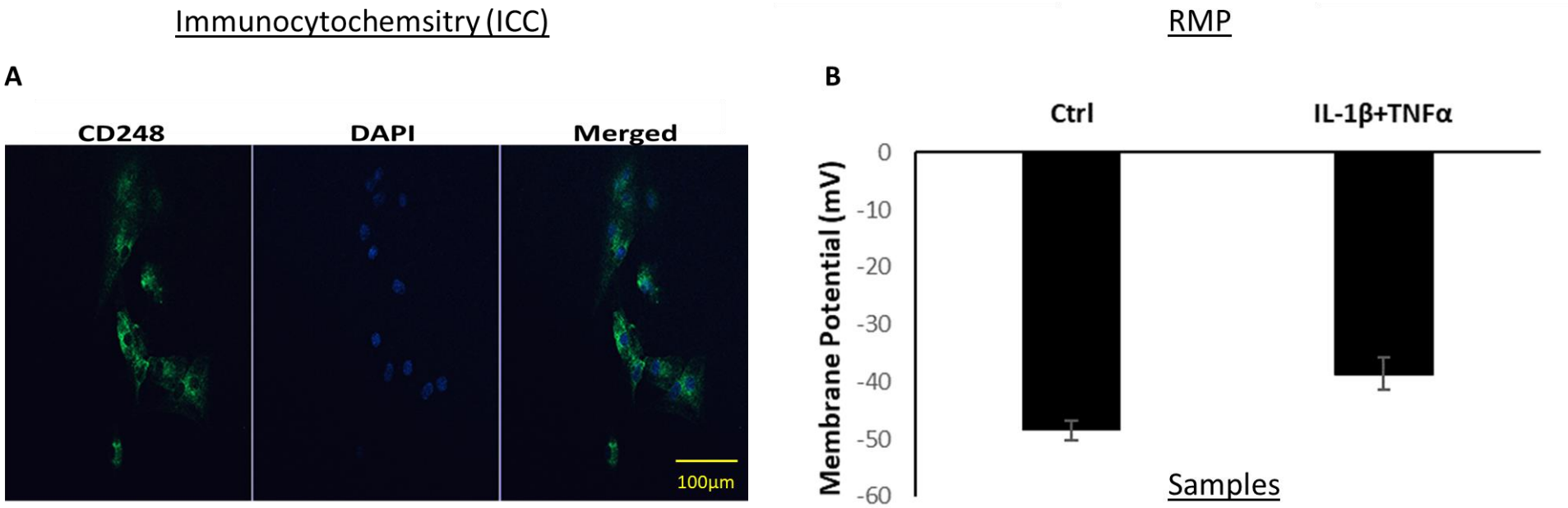

Figure 16: Tissue typing and resting membrane potential (RMP) of FLS cells.
A. *Expression of CD248 in FLS cells with ICC. The concentrations were 1:100 for the primary antibody (CD248) and the secondary antibody concentration was 1:500. The left shows the CD248 alone (green colour) while the middle figure shows the DAPI which is a nuclear counterstain (blue colour) and the right figure shows the final merged CD248 and DAPI. Scale is at 100µm.* ***B.*** *The RMP of FLS cells was decreased (depolarized) following cytokines (IL-1β+TNFα) treatment. The measurements of the RMP were taken from the CAIRN Optopatch amplifier on current clamp (I=0). Data presented in mean±SEM, $p<0.05$, paired- t-test, n=18 for control and n=11 for cytokines treated FLS cells.*

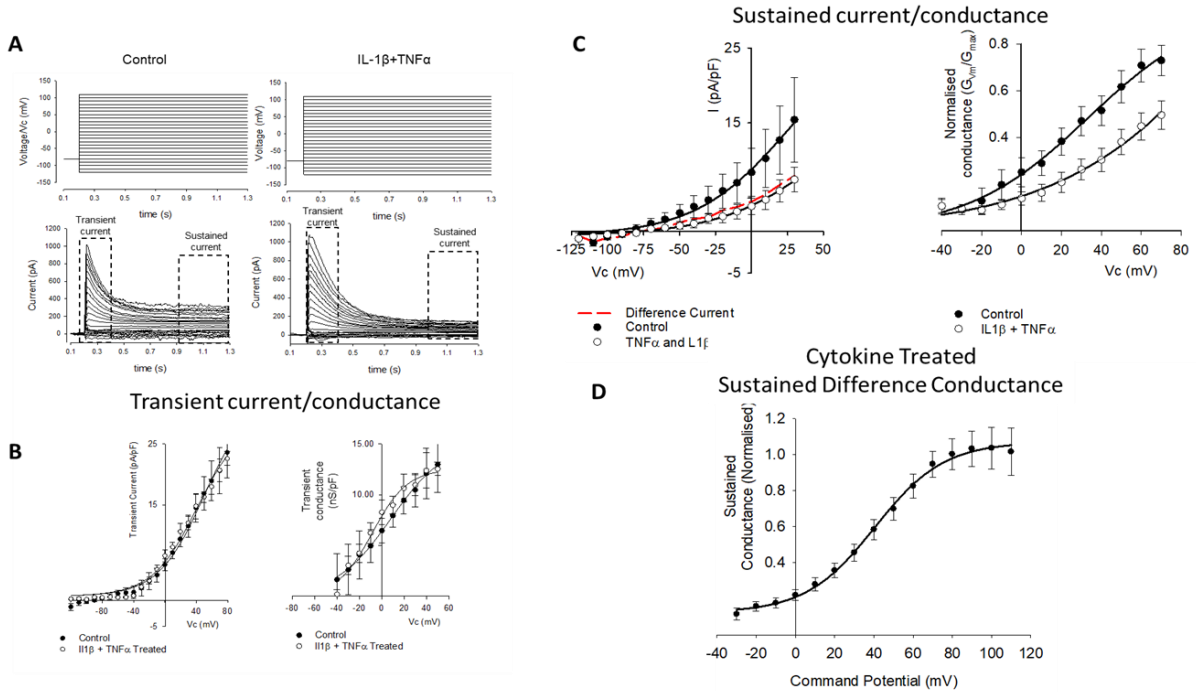

Figure 17: Whole-cell voltage-gated currents from control and cytokine treated FLS.
A. Top panels show the voltage step protocols and the evoked currents are shown below for control (left) and IL-1β+TNFα (right) conditions. Note that FLS exhibit both transient and sustained currents. These phases of current were then *analyzed* separately as indicated. B. Current-voltage curves (left) and Boltzmann transformed conductance voltage curves (right) from the transient currents recorded in a number o*f* experiments such as that illustrated in (A). The solid lines represent Boltzmann fits (see text). There was no significant difference between control and treated transient currents. Data points are shown as mean ± SEM (n=18 for control and n=11 for IL-1β+TNFα). C. Current (left) and conductance (right) curves as (B), but from the sustained currents. The red line in the current-voltage curve is the difference current for control-cytokine treated. D. Difference conductance-voltage curve for the cytokine difference current shown in (C). The line is fit*ted* with a Boltzmann.

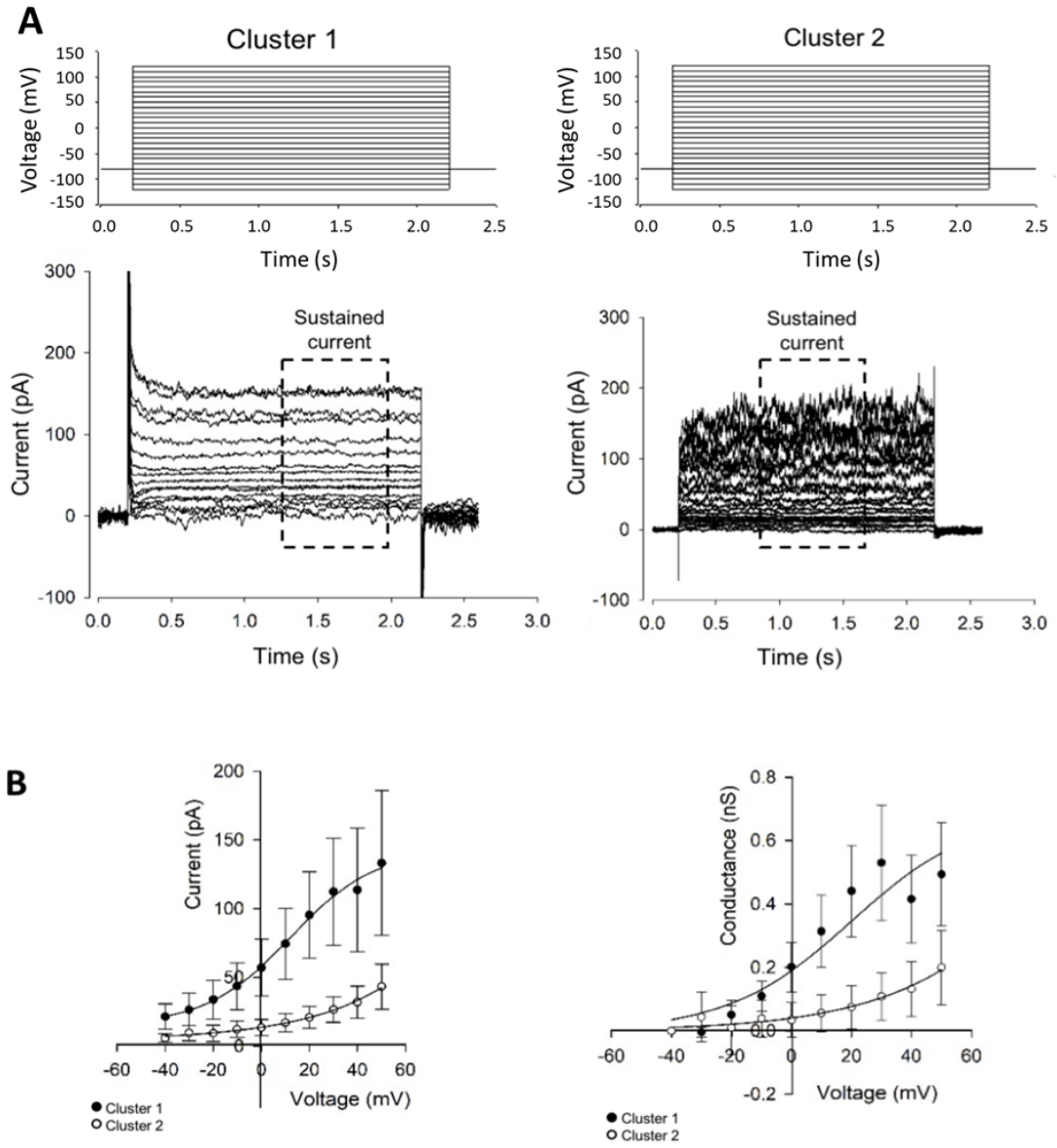

Figure 18: Control and cytokine current family clusters.
K-means cluster analysis shows two clusters of voltage-gated 'sustained' currents. Clusters 1 and 2 significantly associated to control and cytokine treatments. (A) Top panels show the voltage step protocols and the evoked currents are shown below for cluster 1 current family (left) and cluster 2 current family (right) conditions. (B) Left, Current-voltage curve for cluster one and two. Right, Boltzmann transformed conductance voltage curves for cluster one and two current families illustrated in (A). The solid line represents the Boltzmann curve fits to the data. These are significantly different. For this sustained data, a significant association between the cluster and cytokine treatment (Fisher Exact test $p<0.05$, odds ratio 4.5; 95 %CI: 1.98-10.13, n=35) was found.

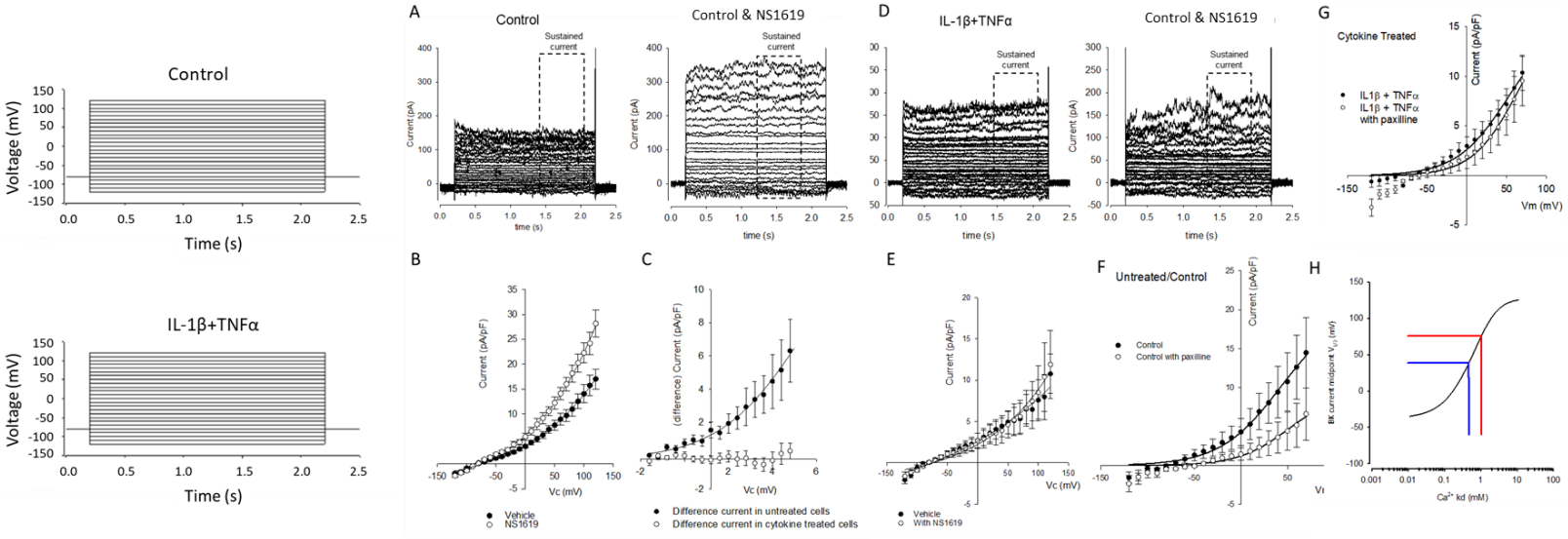

Figure 19: Effects of BK channel drugs on FLS whole-cell currents.
A. Voltage step protocols used with control ± drugs (top) and cytokines (IL-1β+TNFα) ± drugs (bottom). B. Representative examples of untreated (control) cells before (left) and in the presence of 1μM of the BK channel opener NS1619 (left). C. Current-voltage curves from a number of cells such as that shown in (A). Current is significantly greater in the presence of NS1619, $p<0.05$, n= 6 and 6. D. Difference currents for control and cytokine treated cells in the presence of NS1619 (i.e., current in the presence of NS1619- vehicle control. E. Representative raw example current families of cytokine (10ng/ml IL1β+TNFα) treated cells in the absence (left) and presence (right) of 1μM NS1619. F. Current-voltage curves for a number of cells such as that shown in (C). These two curves are not significantly different from each other n= 6 and 6. (G, H) There was no significant different of current amplitude in the presence of the BK inhibitor paxilline (F. control vs cytokine OR G. paxilline vs no paxilline). I. Numerical simulation of data from Clark et al 2017 model. To quantify the degree of change of BK channel modulation taking place with this treatment we used the model of (Clark, Schmidt, Sachse, Boyle, Firestein & Giles, 2017) verbatim with the exception that we varied the inherent BK channel Ca2+ sensitivity parameter kd. In this simulation, the independent variable kd is plotted on the x-axis and the predicted BK current midpoint (V1/2) is plotted on the y-axis. In blue we have added the midpoint we recorded in control conditions, and in red that following cytokine treatment. The complete MATLAB code for this simulation is included in the supplementary data (2).

Comparison of control vs cytokine treated vs young vs old FLS of NGS data

A comparison between all FLS samples (control, cytokine treated, young and old) was done. Again, a multivariate analysis (PCA) was used here with 10 PCs. Figure 20-A shows the scree plot presenting the percentage of explained variance by each dimension. Most of the variabilities are explained by dimension 1 (approximately 66%). The contribution of each sample to the difference between groups is shown in Figure 20-B. T4 (treated sample 4) contributes most to the difference. When comparing the dimensions (PC1, PC2, and PC3) with each other, there was good and clear separation between control and cytokine from young and old as shown by PC1 vs PC2 (Figure 21-A). The other PCs, PC1 with PC3, and PC2 with PC3 did not show such nice separation (Figure 21-B and -C). Figure 21-D shows the 3D plot of all these samples and it shows a clear separation between control and cytokine compared to young and old. The contributing genes to the separation between sample groups using PC1 and PC2 are shown in Table 16.

Table 16: Contributing genes to the difference between all samples in PC1 vs PC2.

PC	Ensemble IDs	Gene name	Gene description	Contribution value
1	ENSRNOG00000001597	Atf2	activating transcription factor 2	0.008799919
1	ENSRNOG00000004556	Dcaf5	DDB1 and CUL4 associated factor 5	0.008808127
1	ENSRNOG00000004577	Fez2	fasciculation and elongation protein zeta 2	0.008797673
1	ENSRNOG00000007224	Bmt2	base methyltransferase of 25S rRNA 2 homolog	0.008795777
1	ENSRNOG00000007333	Wdr20	WD repeat domain 20	0.008799587
1	ENSRNOG00000009781	Dync1i2	dynein cytoplasmic 1 intermediate chain 2	0.008802714
1	ENSRNOG00000010967	Cdc37l1	cell division cycle 37-like 1	0.008810146
1	ENSRNOG00000018176	Rab6a	RAB6A, member RAS oncogene family	0.008798605
1	ENSRNOG00000019649	Cul4a	cullin 4A	0.008796222
1	ENSRNOG00000025269	Slc25a44	solute carrier family 25, member 44	0.00880108
2	ENSRNOG00000000861	Zic3	Zic family member 3	0.04440599
2	ENSRNOG00000003039	Wnt3a	Wnt family member 3A	0.04259736
2	ENSRNOG00000007907	Tmem178a	transmembrane protein 178A	0.04284819
2	ENSRNOG00000016358	Apba2	amyloid-beta precursor protein-binding family A member 2	0.04411142
2	ENSRNOG00000017484	Gja5	gap junction protein, alpha 5	0.0433594

2	ENSRNOG00000017783	Sfrp1	secreted frizzled-related protein 1	0.04421027
2	ENSRNOG00000026902	Lyve1	lymphatic vessel endothelial hyaluronan receptor 1	0.04279164
2	ENSRNOG00000031675	Panx3	pannexin 3	0.04343534
2	ENSRNOG00000052205	Fgf23	fibroblast growth factor 23	0.04429612
2	ENSRNOG00000061614	Olr61	olfactory receptor 61	0.04427828

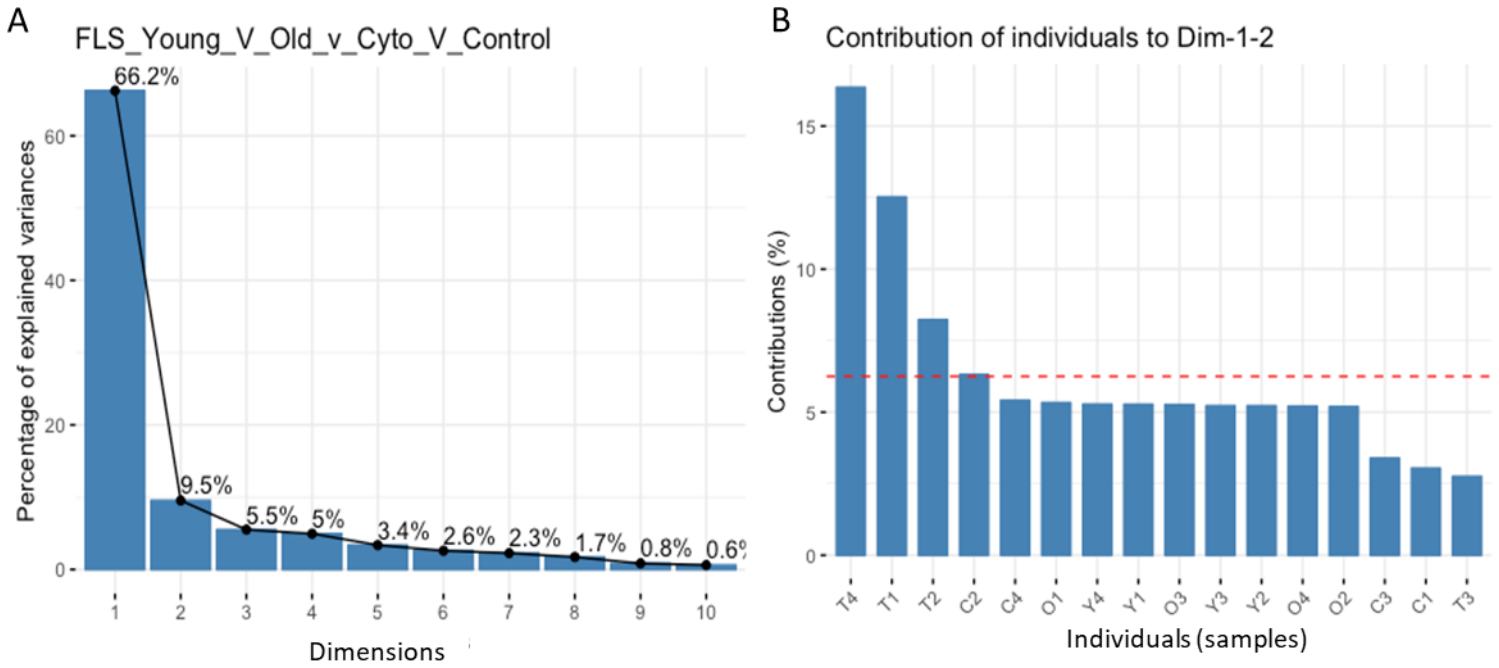

Figure 20: PCA of FLS cells at different conditions and ages.
A. *shows the scree plot for the 10 principle components used to reduce the dimensionality of FLS Young, Old, Control, and Cytokine (IL-1β+TNFα) treated datasets, approximately 22038 variables (genes) reduced to 10 variables (PC) with 16 subjects; 4 young, 4 old, 4 Cytokine treated and 4 Control male rats. PCA Component 1 alone accounts for approximately 66% of the variance in the data.* ***B.*** *Contribution plot showing the relative contributions of each of the sixteen subjects to the variance. The red dotted line indicates the mean contribution. The first 2 subjects contribute most to the variability and the third one contributes least. Individuals are T1, 2, 3, and 4 are cytokine treated, C1, 2, 3, and 4 are Control, Y1, 2, 3, and 4 are Young and O1, 2, 3, and 4 are old FLS samples.*

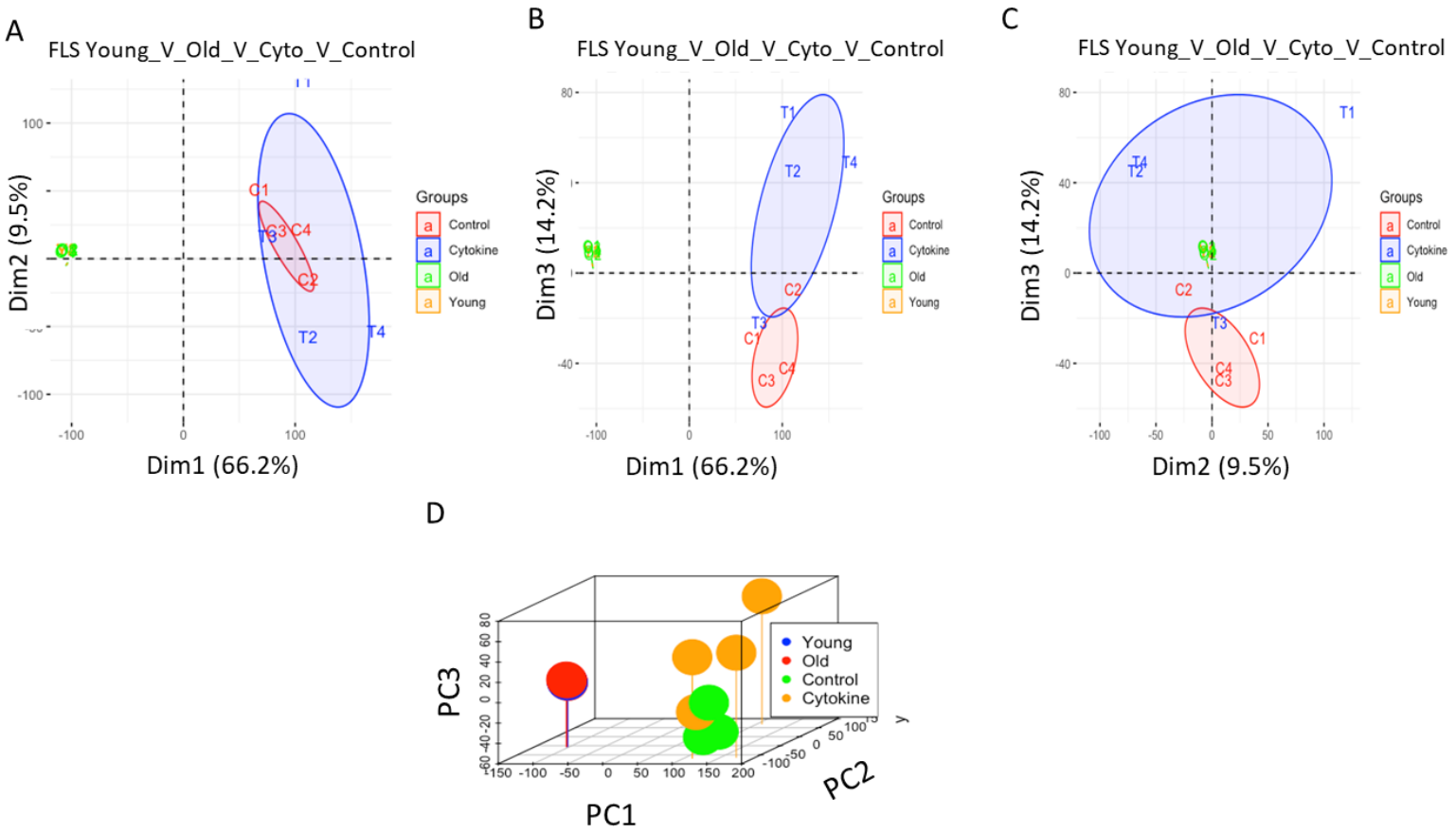

Figure 21: Principle component, k-mean clustering and combined scatter plot of FLS cells at different conditions and ages.
Principle component, k-mean clustering and combined scatter plot. A, B and C show plots of PC1 vs PC2, PC1 vs PC2 and PC2 vs PC3 (Dim=PC). The shaded circles show the unsupervised k mean cluster 95% confidence intervals. Thus, there is a clear statistical separation between young and old from cytokine treated and control samples when combining PC1 and PC2. D. 3D plot showing all three principal components plotted against each other.

3.4 Discussion

In this study, two models were used to investigate the effects of ageing on FLS. Both natural ageing of Wistar rats and an *in vitro* model which was intended to recapitulate some aspects of musculoskeletal inflammageing were used. A number of genetic changes in both were detected. Of particular note is that IL1β and TNFα treatment of FLS cells resulted in profound changes in arthritic, inflammatory and Ca^{2+} regulatory pathways and differential expression of several ion channels. In this model our RNA sequencing and qPCR show an upregulation of KCNMA1 channels and electrophysiological experiments show that while the constitutive activity of the channel is not changed, regulation by voltage and drugs are significantly altered.

Global transcriptomic changes in naturally aged rodents' FLS

The only gene differentially expressed, taking the most rigorous approach, straightforward comparison with BH corrected FDR was Eml1. Eml1 is involved with mitosis (Richards et al., 2014) I are not aware of any previously reported direct role of this in ageing or joint disease, but a loss of this gene is associated with a series of genetic diseases including congenital deafness (Kaplan et al., 1992) and some brain diseases (Oegema et al., 2019). There are also reports of this gene being involved with cancer (De Keersmaecker, 2005). Further investigation will be needed to discover its role in joint ageing. In terms of my multivariate analyses of differential gene expression, several extracellular systems were significantly regulated, focal adhesion, extracellular exosome, extracellular matrix together with RNA processing. This suggests that there have been major changes, perhaps to the entire structure of resulting tissues. That said, transcriptomics always needs a caveat attached that change mRNA whilst probably always important does not necessarily correlate with change of protein, see full discussion [CHAPTER 7] for further discussion of this point.

Ion channel "channelome" changes in naturally aged rodents' FLS

The FDR calculated by Deseq2 for transcriptome-wide comparisons is not useful when investigating changes in a subset of genes, such as ion channel genes, chosen *a priori*. Therefore, here ion channel genes with a p-value below 0.05 were looked for; there were two and interestingly both were members of the KCNK family. Both were upregulated by more than 1.5 log2 fold change. This is a fascinating discovery since this channel was recently reported to be a key regulator of FLS function Clark et al 2018 (Clark et al., 2017).

Tissue typing by ICC

It is important to be able to confirm the type of cells that were used for experiments. For example, in this part of the project, the FLS cells were used and CD248 was used as a marker to identify these cells by ICC. CD248 is a transmembrane glycoprotein. It is dynamically expressed on fibroblasts during tissue development and inflammation. Additionally, it is one of the markers that are used to identify FLS cells (Teicher, 2019). The expression of this marker in FLS cells used in this project was almost in all cells. Also, its expression was increased (log2 fold change was 0.614) in the NGS data in this project. Although ICC of other markers (fibronectin and prolyl 4-hydroxylase) of FLS (Teicher, 2019) could not be done due to technical issues (including costs), the expression level with NGS data was interesting. For example, fibronectin was upregulated with log2 fold change of 0.727 and prolyl 4-hydroxylase was slightly upregulated with log2 fold change of 0.071. This increases the possibility of the high purity of the cell population (FLS) used in this project.

The pathophysiological validity of the 72hr IL1β and TNFα model

There is no established in vitro model of ageing per se, but the treatment of tissue with TNFα and IL1β should recapitulate at least some aspects of inflammageing. In terms of joint tissue, the clear and obvious age-related pathology is arthritis. In *in vitro* studies of inflammatory arthritis, tissues are typically exposed to between 10ng/ml of TNFα and IL1β

for between 2 to 7 days. In the present study, the lower end of the concentration range was used, 10ng and treat for 72hrs (Williams et al., 2011, Stevens et al., 2009, Stevens et al., 2008, Pretzel et al., 2009, De Ceuninck et al., 2004, Williams, 2014). This regime causes will activate inflammatory pathways and yet there will be no cytokine remaining by the time of the electrophysiological experiments that could cause confounding direct effects. FLS cells were treated with the pro-inflammatory cytokines IL1β and TNFα in order to understand the cellular changes that occur when these FLS are subjected to higher-than-normal levels of these cytokines *in vivo*, for example in arthritis. This model has distinct advantages of 3Rs, consistency, reproducibility and allowing the investigation of distinct pathways in isolation but since it is an acute model it may lack some chronic features of *in vivo* models. Our transcriptome analysis demonstrated that pathways were activated in common with arthritis; movement of cells, proliferation and both rheumatoid and osteoarthritis. Taken together with the changes in Ca^{2+} signalling, I show that our *in vitro* model does capture several features of the inflammatory joint phenotype and that FLS have been "activated" as observed in animal models of arthritis.

Causal analysis is a relatively new mathematical technique that allows one to move from the probability of agreement or simple correlation towards the probability of causation in networks (Kramer et al., 2014). The IPA implementation of this identified both IL1β and TNFα as master-regulators of the changes I observe and considering our experimental design included time-matched controls, this strongly supports a suitable dosage and incubation time. Whilst both IL1β and TNFα were identified by IPA as "master regulators", TNFα transcriptome-wide causation was stronger than that of IL1β.

Previous studies of differential expression of membrane ion channels in the synovium

Until very recently, little was known of the FLS ion channel complement (the "channelome") compared to that of another central joint cell, the chondrocyte (Barrett-Jolley

et al., 2010). One of the best-studied families of ion channels in FLS, however, is the Ca^{2+} -activated potassium channel family. The high conductance member of this family termed BK (KCa1.1 or KCNMA1 (Hu et al., 2012a, Tanner et al., 2015b)) and the "intermediate" conductance member ("IK", or KCa3.1) are both expressed and have roles in invasive migration, proliferation, cytokine and MMP release (Friebel et al., 2014, Hu et al., 2012a). Interestingly, inhibitors of BK decrease the signs of joint degeneration in the pristane-induced arthritis model (Tanner et al., 2015b). These channels are therefore potential drug targets to protect against joint degeneration as well as being putative biomarkers. Whilst the BK channel β- subunit (KCNMB1) was slightly increased in transcript abundance in the Lambert *et al.,* 2014 data (Lambert et al., 2014) (similar seen by Huber et al., 2008 (Huber et al., 2008)), both of the two BK α-subunit (KCNMA1) probes on the chip exhibit small decreases in expression. It should be noted that the expression of BK channel β- subunits confer modulation of ion channel activity, in many cases decreasing its sensitivity to, for example, Ca^{2+} ions (Lippiat et al., 2003, Mobasheri et al., 2012).

A recent study by Kondo et al (Kondo et al., 2018) demonstrated human FLS express high levels of both intermediate ($K_{Ca}3.1$) and large (BK/$K_{Ca}1.1$/KCNMA1) Ca^{2+}-activated potassium channels. The other most highly expressed ion channels identified by Kondo et al (2018) (Kondo et al., 2018) were KCNK2, ANO6, ANO10 and KCNK6. KCNK2/6 are members of the two-pore-domain potassium channel family and are particularly thought of as molecular sensors, whereas the ANO (anoctamin) channels are members of the large chloride channel family. The family is relatively understudied compared to potassium channels, but ANO6 (TMEM16F) is, interestingly, thought to be a Ca^{2+}-activated chloride channel as well as a lipid "scramblease"(Scudieri et al., 2015), therefore, likely to be activated in parallel to Ca^{2+}-activated potassium channels.

Changes in BK channels in the present study

The phenotype of FLS current recorded by whole-cell patch-clamp was quite variable in terms of the presence of transient and sustained components of current, as seen in Figure 17. Furthermore, even the sustained current fell into statistically separable clusters, Figure 18. The two "clusters" of sustained current families were present in both control and cytokine treated cells, however, there was a statistically significant correlation between cluster number and cytokine treatment, implying that cytokine treatment tended to push cells into a certain cluster phenotype (in our case, cluster 2). The basis of these different clusters is unknown, but it could represent different states of the same cell type. This hypothesis would fit well with our global transcriptomic analysis that indicated that both proliferative and migratory canonical pathways were activated by cytokines.

Significant increases in RNA expression of the BK α-subunit gene, Kcnma1 was found following cytokine treatment (both by next-generation sequencing (NGS) and qPCR), but there was no overall increase in whole-cell voltage currents in a protocol that would be expected to be heavily dominated by calcium-activated potassium channels. Indeed, in this study the resting membrane potential was depolarised following treatment with cytokines; a phenomenon that could result from either loss of constitutive K^+ conductivity or increase in Cl^- or non-specific channel conductance. The families of currents are, of course, from native cells that also express a number of other ion channels such as TRP channels (for example Trpm7/Trpv2 identified by our NGS) and also other potassium channels, such as the two-pore channel (for example Kcnk2 detected by our NGS) or voltage-gated potassium channels (for example Kcnq5 detected by our NGS). Pro-inflammatory cytokine treatment caused a notable shift in voltage-gated current from left to right which corresponds to reduced activation of current under any reasonable physiological condition. These voltage-activation midpoints ($V_{1/2}$), are in the range expected for BK channels recorded with the presence of intracellular EGTA and thus very low (nanomolar) resting Ca^{2+} concentrations(Cui et al.,

1997). Note that with elevated, thus physiological intracellular Ca^{2+} concentrations, these would likely lie to the left of where they lay in our experiments. However, our patch-clamp conditions allow a more direct comparison between fundamental BK ion channel properties, than for example, sharp-electrode work which would allow change in Ca^{2+} occur simultaneously changes in ion channel properties, and thus be a confounding variable. The difference current between treated and untreated conditions is similar to many common voltage-gated channels, which includes the K_{Ca} which in can be activated by voltage even in the virtual absence of Ca^{2+} ions(Cui et al., 2009). One apparently simple question would be whether the difference current was sensitive to BK channel block, with paxilline. I found that both the BK channel activator (NS-1619) and inhibitor (paxilline) were ineffective following cytokine treatment. This could be for two possible reasons: (i) That there were no longer any KCNMA1 channels expressed; except that would be diametrically opposed to that data I have RNA level (and I would expect to see generally smaller whole-cell currents), so far more likely is (ii) that the channel is still present, but is no longer sensitive to these drugs. This is an exciting interpretation and is strongly supported by the RNA data, since there is a clear shift from RNA-expression of β1 (and β2) subunits to β3 and sensitivity to voltage, calcium AND drugs is well-known to be conveyed by co-expression of the β subunits(Uebele et al., 2000, Yang et al., 2009, McManus et al., 1995). The simple (K^+ channel focussed) FLS electrophysiological model of Clark (Clark et al., 2017) allows using numerical simulation to estimate the change in BK channel Ca^{2+} that would be required to shift the conductance curve by the degree reported in the present work (Figure 19-H). It was found that retaining all the parameters of(Clark et al., 2017) except the Ca^{2+} *kd* itself, data would be the equivalent to increasing *Kd* from 0.46µM to approximately 1.05µM. The upstream pathway (beyond the activation of the cytokine pathway including NFκB etc) for these changes is difficult to identify from these data, especially since there are relatively few ion channel interaction data in the IPA databases. It is notable, however, that there were significant changes in the calcium

signalling pathway (*Figure 14*) and so change in calcium-activated potassium channel expression may follow this, by way of compensatory expression.

Role of ion channels in pro-inflammatory cytokine production and secretion

Ion channels are involved not just in the response to cytokines, but can also contribute to their production. For example, ionotropic NMDA and kainite glutamate receptors contribute to synovial inflammation by increasing expression of the inflammatory cytokine IL-6(Flood et al., 2007) and nicotinic acetylcholine receptor activation reduces the synovial production of IL-6, IL-8, TNFα and several other cytokines(Waldburger et al., 2008, van Maanen et al., 2009). P2X7 is an established conduit for the release of mediators such as IL1β(Mortaz et al., 2012). I saw little P2X7 RNA, but there is evidence that in chondrocytes P2X1, may subserve the same function(Varani et al., 2008) and I detected RNA for this channel only after cytokine treatment. In a previous report inhibition of the small Ca^{2+} activated potassium ion channel decreased the production of cytokines IL-6, IL-8 and MCP1 in response to TGF-1β, but they did not examine secretion of IL1β or TNFα(Friebel et al., 2014). In other-words activation of Ca^{2+} potassium ion channel is essentially a secretion trigger. This result is somewhat counter-intuitive since one would expect activation of a potassium channel to hyperpolarise and decrease secretion. One possible explanation is that activation of Ca^{2+} potassium ion channels draws in additional Ca^{2+} by increasing the driving force for Ca^{2+} entry.

$$Ca^{2+}\ entry\ \alpha\ (Vm\text{-}Eq_{Ca2+})$$

Where negative values are equivalent to the inward driving force for Ca^{2+}, *Vm* is the membrane potential and Eq_{Ca2+} is the equilibrium potential for Ca^{2+}.

Enrichment analysis of FLS cells (ageing and cytokine effects)

For the GOs, it seems that our model of "inflammageing" was close to the real model of ageing (FLS from old rats) when comparing NGS data. For example, focal adhesion, extracellular exosome, and extracellular matrix were all enriched GOs in aged FLS. On the

other hand, the effects of cytokines (10ng/ml IL-1β+TNFα) treatment showed enrichment in genes involved in joint function such as collagens and Mmp2. They were all focused on the extracellular space. As mentioned earlier, the model of "inflammageing" in this study has already captured some features of inflammatory joint phenotype and FLS cells have been activated as observed in animal models of arthritis. A note of caution should be added, to meta-analyses, however. Note that in Figure 20, PCA of four groups Control, Treatment, Young and Old have been shown. Since the Control and Treated are both FLS from Young animals, one would have expected Young and Control to be tightly grouped (or the same), but in fact, in PCA terms over all three dimensions, Young and Old are the most similar and both very different from Control. This implies that in the case of FLS cultured cells, the different strain of rats, time, weather (other confounding factors) may have had a greater effect on the cell phenotype than ageing itself. This could reflect the fact that the cells are first cultured before RNA extraction. It will be interesting to investigate the same phenomenon in the aortic tissue (next chapter) where a similar experimental design has been followed.

3.5 Conclusions

To our knowledge, this is the first report using a combined NGS and patch-clamp electrophysiological approach to (1) understanding the control of potassium channels in inflammageing in joint tissues, (2) to combine such powerful experiments to track changes of the gene expression and ion channels in the inflammatory model of ageing and compare with natural ageing rats. Differences between young and old FLS were found. Also an increased RNA expression of the BK potassium gene KCNMA1 was found, but the constitutive activity of the channel was not increased. The decreased sensitivity to voltage activation and to drugs is likely to be explained by a switch of the RNA expression of β-subunits KCNMB1, 2 and 3. Also, a lot of similarities of enriched GOs between cytokine treated and aged FLS were

detected. In terms of individual gene analysis, Gja1 was decreased with cytokine treatment and increased with the ageing model.

Chapter 4 – Age-related changes in vascular smooth muscle (VSM) of ion channel genes

4.1 Introduction

As an example of a cardiovascular tissue that might change with age, the vascular smooth muscle was chosen. The structure and function have been described in the introduction of chapter 1. In this chapter, two models will be used, the first one is an ageing model in which aged Wistar Kyoto rats will be used and the other model is an inflammageing model where VSMC are isolated from the thoracic aorta, cultured and exposed to cytokines.

With ageing, the balance between pro- and anti-inflammatory cytokines is disturbed. This leads to increased levels of pro-inflammatory cytokine by 2-3 fold compared to normal leading to several age-related diseases (Pedersen, 2006a). Increased levels of cytokines are risk factors for age-related diseases such as cardiovascular diseases (Clarke et al., 2018).

As discussed in Chapter 1, ion channels are important regulators of blood vessels' contractile functions. Several channel types play roles in the vessel's main function. Examples of such channels are K (Kv, KCa, KATP, and inward-rectifier potassium (Kir) channels), Ca signalling, Na (Nav channels), and Cl- (voltage- or Ca2+ dependent) [(Cowled and Fitridge, 2011, Fan et al., 2019, Orlov et al., 2017, Kuriyama et al., 1998). There have been several reports of blood vessel dysfunction associated with ageing [(Laina et al., 2018, Ungvari et al., 2018, Cheng et al., 2019), many of these surround the phenomenon of atherosclerosis, but even allowing for this there are reported cases involving ionic imbalance and VSMC membrane potential changes [(Cheng et al., 2019).

Hypertension, one of the most common diseases of ageing is thought to be genetically determined (Stewart et al., 2017, Brozovich et al., 2016) although the exact mechanisms are often not known. The complex mechanisms of vasorelaxation and the importance of this process to the maintenance of blood pressure mean that there is a constant need to discover new therapeutic targets in VSM.

To investigate this, two complementary models were used. The first model was an "inflammageing" model that was developed by exposing VSMC cells to 10ng/ml IL-1β+TNFα for 72hrs. The second model was a real ageing model where old rats were grown and then used for the study.

Aims

The aims of this chapter were:

- To investigate the change of vascular smooth muscle ion channels with cytokine treatment as a model of inflammageing or ageing itself.
- To investigate whether any other key regulatory genes had a differential expression.
- Finally, are there any genes that were commonly altered in both cytokine treatment and age.

4.2 Materials and methods

Aorta dissection

Aorta tissues from young and old Wistar Kyoto rats were dissected, cleaned with forceps and placed in RNALater, stored at -80^{O}C as described in chapter 2 – materials and methods section RNA extraction, Aorta. These aorta tissues were defrosted later on and RNA was extracted for NGS as described in chapter 2 materials and methods.

Tissue culture

VSMC isolation and culture have already been described in chapter 2 materials and methods. But briefly thoracic aorta was dissected from rat, cleaned and snipped into branches on ice-cold dissection solution, these branches were transferred into low Ca^{++} solution and warmed to 35-37^{O}C for 10 min. After that, branches were digested for 25-30 min at 37^{O}C followed by 3x wash with pre-warmed low-Ca++ solution. Cells were then dispersed by gentle trituration through a sterile plastic Pasteur pipette. Then, connective tissues were discarded and cells were cultured in fresh pre-warmed high glucose 1x DMEM complete media. Once cells grew and became 80-90% confluent, they were passaged and experiments took place after passage 3.

RNA extraction

RNA from aorta tissues and VSMC were extracted as described in chapter 2 – materials and methods. RNA quantity and purity were measured by NanoDrop 2000 Spectrophotometer before submitting samples to the CGR centre for sequencing. The quantities of RNA from Aorta (appendix 5) and VSMC (appendix 8) were measured.

RNA-Sequencing (Next-Generation Sequencing (NGS))

After RNA was extracted as described above, sequencing of large (>200 nucleotides) messenger RNA (mRNA) enriched with polyA-tail was outsourced with a >30M sequencing depth and 50-150bp read length and was run as paired-end. The QC summary of RNA from

FLS samples are shown in appendix 6 and appendix 9 from aorta and VSMC, respectively. Raw data was delivered as FASTQ files containing sequences and quality scores. Then, the quality of reads was checked out by FastQC software that provides Phred quality scores as shown in appendix 7 and appendix 10 for aorta and VSMC, respectively. After that, reads are aligned/mapped, assembled and quantified, and differentially expressed genes are detected as described in chapter 2-materials and methods.

Electrophysiology

Electrophysiology methods with VSMC were similar to those of FLS and described in full in materials and methods of FLS chapter 3, section "Electrophysiology" but briefly, cells were sealed with fire-polished boro-silicate glass pipette filled with intracellular solution. Then, cells that are in the extracellular solution were challenged with a broad range of potentials ranging from -120 to +120mV. The current is recorded in the whole-cell configuration. After that, data were analyzed with different softwares including but not limited to Excel, Sigma Plot, RStudio, Python, and MATLAB. All recordings took place at RT. Solutions described in Chapter 2.

For the ANO1 inhibitor drug (CaCCinh-AO1), the extracellular solution that filled the bath was replaced by an extracellular solution containing the drug at a flow rate of 3ml/min. Then, cells were challenged with the same voltage step protocol (-120 to +120 mV at 10mV increment) and whole-cell currents were recorded within the first 5-10 min of solution replacement.

4.3 Results

Changes in Vascular smooth muscle transcriptome (aorta) with age

Aorta Differentially expressed Genes

The work in this part started with next-generation sequencing of the aorta from young and old rats (ages), aorta dissected, prepared and RNA extraction took place as described in the methods. NGS [FastQC, HiSAT2, and StringTie tools) detected approximately 32695 genes per group. Differential expression testing (CuffDif tools) of all genes identified 441 genes with a p-value for differential <0.05 and 29 genes with Benjamini Hochberg corrected gene expression FDR <0.05. Table 17 shows the top 29 genes with p-value <0.05 and FDR<0.05.

Table 17: Top 29 differentially expressed aorta genes with p-value<0.05 and FDR<0.05.

No.	Gene stable ID	Gene name	Gene description	p_value	q_value
1	ENSRNOG00000002459	Fbxo40	F-box protein 40	5.00E-05	0.02
2	ENSRNOG00000002555	Serpinb7	serpin family B member 7	5.00E-05	0.02
3	ENSRNOG00000002911	Alb	albumin	5.00E-05	0.02
4	ENSRNOG00000003245	Cacng1	calcium voltage-gated channel auxiliary subunit gamma 1	5.00E-05	0.02
5	ENSRNOG00000003435	Mcf2	MCF.2 cell line derived transforming sequence	5.00E-05	0.02
6	ENSRNOG00000004768	Myf5	myogenic factor 5	5.00E-05	0.02
7	ENSRNOG00000006146	Trim54	tripartite motif-containing 54	5.00E-05	0.02
8	ENSRNOG00000006776	Smyd1	SET and MYND domain containing 1	5.00E-05	0.02
9	ENSRNOG00000007059	Atp1b4	ATPase Na+/K+ transporting family member beta 4	5.00E-05	0.02
10	ENSRNOG00000007229	Nr0b2	nuclear receptor subfamily 0, group B, member 2	5.00E-05	0.02
11	ENSRNOG00000008050	Stac3	SH3 and cysteine rich domain 3	5.00E-05	0.02
12	ENSRNOG00000008176	Nppa	natriuretic peptide A	5.00E-05	0.02
13	ENSRNOG00000008210	Ky	kyphoscoliosis peptidase	5.00E-05	0.02
14	ENSRNOG00000008310	Mpo	myeloperoxidase	5.00E-05	0.02
15	ENSRNOG00000010478	LOC500712	Ab1-233	5.00E-05	0.02
16	ENSRNOG00000013552	Scd	stearoyl-CoA desaturase	5.00E-05	0.02
17	ENSRNOG00000015155	Tnnc2	troponin C2, fast skeletal type	5.00E-05	0.02
18	ENSRNOG00000015279	Vtcn1	V-set domain containing T cell activation inhibitor 1	5.00E-05	0.02
19	ENSRNOG00000019390	Klhl40	kelch-like family member 40	5.00E-05	0.02
20	ENSRNOG00000019404	Hhatl	hedgehog acyltransferase-like	5.00E-05	0.02
21	ENSRNOG00000020332	Tnnt3	troponin T3, fast skeletal type	5.00E-05	0.02
22	ENSRNOG00000021789	RGD1565323	similar to OTTMUSP00000000621	5.00E-05	0.02
23	ENSRNOG00000031331	Fpr3	formyl peptide receptor 3	5.00E-05	0.02
24	ENSRNOG00000032461	Bin2a	beta-galactosidase-like protein	5.00E-05	0.02
25	ENSRNOG00000033529	Amy1a	amylase, alpha 1A	5.00E-05	0.02
26	ENSRNOG00000037645	Tceal7	transcription elongation factor A like 7	5.00E-05	0.02
27	ENSRNOG00000042445	AC130970.1		5.00E-05	0.02
28	ENSRNOG00000049695	Myh2	myosin heavy chain 2	5.00E-05	0.02
29	ENSRNOG00000049942	RGD1564899	similar to chromosome 10 open reading frame 71	5.00E-05	0.02

These data were obtained by CuffDiff package.

Functional annotating clustering for those genes on David's Bioinformatics Resources 6.8 returned GOs that were mainly related to the muscle differentiation or function such as "skeletal muscle contraction" (GO:0003009, p=8.28x10-4), "regulation of muscle

contraction" (GO:0006937, p=0.03), "positive regulation of myoblast differentiation" (GO:0045663, 0.04), "skeletal muscle fibre development" (GO:0048741, p=0.04), "troponin complex" (GO:0005861, p=0.01), and "extracellular space" (GO:0005615, p=0.03). No KEGG pathways were significantly enriched but the top to pathways was "Carbohydrate digestion and absorption" with a p-value of $5.2x10^{-2}$, and "cardiac muscle contraction" with a p-value of $9.6x10^{-2}$.

Aorta Differentially expressed ion channel Genes

The primary aim was the discovery of differentially expressed ion channels. Therefore, gene lists were filtered for ion channels grepping the word "channel" in the official Ensemble gene name excluding "intracellular", "tetramerization domain", and "interacting protein". This returned 248 channel genes. Of these 7 were considered differentially expressed (pval<0.05) (Table 18).

Table 18: Differentially expressed channel genes in the aorta.

No.	Ensemble IDs	SYMBOL	p-val	FDR
1	ENSRNOG00000004518	Cacnb1	0.00085	0.238354
2	ENSRNOG00000009797	Aqp3	0.0141	0.999086
3	ENSRNOG00000019750	Kcna1	0.0201	0.999086
4	ENSRNOG00000009686	Aqp7	0.0203	0.999086
5	ENSRNOG00000000805	Gja1	0.02855	0.999086
6	ENSRNOG00000013463	Kcnj8	0.0326	0.999086
7	ENSRNOG00000021128	Kcnj11	0.04445	0.999086

Data obtained by CuffDiff package.

Aorta Multivariate analysis of Genes

To investigate whether there were changes in clusters of genes rather than individual genes, DA-PCA was used. Little population difference was detectable until 4 PCA were used (

Figure 22-A and -B), and so the rest of this section models expression changes with 4 principle components. Given That there are only two groups (young and old), there is only one discriminant function (LD1).

DA-PCA (4 PCs) discriminated the young and old gene populations well (Figure 23-A). The heatmap (Figure 23-B) shows that the 3 control and 2 groups are successfully separated. The mean posterior p-value for the null hypothesis (the groups are undesignable) was statistically significant.

Next, loading values were drawn-out for the discriminant function, which quantifies the relative contribution of all genes to the differences in young and old gene populations. Filteration of all genes took place to return just the top 50 genes and the top 15 of them are displayed in (Figure 23-C). These data show that of all the genes detected in our aorta experiments; the genes contributing most powerfully to the multivariate population difference are shown in Table 19.

Table 19: The most contributing genes to the differences between young and old in aorta samples.

Gene stable ID	Gene name	Gene description
ENSRNOG00000019778	Cavin1	caveolae associated protein 1
ENSRNOG00000002419	Plp1	proteolipid protein 1
ENSRNOG00000003338	Pmp22	peripheral myelin protein 22
ENSRNOG00000029886	Hba-a2	hemoglobin alpha, adult chain 2
ENSRNOG00000012840	Sparc	secreted protein acidic and cysteine-rich
ENSRNOG00000003171	Mpz	myelin protein zero
ENSRNOG00000009439	Eef1a1	eukaryotic translation elongation factor 1 alpha 1
ENSRNOG00000014070	Krt13	keratin 13
ENSRNOG00000003897	Col1a1	collagen type I alpha 1 chain
ENSRNOG00000016945	Pla2g2a	phospholipase A2 group IIA
ENSRNOG00000016516	Mbp	myelin basic protein
ENSRNOG00000006604	Thy1	Thy-1 cell surface antigen
ENSRNOG00000018795	Rpl18a	ribosomal protein L18A
ENSRNOG00000019556	Cd9	CD9 molecule
ENSRNOG00000057569	Ahnak	AHNAK nucleoprotein

Aorta Multivariate analysis of Ion channels

To investigate the population-wide differences in ion channels, the DA-PCA with ion channels was repeated filtering gene lists for the word “channel” in the official gene description. Primarily, the separation between the young and old (Figure 24-A, and B) was not good until 5 principal components were used that showed good discrimination (Figure

25A) with only one discriminant function. Just as with the gene-wide analysis heatmap (Figure 25-B) shows successful separation based on just ion channel expression.

The ion channel loadings of LD1 are shown in Figure 25-C (filtered for the top 50 ion channels) and the top 15 ion channel genes are shown in this figure. These data show that of all the 261 ion channel genes detected in our aorta experiments the genes contributing most to the multivariate ion channel population difference are shown in Table 20.

Table 20: Top 15 channel genes contributing to the differences between young and old Aorta.

Gene ID	Gene name	Gene description
ENSRNOG00000029342	Scn7a	sodium voltage-gated channel alpha subunit 7
ENSRNOG00000006375	Vdac1	voltage-dependent anion channel 1
ENSRNOG00000006639	Scn9a	sodium voltage-gated channel alpha subunit 9
ENSRNOG00000000728	Clic2	chloride intracellular channel 2
ENSRNOG00000019750	Kcna1	potassium voltage-gated channel subfamily A member 1
ENSRNOG00000056697	Kcnab1	potassium voltage-gated channel subfamily A member regulatory beta subunit 1
ENSRNOG00000013463	Kcnj8	potassium voltage-gated channel subfamily J member 8
ENSRNOG00000019277	Vdac3	voltage-dependent anion channel 3
ENSRNOG00000057221	Scn3b	sodium voltage-gated channel beta subunit 3
ENSRNOG00000013505	Vdac2	voltage-dependent anion channel 2
ENSRNOG00000033531	Cacna2d1	calcium voltage-gated channel auxiliary subunit alpha2delta 1
ENSRNOG00000046231	Cacna1s	calcium voltage-gated channel subunit alpha1 S
ENSRNOG00000018285	Kcna2	potassium voltage-gated channel subfamily A member 2
ENSRNOG00000015184	Clic3	chloride intracellular channel 3
ENSRNOG00000012788	Clns1a	chloride nucleotide-sensitive channel 1A

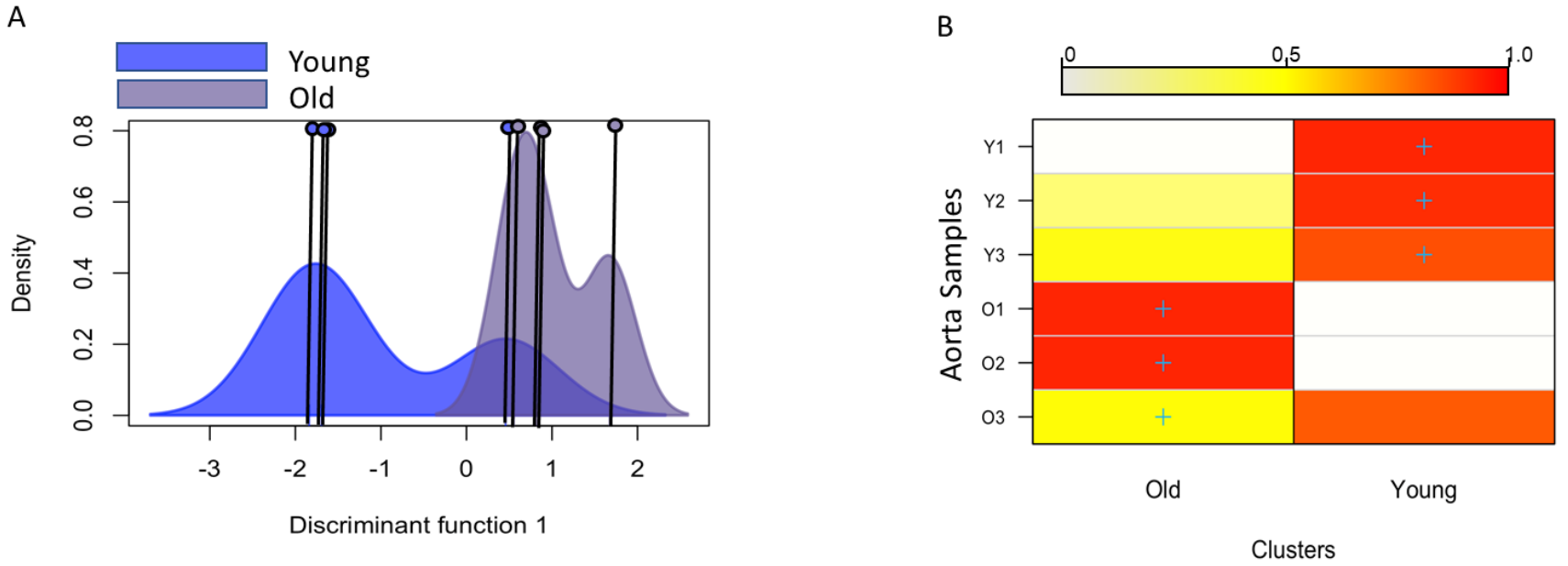

Figure 22: Discriminant Analyses of ageing Effects on Aorta (all genes) - poor discrimination.
A. *Shows the kernel density plots of the discriminant component coordinates for the young and old aorta groups; co-ordinates on the x-axis and density on the y-axis; Individual co-ordinate centre points are illustrated by the vertical line and circle. There is poor discrimination between young and old aorta samples with less than 4 PCs.* ***B.*** *A graphical confusion matrix showing the actual group membership (x-axis) and predicted cluster membership (on the y-axis). Groups were not correctly clustered with probabilities ranging from 0.02 to 0.98.*

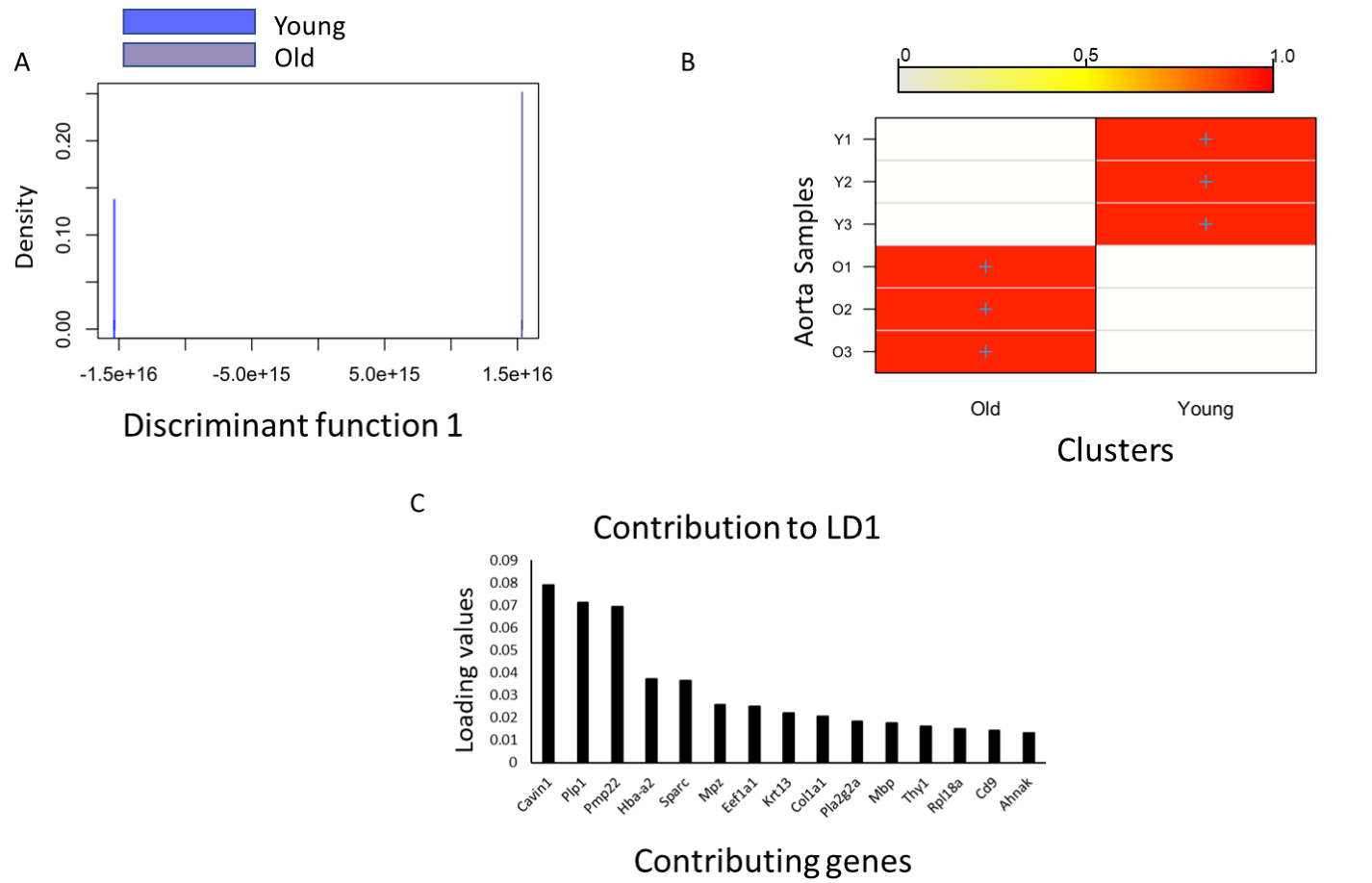

Figure 23: Discriminant Analyses of ageing Effects on Aorta (all genes) - good discrimination.
A. *Shows the kernel density plots of the discriminant component coordinates for the young and old aorta groups; co-ordinates on the x-axis and density on the y-axis; Individual co-ordinate centre points are illustrated by the vertical line and circle. There is clear discrimination between young and old aorta samples with 4 PCs and a probability of belonging of 1.* ***B.*** *A graphical confusion matrix showing the actual group membership (y-axis) and predicted cluster membership (on the y-axis). Groups were correctly clustered with probability 1.* ***C.*** *The contributors to the linear discriminator function in aorta samples (young and old); Cavin1; caveolae associated protein 1, Plp1; proteolipid protein 1, Pmp22; peripheral myelin protein 22, Hba-a2; haemoglobin alpha, adult chain 2, Sparc; secreted protein acidic and cysteine-rich, Mpz; myelin protein zero, Eef1a1; eukaryotic translation elongation factor 1 alpha 1, Krt13; keratin 13, Col1a1; collagen type I alpha 1 chain, Pla2g2a; phospholipase A2 group IIA, Mbp; myelin basic protein, Thy1; Thy-1 cell surface antigen, Rpl18a; ribosomal protein L18A, Cd9; CD9 molecule, and Ahnak; AHNAK nucleoprotein. The x-axis shows contributing genes while the y-axis shows their loading values.*

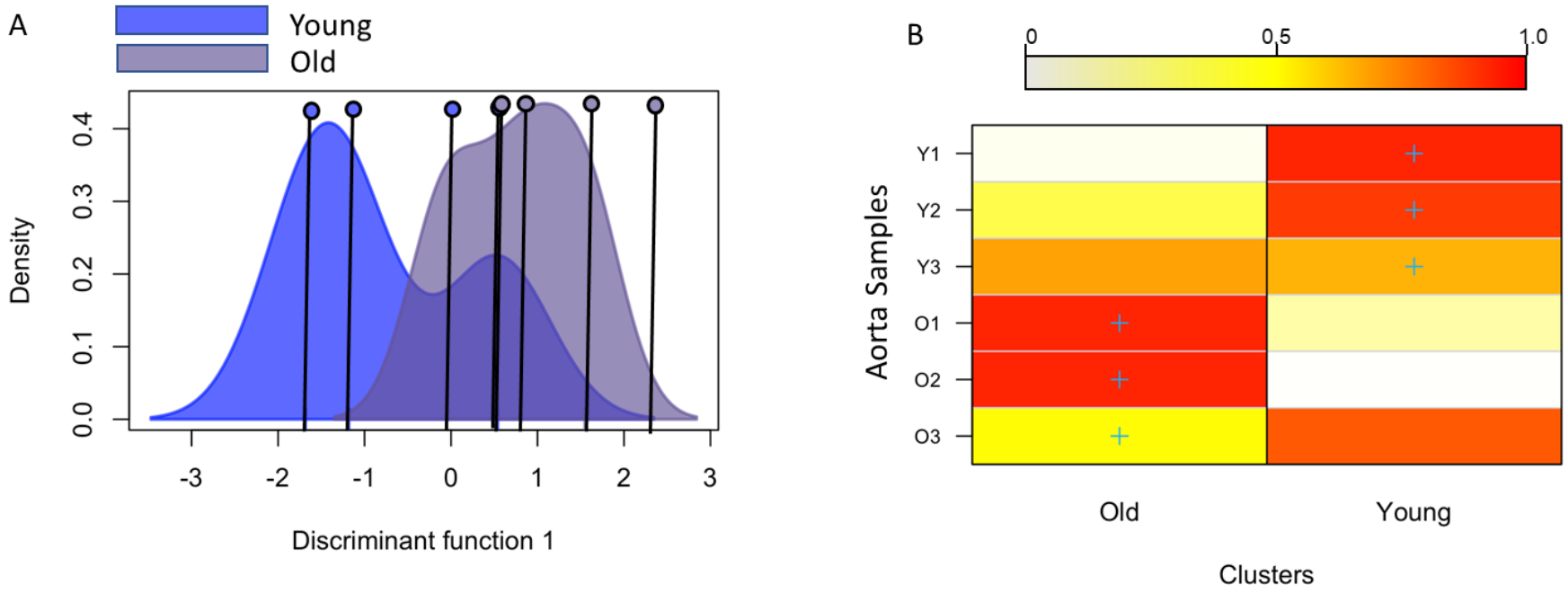

Figure 24:Discriminant Analyses of ageing Effects on Aorta (channel genes) - poor discrimination.
A. Shows the kernel density plots of the discriminant component coordinates for the *young and old* channel groups; co-ordinates on the x-axis and density on the y-axis; Individual co-ordinate centre points are illustrated by the vertical line and circle. There is poor discrimination between young and old aorta samples *with less than 5 PCs*. **B.** A graphical confusion matrix showing the actual group membership (y-axis) and predicted cluster membership (on the y-axis). Groups were not correctly clustered with 0.02 to 0.97 probability.

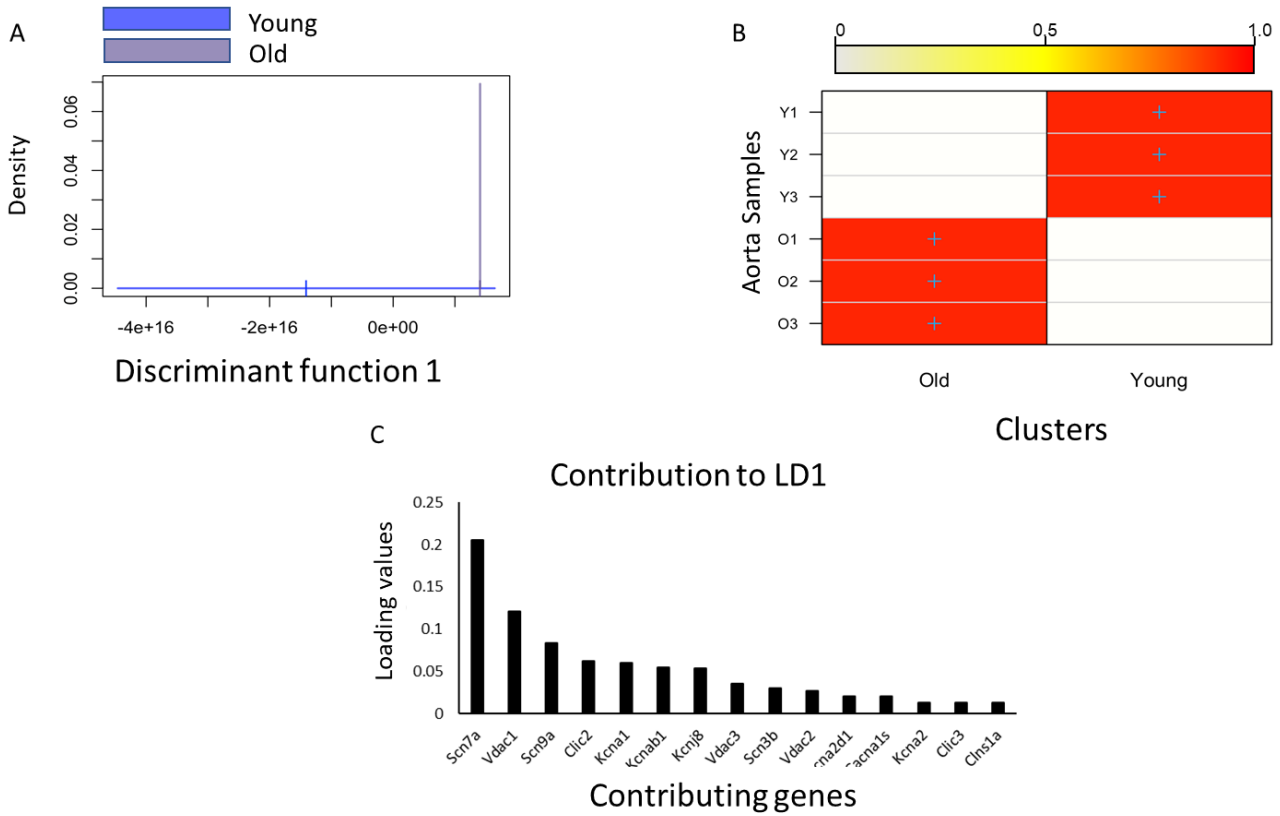

Figure 25:Discriminant Analyses of ageing Effects on Aorta (channel genes) - good discrimination.
A. Shows the kernel density plots of the discriminant component coordinates for the *young and old* aorta channel groups; co-ordinates on the x-axis and density on the y-axis; Individual co-ordinate centre points are illustrated by the vertical line and circle. There is clear discrimination between young and old aorta samples *with 5 PCs*. **B.** A graphical confusion matrix showing the actual group membership (y-axis) and predicted cluster membership (on the y-axis). Groups were correctly clustered with *a* probability of 1. **C.** Ion channel contributors to the linear discriminator function; *Scn7a; sodium voltage-gated channel alpha subunit 7, Vdac1; voltage-dependent anion channel 1, Scn9a; sodium voltage-gated channel alpha subunit 9, Clic2; chloride intracellular channel 2, Kcna1; potassium voltage-gated channel subfamily A member 1, Kcnab1; potassium voltage-gated channel subfamily A member regulatory beta subunit 1, Kcnj8; potassium voltage-gated channel subfamily J member 8, Vdac3; voltage-dependent anion channel 3, Scn3b; sodium voltage-gated channel beta subunit 3, Vdac2; voltage-dependent anion channel 2, Cacna2d1; calcium voltage-gated channel auxiliary subunit alpha2delta 1, Cacna1s; calcium voltage-gated channel subunit alpha1 S, Kcna2; potassium voltage-gated channel subfamily A member 2, Clic3; chloride intracellular channel 3, and Clns1a; chloride nucleotide-sensitive channel 1A.*

Transcriptomic changes in cytokine treated vascular smooth muscle cell (VSMC)

The ageing model is true ageing because rats were at the age of 24+ months (the equivalent of 60+ years of human life) at the time of experiments, but there are a number of limitations with that model (see discussion), so similar analysis to the above with VSMC in culture and cytokine treatment was performed. One strength of this culture model is the ability to do electrophysiology.

VSMC Differentially expressed Genes

This section of work was started by growing VSMC in vitro to be control and treated with 10ng/ml TNFα+IL-1β cytokines for 72hrs. Then, RNA was extracted as described in the method (section RNA extraction) and did next-generation sequencing of these VSMC. NGS detected approximately 22038 genes per group. Differential expression testing of all genes identified 115 genes with a p-value for differential <0.05 and 115 genes with Benjamini Hochberg corrected gene expression FDR <0.05 (Table 21).

Table 21: Differentially expressed genes in VSMC tissue.

Rank	Ensemble Gene ID	Log_2	p-value	q-value	Symbol
1	ENSRNOG00000000805	-1.37492	0.00005	0.0016	Gja1
2	ENSRNOG00000001229	-1.31925	0.00005	0.0016	Col18a1
3	ENSRNOG00000001627	2.5513	0.00005	0.0016	Abi3bp
4	ENSRNOG00000001633	2.54698	0.00005	0.0016	Tfg
5	ENSRNOG00000002525	-3.61343	0.00005	0.0016	Ptgs2
6	ENSRNOG00000003809	-1.7908	0.00005	0.0016	Sat1
7	ENSRNOG00000004210	-1.63214	0.00005	0.0016	Osr1
8	ENSRNOG00000004532	1.28379	0.00005	0.0016	Dipk1b
9	ENSRNOG00000006302	-1.47753	0.00005	0.0016	Gclc
10	ENSRNOG00000006623	1.83443	0.00005	0.0016	Cd302
11	ENSRNOG00000007726	-2.14197	0.00005	0.0016	Mcam
12	ENSRNOG00000008012	2.80961	0.00005	0.0016	Abcb1b
13	ENSRNOG00000009094	2.03807	0.00005	0.0016	Nudt4
14	ENSRNOG00000009779	-2.74207	0.00005	0.0016	Krt8
15	ENSRNOG00000011644	2.4425	0.00005	0.0016	Slc1a7
16	ENSRNOG00000011718	2.50895	0.00005	0.0016	C1rl
17	ENSRNOG00000011796	1.97599	0.00005	0.0016	C1r
18	ENSRNOG00000011971	3.37302	0.00005	0.0016	C1s
19	ENSRNOG00000012868	-1.50957	0.00005	0.0016	Uaca

20	ENSRNOG00000013442	1.49046	0.00005	0.0016	Ciz1
21	ENSRNOG00000013589	3.05591	0.00005	0.0016	Cxcl12
22	ENSRNOG00000014333	2.56278	0.00005	0.0016	Vcam1
23	ENSRNOG00000014532	4.36226	0.00005	0.0016	Lbp
24	ENSRNOG00000016156	-2.49298	0.00005	0.0016	Nptxr
25	ENSRNOG00000017420	-2.04281	0.00005	0.0016	Nudt6
26	ENSRNOG00000019048	3.8891	0.00005	0.0016	Sod2
27	ENSRNOG00000019184	2.28964	0.00005	0.0016	Npr3
28	ENSRNOG00000019422	-3.1011	0.00005	0.0016	Egr1
29	ENSRNOG00000020679	1.47094	0.00005	0.0016	Icam1
30	ENSRNOG00000021802	1.57144	0.00005	0.0016	Isg15
31	ENSRNOG00000026053	-1.35774	0.00005	0.0016	Grem1
32	ENSRNOG00000026951	-1.92488	0.00005	0.0016	Susd5
33	ENSRNOG00000027124	1.96378	0.00005	0.0016	Tdg
34	ENSRNOG00000028892	1.5264	0.00005	0.0016	Prr36
35	ENSRNOG00000031406	3.42862	0.00005	0.0016	Hps3
36	ENSRNOG00000032018	1.63193	0.00005	0.0016	Tmem200b
37	ENSRNOG00000032297	-2.14566	0.00005	0.0016	Msmo1
38	ENSRNOG00000039668	-1.25645	0.00005	0.0016	Col8a1
39	ENSRNOG00000049402	1.65937	0.00005	0.0016	Nbl1
40	ENSRNOG00000049560	1.40386	0.00005	0.0016	Glul
41	ENSRNOG00000049900	-2.07275	0.00005	0.0016	Irf2bp2
42	ENSRNOG00000058068	2.54099	0.00005	0.0016	Obscn
43	ENSRNOG00000001979	-2.01077	0.0001	0.002904	Rcan1
44	ENSRNOG00000016870	1.22926	0.0001	0.002904	Pcif1
45	ENSRNOG00000030118	-1.32044	0.0001	0.002904	Msn
46	ENSRNOG00000033192	1.96112	0.0001	0.002904	Osmr
47	ENSRNOG00000059013	1.37127	0.0001	0.002904	<NA>
48	ENSRNOG00000008529	2.15631	0.00015	0.00392	Foxs1
49	ENSRNOG00000016326	1.73196	0.00015	0.00392	Cx3cl1
50	ENSRNOG00000017765	1.26319	0.00015	0.00392	Net1
51	ENSRNOG00000018748	1.70836	0.00015	0.00392	Slc16a11
52	ENSRNOG00000056819	1.24722	0.00015	0.00392	Susd1
53	ENSRNOG00000000748	-2.35907	0.0002	0.0049	<NA>
54	ENSRNOG00000002403	-1.25204	0.0002	0.0049	Fam129a
55	ENSRNOG00000005924	-1.29616	0.0002	0.0049	Dstnl1
56	ENSRNOG00000013963	1.33671	0.0002	0.0049	Il6st
57	ENSRNOG00000010103	1.08204	0.00025	0.005939	Eif4b
58	ENSRNOG00000014453	-1.13249	0.00025	0.005939	Anxa5
59	ENSRNOG00000002615	1.26214	0.0003	0.006918	Pmm2
60	ENSRNOG00000010797	-2.83425	0.0003	0.006918	Esm1

61	ENSRNOG00000000488	-2.67647	0.00035	0.00784	Hmga1
62	ENSRNOG00000014320	-1.28019	0.00035	0.00784	Inhba
63	ENSRNOG00000011648	-1.1141	0.00045	0.0098	Aqp1
64	ENSRNOG00000027736	-1.29691	0.00045	0.0098	Cnn1
65	ENSRNOG00000033862	2.33425	0.0005	0.010595	Olr836
66	ENSRNOG00000048706	-1.26356	0.0005	0.010595	Nox1
67	ENSRNOG00000002052	1.39993	0.00055	0.011056	Ccdc80
68	ENSRNOG00000007329	-1.22224	0.00055	0.011056	Frmd6
69	ENSRNOG00000010017	1.26807	0.00055	0.011056	Wee1
70	ENSRNOG00000014230	-1.083	0.00055	0.011056	Map1a
71	ENSRNOG00000010170	-1.95337	0.0007	0.01372	Tubb4b
72	ENSRNOG00000060130	1.1218	0.0007	0.01372	Ypel4
73	ENSRNOG00000007799	1.3105	0.00075	0.014342	Fam151a
74	ENSRNOG00000012956	4.01254	0.00075	0.014342	Tgm2
75	ENSRNOG00000005678	-1.00306	0.0008	0.014758	Lamb1
76	ENSRNOG00000015239	1.19588	0.0008	0.014758	Ginm1
77	ENSRNOG00000016695	1.02315	0.0008	0.014758	Mmp2
78	ENSRNOG00000020865	-1.2131	0.00085	0.015498	Ano1
79	ENSRNOG00000021752	-1.19469	0.00095	0.016927	Foxq1
80	ENSRNOG00000015514	-1.14488	0.00095	0.016927	Bcat1
81	ENSRNOG00000014964	2.97864	0.001	0.017422	Hp
82	ENSRNOG00000019162	1.05849	0.001	0.017422	Emc9
83	ENSRNOG00000004912	-1.14024	0.00105	0.018092	Itgav
84	ENSRNOG00000011913	2.4218	0.0012	0.020452	Cp
85	ENSRNOG00000014128	1.11964	0.00125	0.020851	Ecsit
86	ENSRNOG00000020599	1.27651	0.00125	0.020851	Tssk6
87	ENSRNOG00000023226	-1.46104	0.00145	0.023933	S100a10
88	ENSRNOG00000017166	1.1573	0.0015	0.0245	Mycbp
89	ENSRNOG00000005533	1.0638	0.0016	0.0256	LOC686013
90	ENSRNOG00000009274	1.01158	0.0016	0.0256	Fut11
91	ENSRNOG00000016243	-1.15987	0.0017	0.026925	Casq2
92	ENSRNOG00000002146	-0.93539	0.0019	0.029208	Pkd2
93	ENSRNOG00000017852	-1.09098	0.0019	0.029208	Nars
94	ENSRNOG00000033271	1.53996	0.0019	0.029208	<NA>
95	ENSRNOG00000018237	-1.02427	0.002	0.030447	Gstp1
96	ENSRNOG00000012270	1.07023	0.00205	0.030613	Med26
97	ENSRNOG00000033110	1.03323	0.00205	0.030613	Svep1
98	ENSRNOG00000052506	1.18051	0.0022	0.032543	Ak3
99	ENSRNOG00000000466	1.80548	0.00235	0.034119	Hsd17b8
100	ENSRNOG00000052498	0.928334	0.00235	0.034119	Grb14
101	ENSRNOG00000024751	0.987036	0.00245	0.034924	H2afy2

102	ENSRNOG00000015904	-1.73194	0.00255	0.036022	Wfdc1
103	ENSRNOG00000004577	-1.32427	0.0027	0.0378	Fez2
104	ENSRNOG00000042446	1.01227	0.00275	0.038159	Ankrd63
105	ENSRNOG00000003546	-3.02722	0.0028	0.038512	Tnfrsf12a
106	ENSRNOG00000011413	1.06696	0.00295	0.040223	Scp2
107	ENSRNOG00000020716	-0.99421	0.00305	0.040875	Axl
108	ENSRNOG00000045649	1.32266	0.00305	0.040875	Arrdc3
109	ENSRNOG00000008816	0.95582	0.0032	0.042522	Gpnmb
110	ENSRNOG00000002835	0.949708	0.00335	0.044141	Luc7l3
111	ENSRNOG00000014519	1.07198	0.0034	0.044427	Slc35g3
112	ENSRNOG00000019892	-0.9202	0.00365	0.047299	Lrrfip1
113	ENSRNOG00000016885	-1.24797	0.00375	0.048197	Klf6
114	ENSRNOG00000013286	-1.10906	0.0038	0.048442	Pdcl3
115	ENSRNOG00000030170	1.14501	0.0039	0.049316	Krt10

Data obtained by CuffDiff package.

Then, functional annotation clustering and enrichment analysis using David's Bioinformatics Resources 6.8 were done. GOs enriched were "extracellular exosome" (GO:0070062, p=4.83x10-10), "angiogenesis" (GO:0001525, p=7.24x10-8), "extracellular space" (GO:0005615, p=1.18x10-6), "aging" (GO:0007568, p=0.002), and "signal transduction" (GO:0007165, p=0.02).

KEGG pathways returned several statistically significant pathways with p-values of less than 0.05. these pathways are "NF-kappa B signaling pathway" (rno04064, p=0.0022), "TNF signaling pathway" (rno04668, p=0.03) and "Cytokine-cytokine receptor interaction" (rno04060, p= 0.034).

VSMC Differentially expressed ion channel Genes

Filtering gene lists for ion channels grepping the word "channel" in the official Ensemble gene description excluding "intracellular", "tetramerization domain", and "interacting protein". Only 3 ion channel genes were considered differentially expressed (pval<0.05) (Table 22).

Table 22: Differentially expressed ion channel genes in VSMC.

No.	Ensemble Gene ID	Log_2	p-value	q-value	Symbol	Description
1	ENSRNOG00000000805	-1.37492	0.00005	0.0016	Gja1	Gap junction
2	**ENSRNOG00000020865**	**-1.2131**	**0.00085**	**0.015498**	**Ano1**	**Calcium activated chloride channel**
3	ENSRNOG00000002146	-0.93539	0.0019	0.029208	Pkd2	Polycystin 2

This table was obtained by CuffDiff package.

VSMC Multivariate analysis of Genes

To investigate whether there were changes in clusters of genes rather than individual genes, DA-PCA was used. Little population difference was detectable until 4 PCs were used, and so the rest of this section models expression changes with 4 principle components. Since there are only two groups (control and treated) there is only one discriminant function (LD1).

The kernel density plot of DA-PCA shows that with (4 PCs) there is good discrimination of the control and treated gene populations (Figure 26-A). The heatmap (Figure 26-B) shows how well the category of sample is predicted for the two groups (control or cytokine treated). The predicted probability of belonging was successful with greater than 0.9.

Next, loading values for the discriminant function, which quantifies the relative contribution of all genes to the differences in control and treated gene populations, were drawn-out. Then, out of all genes, only the top 50 genes were filtered out and of those the top 15 are displayed in (Figure 26-C). These data show that of all the genes detected in our VSMC experiments the genes contributing most to the multivariate population difference are shown in Table 23.

Table 23: The most contributing genes to the differences between control and cytokine treated VSMC samples.

Ensemble IDs	Gene name	Gene description
ENSRNOG00000047907	LOC100912585	mitogen-activated protein kinase 7-like
ENSRNOG00000037894	<NA>	Unknown gene
ENSRNOG00000014288	Fn1	fibronectin 1
ENSRNOG00000012660	Postn	periostin
ENSRNOG00000020346	Best1	bestrophin 1
ENSRNOG00000001469	Eln	elastin
ENSRNOG00000013987	Sbno2	strawberry notch homolog 2
ENSRNOG00000046836	<NA>	Unknown gene
ENSRNOG00000012579	Tlcd1	TLC domain containing 1
ENSRNOG00000024779	Polr2b	RNA polymerase II subunit B
ENSRNOG00000000506	Tead3	TEA domain transcription factor 3
ENSRNOG00000046313	Basp1	brain abundant, membrane attached signal protein 1
ENSRNOG00000058068	Obscn	obscurin, cytoskeletal calmodulin and titin-interacting RhoGEF
ENSRNOG00000012840	Sparc	secreted protein acidic and cysteine-rich
ENSRNOG00000016488	Pltp	phospholipid transfer protein

VSMC Multivariate analysis of Ion channels

To investigate the population-wide differences in ion channels, the DA-PCA was repeated but with ion channels only. Again, 3 principal components were needed to see good discrimination and there is only one discriminant function. DA-PCA (3 PCs) discriminated the control and treated ion channel populations well (Figure 27-A). Just as with the gene-wide analysis, heatmap (Figure 27-B) shows a successful separation of the samples based on just ion channel expression.

The ion channel loadings of LD1 were filtered for the top 50 ion channels and the top 15 ion channel genes are shown in (Figure 27-C). These data show that of all the ion channel genes detected in our VSMC experiments the genes contributing most to the multivariate ion channel population difference are shown in Table 24.

Table 24: The most contributing ion channel genes to the differences between control and cytokine treated VSMC samples.

Ensemble IDs	Gene name	Gene description
ENSRNOG00000002146	Pkd2	polycystin 2, transient receptor potential cation channel
ENSRNOG00000025489	Pkd2l2	polycystin 2 like 2, transient receptor potential cation channel
ENSRNOG00000014714	Trpv6	transient receptor potential cation channel, subfamily V, member 6
ENSRNOG00000038784	Piezo2	piezo-type mechanosensitive ion channel component 2
ENSRNOG00000010771	Pkd1	polycystin 1, transient receptor potential channel interacting
ENSRNOG00000018109	Clic4	chloride intracellular channel 4
ENSRNOG00000060528	Cacna1g	calcium voltage-gated channel subunit alpha1 G
ENSRNOG00000001270	Hvcn1	hydrogen voltage-gated channel 1
ENSRNOG00000059765	Asic1	acid-sensing ion channel subunit 1
ENSRNOG00000013505	Vdac2	voltage-dependent anion channel 2
ENSRNOG00000015184	Clic3	chloride intracellular channel 3
ENSRNOG00000005985	Kcnma1	potassium calcium-activated channel subfamily M alpha 1
ENSRNOG00000019277	Vdac3	voltage-dependent anion channel 3
ENSRNOG00000033531	Cacna2d1	calcium voltage-gated channel auxiliary subunit alpha2delta 1
ENSRNOG00000007645	Kcnj9	potassium voltage-gated channel subfamily J member 9

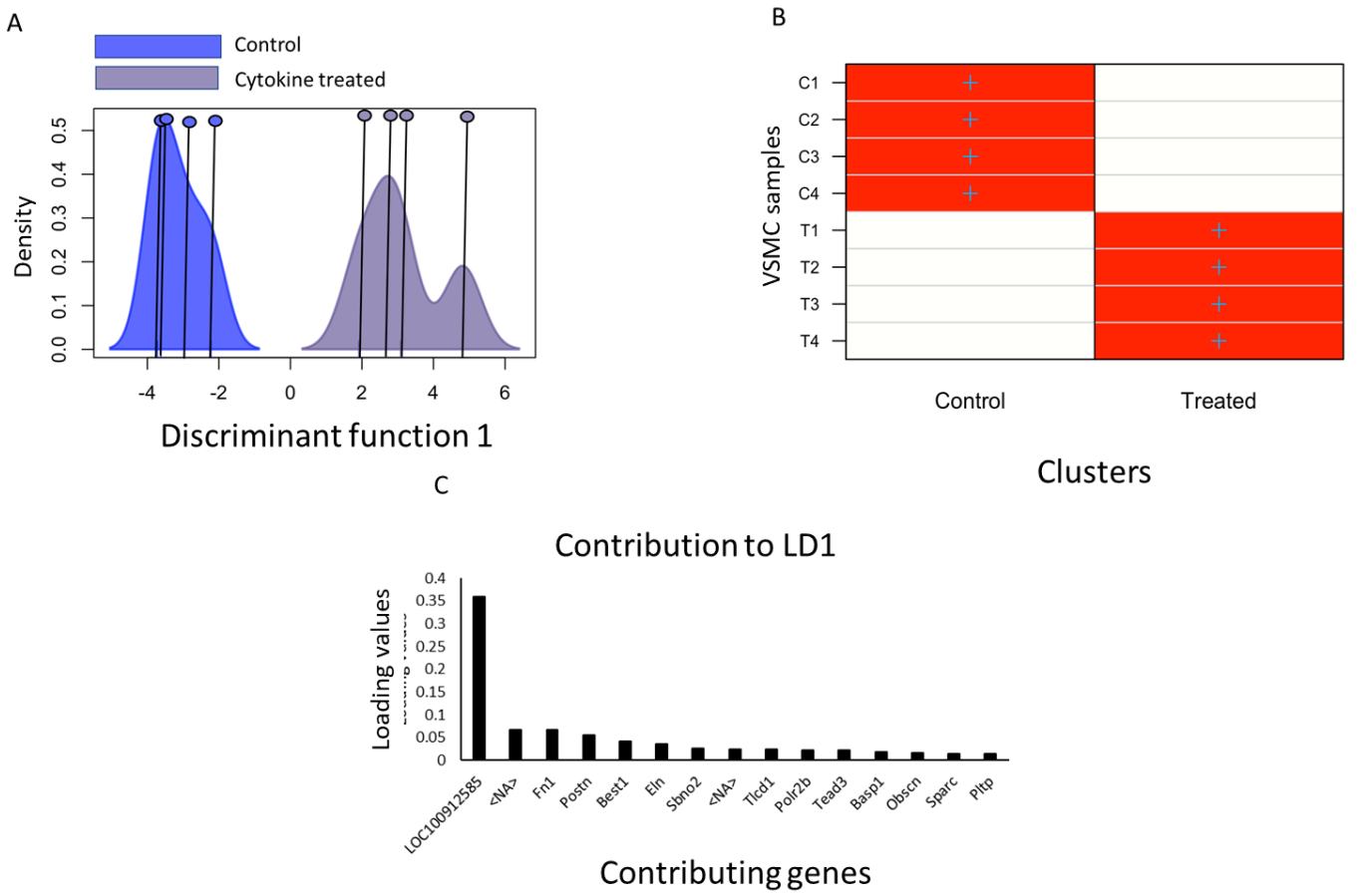

Figure 26: Discriminant Analyses of cytokine effects on VSMC samples (all genes).
A. Shows the kernel density plots of the discriminant component coordinates for the control and treatment groups of VSMC; co-ordinates on the x-axis and density on the y-axis; Individual co-ordinate centre points are illustrated by the vertical line and circle. There is clear discrimination between control and treated VSMC samples. **B.** A graphical confusion matrix showing the actual group membership (y-axis) and predicted cluster membership (on the y-axis). Groups were correctly clustered with *a* probability of 1. **C**. Gene contributors to the linear discriminator function; LOC100912585; mitogen-activated protein kinase 7-like, AABR07068042.1, Fn1; fibronectin 1, Postn; periostin, Best1; bestrophin 1, Eln; elastin, Sbno2; strawberry notch homolog 2, AC133403.1, Tlcd1; TLC domain containing 1, Polr2b; RNA polymerase II subunit B, Tead3; TEA domain transcription factor 3, Basp1; brain abundant, membrane attached signal protein 1, Obscn; obscurin, cytoskeletal calmodulin and titin-interacting RhoGEF, Sparc; secreted protein acidic and cysteine-rich, and Pltp; phospholipid transfer protein.

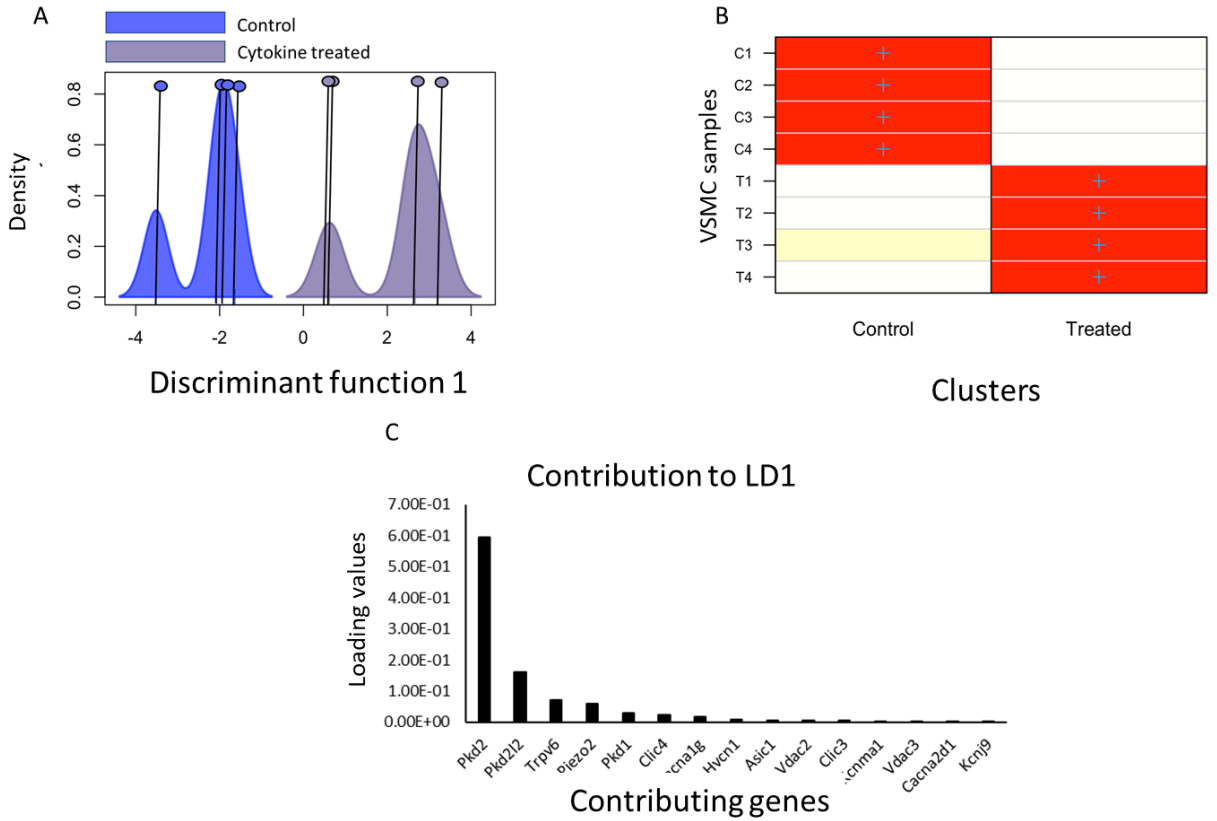

Figure 27: Discriminant Analyses of cytokine effects on VSMC samples (channels genes).
A. *Shows the kernel density plots of the discriminant component coordinates for the channels of the control and treatment groups of VSMC; co-ordinates on the x-axis and density on the y-axis; Individual co-ordinate centre points are illustrated by the vertical line and circle. There is clear discrimination between control and treated VSMC samples.* ***B.*** *A graphical confusion matrix showing the actual group membership (y-axis) and predicted cluster membership (on the y-axis). Groups were correctly clustered with greater than 0.94 probability.* ***C.*** *Gene contributors to the linear discriminator function; Pkd2; polycystin 2, transient receptor potential cation channel, Pkd2l2; polycystin 2 like 2, transient receptor potential cation channel, Trpv6; transient receptor potential cation channel, subfamily V, member 6, Piezo2; piezo-type mechanosensitive ion channel component 2, Pkd1; polycystin 1, transient receptor potential channel interacting, Clic4; chloride intracellular channel 4, Cacna1g; calcium voltage-gated channel subunit alpha1 G, Hvcn1; hydrogen voltage-gated channel 1, Asic1; acid-sensing ion channel subunit 1, Vdac2; voltage-dependent anion channel 2, Clic3; chloride intracellular channel 3, Kcnma1; potassium calcium-activated channel subfamily M alpha 1, Vdac3; voltage-dependent anion channel 3, Cacna2d1; calcium voltage-gated channel auxiliary subunit alpha2delta 1, and Kcnj9; potassium voltage-gated channel subfamily J member 9.*

Electrophysiological changes in cytokine treated vascular smooth muscle cells (VSMC)

One of the advantages of the culture model is it makes cell electrophysiology more practical. In terms of animals needed, for example, it reduces the number required immeasurably. The study of FLS was now repeated using VSMC to see if that ANO1 was differentially expressed and to investigate this by electrophysiology.

Electrophysiological Characterization of VSMC in culture

Patch-clamp electrophysiology was performed on isolated VSMC cells as published previously and described in the methods (section electrophysiology). Whole-cell currents were recorded in voltage-clamp mode patch-clamp with voltage steps applied from a holding potential of -80mV to a range of command potentials (Vc) from -120mV to +120mV. Figure 28-A shows an example representative record from a cell recorded under control conditions. Figure 28-C shows the equivalent in a cytokine treated example. Since CuffDiff suggested that there may be differences in expression of the ANO1 ion channel, the effect of calcium-activated chloride channel (CaCCinh-AO1) inhibitor on these currents in both control and cytokine treated conditions Figure 29-A and Figure 29-C, respectively, was tested.

To get a broad overview of whole-cell properties, the first features analyzed were the slope of the positive phase of the current-voltage curves and reversal potential of this component. Note that this is not a true equilibrium potential but does give an indication of the ion permeabilities contributing to this current-voltage curve. Since there are several groups (control, cytokine treated, control with inhibitor and cytokine (10 ng/ml IL-1β+TNFα) treated with inhibitor), a clustering analysis to detect trends in the ion channel behaviours (Figure 30 (A-E)) took place. A plot of Vrev against slope conductance was created for the rising current phase against each other and then followed by analysis with a k-means clustering script based on Scikit-Learn written in Python 3 by RBJ. The first task with clustering analysis is to determine the optimal number of clusters. This can be done with silhouette analysis. Silhouette analyses (Figure 30-F) shows the optimal numbers of clusters to be 2. There is clearly no separation of control and

cytokine treated data. Most data points in the presence of inhibitor CaCCinh-AO1 cluster into cluster 1 (Figure 31), but most data in the absence of inhibitor fall into cluster 2. To test if this is a significant association, a Fisher Exact test was used. This returned an odds ratio of 4.9 (inhibitor data 4.9x as likely to be clustered together in cluster 1 than in cluster 2), however, this association was not statistically significant ($p=0.09$) and may, therefore, be a chance occurrence. The mean slope conductance in full control conditions (no cytokine and no drug) was 536.5±281.3 pS/pF and not significantly different following cytokine treatment 293.2±86.4pS/pF (Figure 32-A and -B). There was also no significant difference in the Vrev calculated parameter (control; -21.9±26.4mV vs cytokine; 16.3±12.6mV, n=27,26). Following treatment with the 1 µM ion channel inhibitor CaCCinh-AO1, slope conductance was smaller, but not significantly so (164.2±36.5pS/pF). In the presence of cytokine treatment slope conductance was very similar (160.0±39.3pS/pF), but not significant to the equivalent value (above) under control conditions. There was, however, a significant rightward shift of Vrev in the presence of the channel inhibitor (-7.1±5mV, $p<0.05$, n=25,26) and this effect was lost following cytokine treatment of the cells (-20±2.2mV, $p>0.05$, n=26,18).

Current-voltage (I-V) curves of VSMC

As seen in Figure 28 (B and D) and Figure 29 (B and D), VSMC exhibited different phases of currents. These are sustained and peak currents. Both phases were analyzed. In the absence of the CaCCinh-AO1, there was a difference between control and cytokine (10 ng/ml IL-1β+TNFα) treated VSMC. In fact, there was a shift to the left of the I-V curve with sustained current and shift to the right with peak current after cytokine treatment. In the presence of the 1 µM of CaCCinh-AO1, there was a clear shift to the left of the cytokine treated VSMC after -70mV command potential in the sustained current while there were barely any changes with the peak current. The amplitude of the sustained currents in both control and cytokine treated VSMC was increased in the presence of the CaCCinh-AO1 but decreased in both with the peak current.

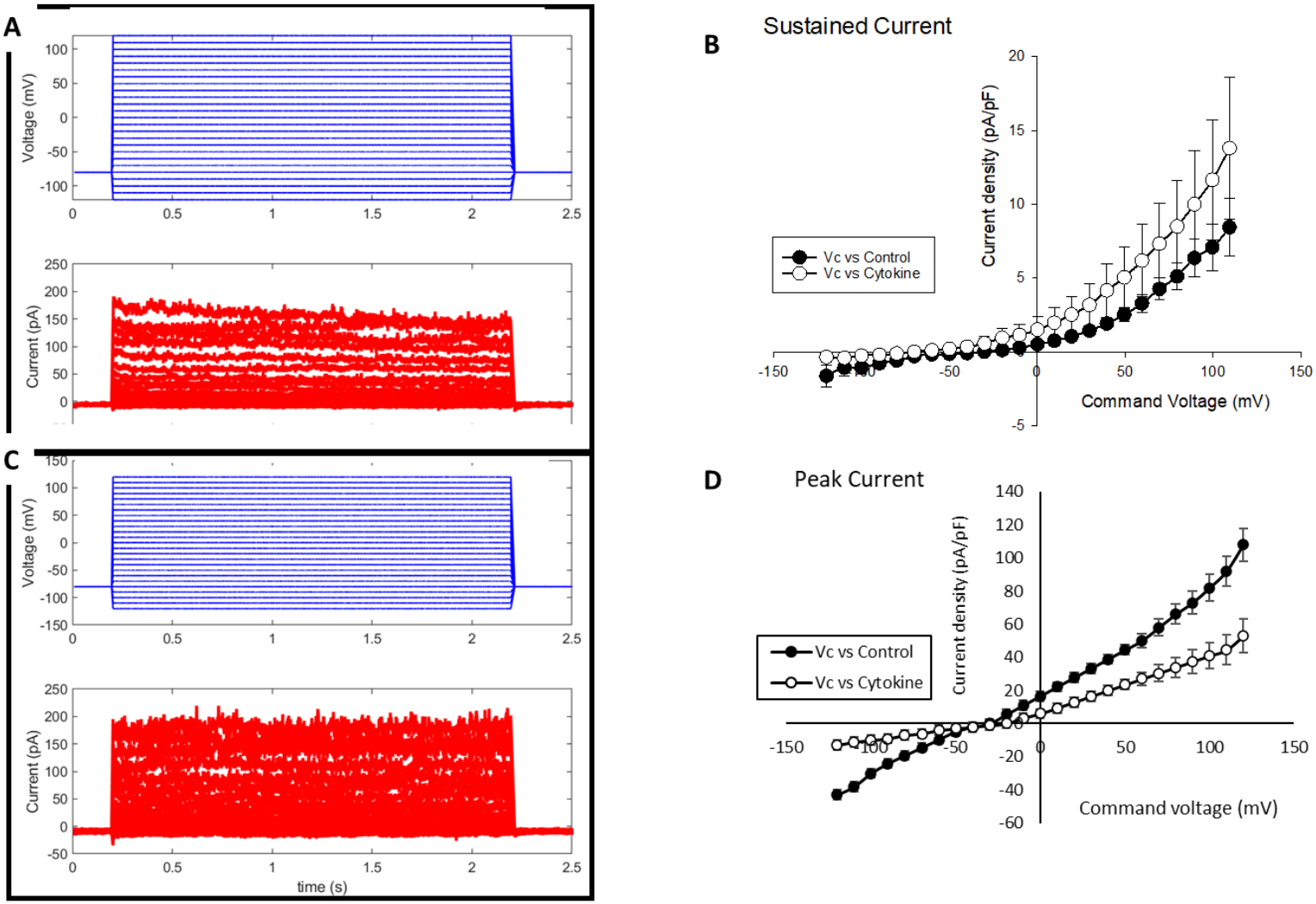

Figure 28: Whole-cell voltage-gated currents from control and cytokine (10ng/ml IL-1β+TNFα) treated VSMC.
A. Top panels show the voltage step protocols and the evoked currents are shown below for control VSMC. Note that VSMC exhibit both sustained and peak currents. These phases were then analyzed separately as indicated. ***B.*** *The* current-voltage curve of the sustained current of control and cytokine treated VSMC. ***C.*** Top panels show the voltage step protocols and the evoked currents are shown below for cytokine treated VSMC. ***D.*** *The* current-voltage curve of the peak current of control and cytokine treated VSMC.

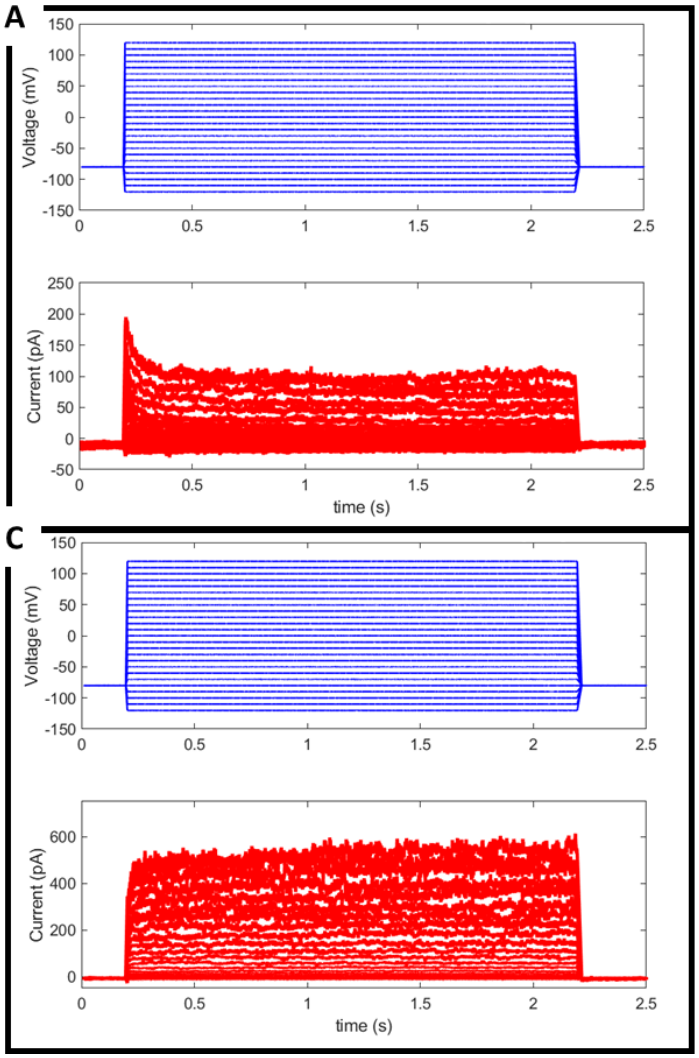

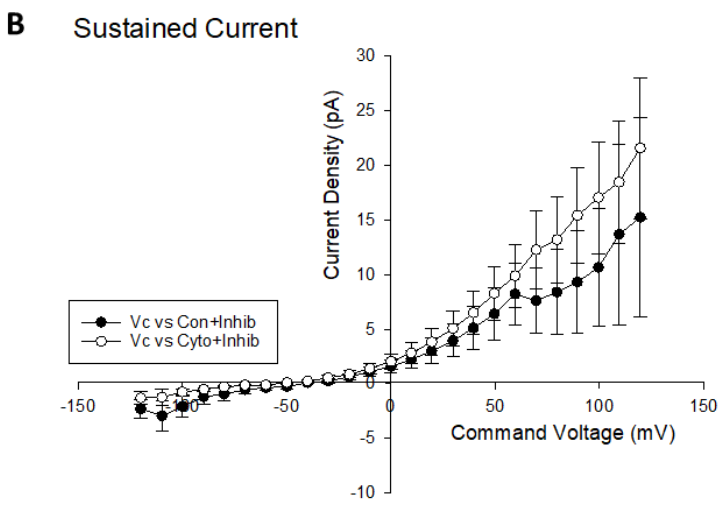

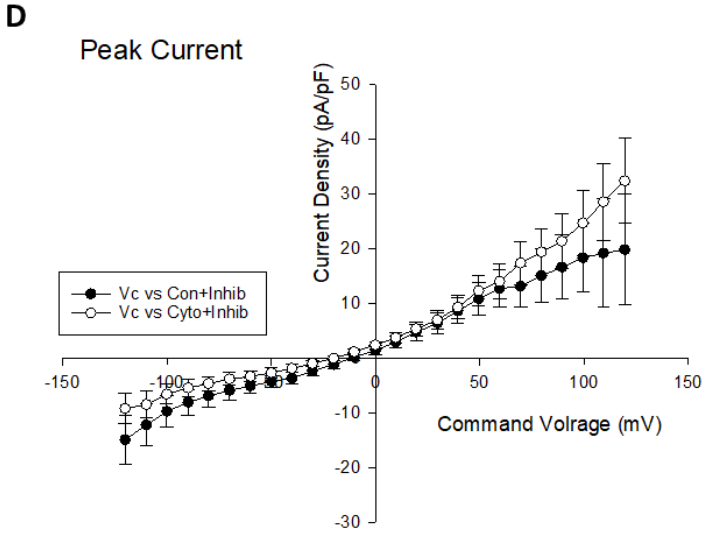

Figure 29: Whole-cell voltage-gated currents from control and cytokine (10ng/ml IL-1β+TNFα) treated VSMC in the presence of CaCCinh-AO1.
A. *Top panels show the voltage step protocols and the evoked currents are shown below for control VSMC plus CaCCinh-AO1.* ***B.*** *The current-voltage curve of the sustained current of control and cytokine treated VSMC in the presence of CaCCinh-AO1. C. Top panels show the voltage step protocols and the evoked currents are shown below for cytokine treated VSMC. D. The current-voltage curve of the peak current of control and cytokine treated VSMC in the presence of CaCCinh-AO1.*

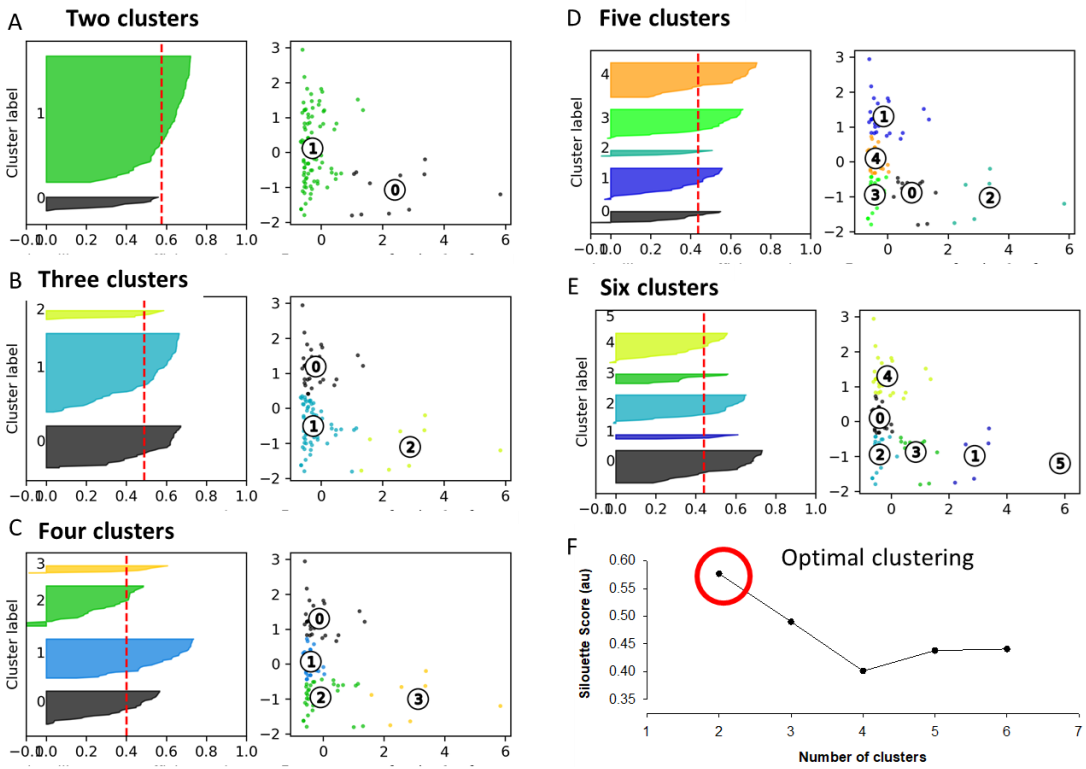

Figure 30: Clustering of electrophysiology data (conductance vs reversal potential) of VSMC.
To look for clusters of cell electrophysiology phenotype, we plot conductance (x-axis) vs Vrev (y-axis) (scaled) of control and cytokines treated (± CaCCinh-AO1), A-E. Then, the script calculates *the* silhouette graph score **(A-E)**. After that, a Chi-square test is used for the association. The best cluster is presented by the red circle in the silhouette graph (**F**). Silhouette analysis is a method to study the separation distance between clusters. The Silhouette value measures how similar an object is to its own cluster compared to other clusters. Clustered data is fit to K means algorithms and then each observed value is clustered with the nearest k mean. The silhouette ranges from -1 to +1. A high value (coefficient) indicates that the object is well matched to its own cluster and poorly matched to the neighbouring clusters. When most objects have high values, then the clustering configuration is appropriate. On the other hand, if many objects have low or negative values, then the clustering configuration may have too many or wrongly clustered. In this study, the silhouette analysis is used to choose an optimal value for n clusters. For the data in this project, the silhouette plot shows that the n cluster value of 4, 5 and 6 are bad choices due to the presence of clusters with below-average silhouette scores and also due to wide fluctuations in the size of the silhouette plots. The thickness of the silhouette plot reflects the size of the cluster. Silhouette analysis shows that the best options are between 2 and 3 clusters. However, (F) shows a high silhouette score (coefficient) for 2 clusters than 3 clusters. Therefore, the optimum clustering is 2 clusters. More details are found in the text. From A-E, on the left side shown is the silhouette plot for the various clusters while on the right side is the visualization of the clustered data. This analysis was done with a script based on Scikit-Learn written in Python 3.

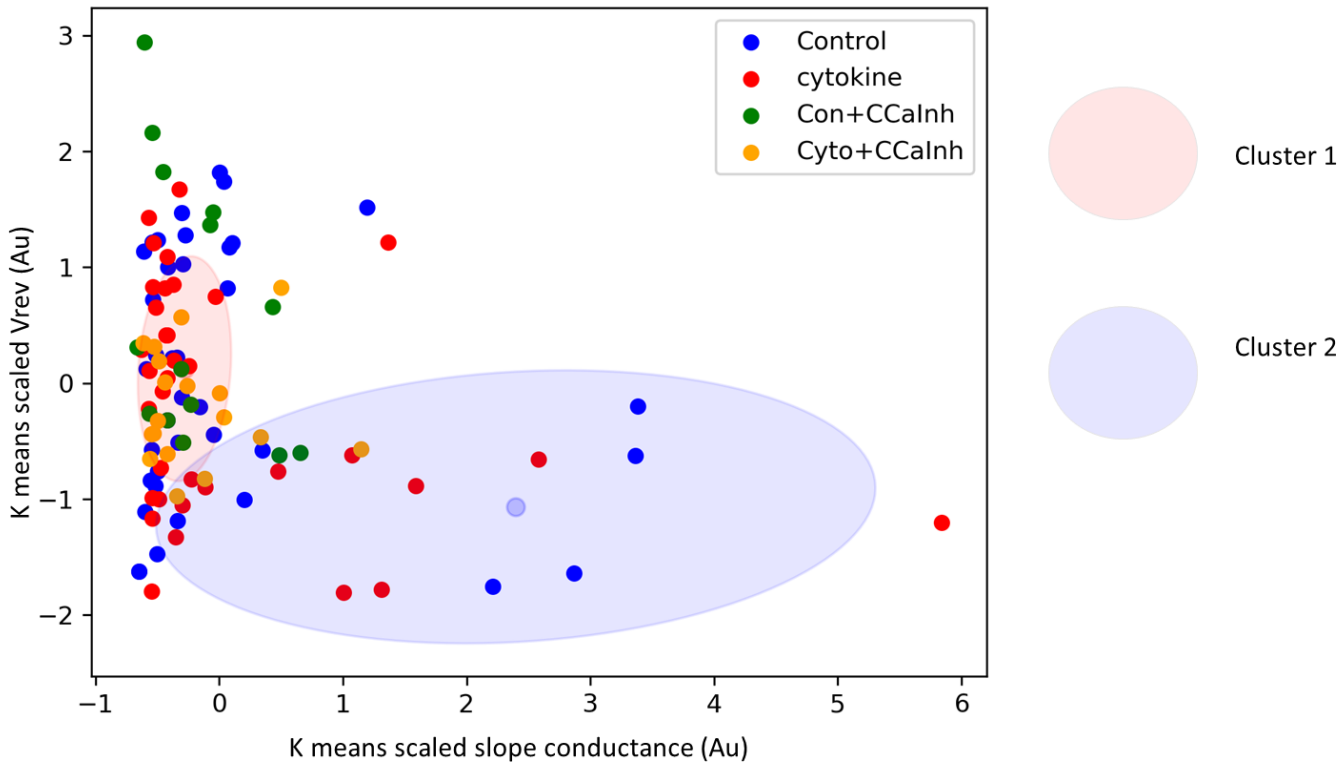

Figure 31: PCA of k means of conductance and Vrev in all VSMC samples of the optimum 2 clusters.
This graph shows the optimum clustering of control and cytokine (10ng/ml IL-1β+TNFα) treated ± CaCCinh-AO1. This is a coloured visualization of the clustered data of the optimum 2 clusters from the previous figure (A) of data from all VSMC samples. The combination of PCA and k means is a way of analysing huge amounts of data. The main steps here are to reduce dimensionality, cluster and visualize data. Therefore, features are taken and projected onto a lower-dimensional space to find the optimal number of components that capture the greatest amount of variance in the data. This step reduces data down to just a few important principal components. Then, cluster data. In this step, the important principal components identified from the first step are fit to the k means algorithms to determine the best number of clusters. The last step is to visualize these data. More details are found in the text. K means of scaled slope conductance is shown on the x-axis while the k means scaled reversal potential (Vrev) are shown on the y-axis. This analysis was done with a script based on Scikit-Learn written in Python 3.

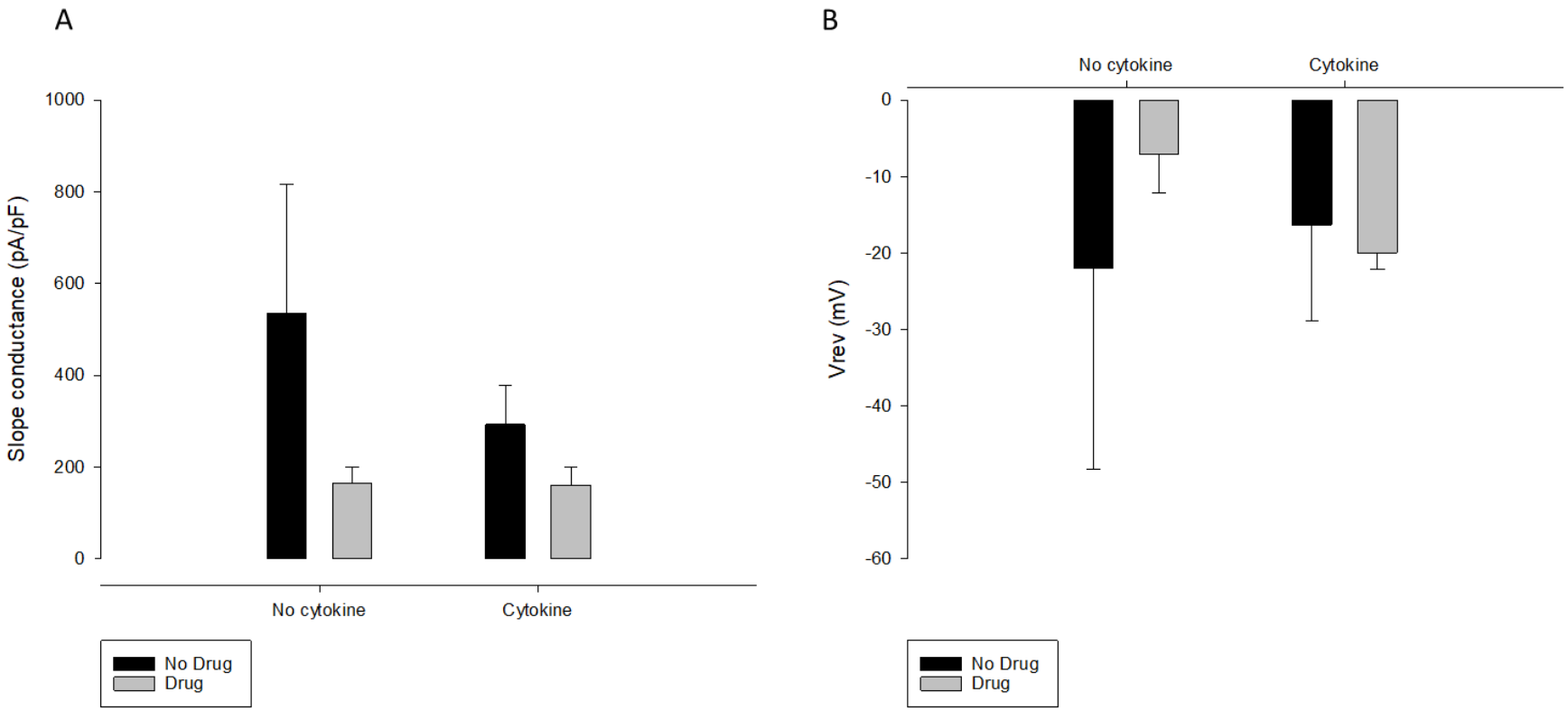

Figure 32: Representation of a broad view of electrophysiological data of VSMC.
A. *Slope conductance (pA/pF) of VSMC samples; control and cytokine (10ng/ml, IL-1β+TNFα, 72hrs) treated VSMC ± CaCCinh-AO1. In the absence of CaCCinh-AO1 (drug), slope conductance of control was 536.5±281.3 pS/pF and following cytokines treatment the slope conductance decreased to 293.2±86.4 pS/pF but was not statistically significant. In the presence of CaCCinh-AO1 (drug), the slope conductance of control was 164.2±36.5 pS/pF and with cytokines treatment was 160.0±39.3 pS/pF and not statistically significant.* ***B.*** *Reversal potential (Vrev in mV) of the same samples ± CaCCinh-AO1. In the absence of CaCCinh-AO1 (drug), the Vrev of control was 21.9 ±26.4 mV and following cytokines treatment was 16.3±12.6 mV but not statistically significant. A significant rightward shift of the Vrev was observed in the presence of CaCCinh-AO1 (drug) with the control (-7.1±5 mV, $p<0.05$, $n=25, 26$) and this effect was lost following cytokines treatment (-20±2.2 mV, $p>0.05$, $n=26, 18$).*

Comparison of Boltzmann parameters in control and cytokine treated VSMC

Since the earlier work with FLS showed changes in potassium conductances, the Boltzmann transformation of current-voltage curves took place and followed by a comparison of these in control and cytokine conditions. There were no significant differences. Gmax: Control 59.5±2.4 pS/pF vs cytokine treated 74.9±6.0 pS/pF. Midpoints: Control 52.9±1.7mV vs treated 63.5±2.2mV. Slopes: Control 26.1±0.4 mV vs treated 25.5±0.4mV. n=25,17 control vs cytokine treated. $P>0.05$ for all parameters.

Analysis of Inward rectified-type currents

A number of potassium channels, namely from the KCNJ family (such as KCNJ8 and KCNJ11 were differentially expressed) exhibit inwardly rectifying currents. That is, currents that are more negative, at negative potentials than would be expected from Ohms law. The presence of these currents in some traces (data not shown) was observed and therefore examined if the presence of these was increased by cytokine. Inward rectification was calculated by subtracting the y=mx+c predicted current at -120mV from the actual current at -120mV. Y=mx+c was calculated in excel from the data in the straight-line portion of the current-voltage curve at -50 to -10mV. The inwardly rectifying current so defined in control conditions was 33.5±32pA/pF, n=27 and 69.5±33.5pA/pF, n=24 after cytokine treatment (not significantly different). These data included many cells that had no inward rectifier current at all (ie., current at -120mV was positive to that predicted from a straight-line as expected for the presence of a dominant voltage-gated, for example, potassium current). To control for this, I analyzed just those cells for which there was a negative inwardly rectifying current. With this caveat, there was a significant reduction in (negative) current following cytokine treatment (control: -5.1±1.2, and cytokine: -1.71±0.6pA/pF, n=7,11, $p<0.05$).

4.5 Discussion

Changes with gene expression in aorta tissues

In this study, the expression of both the channelome and the whole transcriptomic profile of Aorta and VSMC was tested. Also, a functional analysis of the VSMC channels using patch-clamp electrophysiology in the whole-cell configuration was performed. The ageing model itself provides a closer view of the changes that take place in gene expression but lacks pathway-specific details as the input to such changes is limitless due to the presence of different cell populations. On the other hand, the cultured VSMC offers a unique feature in which patch-clamp electrophysiology experiments can be conducted. It also provides inflammation specific pathways on only VSMC that could not be controlled with real aged tissues.

Aorta tissues showed some differentially expressed genes such as Alb, Trim54, Mpo, LOC500712, Scd, Tnnc2, Tnnt3, and Myh2. These genes are mainly involved in the regulation of albumin, binding and stabilizing microtubules, myeloperoxidase, localization to the ECM, biosynthesis of membrane lipids TG and energy homeostasis, cardiac proteins for regulation of muscle growth, muscle fibres and contraction, and proteins responsible for the generation of mechanical force. Such changes may lead to overactivation of muscle growth and muscle fibres leading to cardiac or cardiovascular disorders. One example of such diseases is atherosclerosis. Many factors play roles in the development of this disease. Among these factors is the switch in the VSMC phenotype from contractile to synthetic or even to less differentiated forms of VSMC ((Bennett et al., 2016, Rudijanto, 2007). Different physiological conditions including injury can be involved in this event. Not only this but also other factors such as increased lipid biosynthesis and recruitment of macrophages increased levels of cytokines and growth factors can induce this phenotypic switch (Bennett et al., 2016, Rudijanto, 2007). Some genes such as those mentioned above (Macdonald et al., 2009) were detected in the aorta tissue in this project.

Additionally, functional annotating clustering for these differentially expressed genes took place using David's Bioinformatics Resources 6.8. which enriched extracellular space "p-value of $2.9x10^{-2}$. The KEGG pathways that were enriched by these genes were "Carbohydrate digestion and absorption" with a p-value of $5.2x10^{-2}$, "bile secretion" with a p-value of $8.8x10^{-2}$, and "cardiac muscle contraction" with a p-value of $9.6x10^{-2}$. It is interesting to find out that one of these pathways was related to cardiac muscle contraction although statistically not significant.

Ion channel genes in the aorta

Also, there were some differentially expressed ion channel genes such as calcium channels (Cacnb1), aquaporin channels (Aqp3 and Aqp7), potassium channels (kcna1, kcnj8 and kcnj11), gap junction channel (Gja1), and sodium channel (Scn1b).

These differentially expressed ion channel genes in ageing aorta seem to be responsible for several cellular/tissue functions including their responsibilities for the presence of the pore-forming subunits of the active channels [such as Cancb1 (Williams et al., 1992, Brust et al., 1993, Cohen et al., 2005), and Scn1b (Makita et al., 1994, Qin et al., 2003)], the flow of K^+ ions into the cell (hyperpolarization/repolarization) [such as Kcna1 and kcnj11 (Babenko et al., 1998)], muscle contraction and relaxation [such as kcnj8 that may play role in vasodilation (relaxation) (Kane et al., 2006)], providing energy to the cell during starvation [such as Aqp7 (Agre, 2006)], facilitating water transport [such as Aqp3 (Sasaki et al., 1998, Agre, 2006)] and cell-to-cell communications [such as Gja1 (Cx43) (Rama et al., 2006)]. These should enhance the functions of the cells and the overall health of the tissue and the microenvironment. However, the expression of genes responsible for such functions can be inferred as there is (could be strong) need for them due to loss with ageing.

Changes with gene expression in VSMC

It was not surprising to find out that the enriched KEGG pathways were "NF-kB signalling pathway" with a p-value of 0.0022, "Leukocyte endothelial migration" with a p-value of 0.0058, "TNF

signalling pathway" with a p-value of 0.03 and "Cytokine-cytokine receptor interaction" with a p-value of 0.034 because TNFα (along with IL-1β) was one of the cytokines used in this study to create an inflammatory model of ageing "inflammageing", TNFα interacts with its membrane receptor and can transduce signalling through NF-kB signalling pathway.

Ion channels in VSMC

Only three channel genes were differentially expressed in the VSMC after cytokine (10ng/ml IL-1β+TNFα, 72hrs) treatment. These genes are Gap junction (Gja1), Calcium-activated chloride channel (ANO1), and Polycystin 2 (Pkd2).

Gja1 (Cx43) is an important gene in cell-to-cell communications and it plays a role in VSMC differentiation (Rama et al., 2006). ANO1 has a significant role in controlling smooth muscle contraction (Jensen et al., 2018). Based on the functional significance, it was speculated that the localization of the Pkd2 is in ER of VSMC and it has been suggested that Pkd2 mutation plays a pathogenic role in the complication of the autosomal-dominant polycystic kidney disease (ADPKD) (Torres et al., 2001).

Differences and similarities between Aorta and VSMC

Although, there were some differentially expressed (both p-value and FDR<0.05) genes; 29 genes and 7 channel genes in the aged aorta, they were not like the VSMC which had 115 differentially expressed genes and only 3 channel genes. Also, genes contributed to the differences between the young and old aorta and those between control and cytokine treated VSMC were also different.

The similarities appeared in terms of enriched GOs and individual genes. As mentioned above, aorta GOs showed terms that were mostly related to the muscle contraction/regulation in addition to extracellular space, VSMC GOs were related to signal transduction and angiogenesis. They both shared some extracellular enrichment GOs. For example, extracellular space enriched GO appeared in both in

addition to extracellular exosome and ageing in VSMC. This shows that our model of "inflammageing" was once again able to show some similarities with the real ageing model (old rats).

For individual genes, Gap junction (Gja1) gene was found to be differentially expressed with p-values of 0.02855 and 0.00005 in aorta and VSMC, respectively. Gja1 plays a role in cell to cell communication. With ageing aorta, it seems that the function of this gene is altered which triggered its expression to compensate for the decrease. In VSMC, cells were challenged with cytokine for 72hrs to create the inflammatory model of ageing "inflammageing". This may also have triggered its expression, especially that in the culture system the cells were left to be confluent of 70-80% which allowed the formation of a monolayer of cells, unlike aorta tissue that is multi-layers.

Previous studies on Anoctamin-1 (ANO1, also known as Ca^{2+} activated Chloride channel) expression

Expression of TMEM16A is variable in different tissues as follows; portal vein > thoracic aorta > carotid artery > brain and it was found to be robustly expressed in murine vascular smooth muscle cells (Davis et al., 2010). ANO1; also known as TMEM16A is essential for Ca2+ activated chloride channel conductance in VSM (Jensen et al., 2018). Several studies have been conducted to inhibit this channel. For example, TMEM16A inhibitor called T16A(inh) -A01 was used in a study and found that it inhibited the Ca2+ activated chloride channel current in aorta relaxed murine and human blood vessels (Davis et al., 2013). Also, ANO1 gene was knocked out and the gene was floxed to eliminate the Ca2+ activated chloride channel current and confirmed by comparison of this knocked out mice with WT using patch-clamp electrophysiology. The blood pressure of the knocked out mice in this study was reduced compared to the WT (Heinze et al., 2014). siRNA against TMEM16A was also tested to eliminate the currents from this channel in mice (defined as transgenic mice (TG) in this study). There was no difference in blood pressure and heart rate in TG compared to WT. However, it was suggested that ANO1 modulates the arterial

contractility; at least in part, indirectly by the control of CACNA1C (vascular L-type Ca2+ channel) expression (Jensen et al., 2018).

In this study, a down-regulation (log2 F.C. = -1.2131, p-value=0.00085) of the ANO1 expression after cytokine (10ng/ml IL-1β+TNFα) treatment was observed. Therefore, testing its role on the whole-cell current of the VSMC using its inhibitor (CaCCinh-AO1) seemed interesting. First, the current of the VSMC in both control and cytokine treated cells without the inhibitor was measured. Then, the same cells were challenged with the inhibitor and the currents were measured in a whole-cell configuration of the patch-clamp electrophysiology.

Changes in TMEM16A (AO1) channel electrophysiology

The slope of the positive phase of the current-voltage curves and projection of the reversal potential of this component helps obtain a broad overview and assessment of the whole-cell electrophysiological data. Clustering data usually provide a different way of examination by which close or similar data can be clustered and analyzed together to reduce variabilities within the cluster. Using 2, 3, 4, 5, and 6 Kmeans clustering of slope conductance against reversal potential allowed us to find the optimum cluster with silhouette score which turned out to be 2 clusters in the absence of the CaCCinh-AO1 with an odds ratio of 4.9x and the p-value of association of 0.09 meaning that the association of data to be clustered in cluster 1 (but not cluster 2) in the presence of CaCCinh-AO1 could have occurred by chance. This test of association was done by Fisher Exact test. Then, the analysis of the recordings of VSMC took place.

VSMC like other cells can exhibit different phases of currents. In this study, different phases of currents were noticed; sustained and peak. In order to get a better understanding, analysis of these two phases of currents took place. The sustained current showed a shift to the left after cytokine treatment. This kind of shift in VSMC could be due to the presence of different ion channels such as acid-sensing, sodium, Kv, Kir, BK, channels. The trend was remained even after inhibiting the Ca^{2+} activated chloride

channels with 1 μM CaCCinh-AO1. The current amplitude; however, was slightly increased in the presence of the inhibitor. On the other hand, the peak current showed a shift to right with cytokine treatment but could not sustain that in the presence of CaCCinh-AO1. Instead, the amplitude of the control and cytokine treated currents was decreased with the inhibitor. This means that the cause of such shifts in the first place could be due to the loss of the current toward the sustained current or the activity of other channels such as sodium channels.

Cl^- channels are a major depolarizing mechanism in vascular smooth muscle (Davis et al., 2010). The slope conductance of all conditions (control and cytokine treated VSMC with/out channel blocker (CaCCinh-AO1) was not significantly different from one another. Additionally, the Vrev was not significantly different between control and cytokine treated VSMC except when the CaCCinh-AO1 was used as it showed a significant reduction (control -5.1±1.2 pA/pF and -1.7±-0.6pA/pF) with a p-value<0.05. This could be explained by depolarization of the cell membrane in which intracellular Ca^{2+} concentration increased and K^+ channels closed. This can lead to vasoconstriction which, if persist for a longer time, will lead to hypertension that is one of the age-related diseases.

Conclusion

To our knowledge, this is the first time that NGS is combined with electrophysiology to study aorta (young and old) and VSMC (control with cytokine treated). With NGS data analysis, gene expression of the young aorta was different than the old aorta. Also, cytokine affected gene expression of VSMC. Both ageing and cytokine effects had different gene expression based on the nature of the tissue or cell. However, there were some similarities in terms of GO enrichment in which both were enriched for extracellular space. Also, Gja1 gene was differentially expressed in both aorta and VSMC, this is particularly interesting since it was also elevated in my FLS transcriptomic study. Electrophysiology results showed an increase in sustained currents of both control and cytokine treated VSMC compared to the peak current in the presence of ANO1 inhibitor. Also, inwardly rectifying potassium (such as kcnj8 and kcnj11) channels may have played a significant role in the reduction of the current after cytokine treatment.

Chapter 5 – Paraventricular Nucleus (PVN) of the Hypothalamus

5.1 Introduction

The paraventricular nucleus (PVN) is a key nucleus in the hypothalamus sometime referred to as the "autonomic master controller" (Loewy and McKellar, 1980, Loewy, 1991). It is one of the most important hypothalamic autonomic control centres with a variety of physiological roles ((Feetham et al., 2018)). There are well-established changes in autonomic control in older people (Hotta and Uchida, 2010, Parashar et al., 2016, Fu et al., 2006, Pal et al., 2014), I investigate in this chapter whether I can detect genetic changes that might explain this autonomic change.

The PVN was described in the main Introduction, but briefly, it is composed of magnocellular and parvocellular neurons that can be seen with their respective sub-divisions. subdivisions in (Figure 2**Error! Reference source not found.**). In general terms, the magnocellular sub-division is involved with control of the pituitary and release of hormones to the circulatory system (Ferguson et al., 2008, Swanson and Sawchenko, 1983, Hosoya et al., 1991, Simmons and Swanson, 2008), whereas the parvocellular sub-nucleus contains neurones that project to the medulla and spinal cord and directly control the sympathetic nervous system (Swanson et al., 1980, Coote, 1995, Jansen et al., 1995, Badoer, 1996). This latter function includes control of cardiovascular function (i.e. regulation of blood volume, circadian regulation of blood pressure, cardiovascular response to stress), regulatory functions for hepatic glucose control, circadian pacemaker in mammals, role in osmoregulation and thermoregulation (Feetham et al., 2018, Nunn et al., 2011).

Dysfunction of sympathetic pre-autonomic neurons (usually hyperactivity) has been linked to several serious age-related diseases such as hypertension and heart failure (Julius, 1993). Additionally, there is considerable evidence directly linking ion channel (or their regulators) changes in the PVN with cardiovascular disease, especially heart failure (Zhang et al., 1997, Zhang et al., 1998, Felder et al., 2000, Patel et al., 2000, Julius, 1993).

In this chapter genuine ageing will be used; comparing gene expression between relatively young ~7-8 months old and ~24 months old Wistar rats. Healthy ageing animals rather than one of the hypertensives of other variants were chosen. Changes that will be detected should be genuinely associated with healthy ageing. As in previous chapters, the start will be with the analyses of genome-wide genetic changes and then filter down to the main objective which is to identify any changes in PVN wide ion channel expression. Several ion channels have already been identified in the PVN, by both electrophysiology and by qPCR, and these include such major super-families as the amino acid receptor channels (the primary neurotransmitters of the brain generally), transient receptor potential channels (TRP), potassium channels, sodium channels, voltage-gated Ca2+ channels, and other channels like purinergic membrane receptor family, acid-sensing channels (ASICs), proton-gated voltage insensitive cation channels (Feetham et al., 2018).

Aims

In this chapter, the investigation of transcriptomic changes that take place in the PVN of younger and older Wister rats by RNA-sequencing and bioinformatics will take place. More specifically:

- Is there a detectible over-all difference between transcriptome of young and old PVN transcriptome?
- What genes are significantly changed in the PVN with ageing?
- What functional clusters of genes are associated with PVN ageing?
- Is there a change in overall ion channel gene expression in the PVN with ageing?
- Which specific ion channel genes change with PVN ageing?

5.2 Materials and methods

Tissue

Rats were housed at 22-24°C in a 12 h light/dark cycle-controlled facility with ad libitum access to food and water. Animals were sacrificed by Schedule 1 methods for all in vitro work by my colleague Dr.Fiona O'Brien. Coronal brain slices were prepared using a Brain Slicer Matrix (World Precision Instruments, UK) and the PVN was located based on location and specific markers such as fornix and third ventricle. The PVN was 'punched' out using a 3 mm biopsy punch (Kai Medical, UK) and samples were deep-frozen at -80C in RNA-Later until RNA-extraction.

RNA extraction

PVN tissues were defrosted and RNA was extracted as described in the materials and methods chapter 2.

Next-generation sequencing (RNA-sequencing)

Isolation and preparation of PVN samples must precede the isolation methods. RNA from PVN samples were extracted as described in methods. They were placed in RNALater overnight and then into -80˚C until the experiment. RNA was extracted from these samples as described in materials and methods. RNA samples were sent for sequencing at the Center for Genomic Research (CGR, University of Liverpool, UK) which took place with >30M sequencing depth, 150bp, paired-end. RNA-sequencing data analysis took place as described in the RNA-sequencing pipeline in materials and methods (chapter 2).

RNA-sequencing Quality Control

Before RNA sequencing, RNA isolation was run about 14 times repeating to optimise quality measured by NanoDrop 2000 Spectrophotometer using different methods. After this, different concentrations with good quality RNA were achieved.

Before the sequencing experiments took place, the quantity (Appendix 11) and quality of the submitted RNA samples was checked. Usually, an electropherogram and gel-like image are produced for each sample as presented in Appendix 12.

Once raw data received, they were checked for quality of reads using FastQC software as shown in Appendix 13. These figures show the high quality of reads as their Phred quality scores fall into the green zone >30 which means that the error rate is 1 in 1000bp. Next, these reads were analysed as described in the materials and methods chapter 2. But briefly, they were aligned/mapped to a reference genome with HiSat2 tool (Kim et al., 2015) using a reference genome (Rat Jul. 2014 (RGSC 6.0/rn6)(rn6) database), assembled and quantified using StringTie tool (Pertea et al., 2015) and differentially expressed genes were detected with DESeq2 tool (Trapnell et al., 2010). Using several reference servers such as Genenames.org, HUGO Gene Nomenclature Committee and locally edited script in MATLAB, ion channel genes were filtered/selected and analysed for their gene/transcript abundance and differential expression.

5.3 Results

PVN tissues were harvested from 3 “young” (3-5 months) and 3 “old” (24 months) male Wistar Kyoto rats. Up until culling, animals were visually healthy. After isolation of PVN and extraction of RNA, these samples were sequenced, and the focus was on the analyses of assembled genes rather than individual transcripts. Following rigorous quality control testing (see methods and Appendix), 17397 genes were detected by RNA-sequencing.

Is there a detectible over-all difference between transcriptome of young and old PVN transcriptome?

The standard approach to investigate over-all changes in transcription is to use multivariate analyses. principal components analysis (PCA) was the first to use. This reduced the approximately 17,000 variables (genes) to just 5 variables (5 principal components/dimension); a scree plot shows that nearly 40% of the variance can be accounted for with the first principal component (Figure 33-A). A contributions bar graph illustrates that the young and old subjects contribute relatively similarly to the population variance (Figure 33-B). To investigate natural clustering of young and old phenotypes, the first, second and third principal components were then plotted against each other (Figure 34). Remarkably, (unsupervised) clustering of just the first and second I then plotted component demonstrates significant separation of the two populations (Figure 34-A). There was no separation between groups when plotting principal components 1 and 3 (Figure 34-B), but again statistically significant separation of young and old clusters when plotting principal components 2 and 3 (Figure 34-C). Figure 34-D shows the first three principal components all plotted against each other. This type of analyses is entirely unsupervised and that the groups young and old separate well confirms that there are distinct differences between young and old PVN. Further insight can be gained by using a supervised equivalent to PCA; so-called discriminant analyses of principal components (DAPC). This method allows the user to define the clusters first and then algorithmically search for a single function that optimally discriminates between the two groups.

Applying this technique to our PVN ageing data (Figure 35), a remarkably clear separation of young and old groups with just 3 principal components (Figure 35-A) was found. Bayesian statistics within the DAPC package (Jombart et al., 2010) can then be used to answer the question; if I did not know from which group (young or old) one of our samples came from, how likely is it that our discriminant function would correctly classify it? In the case of the PVN ageing data and 1 discriminant function based on 3 principal components, all samples were successfully classified with greater than 99% accuracy (Figure 35-B). Finally, in this section of the work, an investigation took place to find out the relative contributions of each gene in our dataset to the overall DAPC function. i.e., which cluster of genes is most strongly associated with ageing in the PVN. These are shown in Figure 35-C; the top specific gene was that for production of the apolipoprotein and calmodulin 1.

What genes are significantly changed in the PVN with ageing?

The DAPC shows influential clusters of genes, but now analyses switched to individual genes. Differential expression analysis was carried out using the robust recent DESeq2 tool in R and found that 2577 genes were differentially expressed between the young and old samples, with p-val <0.05. Then, a Benjamini-Hochberg correction was applied to these data to correct for potential multiple comparison errors and calculated "q-values" (aka adjusted p-values or false detection rate, FDR <0.05). Following this procedure, the 811 genes were still found to be differentially expressed. The top 50 differentially expressed genes are given in Table 25 excluding those with absolute $\log_2$ fold change of less than 1.5, equivalent to approximately a 3-fold change.

Table 25: The top 50 differentially expressed genes excluding those with absolute log2 fold change of less than 1.5, equivalent to approximately a 3-fold change.

$\log_2$ change	p-value	padj	symbol	Gene name
-5.5	3.2E-19	5.3E-15	Caps2	calcyphosine 2
-8.4	1.5E-17	1.3E-13	Pmch	pro-melanin-concentrating hormone
1.5	3.7E-15	2.0E-11	Rmdn3	regulator of microtubule dynamics 3

-10.4	4.2E-14	1.7E-10	LOC100911365	Parkinson disease 7 domain-containing protein 1-like
-10.0	1.3E-13	4.4E-10	Brs3	bombesin receptor subtype 3
2.6	1.6E-13	4.4E-10	Hapln1	hyaluronan and proteoglycan link protein 1
-2.3	1.3E-12	3.0E-09	Fbxo36	F-box protein 36
2.1	1.9E-12	3.9E-09	Plekhh1	pleckstrin homology, domain containing H1
-8.9	7.2E-12	1.3E-08	Ttr	transthyretin
-9.9	5.1E-11	7.6E-08	Hcrt	hypocretin neuropeptide precursor
1.6	6.8E-11	9.3E-08	Arrdc3	arrestin domain containing 3
-9.1	1.2E-10	1.5E-07	Prmt6	protein arginine methyltransferase 6
-4.5	5.1E-10	5.8E-07	Tac3	tachykinin 3
-1.6	7.0E-10	7.2E-07	Ifitm3	interferon induced transmembrane protein 3
1.9	8.4E-10	7.7E-07	Mal	mal, T-cell differentiation protein
2.4	1.3E-09	1.1E-06	Tnfaip6	TNF alpha induced protein 6
-2.6	1.5E-09	1.1E-06	Fank1	fibronectin type III and ankyrin repeat domains 1
-1.7	1.8E-09	1.2E-06	RGD1305645	similar to RIKEN cDNA 1500015O10
-8.9	2.0E-09	1.3E-06	Arhgap8	Rho GTPase activating protein 8
-2.9	2.7E-09	1.7E-06	Lrriq1	leucine-rich repeats and IQ motif containing 1
1.6	3.6E-09	2.1E-06	Mtmr2	myotubularin related protein 2
-2.0	3.7E-09	2.1E-06	Syt10	synaptotagmin 10
-2.8	3.8E-09	2.1E-06	Slc44a4	solute carrier family 44, member 4
1.6	4.4E-09	2.3E-06	Trim16	tripartite motif-containing 16
-3.5	5.3E-09	2.6E-06	Lepr	leptin receptor
-9.7	9.9E-09	4.8E-06	Adipoq	adiponectin, C1Q and collagen domain containing
2.2	1.2E-08	5.4E-06	Ugt8	UDP glycosyltransferase 8
-1.6	1.3E-08	5.7E-06	Nppa	natriuretic peptide A
-3.5	1.4E-08	6.0E-06	Gzmm	granzyme M
1.9	2.1E-08	8.7E-06	Plp1	proteolipid protein 1
-2.6	2.2E-08	9.0E-06	Erich2	glutamate-rich 2
-2.4	2.8E-08	1.1E-05	Tekt1	tektin 1
2.5	3.4E-08	1.3E-05	Kcnip3	potassium voltage-gated channel interacting protein 3
-2.8	4.7E-08	1.7E-05	Ccdc190	coiled-coil domain containing 190
-2.5	6.1E-08	2.1E-05	Krt18	keratin 18
-2.7	7.6E-08	2.5E-05	Scn7a	sodium voltage-gated channel alpha subunit 7
-2.2	8.6E-08	2.7E-05	Anxa1	annexin A1

Top 50 genes by p-value; excluding those genes with absolute log2 fold ratio changes of less than 1.5

What functional clusters of genes are associated with PVN ageing?

One of the most useful features of RNA-seq compared to traditional gene-by-gene analyses is the ability to look for functional clusters. This analysis was performed with the GOSeq package in R (Young et

al., 2010). The first step was to correct the differential expression lists for bias associated with very long genes (that are more likely to be detected by RNA-sequencing and thus have greater detection power). This was done by plotting gene length against the probability of a gene being differentially expressed (Figure 36-A) and deriving a probability weighting function that could then be applied as a correction factor for functional enrichment. After this, differentially expressed gene list from this study was submitted to the GO database to investigate enrichment for "biological processes" (Figure 36-B), "molecular functions" (Figure 36-C) and cell compartments (Figure 37-A). In terms of biological processes, interestingly, development was the key processes, and in particular, myelination and neurone ensheathing were significantly enriched. In terms of molecular functions, protein binding, including signalling receptor binding and Ca^{2+} binding were all enriched. Regarding cellular components, the several GO plasma membrane classifications were enriched.

Pathways altered in the ageing PVN were investigated. Given the strict detection criterion *adjusted* p-value <0.05 and >1.5 $\log_2$ fold change (up or down), just two KEGG pathways were significantly enriched (Figure 37-B). The first one termed "neuroactive ligand-receptor interaction" and the second was "phototransduction". The individual differentially expressed genes from these groups were then mapped to the KEGG pathway for neuroactive ligand-receptor interaction (Figure 38) and phototransduction (Figure 39). Several hormones and elements of signal transduction are altered by ageing.

Is there a change in overall ion channel gene expression in the PVN with ageing?

To investigate whether there are clusters of significantly altered ion channel genes in the aged PVN, filtration of our FPKM files (read files) for just those ion channel genes known to be ion channels and subunit proteins took place. In this way, 223 genes were detected. Table 26 shows the top 50 (greatest abundance channel gene reads). Again, I used the DAPC multivariate technique analysis to see whether

there was a pattern of change in over-all ion channel gene expression (Figure 40). Figure 40-A shows the kernel density plot with clear separation of the PVN samples based only on ion channel genes and confirmed by correct prediction using the confusion matrix/ heatmap (Figure 40-B). Figure 40-C shows the channel genes contributing most strongly to this separation; most influential are Scn2a, Kcnd3 and Cacna2d1.

Table 26: Top 50 detected ion channels genes.

Gene ID	pval	Gene description
Scn7a	3.62E-08	Sodium channel protein
Kcnj10	1.68E-06	ATP-sensitive inward rectifier potassium channel 10
Kcng4	9.46E-06	Potassium voltage-gated channel modifier subfamily G member 4 (Potassium voltage-gated channel, subfamily G, member 4 (Predicted))
Cacna2d1	1.78E-05	Voltage-dependent calcium channel subunit alpha-2/delta-1
Kcnk1	5.50E-05	Potassium channel subfamily K member 1 (Inward rectifying potassium channel protein TWIK-1) (rTWIK) (Potassium channel K2P1)
Tmem37	6.69E-05	Voltage-dependent calcium channel gamma-like subunit
Kcns3	0.000108	Potassium voltage-gated channel subfamily S member 3 (Delayed-rectifier K(+) channel alpha subunit 3) (Voltage-gated potassium channel subunit Kv9.3)
Cacnb3	0.000212	Voltage-dependent L-type calcium channel subunit beta-3 (CAB3) (Calcium channel voltage-dependent subunit beta 3)
Scn9a	0.00023	Sodium channel protein type 9 subunit alpha (Peripheral sodium channel 1) (PN1) (Sodium channel protein type IX subunit alpha) (Voltage-gated sodium channel subunit alpha Nav1.7)
Cacna2d2	0.000413	Voltage-dependent calcium channel subunit alpha-2/delta-2
Clcn4	0.000447	Chloride channel protein
Kcnab3	0.000501	Voltage-gated potassium channel subunit beta-3 (K(+) channel subunit beta-3) (Kv-beta-3) (RCK beta3)
Kcna1	0.000859	Potassium voltage-gated channel subfamily A member 1 (RBKI) (RCK1) (Voltage-gated potassium channel subunit Kv1.1)
Scn2a	0.001162	Sodium channel protein
Kcne2	0.003513	Potassium voltage-gated channel subfamily E member 2 (MinK-related peptide 1) (Minimum potassium ion channel-related peptide 1) (Potassium channel subunit beta MiRP1)
Kcnj5	0.004431	G protein-activated inward rectifier potassium channel 4 (GIRK-4) (Cardiac inward rectifier) (CIR) (Heart KATP channel)

Cacna1c	0.005244	Voltage-dependent L-type calcium channel subunit alpha
Kcnn1	0.011869	Small conductance calcium-activated potassium channel protein 1
Scn3a	0.013498	Sodium channel protein
Asic4	0.01575	Acid-sensing ion channel 4 (Amiloride-sensitive cation channel 4, pituitary, isoform CRA_a)
Cacna1b	0.015889	Voltage-dependent N-type calcium channel subunit alpha
Cacfd1	0.01657	Calcium channel flower homolog (Calcium channel flower domain-containing protein 1)
Trpv3	0.016852	Transient receptor potential cation channel, subfamily V, member 3
Kcnc1	0.017028	Potassium voltage-gated channel subfamily C member 1 (NGK2) (RAW2) (Voltage-gated potassium channel subunit Kv3.1) (Voltage-gated potassium channel subunit Kv4)
Kcnd3	0.018429	Potassium voltage-gated channel subfamily D member 3
Kcna3	0.024902	Potassium voltage-gated channel subfamily A member 3 (RCK3) (RGK5) (Voltage-gated potassium channel subunit Kv1.3) (Voltage-gated potassium channel subunit Kv3)
Trpv4	0.025997	Transient receptor potential cation channel subfamily V member 4 (TrpV4) (Osm-9-like TRP channel 4) (OTRPC4) (Vanilloid receptor-related osmotically-activated channel) (VR-OAC)
Catsperg	0.026949	Cation channel sperm-associated auxiliary subunit gamma
Scn1a	0.029337	Sodium channel protein
Kcnt2	0.031272	Potassium channel subfamily T member 2
Kcnk2	0.034713	Potassium channel subfamily K member 2 (Outward rectifying potassium channel protein TREK-1)
Kcnj8	0.039421	ATP-sensitive inward rectifier potassium channel 8 (Inward rectifier K(+) channel Kir6.1) (Potassium channel, inwardly rectifying subfamily J member 8) (uKATP-1)
Kcnab2	0.046071	Voltage-gated potassium channel subunit beta-2
Kcne3	0.04779	Potassium voltage-gated channel subfamily E member 3 (MinK-related peptide 2) (Minimum potassium ion channel-related peptide 2) (Potassium channel subunit beta MiRP2)
Kcnh6	0.048659	Potassium voltage-gated channel subfamily H member 6
Cacng2 Stg	0.049214	Voltage-dependent calcium channel gamma-2 subunit (Neuronal voltage-gated calcium channel gamma-2 subunit) (Stargazin) (Transmembrane AMPAR regulatory protein gamma-2) (TARP gamma-2)
Kcnk13	0.053493	Potassium channel subfamily K member 13 (Potassium channel, subfamily K, member 13)
Kcnc3	0.055728	Potassium voltage-gated channel subfamily C member 3
Kcnh7	0.062349	Potassium voltage-gated channel subfamily H member 7

Scn4b	0.0642	Sodium channel subunit beta-4
Scn5a	0.067009	Sodium channel protein
Scn3b	0.077066	Sodium channel subunit beta-3
Cacnb2	0.08413	Calcium channel, voltage-dependent, beta 2 subunit, isoform CRA_d (Voltage-dependent L-type calcium channel subunit beta-2)
Scnm1	0.084661	Sodium channel modifier 1 (Sodium channel modifier 1 (Predicted), isoform CRA_a)
Clcc1	0.085171	Chloride channel CLIC-like 1, isoform CRA_c (Chloride channel CLIC-like protein 1)
Cngb1	0.08554	Cyclic nucleotide-gated channel beta 1
Clca1	0.092138	Chloride channel accessory 1 (Chloride channel calcium activated 3 (Predicted))
Unc79	0.098502	Unc-79 homolog, NALCN channel complex subunit
Clcn6	0.101184	Chloride channel protein
Kcnh8	0.104129	Potassium voltage-gated channel subfamily H member 8 (Potassium voltage-gated channel, subfamily H, member 8, isoform CRA_b)

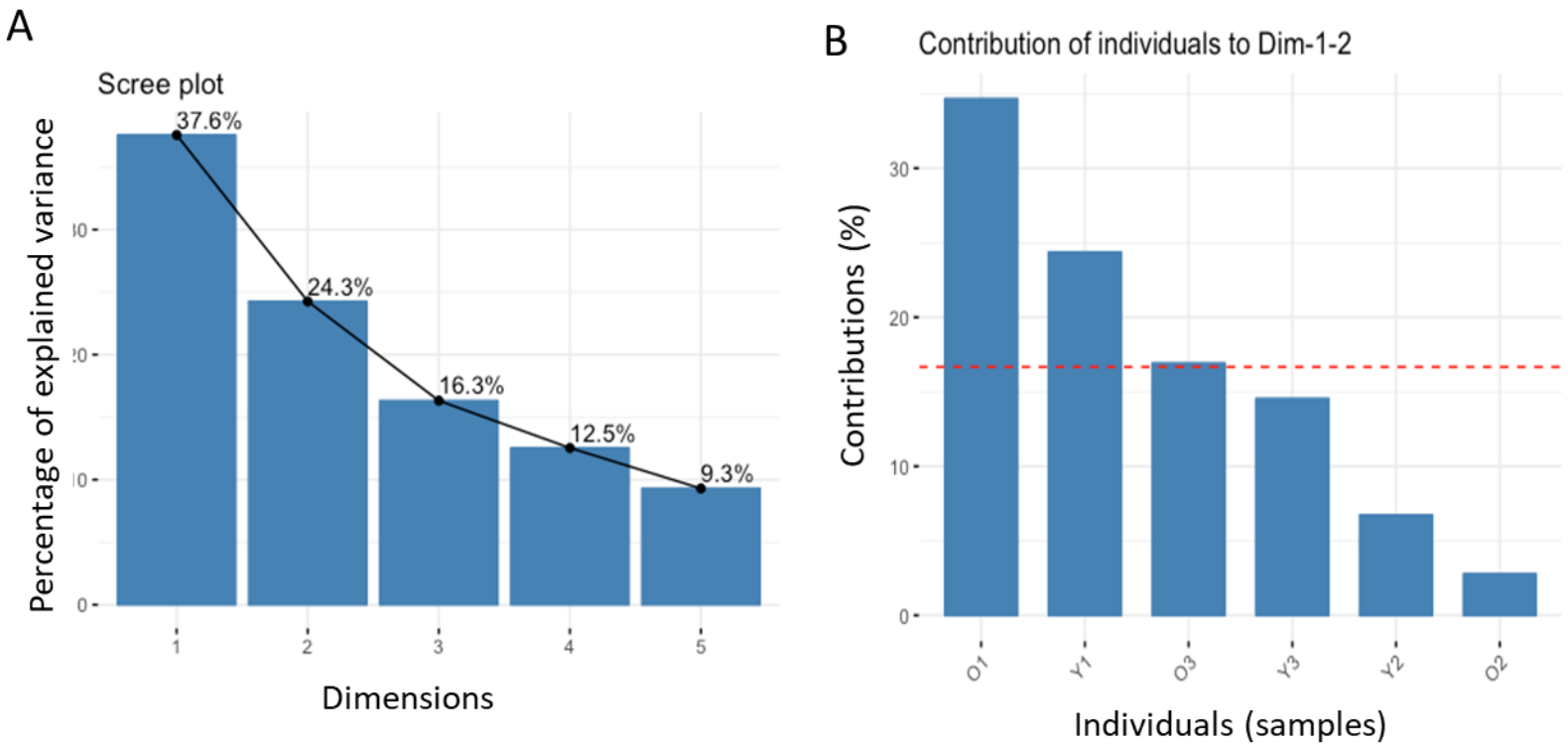

Figure 33: PCA analysis of young and old PVN.

A. *shows the scree plot for the 5 principle components used to reduce the dimensionality of the PVN young old datasets, approximately 16,000 variables (genes) reduced to 5 variables (PC) with 6 subjects; 3 young and 3 old male rats. PCA Component 1 alone accounts for approximately 37% of the variance in the data.* ***B.*** *Contribution plot showing the relative contributions of each of the six subjects to the principal components. The red dotted line indicates the mean contribution. The first Old subject contributes most to the variability and the second contributes least.*

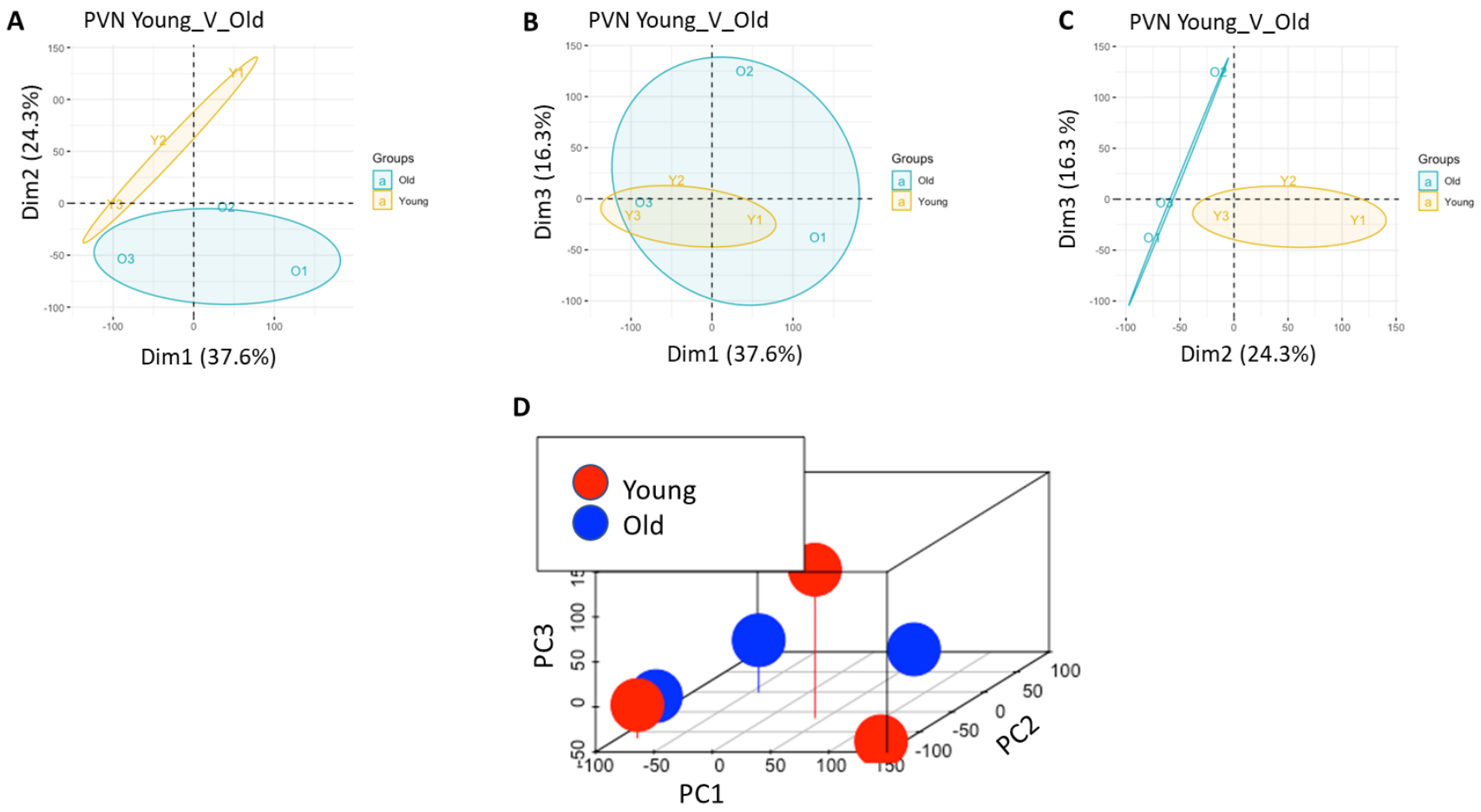

Figure 34: Principle component, k-mean clustering and combined scatter plot of young and old PVN.
A, B *and* ***C*** *show plots of PC1 vs PC2, PC1 vs PC3 and PC2 vs PC3 (Dim=PC). The shaded circles show the unsupervised k mean cluster 95% confidence intervals thus there is a clear statistical separation between young and old when combining PC1 and PC2, or PC2 and 3.* ***D.*** *3D plot showing all three principal components plotted against each other.*

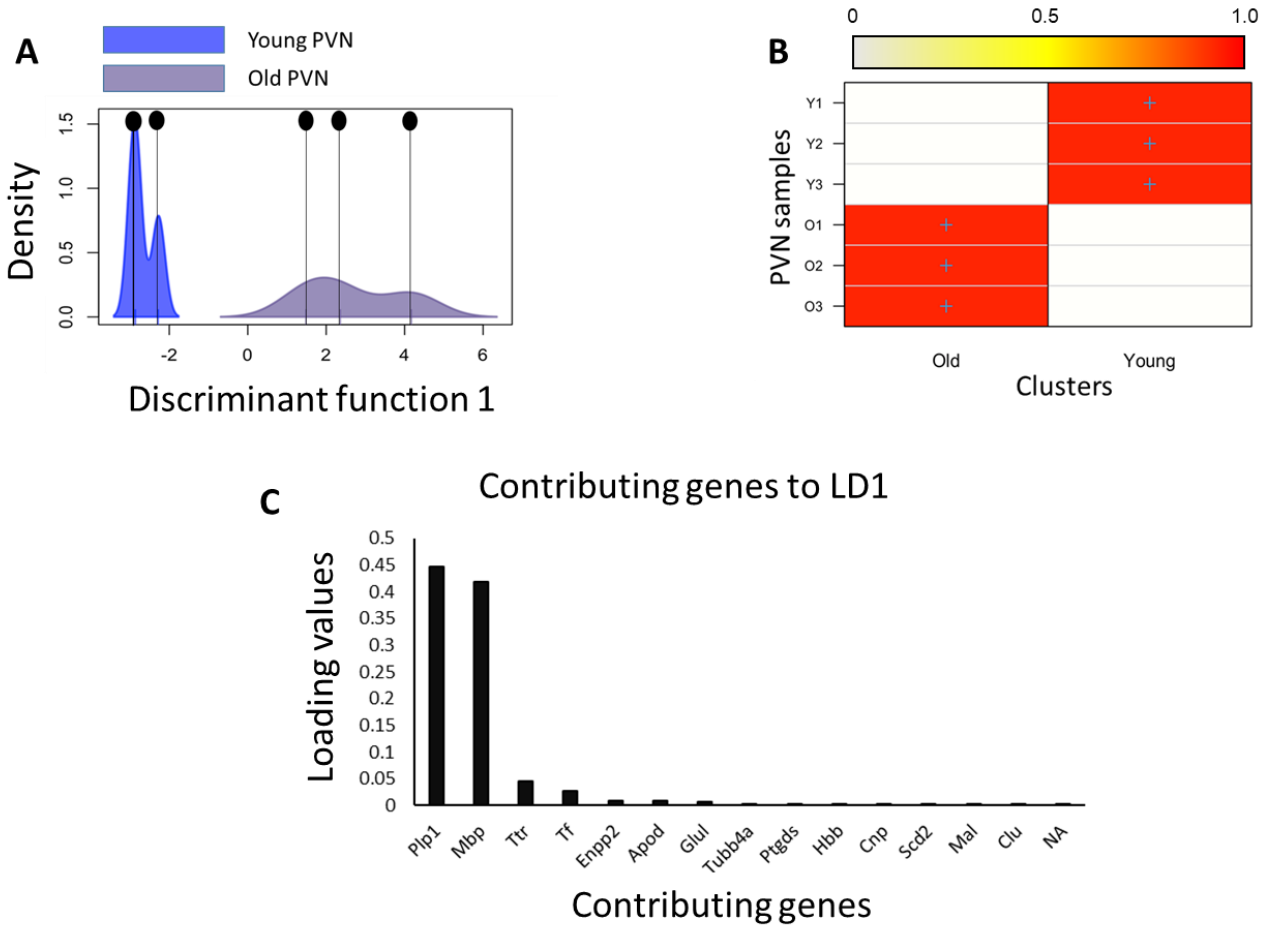

Figure 35: Discriminant (DA-PCA) analysis of ageing effects on PVN (all genes).
A. *Kernel density plots of the discriminant component coordinates for the young and old groups; co-ordinates on the x-axis and density on the y-axis. There is a good clear separation between young and old samples.* ***B.*** *A graphical confusion matrix showing the actual group membership (y-axis) and predicted cluster membership (given by colour and x-axis). All groups are correctly clustered with greater than 0.9 probability.* ***C.*** *The top 15 contributors to the linear discriminator function; Plp1; proteolipid protein 1, Mbp; myelin basic protein, Ttr; transthyretin, Tf; transferrin, Enpp2; ectonucleotide pyrophosphatase/phosphodiesterase 2, Apod; apolipoprotein D, Glul; glutamate-ammonia ligase, Tubb4a; tubulin, beta 4A class IVa, Ptgds; prostaglandin D2 synthase, Hbb; haemoglobin subunit beta, Cnp; 2',3'-cyclic nucleotide 3' phosphodiesterase, Scd2; stearoyl-Coenzyme A desaturase 2, Mal; mal, T-cell differentiation protein, Clu; clusterin, NA; Unidentified gene*.

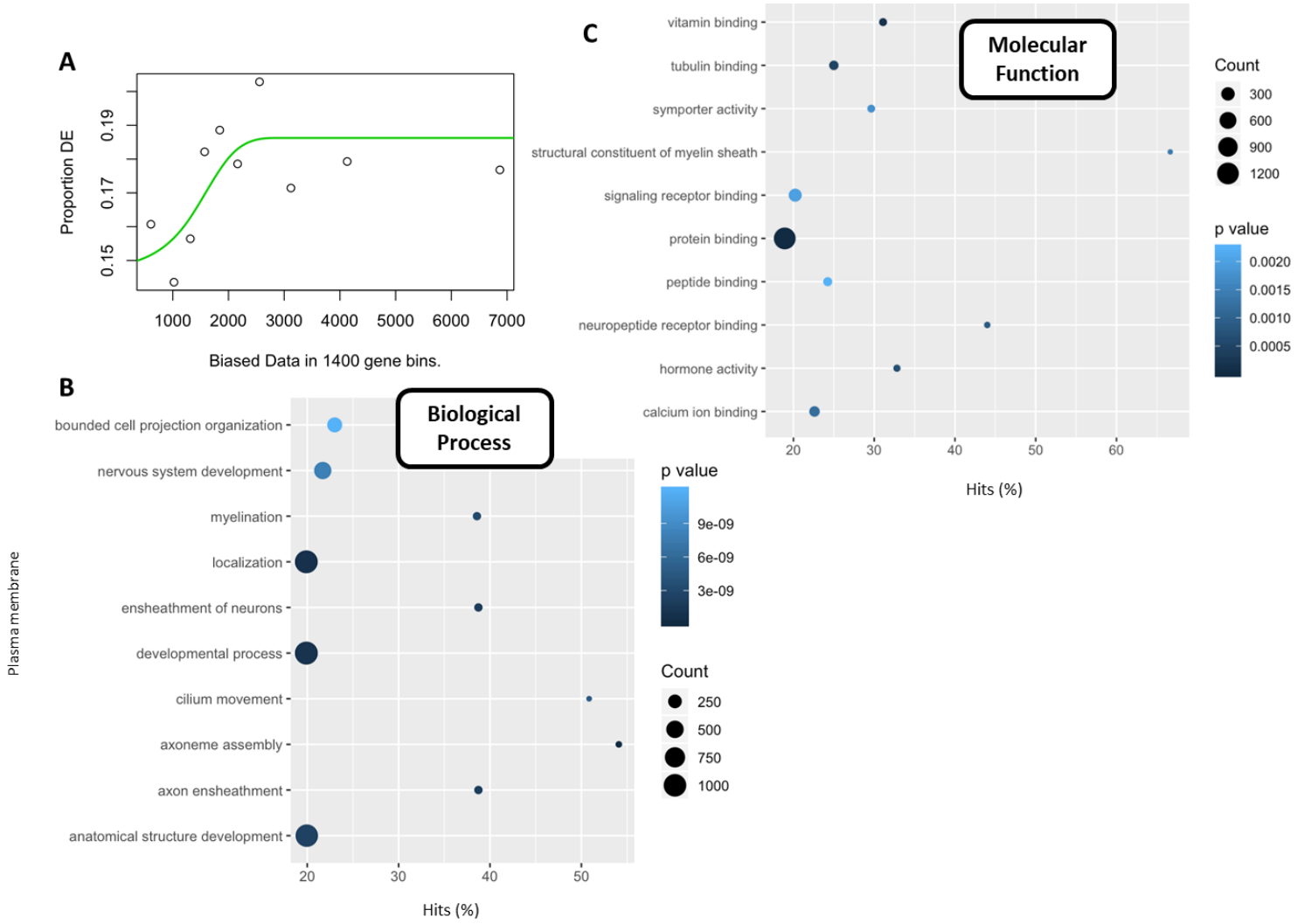

Figure 36: Analysis of Gene Ontology (GOs) of young and old PVN.
A. *Probability weighting function curve relating the length of the gene (x-axis) to the proportion of differentially expressed (DE) genes (y-axis), for that length bias. This curve is fit with the GESEQ package to allow subsequent enrichment analyses to eliminate bias due to the length of the gene.* ***B.*** *Top 10 enriched biological processes (by p-value) between young and old PVN tissue. The x-axis "Hits %", is the number of DE in each category/total number of genes (present) in that category. C. Top 10 enriched molecular functions, all elements as described for A.*

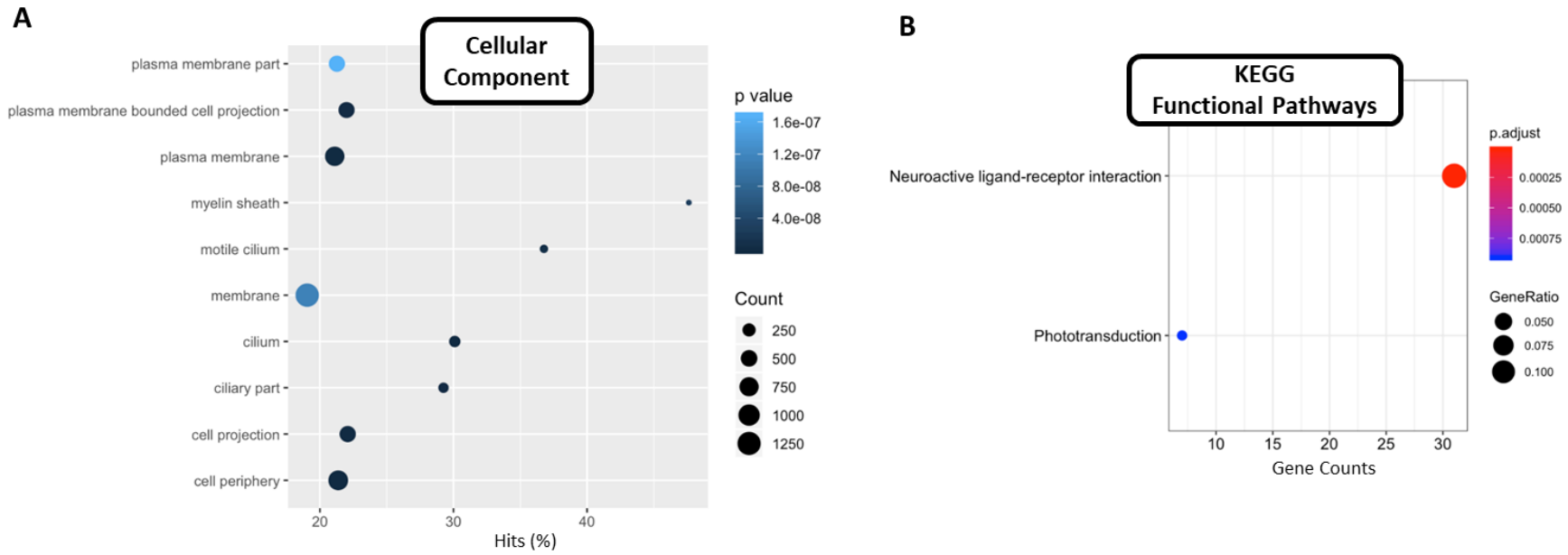

Figure 37:Analysis of GO and functional pathways comparing young and old PVN.
A. *Top 10 enriched cellular components (by p-value) between young and old PVN tissue. The x-axis "Hits %", is the number of DE in each category/total number of genes (present) in that category.* ***B.*** *The significantly enriched KEGG pathways (qualification, FDR/adjusted p-value <0.05). The genes included in these pathways are illustrated in the previous Figure 38.*

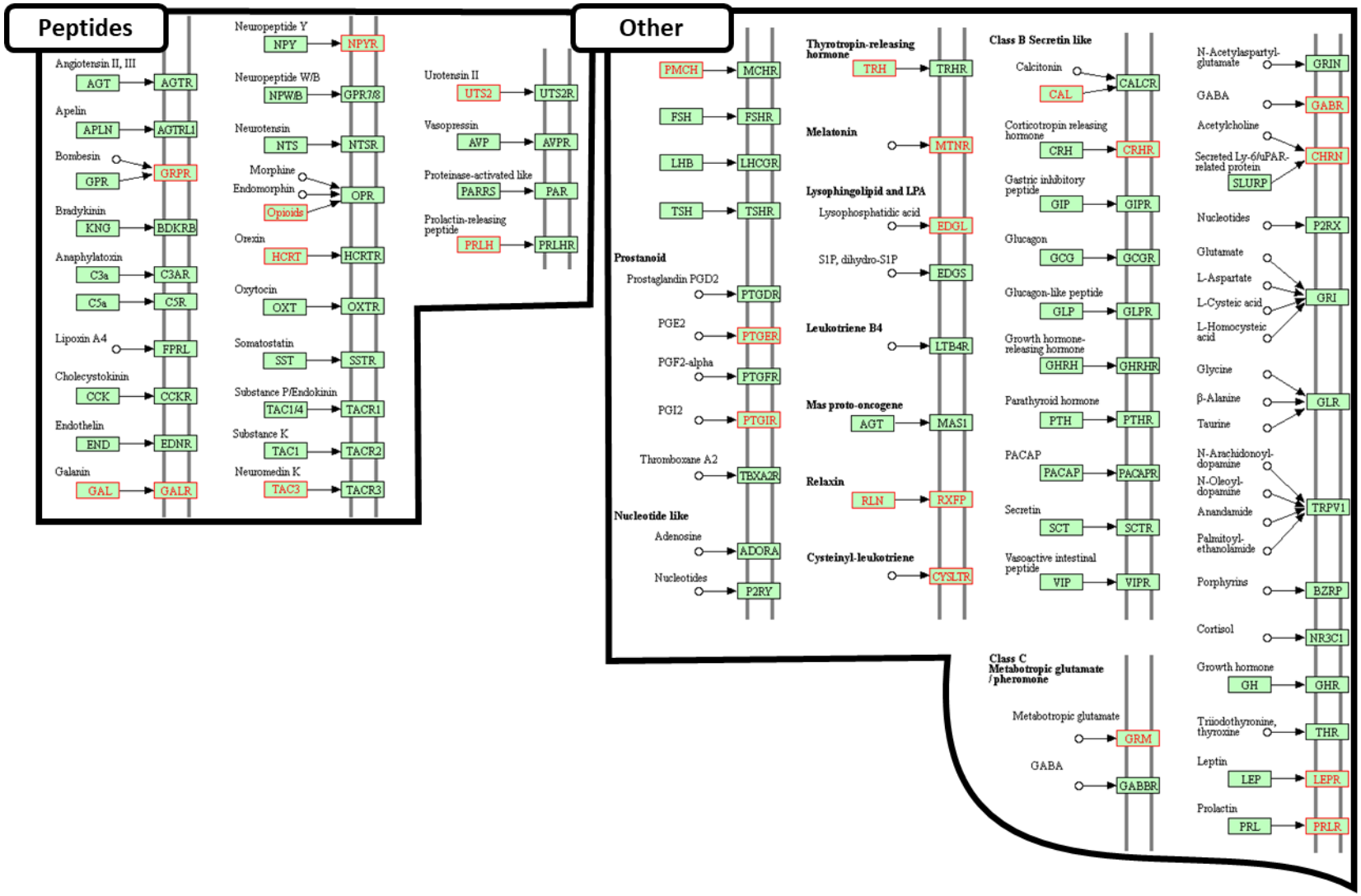

Figure 38: Scheme of the top enriched KEGG pathway comparing young and old PVN.
Several neuropeptides, hormones and prostanoids are changed in the dataset. Official KEGG ID rno04080, P-value 7.05E-08 adjusted p-value 1.83E-05. 31 genes present out of a total in the KEGG database of 261.

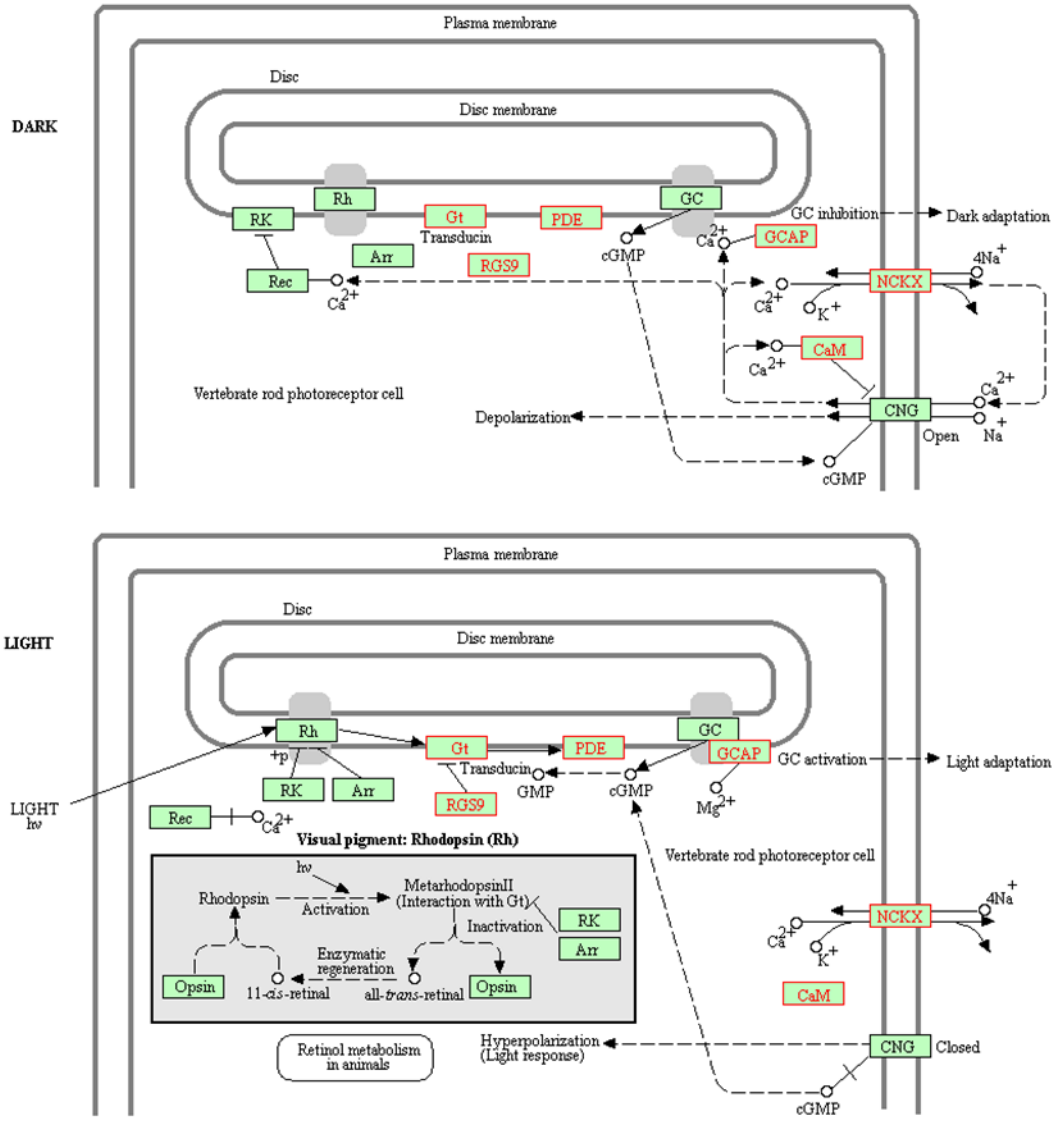

Figure 39: Schema of the second-top enriched KEGG pathway of young and old PVN.
Although classed as "phototransduction", the gene members themselves are all signalling molecules in other contexts too. Official KEGG ID, rno04744. 7/261 genes present. P-value 7.00E-06, adjusted p-value 0.0009.

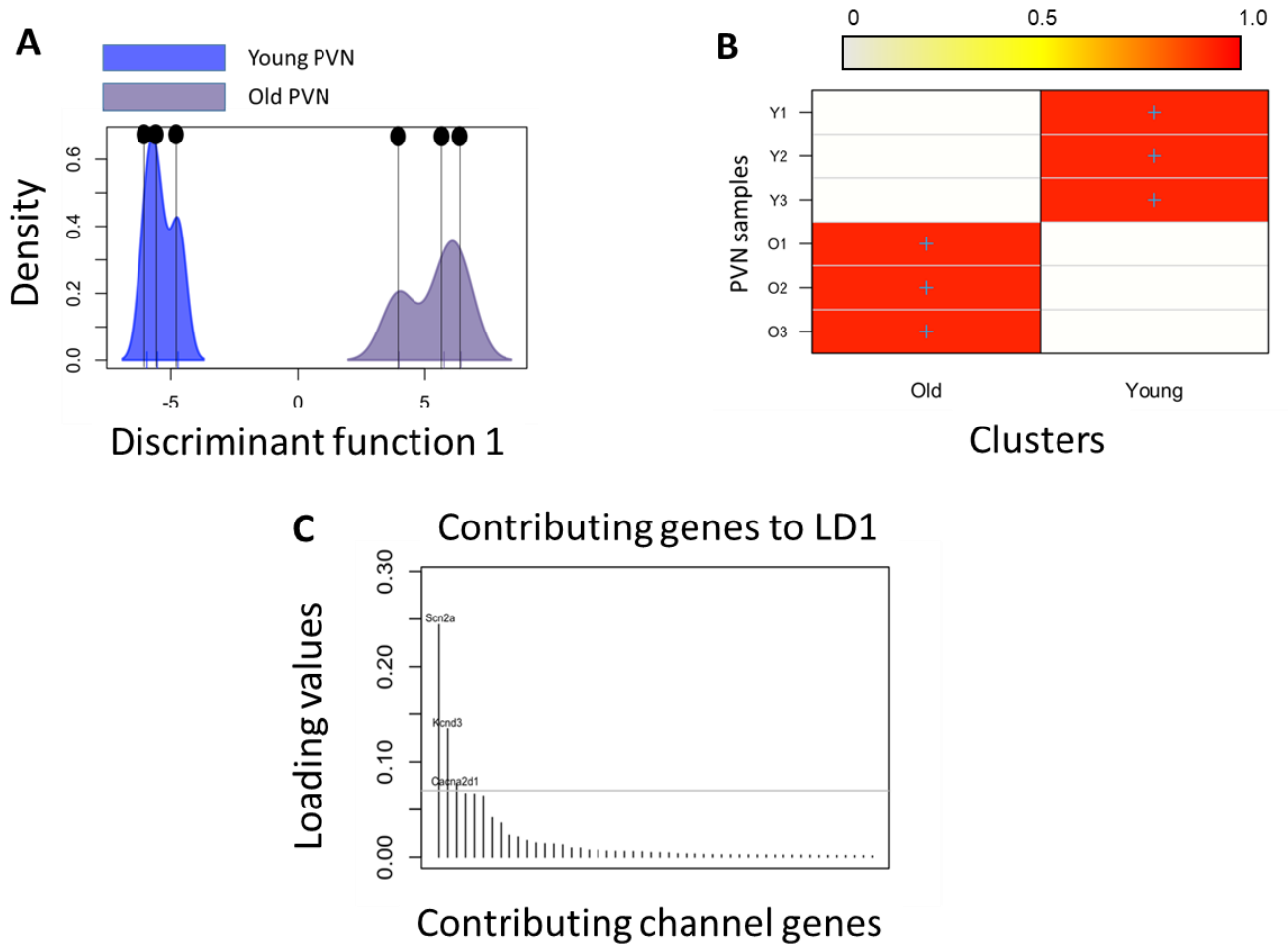

Figure 40: Discriminant Analyses (DA-PCA) of ageing effects on ion channels of young and old PVN.
A. *Kernel density plots of the discriminant component coordinates for the young and old groups; co-ordinates on the x-axis and density on the y-axis. There is a good clear separation between young and old samples based on just their ion channels.* ***B.*** *A graphical confusion matrix showing the actual group membership (x-axis) and predicted cluster membership colouration (y-axis). All groups are correctly clustered with greater than 0.95 probability.* ***C.*** *Loading graph showing the contributions of the most powerful contributors for the discriminant function. The most contributing genes are Scn2a; sodium voltage-gated channel alpha subunit 2, Kcnd3; potassium voltage-gated channel subfamily D member 3, and Cacna2d1: calcium voltage-gated channel auxiliary subunit alpha2delta 1.*

Which specific ion channel genes change with PVN ageing?

In total, 38 ion channel genes were differentially expressed with (pval<0.05) (Table 27). The top 10 channel genes (in terms of $\log_2$ fold change of 1.5, equivalent to approximately a 3-fold change) that were decreased in expression with age are shown in Table 28 while the top 10 channel genes that were increased by ageing are shown on Table 29.

Table 27: The 38 ion channel genes that were differentially expressed (pval<0.05).

Gene ID	Gene description	p-value
Scn7a	Sodium channel protein	3.62E-08
Kcnj10	ATP-sensitive inward rectifier potassium channel 10	1.68E-06
Kcng4	Potassium voltage-gated channel modifier subfamily G member 4 (Potassium voltage-gated channel, subfamily G, member 4 (Predicted))	9.46E-06
Cacna2d1	Voltage-dependent calcium channel subunit alpha-2/delta-1	1.78E-05
Kcnk1	Potassium channel subfamily K member 1 (Inward rectifying potassium channel protein TWIK-1) (rTWIK) (Potassium channel K2P1)	5.50E-05
Tmem37	Voltage-dependent calcium channel gamma-like subunit	6.69E-05
Kcns3	Potassium voltage-gated channel subfamily S member 3 (Delayed-rectifier K(+) channel alpha subunit 3) (Voltage-gated potassium channel subunit Kv9.3)	0.000108
Cacnb3	Voltage-dependent L-type calcium channel subunit beta-3 (CAB3) (Calcium channel voltage-dependent subunit beta 3)	0.000212
Scn9a	Sodium channel protein type 9 subunit alpha (Peripheral sodium channel 1) (PN1) (Sodium channel protein type IX subunit alpha) (Voltage-gated sodium channel subunit alpha Nav1.7)	0.00023
Cacna2d2	Voltage-dependent calcium channel subunit alpha-2/delta-2	0.000413
Clcn4	Chloride channel protein	0.000447
Kcnab3	Voltage-gated potassium channel subunit beta-3 (K(+) channel subunit beta-3) (Kv-beta-3) (RCK beta3)	0.000501
Kcna1	Potassium voltage-gated channel subfamily A member 1 (RBKI) (RCK1) (Voltage-gated potassium channel subunit Kv1.1)	0.000859
Scn2a	Sodium channel protein	0.001162
Kcne2	Potassium voltage-gated channel subfamily E member 2 (MinK-related peptide 1) (Minimum potassium ion channel-related peptide 1) (Potassium channel subunit beta MiRP1)	0.003513
Kcnj5	G protein-activated inward rectifier potassium channel 4 (GIRK-4) (Cardiac inward rectifier) (CIR) (Heart KATP channel)	0.004431
Cacna1c	Voltage-dependent L-type calcium channel subunit alpha	0.005244

Kcnn1	Small conductance calcium-activated potassium channel protein 1	0.011869
Scn3a	Sodium channel protein	0.013498
Asic4	Acid-sensing ion channel 4 (Amiloride-sensitive cation channel 4, pituitary, isoform CRA_a)	0.01575
Cacna1b	Voltage-dependent N-type calcium channel subunit alpha	0.015889
Cacfd1	Calcium channel flower homolog (Calcium channel flower domain-containing protein 1)	0.01657
Trpv3	Transient receptor potential cation channel, subfamily V, member 3	0.016852
Kcnc1	Potassium voltage-gated channel subfamily C member 1 (NGK2) (RAW2) (Voltage-gated potassium channel subunit Kv3.1) (Voltage-gated potassium channel subunit Kv4)	0.017028
Kcnd3	Potassium voltage-gated channel subfamily D member 3	0.018429
Kcna3	Potassium voltage-gated channel subfamily A member 3 (RCK3) (RGK5) (Voltage-gated potassium channel subunit Kv1.3) (Voltage-gated potassium channel subunit Kv3)	0.024902
Trpv4	Transient receptor potential cation channel subfamily V member 4 (TrpV4) (Osm-9-like TRP channel 4) (OTRPC4) (Vanilloid receptor-related osmotically-activated channel) (VR-OAC)	0.025997
Catsperg	Cation channel sperm-associated auxiliary subunit gamma	0.026949
Scn1a	Sodium channel protein	0.029337
Kcnt2	Potassium channel subfamily T member 2	0.031272
Kcnk2	Potassium channel subfamily K member 2 (Outward rectifying potassium channel protein TREK-1)	0.034713
Kcnj8	ATP-sensitive inward rectifier potassium channel 8 (Inward rectifier K(+) channel Kir6.1)	0.039421
Kcnab2	Voltage-gated potassium channel subunit beta-2	0.046071
Kcnj2	Inward rectifier potassium channel 2 (Inward rectifier K(+) channel Kir2.1) (IRK-1) (RBL-IRK1) (Potassium channel, inwardly rectifying subfamily J member 2)	0.046817
Kcne3	Potassium voltage-gated channel subfamily E member 3 (MinK-related peptide 2) (Minimum potassium ion channel-related peptide 2) (Potassium channel subunit beta MiRP2)	0.04779
Kcnh6	Potassium voltage-gated channel subfamily H member 6	0.048659
Cacng2	Voltage-dependent calcium channel gamma-2 subunit (Neuronal voltage-gated calcium channel gamma-2 subunit)	0.049214

10 ion channel genes lowered by log_2 FC with ageing:

Table 28: 10 ion channel genes lowered by log2 FC with ageing.

Gene ID	Gene description	pvalue	log2 F.C.
Scn7a	Sodium channel protein	3.62E-08	-1.977638569
Tmem37	Voltage-dependent calcium channel gamma-like subunit	6.69E-05	-1.459356853
Scn9a	Sodium channel protein type 9 subunit alpha (Peripheral sodium channel 1) (PN1) (Sodium channel protein type IX subunit alpha) (Voltage-gated sodium channel subunit alpha Nav1.7)	0.00023	-1.244866794
Kcne2	Potassium voltage-gated channel subfamily E member 2 (MinK-related peptide 1) (Minimum potassium ion channel-related peptide 1) (Potassium channel subunit beta MiRP1)	0.003513	-1.159645202
Cacna2d1	Voltage-dependent calcium channel subunit alpha-2/delta-1	1.78E-05	-1.144505451
Cacnb3	Voltage-dependent L-type calcium channel subunit beta-3 (CAB3) (Calcium channel voltage-dependent subunit beta 3)	0.000212	-1.004811765
Kcnj5	G protein-activated inward rectifier potassium channel 4 (GIRK-4) (Cardiac inward rectifier) (CIR) (Heart KATP channel)	0.004431	-0.992261906
Trpv4	Transient receptor potential cation channel subfamily V member 4 (TrpV4) (Osm-9-like TRP channel 4) (OTRPC4) (Vanilloid receptor-related osmotically-activated channel) (VR-OAC)	0.025997	-0.940472599
Cacna1c	Voltage-dependent L-type calcium channel subunit alpha	0.005244	-0.926429678
Kcnt2	Potassium channel subfamily T member 2	0.031272	-0.864399306

10 ion channel genes increased by log2 FC with ageing:

Table 29: 10 ion channel genes increased by log2 FC with ageing.

Gene ID	Gene description	pvalue	log2 F.C.
Kcnj10	ATP-sensitive inward rectifier potassium channel 10	1.68E-06	1.548474713
Kcns3	Potassium voltage-gated channel subfamily S member 3 (Delayed-rectifier K(+) channel alpha subunit 3) (Voltage-gated potassium channel subunit Kv9.3)	0.000108	1.526071011
Kcnab3	Voltage-gated potassium channel subunit beta-3 (K(+) channel subunit beta-3) (Kv-beta-3) (RCK beta3)	0.000501	1.321511049
Kcng4	Potassium voltage-gated channel modifier subfamily G member 4 (Potassium voltage-gated channel, subfamily G, member 4 (Predicted))	9.46E-06	1.212143787
Kcnk1	Potassium channel subfamily K member 1 (Inward rectifying potassium channel protein TWIK-1) (rTWIK) (Potassium channel K2P1)	5.50E-05	1.067982226
Trpv3	Transient receptor potential cation channel, subfamily V, member 3	0.016852	0.976391231
Cacna2d2	Voltage-dependent calcium channel subunit alpha-2/delta-2	0.000413	0.973709449
Asic4	Acid-sensing ion channel 4 (Amiloride-sensitive cation channel 4, pituitary, isoform CRA_a)	0.01575	0.950699284

Kcnn1	Small conductance calcium-activated potassium channel protein 1	0.011869	0.899366819
Kcna1	Potassium voltage-gated channel subfamily A member 1 (RBKI) (RCK1) (Voltage-gated potassium channel subunit Kv1.1)	0.000859	0.861476331

5.4 Discussion

In this chapter, RNA-sequencing from young and old rat PVN was carried out. Analysis of these data bioinformatically with a range of the latest powerful genomic tools took place. Major alterations in gene expression generally and also specifically in the expression of ion channel genes were found. In terms of association with functional pathways, KEGG analysis revealed that many genes associated with neuropeptide signalling were altered.

The PVN ageing model

The first point of note from this work is to clarify that genuine ageing is studied here, rats allowed to naturally grow to old age in a way not usually done with laboratory animals for ethical reasons. Our group has a Home Office licence to allow this and as far as I could see there was no evidence of pathology in our old rats. So, this model seems to be healthy ageing. Rodents do suffer a number of age-related diseases just like humans (Bellantuono and Potter, 2016), but in fact, there is little evidence of them naturally developing hypertension. This is interesting since the PVN is a key centre for control of the blood pressure and clearly many genetic changes in the elderly PVN were found. There is a caveat to this study, however, compared to *in vitro* models of ageing in that, by necessity, a punch of whole-tissue was used here. This means that it is expected to have had a mixed population of cells with, for example, glial cells, neurones, blood vessels and ependymal cells present. Despite this, it is noticeable that the majority of changes to see with functional enrichment and pathway analyses are those one might expect associated

with neurones; such as neuropeptide signalling and myelination. RNA-sequencing is still a relatively new technology, but perhaps in future, a study similar to this could be performed which used the even newer technique of *single-cell sequencing* (Ziegenhain et al., 2017). In that way it would theoretically be possible to get profiles of the ageing transcriptome of different types of cells; glia, neurone and so on.

Over-all changes in gene expression

The effective with multivariant analyses to separate the young and old populations based on the transcriptomic data is remarkable. In our aorta and vascular smooth muscle study, for example, many principal components were needed to apply to get good separation, but here the simplest model was effective. The conclusion here is that the elderly PVN is very different from the young PVN. Perhaps changes in the brain are more striking than changes in the peripheral nervous system. Functional clustering revealed that myelination is changed in ageing, it would be interesting to investigate whether this phenomenon also occurs in people. Myelin allows neurones to conduct faster and so loss of myelin could slow conduction rates in the older brain although myelination has been observed throughout life (Callaghan et al., 2014, Peters, 2002, Nasrabady et al., 2018, Hill et al., 2018). The changes in neurotransmitters and receptors ("neuroactive ligand and receptors") are also remarkable since these are the control elements of all neurones and in the future, it may be possible to input these changes into models of paraventricular neurone control (Lewis et al., 2010) to see if these changes contribute to the changes in autonomic control well established in the literature (Hotta and Uchida, 2010, Parashar et al., 2016, Fu et al., 2006, Pal et al., 2014). The changes identified in the GO enrichment are of course associations/correlations, not *causation.* One cannot tell from these data whether the changes contribute towards ageing dysfunction or result from dysfunction. Causal analysis is now possible, however (Kramer et al., 2014, Pearl, 2009) and this is implemented in Ingenuity Pathway Analysis (IPA) software (QIAGEN Inc., https://www.qiagenbioinformatics.com/products/ingenuitypathway-analysis) marketed by Qiagen

(Qiagen Inc., UK). The list of differentially expressed genes is entered into IPA to probe upstream regulator, those factors that could cause the changes to see. IPA returned many of these, but in terms of upstream regulators, TNF was amongst the top hits (activation z-score -3.2, p-value 0.000006). In terms of causal regulators vasopressin, a key PVN regulator involved with activation of the sympathetic nervous system (Rossi and Maliszewska-Scislo, 2008) was also identified to have reduced activity (z-score -3.3, p-value 1.74E-10). Also, there was a reduction in hydrocortisone influence, a key regulator of stress. These changes in upstream causal regulators could be said to be the opposite to that potentially expected in an aged rat.

Changes in ion channel expression (decreases)

The first point of note here is that our data show that there is definitively a change in overall ion channel expression. DAPC shows a clear separation of populations (young versus old) with just 3 PCA. Our tables also show a number of differentially expressed genes in the PVN with ageing.

Among those channels that were lowered by $\log_2$ FC are sodium channels (Scn7a and Scn9a), calcium channels (Tmem37, Cacna2d1, Cacnb3 and Cacna1c), potassium channels (Kcne2, Kcnj5 and Kcnt2) and TRPV4. On the other hand, the top 10 channel genes that were increased by $\log_2$ FC are potassium channels (Kcnj10, Kcns3, Kcnab3, Kcng4, Kcnk1, Kcnn1 and Kcna1), TRPV3, ASIC4 and calcium channel (Cacna2d2). With the ion channels, functional clustering was not done because most channels have quite well-known functions already and the GO databases are not well populated with ion channels. So, for example, of the decreased ion channels, sodium channels are mainly responsible for the rising phase of action potentials (Novakovic et al., 2001).

Sodium ion channels (decreases)

Scn7a and Scn9a are voltage-gated sodium channels and since they are lowered with ageing, this could mean that the rise in action potential is expected to be altered. Scn7a encodes for a common isoform of voltage-gated sodium channels (O'Leary et al., 2016) that play roles in the proper functioning of neurons and muscles during action potential as they direct the diffusion of the Na^+ ions for membrane depolarization. Scn9a has been linked to several human channelopathies such as erythromelalgia, paroxysmal extreme pain disorder (PEPD), and channelopathy-associated insensitivity to pain (Bennett et al., 2019). In summary, these two voltage-gated sodium channels play roles in a proper action potential in neurons and muscles (Vargas-Alarcon et al., 2012).

Calcium ion channels (decreases)

Calcium channels are very critical channels and they carry out important functions at the cellular and tissue levels including the activation of calcium-dependent enzymes, muscle contraction, secretion of neurotransmitters and hormones, and gene transcription (Zamponi, 2016, Simms and Zamponi, 2014, Zamponi et al., 2015). Interestingly, all calcium channels (Tmem37, Cacna2d1, Cacnb3 and Cacna1c) that had lowered expression were voltage-gated channels. Therefore, the release of neurotransmitter may be affected due to the decreased expression of these channels. Less is known about the role of Cacna1c (L-type calcium channels) in the brain. This channel is responsible for prolonged action potential in the cardiac cell (which is also known as DHP receptors), dendrites and dendritic spines of cortical neurons; however, Cacna1c does also play a role in neural stem cell neurogenesis once activated (Zhu et al., 2019a). So, it's change could be linked to the developmental changes identified in the GO biological processes functional mapping. Cacna2d1 regulates calcium current density and activation/inactivation kinetics of the calcium channel and It has also been linked to epilepsy (Vergult et al., 2015). The Cacnb3 gene encodes the regulatory beta subunit of the voltage-gated calcium channel that gives rise to L-type calcium currents (Collin et al., 1994). Therefore, contribute to the regulation of surface expression and gating of calcium

channels and may also play a role in the regulation of transcription factors and calcium transport (O'Leary et al., 2016). TMEM37 is also a Ca ion channel (O'Leary et al., 2016). It is thought that it acts to stabilize the calcium channel in an inactivated (closed) state. It may also modulate calcium current when co-expressed with CACNA1G (O'Leary et al., 2016).

Potassium ion channels (decreases)

Potassium channels that were lowered with ageing in these samples are voltage-gated (kcnj5 and kcne2) and sodium activated (kcnt2). Kcnj5 is Potassium Inwardly Rectifying Channel Subfamily J Member 5. It encodes an integral membrane protein which belongs to one of seven subfamilies of *inward-rectifier potassium channel proteins* now termed potassium channel subfamily J (Doupnik et al., 1995). The encoded protein is a subunit of the potassium channel and has a greater tendency to allow potassium to flow into a cell rather than out of a cell (O'Leary et al., 2016). Kcne2 is potassium voltage-gated channel subfamily E regulatory subunit 2. Their diverse functions include regulating neurotransmitter release and neuronal excitability and cell volume (Pruitt et al., 2007). In non-neuronal tissues, they have roles modulating heart rate, insulin secretion, epithelial electrolyte transport, smooth muscle contraction (Pruitt et al., 2007) which may be replacements for "excitability" in neurones. Interestingly, this gene encodes a member of the potassium channel, voltage-gated that assembles with the KCNH2 gene product, a pore-forming protein, to alter its function and is expressed in nerve cells. This gene was upregulated by a one-fold change in our dataset. The final potassium channel gene differential expressed in ageing PVN tissue is Kcnt2. This is a potassium sodium-activated channel subfamily T member 2. Kcnt2 is an outward rectifying potassium channel and produces rapidly activating outward rectifier K^+ currents (Bhattacharjee et al., 2003). It is unusual in that it is activated by high intracellular sodium and chloride levels (Terrar, 1993, Bhattacharjee et al., 2003, Santi, 2006).

Transient receptor potential ion channels (decreases)

The transient receptor potential cation channel subfamily V member 4 (Trpv4) was also decreased In PVN ageing. Trpv4 is a non-selective calcium permeant cation channel involved in osmotic sensitivity and mechanosensitivity (Garcia-Elias et al., 2008). It is well known in the PVN and has been studied by our group where it links osmolarity to sympathetic activity (Feetham et al., 2015a, Feetham et al., 2015b). Change in this gene with age is very interesting since it may explain some of the changes in the sympathetic activity described earlier, but further experiments will be required to determine how.

Changes in ion channel expression (increases)

10 ion channel genes that were increased by log2 FC; potassium channels (Kcnj10, Kcns3, Kcnab3, Kcng4, Kcnk1, Kcnn1 and Kcna1), TRPV3, ASIC4 and calcium channel (Cacna2d2). In addition to these 10 channel genes, Gja1 was also increased by log2FC of 0.46 which is equivalent to approximately 3-fold change.

Potassium ion channels (increases)

The potassium channels that were increased in PVN with ageing are of different types; voltage-gated potassium channels (Kcnj10, Kcns3, Kcna1, Kcnab3 and Kcng4), calcium-activated potassium channels (Kcnn1), and two-pore domain potassium channel (Kcnk1).

Kcnj10 encodes ATP-sensitive inward rectifier potassium channel 10. It may be responsible for potassium buffering action of glial cells in the brain as these channels are characterized by a greater tendency to *allow potassium to flow into the cell* rather than out of it (Pruitt et al., 2007). Their voltage dependence is regulated by the concentration of extracellular potassium; as external potassium is raised, the voltage range of the channel opening shifts to more positive voltages. The inward rectification is mainly due to the blockage of outward current by internal magnesium (Pruitt et al., 2007). Since these channels may also be involved with control of, or response to, glucose levels in the brain (Rivera-Aponte et al., 2015), their change may also indicate some disturbance to glucose regulation in older rats.

Potassium voltage-gated channel subfamily S member 3 (Kcns3) form the largest and most diversified class of ion channels and are present in both excitable and non-excitable cells (Stocker and Kerschensteiner, 1998). Their main functions are associated with the regulation of the resting membrane potential and the control of the shape and frequency of action potentials (Stocker and Kerschensteiner, 1998). Increased levels of these channels indicate hyperactivity of PVN (Georgiev et al., 2016). Potassium voltage-gated channel subfamily A member 1 (Kcna1) play role in repolarisation of membranes (Pruitt et al., 2007) and its disturbance is another indication of the major changes in neuronal control that appear to have occurred in the older rat brain.

Other ion channels (increases)

Transient receptor potential cation channel, subfamily V, member 3 (TRPV3) is one of the nonselective cation channels that function in a variety of processes such as temperature sensation and vasoregulation (Xu et al., 2002). Increased levels may indicate that dysregulation of temperature sensation as well as vasculature may lead to diseases such as hypertension due to blood vessels abnormality. Acid-sensing ion channel 4 (ASIC4) is expressed in the nervous system (Grunder et al., 2000, Hoshikawa et al., 2017). The pore of the channel through which ions selectively *flow from the extracellular side into the cytoplasm* is formed by the three TM2 regions of the trimer (Hanukoglu, 2017). They are cation channels with high permeability for sodium. In vitro, has no proton-gated channel activity (Grunder et al., 2000). They play roles in mechanosensation, chemosensation, nociception, and regulation of blood volume and pressure. These channels look and function like a tripartite funnel that directs the flow of Na^+ ions into the cytoplasm via the channel pore in the membrane (Hanukoglu, 2017). Since they change in ageing, this may contribute to age-related changes in chronic pain and blood pressure. The alpha-2/delta subunit of voltage-dependent calcium (Cacna2d2) channels was also increased. This channel regulates calcium current density and activation/inactivation kinetics of the calcium channel (Pruitt et al., 2014). Acts as a

regulatory subunit for P/Q-type calcium channel (CACNA1A), N-type (CACNA1B), L-type (CACNA1C OR CACNA1D) and possibly T-type (CACNA1G). Overexpression induces apoptosis (Carboni et al., 2003).

To summarize looking at the overall change in expression of ion channel genes in the ageing PVN, it seems that there is a tendency toward the loss of control of normal action potential, variability in hyperpolarization and depolarization, dysregulation of the osmotic and mechanosensitivity, and abnormal up-regulation of genes responsible for cell-to-cell communications which I may see with ageing. Future analyses will be needed to determine whether these are causal to, or resultant to the well-known neurodegeneration of ageing.

5.5 Conclusions

There are many changes that I have seen in this study with ageing PVN. For the individual gene analysis, it was interesting to find out that Gja1 (a gap junction) gene was upregulated in the old PVN. The functional annotation and pathway analysis showed changes that one might expect associated with neurons such as neuropeptide signalling and myelination which would be interesting to investigate whether this phenomenon also occurs in people. Thus, the elderly (rat) PVN is very different from the young PVN. Perhaps changes in the brain are more striking than changes in the peripheral nervous system.

Chapter 6 – Meta-analysis of NGS data

6.1 Introduction

NGS experiments provide powerful and extremely large amounts of data which can be useful in terms of gene expression studies. In this study, I utilized this technique to study the expression level in three different systems. These are musculoskeletal (FLS and Chondrocytes), cardiovascular (VSMC and Aorta) and nervous (PVN) systems. The expression level of different genes in these systems is expected to be different to suit specific functions according to anatomical locations. I created an "inflammageing" model by exposing rats to cytokines (10ng/ml IL-1β+TNFα) for 72hrs. I also used old rats as a natural ageing model. In this chapter, by comparing these together, considering the appropriate conditions (control vs cytokine) and age (young vs old), I hope to determine how close my inflammageing model to the real ageing model as well as detecting cross-tissue cytokine or age-related differential expression.

Usually, genes do not just change and express their effects individually. They usually affect the expression level of other genes either by upregulation, downregulation or sometimes there are no effects. Therefore, multivariate analysis is necessary, together with looking for changes in networks of genes including signalling pathways.

In this chapter, all samples will be grouped based on their condition, age, or both. Then, a combination of files will take place. Files of samples of the same group will be combined into one file for proper data processing. Next, a run of multivariate analysis for those samples will take place and will compare them with each other to track any significant changes in genes and more specifically the ion channel genes.

Aims

The aims in this chapter were to do a meta-analysis of NGS data by comparing all NGS data obtained from all samples with each other as follows:

- Compare all previous young samples against old samples

- Compare all previous control samples against cytokine (10ng/ml IL-1β+TNFα) treated samples
- Does the cytokine treatment regime follow the natural ageing, therefore; group 1 (Control with young) against group 2 (cytokine (10ng/ml IL-1β+TNFα) treated cells to aged cells/tissues).

6.2 Materials and methods

Next-generation sequencing (NGS)

Analyses were performed on RNA samples described earlier and extracted as described in the methods of chapter 2 and each chapter for specific optimization of the protocol. Chondrocyte RNA-sequencing data (from colleagues) was also added to this analysis. Multivariate analysis was performed for specific groups as follows; 1) young vs old samples, 2) control vs cytokine treated samples, and 3) comparison between two groups; group 1 (control and young) vs group 2 (cytokine and old). The analysis was started with PCA and where appropriate, linear discriminant analysis of PCA (DA-PCA) was used and increased the number of principal components until clear separation was obtained. For DA-PCA, to calculate false detection rate (FDR) data matrices were shuffled 100 or more times in R and the analyses re-run on each detection.

6.3 Results

Multivariate analysis of all young and old samples

In this chapter, a broader overview of the transcriptome profile that changes with ageing models was the goal to obtain. Again, one of the best ways of looking at this is by looking at clustered genes because when gene expression changes it does not have an individual effect. Instead, a group of genes change together, they cluster together, and this can be detected with multivariate analysis.

At the beginning, the multivariate analysis started with a PCA of 20 individuals (samples), 22038 genes and 10 principal components. This generated a scree plot (Figure 41-A) that shows percentages of explained variance by dimensions and 47% of the variance are explained by dimension 1 and samples' (individual) contribution to the difference between the two groups (Figure 41-B). The separation was not clear between PC1 and PC2 (Figure 42-A), PC1 and PC3 (Figure 42-B), or PC2 and PC3 (Figure 42-C) while (Figure 42-D) shows all the three-dimensions (PC1, PC2 and PC3) plotted against each other. An algorithm

is used to tell if the clusters are significant in n umber of dimensional space. Then, supervised multivariate analysis was performed with DA-PCA. As shown in (Figure 43-A), the better separation was obtained with 10 PCs and 1 discriminant function. Thus 10 PCs were used for DA-PCA throughout the rest of the study. To visualize the successful assignment of groups, a heatmap (Figure 43-B) was generated, and this shows that each sample was correctly predicted to its assigned (real) group with prediction probability of belonging (average *p*-value was 0.039). The prediction probability in this part was greater than 0.8, the closer to 1 the higher the accuracy while probability closer to zero is the less likely for a sample to be from that group. To calculate an FDR for this level of significance, a script was used which repeatedly shuffled the data matrix and then re-ran the analysis 1000 simulations of this returned none with mean p-value < 0.04 and so the FDR here is <0.01 and this gave the top 50 contributing genes to this discriminant function as shown on (Table 30) while (Figure 43-C) quantifies the top 15 contributors.

To look at the functions of these genes, a functional annotating clustering in David Bioinformatics Resources 6.8 was done. These genes were explained by 7 clusters with cluster 1 having the highest enrichment score (4.6 a.u.) and these genes were mainly involved with the extracellular space with a p-value of $3.5x10^{-8}$. Also, several pathways were enriched with KEGG pathway including "proteoglycans in cancer" (rno05205, $p=3.9x10^{-4}$), "PI3K-Akt signalling pathway" (rno04151, p=0.02), "Focal adhesion" (rno04510, p=0.03), and "ECM-receptor interaction" (rno04512, p=0.03). Gene ontology (GO) enrichment for young and old samples revealed a list of GOs in which 6 out of top 10 were related to "extracellular". Some of the GOs enrichment will be presented here; for example, "extracellular matrix" (GO: 0031012, p=4.48x10-9), "extracellular space" (GO:0005615, p=6.24x10-7), "ageing" (GO:0007568, p=5.3x10-6), "extracellular exosome" (GO:0070062, p=2.93x10-5), "response to cytokine" (GO:0034097, p=0.001), and "cellular response to interleukine-1" (GO:0071347, p=0.02). Also, protein classification of these genes was sought in David Bioinformatics Resources 6.8 which utilises the InterPro database. This database utilises several other databases to compare identifiable features to functionally classify new proteins. The main

enriched proteins returned were Fibronectin, type II, collagen-binding (IPR000562, p=3.52x10-4), Kringle-like fold[1] (IPR013806, p=0.002) (Patthy et al., 1984), and small leucine-rich proteoglycan, class I, decorin/asporin/byglycan (IPR016352, p=0.009).

Multivariate analysis of channel genes of all young and old samples

Also, DA-PCA for channel genes with 10 PCs to separate groups was performed. It turned out a clear separation (Figure 44-A). Also, a heatmap was generated that shows the correct belonging prediction of each sample to each group (Figure 44-B) with the probability of belonging of greater than 0.8. The top 15 contributing genes to this separation are shown in (Figure 44-C) while the top 50 genes contributing to the difference between all young and old are shown in Table 30

Table 30: top 50 genes contributed to the DA-PCA of all young and old samples.

Ensemble ID	Gene ID	LD1	GENE NAME
ENSRNOG00000001469	Eln	0.13142108	elastin
ENSRNOG00000012660	Postn	0.07869047	periostin
ENSRNOG00000012579	Tlcd1	0.073747397	TLC domain containing 1
ENSRNOG00000019414	Tmem79	0.054747875	transmembrane protein 79
ENSRNOG00000046313	Basp1	0.047793873	brain abundant, membrane attached signal protein 1
ENSRNOG00000046834	C3	0.045407123	complement C3
ENSRNOG00000053025	NA	0.041489768	NA
ENSRNOG00000016539	Mxd3	0.036130552	Max dimerization protein 3
ENSRNOG00000037894	NA	0.035376935	NA
ENSRNOG00000013442	Ciz1	0.021033757	CDKN1A interacting zinc finger protein 1
ENSRNOG00000000506	Tead3	0.017880638	TEA domain transcription factor 3
ENSRNOG00000003357	Col3a1	0.013672632	collagen type III alpha 1 chain
ENSRNOG00000039315	Cfap157	0.012637055	cilia and flagella associated protein 157
ENSRNOG00000024779	Polr2b	0.012610184	RNA polymerase II subunit B
ENSRNOG00000012840	Sparc	0.012275292	secreted protein acidic and cysteine-rich
ENSRNOG00000019992	Cnbd2	0.009221728	cyclic nucleotide binding domain containing 2
ENSRNOG00000048733	Nup62	0.009126601	nucleoporin 62
ENSRNOG00000026053	Grem1	0.008701938	gremlin 1, DAN family BMP antagonist
ENSRNOG00000008415	Nab2	0.008314069	Ngfi-A binding protein 2
ENSRNOG00000003931	Arsg	0.008303714	arylsulfatase G

1 These are domains that fold into large loops that are stabilized by 3 disulfide linkages. Kringle are important in protein-protein interactions.

ENSRNOG00000020389	Capn12	0.007851615	calpain 12
ENSRNOG00000023668	Scyl1	0.007526158	SCY1 like pseudokinase 1
ENSRNOG00000011971	C1s	0.006745817	complement C1s
ENSRNOG00000019052	Ankzf1	0.006590713	ankyrin repeat and zinc finger domain containing 1
ENSRNOG00000017420	Nudt6	0.005775042	nudix hydrolase 6
ENSRNOG00000016460	Clu	0.005549064	clusterin
ENSRNOG00000043451	Spp1	0.005485935	secreted phosphoprotein 1
ENSRNOG00000019162	Emc9	0.005151075	ER membrane protein complex subunit 9
ENSRNOG00000015499	Serinc4	0.005077154	serine incorporator 4
ENSRNOG00000003897	Col1a1	0.004990918	collagen type I alpha 1 chain
ENSRNOG00000016740	Fam210a	0.004720909	family with sequence similarity 210, member A
ENSRNOG00000057040	Spns2	0.004712189	sphingolipid transporter 2
ENSRNOG00000056819	Susd1	0.004396124	sushi domain containing 1
ENSRNOG00000001414	Serpine1	0.004217473	serpin family E member 1
ENSRNOG00000018233	Gas6	0.00406451	growth arrest specific 6
ENSRNOG00000020628	LOC103690068	0.004004462	immortalization up-regulated protein-like
ENSRNOG00000004094	Ptger1	0.003772715	prostaglandin E receptor 1
ENSRNOG00000009439	Eef1a1	0.003736281	eukaryotic translation elongation factor 1 alpha 1
ENSRNOG00000058068	Obscn	0.003647309	obscurin, cytoskeletal calmodulin and titin-interacting RhoGEF
ENSRNOG00000001229	Col18a1	0.003594128	collagen type XVIII alpha 1 chain
ENSRNOG00000054890	Flna	0.003481199	filamin A
ENSRNOG00000058560	Col2a1	0.003419738	collagen type II alpha 1 chain
ENSRNOG00000016488	Pltp	0.003390998	phospholipid transfer protein
ENSRNOG00000017206	Igfbp5	0.003372693	insulin-like growth factor binding protein 5
ENSRNOG00000023493	Creb3l4	0.003239972	cAMP responsive element binding protein 3-like 4
ENSRNOG00000008951	Rasl10a	0.003069361	RAS-like, family 10, member A
ENSRNOG00000019657	Mk1	0.002888024	Mk1 protein
ENSRNOG00000019477	Zmynd15	0.002877551	zinc finger, MYND-type containing 15
ENSRNOG00000008697	Ccn3	0.002804959	cellular communication network factor 3
ENSRNOG00000010529	Thbs2	0.00280402	thrombospondin 2

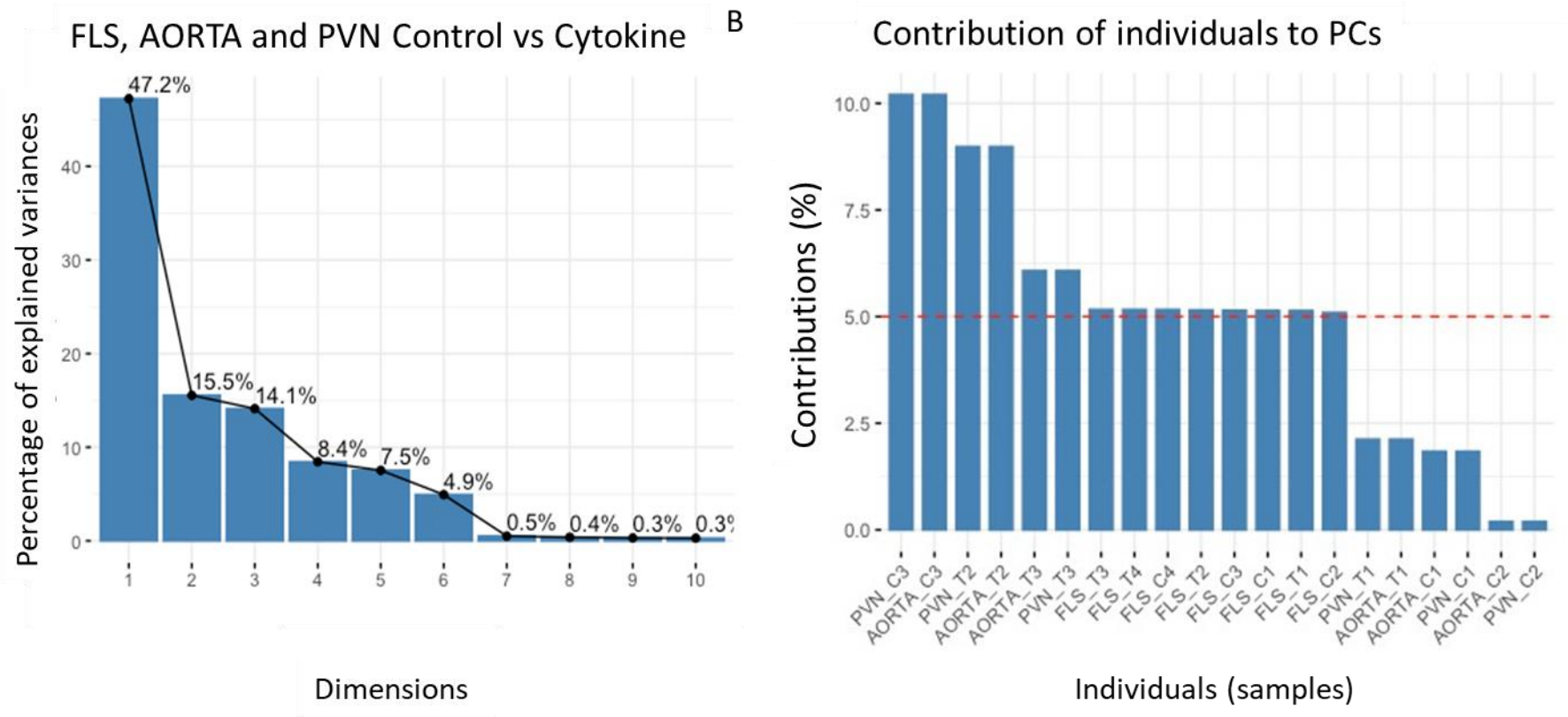

Figure 41: PCA analysis of all young and old of FLS, AORTA, and PVN.
PCA analysis of Young and Old rat FLS, AORTA, and PVN. A. shows the scree plot for the 10 principle components used to reduce the dimensionality of the FLS, AORTA, and PVN young old datasets, approximately 22038 variables (genes) reduced to 10 variables (PC) with 20 subjects; 10 young and 10 old male rats. PCA Component 1 alone accounts for approximately 47% of the variance in the data. B. Contribution plot showing the relative contributions of each of the 20 subjects to the principal components. The red dotted line indicates the mean contribution. The first four subjects contribute most to the variability and the second two contribute least.

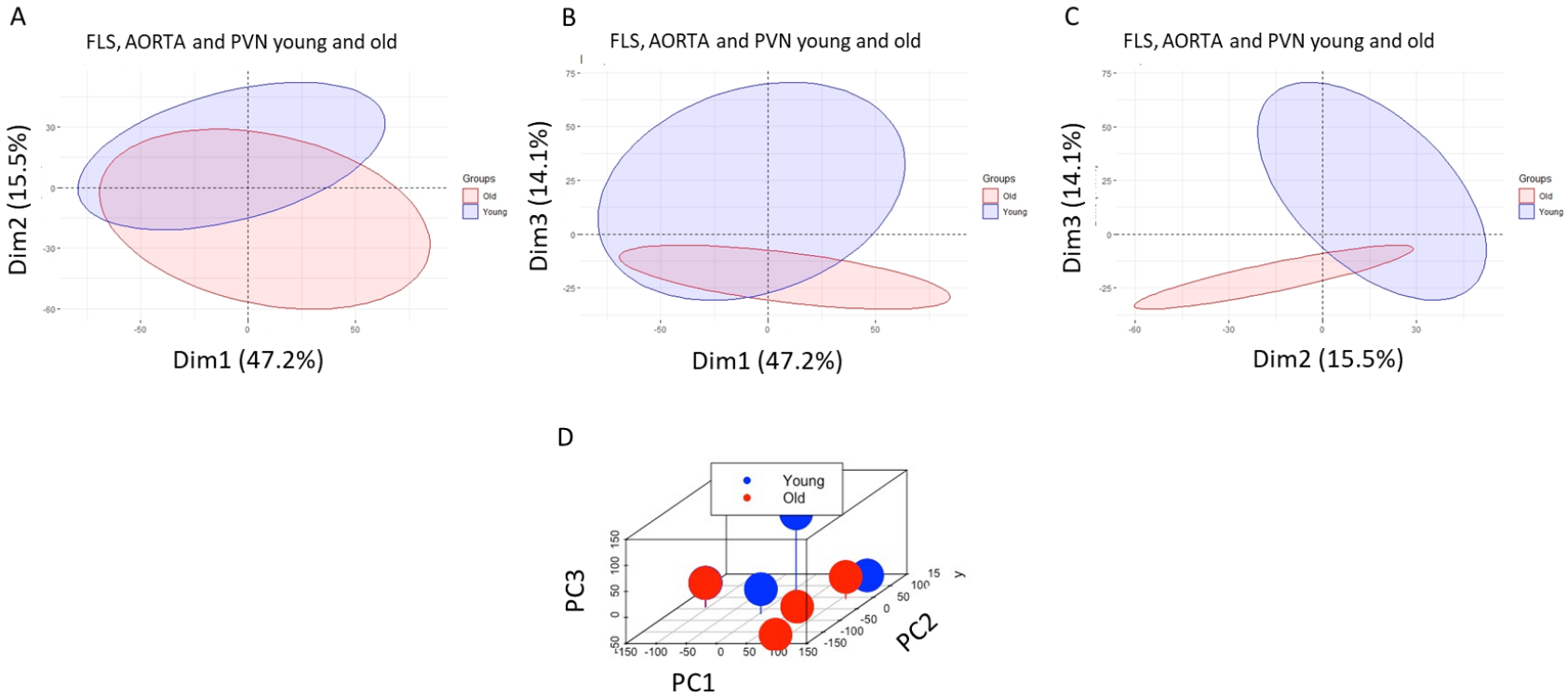

Figure 42: Principle component, k-mean clustering and combined scatter plot of all young and old of FLS, AORTA, and PVN.
A, B *and* ***C*** *show plots of PC1 vs PC2, PC1 vs PC3 and PC2 vs PC3 (Dim=PC). The shaded circles show the unsupervised k mean cluster 95% confidence intervals thus there is no clear statistical separation between young and old when combining PC1 and PC2, PC1 and PC3 or PC2 and PC3.* ***D.*** *3D plot showing all three principal components plotted against each other.*

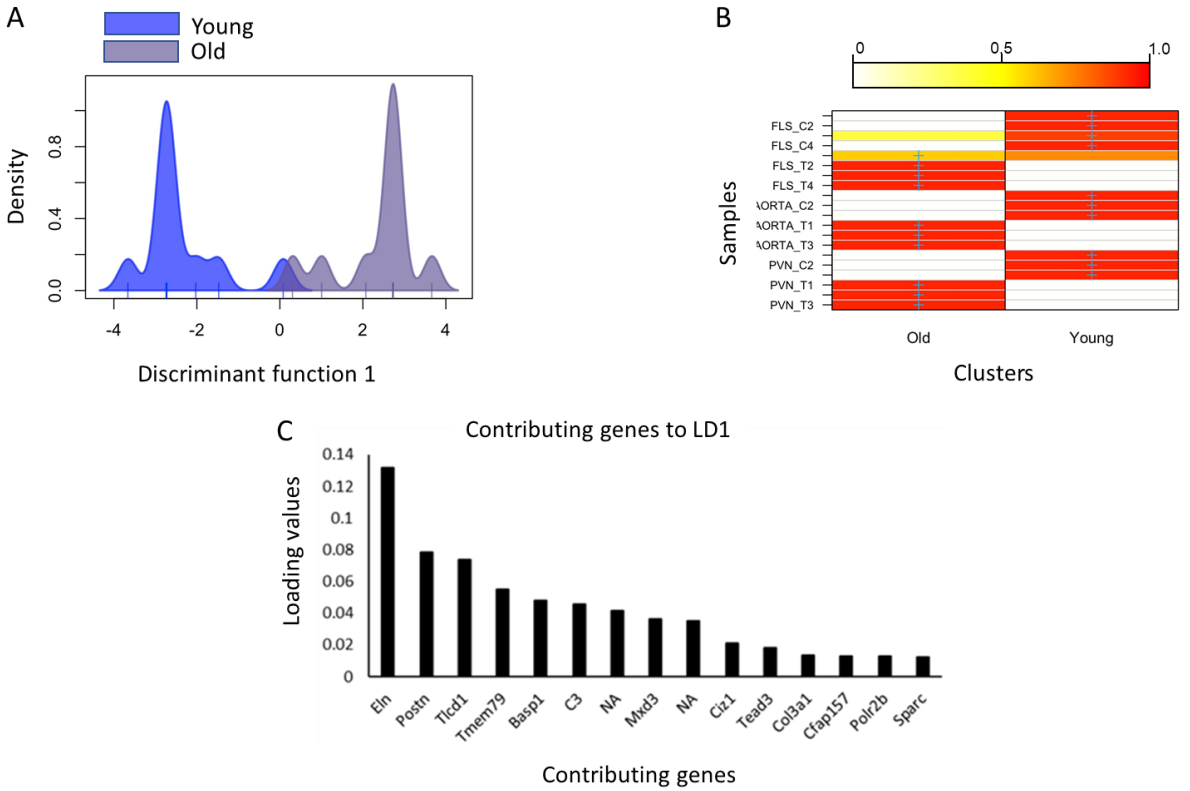

Figure 43: Discriminant Analyses of ageing Effects on all genes of all young and old of FLS, AORTA, and PVN.
A. *Shows the kernel density plots of the discriminant component coordinates for the young and old groups; co-ordinates on the x-axis and density on the y-axis. There is a good clear separation between young and old samples.* ***B.*** *A graphical confusion matrix showing the actual group membership (y-axis) and predicted cluster membership (on the y-axis). All groups are correctly clustered with greater than 0.8 probability except FLS_T1.* ***C.*** *The most powerful contributing genes to the linear discriminator function; Eln; elastin, Postn; periostin, Tlcd1; TLC domain containing 1, Tmem79; transmembrane protein 79, Basp1; brain abundant, membrane attached signal protein 1, C3; complement C3, NA; NA, Mxd3; Max dimerization protein 3, NA; NA, Ciz1; CDKN1A interacting zinc finger protein 1, Tead3; TEA domain transcription factor 3, Col3a1; collagen type III alpha 1 chain, Cfap157; cilia and flagella associated protein 157, Polr2b; RNA polymerase II subunit B, and Sparc; secreted protein acidic and cysteine-rich.*

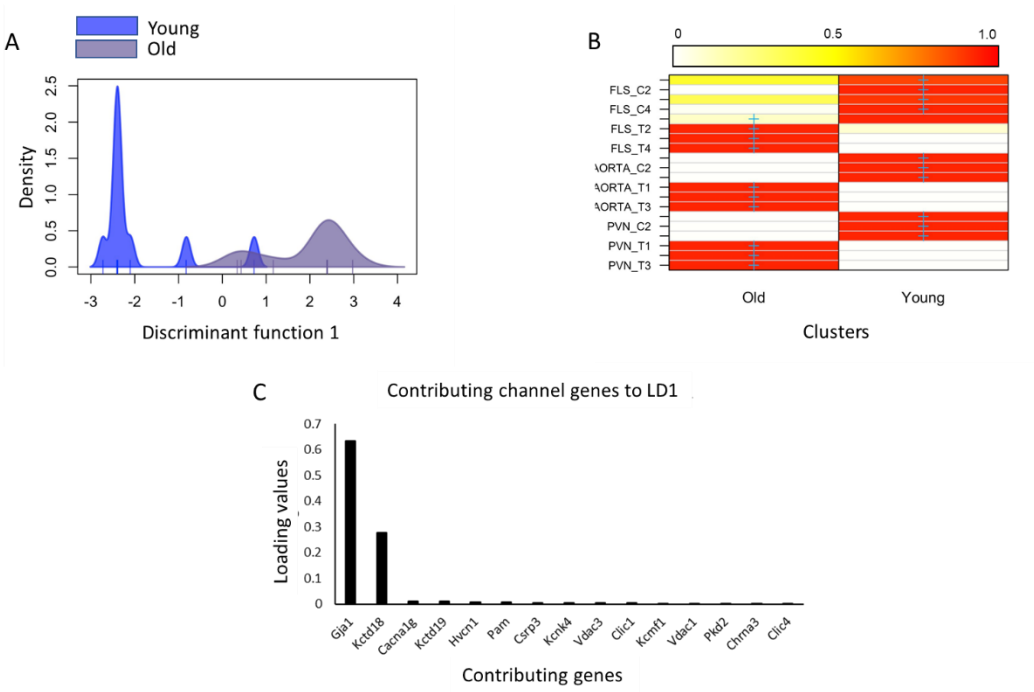

Figure 44: Discriminant Analyses of ageing Effects on channel genes of all young and old of FLS, AORTA, and PVN.
A. *Shows the kernel density plots of the discriminant component coordinates for the young and old groups; co-ordinates on the x-axis and density on the y-axis. There is a good clear separation between young and old samples.* ***B.*** *A graphical confusion matrix showing the actual group membership (y-axis) and predicted cluster membership (on the y-axis). All groups are correctly clustered with greater than 0.8 probability except some FLS samples.* ***C.*** *The most contributing genes to the linear discriminator function; Gja1; gap junction protein, alpha 1, Kctd18; potassium channel tetramerization domain containing 18, Cacna1g; calcium voltage-gated channel subunit alpha1 G, Kctd19; potassium channel tetramerization domain containing 19, Hvcn1; hydrogen voltage-gated channel 1, Pam; peptidylglycine alpha-amidating monooxygenase, Csrp3; cysteine and glycine-rich protein 3, Kcnk4; potassium two pore domain channel subfamily K member 4, Vdac3; voltage-dependent anion channel 3, Clic1; chloride intracellular channel 1, Kcmf1; potassium channel modulatory factor 1, Vdac1; voltage-dependent anion channel 1, Pkd2; polycystin 2, transient receptor potential cation channel, Chrna3; cholinergic receptor nicotinic alpha 3 subunit, Clic4; chloride intracellular channel 4.*

Multivariate analysis of all control and cytokine (10ng/ml TNFα+IL-1β for 72hrs) treated samples

In this multivariate analysis, NGS data from FLS, Aortic VSMC and chondrocytes (unpublished data kindly provided by RBJ group) were included. Again, multivariate analysis was used to separate groups (control vs cytokine treated samples). As before, the start was with PCA, this time with 22 individuals (samples), 22038 genes and 10 components. This PCA with 10 PCs generated a scree plot showing the percentage of explained variance by each dimension. Interestingly, more than 58% of the variance was explained by dimension 1 alone (Figure 45-A). Contributions of each sample (individual) to the separation is shown in (Figure 45-B). The separation between control and cytokine treated groups was not clear between PC1 and PC2 (Figure 46-A), PC1 and PC3 (Figure 46-B) or PC2 and PC3 (Figure 46-C) while Figure 46-D shows the 3D plot of all PCs against each other which again has no obvious clustering. Since the separation with PCA was not clear, A supervised multivariate analysis DA-PCA was done. 17 PCs were the appropriate number for the separation and since there are only two groups, there was only 1 discriminant function. The separation was much better as shown in (Figure 47-A). Also, a heatmap (Figure 47--B) shows belonging of each sample to their group and correct prediction. The predicted probability of belonging was greater than 0.9. The top 50 genes contributing to this separation are shown in Table 31 while (Figure 47-C) shows the top 15 of these contributing genes.

To find out the function of these genes, a functional annotating clustering in David Bioinformatics Resources 6.8 was used. These genes were explained by 10 clusters with cluster 1 having the highest enrichment score of 3.43 and these genes were mainly involved with signalling with a p-value of $1.4x10^{-5}$. Also, KEGG pathway enrichment showed several statistically significant pathways including “ECM-receptor interaction” (rno04512, $p=8.4x10^{-5}$), ”Focal adhesion” (rno04510, p=1.99x10-4), ”Protein digestion and absorption” (rno04974, p=0.002) and “PI3K-Akt signalling pathway” (rno04151, p=0.002). Five out of the top ten of

the main GO enrichments were again related to the extracellular space/matrix, the common GOs will be presented here. For example, ”extracellular matrix” (GO:0031012, p=4.13x10-10), “cell adhesion” (GO:0007155, p=2.98x10-5), “extracellular matrix organization” (GO:0030198, p=7.62x10-5), “angiogenesis” (GO:0001525, p=0.009), “ageing” (GO:0007568, p=0.04), and “cellular response to tumor necrosis factor” (GO:0071356, p=0.04) were the common GOs. The InterPro database revealed “Collagen triple helix repeat” (IPR008160, p=8.4x10-4) and “Fibrillar collagen, C-terminal” (IPR000885, p=0.03).

Multivariate analysis of differentially expressed channel genes of all control and cytokine (10ng/ml TNFα+IL-1β for 72hrs) treated samples

Next, DA-PCA on the data filtered for channel genes with 16 PCs to separate groups was performed. It turned out a clear separation as shown by kernel density plot (Figure 48-A). Again, a heatmap was generated that shows the correct belonging prediction of each sample to each group (Figure 48-B) with a predicted probability of belonging of greater than 0.9. The top 15 contributing genes to this separation are shown on (Figure 48-C) while the top 50 genes contributing to the difference between all control and cytokines are shown in Table 31.

Table 31: Top 50 genes contributing to the DA-PCA in all control and cytokine treated samples.

Ensemble ID	Gene ID	LD1	GENE NAME
ENSRNOG00000037894	AABR07068042.1	0.190076808	NA (NOT A KNOWN GENE)
ENSRNOG00000047907	LOC100912585	0.13849575	mitogen-activated protein kinase 7-like
ENSRNOG00000001469	Eln	0.106064575	elastin
ENSRNOG00000012660	Postn	0.095500481	periostin
ENSRNOG00000020389	Capn12	0.06325397	calpain 12
ENSRNOG00000020346	Best1	0.051078924	bestrophin 1
ENSRNOG00000046313	Basp1	0.034452234	brain abundant, membrane attached signal protein 1
ENSRNOG00000043451	Spp1	0.018173454	secreted phosphoprotein 1
ENSRNOG00000054890	Flna	0.012560313	filamin A
ENSRNOG00000012840	Sparc	0.011580614	secreted protein acidic and cysteine-rich
ENSRNOG00000016740	Fam210a	0.008895896	family with sequence similarity 210, member A
ENSRNOG00000015499	Serinc4	0.008854299	serine incorporator 4
ENSRNOG00000003357	Col3a1	0.008596346	collagen type III alpha 1 chain
ENSRNOG00000013987	Sbno2	0.008295102	strawberry notch homolog 2

ENSRNOG00000016488	Pltp	0.007805867	phospholipid transfer protein
ENSRNOG00000017420	Nudt6	0.007148302	nudix hydrolase 6
ENSRNOG00000046834	C3	0.006931073	complement C3
ENSRNOG00000011971	C1s	0.005502947	complement C1s
ENSRNOG00000000506	Tead3	0.005428161	TEA domain transcription factor 3
ENSRNOG00000053025	AC130391.3	0.005281306	NA (NOT A KNOWN GENE)
ENSRNOG00000008951	Rasl10a	0.004886079	RAS-like, family 10, member A
ENSRNOG00000003897	Col1a1	0.004741078	collagen type I alpha 1 chain
ENSRNOG00000058068	Obscn	0.004578265	obscurin, cytoskeletal calmodulin and titin-interacting RhoGEF
ENSRNOG00000001229	Col18a1	0.004536439	collagen type XVIII alpha 1 chain
ENSRNOG00000012579	Tlcd1	0.00397011	TLC domain containing 1
ENSRNOG00000058618	Dcst2	0.003853329	DC-STAMP domain containing 2
ENSRNOG00000019657	Mk1	0.003501833	Mk1 protein
ENSRNOG00000005695	Mgp	0.003157524	matrix Gla protein
ENSRNOG00000010233	Cald1	0.002827684	caldesmon 1
ENSRNOG00000017628	Tagln	0.002818038	transgelin
ENSRNOG00000045829	Thbs1	0.002813471	thrombospondin 1
ENSRNOG00000013442	Ciz1	0.002738807	CDKN1A interacting zinc finger protein 1
ENSRNOG00000025689	Abhd1	0.002587131	abhydrolase domain containing 1
ENSRNOG00000003931	Arsg	0.002525482	arylsulfatase G
ENSRNOG00000012207	Dst	0.002493232	dystonin
ENSRNOG00000022619	Fth1	0.002461379	ferritin heavy chain 1
ENSRNOG00000002052	Ccdc80	0.002416084	coiled-coil domain containing 80
ENSRNOG00000059504	NA	0.002401354	NA (NOT A KNOWN GENE)
ENSRNOG00000039668	Col8a1	0.002389889	collagen type VIII alpha 1 chain
ENSRNOG00000046005	Scd2	0.002221052	stearoyl-Coenzyme A desaturase 2
ENSRNOG00000018087	Vim	0.002209076	vimentin
ENSRNOG00000026951	Susd5	0.002204525	sushi domain containing 5
ENSRNOG00000024779	Polr2b	0.002167036	RNA polymerase II subunit B
ENSRNOG00000022932	Serhl2	0.002124122	serine hydrolase-like 2
ENSRNOG00000024657	Mfsd4a	0.001941625	major facilitator superfamily domain-containing 4A
ENSRNOG00000014287	Stk11	0.001921727	serine/threonine kinase 11
ENSRNOG00000017206	Igfbp5	0.001885916	insulin-like growth factor binding protein 5
ENSRNOG00000018033	Ddx19a	0.001862009	DEAD-box helicase 19A
ENSRNOG00000010966	Itgb1	0.001768046	integrin subunit beta 1
ENSRNOG00000004860	Myh9l1	0.001693158	myosin, heavy chain 9, non-muscle-like 1

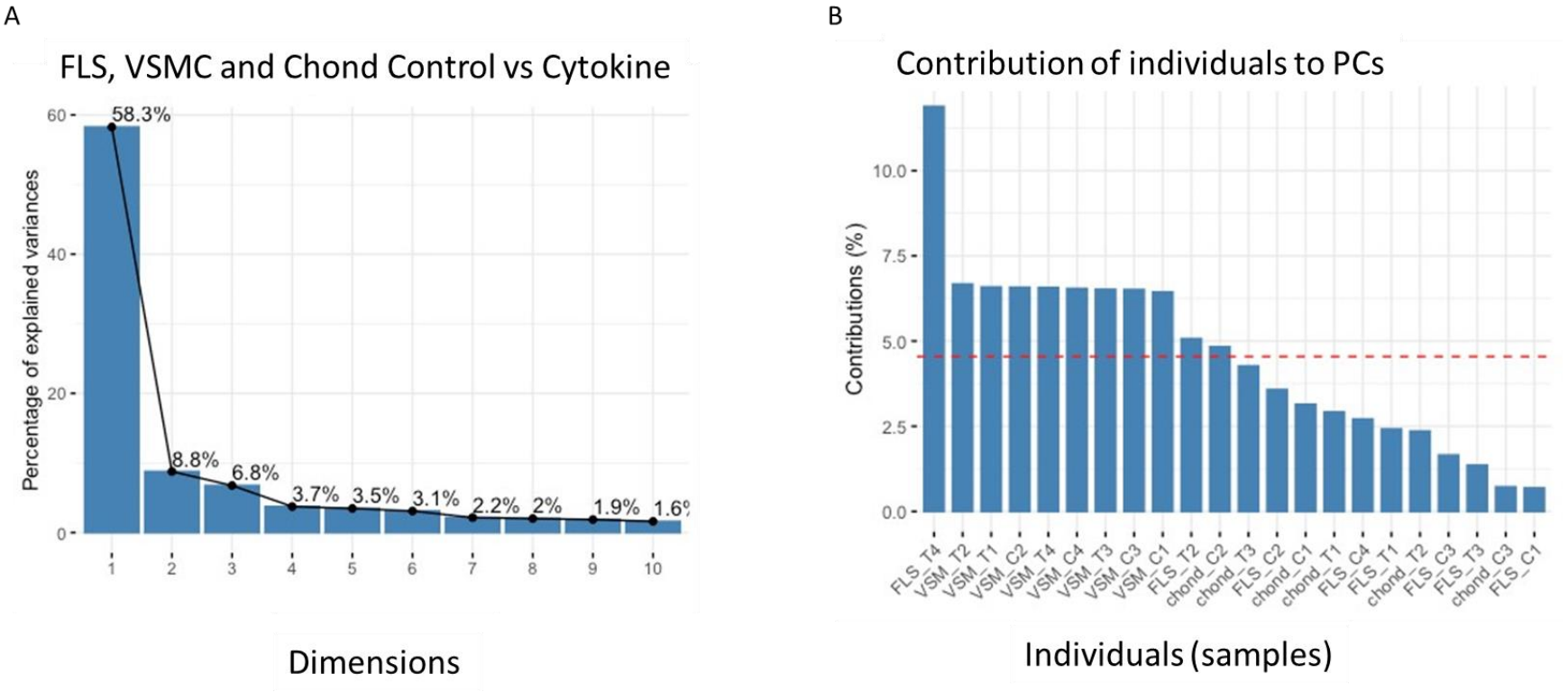

Figure 45: PCA analysis of all control and cytokines treated rats' FLS, VSMC, and chondrocytes.
PCA analysis of Control and Cytokine (IL-1β+TNFα) treated adult rat FLS, VSMC, and chondrocytes. A. shows the scree plot for the 10 principle components used to reduce the dimensionality of the FLS, VSMC, and chondrocytes control and cytokine treated datasets, approximately 22038 variables (genes) reduced to 10 variables (PC) with 22 subjects; 11 control and 11 cytokines treated male rats. PCA Component 1 alone accounts for approximately 58% of the variance in the data. B. Contribution plot showing the relative contributions of each of the 22 subjects to the principal components. The red dotted line indicates the mean contribution. The first subject contributes most to the variability and the second nine contribute least.

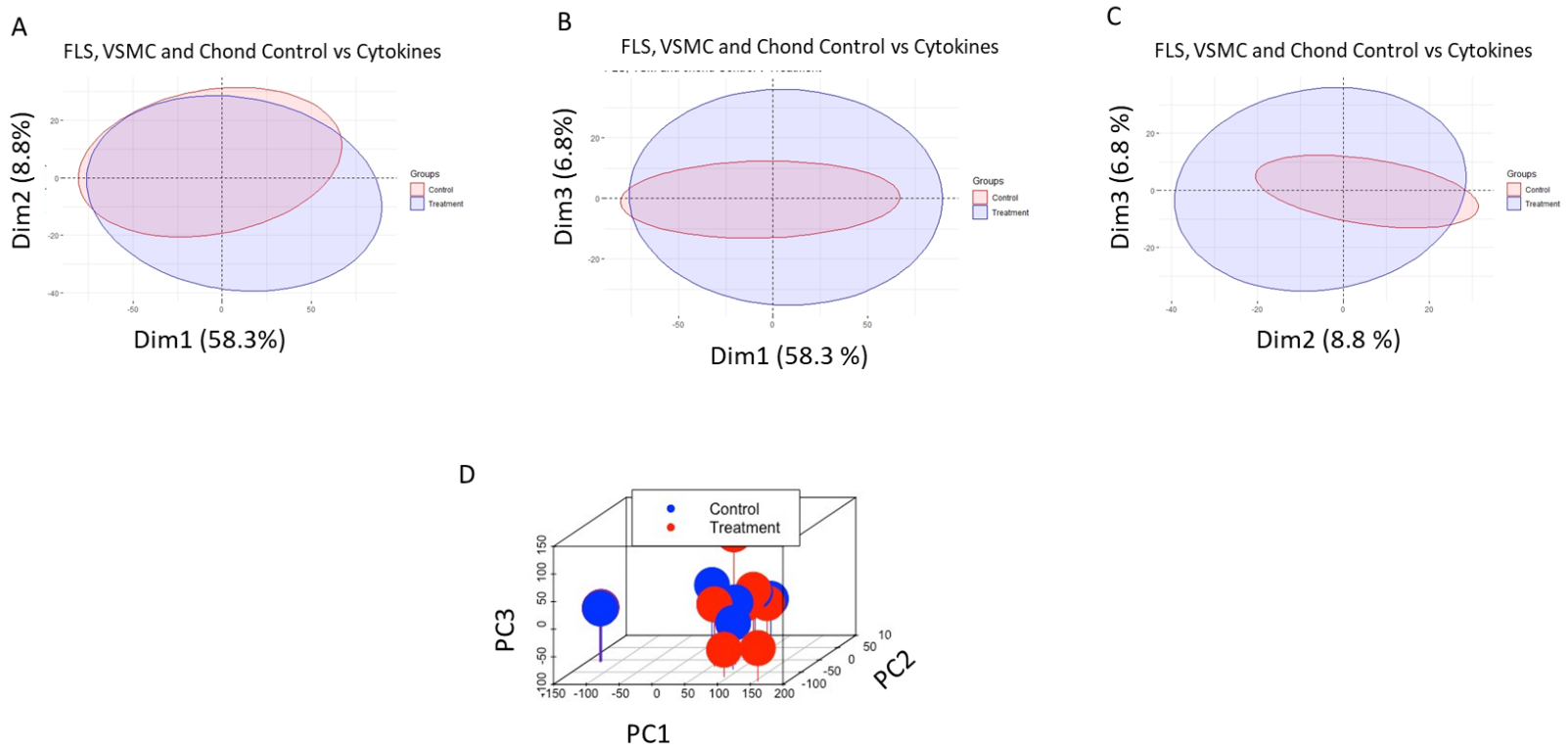

Figure 46: Principle component, k-mean clustering and combined scatter plot of all control and cytokines treated rats' FLS, VSMC, and chondrocytes.
***A, B** and **C** show plots of PC1 vs PC2, PC1 vs PC3 and PC2 vs PC3 (Dim=PC). The shaded circles show the unsupervised k mean cluster 95% confidence intervals thus there is no clear statistical separation between control and cytokine treated when combining PC1 and PC2, PC1 and PC3 or PC2 and 3. **D.** 3D plot showing all three principal components plotted against each other.*

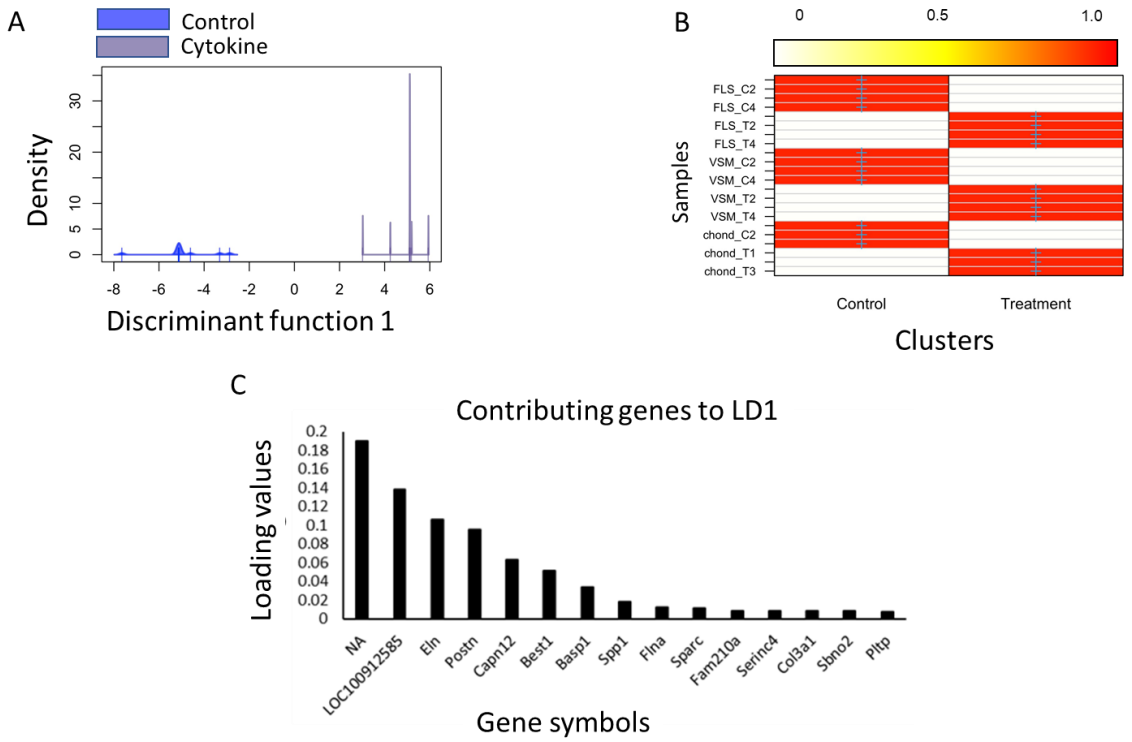

Figure 47: Discriminant Analyses of cytokine Effects on all genes of all control and cytokines treated rats' FLS, VSMC, and chondrocytes.
A. *Shows the kernel density plots of the discriminant component coordinates for the control and cytokine (IL-1β+TNFα) treated groups; co-ordinates on the x-axis and density on the y-axis. There is a clear separation between control and cytokine treated samples.* ***B.*** *A graphical confusion matrix showing the actual group membership (x-axis) and predicted cluster membership (on the y-axis). All groups are correctly clustered with greater than 0.9 probability.* ***C.*** *The most contributing genes to the linear discriminator function; NA; unidentified variant, LOC100912585; mitogen-activated protein kinase 7-like, Eln; elastin, Postn; periostin, Capn12; calpain 12, Best1; bestrophin 1, Basp1; brain abundant, membrane attached signal protein 1, Spp1; secreted phosphoprotein 1, Flna; filamin A, Sparc; secreted protein acidic and cysteine-rich, Fam210a; family with sequence similarity 210, member A, Serinc4; serine incorporator 4, Col3a1; collagen type III alpha 1 chain, Sbno2; strawberry notch homolog 2, Pltp; phospholipid transfer protein.*

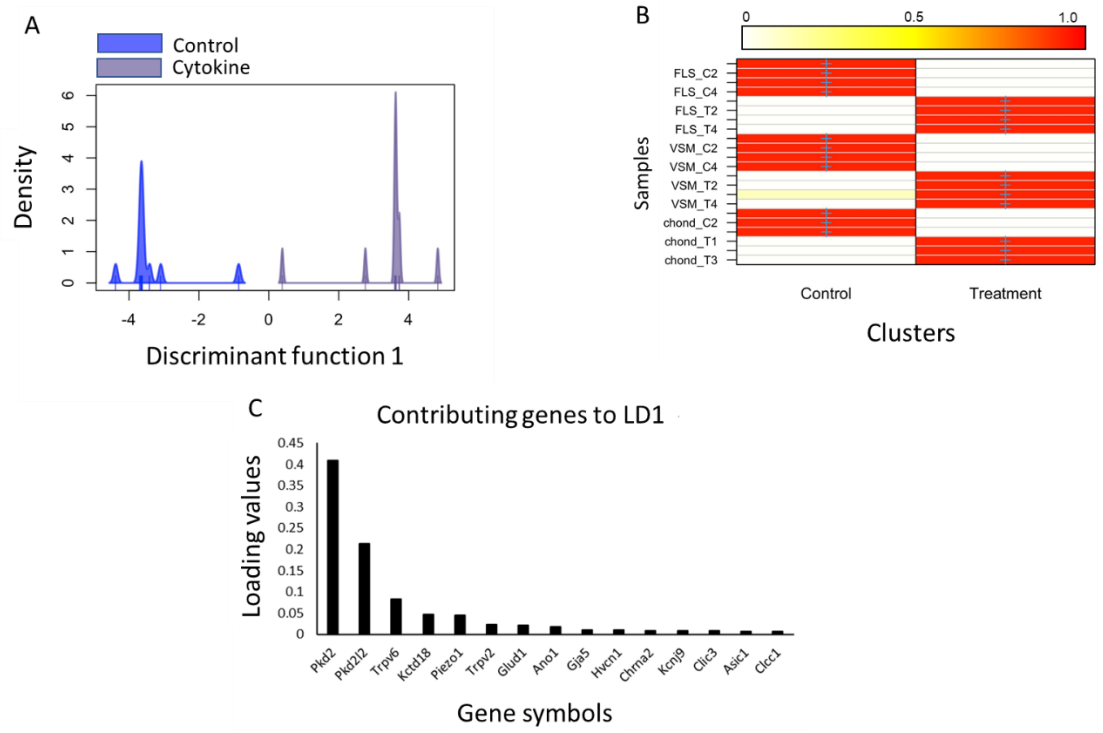

Figure 48: Discriminant Analyses of cytokine Effects on ion channel genes of all control and cytokines treated rats' FLS, VSMC, and chondrocytes.
A. *Shows the kernel density plots of the discriminant component coordinates for the control and cytokine (IL-1β+TNFα) treated groups; co-ordinates on the x-axis and density on the y-axis. There is a clear separation between control and cytokine treated samples.* ***B.*** *A graphical confusion matrix showing the actual group membership (y-axis) and predicted cluster membership (on the y-axis). All groups are correctly clustered with greater than 0.9 probability.* ***C.*** *The most contributing genes to the linear discriminator function; Pkd2; polycystin 2, transient receptor potential cation channel, Pkd2l2; polycystin 2 like 2, transient receptor potential cation channel, Trpv6; transient receptor potential cation channel, subfamily V, member 6, Kctd18; potassium channel tetramerization domain containing 18, Piezo1; piezo-type mechanosensitive ion channel component 1, Trpv2; transient receptor potential cation channel, subfamily V, member 2, Glud1; glutamate dehydrogenase 1, Ano1; anoctamin 1, Gja5; gap junction protein, alpha 5, Hvcn1; hydrogen voltage-gated channel 1, Chrna2; cholinergic receptor nicotinic alpha 2 subunit, Kcnj9; potassium voltage-gated channel subfamily J member 9, Clic3; chloride intracellular channel 3, Asic1; acid-sensing ion channel subunit 1, and Clcc1; chloride channel CLIC-like 1. , and 0.007414555; unidentified variant.*

Multivariate analysis of differentially expressed genes of all control, cytokine (10ng/ml TNFα+IL-1β for 72hrs) treated, young and old samples

Clustering with PCA of 42 individuals (samples), 22038 genes allowed us to reduce the PCs from 22038 to 10 PCs. The generated scree plot showing the percentages of explained variance of each dimension is shown in Figure 49-A with more than 35% of the variance is explained by dimension 1. Also, the contribution of each sample (individual) to the separation between the groups is presented in Figure 49-B. Since the separation was not clear using PC1 and PC2 (Figure 50-A), PC1 and PC3 (Figure 50-B), or PC2 and PC3 (Figure 50-C) while (Figure 50-D) shows the 3D plot of all PCs against each other, therefore I moved to DA-PCA.

A supervised multivariate analysis (DA-PCA) was performed. 27 PCs and 1 discriminant function were needed to obtain good separation as shown in (Figure 51-A). Also, the heatmap (Figure 51-B) was generated that shows group membership of each sample and the probability of correct prediction. The probability of belonging was greater than 0.9 on average. Mean *p*-value for this over-all separation was 0.026 and again the bootstrap method (described earlier) was used to estimate FDR, this time with 100 simulations with the data matrix repeatedly shuffled, none reached statistical significance (therefore FDR<0.01). The top 50 contributing genes to this separation are shown on (Table 32) while (Figure 51-C) shows the top 15 of them.

With functional annotating clustering in David Bioinformatics Resources 6.8, these genes were explained by 7 clusters with cluster 1 having the highest enrichment score of 4.6 and these genes were mainly involved with extracellular space with a p-value of $3.5x10^{-8}$. The following pathways were enriched on KEGG pathway; “Protein digestion and absorption” (rno04974, p=5.52x10-5), “ECM-receptor interaction” (rno04512, p=5.52x10-5), “Focal adhesion” (rno04510, p=1.19x10-4), and ”PI3K-Akt signalling pathway” (rno04151, p=0.001). Again, four out of the top 10 GOs were mainly related to “extracellular”. Examples of GO enriched in this group are “extracellular matrix” (GO:0031012, p=8.58x10-9), “extracellular

space" (GO:0005615, p=3.47x10-8), "collagen fibril organization" (GO:0030199, p=9.49x10-5), "extracellular matrix structural constituent" (GO:0005201, p=1.95x10-4), "angiogenesis" (GO:0001525, p=7.24x10-4), "aging" (GO:0007568, p=0.005), "response to cytokine" (GO:0034097, p=0.02), and "cellular response to tumor necrosis factor" (GO:0071356, p=0.04). The InterPro discovered "Fibrillar collagen, C-terminal" (IPR000885, p=3.28x10-4), "Collagen triple helix repeat" (IPR008160, p=7.37x10-4), some of the epidermal-like growth factor (binding) such as "EGF-like calcium-binding" (IPR001881, p=0.003), and insulin-like growth factors (binding proteins) such as "Insulin-like growth factor binding protein, N-terminal" (IPR009030, p=0.003).

Multivariate analysis of differentially expressed channel genes of all control, cytokine (10ng/ml TNFα+IL-1β for 72hrs) treated, young and old samples

In this analysis, 25 DA-PCA PCs were used to separate groups and this produced clear separation as shown by the Kernel density plot (Figure 52-A). Also, a heatmap shows the correct prediction of each sample belonging to each group (Figure 52-B) was generated and the probability of belonging was greater than 0.9. The top 50 contributing genes to LDA are shown in Table 32 while 15 contributing genes to this separation are shown on (Figure 52-C).

Table 32: Top 50 genes contributing to the LD1 in all groups; control, cytokines (10ng/ml TNFα+IL-1β for 72hrs) treated, young and old samples.

Ensemble IDs	LD1	Gene IDs	Gene description
ENSRNOG00000000506	0.017880638	Tead3	TEA domain transcription factor
ENSRNOG00000001229	0.003594128	Col18a1	collagen type XVIII alpha 1 chain
ENSRNOG00000001414	0.004217473	Serpine1	serpin family E member 1
ENSRNOG00000001469	0.13142108	Eln	elastin
ENSRNOG00000003357	0.013672632	Col3a1	collagen type III alpha 1 chain
ENSRNOG00000003897	0.004990918	Col1a1	collagen type I alpha 1 chain
ENSRNOG00000003931	0.008303714	Arsg	arylsulfatase G
ENSRNOG00000004094	0.003772715	Ptger1	prostaglandin E receptor 1
ENSRNOG00000008415	0.008314069	Nab2	Ngfi-A binding protein 2
ENSRNOG00000008697	0.002804959	Ccn3	cellular communication network factor 3
ENSRNOG00000008951	0.003069361	Rasl10a	RAS-like, family 10, member A
ENSRNOG00000009439	0.003736281	Eef1a1	eukaryotic translation elongation factor 1 alpha 1
ENSRNOG00000010529	0.00280402	Thbs2	thrombospondin 2

ENSRNOG00000011971	0.006745817	C1s	complement C1s
ENSRNOG00000012579	0.073747397	Tlcd1	TLC domain containing 1
ENSRNOG00000012660	0.07869047	Postn	periostin
ENSRNOG00000012840	0.012275292	Sparc	secreted protein acidic and cysteine-rich
ENSRNOG00000013442	0.021033757	Ciz1	CDKN1A interacting zinc finger protein 1
ENSRNOG00000015499	0.005077154	Serinc4	serine incorporator 4
ENSRNOG00000016460	0.005549064	Clu	clusterin
ENSRNOG00000016488	0.003390998	Pltp	phospholipid transfer protein
ENSRNOG00000016539	0.036130552	Mxd3	RAB24, member RAS oncogene family
ENSRNOG00000016740	0.004720909	Fam210a	family with sequence similarity 210, member A
ENSRNOG00000017206	0.003372693	Igfbp5	insulin-like growth factor binding protein 5
ENSRNOG00000017420	0.005775042	Nudt6	nudix hydrolase 6
ENSRNOG00000018233	0.00406451	Gas6	growth arrest specific 6
ENSRNOG00000019052	0.006590713	Ankzf1	ankyrin repeat and zinc finger peptidyl tRNA hydrolase 1
ENSRNOG00000019162	0.005151075	Emc9	ER membrane protein complex subunit 9
ENSRNOG00000019414	0.054747875	Tmem79	transmembrane protein 79
ENSRNOG00000019477	0.002877551	Zmynd15	zinc finger, MYND-type containing 15
ENSRNOG00000019657	0.002888024	Mk1	Mk1 protein
ENSRNOG00000019992	0.009221728	Cnbd2	cyclic nucleotide binding domain containing 2
ENSRNOG00000020389	0.007851615	Capn12	calpain 12
ENSRNOG00000020628	0.004004462	LOC103690068	immortalization up-regulated protein-like
ENSRNOG00000023493	0.003239972	Creb3l4	cAMP responsive element binding protein 3-like 4
ENSRNOG00000023668	0.007526158	Scyl1	SCY1 like pseudokinase 1
ENSRNOG00000024779	0.012610184	Polr2b	RNA polymerase II subunit B
ENSRNOG00000026053	0.008701938	Grem1	gremlin 1, DAN family BMP antagonist
ENSRNOG00000037894	0.035376935	AABR07068042.1	NA (Not a known gene)
ENSRNOG00000039315	0.012637055	Cfap157	cilia and flagella associated protein 157
ENSRNOG00000043451	0.005485935	Spp1	secreted phosphoprotein 1
ENSRNOG00000046313	0.047793873	Basp1	brain abundant, membrane attached signal protein 1
ENSRNOG00000046834	0.045407123	C3	complement C3
ENSRNOG00000048733	0.009126601	Nup62	nucleoporin 62
ENSRNOG00000053025	0.041489768	AC130391.3	NA (Not a known gene)
ENSRNOG00000054890	0.003481199	Flna	filamin A
ENSRNOG00000056819	0.004396124	Susd1	sushi domain containing 1
ENSRNOG00000057040	0.004712189	Spns2	sphingolipid transporter 2
ENSRNOG00000058068	0.003647309	Obscn	obscurin, cytoskeletal calmodulin and titin-interacting RhoGEF
ENSRNOG00000058560	0.003419738	Col2a1	collagen type II alpha 1 chain

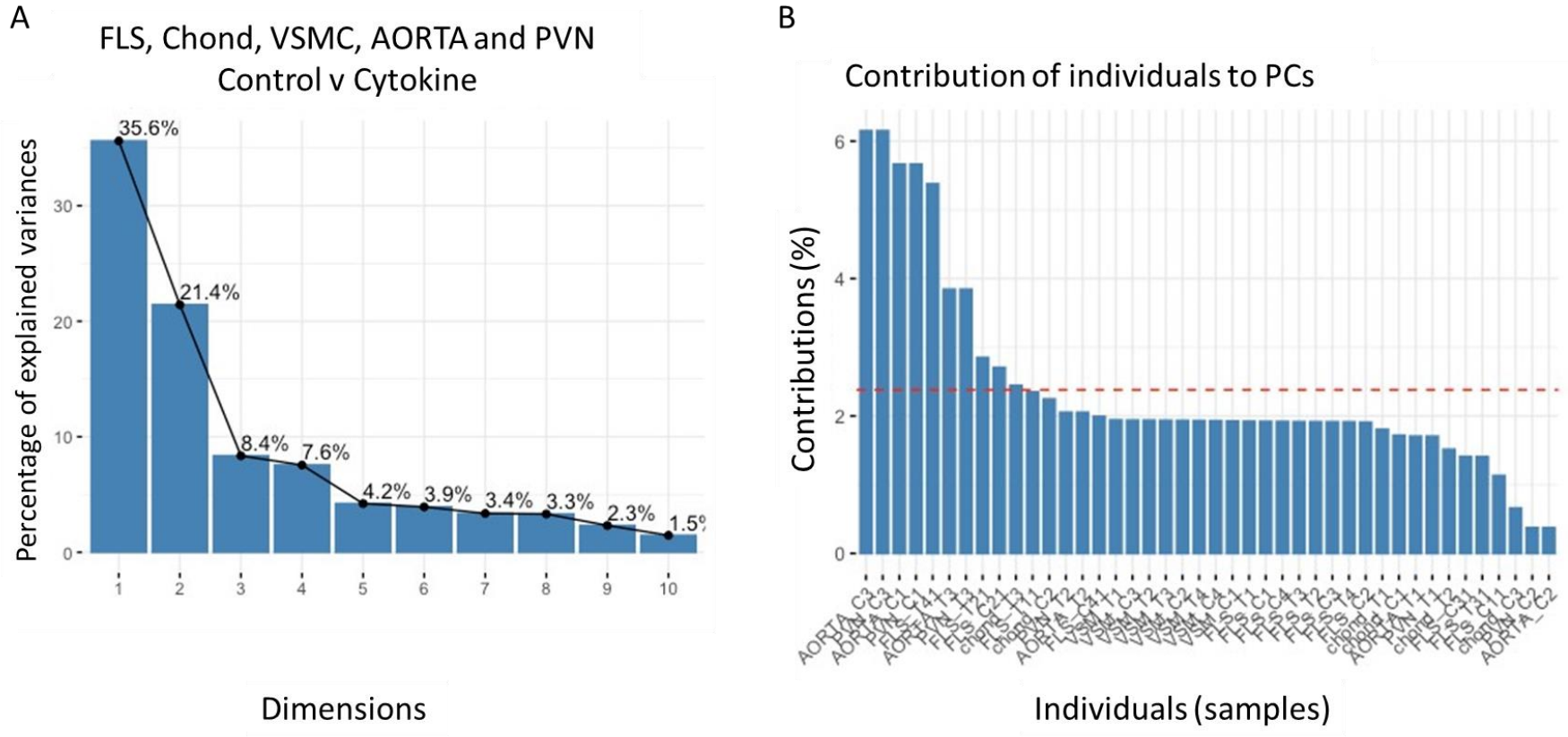

Figure 49: PCA analysis of group 1 (Control + Young) and group 2 (Cytokine (IL-1β+TNFα) treated + Old) rat FLS, Chondrocytes, VSMC, Aorta, and PVN.
A. shows the scree plot for the 10 principle components used to reduce the dimensionality of the groups' datasets, approximately 22038 variables (genes) reduced to 10 variables (PC) with 42 subjects; 21 (group 1) and 21 (group 2) male rats. PCA Component 1 alone accounts for approximately 35% of the variance in the data. B. Contribution plot showing the relative contributions of each of the 42 subjects to principle components. The red dotted line indicates the mean contribution. The first 5 subjects contribute most to the variability and the second four contribute least.

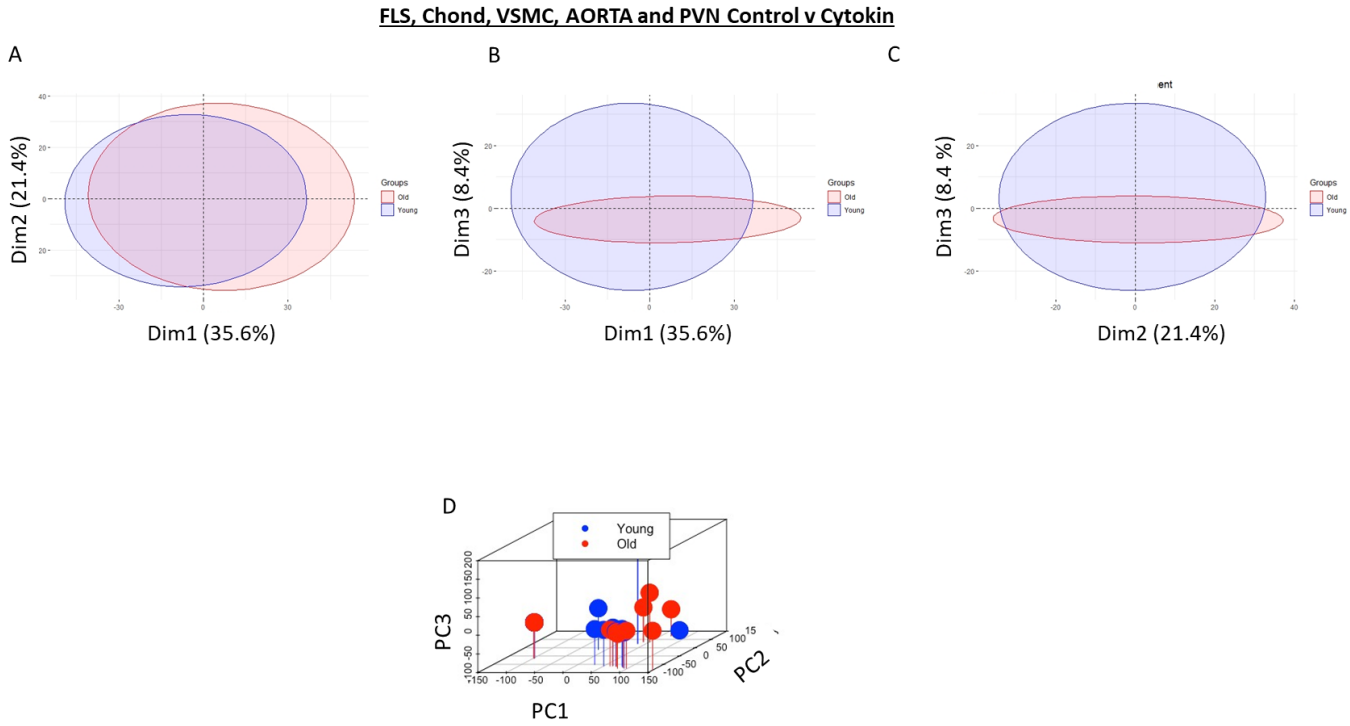

Figure 50: Principle component, k-mean clustering and combined scatter plot of all samples according to their groups.
***A, B** and **C** show plots of PC1 vs PC2, PC1 vs PC3 and PC2 vs PC3 (Dim=PC). The shaded circles show the unsupervised k mean cluster 95% confidence intervals thus there is no clear statistical separation between control and cytokine treated when combining PC1 and PC2, PC1 and PC3 or PC2 and 3. **D.** 3D plot showing all three principal components plotted against each other.*

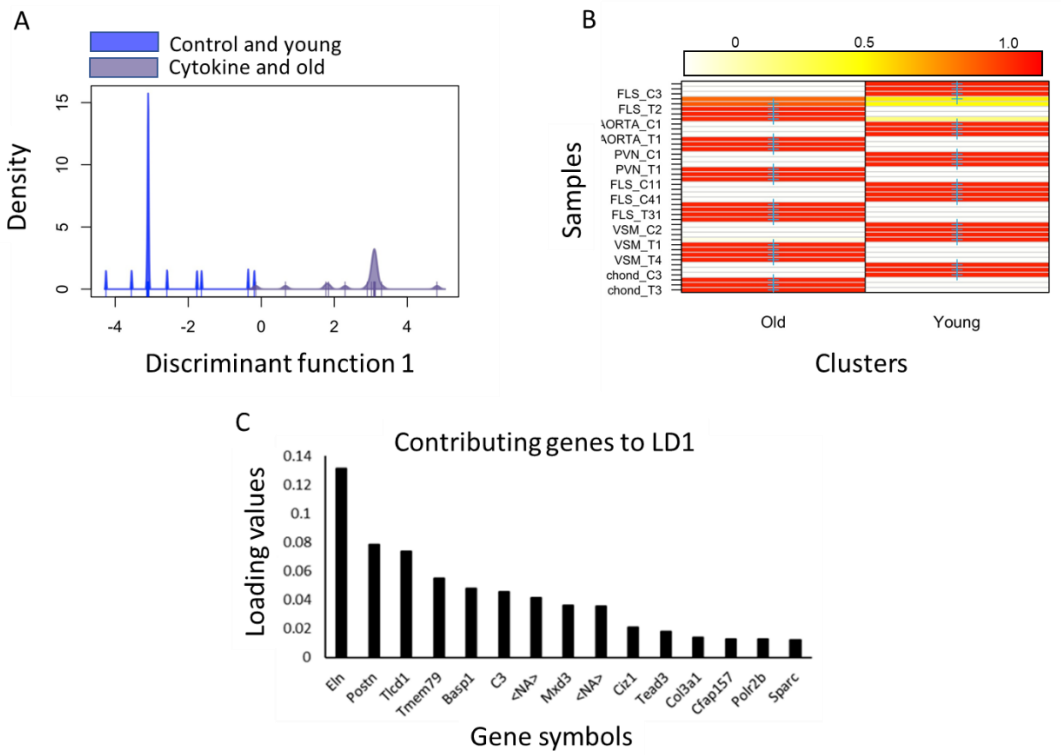

Figure 51: Discriminant Analyses of group 1 (Control + Young) and group 2 (Cytokine (IL-1β+TNFα) treated + Old) rat FLS, Chondrocytes, VSMC, Aorta, and PVN.
A. *Shows the kernel density plots of the discriminant component coordinates for the control and cytokine (IL-1β+TNFα) treated groups; co-ordinates on the x-axis and density on the y-axis. There is a clear separation between group 1 (control and young) and group 2 (cytokine treated and old) samples.* ***B.*** *A graphical confusion matrix showing the actual group membership (y-axis) and predicted cluster membership (on the y-axis). All groups are correctly clustered with greater than 0.9 probability except FLS_C4 and FLS-T1.* ***C.*** *The most powerful contributing genes to the linear discriminator function; Eln; elastin, Postn; periostin, Tlcd1; TLC domain containing 1, Tmem79; transmembrane protein 79, Basp1; brain abundant, membrane attached signal protein 1, C3; complement C3, <NA>; Not a known gene, Mxd3; RAB24, member RAS oncogene family, <NA>; Not a known gene, Ciz1; CDKN1A interacting zinc finger protein 1, Tead3; TEA domain transcription factor 3, Col3a1; collagen type III alpha 1 chain, Cfap157; cilia and flagella associated protein 157, Polr2b; RNA polymerase II subunit B, and Sparc; secreted protein acidic and cysteine-rich.*

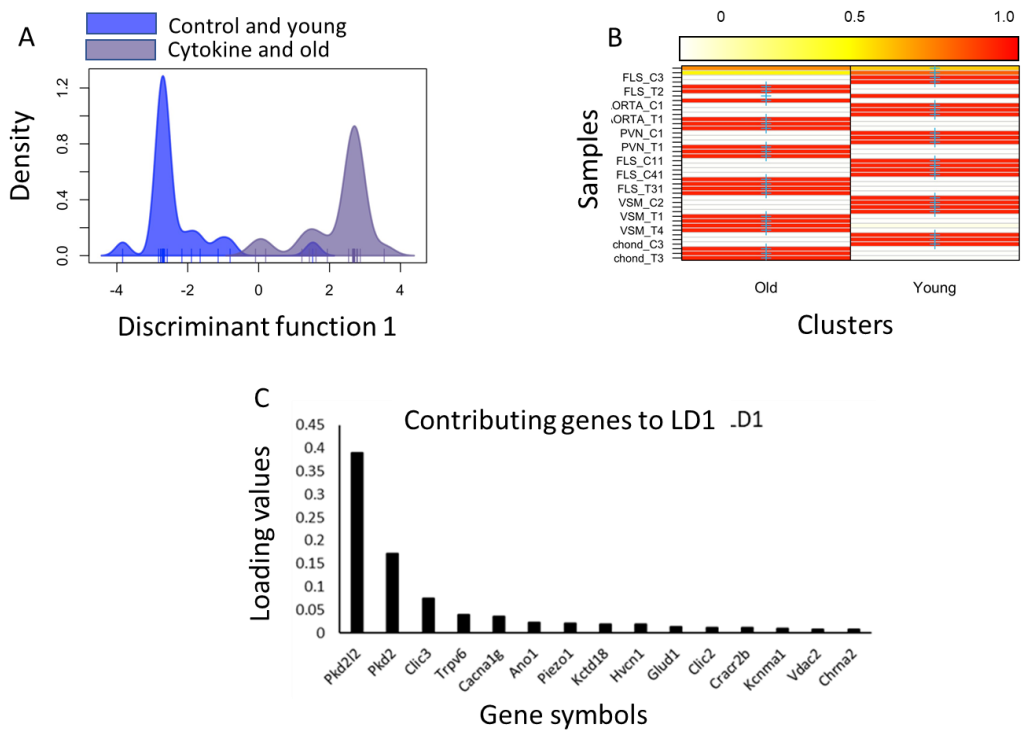

Figure 52: Discriminant Analyses of CHANNELS of group 1 (Control + Young) and group 2 (Cytokine (IL-1β+TNFα) treated + Old) rat FLS, Chondrocytes, VSMC, Aorta, and PVN.
A. *Shows the kernel density plots of the discriminant component coordinates for the control and cytokine (IL-1β+TNFα) treated groups; co-ordinates on the x-axis and density on the y-axis. There is a clear separation between group 1 (control and young) and group 2 (cytokine treated and old) samples.* ***B.*** *A graphical confusion matrix showing the actual group membership (y-axis) and predicted cluster membership (on the y-axis). All groups are correctly clustered with greater than 0.9 probability except FLS_C1, FLS_C2 and FLS-T3.* ***C.*** *The top 15 contributors to the linear discriminator function; Pkd2l2; polycystin 2 like 2, transient receptor potential cation channel, Pkd2; polycystin 2, transient receptor potential cation channel, Clic3; chloride intracellular channel 3, Trpv6; transient receptor potential cation channel, subfamily V, member 6, Cacna1g; calcium voltage-gated channel subunit alpha1 G, Ano1; anoctamin 1, Piezo1; piezo-type mechanosensitive ion channel component 1, Kctd18; potassium channel tetramerization domain containing 18, Hvcn1; hydrogen voltage-gated channel 1, Glud1; glutamate dehydrogenase 1, Clic2; chloride intracellular channel 2, Cracr2b; EF-hand calcium-binding domain-containing protein 4A-like, Kcnma1; potassium calcium-activated channel subfamily M alpha 1, Vdac2; voltage-dependent anion channel 2, and Chrna2; cholinergic receptor nicotinic alpha 2 subunit.*

6.4 Discussion

In this chapter, bioinformatic analyses of all the NGS data from the previous chapters was performed together with a chondrocyte dataset collected in parallel by colleagues. Over-all the most common changes observed were in the extracellular matrix.

The comparison took place by comparing a group containing all young with a group containing all old samples, a group containing all control samples with a group containing all cytokine treated samples, and the last comparison took place by comparing all samples together where control and young samples considered as a group and all cytokine treated and old samples as one group.

With the real aged tissue, there were 20 samples and approximately 22,000 variables (genes). This was reduced to 6 PCs for PCA while DA-PCA method needed 10 PCs to obtain better separation with the groups of samples containing young and old only (FLS, VSMC, and PVN). The next group was of control and cytokine (10ng/ml IL-1β+TNFα) treated samples (FLS, VSMC, and Chondrocytes), 22 samples analysed, 5 PCs were used first for the separation, but it needed more to obtain nice and clear separation with DA-PCA. For the last group that contains all control and young as group 1 and cytokine treated with old samples as group 2, the number of samples was bigger (42 samples). Therefore, 5 PCs with PCA were not enough to obtain a clear separation but 27 PCs produced nicer discrimination. For all samples, they were all represented by 22038 genes.

Differences

First groups for comparison were all young and old samples. In this group, the enrichment was "extracellular space" with a p-value of 3.5×10^{-8}. Extracellular space means, according to "QuickGO" (Ashburner et al., 2000, 2019), any structure that is lying outside the cell that either support or provide biochemical or biomechanical indications for the cells. The same finding was also repeated when

comparing all samples together [group1 (young and control) vs group2 (old and cytokine treated)] while all control and cytokine (10ng/ml IL-1β+TNFα) treated samples had "signalling" enrichment with a p-value of $1.4x10^{-5}$. This may indicate that the largest contribution to the separation between groups of all samples came from all young and old samples whereas groups containing control and cytokine treated cells did not contribute significantly. This may also indicate that the "inflammageing model" that was established in this study did not 100% match the real inflammageing model (*and see later*) although changes have been seen in terms of gene expression and functional analysis with electrophysiology. The reason for that, as hypothesized in this study, was because young FLS and VSMC cells were treated with cytokines to create this model and it seemed that the anti-inflammatory mechanism might have been more efficient in these cells because of their young age in addition to the fact that not all changes that usually take place with ageing had these cells been exposed to.

A final, but important detail on the differences between [*young and old*] vs ["control" *and cytokine treated*] comes from the PCA where all samples were compared, but the age and age model (=cytokine treated) groups were annotated separately. From this it is strikingly apparent that there was, in multivariate PCA terms, a much bigger separation between the combined [*young and old*] group and the [*"control" and cytokine treated*] than there was between either [*young*] vs [*old*] or ["*control*"] vs [*cytokine treated*]. This is interesting because in theory it is expected that [*young*] and ["*control*"] to be near identical even if [*old*] and [*cytokine treated*] were not similar. This is because ["*control*"] was cells from young animals from a similar strain (Wistar versus Wistar Kyoto). One explanation for the difference between [*young*] and ["*control*"] would be that there is a true difference between Wistar and Wistar Kyoto, however, it seems implausible that such a difference would be greater than the difference between ["*control*"] and [*cytokine treated*]. Another, possibility is methodological in that all the ["*control*"] and [*cytokine treated*] RNA came from were cultured cells whilst that of [*young*] and [*old*] came from frozen, non-cultured tissue sections. Both systems have their advantages and disadvantages. Culturing cells

could decrease the numbers of animals required (because 4 animals supply 4 cultures that can be then split to create paired test and control groups, whereas with young and old they need to be 4 animals of each), also since culture experiments have paired samples the statistical power should be greater. Cultured cells also have the advantage of being (more likely to be) a homogenous population of cells compared to whole tissue samples that must contain mixed cell populations. A clear advantage of tissue sections, however, is they are frozen at source and thus there should be none of the phenotypic switching established for long term cultured cells with changes in ion channels and other genes well document (Hdud et al., 2012, Benya and Shaffer, 1982). Culture periods were minimised to ameliorate this issue, but the inference from the PCA is that it may still have been an issue.

Similarities

There were however many other similarities between young and old samples, control and cytokine treated cells, and all samples group1 (control and young) and group2 (cytokine and old). For example, on KEGG pathways, focal adhesion, ECM-receptor interaction and PI3K-Akt signalling pathways were common between the compared groups. Also, GO revealed some similarities as well. For example, extracellular matrix and ageing were commonly enriched GOs in all groups. Also, the "response to tumour necrosis factor" was of noteworthy and was not surprising as this what was used; in addition to IL-1β, to treat cells to create the "inflammageing" model. The InterPro proteins were mainly related to the extracellular proteins such as collagens.

Looking at the genes enriched in these KEGG pathways in this study, it was interesting to see some genes that regulated extracellular space/matrix such as collagens, beta-actin, and Mmp2 contributing to the separation between groups as they had been changed according to treatment or age. These genes could have mediated cell-to-cell communications, played roles in healthy microenvironment between cells, and altered membrane receptor interactions through different receptors including ion channels (i.e. mechanosensitive cation channels such as TRPV4 (Guilak et al., 2010)) that eventually altered intracellular

signalling. Most of the enriched GOs and InterPro proteins were related to ageing and extracellular areas of the cells involving their proteins such as collagens.

Previous studies on some of these genes

Collagens are considered the backbone of tissues which also include other proteins such as laminins and elastin (Karsdal, 2016). The synthesis and degradation of these proteins are tightly regulated to ensure tissues health and homeostasis. Collagens are divided into several subgroups containing fibrillar and networking collagens. The latter were mostly studied (Karsdal, 2016). Some of these collagens such as Col1a1, Col2a1, Col3a1, Col18a1 as well as Mmp2, and Fn1 that were differentially expressed in this project will be covered.

A study conducted on Col1a1 found that collagen fibres were highly straightened with age (Van Gulick et al., 2019, Misra et al., 2007). Also, age-related changes of Col2a1 and Fn1 were observed in a way that they were far more reduced than in the young subjects (Madej et al., 2016). Col3a1 is another gene that participated in the pathway enrichment was reported to be differentially expressed with ageing in other tissues along with inflammatory processes (Sandovici et al., 2016, Misra et al., 2007).

Col18a1 is a naturally occurring agent. It is known for inhibiting angiogenesis and endothelial cell migration. Several hypotheses have been described for that including the blockage of the binding of VEGFA to its receptor (KDR), binding to heparan sulfate proteoglycans involved in the growth factor signalling, and modulation of integrin-dependent endothelial cell migration including integrin itgb1 (Ständker et al., 1997, Kuo et al., 2001).

Matrix metalloproteinase 2 (Mmp2), also changed in most aged samples, is an enzyme responsible for the degradation of native collagen types such as IV, V, VII and X as well denatured collagens and elastins affecting the mechanical properties of the blood vessel wall. It may also play a helpful role in

the migration of VSMC in response to arterial injury which may naturally increase with the age (or inflammatory state) of any older animal (McNulty et al., 2005).

6.5 Conclusions

There are many similarities in the KEGG pathways, GOs and InterPro proteins between young and old compared to control and cytokine treated cells in NGS data in this project. This indicates that the "inflammageing" model that was created in this project is close to the real ageing model presented by the old rats; at least, in terms of gene expression. This also shows that the time (72hrs) and the dose of the cytokine (10ng/ml IL-1β+TNFα) treatment were appropriate based on the above-mentioned data.

Future work

There are a number of interesting directions follow-up studies could take, for example, future studies could;

- Validate the NGS data with mass-spec proteomics where possible
- Validate the pathways and InterPro proteins with proteomics
- Produce functional models to investigate how these changes may affect overall tissue and cell function
- Validate these experimental studies with pre-clinical trials on human subjects, where possible. Biopsy or post-mortem studies would be necessary.

Chapter 7 – General discussion

Next-generation sequencing (NGS) is a powerful technique generating a huge amount of data and allowing insight into global cellular changes that previously were impossible. Therefore, the effects of ageing on FLS, Aorta and PVN cells/tissues' gene expression with NGS were studied. Then, a comparison of the outcomes of within and between groups (cells/tissues) was followed. later on, these experiments were repeated and data analysis with FLS, Chondrocytes (chondrocytes analysis only, raw data from a colleague), and VSMC cells after cytokine (10 ng/ml IL-1β+TNFα, for 72hrs) treatment took place. Next, another comparison took place of all young with all old samples, all control with all cytokine treated cells, and lastly all samples together through grouping them into group 1 (all control and young) against group2 (all cytokine treated and old). NGS data of specific channel genes (i.e. BK in FLS and ANO1 in VSMC) was confirmed with qPCR.

To test the *function* of (potential) differentially expressed ion channels, whole-cell patch-clamp electrophysiology comparing control with cytokine treatment was performed. Then, the effects of drugs on specific channels were tested. the effects of BK channel opener (NS1619) and blocker (paxilline) on FLS cells were examined. The calcium-activated chloride channel (also known as ANO1) blocker (CaCCinh-AO1) was tested in both control and cytokine treated VSMC. It was difficult to test the function of ion channels in PVN because in practice it is only possible to culture neurones from very young animals. Therefore, only NGS was carried out for PVN.

In this project, The main changes in terms of pathways and clusters of biological functions are summarized in Table 33.

Table 33: Summary of the main changes of KEGG pathways and GOs in this project.

NGS data, KEGG pathways and GOs Enrichment			
Cells /tissues	Condition /age	KEGG pathways	GOs
FLS	C vs T	canonical calcium signalling pathway, the rheumatoid and osteoarthritis, and cellular movement and proliferation canonical pathways	extracellular space, extracellular region, integrin-mediated signalling pathway, regulation of the apoptotic process, apoptotic process, immune response, and inflammatory response
	Y vs O	None statistically significant	Focal adhesion, Extracellular exosome, and Extracellular matrix, RNA processing
VSMC	C vs T	NF-kappa B signalling pathway, TNF signalling pathway and Cytokine-cytokine receptor interaction	extracellular exosome, angiogenesis, extracellular space, ageing and signal transduction
Aorta	Y vs O	Carbohydrate digestion and absorption and cardiac muscle contraction	skeletal muscle contraction, regulation of muscle contraction, positive regulation of myoblast differentiation, skeletal muscle fibre development, troponin complex, and extracellular space
PVN	Y vs O	neuroactive ligand-receptor interaction and phototransduction; genes involved were hormones and elements of signal transduction	biological processes; development (myelination and neurone ensheathing), molecular functions; protein binding, including signalling receptor binding and Ca^{2+} binding, cellular components, plasma membrane classifications
Meta-analysis	All C vs T	ECM-receptor interaction, Focal adhesion, Protein digestion and absorption and PI3K-Akt signalling pathways	extracellular matrix, cell adhesion, extracellular matrix organization, angiogenesis, ageing and cellular response to tumour necrosis factor
	All Y vs O	proteoglycans in cancer, PI3K-Akt signalling pathway, Focal adhesion and ECM-receptor interaction	extracellular matrix, and extracellular space, ageing, extracellular exosome, response to cytokine and cellular response to interleukine-1
	All C+Y vs T+O	Protein digestion and absorption, ECM-receptor interaction, Focal adhesion, and PI3K-Akt signalling pathway	extracellular matrix, extracellular space, collagen fibril organization, extracellular matrix structural constituent, angiogenesis, ageing, response to cytokine and cellular response to tumour necrosis factor

Data obtained from Davids Bioinformatics Resources 6.8. Genes were uploaded, enrichment analysis took place and results were obtained. The top enrichments for groups compared with each other were presented in this table.

In this table, although tissue-specific pathways (osteoarthritis for FLS, the contraction for aorta and VSMC and neuroactive ligand-receptor interaction for the PVN) can be seen, the extracellular related enrichments are common among all tissue functions. Examples of genes involved in such enrichments are collagens, beta-actin and Mmp2. However, additionally, in terms of individual gene differential expression, the key gene changed was Gja1. Its level decreased after cytokine treatment in FLS and VSMC (statistically significant) and increased with ageing in FLS, Aorta and PVN (statistically significant). In the following sections, Gja1 and the main changes in the pathways and GOs will be covered.

Gap junctions are membrane channels that allow ions and small molecules to pass through between the cytoplasmic contents of adjacent cells. This kind of communication results in different physiological functions including growth regulation and development, and tissue homeostasis (Fraser et al., 1987, Peters et al., 1994, Goodenough and Paul, 2009, Meşe et al., 2007, Giepmans, 2004). Any abnormal changes in gap junction expression or function result in an impaired cell to cell communication and subsequent disruption of the intracellular signalling leading to diseases such as re-entry arrhythmias of the heart (Watanabe et al., 2004)). It also has been associated with Alzheimer's disease (Kajiwara et al., 2018). Gja1 is expressed in the musculoskeletal system in tissues such as bone, cartilage, skeletal muscle and synovium. Dysfunction of the Gja1 can contribute to the joint diseases such as rheumatoid arthritis, osteoarthritis, skeletal muscle atrophy (reviewed here (Donahue et al., 2017)). Beker et al (Becker et al., 2015) demonstrate that transient downregulation of Gja1 (Cx43) or block of this hemichannel can decrease inflammation. Additionally, innexin genes encoding gap junction subunits have been linked with ageing. Innexin unc-9 loss increases lifespan (longevity) as described in the study on *C.elegans* (Vladis et al., 2019). In this project, downregulation of Gja1 after cytokine (10ng/ml TNFα+IL-β, 72hrs) treatment has been associated with downregulation of some inflammatory markers such as IL-6, CXCL16, CXCL1. Although changes in the expression of different genes have been seen, this downregulation of Gja1 and the inflammatory markers could be attributed to the cells' ability to oppose

the inflammatory mechanisms to restore normal cellular homeostasis after they have been exposed to the inflammatory cytokines for 72hrs. These cells were in fact young, exposed to cytokines and their anti-inflammatory mechanisms may still be effective unlike older cells. Further investigation to find out the pattern of this downregulation of the Gja1 in response to such cytokines is needed.

For the ageing tissues/cells, the opposite has been seen in terms of Gja1 expression level. It was increased compared to the young. These old rats were visually healthy but biochemically may have not reached the chronic low-grade pro-inflammatory status in which pro-inflammatory cytokine levels are 2-3-fold above normal levels. Gja1 levels are tightly regulated and Gja1 has a short half-life of about 3.5hrs. In case of rapid response is needed, the rate of Gja1 synthesis increases while the degradation of this protein is inhibited (Ribeiro-Rodrigues et al., 2017). Ageing can affect the expression of several genes and proteins. Therefore, the hypothesis that was made here was that the increased level of Gja1 associated with ageing in this study could be attributed to the inhibited degradation or increased rate of synthesis of this gene. Further investigation of the synthesis, degradation, and functions of this gene as well as its related protein in the process of ageing is required.

For the channel families, variabilities in gene expression have been observed. Important and interesting changes in ion channels discovered in this project will be covered.

K^+ channels are important channels in almost all cells. Inwardly rectifying potassium channels were upregulated in VSMC following cytokines treatment in this project. These channels allow potassium ions to flow into rather than out of the cell. When hyperpolarization of the VSMC takes place, this type of channels becomes activated. As a result, more K^+ ions move into the cell from the extracellular space to neutralize the hyperpolarization trigger. These channels are also important players in the equilibrium potential of potassium. (Cowled and Fitridge, 2011). Rarely, this type of channels conducts small outward rectifying K^+ currents when the membrane potential is more negative than the equilibrium potential of

the K^+ ions. This usually involves other types of channels such as $3Na^+/2K^+$ ATPase channels (Cowled and Fitridge, 2011). Upregulation of inwardly rectifying potassium channels following cytokines treatment in VSMC could be due to activation of an inflammatory pathway. Additionally, this type of channels may play a critical role in vasodilation and regulation of the sympathetic nervous system leading to blood pressure regulation as suggested by Geraldes et al (Geraldes et al., 2014). Moreover, these channels were upregulated in the ageing aorta. Therefore, upregulation of inwardly rectifying potassium channels could an indicator of ageing of VSMC.

Two pore domain potassium channels were upregulated following cytokines treatment in FLS. These channels are responsible for controlling the membrane potential of chondrocytes (Clark et al., 2011) and dorsal root ganglion (Kim et al., 2012). Also, these channels have been linked to pain and inflammation (Qiu et al., 2020). Besides, these channels are sensitive to the pH (Lesage and Lazdunski, 2000). Expression of acid-sensing channels has also been changed in FLS cells in this project. Upregulation of two-pore domain potassium channels following cytokines treatment could be an indicator of ageing especially, that it has been associated with upregulation of these channels in the ageing FLS in this study.

Acid-sensing channels (ASICs) were also upregulated in FLS following cytokines treatment. ASICs are a family of extracellular H+-activated ligated-gated ion channels. These channels play significant roles in the physiology and pathology of several conditions. These channels have been reported to regulate cell apoptosis, differentiation and autophagy. Not only this but also have been involved in degenerative disorders such as Parkinson's disease and arthritis (Zhou et al., 2016). In addition to upregulation of ASICs following cytokines treatment, these channels were upregulated in ageing FLS. Therefore, it seems that upregulation of ASICs following cytokines treatment could be an indicator of ageing in FLS cells.

For the GOs enrichment, the effects of both cytokine (10ng/ml TNFα+IL-β, 72hrs) treatment and ageing resulted in enrichment of extracellular space/matrix genes in this project. TNFα along with IL-1β

has been shown to play roles in the classically age-related disease osteoarthritis, through chondrocytes which respond to such cytokines stimulus through the production of catabolism of type II collagen and proteoglycan which compromises the extracellular matrix integrity and tissue homeostasis (Goldring and Goldring, 2007). TNFα also promotes the production of other cytokines and chemokines from other cells such as synoviocytes which ensures the renewal of the inflammatory mediators (Lee et al., 2011). Also, TNFα has been associated with loss of type II collagen (Lee et al., 2011). Age-related changes in the extracellular matrix are among the common changes that elderly experience (Li et al., 2013). Mainly, chondrocytes play major roles in the maintenance of the homeostasis of the articular joints. This function is altered with ageing leading to the impaired ability for chondrocytes to maintain the extracellular matrix. Not only this but also, the synthetic ability of the chondrocyte is decreased as well while proteoglycans become smaller and irregular (Li et al., 2013). Together, our results showed similarities between inflammageing model and the natural ageing in several ways. Inflammatory cytokines affect not only the intracellular signalling but also the extracellular space/matrix. Ageing also affects the extracellular space/matrix leading to altered cellular/tissue functions.

Future work

- For FLS,
    - Tissue typing can be carried out by flow cytometry (FC) which could detect population differences, even after just passage 3. Our present analysis only takes into account the one, majority, cell type being present. Cell separation techniques would probably allow reduced variance within groups and thus increase the possibility of seeing between-group variability. To do this, I will need CD90.2 and CD248 markers for FLS cells and macrophages CD14, CD16 or CD68 (Hardy et al., 2013). Do FC using these antibodies as well as light scatter to separate cells (Jayasuriya et al., 2018). Then, pull FLS with anti-FITC microbeads as described here (Hamada et al., 2013). Again, repeat the FC to confirm the purity of cells but having only one population of cells which FLS.
    - Tissue-specific knock out (KO) of BK channel in FLS cells from articular joints because BK activation has been associated with increased migration and invasion in RA disease. Therefore, KO of this channel is expected to limit this these functions and improve the prognosis of this disease (Hu et al., 2012b, Pethő et al., 2016, Tanner et al., 2015a). To do tissue-specific BK channel KO,

      FLS specific gene is selected. Then, the promoter of this gene is cloned into the plasmid that will drive the expression of the Cas-9 enzyme and gRNA that will direct the enzyme to the BK gene. The expression of this plasmid will only occur in the FLS cells and via the gRNA, cleavage at the BK channel gene will result in tissue-specific BK KO. The insertion and expression of the CRISPR/Cas9 machinery will occur at the zygote level (Meltzer et al., 2019). Although the in vitro method has a success rate of 1-10% in which the

environment is more controlled, the in vivo KO is expected to be more challenging because the input will be from different environments that I can barely control.

- For Aorta and VSMC
    - Also, single-cell RNA-sequencing would allow greater resolution from aortic tissue itself (see below "PVN").
    - Investigating the inherent changes in the contractile force and phenotype of the VSMC cells using a photoelasticity-based method using retardation that is related to the difference between the first and the second principal stress as well as their orientation. Cells are first treated with calyculin A and Y-27632 which produce large and small cell retardation. Actin filaments of the cell co-localize with areas of high retardation. Treated cells will have different retardation compared to the control. As cells grow in passage number, the retardation of contractile cells decreases because cell switch to synthetic phenotype (Sugita et al., 2019).
- For PVN,
    - With ageing, TRPV3 channel is thermosensitive in the PVN (reviewed here (Caterina, 2007)). Further investigation of how it's upregulation in ageing would be interesting; perhaps by targeted up-regulation in vivo using small activating RNA method(Kwok et al., 2019). Or indeed computationally using the model of Feetham *et al.* (Feetham et al., 2015b). Technically patch-clamp validation experiments of the PVN changes would be difficult. Old brain tissue is rarely used due to the technical difficulty and even isolation of neurones from older brains is rarely achieved successfully.
    - Single-cell next-generation sequencing (Hwang et al., 2018, Haque et al., 2017, Stevenson and Uversky, 2019, Anaparthy et al., 2019). This technique requires some method of cell isolation, perhaps microfluidics (Ma et al., 2017, Demaree et al., 2018) and then each

cell's RNA is individually amplified and sequenced. This would be ideal for the PVN study, but it is currently very expensive (3x the price of NGS). It would allow separation of neurones and glia (and perhaps other minor cell types such as blood vessel cells) and may also allow the separation of different types of neurones. For model parameterisation (e.g., (Feetham et al., 2015b)) it would impart tremendous scientific power to detect different cell properties (expression profiles) with age.

Conclusions

Our powerful bioinformatics approach using the inflammatory model of ageing "inflammageing" showed many similarities with the natural ageing model (old rats) presented by the enrichment of different KEGG pathways and GOs. Extracellular matrix/space and ageing were among the most common enriched GOs. Although expression of common sets of ion channels has not been found to be linked with ageing in this study, expression of some ion channel families can be counted as indicators of ageing. Common patterns of Gja1 gene expression is very interesting especially in light of recent findings that knockdown of gap junctions resulted in the extension of lifespan in worms. The roles that these gap junctions play with ageing process require further investigations. All our data will be publicly shared and together with our novel analyses pipeline, this work will be a valuable resource for ageing research**.**

Appendix

Appendix 1: Quantities of RNA of FLS young and old samples.

Sample ID	Sample name	Total quantity (ng)
18141_1	FLS_Y1C1	24552
18141_2	FLS_Y3C	37950
18141_3	FLS_Y6C	30636
18141_4	FLS_Y4C1	32400
18141_5	FLS_O1C2	31188
18141_6	FLS_O2C2	25608
18141_7	FLS_O5C1	27324
18141_8	FLS_O4C1	17388

Concentrations (quantities) of RNA from FLS young and old samples. The quantities (ng) were high (the last column). Young samples are FLS_Y1C1, FLS_Y3C, FLS_Y6C and FLS_Y4C1 while old samples are FLS_O1C2, FLS_O2C2, FLS_O5C1 and FLS_O4C1.

Appendix 2: Representatives of gel-like image and electropherogram of RNA samples.

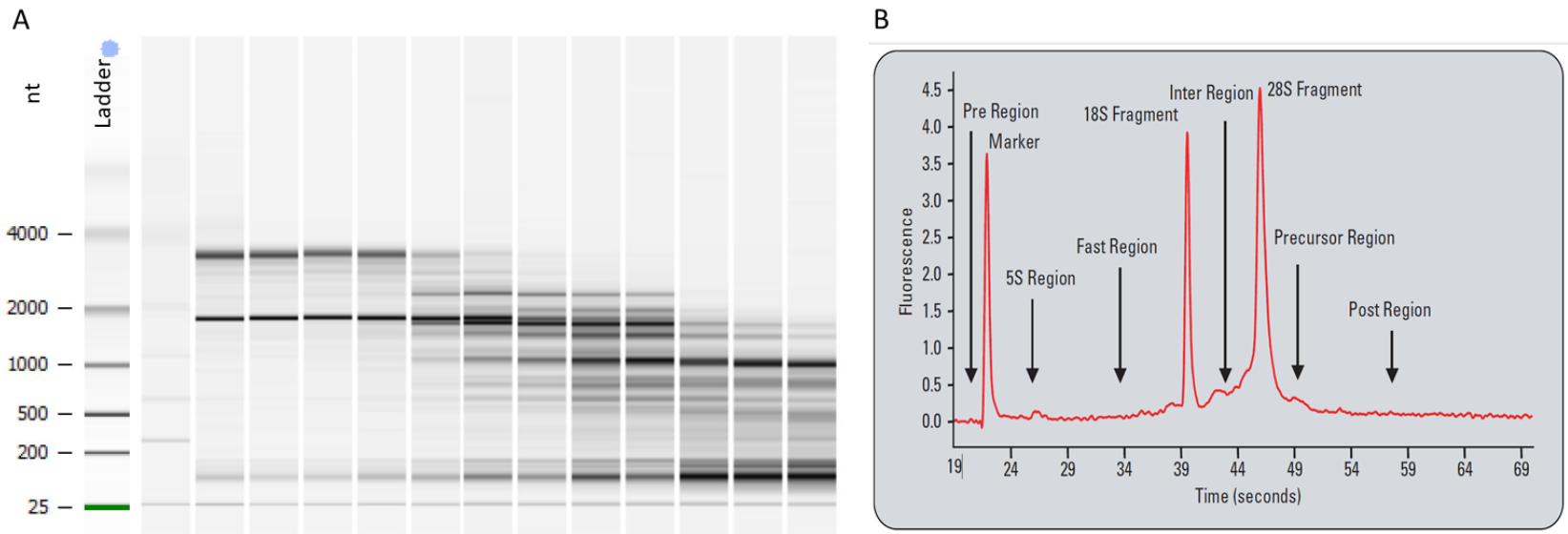

Gel-like image and electropherogram of RNA samles. A. A total RNA sample was degraded for different times. Then, analyzed on Agilent 2100 Bioanalyzer. As we move to the right, there is a shift toward more small fragments as the degradation progresses. **B.** Electropherogram detailing the regions that are indicative of RNA quality.

Appendix 3: Gel-like image of RNA of young and old FLS samples.

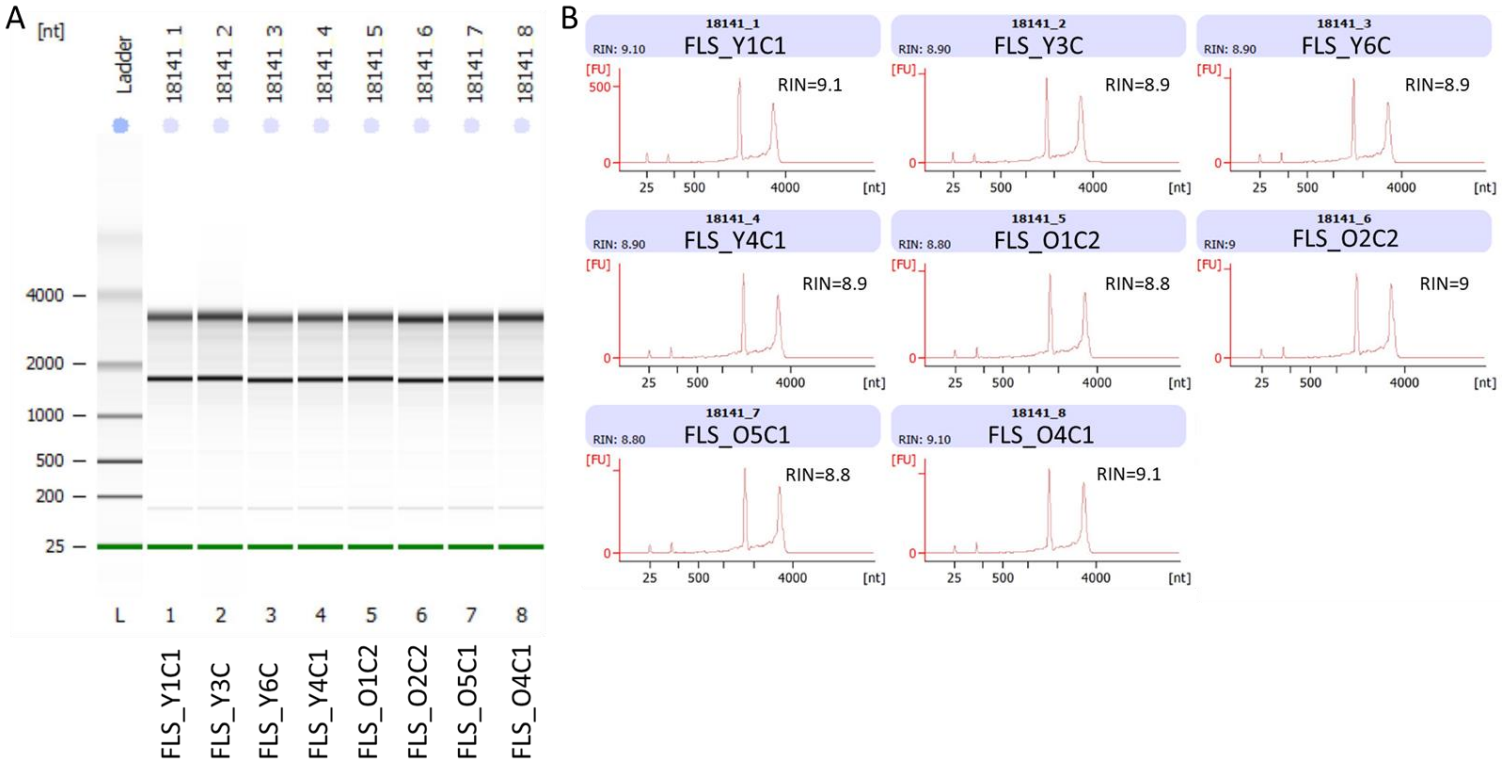

Gel-like electrophoresis of FLS young and old samples. **A.** Bands of the ribosomal subunits (18S and 28S) are shown around 2000 and 4000 nt, respectively. X-axis shows ladder (L) and FLS samples while y-axis presents nucleotides (nt). **B.** Electropherograms of RNA QC from PVN young and old samples. RNA integrity number is shown in the right side of each sample's graph. 18S (at ~2000nt) and 28S (~4000nt) peaks are shown in the figure where (x-axis) represents nucleotides (nt) and (y-axis) represents the fluorescence unit (FU). Young samples are FLS_Y1C1, FLS_Y3C, FLS_Y6C and FLS_Y4C1 while old samples are FLS_O1C2, FLS_O2C2, FLS_O5C1 and FLS_O4C1.

Appendix 4: QC summary of young and old FLS reads.

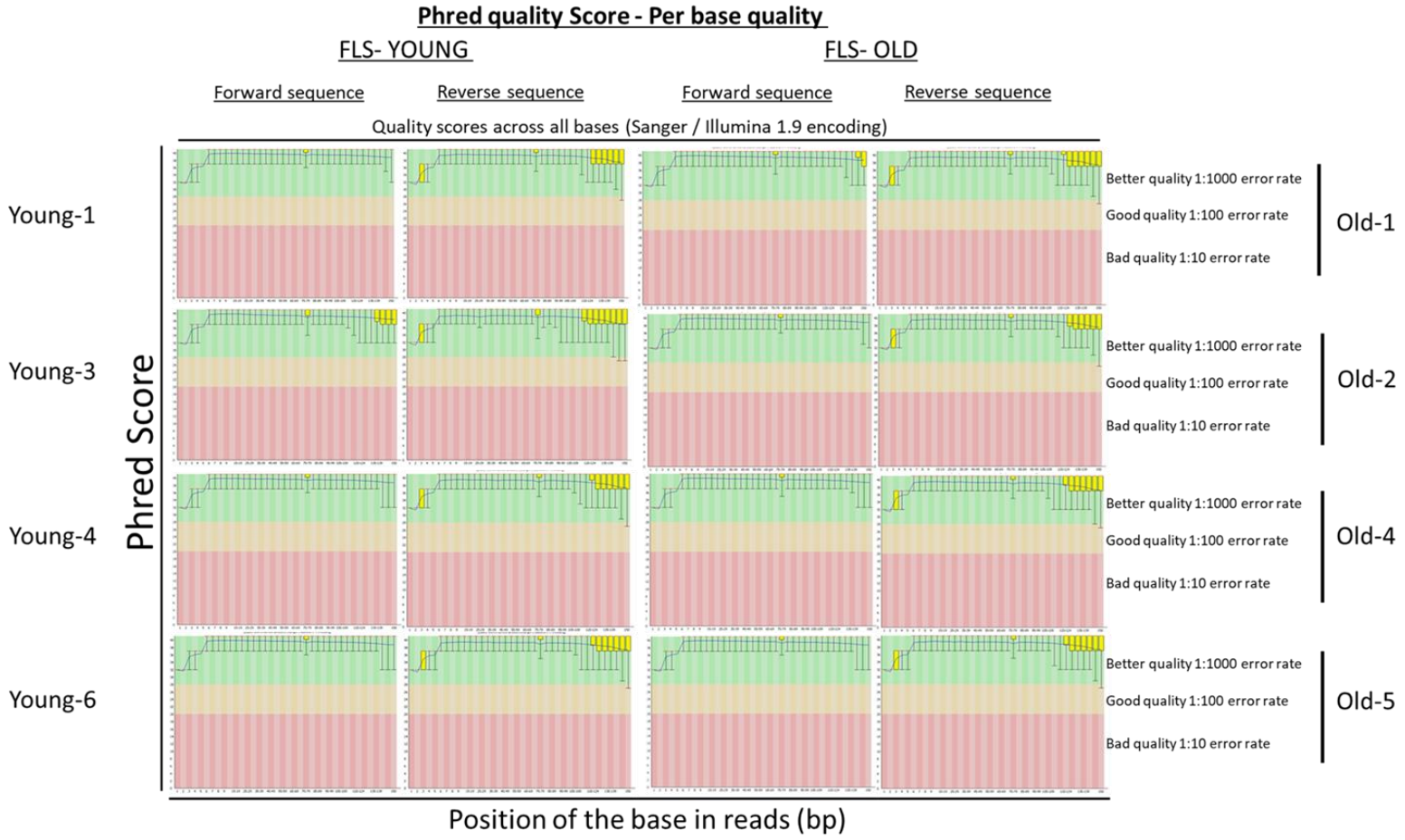

Per base quality-Phred quality score of young and old FLS reads. The Phred score is greater than 30 which reflects high quality reads (green area), more accurate and there is less rate of error (<1:1000). X-axis represents the position of the base pair in read and y-axis is the phred score from 1-40. Once quality hits the green zone, it is not necessary to show higher scores which can reach 60.

Appendix 5: Quantities of Aorta RNA samples.

		Quantity for DNase treatment	Volume for DNase treatment	RNAClean XP purification	Elution volume	Volume remaining	Total quantity
ID	Sample name	(ng)	(ul)	(1: 1.8 ratio)	(ul)	(ul)	(ng)
19191_11	AORTA-YOUNG-1	15	18	Yes	9	7	1.23
19191_14	AORTA-YOUNG-4	189	18	Yes	9	7	35
19191_15	AORTA-YOUNG-5	472	18	Yes	9	7	123.2
19191_16	AORTA-OLD-1	16	18	Yes	9	7	19.7
19191_17	AORTA-OLD-2	239	18	Yes	9	7	51.7
19191_19	AORTA-OLD-4	196	18	Yes	9	7	4.73

Concentrations (quantities) of RNA from Aorta young and old samples. The quantities (ng) were low. Samples were DNase treated, cleaned with RNAClean XP purification kit, and eluted in 9 µl. The final quantities are shown on the last column. Young aorta samples are AORTA-YOUNG-1, AORTA-YOUNG-4 and AORTA-YOUNG-5 while old are AORTA-OLD-1, AORTA-OLD-2 and AORTA-OLD-4.

Appendix 6: QC summary of RNA of young and old Aorta samples.

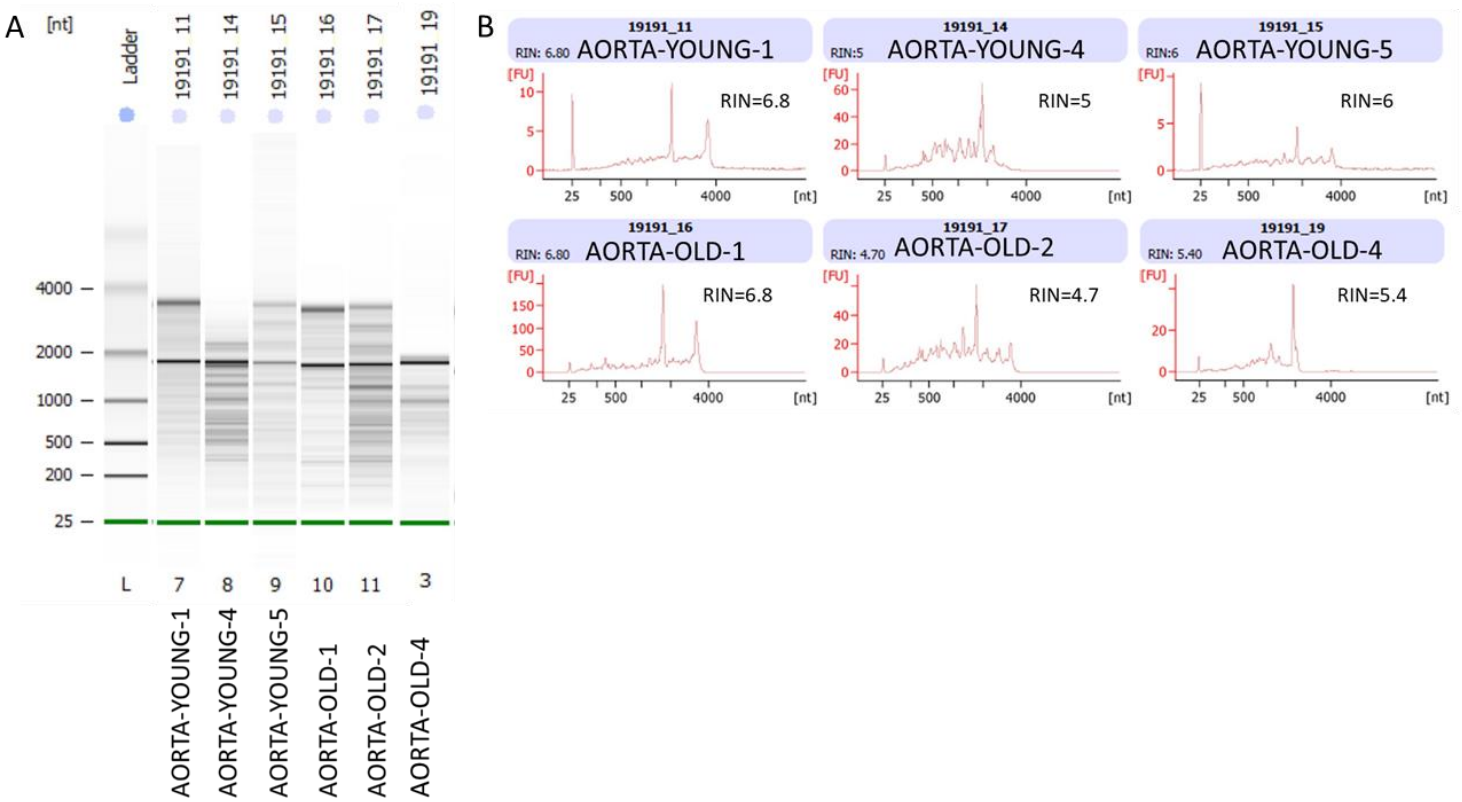

Quality check of RNA of young and old Aorta samples. **A.** Gel-like electrophoresis of Aorta young and old samples. Bands of the ribosomal subunits (18S and 28S) are shown around 2000 and 4000 nt, respectively. X-axis shows ladder (L) and Aorta samples while y-axis presents nucleotides (nt). **B.** Electropherograms of RNA QC from Aorta young and old samples. RNA integrity number is shown in the right side of each sample's graph. 18S (at ~2000nt) and 28S (~4000nt) peaks are shown in the figure where (x-axis) represents nucleotides (nt) and (y-axis) represents the fluorescence unit (FU). AORTA-YOUNG-1, AORTA-YOUNG-4 and AORTA-YOUNG-5 while old are AORTA-OLD-1, AORTA-OLD-2 and AORTA-OLD-4.

Appendix 7: QC check of Aorta reads.

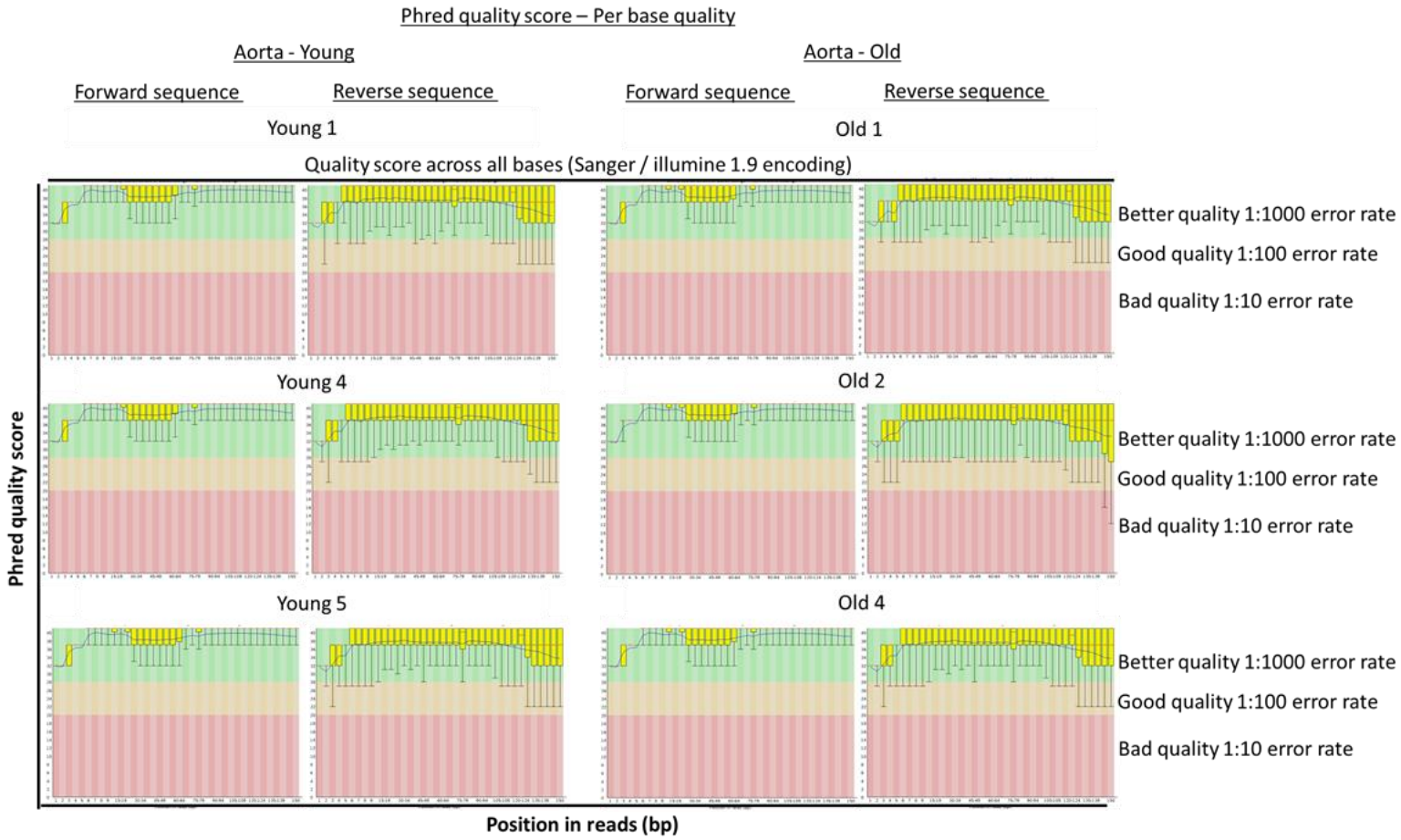

QC summary of young and old Aorta reads. Per base quality-Phred quality score of young and old Aorta reads. The Phred score is greater than 30 which reflects high quality reads (green area), more accurate and there is less rate of error (<1:1000). X-axis represents the position of the base pair in read and y-axis is the phred score from 1-40. Once quality hits the green zone, it is not necessary to show higher scores which can reach 60.

Appendix 8: Quantities of VSMC RNA samples.

Sample ID	Sample name	Total quantity (ng)
18141_9	VSMC_17C	58392
18141_10	VSMC_17T	33132
18141_11	VSMC_18C	3600
18141_12	VSMC_18T	7452
18141_13	VSMC_13C	4882
18141_14	VSMC_13T	8446
18141_15	VSMC_12C	7500
18141_16	VSMC_12T	11178

Concentrations (quantities) of RNA from VSMC control and cytokine treated samples. The quantities (ng) were high. Control samples of VSMC are VSMC_17C, VSMC_18C, VSMC_13C and VSMC_12C while cytokines treated VSMC are VSMC_17T, VSMC_18T, VSMC_13T and VSMC_12T.

Appendix 9: Gel-like image of RNA of control and cytokine treated VSMC samples.

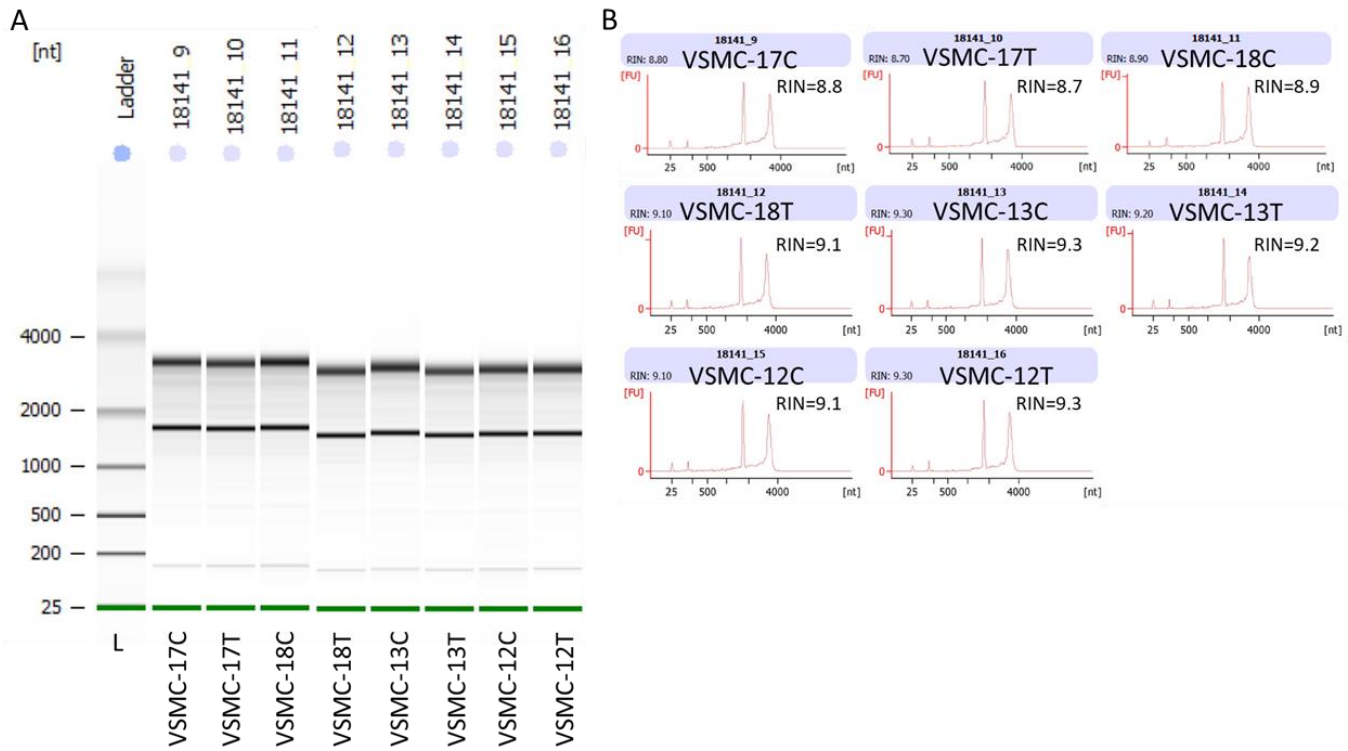

Quality check of RNA of young and old VSMC samples . A. Gel-like electrophoresis of VSMC of young and old samples. Bands of the ribosomal subunits (18S and 28S) are shown around 2000 and 4000 nt, respectively. X-axis shows ladder (L) and VSMC samples while y-axis presents nucleotides (nt). **B.** Electropherograms of RNA QC from VSMC young and old samples. RNA integrity number is shown in the right side of each sample's graph. 18S (at ~2000nt) and 28S (~4000nt) peaks are shown in the figure where (x-axis) represents nucleotides (nt) and (y-axis) represents the fluorescence unit (FU). 17C, 18C, 13C, AND 12C are control samples whereas 17T, 18T, 13T, and 12T are cytokine treated samples. Control samples of VSMC are VSMC_17C, VSMC_18C, VSMC_13C and VSMC_12C while cytokines treated VSMC are VSMC_17T, VSMC_18T, VSMC_13T and VSMC_12T.

Appendix 10: QC summary of control and cytokine treated VSMC reads.

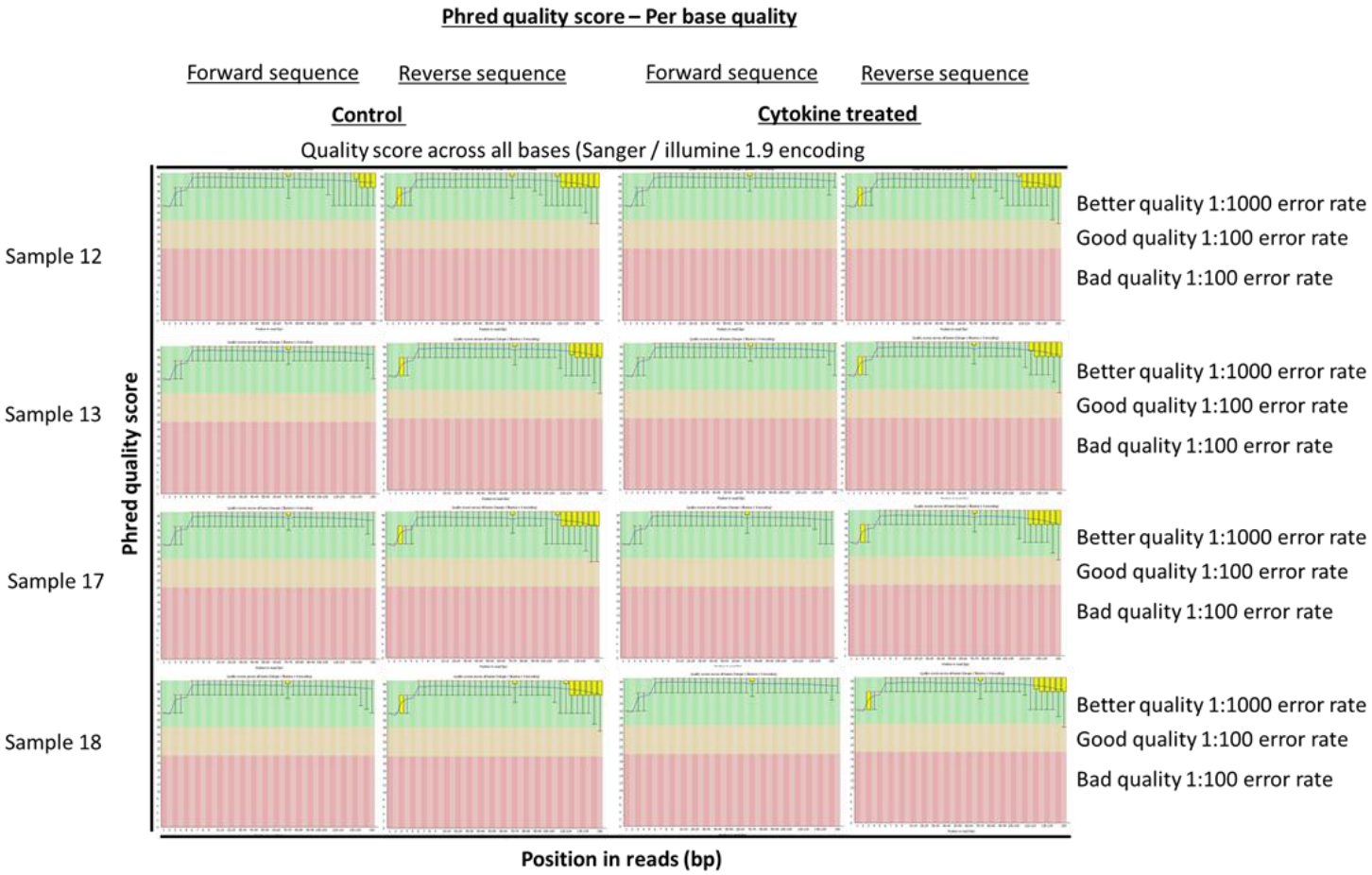

Per base quality-Phred quality score of young and old Aorta reads. The Phred score is greater than 30 which reflects high quality reads (green area), more accurate and there is less rate of error (<1:1000). X-axis represents the position of the base pair in read and y-axis is the phred score from 1-40. Once quality hits the green zone, it is not necessary to show higher scores which can reach 60.

Appendix 11: Quantities of PVN samples.

		Quantity for	Volume for	RNAClean XP	Elution	Volume	Total
		DNase treatment	DNase treatment	purification	volume	remaining	quantity
ID	Sample name	(ng)	(ul)	(1: 1.8 ratio)	(ul)	(ul)	(ng)
19191_1	PVN-YOUNG-1	407	18	Yes	9	7	86.1
19191_3	PVN-YOUNG-3	225	18	Yes	9	7	40.9
19191_4	PVN-YOUNG-4	396	18	Yes	9	7	94.5
19191_8	PVN-OLD-3	19	18	Yes	9	7	1.4
19191_9	PVN-OLD-4	72	18	Yes	9	7	2.79
19191_10	PVN-OLD-5	28	18	Yes	9	7	1.65

Concentrations (quantities) of RNA from PVN young and old samples. The quantities (ng) were low. Samples were DNase treated, cleaned with RNAClean XP purification kit, and eluted in 9 µl. The final quantities are shown on the last column.

Appendix 12: QC summary of RNA of PVN young and old samples.

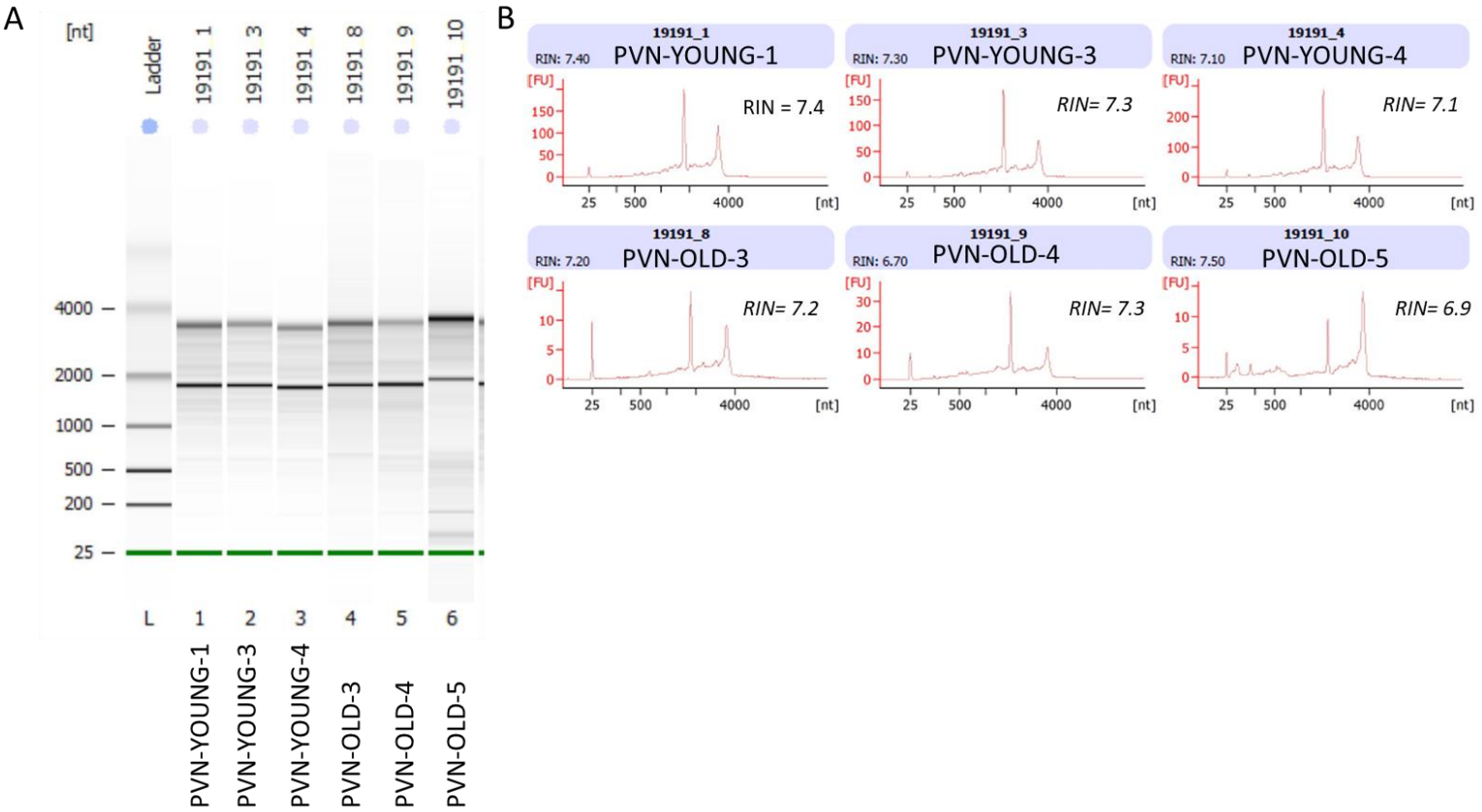

Gel-like electrophoresis and electropherogram of PVN young and old samples. A. Bands of the ribosomal subunits (18S and 28S) are shown around 2000 and 4000 nt, respectively. X-axis shows ladder (L) and PVN samples while y-axis presents nucleotides (nt). **B.** Electropherograms of RNA QC from PVN young and old samples. RNA integrity number is shown in the right side of each sample's graph. 18S (at ~2000nt) and 28S (~4000nt) peaks are shown in the figure where (x-axis) represents nucleotides (nt) and (y-axis) represents the fluorescence unit (FU).

Appendix 13: Summary of QC of PVN young and old reads.

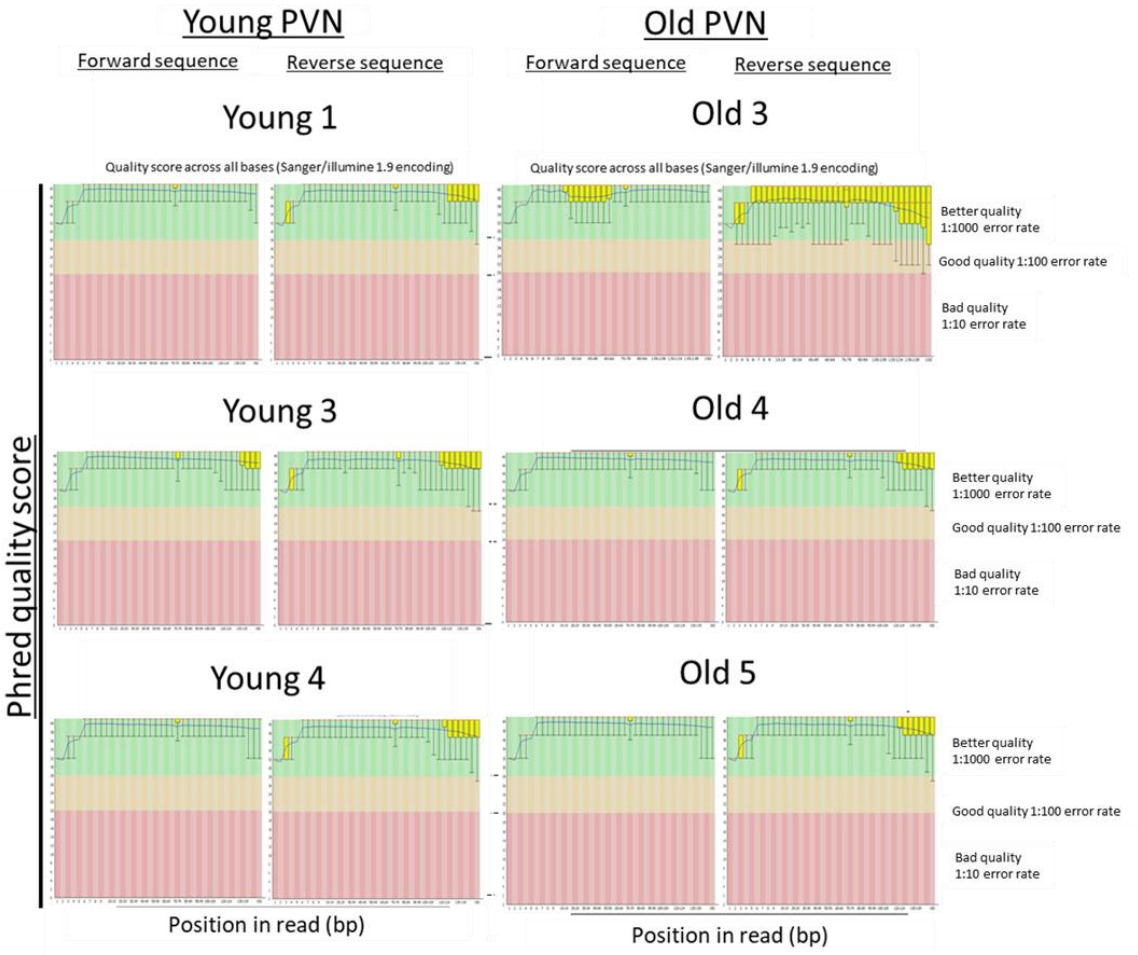

Per base quality-Phred quality score of young and old PVN reads. The Phred score is greater than 30 which reflects high quality reads (green area), more accurate and there is less rate of error (<1 in 1000). X-axis represents the position of the base pair in read. Each read is 150bp. Y-axis is the phred score from 1-40. once quality hits the green zone, it is not necessary to show higher scores which can reach 60.

References

2019. The Gene Ontology Resource: 20 years and still GOing strong. *Nucleic Acids Research,* 47**,** D330-D338.

ABDUL KADIR, L., STACEY, M. & BARRETT-JOLLEY, R. 2018. Emerging Roles of the Membrane Potential: Action Beyond the Action Potential. *Frontiers in Physiology,* 9.

ACKERMANN, M., CHAO, L., BERGSTROM, C. T. & DOEBELI, M. 2007. On the evolutionary origin of aging. *Aging Cell,* 6**,** 235-244.

AGRE, P. 2006. The Aquaporin Water Channels. 3**,** 5-13.

AHMED, M. S., IKRAM, S., BIBI, N. & MIR, A. 2017. Hutchinson–Gilford Progeria Syndrome: A Premature Aging Disease. *Molecular Neurobiology*.

AKHURST, R. J. & HATA, A. 2012. Targeting the TGFβ signalling pathway in disease. *Nature Reviews Drug Discovery,* 11**,** 790-811.

ALBARWANI, S. A., MANSOUR, F., KHAN, A. A., AL-LAWATI, I., AL-KAABI, A., AL-BUSAIDI, A.-M., AL-HADHRAMI, S., AL-HUSSEINI, I., AL-SIYABI, S. & TANIRA, M. O. 2016. Aging Reduces L-Type Calcium Channel Current and the Vasodilatory Response of Small Mesenteric Arteries to Calcium Channel Blockers. *Frontiers in Physiology,* 7.

AMIN, A. S., TAN, H. L. & WILDE, A. A. 2010. Cardiac ion channels in health and disease. *Heart Rhythm,* 7**,** 117-26.

ANAPARTHY, N., HO, Y. J., MARTELOTTO, L., HAMMELL, M. & HICKS, J. 2019. Single-Cell Applications of Next-Generation Sequencing. *Cold Spring Harb Perspect Med,* 9.

ANGULO, E., NOE, V., CASADO, V., MALLOL, J., GOMEZ-ISLA, T., LLUIS, C., FERRER, I., CIUDAD, C. J. & FRANCO, R. 2004. Up-regulation of the Kv3.4 potassium channel subunit in early stages of Alzheimer's disease. *J Neurochem,* 91**,** 547-57.

ANON 2000. Recommendations for the medical management of osteoarthritis of the hip and knee: 2000 update. American College of Rheumatology Subcommittee on Osteoarthritis Guidelines. *Arthritis Rheum,* 43**,** 1905-15.

ARITA, M., OHIRA, T., SUN, Y. P., ELANGOVAN, S., CHIANG, N. & SERHAN, C. N. 2007. Resolvin E1 selectively interacts with leukotriene B4 receptor BLT1 and ChemR23 to regulate inflammation. *J Immunol,* 178**,** 3912-7.

ARMSTRONG, M. E., ALEXANDER, H. D., RITCHIE, J. L., MCMILLAN, S. A. & REA, I. M. 2001. Age-related alterations in basal expression and in vitro, tumour necrosis factor alpha mediated, upregulation of CD11b. *Gerontology,* 47**,** 180-5.

ASHBURNER, M., BALL, C. A., BLAKE, J. A., BOTSTEIN, D., BUTLER, H., CHERRY, J. M., DAVIS, A. P., DOLINSKI, K., DWIGHT, S. S., EPPIG, J. T., HARRIS, M. A., HILL, D. P., ISSEL-TARVER, L., KASARSKIS, A., LEWIS, S., MATESE, J. C., RICHARDSON, J. E., RINGWALD, M., RUBIN, G. M. & SHERLOCK, G. 2000. Gene Ontology: tool for the unification of biology. *Nature Genetics,* 25**,** 25-29.

ASPINALL, R. 2006. T cell development, ageing and Interleukin-7. *Mech Ageing Dev,* 127**,** 572-8.

BABENKO, A. P., GONZALEZ, G., AGUILAR-BRYAN, L. & BRYAN, J. 1998. Reconstituted Human Cardiac KATP Channels : Functional Identity With the Native Channels From the Sarcolemma of Human Ventricular Cells. 83**,** 1132-1143.

BADOER, E. 1996. Cardiovascular role of parvocellular neurons in the paraventricular nucleus of the hypothalamus. *News in Physiological Sciences,* 11**,** 43-47.

BAE, E., CHA, R. H., KIM, Y. C., AN, J. N., KIM, D. K., YOO, K. D., LEE, S. M., KIM, M. H., PARK, J. T., KANG, S. W., PARK, J. Y., LIM, C. S., KIM, Y. S., YANG, S. H. & LEE, J. P. 2017. Circulating TNF receptors predict cardiovascular disease in patients with chronic kidney disease. *Medicine (Baltimore),* 96**,** e6666.

BARDAK, S., TURGUTALP, K., KOYUNCU, M. B., HARI, H., HELVACI, I., OVLA, D., HOROZ, M., DEMIR, S. & KIYKIM, A. 2017. Community-acquired hypokalemia in elderly patients: related factors and clinical outcomes. *Int Urol Nephrol,* 49**,** 483-489.

BARRETT-JOLLEY, R., LEWIS, R., FALLMAN, R. & MOBASHERI, A. 2010. The Emerging Chondrocyte Channelome. *Frontiers in Physiology,* 1**,** 1-11.

BARTOK, B. & FIRESTEIN, G. S. 2010. Fibroblast-like synoviocytes: key effector cells in rheumatoid arthritis. *Immunological Reviews,* 233**,** 233-255.

BAUER, J. 1989. Regulation of interleukin 6 receptor expression in human monocytes and monocyte-derived macrophages. Comparison with the expression in human hepatocytes. *Journal of Experimental Medicine,* 170**,** 1537-1549.

BAUGE, C., GIRARD, N., LHUISSIER, E., BAZILLE, C. & BOUMEDIENE, K. 2014. Regulation and Role of TGFbeta Signaling Pathway in Aging and Osteoarthritis Joints. *Aging Dis,* 5**,** 394-405.

BECKER, D. L., PHILLIPS, A. R., DUFT, B. J., KIM, Y. & GREEN, C. R. 2015. Translating connexin biology into therapeutics.

BEHR, E. R., DALAGEORGOU, C., CHRISTIANSEN, M., SYRRIS, P., HUGHES, S., TOME ESTEBAN, M. T., ROWLAND, E., JEFFERY, S. & MCKENNA, W. J. 2008. Sudden arrhythmic death syndrome: familial evaluation identifies inheritable heart disease in the majority of families. *Eur Heart J,* 29**,** 1670-80.

BELLANTUONO, I. & POTTER, P. K. 2016. Modelling ageing and age-related disease. *Drug Discovery Today: Disease Models,* 20**,** 27-32.

BELLOCQ, C., VAN GINNEKEN, A. C., BEZZINA, C. R., ALDERS, M., ESCANDE, D., MANNENS, M. M., BARO, I. & WILDE, A. A. 2004. Mutation in the KCNQ1 gene leading to the short QT-interval syndrome. *Circulation,* 109**,** 2394-7.

BENNETT, D. L., CLARK, A. J., HUANG, J., WAXMAN, S. G. & DIB-HAJJ, S. D. 2019. The Role of Voltage-Gated Sodium Channels in Pain Signaling. *Physiol Rev,* 99**,** 1079-1151.

BENNETT, M. R., SINHA, S. & OWENS, G. K. 2016. Vascular Smooth Muscle Cells in Atherosclerosis. *Circulation Research,* 118**,** 692-702.

BENYA, P. D. & SHAFFER, J. D. 1982. Dedifferentiated chondrocytes reexpress the differentiated collagen phenotype when cultured in agarose gels. *Cell,* 30**,** 215-24.

BERENBAUM, F. 2013. Osteoarthritis as an inflammatory disease (osteoarthritis is not osteoarthrosis!). *Osteoarthritis and Cartilage,* 21**,** 16-21.

BHATTACHARJEE, A., JOINER, W. J., WU, M., YANG, Y., SIGWORTH, F. J. & KACZMAREK, L. K. 2003. Slick (Slo2.1), a Rapidly-Gating Sodium-Activated Potassium Channel Inhibited by ATP. *The Journal of Neuroscience,* 23**,** 11681-11691.

BODA, E., HOXHA, E., PINI, A., MONTAROLO, F. & TEMPIA, F. 2012. Brain expression of Kv3 subunits during development, adulthood and aging and in a murine model of Alzheimer's disease. *J Mol Neurosci,* 46**,** 606-15.

BODMAN, M. A. & VARACALLO, M. 2019. Diabetic Neuropathy. *StatPearls.* Treasure Island (FL).

BORASCHI, D., ITALIANI, P., WEIL, S. & MARTIN, M. U. 2018. The family of the interleukin-1 receptors. *Immunol Rev,* 281**,** 197-232.

BOSCO, P., FERRI, R., SALLUZZO, M. G., CASTELLANO, S., SIGNORELLI, M., NICOLETTI, F., NUOVO, S. D., DRAGO, F. & CARACI, F. 2013. Role of the Transforming-Growth-Factor-beta1 Gene in Late-Onset Alzheimer's Disease: Implications for the Treatment. *Curr Genomics,* 14**,** 147-56.

BROZOVICH, F. V., NICHOLSON, C. J., DEGEN, C. V., GAO, Y. Z., AGGARWAL, M. & MORGAN, K. G. 2016. Mechanisms of Vascular Smooth Muscle Contraction and the Basis for Pharmacologic Treatment of Smooth Muscle Disorders. *Pharmacological Reviews,* 68**,** 476-532.

BRUST, P. F., SIMERSON, S., MCCUE, A. F., DEAL, C. R., SCHOONMAKER, S., WILLIAMS, M. E., VELICELEBI, G., JOHNSON, E. C., HARPOLD, M. M. & ELLIS, S. B. 1993. Human neuronal voltage-dependent

calcium channels: studies on subunit structure and role in channel assembly. *Neuropharmacology,* 32**,** 1089-102.

BRUUNSGAARD, H. 2002. Effects of tumor necrosis factor-alpha and interleukin-6 in elderly populations. *Eur Cytokine Netw,* 13**,** 389-91.

BRUUNSGAARD, H., ANDERSEN-RANBERG, K., HJELMBORG, J. V. B., PEDERSEN, B. K. & JEUNE, B. 2003a. Elevated levels of tumor necrosis factor alpha and mortality in centenarians. 115**,** 278-283.

BRUUNSGAARD, H., LADELUND, S., PEDERSEN, A. N., SCHROLL, M., JORGENSEN, T. & PEDERSEN, B. K. 2003b. Predicting death from tumour necrosis factor-alpha and interleukin-6 in 80-year-old people. *Clin Exp Immunol,* 132**,** 24-31.

BRUUNSGAARD, H., SKINHOJ, P., PEDERSEN, A. N., SCHROLL, M. & PEDERSEN, B. K. 2000. Ageing, tumour necrosis factor-alpha (TNF-alpha) and atherosclerosis. *Clin Exp Immunol,* 121**,** 255-60.

BURKE, D., KIERNAN, M. C. & BOSTOCK, H. 2001. Excitability of human axons. *Clin Neurophysiol,* 112**,** 1575-85.

BURKS, T. N. & COHN, R. D. 2011. Role of TGF-beta signaling in inherited and acquired myopathies. *Skelet Muscle,* 1**,** 19.

BURMESTER, G. R., DIMITRIU-BONA, A., WATERS, S. J. & WINCHESTER, R. J. 1983. Identification of three major synovial lining cell populations by monoclonal antibodies directed to Ia antigens and antigens associated with monocytes/macrophages and fibroblasts. *Scand J Immunol,* 17**,** 69-82.

CAMPBELL, L. M., MAXWELL, P. J. & WAUGH, D. J. 2013. Rationale and Means to Target Pro-Inflammatory Interleukin-8 (CXCL8) Signaling in Cancer. *Pharmaceuticals (Basel),* 6**,** 929-59.

CANNON, S. C. 2015. Channelopathies of skeletal muscle excitability. *Compr Physiol,* 5**,** 761-90.

CARBONI, G. L., GAO, B., NISHIZAKI, M., XU, K., MINNA, J. D., ROTH, J. A. & JI, L. 2003. CACNA2D2-mediated apoptosis in NSCLC cells is associated with alterations of the intracellular calcium signaling and disruption of mitochondria membrane integrity. *Oncogene,* 22**,** 615-626.

CARRIERI, G., MARZI, E., OLIVIERI, F., MARCHEGIANI, F., CAVALLONE, L., CARDELLI, M., GIOVAGNETTI, S., STECCONI, R., MOLENDINI, C., TRAPASSI, C., DE BENEDICTIS, G., KLETSAS, D. & FRANCESCHI, C. 2004. The G/C915 polymorphism of transforming growth factor β1 is associated with human longevity: a study in Italian centenarians. *Aging Cell,* 3**,** 443-448.

CARUSO, C., CANDORE, G., CIGNA, D., DILORENZO, G., SIRECI, G., DIELI, F. & SALERNO, A. 1996. Cytokine production pathway in the elderly. *Immunol Res,* 15**,** 84-90.

CARVALHO-DE-SOUZA, J. L., VARANDA, W. A., TOSTES, R. C. & CHIGNALIA, A. Z. 2013. BK Channels in Cardiovascular Diseases and Aging. *Aging Dis,* 4**,** 38-49.

CASTRO, D. & SHARMA, S. 2019. Hypokalemia. *StatPearls.* Treasure Island (FL).

CATERINA, M. J. 2007. Transient receptor potential ion channels as participants in thermosensation and thermoregulation. *American Journal of Physiology-Regulatory, Integrative and Comparative Physiology,* 292**,** R64-R76.

CAVALLONE, L., BONAFE, M., OLIVIERI, F., CARDELLI, M., MARCHEGIANI, F., GIOVAGNETTI, S., DI STASIO, G., GIAMPIERI, C., MUGIANESI, E., STECCONI, R., SCIACCA, F., GRIMALDI, L. M., DE BENEDICTIS, G., LIO, D., CARUSO, C. & FRANCESCHI, C. 2003. The role of IL-1 gene cluster in longevity: a study in Italian population. *Mech Ageing Dev,* 124**,** 533-8.

CHAKROBORTY, S. & STUTZMANN, G. E. 2014. Calcium channelopathies and Alzheimer's disease: insight into therapeutic success and failures. *Eur J Pharmacol,* 739**,** 83-95.

CHATTERJEE, A., SHARMA, A., CHEN, M., TOY, R., MOTTOLA, G. & CONTE, M. S. 2014. The pro-resolving lipid mediator maresin 1 (MaR1) attenuates inflammatory signaling pathways in vascular smooth muscle and endothelial cells. *PLoS One,* 9**,** e113480.

CHENG, J., WEN, J., WANG, N., WANG, C., XU, Q. & YANG, Y. 2019. Ion Channels and Vascular Diseases. *Arteriosclerosis, Thrombosis, and Vascular Biology,* 39.

CHENG, W., SUN, C. & ZHENG, J. 2010. Heteromerization of TRP channel subunits: extending functional diversity. *Protein & Cell,* 1**,** 802-810.

CHIURCHIU, V., LEUTI, A. & MACCARRONE, M. 2018. Bioactive Lipids and Chronic Inflammation: Managing the Fire Within. *Front Immunol,* 9**,** 38.

CHRISTOPHER, DEREK & CHARLES 2014. Proresolving Lipid Mediators and Mechanisms in the Resolution of Acute Inflammation. *Immunity,* 40**,** 315-327.

CHRYSAFIDES, S. M. & SHARMA, S. 2019. Physiology, Resting Potential. *StatPearls.* Treasure Island (FL).

CHUNG, H. Y., CESARI, M., ANTON, S., MARZETTI, E., GIOVANNINI, S., SEO, A. Y., CARTER, C., YU, B. P. & LEEUWENBURGH, C. 2009. Molecular inflammation: underpinnings of aging and age-related diseases. *Ageing Res Rev,* 8**,** 18-30.

CHUNG, K. F. 2009. Cytokines. Elsevier.

CLARK, R. B., SCHMIDT, T. A., SACHSE, F. B., BOYLE, D., FIRESTEIN, G. S. & GILES, W. R. 2017. Cellular electrophysiological principles that modulate secretion from synovial fibroblasts. *J Physiol,* 595**,** 635-645.

CLARKE, R., VALDES-MARQUEZ, E., HILL, M., GORDON, J., FARRALL, M., HAMSTEN, A., WATKINS, H. & HOPEWELL, J. C. 2018. Plasma cytokines and risk of coronary heart disease in the PROCARDIS study. *Open Heart,* 5**,** e000807.

COHEN, R. M., FOELL, J. D., BALIJEPALLI, R. C., SHAH, V., HELL, J. W. & KAMP, T. J. 2005. Unique modulation of L-type Ca2+ channels by short auxiliary beta1d subunit present in cardiac muscle. *Am J Physiol Heart Circ Physiol,* 288**,** H2363-74.

COLLIN, T., LORY, P., TAVIAUX, S., COURTIEU, C., GUILBAULT, P., BERTA, P. & NARGEOT, J. 1994. Cloning, chromosomal location and functional expression of the human voltage-dependent calcium-channel beta3 subunit. 220**,** 257-262.

COLLINS, J. S., PERRY, R. T., WATSON, B., JR., HARRELL, L. E., ACTON, R. T., BLACKER, D., ALBERT, M. S., TANZI, R. E., BASSETT, S. S., MCINNIS, M. G., CAMPBELL, R. D. & GO, R. C. 2000. Association of a haplotype for tumor necrosis factor in siblings with late-onset Alzheimer disease: the NIMH Alzheimer Disease Genetics Initiative. *Am J Med Genet,* 96**,** 823-30.

COMMINS, S., STEINKE, J. W. & BORISH, L. 2008. The extended IL-10 superfamily: IL-10, IL-19, IL-20, IL-22, IL-24, IL-26, IL-28, and IL-29. *Journal of Allergy and Clinical Immunology,* 121**,** 1108-1111.

COOTE, J. H. 1995. Cardiovascular function of the paraventricular nucleus of the hypothalamus. *Biological Signals,* 4**,** 142-149.

COOTE, J. H. 2005. A role for the paraventricular nucleus of the hypothalamus in the autonomic control of heart and kidney. *Experimental physiology,* 90**,** 169-73.

COOTE, J. H. 2007. Landmarks in understanding the central nervous control of the cardiovascular system. *Experimental Physiology,* 92**,** 3-18.

COWLED, P. & FITRIDGE, R. 2011. Pathophysiology of Reperfusion Injury. *In:* FITRIDGE, R. & THOMPSON, M. (eds.) *Mechanisms of Vascular Disease: A Reference Book for Vascular Specialists.* Adelaide (AU).

CUI, J., COX, D. H. & ALDRICH, R. W. 1997. Intrinsic voltage dependence and Ca2+ regulation of mslo large conductance Ca-activated K+ channels. *J Gen Physiol,* 109**,** 647-73.

CUI, J., YANG, H. & LEE, U. S. 2009. Molecular mechanisms of BK channel activation. *Cell Mol Life Sci,* 66**,** 852-75.

DANE, E. L. & GRINSTAFF, M. W. 2012. Poly-amido-saccharides: Synthesis via Anionic Polymerization of a β-Lactam Sugar Monomer. 134**,** 16255-16264.

DANIIL, G., FERNANDES-ROSA, F. L., CHEMIN, J., BLESNEAC, I., BELTRAND, J., POLAK, M., JEUNEMAITRE, X., BOULKROUN, S., AMAR, L., STROM, T. M., LORY, P. & ZENNARO, M. C. 2016. CACNA1H Mutations Are Associated With Different Forms of Primary Aldosteronism. *EBioMedicine,* 13**,** 225-236.

DAVIS, A. J., FORREST, A. S., JEPPS, T. A., VALENCIK, M. L., WIWCHAR, M., SINGER, C. A., SONES, W. R., GREENWOOD, I. A. & LEBLANC, N. 2010. Expression profile and protein translation of TMEM16A in murine smooth muscle. *Am J Physiol Cell Physiol,* 299**,** C948-59.

DAVIS, A. J., SHI, J., PRITCHARD, H. A., CHADHA, P. S., LEBLANC, N., VASILIKOSTAS, G., YAO, Z., VERKMAN, A. S., ALBERT, A. P. & GREENWOOD, I. A. 2013. Potent vasorelaxant activity of the TMEM16A inhibitor T16A(inh) -A01. *Br J Pharmacol,* 168**,** 773-84.

DAY, M. J. 2010. Ageing, immunosenescence and inflammageing in the dog and cat. *J Comp Pathol,* 142 S1**,** S60-9.

DE CEUNINCK, F., DASSENCOURT, L. & ANRACT, P. 2004. The inflammatory side of human chondrocytes unveiled by antibody microarrays. *Biochem Biophys Res Commun,* 323**,** 960-9.

DE HOOGE, A. S., VAN DE LOO, F. A., BENNINK, M. B., ARNTZ, O. J., DE HOOGE, P. & VAN DEN BERG, W. B. 2005. Male IL-6 gene knock out mice developed more advanced osteoarthritis upon aging. *Osteoarthritis Cartilage,* 13**,** 66-73.

DE KEERSMAECKER, K. 2005. Fusion of EML1 to ABL1 in T-cell acute lymphoblastic leukemia with cryptic t(9;14)(q34;q32). 105**,** 4849-4852.

DEMAREE, B., WEISGERBER, D., LAN, F. & ABATE, A. R. 2018. An Ultrahigh-throughput Microfluidic Platform for Single-cell Genome Sequencing. *Journal of Visualized Experiments*.

DEUTCH, A. Y. & WINDER, D. G. 2006. A channel to neurodegeneration. *Nat Med,* 12**,** 17-8.

DI IORIO, A., FERRUCCI, L., SPARVIERI, E., CHERUBINI, A., VOLPATO, S., CORSI, A., BONAFE, M., FRANCESCHI, C., ABATE, G. & PAGANELLI, R. 2003. Serum IL-1beta levels in health and disease: a population-based study. 'The InCHIANTI study'. *Cytokine,* 22**,** 198-205.

DIDION, S. P., KINZENBAW, D. A., SCHRADER, L. I., CHU, Y. & FARACI, F. M. 2009. Endogenous Interleukin-10 Inhibits Angiotensin II-Induced Vascular Dysfunction. 54**,** 619-624.

DINARELLO, C. A. 2006. Interleukin 1 and interleukin 18 as mediators of inflammation and the aging process. *Am J Clin Nutr,* 83**,** 447S-455S.

DINARELLO, C. A. 2018. Overview of the IL-1 family in innate inflammation and acquired immunity. *Immunol Rev,* 281**,** 8-27.

DINARELLO, C. A., NOLD-PETRY, C., NOLD, M., FUJITA, M., LI, S., KIM, S. & BUFLER, P. 2016. Suppression of innate inflammation and immunity by interleukin-37. *Eur J Immunol,* 46**,** 1067-81.

DONAHUE, H. J., QU, R. W. & GENETOS, D. C. 2017. Joint diseases: from connexins to gap junctions. *Nature Reviews Rheumatology,* 14**,** 42-51.

DONG, C. 2008. Regulation and pro-inflammatory function of interleukin-17 family cytokines. 226**,** 80-86.

DOUPNIK, C. A., DAVIDSON, N. & LESTER, H. A. 1995. The inward rectifier potassium channel family. 5**,** 268-277.

DOYLE, K. P., CEKANAVICIUTE, E., MAMER, L. E. & BUCKWALTER, M. S. 2010. TGFbeta signaling in the brain increases with aging and signals to astrocytes and innate immune cells in the weeks after stroke. *J Neuroinflammation,* 7**,** 62.

DOYLE, S. L., OZAKI, E., BRENNAN, K., HUMPHRIES, M. M., MULFAUL, K., KEANEY, J., KENNA, P. F., MAMINISHKIS, A., KIANG, A. S., SAUNDERS, S. P., HAMS, E., LAVELLE, E. C., GARDINER, C., FALLON, P. G., ADAMSON, P., HUMPHRIES, P. & CAMPBELL, M. 2014. IL-18 attenuates experimental choroidal neovascularization as a potential therapy for wet age-related macular degeneration. *Sci Transl Med,* 6**,** 230ra44.

EKKENS, M. J., SHEDLOCK, D. J., JUNG, E., TROY, A., PEARCE, E. L., SHEN, H. & PEARCE, E. J. 2007. Th1 and Th2 cells help CD8 T-cell responses. *Infect Immun,* 75**,** 2291-6.

ENYEDI, P. & CZIRJAK, G. 2010. Molecular background of leak K+ currents: two-pore domain potassium channels. *Physiol Rev,* 90**,** 559-605.

ERRO, R., BHATIA, K. P., ESPAY, A. J. & STRIANO, P. 2017. The epileptic and nonepileptic spectrum of paroxysmal dyskinesias: Channelopathies, synaptopathies, and transportopathies. *Mov Disord,* 32**,** 310-318.

ERSHLER, W. B. 1993. Interleukin-6: a cytokine for gerontologists. *J Am Geriatr Soc,* 41**,** 176-81.

ETCHEBERRIGARAY, R., ITO, E., OKA, K., TOFEL-GREHL, B., GIBSON, G. E. & ALKON, D. L. 1993. Potassium channel dysfunction in fibroblasts identifies patients with Alzheimer disease. *Proc Natl Acad Sci U S A,* 90**,** 8209-13.

EWING, B. & GREEN, P. 1998. Base-Calling of Automated Sequencer Traces UsingPhred.II. Error Probabilities. *Genome Research,* 8**,** 186-194.

EWING, B., HILLIER, L., WENDL, M. C. & GREEN, P. 1998. Base-Calling of Automated Sequencer Traces UsingPhred. I. Accuracy Assessment. *Genome Research,* 8**,** 175-185.

FAN, G., CUI, Y., GOLLASCH, M. & KASSMANN, M. 2019. Elementary calcium signaling in arterial smooth muscle. *Channels,* 13**,** 505-519.

FARAJNIA, S., MEIJER, J. H. & MICHEL, S. 2015. Age-related changes in large-conductance calcium-activated potassium channels in mammalian circadian clock neurons. 36**,** 2176-2183.

FEETHAM, C. H., NUNN, N. & BARRETT-JOLLEY, R. 2015a. The depressor response to intracerebroventricular hypotonic saline is sensitive to TRPV4 antagonist RN1734. *Front Pharmacol,* 6**,** 83.

FEETHAM, C. H., NUNN, N., LEWIS, R., DART, C. & BARRETT-JOLLEY, R. 2015b. TRPV4 and KCa ion channels functionally couple as osmosensors in the paraventricular nucleus. *Br J Pharmacol,* 172**,** 1753-68.

FEETHAM, C. H., O'BRIEN, F. & BARRETT-JOLLEY, R. 2018. Ion Channels in the Paraventricular Hypothalamic Nucleus (PVN); Emerging Diversity and Functional Roles. *Frontiers in Physiology,* 9.

FELDER, R. B., FRANCIS, J., WEISS, R. M., ZHANG, Z. H., WEI, S. G. & JOHNSON, A. K. Neurohumoral regulation in ischemia-induced heart failure - Role of the forebrain. *In:* CHAPLEAU, M. W. & ABBOUD, F. M., eds., Aug 23-27 2000 Iowa City, Iowa. 444-453.

FERGUSON, A. V., LATCHFORD, K. J. & SAMSON, W. K. 2008. The paraventricular nucleus of the hypothalamus – a potential target for integrative treatment of autonomic dysfunction. *Expert Opinion on Therapeutic Targets,* 12**,** 717-727.

FERNANDEZ-FALGUERAS, A., SARQUELLA-BRUGADA, G., BRUGADA, J., BRUGADA, R. & CAMPUZANO, O. 2017. Cardiac Channelopathies and Sudden Death: Recent Clinical and Genetic Advances. *Biology (Basel),* 6.

FERRUCCI, L., CORSI, A., LAURETANI, F., BANDINELLI, S., BARTALI, B., TAUB, D. D., GURALNIK, J. M. & LONGO, D. L. 2005. The origins of age-related proinflammatory state. *Blood,* 105**,** 2294-2299.

FERRUCCI, L. & FABBRI, E. 2018. Inflammageing: chronic inflammation in ageing, cardiovascular disease, and frailty. *Nature Reviews Cardiology,* 15**,** 505-522.

FICHTLSCHERER, S., BREUER, S., HEESCHEN, C., DIMMELER, S. & ZEIHER, A. M. 2004. Interleukin-10 serum levels and systemic endothelial vasoreactivity in patients with coronary artery disease. *Journal of the American College of Cardiology,* 44**,** 44-49.

FLAK, J. N., MYERS, B., SOLOMON, M. B., MCKLVEEN, J. M., KRAUSE, E. G. & HERMAN, J. P. 2014. Role of paraventricular nucleus-projecting norepinephrine/epinephrine neurons in acute and chronic stress. *Eur J Neurosci,* 39**,** 1903-11.

FLAK, J. N., OSTRANDER, M. M., TASKER, J. G. & HERMAN, J. P. 2009. Chronic stress-induced neurotransmitter plasticity in the PVN. *J Comp Neurol,* 517**,** 156-65.

FLOOD, S., PARRI, R., WILLIAMS, A., DUANCE, V. & MASON, D. 2007. Modulation of interleukin-6 and matrix metalloproteinase 2 expression in human fibroblast-like synoviocytes by functional ionotropic glutamate receptors. *Arthritis Rheum,* 56**,** 2523-34.

FRANCESCHI, C. & CAMPISI, J. 2014. Chronic inflammation (inflammaging) and its potential contribution to age-associated diseases. *J Gerontol A Biol Sci Med Sci,* 69 Suppl 1**,** S4-9.

FRANCESCHI, C., CAPRI, M., MONTI, D., GIUNTA, S., OLIVIERI, F., SEVINI, F., PANOURGIA, M. P., INVIDIA, L., CELANI, L., SCURTI, M., CEVENINI, E., CASTELLANI, G. C. & SALVIOLI, S. 2007a. Inflammaging and anti-inflammaging: A systemic perspective on aging and longevity emerged from studies in humans. *Mechanisms of Ageing and Development,* 128**,** 92-105.

FRANCESCHI, C., CAPRI, M., MONTI, D., GIUNTA, S., OLIVIERI, F., SEVINI, F., PANOURGIA, M. P., INVIDIA, L., CELANI, L., SCURTI, M., CEVENINI, E., CASTELLANI, G. C. & SALVIOLI, S. 2007b. Inflammaging and anti-inflammaging: A systemic perspective on aging and longevity emerged from studies in humans. *Mech Ageing Devel,* 128**,** 92-105.

FRASER, S., GREEN, C., BODE, H. & GILULA, N. 1987. Selective disruption of gap junctional communication interferes with a patterning process in hydra. 237**,** 49-55.

FRAYLING, T. M., RAFIQ, S., MURRAY, A., HURST, A. J., WEEDON, M. N., HENLEY, W., BANDINELLI, S., CORSI, A. M., FERRUCCI, L., GURALNIK, J. M., WALLACE, R. B. & MELZER, D. 2007. An interleukin-18 polymorphism is associated with reduced serum concentrations and better physical functioning in older people. *J Gerontol A Biol Sci Med Sci,* 62**,** 73-8.

FREDMAN, G., HELLMANN, J., PROTO, J. D., KURIAKOSE, G., COLAS, R. A., DORWEILER, B., CONNOLLY, E. S., SOLOMON, R., JONES, D. M., HEYER, E. J., SPITE, M. & TABAS, I. 2016. An imbalance between specialized pro-resolving lipid mediators and pro-inflammatory leukotrienes promotes instability of atherosclerotic plaques. *Nature Communications,* 7**,** 12859.

FRIEBEL, K., SCHONHERR, R., KINNE, R. W. & KUNISCH, E. 2014. Functional role of the KCa3.1 potassium channel in synovial fibroblasts from rheumatoid arthritis patients. *J Cell Physiol*.

FRIEBEL, K., SCHÖNHERR, R., KINNE, R. W. & KUNISCH, E. 2015. Functional role of the KCa3.1 potassium channel in synovial fibroblasts from rheumatoid arthritis patients. 230**,** 1677-1688.

FU, C. H., YANG, C. C. & KUO, T. B. 2006. Age-related changes in cerebral hemodynamics and their correlations with cardiac autonomic functions. *Neurol Res,* 28**,** 871-6.

GAFFEN, S. L. 2009. The role of interleukin-17 in the pathogenesis of rheumatoid arthritis. *Curr Rheumatol Rep,* 11**,** 365-70.

GALIONE, A. & DAVIS, L. C. 2018. Revealing the secrets of secretion. *Elife,* 7.

GANGEMI, S. 2003. Increased circulating Interleukin-18 levels in centenarians with no signs of vascular disease: another paradox of longevity? 38**,** 669-672.

GARCIA-ELIAS, A., LORENZO, I. M., VICENTE, R. & VALVERDE, M. A. 2008. IP3 Receptor Binds to and Sensitizes TRPV4 Channel to Osmotic Stimuli via a Calmodulin-binding Site. 283**,** 31284-31288.

GARLANDA, C., DINARELLO, C. A. & MANTOVANI, A. 2013. The interleukin-1 family: back to the future. *Immunity,* 39**,** 1003-18.

GARRETT-SINHA, L. A., JOHN, S. & GAFFEN, S. L. 2008. IL-17 and the Th17 lineage in systemic lupus erythematosus. *Curr Opin Rheumatol,* 20**,** 519-25.

GAVRILOV, L. A. & GAVRILOVA, N. S. 2002. Evolutionary Theories of Aging and Longevity. *The Scientific World JOURNAL,* 2**,** 339-356.

GEORGIEV, D., YOSHIHARA, T., KAWABATA, R., MATSUBARA, T., TSUBOMOTO, M., MINABE, Y., LEWIS, D. A. & HASHIMOTO, T. 2016. Cortical Gene Expression After a Conditional Knockout of 67 kDa Glutamic Acid Decarboxylase in Parvalbumin Neurons. *Schizophrenia Bulletin,* 42**,** 992-1002.

GIEPMANS, B. 2004. Gap junctions and connexin-interacting proteins. 62**,** 233-245.

GILLIS, S. & WATSON, J. 1981. Interleukin-2 dependent culture of cytolytic T cell lines. *Immunol Rev,* 54**,** 81-109.

GIUDICESSI, J. R., YE, D., KRITZBERGER, C. J., NESTERENKO, V. V., TESTER, D. J., ANTZELEVITCH, C. & ACKERMAN, M. J. 2012. Novel mutations in the KCND3-encoded Kv4.3 K+ channel associated with autopsy-negative sudden unexplained death. *Hum Mutat,* 33**,** 989-97.

GOLDRING, M. B. & GOLDRING, S. R. 2007. Osteoarthritis. *Journal of Cellular Physiology,* 213**,** 626-634.

GOODENOUGH, D. A. & PAUL, D. L. 2009. Gap Junctions. 1**,** a002576-a002576.

GREENWOOD, M. P., GREENWOOD, M., ROMANOVA, E. V., MECAWI, A. S., PATERSON, A., SARENAC, O., JAPUNDŽIĆ-ŽIGON, N., ANTUNES-RODRIGUES, J., PATON, J. F. R., SWEEDLER, J. V. & MURPHY, D. 2018. The effects of aging on biosynthetic processes in the rat hypothalamic osmoregulatory neuroendocrine system. *Neurobiology of Aging,* 65**,** 178-191.

GRIDER, M. H., BELCEA, C. Q., COVINGTON, B. P. & SHARMA, S. 2019. Neuroanatomy, Nodes of Ranvier. *StatPearls.* Treasure Island (FL).

GRIDER, M. H. & GLAUBENSKLEE, C. S. 2019. Physiology, Action Potential. *StatPearls.* Treasure Island (FL).

GRUBB, B. D. 2004. Activation of sensory neurons in the arthritic joint. *Novartis Found Symp,* 260**,** 28-36; discussion 36-48, 100-4, 277-9.

GRUNDER, S., GEISSLER, H. S., BASSLER, E. L. & RUPPERSBERG, J. P. 2000. A new member of acid-sensing ion channels from pituitary gland. *Neuroreport,* 11**,** 1607-11.

GUI, Y. X., WAN, Y., XIAO, Q., WANG, Y., WANG, G. & CHEN, S. D. 2011. Verification of expressions of Kir2 as potential peripheral biomarkers in lymphocytes from patients with Parkinson's disease. *Neurosci Lett,* 505**,** 104-8.

GUILAK, F., LEDDY, H. A. & LIEDTKE, W. 2010. Transient receptor potential vanilloid 4: The sixth sense of the musculoskeletal system? *Annals of the New York Academy of Sciences,* 1192**,** 404-409.

HAN, G., LI, F., SINGH, T. P., WOLF, P. & WANG, X. J. 2012. The pro-inflammatory role of TGFbeta1: a paradox? *Int J Biol Sci,* 8**,** 228-35.

HANUKOGLU, I. 2017. ASIC and ENaC type sodium channels: conformational states and the structures of the ion selectivity filters. *The FEBS Journal,* 284**,** 525-545.

HAQUE, A., ENGEL, J., TEICHMANN, S. A. & LÖNNBERG, T. 2017. A practical guide to single-cell RNA-sequencing for biomedical research and clinical applications. *Genome Medicine,* 9.

HARMS, R. Z., YARDE, D. N., GUINN, Z., LORENZO-ARTEAGA, K. M., CORLEY, K. P., CABRERA, M. S. & SARVETNICK, N. E. 2015. Increased expression of IL-18 in the serum and islets of type 1 diabetics. *Mol Immunol,* 64**,** 306-312.

HDUD, I. M., EL-SHAFEI, A. A., LOUGHNA, P., BARRETT-JOLLEY, R. & MOBASHERI, A. 2012. Expression of transient receptor potential vanilloid (TRPV) channels in different passages of articular chondrocytes. *International Journal of Molecular Sciences,* 13**,** 4433-4445.

HE, W., LIU, W., CHEW, C. S., BAKER, S. S., BAKER, R. D., FORTE, J. G. & ZHU, L. 2011. Acid secretion-associated translocation of KCNJ15 in gastric parietal cells. *Am J Physiol Gastrointest Liver Physiol,* 301**,** G591-600.

HEINZE, C., SENIUK, A., SOKOLOV, M. V., HUEBNER, A. K., KLEMENTOWICZ, A. E., SZIJÁRTÓ, I. A., SCHLEIFENBAUM, J., VITZTHUM, H., GOLLASCH, M., EHMKE, H., SCHROEDER, B. C. & HÜBNER, C. A. 2014. Disruption of vascular Ca2+-activated chloride currents lowers blood pressure. 124**,** 675-686.

HERNANDEZ, C. M. & RICHARDS, J. R. 2019. Physiology, Sodium Channels. *StatPearls.* Treasure Island (FL).

HIROKAWA, K., UTSUYAMA, M., HAYASHI, Y., KITAGAWA, M., MAKINODAN, T. & FULOP, T. 2013. Slower immune system aging in women versus men in the Japanese population. *Immunity & Ageing,* 10**,** 19.

HOSHIKAWA, M., KATO, A., HOJO, H., SHIBATA, Y., KUMAMOTO, N., WATANABE, M. & UGAWA, S. 2017. Distribution of ASIC4 transcripts in the adult wild-type mouse brain. *Neuroscience Letters*.

HOSOYA, Y., SUGIURA, Y., OKADO, N., LOEWY, A. & KOHNO, K. 1991. Descending input from the hypothalamic paraventricular nucleus to sympathetic preganglionic neurons in the rat. *Experimental Brain Research,* 85**,** 10-20.

HOTTA, H. & UCHIDA, S. 2010. Aging of the autonomic nervous system and possible improvements in autonomic activity using somatic afferent stimulation. *Geriatr Gerontol Int,* 10 Suppl 1**,** S127-36.

HU, X., LARAGIONE, T., SUN, L., KOSHY, S., JONES, K. R., ISMAILOV, II, YOTNDA, P., HORRIGAN, F. T., GULKO, P. S. & BEETON, C. 2012a. KCa1.1 potassium channels regulate key proinflammatory and invasive

properties of fibroblast-like synoviocytes in rheumatoid arthritis. *Journal of biological chemistry,* 287**,** 4014-22.

HU, X., LARAGIONE, T., SUN, L., KOSHY, S., JONES, K. R., ISMAILOV, I. I., YOTNDA, P., HORRIGAN, F. T., GULKO, P. S. & BEETON, C. 2012b. KCa1.1 Potassium Channels Regulate Key Proinflammatory and Invasive Properties of Fibroblast-like Synoviocytes in Rheumatoid Arthritis. 287**,** 4014-4022.

HUBER, R., HUMMERT, C., GAUSMANN, U., POHLERS, D., KOCZAN, D., GUTHKE, R. & KINNE, R. W. 2008. Identification of intra-group, inter-individual, and gene-specific variances in mRNA expression profiles in the rheumatoid arthritis synovial membrane. *Arthritis Res Ther,* 10**,** R98.

HUI, A. Y., MCCARTY, W. J., MASUDA, K., FIRESTEIN, G. S. & SAH, R. L. 2012. A systems biology approach to synovial joint lubrication in health, injury, and disease. *Wiley Interdiscip Rev Syst Biol Med,* 4**,** 15-37.

HWANG, B., LEE, J. H. & BANG, D. 2018. Single-cell RNA sequencing technologies and bioinformatics pipelines. *Experimental & Molecular Medicine,* 50.

IMBRICI, P., LIANTONIO, A., CAMERINO, G. M., DE BELLIS, M., CAMERINO, C., MELE, A., GIUSTINO, A., PIERNO, S., DE LUCA, A., TRICARICO, D., DESAPHY, J. F. & CONTE, D. 2016. Therapeutic Approaches to Genetic Ion Channelopathies and Perspectives in Drug Discovery. *Front Pharmacol,* 7**,** 121.

IORGA, A. & HOROWITZ, B. Z. 2019. Phenytoin Toxicity. *StatPearls.* Treasure Island (FL).

IWANAGA, T., SHIKICHI, M., KITAMURA, H., YANASE, H. & NOZAWA-INOUE, K. 2000. Morphology and functional roles of synoviocytes in the joint. *Arch Histol Cytol,* 63**,** 17-31.

JANSEN, A. S. P., WESSENDORF, M. W. & LOEWY, A. D. 1995. Transneuronal Labeling of Cns Neuropeptide and Monoamine Neurons after Pseudorabies Virus Injections into the Stellate Ganglion. *Brain Research,* 683**,** 1-24.

JAVIER CAMACHO, J., CHÁVEZ-LÓPEZ, M., ZÚÑIGA-GARCÍA, V., PÉREZ-CARREÓN, J., AVALOS-FUENTES, A. & ESCOBAR, Y. 2016. Eag1 channels as potential early-stage biomarkers of hepatocellular carcinoma. *Biologics: Targets and Therapy,* Volume 10**,** 139-148.

JEFFERIS, B. J., PAPACOSTA, O., OWEN, C. G., WANNAMETHEE, S. G., HUMPHRIES, S. E., WOODWARD, M., LENNON, L. T., THOMSON, A., WELSH, P., RUMLEY, A., LOWE, G. D. & WHINCUP, P. H. 2011. Interleukin 18 and coronary heart disease: prospective study and systematic review. *Atherosclerosis,* 217**,** 227-33.

JENSEN, A. B., JOERGENSEN, H. B., DAM, V. S., KAMAEV, D., BOEDTKJER, D., FÜCHTBAUER, E.-M., AALKJAER, C. & MATCHKOV, V. V. 2018. Variable Contribution of TMEM16A to Tone in Murine Arterial Vasculature. *Basic & Clinical Pharmacology & Toxicology*.

JENTSCH, T. J. & GUNTHER, W. 1997. Chloride channels: an emerging molecular picture. *Bioessays,* 19**,** 117-26.

JENTSCH, T. J., STEIN, V., WEINREICH, F. & ZDEBIK, A. A. 2002. Molecular Structure and Physiological Function of Chloride Channels. *Physiological Reviews,* 82**,** 503-568.

JI, M. J. & HONG, J. H. 2019. An overview of carbonic anhydrases and membrane channels of synoviocytes in inflamed joints. *J Enzyme Inhib Med Chem,* 34**,** 1615-1622.

JIANG, Y., PICO, A., CADENE, M., CHAIT, B. T. & MACKINNON, R. 2001. Structure of the RCK domain from the E. coli K+ channel and demonstration of its presence in the human BK channel. *Neuron,* 29**,** 593-601.

JOMBART, T., DEVILLARD, S. & BALLOUX, F. 2010. Discriminant analysis of principal components: a new method for the analysis of genetically structured populations. *BMC Genet,* 11**,** 94.

JULIUS, S. 1993. Sympathetic Hyperactivity and Coronary Risk in Hypertension. *Hypertension,* 21**,** 886-893.

JYLHA, M., PAAVILAINEN, P., LEHTIMAKI, T., GOEBELER, S., KARHUNEN, P. J., HERVONEN, A. & HURME, M. 2007. Interleukin-1 receptor antagonist, interleukin-6, and C-reactive protein as predictors of mortality in nonagenarians: the vitality 90+ study. *J Gerontol A Biol Sci Med Sci,* 62**,** 1016-21.

KAJIWARA, Y., WANG, E., WANG, M., SIN, W. C., BRENNAND, K. J., SCHADT, E., NAUS, C. C., BUXBAUM, J. & ZHANG, B. 2018. GJA1 (connexin43) is a key regulator of Alzheimer's disease pathogenesis. *Acta Neuropathol Commun,* 6**,** 144.

KANE, G. C., LAM, C. F., O'COCHLAIN, F., HODGSON, D. M., REYES, S., LIU, X. K., MIKI, T., SEINO, S., KATUSIC, Z. S. & TERZIC, A. 2006. Gene knockout of the KCNJ8-encoded Kir6.1 K(ATP) channel imparts fatal susceptibility to endotoxemia. *FASEB J,* 20**,** 2271-80.

KANG, Y. M., HE, R. L., YANG, L. M., QIN, D. N., GUGGILAM, A., ELKS, C., YAN, N., GUO, Z. & FRANCIS, J. 2009. Brain tumour necrosis factor-alpha modulates neurotransmitters in hypothalamic paraventricular nucleus in heart failure. *Cardiovasc Res,* 83**,** 737-46.

KAPLAN, J., GERBER, S., BONNEAU, D., ROZET, J. M., DELRIEU, O., BRIARD, M. L., DOLLFUS, H., GHAZI, I., DUFIER, J. L., FRÉZAL, J. & MUNNICH, A. 1992. A gene for usher syndrome type I (USH1A) maps to chromosome 14q. 14**,** 979-987.

KARIMI, A. & MILEWICZ, D. M. 2016. Structure of the Elastin-Contractile Units in the Thoracic Aorta and How Genes That Cause Thoracic Aortic Aneurysms and Dissections Disrupt This Structure. *Canadian Journal of Cardiology,* 32**,** 26-34.

KARSDAL, M. A. 2016. Collagens - Introduction.

KIM, D., LANGMEAD, B. & SALZBERG, S. L. 2015. HISAT: a fast spliced aligner with low memory requirements. *Nature Methods,* 12**,** 357-360.

KIM, J. B. 2014. Channelopathies. *Korean J Pediatr,* 57**,** 1-18.

KINZENBAW, D. A., CHU, Y., PEÑA SILVA, R. A., DIDION, S. P. & FARACI, F. M. 2013. Interleukin-10 protects against aging-induced endothelial dysfunction. *Physiological Reports,* 1**,** e00149.

KIRKWOOD, T. B. L. 1977. Evolution of ageing. *Nature,* 270**,** 301-304.

KIRKWOOD, T. B. L. & HOLLIDAY, R. 1979. The Evolution of Ageing and Longevity. 205**,** 531-546.

KONDO, C., CLARK, R. B., KIM, T. Y., BELKE, D., BANDERALI, U., SZERENCSEI, R. T., JALLOUL, A. H., SCHNETKAMP, P. P. M., SPITZER, K. W. & GILES, W. R. 2018. ATP triggers a robust intracellular [Ca(2+)]-mediated signalling pathway in human synovial fibroblasts. *Exp Physiol,* 103**,** 1101-1122.

KORN, T., BETTELLI, E., OUKKA, M. & KUCHROO, V. K. 2009. IL-17 and Th17 Cells. *Annu Rev Immunol,* 27**,** 485-517.

KOTIPOYINA, H. R. & WARRINGTON, S. J. 2019. Tetrodotoxin Toxicity. *StatPearls.* Treasure Island (FL).

KRAMER, A., GREEN, J., POLLARD, J., JR. & TUGENDREICH, S. 2014. Causal analysis approaches in Ingenuity Pathway Analysis. *Bioinformatics,* 30**,** 523-30.

KRIEGLSTEIN, K., MIYAZONO, K., TEN DIJKE, P. & UNSICKER, K. 2012. TGF-beta in aging and disease. *Cell Tissue Res,* 347**,** 5-9.

KRISHNAMOORTHY, N., BURKETT, P. R., DALLI, J., ABDULNOUR, R. E., COLAS, R., RAMON, S., PHIPPS, R. P., PETASIS, N. A., KUCHROO, V. K., SERHAN, C. N. & LEVY, B. D. 2015. Cutting edge: maresin-1 engages regulatory T cells to limit type 2 innate lymphoid cell activation and promote resolution of lung inflammation. *J Immunol,* 194**,** 863-7.

KUBICZKOVA, L., SEDLARIKOVA, L., HAJEK, R. & SEVCIKOVA, S. 2012. TGF-beta - an excellent servant but a bad master. *J Transl Med,* 10**,** 183.

KUMAHASHI, N., NAITOU, K., NISHI, H., OAE, K., WATANABE, Y., KUWATA, S., OCHI, M., IKEDA, M. & UCHIO, Y. 2011. Correlation of changes in pain intensity with synovial fluid adenosine triphosphate levels after treatment of patients with osteoarthritis of the knee with high-molecular-weight hyaluronic acid. *The Knee,* 18**,** 160-164.

KUO, C. J., LAMONTAGNE, K. R., GARCIA-CARDEÑA, G., ACKLEY, B. D., KALMAN, D., PARK, S., CHRISTOFFERSON, R., KAMIHARA, J., DING, Y.-H., LO, K.-M., GILLIES, S., FOLKMAN, J., MULLIGAN, R. C. & JAVAHERIAN, K. 2001. Oligomerization-Dependent Regulation of Motility and Morphogenesis by the Collagen Xviii Nc1/Endostatin Domain. 152**,** 1233-1246.

KURIYAMA, H., KITAMURA, K., ITOH, T. & INOUE, R. 1998. Physiological features of visceral smooth muscle cells, with special reference to receptors and ion channels. *Physiol Rev,* 78**,** 811-920.

LAINA, A., STELLOS, K. & STAMATELOPOULOS, K. 2018. Vascular ageing: Underlying mechanisms and clinical implications. *Experimental Gerontology,* 109**,** 16-30.

LAKOSKI, S. G., LIU, Y., BROSNIHAN, K. B. & HERRINGTON, D. M. 2008. Interleukin-10 concentration and coronary heart disease (CHD) event risk in the estrogen replacement and atherosclerosis (ERA) study. *Atherosclerosis,* 197**,** 443-447.

LAMBERT, C., DUBUC, J.-E., MONTELL, E., VERGÉS, J., MUNAUT, C., NOËL, A. & HENROTIN, Y. 2014. Gene Expression Pattern of Cells From Inflamed and Normal Areas of Osteoarthritis Synovial Membrane. *Arthritis & Rheumatology,* 66**,** 960-968.

LANG, F. & HOFFMANN, E. K. 2013. CrossTalk proposal: Cell volume changes are an essential step in the cell death machinery. *J Physiol,* 591**,** 6119-21.

LATORRE, R. & BRAUCHI, S. 2006. Large conductance Ca2+-activated K+ (BK) channel: activation by Ca2+ and voltage. *Biol Res,* 39**,** 385-401.

LAURENCE, A., TATO, C. M., DAVIDSON, T. S., KANNO, Y., CHEN, Z., YAO, Z., BLANK, R. B., MEYLAN, F., SIEGEL, R., HENNIGHAUSEN, L., SHEVACH, E. M. & O'SHEA J, J. 2007. Interleukin-2 signaling via STAT5 constrains T helper 17 cell generation. *Immunity,* 26**,** 371-81.

LEE, J. C. & CHOE, S. Y. 2014. Age-related changes in the distribution of transient receptor potential vanilloid 4 channel (TRPV4) in the central nervous system of rats. *J Mol Histol,* 45**,** 497-505.

LEE, J. S., LEE, W. W., KIM, S. H., KANG, Y., LEE, N., SHIN, M. S., KANG, S. W. & KANG, I. 2011a. Age-associated alteration in naive and memory Th17 cell response in humans. *Clin Immunol,* 140**,** 84-91.

LEE, S. W., SONG, Y. S., LEE, S. Y., YOON, Y. G., LEE, S. H., PARK, B. S., YUN, I., CHOI, H., KIM, K., CHUNG, W. T. & YOO, Y. H. 2011b. Downregulation of Protein Kinase CK2 Activity Facilitates Tumor Necrosis Factor-α-Mediated Chondrocyte Death through Apoptosis and Autophagy. *PLoS ONE,* 6**,** e19163.

LEVINE, J. D. & ALESSANDRI-HABER, N. 2007. TRP channels: Targets for the relief of pain. *Biochimica et Biophysica Acta (BBA) - Molecular Basis of Disease,* 1772**,** 989-1003.

LEWIS, R., ASPLIN, K. E., BRUCE, G., DART, C., MOBASHERI, A. & BARRETT-JOLLEY, R. 2011a. The Role of the Membrane Potential in Chondrocyte Volume Regulation. *Journal of Cellular Physiology,* 226**,** 2979-2986.

LEWIS, R. & BARRETT-JOLLEY, R. 2015. Changes in Membrane Receptors and Ion Channels as Potential Biomarkers for Osteoarthritis. *Front Physiol,* 6**,** 357.

LEWIS, R., FEETHAM, C. H. & BARRETT-JOLLEY, R. 2011b. Cell Volume Regulation in Chondrocytes. *Cellular Physiology and Biochemistry,* 28**,** 1111-1122.

LEWIS, R., MAY, H., MOBASHERI, A. & BARRETT-JOLLEY, R. 2013. Chondrocyte channel transcriptomics: do microarray data fit with expression and functional data? *Channels (Austin),* 7**,** 459-67.

LEWIS, R., MILLS, A. & BARRETT-JOLLEY, R. 2010. Models Of Paraventricular Nucleus (PVN) Sympathetic Neurone Modulation by Glucose and Hypoglycaemia. *Biophysical Journal - BIOPHYS J,* 98.

LI, Y., WEI, X., ZHOU, J. & WEI, L. 2013. The Age-Related Changes in Cartilage and Osteoarthritis. *BioMed Research International,* 2013**,** 1-12.

LI, Y., ZHAO, Z., CAI, J., GU, B., LV, Y. & ZHAO, L. 2017. The Frequency-Dependent Aerobic Exercise Effects of Hypothalamic GABAergic Expression and Cardiovascular Functions in Aged Rats. *Frontiers in Aging Neuroscience,* 9.

LI, Y. F., CORNISH, K. G. & PATEL, K. P. 2003. Alteration of NMDA NR1 receptors within the paraventricular nucleus of hypothalamus in rats with heart failure. *Circulation Research,* 93**,** 990-997.

LI, Y. F., JACKSON, K. L., STERN, J. E., RABELER, B. & PATEL, K. P. 2006a. Interaction between glutamate and GABA systems in the integration of sympathetic outflow by the paraventricular nucleus of the

hypothalamus. *American Journal of Physiology-Heart and Circulatory Physiology,* 291**,** H2847-H2856.

LI, Y. F. & PATEL, K. P. Paraventricular nucleus of the hypothalamus and elevated sympathetic activity in heart failure: the altered inhibitory mechanisms. Apr 20-24 2002 New Orleans, Louisiana. 17-26.

LI, Y. F. & PATEL, K. P. 2003. Paraventricular nucleus of the hypothalamus and elevated sympathetic activity in heart failure: the altered inhibitory mechanisms. *Acta Physio Scand,* 177**,** 17-26.

LI, Y. F., WANG, W., MAYHAN, W. G. & PATEL, K. P. 2006b. Angiotensin-mediated increase in renal sympathetic nerve discharge within the PVN: role of nitric oxide. *American Journal of Physiology-Regulatory Integrative and Comparative Physiology,* 290**,** R1035-R1043.

LIAO, Z., DONG, J., WU, W., YANG, T., WANG, T., GUO, L., CHEN, L., XU, D. & WEN, F. 2012. Resolvin D1 attenuates inflammation in lipopolysaccharide-induced acute lung injury through a process involving the PPARγ/NF-κB pathway. *Respiratory Research,* 13**,** 110.

LIO, D. 2003. Inflammation, genetics, and longevity: further studies on the protective effects in men of IL-10 -1082 promoter SNP and its interaction with TNF-alpha -308 promoter SNP. *Journal of Medical Genetics,* 40**,** 296-299.

LIPPIAT, J. D., STANDEN, N. B., HARROW, I. D., PHILLIPS, S. C. & DAVIES, N. W. 2003. Properties of BK(Ca) channels formed by bicistronic expression of hSloalpha and beta1-4 subunits in HEK293 cells. *The Journal of membrane biology,* 192**,** 141-8.

LIU, L. & CHAN, C. 2014. The role of inflammasome in Alzheimer's disease. *Ageing Res Rev,* 15**,** 6-15.

LOEWY, A. 1991. Forebrain nuclei involved in autonomic control. *Progress in brain research,* 87**,** 253.

LOEWY, A. D. & MCKELLAR, S. 1980. The neuroanatomical basis of central cardiovascular control. *Fed.Proc.,* 39**,** 2495-2503.

LONG, S. B., CAMPBELL, E. B. & MACKINNON, R. 2005a. Crystal structure of a mammalian voltage-dependent Shaker family K+ channel. *Science,* 309**,** 897-903.

LONG, S. B., CAMPBELL, E. B. & MACKINNON, R. 2005b. Voltage sensor of Kv1.2: structural basis of electromechanical coupling. *Science,* 309**,** 903-8.

LOVICK, T. A. & COOTE, J. H. 1988. Effects of volume loading on paraventriculo-spinal neurones in the rat. *J Auton Nerv Syst,* 25**,** 135-40.

LOVICK, T. A. & COOTE, J. H. 1989. Circulating atrial natriuretic factor activates vagal afferent inputs to paraventriculo-spinal neurones in the rat. *J Auton Nerv Syst,* 26**,** 129-34.

LOVICK, T. A., MALPAS, S. & MAHONY, M. T. 1993. Renal vasodilatation in response to acute volume load is attenuated following lesions of parvocellular neurones in the paraventricular nucleus in rats. *Journal of the Autonomic Nervous System,* 43**,** 247-256.

LYTTON, J. 2007. Na+/Ca2+ exchangers: three mammalian gene families control Ca2+ transport. *Biochem J,* 406**,** 365-82.

MA, S., MURPHY, T. W. & LU, C. 2017. Microfluidics for genome-wide studies involving next generation sequencing. *Biomicrofluidics,* 11**,** 021501.

MACDONALD, M. L. E., VAN ECK, M., HILDEBRAND, R. B., WONG, B. W. C., BISSADA, N., RUDDLE, P., KONTUSH, A., HUSSEIN, H., POULADI, M. A., CHAPMAN, M. J., FIEVET, C., VAN BERKEL, T. J. C., STAELS, B., MCMANUS, B. M. & HAYDEN, M. R. 2009. Despite Antiatherogenic Metabolic Characteristics, SCD1-Deficient Mice Have Increased Inflammation and Atherosclerosis. 29**,** 341-347.

MACKINNON, R., HEGINBOTHAM, L. & ABRAMSON, T. 1990. Mapping the receptor site for charybdotoxin, a pore-blocking potassium channel inhibitor. *Neuron,* 5**,** 767-71.

MACKINNON, R. & MILLER, C. 1989. Mutant potassium channels with altered binding of charybdotoxin, a pore-blocking peptide inhibitor. *Science,* 245**,** 1382-5.

MADEJ, W., VAN CAAM, A., BLANEY DAVIDSON, E. N., HANNINK, G., BUMA, P. & VAN DER KRAAN, P. M. 2016. Ageing is associated with reduction of mechanically-induced activation of Smad2/3P signaling in articular cartilage. 24**,** 146-157.

MAEZAWA, I., JENKINS, D. P., JIN, B. E. & WULFF, H. 2012. Microglial KCa3.1 Channels as a Potential Therapeutic Target for Alzheimer's Disease. *International Journal of Alzheimer's Disease,* 2012**,** 1-8.

MAGGIO, M., GURALNIK, J. M., LONGO, D. L. & FERRUCCI, L. 2006. Interleukin-6 in aging and chronic disease: a magnificent pathway. *J Gerontol A Biol Sci Med Sci,* 61**,** 575-84.

MAKITA, N., BENNETT, P. B., JR. & GEORGE, A. L., JR. 1994. Voltage-gated Na+ channel beta 1 subunit mRNA expressed in adult human skeletal muscle, heart, and brain is encoded by a single gene. *J Biol Chem,* 269**,** 7571-8.

MALLAT, Z., GOJOVA, A., MARCHIOL-FOURNIGAULT, C., ESPOSITO, B., KAMATE, C., MERVAL, R., FRADELIZI, D. & TEDGUI, A. 2001. Inhibition of transforming growth factor-beta signaling accelerates atherosclerosis and induces an unstable plaque phenotype in mice. *Circ Res,* 89**,** 930-4.

MALLAT, Z., HEYMES, C., CORBAZ, A., LOGEART, D., ALOUANI, S., COHEN-SOLAL, A., SEIDLER, T., HASENFUSS, G., CHVATCHKO, Y., SHAH, A. M. & TEDGUI, A. 2004. Evidence for altered interleukin 18 (IL)-18 pathway in human heart failure. *FASEB J,* 18**,** 1752-4.

MANSOUR, F. A., HASSAN, M. O., KHAN, A. A. & ALBARWANI, S. 2016. Aging Down Regulates L-Type Voltage-gated Calcium Channels in Resistance Coronary Arteries. *Faseb Journal,* 30.

MARCON, R., BENTO, A. F., DUTRA, R. C., BICCA, M. A., LEITE, D. F. & CALIXTO, J. B. 2013. Maresin 1, a proresolving lipid mediator derived from omega-3 polyunsaturated fatty acids, exerts protective actions in murine models of colitis. *J Immunol,* 191**,** 4288-98.

MARTIN, D. S. & HAYWOOD, J. R. 1993. Hemodynamic responses to paraventricular nucleus disinhibition with bicuculline in conscious rats. *American Journal of Physiology- Heart and Circulatory Physiology,* 265**,** H1727-H1733.

MARTIN, D. S., SEGURA, T. & HAYWOOD, J. R. 1991. Cardiovascular responses to bicuculline in the paraventricular nucleus of the rat. *Hypertension,* 18**,** 48-55.

MARTIN, S. J. 2016. Cell death and inflammation: the case for IL-1 family cytokines as the canonical DAMPs of the immune system. *The FEBS Journal,* 283**,** 2599-2615.

MARTINEZ, A. H. & MOHIUDDIN, S. S. 2019. Biochemistry, Chloride Channels. *StatPearls.* Treasure Island (FL).

MARTINSEN, A., DESSY, C. & MOREL, N. 2014. Regulation of calcium channels in smooth muscle: New insights into the role of myosin light chain kinase. 8**,** 402-413.

MCCUSKER, S. M., CURRAN, M. D., DYNAN, K. B., MCCULLAGH, C. D., URQUHART, D. D., MIDDLETON, D., PATTERSON, C. C., MCILROY, S. P. & PETER PASSMORE, A. 2001. Association between polymorphism in regulatory region of gene encoding tumour necrosis factor α and risk of Alzheimer's disease and vascular dementia: a case-control study. 357**,** 436-439.

MCKENZIE, B. S., KASTELEIN, R. A. & CUA, D. J. 2006. Understanding the IL-23-IL-17 immune pathway. *Trends Immunol,* 27**,** 17-23.

MCMANUS, O. B., HELMS, L. M., PALLANCK, L., GANETZKY, B., SWANSON, R. & LEONARD, R. J. 1995. Functional role of the beta subunit of high conductance calcium-activated potassium channels. *Neuron,* 14**,** 645-50.

MCNERLAN, S. E., ARMSTRONG, M., ROSS, O. A. & MAEVE REA, I. 2009. Cytokine Expression and Production Changes in Very Old Age. *In:* FULOP, T., FRANCESCHI, C., HIROKAWA, K. & PAWELEC, G. (eds.) *Handbook on Immunosenescence: Basic Understanding and Clinical Applications.* Dordrecht: Springer Netherlands.

MCNERLAN, S. E., REA, I. M. & ALEXANDER, H. D. 2002. A whole blood method for measurement of intracellular TNF-alpha, IFN-gamma and IL-2 expression in stimulated CD3+ lymphocytes: differences between young and elderly subjects. *Exp Gerontol,* 37**,** 227-34.

MCNULTY, M., SPIERS, P., MCGOVERN, E. & FEELY, J. 2005. Aging is associated with increased matrix metalloproteinase-2 activity in the human aorta. 18**,** 504-509.

MEDVEDEV, Z. A. 1990. AN ATTEMPT AT A RATIONAL CLASSIFICATION OF THEORIES OF AGEING. *Biological Reviews,* 65**,** 375-398.

MEERA, P., WALLNER, M., SONG, M. & TORO, L. 1997. Large conductance voltage- and calcium-dependent K+ channel, a distinct member of voltage-dependent ion channels with seven N-terminal transmembrane segments (S0-S6), an extracellular N terminus, and an intracellular (S9-S10) C terminus. 94**,** 14066-14071.

MEKLI, K., MARSHALL, A., NAZROO, J., VANHOUTTE, B. & PENDLETON, N. 2015. Genetic variant of Interleukin-18 gene is associated with the Frailty Index in the English Longitudinal Study of Ageing. 44**,** 938-942.

MENDONCA, M. M., SANTANA, J. S., DA CRUZ, K. R., IANZER, D., GHEDINI, P. C., NALIVAIKO, E., FONTES, M. A. P., FERREIRA, R. N., PEDRINO, G. R., COLUGNATI, D. B. & XAVIER, C. H. 2018. Involvement of GABAergic and Adrenergic Neurotransmissions on Paraventricular Nucleus of Hypothalamus in the Control of Cardiac Function. *Front Physiol,* 9**,** 670.

MEŞE, G., RICHARD, G. & WHITE, T. W. 2007. Gap Junctions: Basic Structure and Function. *Journal of Investigative Dermatology,* 127**,** 2516-2524.

MISRA, V., LEE, H., SINGH, A., HUANG, K., THIMMULAPPA, R. K., MITZNER, W., BISWAL, S. & TANKERSLEY, C. G. 2007. Global expression profiles from C57BL/6J and DBA/2J mouse lungs to determine aging-related genes. 31**,** 429-440.

MITNITSKI, A., COLLERTON, J., MARTIN-RUIZ, C., JAGGER, C., VON ZGLINICKI, T., ROCKWOOD, K. & KIRKWOOD, T. B. L. 2015. Age-related frailty and its association with biological markers of ageing. *BMC Medicine,* 13.

MOBASHERI, A., LEWIS, R., FERREIRA-MENDES, A., RUFINO, A., DART, C. & BARRETT-JOLLEY, R. 2012. Potassium channels in articular chondrocytes. *Channels,* 6**,** 416-425.

MOCZYDLOWSKI, E., LUCCHESI, K. & RAVINDRAN, A. 1988. An emerging pharmacology of peptide toxins targeted against potassium channels. *J Membr Biol,* 105**,** 95-111.

MONK, B. A. & GEORGE, S. J. 2015. The Effect of Ageing on Vascular Smooth Muscle Cell Behaviour--A Mini-Review. *Gerontology,* 61**,** 416-26.

MORTAZ, E., ADCOCK, I. M., SHAFEI, H., MASJEDI, M. R. & FOLKERTS, G. 2012. Role of P2X7 Receptors in Release of IL-1β: A Possible Mediator of Pulmonary Inflammation. *Tanaffos,* 11**,** 6-11.

MORTH, J. P., PEDERSEN, B. P., TOUSTRUP-JENSEN, M. S., SORENSEN, T. L., PETERSEN, J., ANDERSEN, J. P., VILSEN, B. & NISSEN, P. 2007. Crystal structure of the sodium-potassium pump. *Nature,* 450**,** 1043-9.

MOSKALEV, A., ALIPER, A., SMIT-MCBRIDE, Z., BUZDIN, A. & ZHAVORONKOV, A. 2014. Genetics and epigenetics of aging and longevity. 13**,** 1063-1077.

MOSMANN, T. R. & SAD, S. 1996. The expanding universe of T-cell subsets: Th1, Th2 and more. *Immunol Today,* 17**,** 138-46.

MUELLER, O., LIGHTFOOT, S., SCHROEDER, A. <RNA Integrity Number (RIN) - Standardization of RNA Quality Control.pdf>.

MUN, M. J., KIM, J. H., CHOI, J. Y. & JANG, W. C. 2016. Genetic polymorphisms of interleukin genes and the risk of Alzheimer's disease: An update meta-analysis. *Meta Gene,* 8**,** 1-10.

NATHAN, C. 2002. Points of control in inflammation. *Nature,* 420**,** 846-52.

NGUYEN, T. P. & TAYLOR, R. S. 2019. Guillain Barre Syndrome. *StatPearls.* Treasure Island (FL).

NGUYEN, V., MENDELSOHN, A. & LARRICK, J. W. 2017. Interleukin-7 and Immunosenescence. *J Immunol Res,* 2017**,** 4807853.

NIISSALO, S., LI, T. F., SANTAVIRTA, S., TAKAGI, M., HIETANEN, J. & KONTTINEN, Y. T. 2002. Dense innervation in pseudocapsular tissue compared to aneural interface tissue in loose totally replaced hips. *J Rheumatol,* 29**,** 796-803.

NILSSON, L., SZYMANOWSKI, A., SWAHN, E. & JONASSON, L. 2013. Soluble TNF receptors are associated with infarct size and ventricular dysfunction in ST-elevation myocardial infarction. *PLoS One,* 8**,** e55477.

NOLD, M. F., NOLD-PETRY, C. A., ZEPP, J. A., PALMER, B. E., BUFLER, P. & DINARELLO, C. A. 2010. IL-37 is a fundamental inhibitor of innate immunity. *Nature Immunology,* 11**,** 1014-1022.

NOSS, E. H. & BRENNER, M. B. 2008. The role and therapeutic implications of fibroblast-like synoviocytes in inflammation and cartilage erosion in rheumatoid arthritis. *Immunological Reviews,* 223**,** 252-270.

NOVAKOVIC, S. D., EGLEN, R. M. & HUNTER, J. C. 2001. Regulation of Na+ channel distribution in the nervous system. 24**,** 473-478.

NUNN, N., WOMACK, M., DART, C. & BARRETT-JOLLEY, R. 2011. Function and pharmacology of spinally-projecting sympathetic pre-autonomic neurones in the paraventricular nucleus of the hypothalamus. *Current neuropharmacology,* 9**,** 262-77.

O'LEARY, N. A., WRIGHT, M. W., BRISTER, J. R., CIUFO, S., HADDAD, D., MCVEIGH, R., RAJPUT, B., ROBBERTSE, B., SMITH-WHITE, B., AKO-ADJEI, D., ASTASHYN, A., BADRETDIN, A., BAO, Y., BLINKOVA, O., BROVER, V., CHETVERNIN, V., CHOI, J., COX, E., ERMOLAEVA, O., FARRELL, C. M., GOLDFARB, T., GUPTA, T., HAFT, D., HATCHER, E., HLAVINA, W., JOARDAR, V. S., KODALI, V. K., LI, W., MAGLOTT, D., MASTERSON, P., MCGARVEY, K. M., MURPHY, M. R., O'NEILL, K., PUJAR, S., RANGWALA, S. H., RAUSCH, D., RIDDICK, L. D., SCHOCH, C., SHKEDA, A., STORZ, S. S., SUN, H., THIBAUD-NISSEN, F., TOLSTOY, I., TULLY, R. E., VATSAN, A. R., WALLIN, C., WEBB, D., WU, W., LANDRUM, M. J., KIMCHI, A., TATUSOVA, T., DICUCCIO, M., KITTS, P., MURPHY, T. D. & PRUITT, K. D. 2016. Reference sequence (RefSeq) database at NCBI: current status, taxonomic expansion, and functional annotation. *Nucleic Acids Research,* 44**,** D733-D745.

O'MAHONY, L., HOLLAND, J., JACKSON, J., FEIGHERY, C., HENNESSY, T. P. & MEALY, K. 1998. Quantitative intracellular cytokine measurement: age-related changes in proinflammatory cytokine production. *Clin Exp Immunol,* 113**,** 213-9.

O'MALLEY, H. A. & ISOM, L. L. 2015. Sodium channel beta subunits: emerging targets in channelopathies. *Annu Rev Physiol,* 77**,** 481-504.

O'QUINN, D. B., PALMER, M. T., LEE, Y. K. & WEAVER, C. T. 2008. Emergence of the Th17 pathway and its role in host defense. *Adv Immunol,* 99**,** 115-63.

OEGEMA, R., MCGILLIVRAY, G., LEVENTER, R., LE MOING, A. G., BAHI-BUISSON, N., BARNICOAT, A., MANDELSTAM, S., FRANCIS, D., FRANCIS, F., MANCINI, G. M. S., SAVELBERG, S., HAAFTEN, G., MANKAD, K. & LEQUIN, M. H. 2019. EML1- associated brain overgrowth syndrome with ribbon-like heterotopia. *American Journal of Medical Genetics Part C: Seminars in Medical Genetics*.

OKAMOTO, K., IWASAKI, N., DOI, K., NOIRI, E., IWAMOTO, Y., UCHIGATA, Y., FUJITA, T. & TOKUNAGA, K. 2012. Inhibition of glucose-stimulated insulin secretion by KCNJ15, a newly identified susceptibility gene for type 2 diabetes. *Diabetes,* 61**,** 1734-41.

OKAMOTO, K., IWASAKI, N., NISHIMURA, C., DOI, K., NOIRI, E., NAKAMURA, S., TAKIZAWA, M., OGATA, M., FUJIMAKI, R., GRARUP, N., PISINGER, C., BORCH-JOHNSEN, K., LAURITZEN, T., SANDBAEK, A., HANSEN, T., YASUDA, K., OSAWA, H., NANJO, K., KADOWAKI, T., KASUGA, M., PEDERSEN, O., FUJITA, T., KAMATANI, N., IWAMOTO, Y. & TOKUNAGA, K. 2010. Identification of KCNJ15 as a Susceptibility Gene in Asian Patients with Type 2 Diabetes Mellitus. 86**,** 54-64.

ORLOV, S. N., GUSAKOVA, S. V., SMAGLII, L. V., KOLTSOVA, S. V. & SIDORENKO, S. V. 2017. Vasoconstriction triggered by hydrogen sulfide: Evidence for Na(+),K(+),2Cl(-)cotransport and L-type Ca(2+) channel-mediated pathway. *Biochem Biophys Rep,* 12**,** 220-227.

ORLOV, S. N., MODEL, M. A. & GRYGORCZYK, R. 2013. CrossTalk opposing view: The triggering and progression of the cell death machinery can occur without cell volume perturbations. *J Physiol,* 591**,** 6123-5.

OUYANG, W., RUTZ, S., CRELLIN, N. K., VALDEZ, P. A. & HYMOWITZ, S. G. 2011. Regulation and functions of the IL-10 family of cytokines in inflammation and disease. *Annu Rev Immunol,* 29**,** 71-109.

PAL, R., SINGH, S. N., CHATTERJEE, A. & SAHA, M. 2014. Age-related changes in cardiovascular system, autonomic functions, and levels of BDNF of healthy active males: role of yogic practice. *Age (Dordr),* 36**,** 9683.

PARASHAR, R., AMIR, M., PAKHARE, A., RATHI, P. & CHAUDHARY, L. 2016. Age Related Changes in Autonomic Functions. *J Clin Diagn Res,* 10**,** CC11-5.

PASSTOORS, W. M., BOER, J. M., GOEMAN, J. J., VAN DEN AKKER, E. B., DEELEN, J., ZWAAN, B. J., SCARBOROUGH, A., VAN DER BREGGEN, R., VOSSEN, R. H. A. M., HOUWING-DUISTERMAAT, J. J., VAN OMMEN, G. J. B., WESTENDORP, R. G. J., VAN HEEMST, D., DE CRAEN, A. J. M., WHITE, A. J., GUNN, D. A., BEEKMAN, M. & SLAGBOOM, P. E. 2012. Transcriptional Profiling of Human Familial Longevity Indicates a Role for ASF1A and IL7R. 7**,** e27759.

PASSTOORS, W. M., VAN DEN AKKER, E. B., DEELEN, J., MAIER, A. B., VAN DER BREGGEN, R., JANSEN, R., TROMPET, S., VAN HEEMST, D., DERHOVANESSIAN, E., PAWELEC, G., VAN OMMEN, G. J., SLAGBOOM, P. E. & BEEKMAN, M. 2015. IL7R gene expression network associates with human healthy ageing. *Immun Ageing,* 12**,** 21.

PASTRANA, J. L., SHA, X., VIRTUE, A., MAI, J., CUETO, R., LEE, I. A., WANG, H. & YANG, X. F. 2012. Regulatory T cells and Atherosclerosis. *J Clin Exp Cardiolog,* 2012**,** 2.

PATEL, K. P., ZHANG, K., KENNEY, M. J., WEISS, M. & MAYHAN, W. G. 2000. Neuronal expression of Fos protein in the hypothalamus of rats with heart failure. *Brain Research,* 865**,** 27-34.

PATTHY, L., TREXLER, M., VÁLI, Z., BÁNYAI, L. & VÁRADI, A. 1984. Kringles: modules specialized for protein binding. 171**,** 131-136.

PEARL, J. 2009. Causal inference in statistics: An overview. *Statistics Surveys,* 3**,** 96-146.

PEDERSEN, B. K. 2006a. The anti-inflammatory effect of exercise: its role in diabetes and cardiovascular disease control. *Essays in Biochemistry, Vol 42,* 42**,** 105-117.

PEDERSEN, B. K. 2006b. The anti-inflammatory effect of exercise: its role in diabetes and cardiovascular disease control. *Essays Biochem,* 42**,** 105-17.

PERTEA, M., PERTEA, G. M., ANTONESCU, C. M., CHANG, T.-C., MENDELL, J. T. & SALZBERG, S. L. 2015. StringTie enables improved reconstruction of a transcriptome from RNA-seq reads. *Nature Biotechnology,* 33**,** 290-295.

PES, G. M., LIO, D., CARRU, C., DEIANA, L., BAGGIO, G., FRANCESCHI, C., FERRUCCI, L., OLIVERI, F., SCOLA, L., CRIVELLO, A., CANDORE, G., COLONNA-ROMANO, G. & CARUSO, C. 2004. Association between longevity and cytokine gene polymorphisms. A study in Sardinian centenarians. *Aging Clin Exp Res,* 16**,** 244-8.

PETERS, N. S., SEVERS, N. J., ROTHERY, S. M., LINCOLN, C., YACOUB, M. H. & GREEN, C. R. 1994. Spatiotemporal relation between gap junctions and fascia adherens junctions during postnatal development of human ventricular myocardium. 90**,** 713-725.

PI, Y., GOLDENTHAL, M. J. & MARIN-GARCIA, J. 2007. Mitochondrial channelopathies in aging. *J Mol Med (Berl),* 85**,** 937-51.

PINTO, E. 2007. Blood pressure and ageing. *Postgraduate Medical Journal,* 83**,** 109-114.

PLANELLS-CASES, R. & JENTSCH, T. J. 2009. Chloride channelopathies. *Biochim Biophys Acta,* 1792**,** 173-89.

PRETZEL, D., POHLERS, D., WEINERT, S. & KINNE, R. W. 2009. In vitro model for the analysis of synovial fibroblast-mediated degradation of intact cartilage. *Arthritis Res Ther,* 11**,** R25.

PRUITT, K. D., BROWN, G. R., HIATT, S. M., THIBAUD-NISSEN, F., ASTASHYN, A., ERMOLAEVA, O., FARRELL, C. M., HART, J., LANDRUM, M. J., MCGARVEY, K. M., MURPHY, M. R., O'LEARY, N. A., PUJAR, S., RAJPUT, B., RANGWALA, S. H., RIDDICK, L. D., SHKEDA, A., SUN, H., TAMEZ, P., TULLY, R. E., WALLIN, C., WEBB, D., WEBER, J., WU, W., DICUCCIO, M., KITTS, P., MAGLOTT, D. R., MURPHY, T. D. & OSTELL, J. M. 2014. RefSeq: an update on mammalian reference sequences. 42**,** D756-D763.

PRUITT, K. D., TATUSOVA, T. & MAGLOTT, D. R. 2007. NCBI reference sequences (RefSeq): a curated non-redundant sequence database of genomes, transcripts and proteins. *Nucleic Acids Research,* 35**,** D61-D65.

QIN, N., D'ANDREA, M. R., LUBIN, M. L., SHAFAEE, N., CODD, E. E. & CORREA, A. M. 2003. Molecular cloning and functional expression of the human sodium channel beta1B subunit, a novel splicing variant of the beta1 subunit. *Eur J Biochem,* 270**,** 4762-70.

RAMA, A., MATSUSHITA, T., CHAROLIDI, N., ROTHERY, S., DUPONT, E. & SEVERS, N. J. 2006. Up-regulation of connexin43 correlates with increased synthetic activity and enhanced contractile differentiation in TGF-β-treated human aortic smooth muscle cells. 85**,** 375-386.

RAMON, S., GAO, F., SERHAN, C. N. & PHIPPS, R. P. 2012. Specialized proresolving mediators enhance human B cell differentiation to antibody-secreting cells. *J Immunol,* 189**,** 1036-42.

RAMSEY, I. S., DELLING, M. & CLAPHAM, D. E. 2006. AN INTRODUCTION TO TRP CHANNELS. *Annual Review of Physiology,* 68**,** 619-647.

RAO, V., KAJA, S., AND GENTILE, S. 2016. Ion channels in Aging and Age-related Diseases.

REA, I. M., GIBSON, D. S., MCGILLIGAN, V., MCNERLAN, S. E., ALEXANDER, H. D. & ROSS, O. A. 2018. Age and Age-Related Diseases: Role of Inflammation Triggers and Cytokines. *Front Immunol,* 9**,** 586.

REA, I. M., STEWART, M., CAMPBELL, P., ALEXANDER, H. D., CROCKARD, A. D. & MORRIS, T. C. 1996. Changes in lymphocyte subsets, interleukin 2, and soluble interleukin 2 receptor in old and very old age. *Gerontology,* 42**,** 69-78.

RECCHIUTI, A. & SERHAN, C. N. 2012. Pro-Resolving Lipid Mediators (SPMs) and Their Actions in Regulating miRNA in Novel Resolution Circuits in Inflammation. *Front Immunol,* 3**,** 298.

REDDY, M. M. & KAR, S. S. 2019. Unconditional probability of dying and age-specific mortality rate because of major non-communicable diseases in India: Time trends from 2001 to 2013. *Journal of postgraduate medicine,* 65**,** 11-17.

RICHARDS, M. W., LAW, E. W. P., RENNALLS, L. P., BUSACCA, S., O'REGAN, L., FRY, A. M., FENNELL, D. A. & BAYLISS, R. 2014. Crystal structure of EML1 reveals the basis for Hsp90 dependence of oncogenic EML4-ALK by disruption of an atypical -propeller domain. *Proceedings of the National Academy of Sciences,* 111**,** 5195-5200.

RIDKER, P. M., RIFAI, N., PFEFFER, M., SACKS, F., LEPAGE, S. & BRAUNWALD, E. 2000. Elevation of tumor necrosis factor-alpha and increased risk of recurrent coronary events after myocardial infarction. *Circulation,* 101**,** 2149-53.

RINK, L., CAKMAN, I. & KIRCHNER, H. 1998. Altered cytokine production in the elderly. *Mech Ageing Dev,* 102**,** 199-209.

RIVERA-APONTE, D. E., MÉNDEZ-GONZÁLEZ, M. P., RIVERA-PAGÁN, A. F., KUCHERYAVYKH, Y. V., KUCHERYAVYKH, L. Y., SKATCHKOV, S. N. & EATON, M. J. 2015. Hyperglycemia reduces functional expression of astrocytic Kir4.1 channels and glial glutamate uptake. *Neuroscience,* 310**,** 216-223.

ROBERTSON, D. W. & STEINBERG, M. I. 1990. Potassium channel modulators: scientific applications and therapeutic promise. *J Med Chem,* 33**,** 1529-41.

ROSASCO, M. G. & GORDON, S. E. 2017. TRP Channels: What Do They Look Like? *In:* ND & EMIR, T. L. R. (eds.) *Neurobiology of TRP Channels.* Boca Raton (FL).

ROSS, O. 2003. Study of age-association with cytokine gene polymorphisms in an aged Irish population. *Mechanisms of Ageing and Development,* 124**,** 199-206.

RUBENHAGEN, R., SCHUTTRUMPF, J. P., STURMER, K. M. & FROSCH, K. H. 2012. Interleukin-7 levels in synovial fluid increase with age and MMP-1 levels decrease with progression of osteoarthritis. *Acta Orthop,* 83**,** 59-64.

RUDIJANTO, A. 2007. The role of vascular smooth muscle cells on the pathogenesis of atherosclerosis. *Acta Med Indones,* 39**,** 86-93.

RUPARELIA, N., CHAI, J. T., FISHER, E. A. & CHOUDHURY, R. P. 2017. Inflammatory processes in cardiovascular disease: a route to targeted therapies. *Nat Rev Cardiol,* 14**,** 133-144.

SANDER, S. E., LEMM, C., LANGE, N., HAMANN, M. & RICHTER, A. 2012. Retigabine, a K(V)7 (KCNQ) potassium channel opener, attenuates L-DOPA-induced dyskinesias in 6-OHDA-lesioned rats. *Neuropharmacology,* 62**,** 1052-61.

SANDOVICI, I., HAMMERLE, C. M., COOPER, W. N., SMITH, N. H., TARRY-ADKINS, J. L., DUNMORE, B. J., BAUER, J., ANDREWS, S. R., YEO, G. S. H., OZANNE, S. E. & CONSTÂNCIA, M. 2016. Ageing is associated with molecular signatures of inflammation and type 2 diabetes in rat pancreatic islets. 59**,** 502-511.

SANSONI, P., VESCOVINI, R., FAGNONI, F., BIASINI, C., ZANNI, F., ZANLARI, L., TELERA, A., LUCCHINI, G., PASSERI, G., MONTI, D., FRANCESCHI, C. & PASSERI, M. 2008. The immune system in extreme longevity. *Experimental Gerontology,* 43**,** 61-65.

SANTI, C. M. 2006. Opposite Regulation of Slick and Slack K+ Channels by Neuromodulators. *Journal of Neuroscience,* 26**,** 5059-5068.

SASAKI, S., ISHIBASHI, K. & MARUMO, F. 1998. Aquaporin-2 and -3: representatives of two subgroups of the aquaporin family colocalized in the kidney collecting duct. *Annu Rev Physiol,* 60**,** 199-220.

SCANZELLO, C. R. & GOLDRING, S. R. 2012. The role of synovitis in osteoarthritis pathogenesis. *Bone,* 51**,** 249-57.

SCHELLER, J., CHALARIS, A., SCHMIDT-ARRAS, D. & ROSE-JOHN, S. 2011. The pro- and anti-inflammatory properties of the cytokine interleukin-6. *Biochimica et Biophysica Acta (BBA) - Molecular Cell Research,* 1813**,** 878-888.

SCHOLZ, A. 2002. Mechanisms of (local) anaesthetics on voltage-gated sodium and other ion channels. *Br J Anaesth,* 89**,** 52-61.

SCHREIBER, M. 1998. Slo3, a Novel pH-sensitive K+ Channel from Mammalian Spermatocytes. 273**,** 3509-3516.

SCUDIERI, P., CACI, E., VENTURINI, A., SONDO, E., PIANIGIANI, G., MARCHETTI, C., RAVAZZOLO, R., PAGANI, F. & GALIETTA, L. J. V. 2015. Ion channel and lipid scramblase activity associated with expression of TMEM16F/ANO6 isoforms. *Journal of Physiology-London,* 593**,** 3829-3848.

SELLAM, J. & BERENBAUM, F. 2010. The role of synovitis in pathophysiology and clinical symptoms of osteoarthritis. *Nat Rev Rheumatol,* 6**,** 625-35.

SERHAN, C. N. 2014. Pro-resolving lipid mediators are leads for resolution physiology. *Nature,* 510**,** 92-101.

SERHAN, C. N., CHIANG, N. & DALLI, J. 2018. New pro-resolving n-3 mediators bridge resolution of infectious inflammation to tissue regeneration. *Mol Aspects Med,* 64**,** 1-17.

SESTI, F. 2016. Oxidation of K+Channels in Aging and Neurodegeneration. 7**,** 130.

SHAMIM, D. & LASKOWSKI, M. 2017. Inhibition of Inflammation Mediated Through the Tumor Necrosis Factor alpha Biochemical Pathway Can Lead to Favorable Outcomes in Alzheimer Disease. *J Cent Nerv Syst Dis,* 9**,** 1179573517722512.

SHIH, C. D., AU, L. C. & CHAN, J. Y. 2003. Differential role of leptin receptors at the hypothalamic paraventricular nucleus in tonic regulation of food intake and cardiovascular functions. *J Biomed Sci,* 10**,** 367-78.

SHOCK, N. W. 1964. Ageing: The Biology of Senescence. *Journal of Gerontology,* 19**,** 521-522.
SHORTER, E., SANNICANDRO, A. J., POULET, B. & GOLJANEK-WHYSALL, K. 2019. Skeletal Muscle Wasting and Its Relationship With Osteoarthritis: a Mini-Review of Mechanisms and Current Interventions. *Current Rheumatology Reports,* 21.
SHOU, X., LIN, J., XIE, C., WANG, Y. & SUN, C. 2017. Plasma IL-37 Elevated in Patients with Chronic Heart Failure and Predicted Major Adverse Cardiac Events: A 1-Year Follow-Up Study. *Dis Markers,* 2017**,** 9134079.
SIMMONS, D. M. & SWANSON, L. W. 2008. High-resolution paraventricular nucleus serial section model constructed within a traditional rat brain atlas. 438**,** 85-89.
SIMMS, B. A. & ZAMPONI, G. W. 2014. Neuronal voltage-gated calcium channels: structure, function, and dysfunction. *Neuron,* 82**,** 24-45.
SIMON, L. V., HASHMI, M. F. & FARRELL, M. W. 2019. Hyperkalemia. *StatPearls.* Treasure Island (FL).
SIMS, J. E. & SMITH, D. E. 2010. The IL-1 family: regulators of immunity. *Nat Rev Immunol,* 10**,** 89-102.
SMITH, D. E. 2011. The biological paths of IL-1 family members IL-18 and IL-33. *J Leukoc Biol,* 89**,** 383-92.
SONG, M. Y. & YUAN, J. X. 2010. Introduction to TRP channels: structure, function, and regulation. *Adv Exp Med Biol,* 661**,** 99-108.
SPITE, M., NORLING, L. V., SUMMERS, L., YANG, R., COOPER, D., PETASIS, N. A., FLOWER, R. J., PERRETTI, M. & SERHAN, C. N. 2009. Resolvin D2 is a potent regulator of leukocytes and controls microbial sepsis. *Nature,* 461**,** 1287-1291.
STÄNDKER, L., SCHRADER, M., KANSE, S. M., JÜRGENS, M., FORSSMANN, W.-G. & PREISSNER, K. T. 1997. Isolation and characterization of the circulating form of human endostatin. 420**,** 129-133.
STATLAND, J., PHILLIPS, L. & TRIVEDI, J. R. 2014. Muscle channelopathies. *Neurol Clin,* 32**,** 801-15, x.
STEVENS, A. L., WISHNOK, J. S., CHAI, D. H., GRODZINSKY, A. J. & TANNENBAUM, S. R. 2008. A sodium dodecyl sulfate-polyacrylamide gel electrophoresis-liquid chromatography tandem mass spectrometry analysis of bovine cartilage tissue response to mechanical compression injury and the inflammatory cytokines tumor necrosis factor alpha and interleukin-1beta. *Arthritis Rheum,* 58**,** 489-500.
STEVENS, A. L., WISHNOK, J. S., WHITE, F. M., GRODZINSKY, A. J. & TANNENBAUM, S. R. 2009. Mechanical injury and cytokines cause loss of cartilage integrity and upregulate proteins associated with catabolism, immunity, inflammation, and repair. *Mol Cell Proteomics,* 8**,** 1475-89.
STEVENSON, K. & UVERSKY, V. N. 2019. Single-cell RNA-Seq: a next generation sequencing tool for a high-resolution view of the individual cell. *J Biomol Struct Dyn***,** 1-6.
STEWART, J., MANMATHAN, G. & WILKINSON, P. 2017. Primary prevention of cardiovascular disease: A review of contemporary guidance and literature. *JRSM Cardiovascular Disease,* 6**,** 204800401668721.
STOCKER, M. & KERSCHENSTEINER, D. 1998. Cloning and Tissue Distribution of Two New Potassium Channel α-Subunits from Rat Brain. 248**,** 927-934.
STOJILKOVIC, S. S., TABAK, J. & BERTRAM, R. 2010. Ion channels and signaling in the pituitary gland. *Endocr Rev,* 31**,** 845-915.
SUGITA, S., MIZUTANI, E., HOZAKI, M., NAKAMURA, M. & MATSUMOTO, T. 2019. Photoelasticity-based evaluation of cellular contractile force for phenotypic discrimination of vascular smooth muscle cells. *Scientific Reports,* 9.
SUTTON, S., CLUTTERBUCK, A., HARRIS, P., GENT, T., FREEMAN, S., FOSTER, N., BARRETT-JOLLEY, R. & MOBASHERI, A. 2009. The contribution of the synovium, synovial derived inflammatory cytokines and neuropeptides to the pathogenesis of osteoarthritis. *Vet J,* 179**,** 10-24.
SWANSON, L. W. & SAWCHENKO, P. E. 1983. Hypothalamic Integration - Organization of the Paraventricular and Supraoptic Nuclei. *Annual Review of Neuroscience,* 6**,** 269-324.

SWANSON, L. W., SAWCHENKO, P. E., WIEGAND, S. J. & PRICE, J. L. 1980. Separate Neurons in the Paraventricular Nucleus Project to the Median-Eminence and to the Medulla or Spinal-Cord. *Brain Research,* 198**,** 190-195.

SWARTZ, K. J. 2007. Tarantula toxins interacting with voltage sensors in potassium channels. *Toxicon,* 49**,** 213-30.

SWARTZ, K. J. & MACKINNON, R. 1997. Hanatoxin Modifies the Gating of a Voltage-Dependent K+ Channel through Multiple Binding Sites. *Neuron,* 18**,** 665-673.

TANAKA, T., NARAZAKI, M. & KISHIMOTO, T. 2014. IL-6 in Inflammation, Immunity, and Disease. *Cold Spring Harbor Perspectives in Biology,* 6**,** a016295-a016295.

TANG, C.-Y. & CHEN, T.-Y. 2011. Physiology and Pathophysiology of CLC-1: Mechanisms of a Chloride Channel Disease, Myotonia. 2011**,** 1-10.

TANNER, M. R., HU, X., HUQ, R., TAJHYA, R. B., SUN, L., KHAN, F. S., LARAGIONE, T., HORRIGAN, F. T., GULKO, P. S. & BEETON, C. 2015a. KCa1.1 Inhibition Attenuates Fibroblast-like Synoviocyte Invasiveness and Ameliorates Disease in Rat Models of Rheumatoid Arthritis. *Arthritis Rheumatol,* 67**,** 96-106.

TANNER, M. R., HU, X., HUQ, R., TAJHYA, R. B., SUN, L., KHAN, F. S., LARAGIONE, T., HORRIGAN, F. T., GULKO, P. S. & BEETON, C. 2015b. KCa1.1 Inhibition Attenuates Fibroblast-like Synoviocyte Invasiveness and Ameliorates Disease in Rat Models of Rheumatoid Arthritis. *Arthritis & Rheumatology,* 67**,** 96-106.

TERRAR, D. A. 1993. Structure and function of calcium channels and the actions of anaesthetics. *Br J Anaesth,* 71**,** 39-46.

THOMAS, K., RAFIQ, S., FRAYLING, T. M., EBRAHIM, S., KUMARI, M., GALLACHER, J., FERRUCCI, L., BANDINELLI, S., WALLACE, R. B., MELZER, D., MARTIN, R. M. & BEN-SHLOMO, Y. 2009. Interleukin-18 polymorphism and physical functioning in older people: a replication study and meta-analysis. *J Gerontol A Biol Sci Med Sci,* 64**,** 1177-82.

TIAN, C., ZHU, R., ZHU, L., QIU, T., CAO, Z. & KANG, T. 2014. Potassium channels: structures, diseases, and modulators. *Chem Biol Drug Des,* 83**,** 1-26.

TORP, K. D. & SIMON, L. V. 2019. Lidocaine Toxicity. *StatPearls.* Treasure Island (FL).

TORRES, V. E., CAI, Y., CHEN, X., WU, G. Q., GENG, L., CLEGHORN, K. A., JOHNSON, C. M. & SOMLO, S. 2001. Vascular expression of polycystin-2. *J Am Soc Nephrol,* 12**,** 1-9.

TRAN, D. Q. 2012. TGF-beta: the sword, the wand, and the shield of FOXP3(+) regulatory T cells. *J Mol Cell Biol,* 4**,** 29-37.

TRAPNELL, C., WILLIAMS, B. A., PERTEA, G., MORTAZAVI, A., KWAN, G., VAN BAREN, M. J., SALZBERG, S. L., WOLD, B. J. & PACHTER, L. 2010. Transcript assembly and quantification by RNA-Seq reveals unannotated transcripts and isoform switching during cell differentiation. *Nature Biotechnology,* 28**,** 511-515.

TROMPET, S., DE CRAEN, A. J. M., SLAGBOOM, P., SHEPHERD, J., BLAUW, G. J., MURPHY, M. B., BOLLEN, E. L. E. M., BUCKLEY, B. M., FORD, I., GAW, A., MACFARLANE, P. W., PACKARD, C. J., STOTT, D. J., JUKEMA, J. W. & WESTENDORP, R. G. J. 2008. Genetic variation in the interleukin-1 -converting enzyme associates with cognitive function. The PROSPER study. *Brain,* 131**,** 1069-1077.

TURGUTALP, K., BARDAK, S., HELVACı, I., İŞGÜZAR, G., PAYAS, E., DEMIR, S. & KıYKıM, A. 2016. Community-acquired hyperkalemia in elderly patients: risk factors and clinical outcomes. 38**,** 1405-1412.

UCAR, D., MARQUEZ, E. J., CHUNG, C. H., MARCHES, R., ROSSI, R. J., UYAR, A., WU, T. C., GEORGE, J., STITZEL, M. L., PALUCKA, A. K., KUCHEL, G. A. & BANCHEREAU, J. 2017. The chromatin accessibility signature of human immune aging stems from CD8(+) T cells. *J Exp Med,* 214**,** 3123-3144.

UEBELE, V. N., LAGRUTTA, A., WADE, T., FIGUEROA, D. J., LIU, Y., MCKENNA, E., AUSTIN, C. P., BENNETT, P. B. & SWANSON, R. 2000. Cloning and functional expression of two families of beta-subunits of the large conductance calcium-activated K+ channel. *J Biol Chem,* 275**,** 23211-8.

ULBRICHT, W. 2005. Sodium Channel Inactivation: Molecular Determinants and Modulation. 85**,** 1271-1301.

UNGVARI, Z., TARANTINI, S., DONATO, A. J., GALVAN, V. & CSISZAR, A. 2018. Mechanisms of Vascular Aging. *Circulation Research,* 123**,** 849-867.

VAISHALI, M. P. & SATYA, P. G. 2016. Studies on Chloride Channels and their Modulators. *Current Topics in Medicinal Chemistry,* 16**,** 1862-1876.

VAN DER HEIJDEN, T., BOT, I. & KUIPER, J. 2019. The IL-12 cytokine family in cardiovascular diseases. *Cytokine,* 122**,** 154188.

VAN GULICK, L., SABY, C., MORJANI, H. & BELJEBBAR, A. 2019. Age-related changes in molecular organization of type I collagen in tendon as probed by polarized SHG and Raman microspectroscopy. *Scientific Reports,* 9.

VAN MAANEN, M. A., STOOF, S. P., VAN DER ZANDEN, E. P., DE JONGE, W. J., JANSSEN, R. A., FISCHER, D. F., VANDEGHINSTE, N., BRYS, R., VERVOORDELDONK, M. J. & TAK, P. P. 2009. The alpha7 nicotinic acetylcholine receptor on fibroblast-like synoviocytes and in synovial tissue from rheumatoid arthritis patients: a possible role for a key neurotransmitter in synovial inflammation. *Arthritis Rheum,* 60**,** 1272-81.

VARANI, K., DE MATTEI, M., VINCENZI, F., TOSI, A., GESSI, S., MERIGHI, S., PELLATI, A., MASIERI, F., ONGARO, A. & BOREA, P. A. 2008. Pharmacological characterization of P2X1 and P2X3 purinergic receptors in bovine chondrocytes. *Osteoarthritis Cartilage,* 16**,** 1421-9.

VARGAS-ALARCON, G., ALVAREZ-LEON, E., FRAGOSO, J.-M., VARGAS, A., MARTINEZ, A., VALLEJO, M. & MARTINEZ-LAVIN, M. 2012. A SCN9A gene-encoded dorsal root ganglia sodium channel polymorphism associated with severe fibromyalgia. *BMC Musculoskeletal Disorders,* 13**,** 23.

VASILAKI, A., VAN DER MEULEN, J. H., LARKIN, L., HARRISON, D. C., PEARSON, T., VAN REMMEN, H., RICHARDSON, A., BROOKS, S. V., JACKSON, M. J. & MCARDLE, A. 2010. The age-related failure of adaptive responses to contractile activity in skeletal muscle is mimicked in young mice by deletion of Cu,Zn superoxide dismutase. 9**,** 979-990.

VERGULT, S., DHEEDENE, A., MEURS, A., FAES, F., ISIDOR, B., JANSSENS, S., GAUTIER, A., LE CAIGNEC, C. & MENTEN, B. 2015. Genomic aberrations of the CACNA2D1 gene in three patients with epilepsy and intellectual disability. 23**,** 628-632.

VON BANCHET, G. S., RICHTER, J., HUCKEL, M., ROSE, C., BRAUER, R. & SCHAIBLE, H. G. 2007. Fibroblast-like synovial cells from normal and inflamed knee joints differently affect the expression of pain-related receptors in sensory neurones: a co-culture study. *Arthritis Res Ther,* 9**,** R6.

WALDBURGER, J. M., BOYLE, D. L., PAVLOV, V. A., TRACEY, K. J. & FIRESTEIN, G. S. 2008. Acetylcholine regulation of synoviocyte cytokine expression by the alpha7 nicotinic receptor. *Arthritis Rheum,* 58**,** 3439-49.

WALSTON, J. D. 2012. Sarcopenia in older adults. *Current Opinion in Rheumatology,* 24**,** 623-627.

WANG, H. & WOOLF, C. J. 2005. Pain TRPs. *Neuron,* 46**,** 9-12.

WANG, J., OU, S. W. & WANG, Y. J. 2017. Distribution and function of voltage-gated sodium channels in the nervous system. *Channels (Austin),* 11**,** 534-554.

WANG, S., HU, L. F., YANG, Y., DING, J. H. & HU, G. 2005. Studies of ATP-sensitive potassium channels on 6-hydroxydopamine and haloperidol rat models of Parkinson's disease: implications for treating Parkinson's disease? *Neuropharmacology,* 48**,** 984-92.

WANG, T. 2015. TNF-alpha G308A polymorphism and the susceptibility to Alzheimer's disease: an updated meta-analysis. *Arch Med Res,* 46**,** 24-30 e1.

WANG, X.-Y., HURME, M., JYLHÄ, M. & HERVONEN, A. 2001. Lack of association between human longevity and polymorphisms of IL-1 cluster, IL-6, IL-10 and TNF-α genes in Finnish nonagenarians. *Mechanisms of Ageing and Development,* 123**,** 29-38.

WATANABE, M., ICHINOSE, S. & SUNAMORI, M. 2004. Age-related changes in gap junctional protein of the rat heart. *Exp Clin Cardiol,* 9**,** 130-2.

WEI, A., JEGLA, T. & SALKOFF, L. 1996. Eight potassium channel families revealed by the C. elegans genome project. *Neuropharmacology,* 35**,** 805-29.

WEI, X. & RICHARDS, J. R. 2019. Physiology, Cardiac Repolarization Dispersion and Reserve. *StatPearls.* Treasure Island (FL).

WEINERT, B. T. & TIMIRAS, P. S. 2003. Invited Review: Theories of aging. *Journal of Applied Physiology,* 95**,** 1706-1716.

WEINGARTH, M., PROKOFYEV, A., VAN DER CRUIJSEN, E. A., NAND, D., BONVIN, A. M., PONGS, O. & BALDUS, M. 2013. Structural determinants of specific lipid binding to potassium channels. *J Am Chem Soc,* 135**,** 3983-8.

WELSH, P., MURRAY, H. M., FORD, I., TROMPET, S., DE CRAEN, A. J. M., JUKEMA, J. W., STOTT, D. J., MCINNES, I. B., PACKARD, C. J., WESTENDORP, R. G. J. & SATTAR, N. 2011. Circulating Interleukin-10 and Risk of Cardiovascular Events. *Arteriosclerosis, Thrombosis, and Vascular Biology,* 31**,** 2338-2344.

WESTENDORP, R. G., LANGERMANS, J. A., HUIZINGA, T. W., VERWEIJ, C. L. & STURK, A. 1997. Genetic influence on cytokine production in meningococcal disease. *Lancet,* 349**,** 1912-3.

WIBBERLEY, A., STAUNTON, C. A., FEETHAM, C. H., VERENINOV, A. A. & BARRETT-JOLLEY, R. 2015. An In Vitro Model of Skeletal Muscle Volume Regulation. *PLOS ONE,* 10**,** e0127889.

WIECZOROWSKA-TOBIS, K., NIEMIR, Z. I., PODKOWKA, R., KORYBALSKA, K., MOSSAKOWSKA, M. & BREBOROWICZ, A. 2006. Can an increased level of circulating IL-8 be a predictor of human longevity? *Med Sci Monit,* 12**,** Cr118-21.

WILDERS, R. 2012. Cardiac ion channelopathies and the sudden infant death syndrome. *ISRN Cardiol,* 2012**,** 846171.

WILLIAMS, A. 2014. Proteomic studies of an explant

model of equine articular cartilage in response to proinflammatory and anti-inflammatory stimuli. *PhD Thesis University of Nottingham*.

WILLIAMS, A., SMITH, J. R., ALLAWAY, D., HARRIS, P., LIDDELL, S. & MOBASHERI, A. 2011. Strategies for optimising proteomic studies of the cartilage secretome: establishing the time course for protein release and evaluating responses of explant cultures to il-1 beta, tnf-alpha and carprofen. *Osteoarthritis and Cartilage,* 19**,** S209-S209.

WILLIAMS, M. E., FELDMAN, D. H., MCCUE, A. F., BRENNER, R., VELICELEBI, G., ELLIS, S. B. & HARPOLD, M. M. 1992. Structure and functional expression of alpha 1, alpha 2, and beta subunits of a novel human neuronal calcium channel subtype. *Neuron,* 8**,** 71-84.

WRIGHT, S. H. 2004. Generation of resting membrane potential. *Adv Physiol Educ,* 28**,** 139-42.

WU, C., YANG, K., LIU, Q., WAKUI, M., JIN, G. Z., ZHEN, X. & WU, J. 2010. Tetrahydroberberine blocks ATP-sensitive potassium channels in dopamine neurons acutely-dissociated from rat substantia nigra pars compacta. *Neuropharmacology,* 59**,** 567-72.

XU, H., RAMSEY, I. S., KOTECHA, S. A., MORAN, M. M., CHONG, J. A., LAWSON, D., GE, P., LILLY, J., SILOS-SANTIAGO, I., XIE, Y., DISTEFANO, P. S., CURTIS, R. & CLAPHAM, D. E. 2002. TRPV3 is a calcium-permeable temperature-sensitive cation channel. *Nature,* 418**,** 181-186.

YANG, C. T., ZENG, X. H., XIA, X. M. & LINGLE, C. J. 2009. Interactions between beta subunits of the KCNMB family and Slo3: beta4 selectively modulates Slo3 expression and function. *PLoS One,* 4**,** e6135.

YANG, Q., WANG, E.-Y., JIA, H.-W. & WANG, Y.-P. 2016. Association between polymorphisms in transforming growth factor-β1 and sporadic Alzheimer's disease in a Chinese population. *International Journal of Neuroscience,* 126**,** 979-984.

YOSHIMURA, A., WAKABAYASHI, Y. & MORI, T. 2010. Cellular and molecular basis for the regulation of inflammation by TGF-beta. *J Biochem,* 147**,** 781-92.

YOUNG, M. D., WAKEFIELD, M. J., SMYTH, G. K. & OSHLACK, A. 2010. Gene ontology analysis for RNA-seq: accounting for selection bias. *Genome Biol,* 11**,** R14.

YU, F. H. & CATTERALL, W. A. 2003. Overview of the voltage-gated sodium channel family. *Genome Biol,* 4**,** 207.

YU, F. H., YAROV-YAROVOY, V., GUTMAN, G. A. & CATTERALL, W. A. 2005. Overview of molecular relationships in the voltage-gated ion channel superfamily. *Pharmacol Rev,* 57**,** 387-95.

ZAMBRANO-ZARAGOZA, J. F., ROMO-MARTINEZ, E. J., DURAN-AVELAR MDE, J., GARCIA-MAGALLANES, N. & VIBANCO-PEREZ, N. 2014. Th17 cells in autoimmune and infectious diseases. *Int J Inflam,* 2014**,** 651503.

ZAMPONI, G. W. 2016. Targeting voltage-gated calcium channels in neurological and psychiatric diseases. *Nat Rev Drug Discov,* 15**,** 19-34.

ZAMPONI, G. W. 2017. A Crash Course in Calcium Channels. *ACS Chem Neurosci,* 8**,** 2583-2585.

ZAMPONI, G. W., STRIESSNIG, J., KOSCHAK, A. & DOLPHIN, A. C. 2015. The Physiology, Pathology, and Pharmacology of Voltage-Gated Calcium Channels and Their Future Therapeutic Potential. *Pharmacol Rev,* 67**,** 821-70.

ZHANG, J. M. & AN, J. 2007. Cytokines, inflammation, and pain. *Int Anesthesiol Clin,* 45**,** 27-37.

ZHANG, K., MAYHAN, W. G. & PATEL, K. P. 1997. Nitric oxide within the paraventricular nucleus mediates changes in renal sympathetic nerve activity. *American Journal of Physiology-Regulatory Integrative and Comparative Physiology,* 273**,** R864-R872.

ZHANG, K., ZUCKER, I. H. & PATEL, K. P. 1998. Altered number of diaphorase (NOS) positive neurons in the hypothalamus of rats with heart failure. *Brain Research,* 786**,** 219-225.

ZHANG, P., WU, X., LI, G., HE, Q., DAI, H., AI, C. & SHI, J. 2017. Tumor necrosis factor-alpha gene polymorphisms and susceptibility to ischemic heart disease: A systematic review and meta-analysis. *Medicine (Baltimore),* 96**,** e6569.

ZHENG, C., ZHOU, X. W. & WANG, J. Z. 2016. The dual roles of cytokines in Alzheimer's disease: update on interleukins, TNF-alpha, TGF-beta and IFN-gamma. *Transl Neurodegener,* 5**,** 7.

ZHU, R., SUN, Z., LI, C., RAMAKRISHNA, S., CHIU, K. & HE, L. 2019a. Electrical stimulation affects neural stem cell fate and function in vitro. *Exp Neurol,* 319**,** 112963.

ZHU, Y., QU, J., HE, L., ZHANG, F., ZHOU, Z., YANG, S. & ZHOU, Y. 2019b. Calcium in Vascular Smooth Muscle Cell Elasticity and Adhesion: Novel Insights Into the Mechanism of Action. *Frontiers in Physiology,* 10.

ZIEGENHAIN, C., VIETH, B., PAREKH, S., REINIUS, B., GUILLAUMET-ADKINS, A., SMETS, M., LEONHARDT, H., HEYN, H., HELLMANN, I. & ENARD, W. 2017. Comparative Analysis of Single-Cell RNA Sequencing Methods. *Molecular Cell,* 65**,** 631-643.e4.

ZUVICH, R. L., MCCAULEY, J. L., OKSENBERG, J. R., SAWCER, S. J., DE JAGER, P. L., INTERNATIONAL MULTIPLE SCLEROSIS GENETICS, C., AUBIN, C., CROSS, A. H., PICCIO, L., AGGARWAL, N. T., EVANS, D., HAFLER, D. A., COMPSTON, A., HAUSER, S. L., PERICAK-VANCE, M. A. & HAINES, J. L. 2010. Genetic variation in the IL7RA/IL7 pathway increases multiple sclerosis susceptibility. *Hum Genet,* 127**,** 525-35.

ZYKOV, M. V., BARBARASH, O. L., KASHTALAP, V. V., KUTIKHIN, A. G. & BARBARASH, L. S. 2016. Interleukin-12 serum level has prognostic value in patients with ST-segment elevation myocardial infarction. *Heart & Lung,* 45**,** 336-340.

2019. The Gene Ontology Resource: 20 years and still GOing strong. *Nucleic Acids Research,* 47**,** D330-D338.

ABDUL KADIR, L., STACEY, M. & BARRETT-JOLLEY, R. 2018. Emerging Roles of the Membrane Potential: Action Beyond the Action Potential. *Frontiers in Physiology,* 9.

ACKERMANN, M., CHAO, L., BERGSTROM, C. T. & DOEBELI, M. 2007. On the evolutionary origin of aging. *Aging Cell,* 6**,** 235-244.

AGRE, P. 2006. The Aquaporin Water Channels. 3**,** 5-13.

AHMED, M. S., IKRAM, S., BIBI, N. & MIR, A. 2017. Hutchinson–Gilford Progeria Syndrome: A Premature Aging Disease. *Molecular Neurobiology*.

ALBARWANI, S. A., MANSOUR, F., KHAN, A. A., AL-LAWATI, I., AL-KAABI, A., AL-BUSAIDI, A.-M., AL-HADHRAMI, S., AL-HUSSEINI, I., AL-SIYABI, S. & TANIRA, M. O. 2016. Aging Reduces L-Type Calcium Channel Current and the Vasodilatory Response of Small Mesenteric Arteries to Calcium Channel Blockers. *Frontiers in Physiology,* 7.

AMIN, A. S., TAN, H. L. & WILDE, A. A. 2010. Cardiac ion channels in health and disease. *Heart Rhythm,* 7**,** 117-26.

ANAPARTHY, N., HO, Y. J., MARTELOTTO, L., HAMMELL, M. & HICKS, J. 2019. Single-Cell Applications of Next-Generation Sequencing. *Cold Spring Harb Perspect Med,* 9.

ANGULO, E., NOE, V., CASADO, V., MALLOL, J., GOMEZ-ISLA, T., LLUIS, C., FERRER, I., CIUDAD, C. J. & FRANCO, R. 2004. Up-regulation of the Kv3.4 potassium channel subunit in early stages of Alzheimer's disease. *J Neurochem,* 91**,** 547-57.

ANON 2000. Recommendations for the medical management of osteoarthritis of the hip and knee: 2000 update. American College of Rheumatology Subcommittee on Osteoarthritis Guidelines. *Arthritis Rheum,* 43**,** 1905-15.

ARMSTRONG, M. E., ALEXANDER, H. D., RITCHIE, J. L., MCMILLAN, S. A. & REA, I. M. 2001. Age-related alterations in basal expression and in vitro, tumour necrosis factor alpha mediated, upregulation of CD11b. *Gerontology,* 47**,** 180-5.

ASHBURNER, M., BALL, C. A., BLAKE, J. A., BOTSTEIN, D., BUTLER, H., CHERRY, J. M., DAVIS, A. P., DOLINSKI, K., DWIGHT, S. S., EPPIG, J. T., HARRIS, M. A., HILL, D. P., ISSEL-TARVER, L., KASARSKIS, A., LEWIS, S., MATESE, J. C., RICHARDSON, J. E., RINGWALD, M., RUBIN, G. M. & SHERLOCK, G. 2000. Gene Ontology: tool for the unification of biology. *Nature Genetics,* 25**,** 25-29.

BABENKO, A. P., GONZALEZ, G., AGUILAR-BRYAN, L. & BRYAN, J. 1998. Reconstituted Human Cardiac KATP Channels : Functional Identity With the Native Channels From the Sarcolemma of Human Ventricular Cells. 83**,** 1132-1143.

BADOER, E. 1996. Cardiovascular role of parvocellular neurons in the paraventricular nucleus of the hypothalamus. *News in Physiological Sciences,* 11**,** 43-47.

BAE, E., CHA, R. H., KIM, Y. C., AN, J. N., KIM, D. K., YOO, K. D., LEE, S. M., KIM, M. H., PARK, J. T., KANG, S. W., PARK, J. Y., LIM, C. S., KIM, Y. S., YANG, S. H. & LEE, J. P. 2017. Circulating TNF receptors predict cardiovascular disease in patients with chronic kidney disease. *Medicine (Baltimore),* 96**,** e6666.

BARDAK, S., TURGUTALP, K., KOYUNCU, M. B., HARI, H., HELVACI, I., OVLA, D., HOROZ, M., DEMIR, S. & KIYKIM, A. 2017. Community-acquired hypokalemia in elderly patients: related factors and clinical outcomes. *Int Urol Nephrol,* 49**,** 483-489.

BARRETT-JOLLEY, R., LEWIS, R., FALLMAN, R. & MOBASHERI, A. 2010. The Emerging Chondrocyte Channelome. *Frontiers in Physiology,* 1**,** 1-11.

BARTOK, B. & FIRESTEIN, G. S. 2010. Fibroblast-like synoviocytes: key effector cells in rheumatoid arthritis. *Immunological Reviews,* 233**,** 233-255.

BECKER, D. L., PHILLIPS, A. R., DUFT, B. J., KIM, Y. & GREEN, C. R. 2015. Translating connexin biology into therapeutics.

BEETON, C. 2017. KCa1.1 channels as therapeutic targets for rheumatoid arthritis. *Expert Opin Ther Targets,* 21**,** 1077-1081.

BEHR, E. R., DALAGEORGOU, C., CHRISTIANSEN, M., SYRRIS, P., HUGHES, S., TOME ESTEBAN, M. T., ROWLAND, E., JEFFERY, S. & MCKENNA, W. J. 2008. Sudden arrhythmic death syndrome: familial evaluation identifies inheritable heart disease in the majority of families. *Eur Heart J,* 29**,** 1670-80.

BELLANTUONO, I. & POTTER, P. K. 2016. Modelling ageing and age-related disease. *Drug Discovery Today: Disease Models,* 20**,** 27-32.

BELLOCQ, C., VAN GINNEKEN, A. C., BEZZINA, C. R., ALDERS, M., ESCANDE, D., MANNENS, M. M., BARO, I. & WILDE, A. A. 2004. Mutation in the KCNQ1 gene leading to the short QT-interval syndrome. *Circulation,* 109**,** 2394-7.

BENNETT, D. L., CLARK, A. J., HUANG, J., WAXMAN, S. G. & DIB-HAJJ, S. D. 2019. The Role of Voltage-Gated Sodium Channels in Pain Signaling. *Physiol Rev,* 99**,** 1079-1151.

BENNETT, M. R., SINHA, S. & OWENS, G. K. 2016. Vascular Smooth Muscle Cells in Atherosclerosis. *Circulation Research,* 118**,** 692-702.

BENYA, P. D. & SHAFFER, J. D. 1982. Dedifferentiated chondrocytes reexpress the differentiated collagen phenotype when cultured in agarose gels. *Cell,* 30**,** 215-24.

BERENBAUM, F. 2013. Osteoarthritis as an inflammatory disease (osteoarthritis is not osteoarthrosis!). *Osteoarthritis and Cartilage,* 21**,** 16-21.

BHATTACHARJEE, A., JOINER, W. J., WU, M., YANG, Y., SIGWORTH, F. J. & KACZMAREK, L. K. 2003. Slick (Slo2.1), a Rapidly-Gating Sodium-Activated Potassium Channel Inhibited by ATP. *The Journal of Neuroscience,* 23**,** 11681-11691.

BODA, E., HOXHA, E., PINI, A., MONTAROLO, F. & TEMPIA, F. 2012. Brain expression of Kv3 subunits during development, adulthood and aging and in a murine model of Alzheimer's disease. *J Mol Neurosci,* 46**,** 606-15.

BODMAN, M. A. & VARACALLO, M. 2019. Diabetic Neuropathy. *StatPearls.* Treasure Island (FL).

BROZOVICH, F. V., NICHOLSON, C. J., DEGEN, C. V., GAO, Y. Z., AGGARWAL, M. & MORGAN, K. G. 2016. Mechanisms of Vascular Smooth Muscle Contraction and the Basis for Pharmacologic Treatment of Smooth Muscle Disorders. *Pharmacological Reviews,* 68**,** 476-532.

BRUST, P. F., SIMERSON, S., MCCUE, A. F., DEAL, C. R., SCHOONMAKER, S., WILLIAMS, M. E., VELICELEBI, G., JOHNSON, E. C., HARPOLD, M. M. & ELLIS, S. B. 1993. Human neuronal voltage-dependent calcium channels: studies on subunit structure and role in channel assembly. *Neuropharmacology,* 32**,** 1089-102.

BRUUNSGAARD, H. 2002. Effects of tumor necrosis factor-alpha and interleukin-6 in elderly populations. *Eur Cytokine Netw,* 13**,** 389-91.

BRUUNSGAARD, H., ANDERSEN-RANBERG, K., HJELMBORG, J. V. B., PEDERSEN, B. K. & JEUNE, B. 2003a. Elevated levels of tumor necrosis factor alpha and mortality in centenarians. 115**,** 278-283.

BRUUNSGAARD, H., LADELUND, S., PEDERSEN, A. N., SCHROLL, M., JORGENSEN, T. & PEDERSEN, B. K. 2003b. Predicting death from tumour necrosis factor-alpha and interleukin-6 in 80-year-old people. *Clin Exp Immunol,* 132**,** 24-31.

BRUUNSGAARD, H., SKINHOJ, P., PEDERSEN, A. N., SCHROLL, M. & PEDERSEN, B. K. 2000. Ageing, tumour necrosis factor-alpha (TNF-alpha) and atherosclerosis. *Clin Exp Immunol,* 121**,** 255-60.

BURKE, D., KIERNAN, M. C. & BOSTOCK, H. 2001. Excitability of human axons. *Clin Neurophysiol,* 112**,** 1575-85.

BURMESTER, G. R., DIMITRIU-BONA, A., WATERS, S. J. & WINCHESTER, R. J. 1983. Identification of three major synovial lining cell populations by monoclonal antibodies directed to Ia antigens and antigens associated with monocytes/macrophages and fibroblasts. *Scand J Immunol,* 17**,** 69-82.

CALLAGHAN, M. F., FREUND, P., DRAGANSKI, B., ANDERSON, E., CAPPELLETTI, M., CHOWDHURY, R., DIEDRICHSEN, J., FITZGERALD, T. H. B., SMITTENAAR, P., HELMS, G., LUTTI, A. & WEISKOPF, N.

2014. Widespread age-related differences in the human brain microstructure revealed by quantitative magnetic resonance imaging. 35**,** 1862-1872.
CANNON, S. C. 2015. Channelopathies of skeletal muscle excitability. *Compr Physiol,* 5**,** 761-90.
CARBONI, G. L., GAO, B., NISHIZAKI, M., XU, K., MINNA, J. D., ROTH, J. A. & JI, L. 2003. CACNA2D2-mediated apoptosis in NSCLC cells is associated with alterations of the intracellular calcium signaling and disruption of mitochondria membrane integrity. *Oncogene,* 22**,** 615-626.
CARVALHO-DE-SOUZA, J. L., VARANDA, W. A., TOSTES, R. C. & CHIGNALIA, A. Z. 2013. BK Channels in Cardiovascular Diseases and Aging. *Aging Dis,* 4**,** 38-49.
CASTRO, D. & SHARMA, S. 2019. Hypokalemia. *StatPearls.* Treasure Island (FL).
CATERINA, M. J. 2007. Transient receptor potential ion channels as participants in thermosensation and thermoregulation. *American Journal of Physiology-Regulatory, Integrative and Comparative Physiology,* 292**,** R64-R76.
CATTERALL, W. A. 2011. Voltage-Gated Calcium Channels. *Cold Spring Harbor Perspectives in Biology,* 3**,** a003947-a003947.
CAVALLONE, L., BONAFE, M., OLIVIERI, F., CARDELLI, M., MARCHEGIANI, F., GIOVAGNETTI, S., DI STASIO, G., GIAMPIERI, C., MUGIANESI, E., STECCONI, R., SCIACCA, F., GRIMALDI, L. M., DE BENEDICTIS, G., LIO, D., CARUSO, C. & FRANCESCHI, C. 2003. The role of IL-1 gene cluster in longevity: a study in Italian population. *Mech Ageing Dev,* 124**,** 533-8.
CHAKROBORTY, S. & STUTZMANN, G. E. 2014. Calcium channelopathies and Alzheimer's disease: insight into therapeutic success and failures. *Eur J Pharmacol,* 739**,** 83-95.
CHENG, J., WEN, J., WANG, N., WANG, C., XU, Q. & YANG, Y. 2019. Ion Channels and Vascular Diseases. *Arteriosclerosis, Thrombosis, and Vascular Biology,* 39.
CHENG, W., SUN, C. & ZHENG, J. 2010. Heteromerization of TRP channel subunits: extending functional diversity. *Protein & Cell,* 1**,** 802-810.
CHRYSAFIDES, S. M. & SHARMA, S. 2019. Physiology, Resting Potential. *StatPearls.* Treasure Island (FL).
CHUNG, K. F. 2009. Cytokines. Elsevier.
CLARK, R. B., KONDO, C., BELKE, D. D. & GILES, W. R. 2011. Two-pore domain K + channels regulate membrane potential of isolated human articular chondrocytes. 589**,** 5071-5089.
CLARK, R. B., SCHMIDT, T. A., SACHSE, F. B., BOYLE, D., FIRESTEIN, G. S. & GILES, W. R. 2017. Cellular electrophysiological principles that modulate secretion from synovial fibroblasts. *J Physiol,* 595**,** 635-645.
CLARKE, R., VALDES-MARQUEZ, E., HILL, M., GORDON, J., FARRALL, M., HAMSTEN, A., WATKINS, H. & HOPEWELL, J. C. 2018. Plasma cytokines and risk of coronary heart disease in the PROCARDIS study. *Open Heart,* 5**,** e000807.
COHEN, R. M., FOELL, J. D., BALIJEPALLI, R. C., SHAH, V., HELL, J. W. & KAMP, T. J. 2005. Unique modulation of L-type Ca2+ channels by short auxiliary beta1d subunit present in cardiac muscle. *Am J Physiol Heart Circ Physiol,* 288**,** H2363-74.
COLLIN, T., LORY, P., TAVIAUX, S., COURTIEU, C., GUILBAULT, P., BERTA, P. & NARGEOT, J. 1994. Cloning, chromosomal location and functional expression of the human voltage-dependent calcium-channel beta3 subunit. 220**,** 257-262.
COLLINS, J. S., PERRY, R. T., WATSON, B., JR., HARRELL, L. E., ACTON, R. T., BLACKER, D., ALBERT, M. S., TANZI, R. E., BASSETT, S. S., MCINNIS, M. G., CAMPBELL, R. D. & GO, R. C. 2000. Association of a haplotype for tumor necrosis factor in siblings with late-onset Alzheimer disease: the NIMH Alzheimer Disease Genetics Initiative. *Am J Med Genet,* 96**,** 823-30.
COOTE, J. H. 1995. Cardiovascular function of the paraventricular nucleus of the hypothalamus. *Biological Signals,* 4**,** 142-149.
COOTE, J. H. 2005. A role for the paraventricular nucleus of the hypothalamus in the autonomic control of heart and kidney. *Experimental physiology,* 90**,** 169-73.

COOTE, J. H. 2007. Landmarks in understanding the central nervous control of the cardiovascular system. *Experimental Physiology,* 92**,** 3-18.

COWLED, P. & FITRIDGE, R. 2011. Pathophysiology of Reperfusion Injury. *In:* FITRIDGE, R. & THOMPSON, M. (eds.) *Mechanisms of Vascular Disease: A Reference Book for Vascular Specialists.* Adelaide (AU).

CUI, J., COX, D. H. & ALDRICH, R. W. 1997. Intrinsic voltage dependence and Ca2+ regulation of mslo large conductance Ca-activated K+ channels. *J Gen Physiol,* 109**,** 647-73.

CUI, J., YANG, H. & LEE, U. S. 2009. Molecular mechanisms of BK channel activation. *Cell Mol Life Sci,* 66**,** 852-75.

DANE, E. L. & GRINSTAFF, M. W. 2012. Poly-amido-saccharides: Synthesis via Anionic Polymerization of a β-Lactam Sugar Monomer. 134**,** 16255-16264.

DANIIL, G., FERNANDES-ROSA, F. L., CHEMIN, J., BLESNEAC, I., BELTRAND, J., POLAK, M., JEUNEMAITRE, X., BOULKROUN, S., AMAR, L., STROM, T. M., LORY, P. & ZENNARO, M. C. 2016. CACNA1H Mutations Are Associated With Different Forms of Primary Aldosteronism. *EBioMedicine,* 13**,** 225-236.

DAVIS, A. J., FORREST, A. S., JEPPS, T. A., VALENCIK, M. L., WIWCHAR, M., SINGER, C. A., SONES, W. R., GREENWOOD, I. A. & LEBLANC, N. 2010. Expression profile and protein translation of TMEM16A in murine smooth muscle. *Am J Physiol Cell Physiol,* 299**,** C948-59.

DAVIS, A. J., SHI, J., PRITCHARD, H. A., CHADHA, P. S., LEBLANC, N., VASILIKOSTAS, G., YAO, Z., VERKMAN, A. S., ALBERT, A. P. & GREENWOOD, I. A. 2013. Potent vasorelaxant activity of the TMEM16A inhibitor T16A(inh) -A01. *Br J Pharmacol,* 168**,** 773-84.

DAY, M. J. 2010. Ageing, immunosenescence and inflammageing in the dog and cat. *J Comp Pathol,* 142 S1**,** S60-9.

DE CEUNINCK, F., DASSENCOURT, L. & ANRACT, P. 2004. The inflammatory side of human chondrocytes unveiled by antibody microarrays. *Biochem Biophys Res Commun,* 323**,** 960-9.

DE HOOGE, A. S., VAN DE LOO, F. A., BENNINK, M. B., ARNTZ, O. J., DE HOOGE, P. & VAN DEN BERG, W. B. 2005. Male IL-6 gene knock out mice developed more advanced osteoarthritis upon aging. *Osteoarthritis Cartilage,* 13**,** 66-73.

DE KEERSMAECKER, K. 2005. Fusion of EML1 to ABL1 in T-cell acute lymphoblastic leukemia with cryptic t(9;14)(q34;q32). 105**,** 4849-4852.

DEMAREE, B., WEISGERBER, D., LAN, F. & ABATE, A. R. 2018. An Ultrahigh-throughput Microfluidic Platform for Single-cell Genome Sequencing. *Journal of Visualized Experiments*.

DEUTCH, A. Y. & WINDER, D. G. 2006. A channel to neurodegeneration. *Nat Med,* 12**,** 17-8.

DI IORIO, A., FERRUCCI, L., SPARVIERI, E., CHERUBINI, A., VOLPATO, S., CORSI, A., BONAFE, M., FRANCESCHI, C., ABATE, G. & PAGANELLI, R. 2003. Serum IL-1beta levels in health and disease: a population-based study. 'The InCHIANTI study'. *Cytokine,* 22**,** 198-205.

DONAHUE, H. J., QU, R. W. & GENETOS, D. C. 2017. Joint diseases: from connexins to gap junctions. *Nature Reviews Rheumatology,* 14**,** 42-51.

DOUPNIK, C. A., DAVIDSON, N. & LESTER, H. A. 1995. The inward rectifier potassium channel family. 5**,** 268-277.

ENYEDI, P. & CZIRJAK, G. 2010. Molecular background of leak K+ currents: two-pore domain potassium channels. *Physiol Rev,* 90**,** 559-605.

ERRO, R., BHATIA, K. P., ESPAY, A. J. & STRIANO, P. 2017. The epileptic and nonepileptic spectrum of paroxysmal dyskinesias: Channelopathies, synaptopathies, and transportopathies. *Mov Disord,* 32**,** 310-318.

ETCHEBERRIGARAY, R., ITO, E., OKA, K., TOFEL-GREHL, B., GIBSON, G. E. & ALKON, D. L. 1993. Potassium channel dysfunction in fibroblasts identifies patients with Alzheimer disease. *Proc Natl Acad Sci U S A,* 90**,** 8209-13.

EWING, B. & GREEN, P. 1998. Base-Calling of Automated Sequencer Traces UsingPhred.II. Error Probabilities. *Genome Research,* 8**,** 186-194.

EWING, B., HILLIER, L., WENDL, M. C. & GREEN, P. 1998. Base-Calling of Automated Sequencer Traces UsingPhred. I. Accuracy Assessment. *Genome Research,* 8**,** 175-185.

FAN, G., CUI, Y., GOLLASCH, M. & KASSMANN, M. 2019. Elementary calcium signaling in arterial smooth muscle. *Channels,* 13**,** 505-519.

FARAJNIA, S., MEIJER, J. H. & MICHEL, S. 2015. Age-related changes in large-conductance calcium-activated potassium channels in mammalian circadian clock neurons. 36**,** 2176-2183.

FEETHAM, C. H., NUNN, N. & BARRETT-JOLLEY, R. 2015a. The depressor response to intracerebroventricular hypotonic saline is sensitive to TRPV4 antagonist RN1734. *Front Pharmacol,* 6**,** 83.

FEETHAM, C. H., NUNN, N., LEWIS, R., DART, C. & BARRETT-JOLLEY, R. 2015b. TRPV4 and KCa ion channels functionally couple as osmosensors in the paraventricular nucleus. *Br J Pharmacol,* 172**,** 1753-68.

FEETHAM, C. H., O'BRIEN, F. & BARRETT-JOLLEY, R. 2018. Ion Channels in the Paraventricular Hypothalamic Nucleus (PVN); Emerging Diversity and Functional Roles. *Frontiers in Physiology,* 9.

FELDER, R. B., FRANCIS, J., WEISS, R. M., ZHANG, Z. H., WEI, S. G. & JOHNSON, A. K. Neurohumoral regulation in ischemia-induced heart failure - Role of the forebrain. *In:* CHAPLEAU, M. W. & ABBOUD, F. M., eds., Aug 23-27 2000 Iowa City, Iowa. 444-453.

FERGUSON, A. V., LATCHFORD, K. J. & SAMSON, W. K. 2008. The paraventricular nucleus of the hypothalamus – a potential target for integrative treatment of autonomic dysfunction. *Expert Opinion on Therapeutic Targets,* 12**,** 717-727.

FERNANDEZ-FALGUERAS, A., SARQUELLA-BRUGADA, G., BRUGADA, J., BRUGADA, R. & CAMPUZANO, O. 2017. Cardiac Channelopathies and Sudden Death: Recent Clinical and Genetic Advances. *Biology (Basel),* 6.

FERRUCCI, L., CORSI, A., LAURETANI, F., BANDINELLI, S., BARTALI, B., TAUB, D. D., GURALNIK, J. M. & LONGO, D. L. 2005. The origins of age-related proinflammatory state. *Blood,* 105**,** 2294-2299.

FERRUCCI, L. & FABBRI, E. 2018. Inflammageing: chronic inflammation in ageing, cardiovascular disease, and frailty. *Nature Reviews Cardiology,* 15**,** 505-522.

FLAK, J. N., MYERS, B., SOLOMON, M. B., MCKLVEEN, J. M., KRAUSE, E. G. & HERMAN, J. P. 2014. Role of paraventricular nucleus-projecting norepinephrine/epinephrine neurons in acute and chronic stress. *Eur J Neurosci,* 39**,** 1903-11.

FLAK, J. N., OSTRANDER, M. M., TASKER, J. G. & HERMAN, J. P. 2009. Chronic stress-induced neurotransmitter plasticity in the PVN. *J Comp Neurol,* 517**,** 156-65.

FLOOD, S., PARRI, R., WILLIAMS, A., DUANCE, V. & MASON, D. 2007. Modulation of interleukin-6 and matrix metalloproteinase 2 expression in human fibroblast-like synoviocytes by functional ionotropic glutamate receptors. *Arthritis Rheum,* 56**,** 2523-34.

FRANCESCHI, C. & CAMPISI, J. 2014. Chronic inflammation (inflammaging) and its potential contribution to age-associated diseases. *J Gerontol A Biol Sci Med Sci,* 69 Suppl 1**,** S4-9.

FRANCESCHI, C., CAPRI, M., MONTI, D., GIUNTA, S., OLIVIERI, F., SEVINI, F., PANOURGIA, M. P., INVIDIA, L., CELANI, L., SCURTI, M., CEVENINI, E., CASTELLANI, G. C. & SALVIOLI, S. 2007a. Inflammaging and anti-inflammaging: A systemic perspective on aging and longevity emerged from studies in humans. *Mech Ageing Devel,* 128**,** 92-105.

FRANCESCHI, C., CAPRI, M., MONTI, D., GIUNTA, S., OLIVIERI, F., SEVINI, F., PANOURGIA, M. P., INVIDIA, L., CELANI, L., SCURTI, M., CEVENINI, E., CASTELLANI, G. C. & SALVIOLI, S. 2007b. Inflammaging and anti-inflammaging: A systemic perspective on aging and longevity emerged from studies in humans. *Mechanisms of Ageing and Development,* 128**,** 92-105.

FRASER, S., GREEN, C., BODE, H. & GILULA, N. 1987. Selective disruption of gap junctional communication interferes with a patterning process in hydra. 237**,** 49-55.

FRIEBEL, K., SCHONHERR, R., KINNE, R. W. & KUNISCH, E. 2014. Functional role of the KCa3.1 potassium channel in synovial fibroblasts from rheumatoid arthritis patients. *J Cell Physiol*.

FRIEBEL, K., SCHÖNHERR, R., KINNE, R. W. & KUNISCH, E. 2015. Functional role of the KCa3.1 potassium channel in synovial fibroblasts from rheumatoid arthritis patients. 230**,** 1677-1688.

FU, C. H., YANG, C. C. & KUO, T. B. 2006. Age-related changes in cerebral hemodynamics and their correlations with cardiac autonomic functions. *Neurol Res,* 28**,** 871-6.

GARCIA-ELIAS, A., LORENZO, I. M., VICENTE, R. & VALVERDE, M. A. 2008. IP3 Receptor Binds to and Sensitizes TRPV4 Channel to Osmotic Stimuli via a Calmodulin-binding Site. 283**,** 31284-31288.

GAVRILOV, L. A. & GAVRILOVA, N. S. 2002. Evolutionary Theories of Aging and Longevity. *The Scientific World JOURNAL,* 2**,** 339-356.

GEORGIEV, D., YOSHIHARA, T., KAWABATA, R., MATSUBARA, T., TSUBOMOTO, M., MINABE, Y., LEWIS, D. A. & HASHIMOTO, T. 2016. Cortical Gene Expression After a Conditional Knockout of 67 kDa Glutamic Acid Decarboxylase in Parvalbumin Neurons. *Schizophrenia Bulletin,* 42**,** 992-1002.

GERALDES, V., GONÇALVES-ROSA, N., LIU, B., PATON, J. F. R. & ROCHA, I. 2014. Chronic depression of hypothalamic paraventricular neuronal activity produces sustained hypotension in hypertensive rats. 99**,** 89-100.

GIEPMANS, B. 2004. Gap junctions and connexin-interacting proteins. 62**,** 233-245.

GOLDRING, M. B. & GOLDRING, S. R. 2007. Osteoarthritis. *Journal of Cellular Physiology,* 213**,** 626-634.

GOODENOUGH, D. A. & PAUL, D. L. 2009. Gap Junctions. 1**,** a002576-a002576.

GREENWOOD, M. P., GREENWOOD, M., ROMANOVA, E. V., MECAWI, A. S., PATERSON, A., SARENAC, O., JAPUNDŽIĆ-ŽIGON, N., ANTUNES-RODRIGUES, J., PATON, J. F. R., SWEEDLER, J. V. & MURPHY, D. 2018. The effects of aging on biosynthetic processes in the rat hypothalamic osmoregulatory neuroendocrine system. *Neurobiology of Aging,* 65**,** 178-191.

GRIDER, M. H., BELCEA, C. Q., COVINGTON, B. P. & SHARMA, S. 2019. Neuroanatomy, Nodes of Ranvier. *StatPearls.* Treasure Island (FL).

GRIDER, M. H. & GLAUBENSKLEE, C. S. 2019. Physiology, Action Potential. *StatPearls.* Treasure Island (FL).

GRUBB, B. D. 2004. Activation of sensory neurons in the arthritic joint. *Novartis Found Symp,* 260**,** 28-36; discussion 36-48, 100-4, 277-9.

GRUNDER, S., GEISSLER, H. S., BASSLER, E. L. & RUPPERSBERG, J. P. 2000. A new member of acid-sensing ion channels from pituitary gland. *Neuroreport,* 11**,** 1607-11.

GUI, Y. X., WAN, Y., XIAO, Q., WANG, Y., WANG, G. & CHEN, S. D. 2011. Verification of expressions of Kir2 as potential peripheral biomarkers in lymphocytes from patients with Parkinson's disease. *Neurosci Lett,* 505**,** 104-8.

GUILAK, F., LEDDY, H. A. & LIEDTKE, W. 2010. Transient receptor potential vanilloid 4: The sixth sense of the musculoskeletal system? *Annals of the New York Academy of Sciences,* 1192**,** 404-409.

HAMADA, T., SAKAI, T., HIRAIWA, H., NAKASHIMA, M., ONO, Y., MITSUYAMA, H. & ISHIGURO, N. 2013. Surface markers and gene expression to characterize the differentiation of monolayer expanded human articular chondrocytes. *Nagoya J Med Sci,* 75**,** 101-11.

HANUKOGLU, I. 2017. ASIC and ENaC type sodium channels: conformational states and the structures of the ion selectivity filters. *The FEBS Journal,* 284**,** 525-545.

HAQUE, A., ENGEL, J., TEICHMANN, S. A. & LÖNNBERG, T. 2017. A practical guide to single-cell RNA-sequencing for biomedical research and clinical applications. *Genome Medicine,* 9.

HARDY, R. S., HÜLSO, C., LIU, Y., GASPARINI, S. J., FONG-YEE, C., TU, J., STONER, S., STEWART, P. M., RAZA, K., COOPER, M. S., SEIBEL, M. J. & ZHOU, H. 2013. Characterisation of fibroblast-like synoviocytes from a murine model of joint inflammation. *Arthritis Research & Therapy,* 15**,** R24.

HDUD, I. M., EL-SHAFEI, A. A., LOUGHNA, P., BARRETT-JOLLEY, R. & MOBASHERI, A. 2012. Expression of transient receptor potential vanilloid (TRPV) channels in different passages of articular chondrocytes. *International Journal of Molecular Sciences,* 13**,** 4433-4445.

HE, W., LIU, W., CHEW, C. S., BAKER, S. S., BAKER, R. D., FORTE, J. G. & ZHU, L. 2011. Acid secretion-associated translocation of KCNJ15 in gastric parietal cells. *Am J Physiol Gastrointest Liver Physiol,* 301**,** G591-600.

HEINZE, C., SENIUK, A., SOKOLOV, M. V., HUEBNER, A. K., KLEMENTOWICZ, A. E., SZIJÁRTÓ, I. A., SCHLEIFENBAUM, J., VITZTHUM, H., GOLLASCH, M., EHMKE, H., SCHROEDER, B. C. & HÜBNER, C. A. 2014. Disruption of vascular Ca2+-activated chloride currents lowers blood pressure. 124**,** 675-686.

HERNANDEZ, C. M. & RICHARDS, J. R. 2019. Physiology, Sodium Channels. *StatPearls.* Treasure Island (FL).

HILL, R. A., LI, A. M. & GRUTZENDLER, J. 2018. Lifelong cortical myelin plasticity and age-related degeneration in the live mammalian brain. *Nature Neuroscience,* 21**,** 683-695.

HOSHIKAWA, M., KATO, A., HOJO, H., SHIBATA, Y., KUMAMOTO, N., WATANABE, M. & UGAWA, S. 2017. Distribution of ASIC4 transcripts in the adult wild-type mouse brain. *Neuroscience Letters*.

HOSOYA, Y., SUGIURA, Y., OKADO, N., LOEWY, A. & KOHNO, K. 1991. Descending input from the hypothalamic paraventricular nucleus to sympathetic preganglionic neurons in the rat. *Experimental Brain Research,* 85**,** 10-20.

HOTTA, H. & UCHIDA, S. 2010. Aging of the autonomic nervous system and possible improvements in autonomic activity using somatic afferent stimulation. *Geriatr Gerontol Int,* 10 Suppl 1**,** S127-36.

HU, X., LARAGIONE, T., SUN, L., KOSHY, S., JONES, K. R., ISMAILOV, II, YOTNDA, P., HORRIGAN, F. T., GULKO, P. S. & BEETON, C. 2012a. KCa1.1 potassium channels regulate key proinflammatory and invasive properties of fibroblast-like synoviocytes in rheumatoid arthritis. *Journal of biological chemistry,* 287**,** 4014-22.

HU, X., LARAGIONE, T., SUN, L., KOSHY, S., JONES, K. R., ISMAILOV, I. I., YOTNDA, P., HORRIGAN, F. T., GULKO, P. S. & BEETON, C. 2012b. KCa1.1 Potassium Channels Regulate Key Proinflammatory and Invasive Properties of Fibroblast-like Synoviocytes in Rheumatoid Arthritis. 287**,** 4014-4022.

HUBER, R., HUMMERT, C., GAUSMANN, U., POHLERS, D., KOCZAN, D., GUTHKE, R. & KINNE, R. W. 2008. Identification of intra-group, inter-individual, and gene-specific variances in mRNA expression profiles in the rheumatoid arthritis synovial membrane. *Arthritis Res Ther,* 10**,** R98.

HUI, A. Y., MCCARTY, W. J., MASUDA, K., FIRESTEIN, G. S. & SAH, R. L. 2012. A systems biology approach to synovial joint lubrication in health, injury, and disease. *Wiley Interdiscip Rev Syst Biol Med,* 4**,** 15-37.

HWANG, B., LEE, J. H. & BANG, D. 2018. Single-cell RNA sequencing technologies and bioinformatics pipelines. *Experimental & Molecular Medicine,* 50.

IMBRICI, P., LIANTONIO, A., CAMERINO, G. M., DE BELLIS, M., CAMERINO, C., MELE, A., GIUSTINO, A., PIERNO, S., DE LUCA, A., TRICARICO, D., DESAPHY, J. F. & CONTE, D. 2016. Therapeutic Approaches to Genetic Ion Channelopathies and Perspectives in Drug Discovery. *Front Pharmacol,* 7**,** 121.

IORGA, A. & HOROWITZ, B. Z. 2019. Phenytoin Toxicity. *StatPearls.* Treasure Island (FL).

IWANAGA, T., SHIKICHI, M., KITAMURA, H., YANASE, H. & NOZAWA-INOUE, K. 2000. Morphology and functional roles of synoviocytes in the joint. *Arch Histol Cytol,* 63**,** 17-31.

JANSEN, A. S. P., WESSENDORF, M. W. & LOEWY, A. D. 1995. Transneuronal Labeling of Cns Neuropeptide and Monoamine Neurons after Pseudorabies Virus Injections into the Stellate Ganglion. *Brain Research,* 683**,** 1-24.

JAVIER CAMACHO, J., CHÁVEZ-LÓPEZ, M., ZÚÑIGA-GARCÍA, V., PÉREZ-CARREÓN, J., AVALOS-FUENTES, A. & ESCOBAR, Y. 2016. Eag1 channels as potential early-stage biomarkers of hepatocellular carcinoma. *Biologics: Targets and Therapy,* Volume 10**,** 139-148.

JAYASURIYA, C. T., HU, N., LI, J., LEMME, N., TEREK, R., EHRLICH, M. G. & CHEN, Q. 2018. Molecular characterization of mesenchymal stem cells in human osteoarthritis cartilage reveals contribution to the OA phenotype. *Sci Rep,* 8**,** 7044.

JENSEN, A. B., JOERGENSEN, H. B., DAM, V. S., KAMAEV, D., BOEDTKJER, D., FÜCHTBAUER, E.-M., AALKJAER, C. & MATCHKOV, V. V. 2018. Variable Contribution of TMEM16A to Tone in Murine Arterial Vasculature. *Basic & Clinical Pharmacology & Toxicology*.

JENTSCH, T. J. & GUNTHER, W. 1997. Chloride channels: an emerging molecular picture. *Bioessays,* 19**,** 117-26.

JENTSCH, T. J., STEIN, V., WEINREICH, F. & ZDEBIK, A. A. 2002. Molecular Structure and Physiological Function of Chloride Channels. *Physiological Reviews,* 82**,** 503-568.

JI, M. J. & HONG, J. H. 2019. An overview of carbonic anhydrases and membrane channels of synoviocytes in inflamed joints. *J Enzyme Inhib Med Chem,* 34**,** 1615-1622.

JIANG, Y., PICO, A., CADENE, M., CHAIT, B. T. & MACKINNON, R. 2001. Structure of the RCK domain from the E. coli K+ channel and demonstration of its presence in the human BK channel. *Neuron,* 29**,** 593-601.

JOMBART, T., DEVILLARD, S. & BALLOUX, F. 2010. Discriminant analysis of principal components: a new method for the analysis of genetically structured populations. *BMC Genet,* 11**,** 94.

JULIUS, S. 1993. Sympathetic Hyperactivity and Coronary Risk in Hypertension. *Hypertension,* 21**,** 886-893.

JYLHA, M., PAAVILAINEN, P., LEHTIMAKI, T., GOEBELER, S., KARHUNEN, P. J., HERVONEN, A. & HURME, M. 2007. Interleukin-1 receptor antagonist, interleukin-6, and C-reactive protein as predictors of mortality in nonagenarians: the vitality 90+ study. *J Gerontol A Biol Sci Med Sci,* 62**,** 1016-21.

KAJIWARA, Y., WANG, E., WANG, M., SIN, W. C., BRENNAND, K. J., SCHADT, E., NAUS, C. C., BUXBAUM, J. & ZHANG, B. 2018. GJA1 (connexin43) is a key regulator of Alzheimer's disease pathogenesis. *Acta Neuropathol Commun,* 6**,** 144.

KANE, G. C., LAM, C. F., O'COCHLAIN, F., HODGSON, D. M., REYES, S., LIU, X. K., MIKI, T., SEINO, S., KATUSIC, Z. S. & TERZIC, A. 2006. Gene knockout of the KCNJ8-encoded Kir6.1 K(ATP) channel imparts fatal susceptibility to endotoxemia. *FASEB J,* 20**,** 2271-80.

KANG, Y. M., HE, R. L., YANG, L. M., QIN, D. N., GUGGILAM, A., ELKS, C., YAN, N., GUO, Z. & FRANCIS, J. 2009. Brain tumour necrosis factor-alpha modulates neurotransmitters in hypothalamic paraventricular nucleus in heart failure. *Cardiovasc Res,* 83**,** 737-46.

KAPLAN, J., GERBER, S., BONNEAU, D., ROZET, J. M., DELRIEU, O., BRIARD, M. L., DOLLFUS, H., GHAZI, I., DUFIER, J. L., FRÉZAL, J. & MUNNICH, A. 1992. A gene for usher syndrome type I (USH1A) maps to chromosome 14q. 14**,** 979-987.

KARIMI, A. & MILEWICZ, D. M. 2016. Structure of the Elastin-Contractile Units in the Thoracic Aorta and How Genes That Cause Thoracic Aortic Aneurysms and Dissections Disrupt This Structure. *Canadian Journal of Cardiology,* 32**,** 26-34.

KARSDAL, M. A. 2016. Collagens - Introduction.

KIM, D., LANGMEAD, B. & SALZBERG, S. L. 2015. HISAT: a fast spliced aligner with low memory requirements. *Nature Methods,* 12**,** 357-360.

KIM, G.-T., CHO, Y.-W., TAK, H.-M., LEE, J.-S., KIM, E.-J., HAN, J. & KANG, D. 2012. Age-related changes in two-pore domain acid-sensitive K+ channel expression in rat dorsal root ganglion neurons. 39**,** 43-48.

KIM, J. B. 2014. Channelopathies. *Korean J Pediatr,* 57**,** 1-18.

KIRKWOOD, T. B. L. 1977. Evolution of ageing. *Nature,* 270**,** 301-304.

KIRKWOOD, T. B. L. & HOLLIDAY, R. 1979. The Evolution of Ageing and Longevity. 205**,** 531-546.

KONDO, C., CLARK, R. B., KIM, T. Y., BELKE, D., BANDERALI, U., SZERENCSEI, R. T., JALLOUL, A. H., SCHNETKAMP, P. P. M., SPITZER, K. W. & GILES, W. R. 2018. ATP triggers a robust intracellular [Ca(2+)]-mediated signalling pathway in human synovial fibroblasts. *Exp Physiol,* 103**,** 1101-1122.

KOTIPOYINA, H. R. & WARRINGTON, S. J. 2019. Tetrodotoxin Toxicity. *StatPearls.* Treasure Island (FL).

KRAMER, A., GREEN, J., POLLARD, J., JR. & TUGENDREICH, S. 2014. Causal analysis approaches in Ingenuity Pathway Analysis. *Bioinformatics,* 30**,** 523-30.

KUMAHASHI, N., NAITOU, K., NISHI, H., OAE, K., WATANABE, Y., KUWATA, S., OCHI, M., IKEDA, M. & UCHIO, Y. 2011. Correlation of changes in pain intensity with synovial fluid adenosine triphosphate levels after treatment of patients with osteoarthritis of the knee with high-molecular-weight hyaluronic acid. *The Knee,* 18**,** 160-164.

KUO, C. J., LAMONTAGNE, K. R., GARCIA-CARDEÑA, G., ACKLEY, B. D., KALMAN, D., PARK, S., CHRISTOFFERSON, R., KAMIHARA, J., DING, Y.-H., LO, K.-M., GILLIES, S., FOLKMAN, J., MULLIGAN, R. C. & JAVAHERIAN, K. 2001. Oligomerization-Dependent Regulation of Motility and Morphogenesis by the Collagen Xviii Nc1/Endostatin Domain. 152**,** 1233-1246.

KURIYAMA, H., KITAMURA, K., ITOH, T. & INOUE, R. 1998. Physiological features of visceral smooth muscle cells, with special reference to receptors and ion channels. *Physiol Rev,* 78**,** 811-920.

KWOK, A., RAULF, N. & HABIB, N. 2019. Developing small activating RNA as a therapeutic: current challenges and promises. *Ther Deliv,* 10**,** 151-164.

LAINA, A., STELLOS, K. & STAMATELOPOULOS, K. 2018. Vascular ageing: Underlying mechanisms and clinical implications. *Experimental Gerontology,* 109**,** 16-30.

LAMBERT, C., DUBUC, J.-E., MONTELL, E., VERGÉS, J., MUNAUT, C., NOËL, A. & HENROTIN, Y. 2014. Gene Expression Pattern of Cells From Inflamed and Normal Areas of Osteoarthritis Synovial Membrane. *Arthritis & Rheumatology,* 66**,** 960-968.

LANG, F. & HOFFMANN, E. K. 2013. CrossTalk proposal: Cell volume changes are an essential step in the cell death machinery. *J Physiol,* 591**,** 6119-21.

LATORRE, R. & BRAUCHI, S. 2006. Large conductance Ca2+-activated K+ (BK) channel: activation by Ca2+ and voltage. *Biol Res,* 39**,** 385-401.

LEE, J. C. & CHOE, S. Y. 2014. Age-related changes in the distribution of transient receptor potential vanilloid 4 channel (TRPV4) in the central nervous system of rats. *J Mol Histol,* 45**,** 497-505.

LEE, S. W., SONG, Y. S., LEE, S. Y., YOON, Y. G., LEE, S. H., PARK, B. S., YUN, I., CHOI, H., KIM, K., CHUNG, W. T. & YOO, Y. H. 2011. Downregulation of Protein Kinase CK2 Activity Facilitates Tumor Necrosis Factor-α-Mediated Chondrocyte Death through Apoptosis and Autophagy. *PLoS ONE,* 6**,** e19163.

LESAGE, F. & LAZDUNSKI, M. 2000. Molecular and functional properties of two-pore-domain potassium channels. *American Journal of Physiology-Renal Physiology,* 279**,** F793-F801.

LEVINE, J. D. & ALESSANDRI-HABER, N. 2007. TRP channels: Targets for the relief of pain. *Biochimica et Biophysica Acta (BBA) - Molecular Basis of Disease,* 1772**,** 989-1003.

LEWIS, R., ASPLIN, K. E., BRUCE, G., DART, C., MOBASHERI, A. & BARRETT-JOLLEY, R. 2011a. The Role of the Membrane Potential in Chondrocyte Volume Regulation. *Journal of Cellular Physiology,* 226**,** 2979-2986.

LEWIS, R. & BARRETT-JOLLEY, R. 2015. Changes in Membrane Receptors and Ion Channels as Potential Biomarkers for Osteoarthritis. *Front Physiol,* 6**,** 357.

LEWIS, R., FEETHAM, C. H. & BARRETT-JOLLEY, R. 2011b. Cell Volume Regulation in Chondrocytes. *Cellular Physiology and Biochemistry,* 28**,** 1111-1122.

LEWIS, R., MILLS, A. & BARRETT-JOLLEY, R. 2010. Models Of Paraventricular Nucleus (PVN) Sympathetic Neurone Modulation by Glucose and Hypoglycaemia. *Biophysical Journal - BIOPHYS J,* 98.

LI, Y., WEI, X., ZHOU, J. & WEI, L. 2013. The Age-Related Changes in Cartilage and Osteoarthritis. *BioMed Research International,* 2013**,** 1-12.

LI, Y., ZHAO, Z., CAI, J., GU, B., LV, Y. & ZHAO, L. 2017. The Frequency-Dependent Aerobic Exercise Effects of Hypothalamic GABAergic Expression and Cardiovascular Functions in Aged Rats. *Frontiers in Aging Neuroscience,* 9.

LI, Y. F., CORNISH, K. G. & PATEL, K. P. 2003. Alteration of NMDA NR1 receptors within the paraventricular nucleus of hypothalamus in rats with heart failure. *Circulation Research,* 93**,** 990-997.

LI, Y. F., JACKSON, K. L., STERN, J. E., RABELER, B. & PATEL, K. P. 2006a. Interaction between glutamate and GABA systems in the integration of sympathetic outflow by the paraventricular nucleus of the

hypothalamus. *American Journal of Physiology-Heart and Circulatory Physiology,* 291**,** H2847-H2856.

LI, Y. F. & PATEL, K. P. Paraventricular nucleus of the hypothalamus and elevated sympathetic activity in heart failure: the altered inhibitory mechanisms. Apr 20-24 2002 New Orleans, Louisiana. 17-26.

LI, Y. F. & PATEL, K. P. 2003. Paraventricular nucleus of the hypothalamus and elevated sympathetic activity in heart failure: the altered inhibitory mechanisms. *Acta Physio Scand,* 177**,** 17-26.

LI, Y. F., WANG, W., MAYHAN, W. G. & PATEL, K. P. 2006b. Angiotensin-mediated increase in renal sympathetic nerve discharge within the PVN: role of nitric oxide. *American Journal of Physiology-Regulatory Integrative and Comparative Physiology,* 290**,** R1035-R1043.

LIPPIAT, J. D., STANDEN, N. B., HARROW, I. D., PHILLIPS, S. C. & DAVIES, N. W. 2003. Properties of BK(Ca) channels formed by bicistronic expression of hSloalpha and beta1-4 subunits in HEK293 cells. *The Journal of membrane biology,* 192**,** 141-8.

LOEWY, A. 1991. Forebrain nuclei involved in autonomic control. *Progress in brain research,* 87**,** 253.

LOEWY, A. D. & MCKELLAR, S. 1980. The neuroanatomical basis of central cardiovascular control. *Fed.Proc.,* 39**,** 2495-2503.

LONG, S. B., CAMPBELL, E. B. & MACKINNON, R. 2005a. Crystal structure of a mammalian voltage-dependent Shaker family K+ channel. *Science,* 309**,** 897-903.

LONG, S. B., CAMPBELL, E. B. & MACKINNON, R. 2005b. Voltage sensor of Kv1.2: structural basis of electromechanical coupling. *Science,* 309**,** 903-8.

LOVICK, T. A. & COOTE, J. H. 1988. Effects of volume loading on paraventriculo-spinal neurones in the rat. *J Auton Nerv Syst,* 25**,** 135-40.

LOVICK, T. A. & COOTE, J. H. 1989. Circulating atrial natriuretic factor activates vagal afferent inputs to paraventriculo-spinal neurones in the rat. *J Auton Nerv Syst,* 26**,** 129-34.

LOVICK, T. A., MALPAS, S. & MAHONY, M. T. 1993. Renal vasodilatation in response to acute volume load is attenuated following lesions of parvocellular neurones in the paraventricular nucleus in rats. *Journal of the Autonomic Nervous System,* 43**,** 247-256.

LYTTON, J. 2007. Na+/Ca2+ exchangers: three mammalian gene families control Ca2+ transport. *Biochem J,* 406**,** 365-82.

MA, S., MURPHY, T. W. & LU, C. 2017. Microfluidics for genome-wide studies involving next generation sequencing. *Biomicrofluidics,* 11**,** 021501.

MACDONALD, M. L. E., VAN ECK, M., HILDEBRAND, R. B., WONG, B. W. C., BISSADA, N., RUDDLE, P., KONTUSH, A., HUSSEIN, H., POULADI, M. A., CHAPMAN, M. J., FIEVET, C., VAN BERKEL, T. J. C., STAELS, B., MCMANUS, B. M. & HAYDEN, M. R. 2009. Despite Antiatherogenic Metabolic Characteristics, SCD1-Deficient Mice Have Increased Inflammation and Atherosclerosis. 29**,** 341-347.

MACKINNON, R., HEGINBOTHAM, L. & ABRAMSON, T. 1990. Mapping the receptor site for charybdotoxin, a pore-blocking potassium channel inhibitor. *Neuron,* 5**,** 767-71.

MACKINNON, R. & MILLER, C. 1989. Mutant potassium channels with altered binding of charybdotoxin, a pore-blocking peptide inhibitor. *Science,* 245**,** 1382-5.

MADEJ, W., VAN CAAM, A., BLANEY DAVIDSON, E. N., HANNINK, G., BUMA, P. & VAN DER KRAAN, P. M. 2016. Ageing is associated with reduction of mechanically-induced activation of Smad2/3P signaling in articular cartilage. 24**,** 146-157.

MAEZAWA, I., JENKINS, D. P., JIN, B. E. & WULFF, H. 2012. Microglial KCa3.1 Channels as a Potential Therapeutic Target for Alzheimer's Disease. *International Journal of Alzheimer's Disease,* 2012**,** 1-8.

MAKITA, N., BENNETT, P. B., JR. & GEORGE, A. L., JR. 1994. Voltage-gated Na+ channel beta 1 subunit mRNA expressed in adult human skeletal muscle, heart, and brain is encoded by a single gene. *J Biol Chem,* 269**,** 7571-8.

MANSOUR, F. A., HASSAN, M. O., KHAN, A. A. & ALBARWANI, S. 2016. Aging Down Regulates L-Type Voltage-gated Calcium Channels in Resistance Coronary Arteries. *Faseb Journal,* 30.

MARTIN, D. S. & HAYWOOD, J. R. 1993. Hemodynamic responses to paraventricular nucleus disinhibition with bicuculline in conscious rats. *American Journal of Physiology- Heart and Circulatory Physiology,* 265**,** H1727-H1733.

MARTIN, D. S., SEGURA, T. & HAYWOOD, J. R. 1991. Cardiovascular responses to bicuculline in the paraventricular nucleus of the rat. *Hypertension,* 18**,** 48-55.

MARTINEZ, A. H. & MOHIUDDIN, S. S. 2019. Biochemistry, Chloride Channels. *StatPearls.* Treasure Island (FL).

MARTINSEN, A., DESSY, C. & MOREL, N. 2014. Regulation of calcium channels in smooth muscle: New insights into the role of myosin light chain kinase. 8**,** 402-413.

MCCUSKER, S. M., CURRAN, M. D., DYNAN, K. B., MCCULLAGH, C. D., URQUHART, D. D., MIDDLETON, D., PATTERSON, C. C., MCILROY, S. P. & PETER PASSMORE, A. 2001. Association between polymorphism in regulatory region of gene encoding tumour necrosis factor α and risk of Alzheimer's disease and vascular dementia: a case-control study. 357**,** 436-439.

MCMANUS, O. B., HELMS, L. M., PALLANCK, L., GANETZKY, B., SWANSON, R. & LEONARD, R. J. 1995. Functional role of the beta subunit of high conductance calcium-activated potassium channels. *Neuron,* 14**,** 645-50.

MCNERLAN, S. E., REA, I. M. & ALEXANDER, H. D. 2002. A whole blood method for measurement of intracellular TNF-alpha, IFN-gamma and IL-2 expression in stimulated CD3+ lymphocytes: differences between young and elderly subjects. *Exp Gerontol,* 37**,** 227-34.

MCNULTY, M., SPIERS, P., MCGOVERN, E. & FEELY, J. 2005. Aging is associated with increased matrix metalloproteinase-2 activity in the human aorta. 18**,** 504-509.

MEDVEDEV, Z. A. 1990. AN ATTEMPT AT A RATIONAL CLASSIFICATION OF THEORIES OF AGEING. *Biological Reviews,* 65**,** 375-398.

MEERA, P., WALLNER, M., SONG, M. & TORO, L. 1997. Large conductance voltage- and calcium-dependent K+ channel, a distinct member of voltage-dependent ion channels with seven N-terminal transmembrane segments (S0-S6), an extracellular N terminus, and an intracellular (S9-S10) C terminus. 94**,** 14066-14071.

MELTZER, H., MAROM, E., ALYAGOR, I., MAYSELESS, O., BERKUN, V., SEGAL-GILBOA, N., UNGER, T., LUGINBUHL, D. & SCHULDINER, O. 2019. Tissue-specific (ts)CRISPR as an efficient strategy for in vivo screening in Drosophila. *Nature Communications,* 10.

MENDONCA, M. M., SANTANA, J. S., DA CRUZ, K. R., IANZER, D., GHEDINI, P. C., NALIVAIKO, E., FONTES, M. A. P., FERREIRA, R. N., PEDRINO, G. R., COLUGNATI, D. B. & XAVIER, C. H. 2018. Involvement of GABAergic and Adrenergic Neurotransmissions on Paraventricular Nucleus of Hypothalamus in the Control of Cardiac Function. *Front Physiol,* 9**,** 670.

MEŞE, G., RICHARD, G. & WHITE, T. W. 2007. Gap Junctions: Basic Structure and Function. *Journal of Investigative Dermatology,* 127**,** 2516-2524.

MISRA, V., LEE, H., SINGH, A., HUANG, K., THIMMULAPPA, R. K., MITZNER, W., BISWAL, S. & TANKERSLEY, C. G. 2007. Global expression profiles from C57BL/6J and DBA/2J mouse lungs to determine aging-related genes. 31**,** 429-440.

MOBASHERI, A., LEWIS, R., FERREIRA-MENDES, A., RUFINO, A., DART, C. & BARRETT-JOLLEY, R. 2012. Potassium channels in articular chondrocytes. *Channels,* 6**,** 416-425.

MOCZYDLOWSKI, E., LUCCHESI, K. & RAVINDRAN, A. 1988. An emerging pharmacology of peptide toxins targeted against potassium channels. *J Membr Biol,* 105**,** 95-111.

MONK, B. A. & GEORGE, S. J. 2015. The Effect of Ageing on Vascular Smooth Muscle Cell Behaviour--A Mini-Review. *Gerontology,* 61**,** 416-26.

MORTAZ, E., ADCOCK, I. M., SHAFEI, H., MASJEDI, M. R. & FOLKERTS, G. 2012. Role of P2X7 Receptors in Release of IL-1β: A Possible Mediator of Pulmonary Inflammation. *Tanaffos,* 11**,** 6-11.

MORTH, J. P., PEDERSEN, B. P., TOUSTRUP-JENSEN, M. S., SORENSEN, T. L., PETERSEN, J., ANDERSEN, J. P., VILSEN, B. & NISSEN, P. 2007. Crystal structure of the sodium-potassium pump. *Nature,* 450**,** 1043-9.

MOSKALEV, A., ALIPER, A., SMIT-MCBRIDE, Z., BUZDIN, A. & ZHAVORONKOV, A. 2014. Genetics and epigenetics of aging and longevity. 13**,** 1063-1077.

MUELLER, O., LIGHTFOOT, S., SCHROEDER, A. <RNA Integrity Number (RIN) - Standardization of RNA Quality Control.pdf>.

MUN, M. J., KIM, J. H., CHOI, J. Y. & JANG, W. C. 2016. Genetic polymorphisms of interleukin genes and the risk of Alzheimer's disease: An update meta-analysis. *Meta Gene,* 8**,** 1-10.

NASRABADY, S. E., RIZVI, B., GOLDMAN, J. E. & BRICKMAN, A. M. 2018. White matter changes in Alzheimer's disease: a focus on myelin and oligodendrocytes. *Acta Neuropathologica Communications,* 6.

NGUYEN, T. P. & TAYLOR, R. S. 2019. Guillain Barre Syndrome. *StatPearls.* Treasure Island (FL).

NICHOLS, C. G., SINGH, G. K. & GRANGE, D. K. 2013. KATP Channels and Cardiovascular Disease: Suddenly a Syndrome. 112**,** 1059-1072.

NIISSALO, S., LI, T. F., SANTAVIRTA, S., TAKAGI, M., HIETANEN, J. & KONTTINEN, Y. T. 2002. Dense innervation in pseudocapsular tissue compared to aneural interface tissue in loose totally replaced hips. *J Rheumatol,* 29**,** 796-803.

NILSSON, L., SZYMANOWSKI, A., SWAHN, E. & JONASSON, L. 2013. Soluble TNF receptors are associated with infarct size and ventricular dysfunction in ST-elevation myocardial infarction. *PLoS One,* 8**,** e55477.

NOSS, E. H. & BRENNER, M. B. 2008. The role and therapeutic implications of fibroblast-like synoviocytes in inflammation and cartilage erosion in rheumatoid arthritis. *Immunological Reviews,* 223**,** 252-270.

NOVAKOVIC, S. D., EGLEN, R. M. & HUNTER, J. C. 2001. Regulation of Na+ channel distribution in the nervous system. 24**,** 473-478.

NUNN, N., WOMACK, M., DART, C. & BARRETT-JOLLEY, R. 2011. Function and pharmacology of spinally-projecting sympathetic pre-autonomic neurones in the paraventricular nucleus of the hypothalamus. *Current neuropharmacology,* 9**,** 262-77.

O'LEARY, N. A., WRIGHT, M. W., BRISTER, J. R., CIUFO, S., HADDAD, D., MCVEIGH, R., RAJPUT, B., ROBBERTSE, B., SMITH-WHITE, B., AKO-ADJEI, D., ASTASHYN, A., BADRETDIN, A., BAO, Y., BLINKOVA, O., BROVER, V., CHETVERNIN, V., CHOI, J., COX, E., ERMOLAEVA, O., FARRELL, C. M., GOLDFARB, T., GUPTA, T., HAFT, D., HATCHER, E., HLAVINA, W., JOARDAR, V. S., KODALI, V. K., LI, W., MAGLOTT, D., MASTERSON, P., MCGARVEY, K. M., MURPHY, M. R., O'NEILL, K., PUJAR, S., RANGWALA, S. H., RAUSCH, D., RIDDICK, L. D., SCHOCH, C., SHKEDA, A., STORZ, S. S., SUN, H., THIBAUD-NISSEN, F., TOLSTOY, I., TULLY, R. E., VATSAN, A. R., WALLIN, C., WEBB, D., WU, W., LANDRUM, M. J., KIMCHI, A., TATUSOVA, T., DICUCCIO, M., KITTS, P., MURPHY, T. D. & PRUITT, K. D. 2016. Reference sequence (RefSeq) database at NCBI: current status, taxonomic expansion, and functional annotation. *Nucleic Acids Research,* 44**,** D733-D745.

O'MAHONY, L., HOLLAND, J., JACKSON, J., FEIGHERY, C., HENNESSY, T. P. & MEALY, K. 1998. Quantitative intracellular cytokine measurement: age-related changes in proinflammatory cytokine production. *Clin Exp Immunol,* 113**,** 213-9.

O'MALLEY, H. A. & ISOM, L. L. 2015. Sodium channel beta subunits: emerging targets in channelopathies. *Annu Rev Physiol,* 77**,** 481-504.

OEGEMA, R., MCGILLIVRAY, G., LEVENTER, R., LE MOING, A. G., BAHI-BUISSON, N., BARNICOAT, A., MANDELSTAM, S., FRANCIS, D., FRANCIS, F., MANCINI, G. M. S., SAVELBERG, S., HAAFTEN, G.,

MANKAD, K. & LEQUIN, M. H. 2019. EML1- associated brain overgrowth syndrome with ribbon-like heterotopia. *American Journal of Medical Genetics Part C: Seminars in Medical Genetics*.

OKAMOTO, K., IWASAKI, N., DOI, K., NOIRI, E., IWAMOTO, Y., UCHIGATA, Y., FUJITA, T. & TOKUNAGA, K. 2012. Inhibition of glucose-stimulated insulin secretion by KCNJ15, a newly identified susceptibility gene for type 2 diabetes. *Diabetes,* 61**,** 1734-41.

OKAMOTO, K., IWASAKI, N., NISHIMURA, C., DOI, K., NOIRI, E., NAKAMURA, S., TAKIZAWA, M., OGATA, M., FUJIMAKI, R., GRARUP, N., PISINGER, C., BORCH-JOHNSEN, K., LAURITZEN, T., SANDBAEK, A., HANSEN, T., YASUDA, K., OSAWA, H., NANJO, K., KADOWAKI, T., KASUGA, M., PEDERSEN, O., FUJITA, T., KAMATANI, N., IWAMOTO, Y. & TOKUNAGA, K. 2010. Identification of KCNJ15 as a Susceptibility Gene in Asian Patients with Type 2 Diabetes Mellitus. 86**,** 54-64.

ORLOV, S. N., GUSAKOVA, S. V., SMAGLII, L. V., KOLTSOVA, S. V. & SIDORENKO, S. V. 2017. Vasoconstriction triggered by hydrogen sulfide: Evidence for Na(+),K(+),2Cl(-)cotransport and L-type Ca(2+) channel-mediated pathway. *Biochem Biophys Rep,* 12**,** 220-227.

ORLOV, S. N., MODEL, M. A. & GRYGORCZYK, R. 2013. CrossTalk opposing view: The triggering and progression of the cell death machinery can occur without cell volume perturbations. *J Physiol,* 591**,** 6123-5.

PAL, R., SINGH, S. N., CHATTERJEE, A. & SAHA, M. 2014. Age-related changes in cardiovascular system, autonomic functions, and levels of BDNF of healthy active males: role of yogic practice. *Age (Dordr),* 36**,** 9683.

PARASHAR, R., AMIR, M., PAKHARE, A., RATHI, P. & CHAUDHARY, L. 2016. Age Related Changes in Autonomic Functions. *J Clin Diagn Res,* 10**,** CC11-5.

PATEL, K. P., ZHANG, K., KENNEY, M. J., WEISS, M. & MAYHAN, W. G. 2000. Neuronal expression of Fos protein in the hypothalamus of rats with heart failure. *Brain Research,* 865**,** 27-34.

PATTHY, L., TREXLER, M., VÁLI, Z., BÁNYAI, L. & VÁRADI, A. 1984. Kringles: modules specialized for protein binding. 171**,** 131-136.

PEARL, J. 2009. Causal inference in statistics: An overview. *Statistics Surveys,* 3**,** 96-146.

PECANHA, F. M., WIGGERS, G. A., BRIONES, A. M., PEREZ-GIRON, J. V., MIGUEL, M., GARCIA-REDONDO, A. B., VASSALLO, D. V., ALONSO, M. J. & SALAICES, M. 2010. The role of cyclooxygenase (COX)-2 derived prostanoids on vasoconstrictor responses to phenylephrine is increased by exposure to low mercury concentration. *J Physiol Pharmacol,* 61**,** 29-36.

PEDERSEN, B. K. 2006a. The anti-inflammatory effect of exercise: its role in diabetes and cardiovascular disease control. *Essays in Biochemistry, Vol 42,* 42**,** 105-117.

PEDERSEN, B. K. 2006b. The anti-inflammatory effect of exercise: its role in diabetes and cardiovascular disease control. *Essays Biochem,* 42**,** 105-17.

PERTEA, M., PERTEA, G. M., ANTONESCU, C. M., CHANG, T.-C., MENDELL, J. T. & SALZBERG, S. L. 2015. StringTie enables improved reconstruction of a transcriptome from RNA-seq reads. *Nature Biotechnology,* 33**,** 290-295.

PETERS, A. 2002. The effects of normal aging on myelin and nerve fibers: a review. *J Neurocytol,* 31**,** 581-93.

PETERS, N. S., SEVERS, N. J., ROTHERY, S. M., LINCOLN, C., YACOUB, M. H. & GREEN, C. R. 1994. Spatiotemporal relation between gap junctions and fascia adherens junctions during postnatal development of human ventricular myocardium. 90**,** 713-725.

PETHŐ, Z., TANNER, M. R., TAJHYA, R. B., HUQ, R., LARAGIONE, T., PANYI, G., GULKO, P. S. & BEETON, C. 2016. Different expression of β subunits of the KCa1.1 channel by invasive and non-invasive human fibroblast-like synoviocytes. 18.

PI, Y., GOLDENTHAL, M. J. & MARIN-GARCIA, J. 2007. Mitochondrial channelopathies in aging. *J Mol Med (Berl),* 85**,** 937-51.

PINTO, E. 2007. Blood pressure and ageing. *Postgraduate Medical Journal,* 83**,** 109-114.

PLANELLS-CASES, R. & JENTSCH, T. J. 2009. Chloride channelopathies. *Biochim Biophys Acta,* 1792**,** 173-89.

PRETZEL, D., POHLERS, D., WEINERT, S. & KINNE, R. W. 2009. In vitro model for the analysis of synovial fibroblast-mediated degradation of intact cartilage. *Arthritis Res Ther,* 11**,** R25.

PRUITT, K. D., BROWN, G. R., HIATT, S. M., THIBAUD-NISSEN, F., ASTASHYN, A., ERMOLAEVA, O., FARRELL, C. M., HART, J., LANDRUM, M. J., MCGARVEY, K. M., MURPHY, M. R., O'LEARY, N. A., PUJAR, S., RAJPUT, B., RANGWALA, S. H., RIDDICK, L. D., SHKEDA, A., SUN, H., TAMEZ, P., TULLY, R. E., WALLIN, C., WEBB, D., WEBER, J., WU, W., DICUCCIO, M., KITTS, P., MAGLOTT, D. R., MURPHY, T. D. & OSTELL, J. M. 2014. RefSeq: an update on mammalian reference sequences. 42**,** D756-D763.

PRUITT, K. D., TATUSOVA, T. & MAGLOTT, D. R. 2007. NCBI reference sequences (RefSeq): a curated non-redundant sequence database of genomes, transcripts and proteins. *Nucleic Acids Research,* 35**,** D61-D65.

QIN, N., D'ANDREA, M. R., LUBIN, M. L., SHAFAEE, N., CODD, E. E. & CORREA, A. M. 2003. Molecular cloning and functional expression of the human sodium channel beta1B subunit, a novel splicing variant of the beta1 subunit. *Eur J Biochem,* 270**,** 4762-70.

QIU, Y., HUANG, L., FU, J., HAN, C., FANG, J., LIAO, P., CHEN, Z., MO, Y., SUN, P., LIAO, D., YANG, L., WANG, J., ZHANG, Q., LIU, J., LIU, F., LIU, T., HUANG, W., YANG, H. & JIANG, R. 2020. A TREK Channel Family Activator with Well-Defined Structure-Activation Relationship for Pain and Neurogenic Inflammation. *J Med Chem*.

RAMA, A., MATSUSHITA, T., CHAROLIDI, N., ROTHERY, S., DUPONT, E. & SEVERS, N. J. 2006. Up-regulation of connexin43 correlates with increased synthetic activity and enhanced contractile differentiation in TGF-β-treated human aortic smooth muscle cells. 85**,** 375-386.

RAMSEY, I. S., DELLING, M. & CLAPHAM, D. E. 2006. AN INTRODUCTION TO TRP CHANNELS. *Annual Review of Physiology,* 68**,** 619-647.

RAO, V., KAJA, S., AND GENTILE, S. 2016. Ion channels in Aging and Age-related Diseases.

REA, I. M., GIBSON, D. S., MCGILLIGAN, V., MCNERLAN, S. E., ALEXANDER, H. D. & ROSS, O. A. 2018. Age and Age-Related Diseases: Role of Inflammation Triggers and Cytokines. *Front Immunol,* 9**,** 586.

REDDY, M. M. & KAR, S. S. 2019. Unconditional probability of dying and age-specific mortality rate because of major non-communicable diseases in India: Time trends from 2001 to 2013. *Journal of postgraduate medicine,* 65**,** 11-17.

RIBEIRO-RODRIGUES, T. M., MARTINS-MARQUES, T., MOREL, S., KWAK, B. R. & GIRAO, H. 2017. Role of connexin 43 in different forms of intercellular communication - gap junctions, extracellular vesicles and tunnelling nanotubes. *J Cell Sci,* 130**,** 3619-3630.

RICHARDS, M. W., LAW, E. W. P., RENNALLS, L. P., BUSACCA, S., O'REGAN, L., FRY, A. M., FENNELL, D. A. & BAYLISS, R. 2014. Crystal structure of EML1 reveals the basis for Hsp90 dependence of oncogenic EML4-ALK by disruption of an atypical -propeller domain. *Proceedings of the National Academy of Sciences,* 111**,** 5195-5200.

RIDKER, P. M., RIFAI, N., PFEFFER, M., SACKS, F., LEPAGE, S. & BRAUNWALD, E. 2000. Elevation of tumor necrosis factor-alpha and increased risk of recurrent coronary events after myocardial infarction. *Circulation,* 101**,** 2149-53.

RIVERA-APONTE, D. E., MÉNDEZ-GONZÁLEZ, M. P., RIVERA-PAGÁN, A. F., KUCHERYAVYKH, Y. V., KUCHERYAVYKH, L. Y., SKATCHKOV, S. N. & EATON, M. J. 2015. Hyperglycemia reduces functional expression of astrocytic Kir4.1 channels and glial glutamate uptake. *Neuroscience,* 310**,** 216-223.

ROBERTSON, D. W. & STEINBERG, M. I. 1990. Potassium channel modulators: scientific applications and therapeutic promise. *J Med Chem,* 33**,** 1529-41.

ROSASCO, M. G. & GORDON, S. E. 2017. TRP Channels: What Do They Look Like? *In:* ND & EMIR, T. L. R. (eds.) *Neurobiology of TRP Channels.* Boca Raton (FL).

ROSSI, N. F. & MALISZEWSKA-SCISLO, M. 2008. Role of paraventricular nucleus vasopressin V1A receptors in the response to endothelin 1 activation of the subfornical organ in the rat. *J Physiol Pharmacol,* 59 Suppl 8**,** 47-59.

RUDIJANTO, A. 2007. The role of vascular smooth muscle cells on the pathogenesis of atherosclerosis. *Acta Med Indones,* 39**,** 86-93.

RUPARELIA, N., CHAI, J. T., FISHER, E. A. & CHOUDHURY, R. P. 2017. Inflammatory processes in cardiovascular disease: a route to targeted therapies. *Nat Rev Cardiol,* 14**,** 133-144.

SANDER, S. E., LEMM, C., LANGE, N., HAMANN, M. & RICHTER, A. 2012. Retigabine, a K(V)7 (KCNQ) potassium channel opener, attenuates L-DOPA-induced dyskinesias in 6-OHDA-lesioned rats. *Neuropharmacology,* 62**,** 1052-61.

SANDOVICI, I., HAMMERLE, C. M., COOPER, W. N., SMITH, N. H., TARRY-ADKINS, J. L., DUNMORE, B. J., BAUER, J., ANDREWS, S. R., YEO, G. S. H., OZANNE, S. E. & CONSTÂNCIA, M. 2016. Ageing is associated with molecular signatures of inflammation and type 2 diabetes in rat pancreatic islets. 59**,** 502-511.

SANTI, C. M. 2006. Opposite Regulation of Slick and Slack K+ Channels by Neuromodulators. *Journal of Neuroscience,* 26**,** 5059-5068.

SASAKI, S., ISHIBASHI, K. & MARUMO, F. 1998. Aquaporin-2 and -3: representatives of two subgroups of the aquaporin family colocalized in the kidney collecting duct. *Annu Rev Physiol,* 60**,** 199-220.

SAWCHENKO, P. E. & SWANSON, L. W. 1982. Immunohistochemical identification of neurons in the paraventricular nucleus of the hypothalamus that project to the medulla or to the spinal cord in the rat. *Journal of Comparative Neurology,* 205**,** 260-272.

SCANZELLO, C. R. & GOLDRING, S. R. 2012. The role of synovitis in osteoarthritis pathogenesis. *Bone,* 51**,** 249-57.

SCHELLER, J., CHALARIS, A., SCHMIDT-ARRAS, D. & ROSE-JOHN, S. 2011. The pro- and anti-inflammatory properties of the cytokine interleukin-6. *Biochimica et Biophysica Acta (BBA) - Molecular Cell Research,* 1813**,** 878-888.

SCHOLZ, A. 2002. Mechanisms of (local) anaesthetics on voltage-gated sodium and other ion channels. *Br J Anaesth,* 89**,** 52-61.

SCHREIBER, M. 1998. Slo3, a Novel pH-sensitive K+ Channel from Mammalian Spermatocytes. 273**,** 3509-3516.

SCUDIERI, P., CACI, E., VENTURINI, A., SONDO, E., PIANIGIANI, G., MARCHETTI, C., RAVAZZOLO, R., PAGANI, F. & GALIETTA, L. J. V. 2015. Ion channel and lipid scramblase activity associated with expression of TMEM16F/ANO6 isoforms. *Journal of Physiology-London,* 593**,** 3829-3848.

SELLAM, J. & BERENBAUM, F. 2010. The role of synovitis in pathophysiology and clinical symptoms of osteoarthritis. *Nat Rev Rheumatol,* 6**,** 625-35.

SESTI, F. 2016. Oxidation of K+Channels in Aging and Neurodegeneration. 7**,** 130.

SHAMIM, D. & LASKOWSKI, M. 2017. Inhibition of Inflammation Mediated Through the Tumor Necrosis Factor alpha Biochemical Pathway Can Lead to Favorable Outcomes in Alzheimer Disease. *J Cent Nerv Syst Dis,* 9**,** 1179573517722512.

SHIH, C. D., AU, L. C. & CHAN, J. Y. 2003. Differential role of leptin receptors at the hypothalamic paraventricular nucleus in tonic regulation of food intake and cardiovascular functions. *J Biomed Sci,* 10**,** 367-78.

SHOCK, N. W. 1964. Ageing: The Biology of Senescence. *Journal of Gerontology,* 19**,** 521-522.

SHORTER, E., SANNICANDRO, A. J., POULET, B. & GOLJANEK-WHYSALL, K. 2019. Skeletal Muscle Wasting and Its Relationship With Osteoarthritis: a Mini-Review of Mechanisms and Current Interventions. *Current Rheumatology Reports,* 21.

SIMMONS, D. M. & SWANSON, L. W. 2008. High-resolution paraventricular nucleus serial section model constructed within a traditional rat brain atlas. 438**,** 85-89.

SIMMS, B. A. & ZAMPONI, G. W. 2014. Neuronal voltage-gated calcium channels: structure, function, and dysfunction. *Neuron,* 82**,** 24-45.

SIMON, L. V., HASHMI, M. F. & FARRELL, M. W. 2019. Hyperkalemia. *StatPearls.* Treasure Island (FL).

SIMS, J. E. & SMITH, D. E. 2010. The IL-1 family: regulators of immunity. *Nat Rev Immunol,* 10**,** 89-102.

SONG, M. Y. & YUAN, J. X. 2010. Introduction to TRP channels: structure, function, and regulation. *Adv Exp Med Biol,* 661**,** 99-108.

STÄNDKER, L., SCHRADER, M., KANSE, S. M., JÜRGENS, M., FORSSMANN, W.-G. & PREISSNER, K. T. 1997. Isolation and characterization of the circulating form of human endostatin. 420**,** 129-133.

STATLAND, J., PHILLIPS, L. & TRIVEDI, J. R. 2014. Muscle channelopathies. *Neurol Clin,* 32**,** 801-15, x.

STEVENS, A. L., WISHNOK, J. S., CHAI, D. H., GRODZINSKY, A. J. & TANNENBAUM, S. R. 2008. A sodium dodecyl sulfate-polyacrylamide gel electrophoresis-liquid chromatography tandem mass spectrometry analysis of bovine cartilage tissue response to mechanical compression injury and the inflammatory cytokines tumor necrosis factor alpha and interleukin-1beta. *Arthritis Rheum,* 58**,** 489-500.

STEVENS, A. L., WISHNOK, J. S., WHITE, F. M., GRODZINSKY, A. J. & TANNENBAUM, S. R. 2009. Mechanical injury and cytokines cause loss of cartilage integrity and upregulate proteins associated with catabolism, immunity, inflammation, and repair. *Mol Cell Proteomics,* 8**,** 1475-89.

STEVENSON, K. & UVERSKY, V. N. 2019. Single-cell RNA-Seq: a next generation sequencing tool for a high-resolution view of the individual cell. *J Biomol Struct Dyn***,** 1-6.

STEWART, J., MANMATHAN, G. & WILKINSON, P. 2017. Primary prevention of cardiovascular disease: A review of contemporary guidance and literature. *JRSM Cardiovascular Disease,* 6**,** 204800401668721.

STOCKER, M. & KERSCHENSTEINER, D. 1998. Cloning and Tissue Distribution of Two New Potassium Channel α-Subunits from Rat Brain. 248**,** 927-934.

STOJILKOVIC, S. S., TABAK, J. & BERTRAM, R. 2010. Ion channels and signaling in the pituitary gland. *Endocr Rev,* 31**,** 845-915.

SUGITA, S., MIZUTANI, E., HOZAKI, M., NAKAMURA, M. & MATSUMOTO, T. 2019. Photoelasticity-based evaluation of cellular contractile force for phenotypic discrimination of vascular smooth muscle cells. *Scientific Reports,* 9.

SUTTON, S., CLUTTERBUCK, A., HARRIS, P., GENT, T., FREEMAN, S., FOSTER, N., BARRETT-JOLLEY, R. & MOBASHERI, A. 2009. The contribution of the synovium, synovial derived inflammatory cytokines and neuropeptides to the pathogenesis of osteoarthritis. *Vet J,* 179**,** 10-24.

SWANSON, L. W. & SAWCHENKO, P. E. 1983. Hypothalamic Integration - Organization of the Paraventricular and Supraoptic Nuclei. *Annual Review of Neuroscience,* 6**,** 269-324.

SWANSON, L. W., SAWCHENKO, P. E., WIEGAND, S. J. & PRICE, J. L. 1980. Separate Neurons in the Paraventricular Nucleus Project to the Median-Eminence and to the Medulla or Spinal-Cord. *Brain Research,* 198**,** 190-195.

SWARTZ, K. J. 2007. Tarantula toxins interacting with voltage sensors in potassium channels. *Toxicon,* 49**,** 213-30.

SWARTZ, K. J. & MACKINNON, R. 1997. Hanatoxin Modifies the Gating of a Voltage-Dependent K+ Channel through Multiple Binding Sites. *Neuron,* 18**,** 665-673.

TANG, C.-Y. & CHEN, T.-Y. 2011. Physiology and Pathophysiology of CLC-1: Mechanisms of a Chloride Channel Disease, Myotonia. 2011**,** 1-10.

TANNER, M. R., HU, X., HUQ, R., TAJHYA, R. B., SUN, L., KHAN, F. S., LARAGIONE, T., HORRIGAN, F. T., GULKO, P. S. & BEETON, C. 2015a. KCa1.1 Inhibition Attenuates Fibroblast-like Synoviocyte Invasiveness and Ameliorates Disease in Rat Models of Rheumatoid Arthritis. *Arthritis & Rheumatology,* 67**,** 96-106.

TANNER, M. R., HU, X., HUQ, R., TAJHYA, R. B., SUN, L., KHAN, F. S., LARAGIONE, T., HORRIGAN, F. T., GULKO, P. S. & BEETON, C. 2015b. KCa1.1 Inhibition Attenuates Fibroblast-like Synoviocyte Invasiveness and Ameliorates Disease in Rat Models of Rheumatoid Arthritis. *Arthritis Rheumatol,* 67**,** 96-106.

TEICHER, B. A. 2019. CD248: A therapeutic target in cancer and fibrotic diseases. *Oncotarget,* 10**,** 993-1009.

TERRAR, D. A. 1993. Structure and function of calcium channels and the actions of anaesthetics. *Br J Anaesth,* 71**,** 39-46.

TIAN, C., ZHU, R., ZHU, L., QIU, T., CAO, Z. & KANG, T. 2014. Potassium channels: structures, diseases, and modulators. *Chem Biol Drug Des,* 83**,** 1-26.

TORP, K. D. & SIMON, L. V. 2019. Lidocaine Toxicity. *StatPearls.* Treasure Island (FL).

TORRES, V. E., CAI, Y., CHEN, X., WU, G. Q., GENG, L., CLEGHORN, K. A., JOHNSON, C. M. & SOMLO, S. 2001. Vascular expression of polycystin-2. *J Am Soc Nephrol,* 12**,** 1-9.

TRAPNELL, C., WILLIAMS, B. A., PERTEA, G., MORTAZAVI, A., KWAN, G., VAN BAREN, M. J., SALZBERG, S. L., WOLD, B. J. & PACHTER, L. 2010. Transcript assembly and quantification by RNA-Seq reveals unannotated transcripts and isoform switching during cell differentiation. *Nature Biotechnology,* 28**,** 511-515.

TROMPET, S., DE CRAEN, A. J. M., SLAGBOOM, P., SHEPHERD, J., BLAUW, G. J., MURPHY, M. B., BOLLEN, E. L. E. M., BUCKLEY, B. M., FORD, I., GAW, A., MACFARLANE, P. W., PACKARD, C. J., STOTT, D. J., JUKEMA, J. W. & WESTENDORP, R. G. J. 2008. Genetic variation in the interleukin-1 -converting enzyme associates with cognitive function. The PROSPER study. *Brain,* 131**,** 1069-1077.

TURGUTALP, K., BARDAK, S., HELVACı, I., İŞGÜZAR, G., PAYAS, E., DEMIR, S. & KıYKıM, A. 2016. Community-acquired hyperkalemia in elderly patients: risk factors and clinical outcomes. 38**,** 1405-1412.

UEBELE, V. N., LAGRUTTA, A., WADE, T., FIGUEROA, D. J., LIU, Y., MCKENNA, E., AUSTIN, C. P., BENNETT, P. B. & SWANSON, R. 2000. Cloning and functional expression of two families of beta-subunits of the large conductance calcium-activated K+ channel. *J Biol Chem,* 275**,** 23211-8.

ULBRICHT, W. 2005. Sodium Channel Inactivation: Molecular Determinants and Modulation. 85**,** 1271-1301.

UNGVARI, Z., TARANTINI, S., DONATO, A. J., GALVAN, V. & CSISZAR, A. 2018. Mechanisms of Vascular Aging. *Circulation Research,* 123**,** 849-867.

VAISHALI, M. P. & SATYA, P. G. 2016. Studies on Chloride Channels and their Modulators. *Current Topics in Medicinal Chemistry,* 16**,** 1862-1876.

VAN GULICK, L., SABY, C., MORJANI, H. & BELJEBBAR, A. 2019. Age-related changes in molecular organization of type I collagen in tendon as probed by polarized SHG and Raman microspectroscopy. *Scientific Reports,* 9.

VAN MAANEN, M. A., STOOF, S. P., VAN DER ZANDEN, E. P., DE JONGE, W. J., JANSSEN, R. A., FISCHER, D. F., VANDEGHINSTE, N., BRYS, R., VERVOORDELDONK, M. J. & TAK, P. P. 2009. The alpha7 nicotinic acetylcholine receptor on fibroblast-like synoviocytes and in synovial tissue from rheumatoid arthritis patients: a possible role for a key neurotransmitter in synovial inflammation. *Arthritis Rheum,* 60**,** 1272-81.

VARANI, K., DE MATTEI, M., VINCENZI, F., TOSI, A., GESSI, S., MERIGHI, S., PELLATI, A., MASIERI, F., ONGARO, A. & BOREA, P. A. 2008. Pharmacological characterization of P2X1 and P2X3 purinergic receptors in bovine chondrocytes. *Osteoarthritis Cartilage,* 16**,** 1421-9.

VARGAS-ALARCON, G., ALVAREZ-LEON, E., FRAGOSO, J.-M., VARGAS, A., MARTINEZ, A., VALLEJO, M. & MARTINEZ-LAVIN, M. 2012. A SCN9A gene-encoded dorsal root ganglia sodium channel polymorphism associated with severe fibromyalgia. *BMC Musculoskeletal Disorders,* 13**,** 23.

VASILAKI, A., VAN DER MEULEN, J. H., LARKIN, L., HARRISON, D. C., PEARSON, T., VAN REMMEN, H., RICHARDSON, A., BROOKS, S. V., JACKSON, M. J. & MCARDLE, A. 2010. The age-related failure of

adaptive responses to contractile activity in skeletal muscle is mimicked in young mice by deletion of Cu,Zn superoxide dismutase. 9**,** 979-990.
VERGULT, S., DHEEDENE, A., MEURS, A., FAES, F., ISIDOR, B., JANSSENS, S., GAUTIER, A., LE CAIGNEC, C. & MENTEN, B. 2015. Genomic aberrations of the CACNA2D1 gene in three patients with epilepsy and intellectual disability. 23**,** 628-632.
VLADIS, N. A., FISCHER, K. E., DIGALAKI, E., MARCU, D.-C., BIMPOS, M. N., GREER, P., AYRES, A., LI, Q. & BUSCH, K. E. 2019. Gap junctions in theC. elegansnervous system regulate ageing and lifespan.
VON BANCHET, G. S., RICHTER, J., HUCKEL, M., ROSE, C., BRAUER, R. & SCHAIBLE, H. G. 2007. Fibroblast-like synovial cells from normal and inflamed knee joints differently affect the expression of pain-related receptors in sensory neurones: a co-culture study. *Arthritis Res Ther,* 9**,** R6.
WALDBURGER, J. M., BOYLE, D. L., PAVLOV, V. A., TRACEY, K. J. & FIRESTEIN, G. S. 2008. Acetylcholine regulation of synoviocyte cytokine expression by the alpha7 nicotinic receptor. *Arthritis Rheum,* 58**,** 3439-49.
WALSTON, J. D. 2012. Sarcopenia in older adults. *Current Opinion in Rheumatology,* 24**,** 623-627.
WANG, H. & WOOLF, C. J. 2005. Pain TRPs. *Neuron,* 46**,** 9-12.
WANG, J., OU, S. W. & WANG, Y. J. 2017. Distribution and function of voltage-gated sodium channels in the nervous system. *Channels (Austin),* 11**,** 534-554.
WANG, S., HU, L. F., YANG, Y., DING, J. H. & HU, G. 2005. Studies of ATP-sensitive potassium channels on 6-hydroxydopamine and haloperidol rat models of Parkinson's disease: implications for treating Parkinson's disease? *Neuropharmacology,* 48**,** 984-92.
WANG, T. 2015. TNF-alpha G308A polymorphism and the susceptibility to Alzheimer's disease: an updated meta-analysis. *Arch Med Res,* 46**,** 24-30 e1.
WATANABE, M., ICHINOSE, S. & SUNAMORI, M. 2004. Age-related changes in gap junctional protein of the rat heart. *Exp Clin Cardiol,* 9**,** 130-2.
WEI, A., JEGLA, T. & SALKOFF, L. 1996. Eight potassium channel families revealed by the C. elegans genome project. *Neuropharmacology,* 35**,** 805-29.
WEI, X. & RICHARDS, J. R. 2019. Physiology, Cardiac Repolarization Dispersion and Reserve. *StatPearls.* Treasure Island (FL).
WEINERT, B. T. & TIMIRAS, P. S. 2003. Invited Review: Theories of aging. *Journal of Applied Physiology,* 95**,** 1706-1716.
WEINGARTH, M., PROKOFYEV, A., VAN DER CRUIJSEN, E. A., NAND, D., BONVIN, A. M., PONGS, O. & BALDUS, M. 2013. Structural determinants of specific lipid binding to potassium channels. *J Am Chem Soc,* 135**,** 3983-8.
WESTENDORP, R. G., LANGERMANS, J. A., HUIZINGA, T. W., VERWEIJ, C. L. & STURK, A. 1997. Genetic influence on cytokine production in meningococcal disease. *Lancet,* 349**,** 1912-3.
WIBBERLEY, A., STAUNTON, C. A., FEETHAM, C. H., VERENINOV, A. A. & BARRETT-JOLLEY, R. 2015. An In Vitro Model of Skeletal Muscle Volume Regulation. *PLOS ONE,* 10**,** e0127889.
WILDERS, R. 2012. Cardiac ion channelopathies and the sudden infant death syndrome. *ISRN Cardiol,* 2012**,** 846171.
WILLIAMS, A. 2014. Proteomic studies of an explant

model of equine articular cartilage in response to proinflammatory and anti-inflammatory stimuli. *PhD Thesis University of Nottingham*.
WILLIAMS, A., SMITH, J. R., ALLAWAY, D., HARRIS, P., LIDDELL, S. & MOBASHERI, A. 2011. Strategies for optimising proteomic studies of the cartilage secretome: establishing the time course for protein release and evaluating responses of explant cultures to il-1 beta, tnf-alpha and carprofen. *Osteoarthritis and Cartilage,* 19**,** S209-S209.

WILLIAMS, M. E., FELDMAN, D. H., MCCUE, A. F., BRENNER, R., VELICELEBI, G., ELLIS, S. B. & HARPOLD, M. M. 1992. Structure and functional expression of alpha 1, alpha 2, and beta subunits of a novel human neuronal calcium channel subtype. *Neuron,* 8**,** 71-84.

WRIGHT, S. H. 2004. Generation of resting membrane potential. *Adv Physiol Educ,* 28**,** 139-42.

WU, C., YANG, K., LIU, Q., WAKUI, M., JIN, G. Z., ZHEN, X. & WU, J. 2010. Tetrahydroberberine blocks ATP-sensitive potassium channels in dopamine neurons acutely-dissociated from rat substantia nigra pars compacta. *Neuropharmacology,* 59**,** 567-72.

WULFF, H., CASTLE, N. A. & PARDO, L. A. 2009. Voltage-gated potassium channels as therapeutic targets. 8**,** 982-1001.

XU, H., RAMSEY, I. S., KOTECHA, S. A., MORAN, M. M., CHONG, J. A., LAWSON, D., GE, P., LILLY, J., SILOS-SANTIAGO, I., XIE, Y., DISTEFANO, P. S., CURTIS, R. & CLAPHAM, D. E. 2002. TRPV3 is a calcium-permeable temperature-sensitive cation channel. *Nature,* 418**,** 181-186.

YANG, C. T., ZENG, X. H., XIA, X. M. & LINGLE, C. J. 2009. Interactions between beta subunits of the KCNMB family and Slo3: beta4 selectively modulates Slo3 expression and function. *PLoS One,* 4**,** e6135.

YANG, H., ZHANG, G. & CUI, J. 2015. BK channels: multiple sensors, one activation gate. 6.

YOUNG, M. D., WAKEFIELD, M. J., SMYTH, G. K. & OSHLACK, A. 2010. Gene ontology analysis for RNA-seq: accounting for selection bias. *Genome Biol,* 11**,** R14.

YU, F. H. & CATTERALL, W. A. 2003. Overview of the voltage-gated sodium channel family. *Genome Biol,* 4**,** 207.

YU, F. H., YAROV-YAROVOY, V., GUTMAN, G. A. & CATTERALL, W. A. 2005. Overview of molecular relationships in the voltage-gated ion channel superfamily. *Pharmacol Rev,* 57**,** 387-95.

ZAMPONI, G. W. 2016. Targeting voltage-gated calcium channels in neurological and psychiatric diseases. *Nat Rev Drug Discov,* 15**,** 19-34.

ZAMPONI, G. W. 2017. A Crash Course in Calcium Channels. *ACS Chem Neurosci,* 8**,** 2583-2585.

ZAMPONI, G. W., STRIESSNIG, J., KOSCHAK, A. & DOLPHIN, A. C. 2015. The Physiology, Pathology, and Pharmacology of Voltage-Gated Calcium Channels and Their Future Therapeutic Potential. *Pharmacol Rev,* 67**,** 821-70.

ZHANG, J. M. & AN, J. 2007. Cytokines, inflammation, and pain. *Int Anesthesiol Clin,* 45**,** 27-37.

ZHANG, K., MAYHAN, W. G. & PATEL, K. P. 1997. Nitric oxide within the paraventricular nucleus mediates changes in renal sympathetic nerve activity. *American Journal of Physiology-Regulatory Integrative and Comparative Physiology,* 273**,** R864-R872.

ZHANG, K., ZUCKER, I. H. & PATEL, K. P. 1998. Altered number of diaphorase (NOS) positive neurons in the hypothalamus of rats with heart failure. *Brain Research,* 786**,** 219-225.

ZHANG, P., WU, X., LI, G., HE, Q., DAI, H., AI, C. & SHI, J. 2017. Tumor necrosis factor-alpha gene polymorphisms and susceptibility to ischemic heart disease: A systematic review and meta-analysis. *Medicine (Baltimore),* 96**,** e6569.

ZHENG, C., ZHOU, X. W. & WANG, J. Z. 2016. The dual roles of cytokines in Alzheimer's disease: update on interleukins, TNF-alpha, TGF-beta and IFN-gamma. *Transl Neurodegener,* 5**,** 7.

ZHOU, R. P., WU, X. S., WANG, Z. S., XIE, Y. Y., GE, J. F. & CHEN, F. H. 2016. Novel Insights into Acid-Sensing Ion Channels: Implications for Degenerative Diseases. *Aging Dis,* 7**,** 491-501.

ZHU, R., SUN, Z., LI, C., RAMAKRISHNA, S., CHIU, K. & HE, L. 2019a. Electrical stimulation affects neural stem cell fate and function in vitro. *Exp Neurol,* 319**,** 112963.

ZHU, Y., QU, J., HE, L., ZHANG, F., ZHOU, Z., YANG, S. & ZHOU, Y. 2019b. Calcium in Vascular Smooth Muscle Cell Elasticity and Adhesion: Novel Insights Into the Mechanism of Action. *Frontiers in Physiology,* 10.

ZIEGENHAIN, C., VIETH, B., PAREKH, S., REINIUS, B., GUILLAUMET-ADKINS, A., SMETS, M., LEONHARDT, H., HEYN, H., HELLMANN, I. & ENARD, W. 2017. Comparative Analysis of Single-Cell RNA Sequencing Methods. *Molecular Cell,* 65**,** 631-643.e4.

frontiers in Physiology

ORIGINAL RESEARCH
published: 24 March 2020
doi: 10.3389/fphys.2020.00226

Pro-inflammatory Cytokines Drive Deregulation of Potassium Channel Expression in Primary Synovial Fibroblasts

*Omar Haidar[1], Nathanael O'Neill[1], Caroline A. Staunton[1], Selvan Bavan[1], Fiona O'Brien[1], Sarah Zouggari[1], Umar Sharif[1], Ali Mobasheri[2,3,4,5], Kosuke Kumagai[1,6] and Richard Barrett-Jolley[1,5]**

[1] Institute of Ageing and Chronic Disease, University of Liverpool, Liverpool, United Kingdom, [2] Research Unit of Medical Imaging, Physics and Technology, University of Oulu, Oulu, Finland, [3] Department of Regenerative Medicine, State Research Institute Centre for Innovative Medicine, Vilnius, Lithuania, [4] Department of Orthopedics and Department of Rheumatology & Clinical Immunology, UMC Utrecht, Utrecht, Netherlands, [5] Versus Arthritis Centre for Sport, Exercise and Osteoarthritis Research, Queen's Medical Centre, Nottingham, United Kingdom, [6] Department of Orthopaedic Surgery, Shiga University of Medical Science, Shiga, Japan

OPEN ACCESS

Edited by:
J. David Spafford, University of Waterloo, Canada

Reviewed by:
Christine Beeton, Baylor College of Medicine, United States
Robert Brenner, The University of Texas Health Science Center at San Antonio, United States

***Correspondence:**
Richard Barrett-Jolley
RBJ@Liverpool.ac.uk

Specialty section:
This article was submitted to Membrane Physiology and Membrane Biophysics, a section of the journal Frontiers in Physiology

Received: *03 September 2019*
Accepted: *27 February 2020*
Published: *24 March 2020*

Citation:
Haidar O, O'Neill N, Staunton CA, Bavan S, O'Brien F, Zouggari S, Sharif U, Mobasheri A, Kumagai K and Barrett-Jolley R (2020) Pro-inflammatory Cytokines Drive Deregulation of Potassium Channel Expression in Primary Synovial Fibroblasts. Front. Physiol. 11:226. doi: 10.3389/fphys.2020.00226

The synovium secretes synovial fluid, but is also richly innervated with nociceptors and acts as a gateway between avascular joint tissues and the circulatory system. Resident fibroblast-like synoviocytes' (FLS) calcium-activated potassium channels (K_{Ca}) change in activity in arthritis models and this correlates with FLS *activation*.

Objective: To investigate this activation in an *in vitro* model of inflammatory arthritis; 72 h treatment with cytokines TNFα and IL1β.

Methods: FLS cells were isolated from rat synovial membranes. We analyzed global changes in FLS mRNA by RNA-sequencing, then focused on FLS ion channel genes and the corresponding FLS electrophysiological phenotype and finally modeling data with ingenuity pathway analysis (IPA) and MATLAB.

Results: IPA showed significant activation of inflammatory, osteoarthritic and calcium signaling canonical pathways by cytokines, and we identified ∼200 channel gene transcripts. The large K_{Ca} (BK) channel consists of the pore forming Kcnma1 together with β-subunits. Following cytokine treatment, a significant increase in Kcnma1 RNA abundance was detected by qPCR and changes in several ion channels were detected by RNA-sequencing, including a loss of BK channel β-subunit expression Kcnmb1/2 and an increase in Kcnmb3. In electrophysiological experiments, there was a decrease in over-all current density at 20 mV without change in chord conductance at this potential.

Conclusion: TNFα and IL1β treatment of FLS *in vitro* recapitulated several common features of inflammatory arthritis at the transcriptomic level, including increase in Kcnma1 and Kcnmb3 gene expression.

Keywords: TNFα, IL1β, inflammation, synovial fibroblast, ion channel

INTRODUCTION

Rheumatoid arthritis (RA) and osteoarthritis (OA) are degenerative diseases that target articular joint structures resulting in pain, loss of function and frequent disability. Whilst RA is an established inflammatory condition, the contribution of inflammatory processes to OA was less well known until recently. Mediators of inflammation (i.e., including pro-inflammatory cytokines) contribute to the development of synovitis, which is known to drive disease progression in RA. In contrast, it is thought that in OA, synovitis can be caused by the release of cartilage fragments and meniscal damage that in turn, activate synovial lining cells (Fernandez-Madrid et al., 1995; Roemer et al., 2013; Mathiessen and Conaghan, 2017). How inflammation drives joint destruction is not fully known. One feature of synovitis, however, is the presence of major pro-inflammatory cytokines, such as interleukin-1β (IL-1β), tumor necrosis factor alpha (TNFα), and interleukin 6 (IL-6), resulting in suppression of collagen and proteoglycan synthesis, increased inflammatory signaling, and protease expression and activation (Martel-Pelletier et al., 1999).

Management of arthritis has significantly improved in recent years', however, remission is rarely achieved, and many patients remain unresponsive to conventional and/or biologic treatments. In addition, current therapies and treatments are associated with notable side effects that can pose great challenges for long-term treatment, especially in patients with cardiovascular co-morbidities. For example, some drugs can increase the risk of cardiovascular disease or significantly impair immune responses, rendering patients more susceptible to infections and cancer (Kahlenberg and Fox, 2011). Therefore, new therapeutic options and novel targets are needed that lead to pronounced improvement without inducing unwanted side effects and thus avoiding the need for joint replacement.

The synovium is the major barrier between the joint and the systemic circulation and plays a role in maintaining the health of articular cartilage (Sutton et al., 2009; Berenbaum, 2013). The synovium lubricates the articular surfaces and provides nutrients for chondrocytes within the avascular cartilage; it has been suggested that catabolic enzymes such as matrix metalloproteinase (MMPs) are produced by synovial cells and diffuse into the cartilage. The intimal lining layer of the synovium produces lubricious synovial fluid and is composed of two cell types in relatively equal proportions: Type A or macrophage-like synovial cells and Type B or fibroblasts like synoviocytes (FLS). FLS cells contribute to the structural integrity of the joints by controlling the composition of the synovial fluid and extracellular matrix (ECM) of the joint. The synovial environment changes physically, chemically, and physiologically with injury or the onset of disease and is thought to be a mediator in arthritis pain (Grubb, 2004; Sellam and Berenbaum, 2010; Kumahashi et al., 2011). FLS cells have been implicated in arthritis as they exhibit a transformed phenotype with increased invasiveness and production of various pro-inflammatory mediators that perpetrate inflammation and proteases that contribute to cartilage destruction (Noss and Brenner, 2008; Bartok and Firestein, 2010). Understanding the biology and regulation of FLS cells provides insight into the pathogenesis of inflammatory arthritis. FLS cells could potentially be targeted pharmacologically to produce increased volumes of synovial fluid as an alternative to intra-articular hyaluronan or synthetic fluid injection therapies. They are also a plausible analgesic target because they may interact with sensory neurons and have been described as "amplifiers" of neuropeptide mediated inflammation and pain.

To deepen our understanding of the synovium in the context of synovial joint health and disease, the electrophysiological profile of FLS cells needs to be characterized, along with the ion channels that are present. Ion channels are an essential component of any cell membrane that controls ion movement in and out of the cell and play an important role in a multitude of cell regulating processes, typically by modulating the membrane potential. Electrophysiological techniques have been used to characterize the biophysical properties of a number of different FLS preparations, including mouse, rabbit, bovine and human (Large et al., 2010; Friebel et al., 2014; Clark et al., 2017). The best available whole-cell mathematical model of the FLS is heavily dominated by a Ca^{2+}-activated potassium conductance, with small added components of inward rectifiers, background and leak. A recent study by Kondo et al. (2018) demonstrated that human FLS express high levels of Ca^{2+}-activated potassium channels and these ion channels were also identified in both RA-derived and rodent model FLS studies. Typically, Ca^{2+}-activated channels couple with Ca^{2+} entry channels such as transient receptor potential (TRP) channels; they are both activated by the Ca^{2+} ions that enter and maintain the membrane potential hyperpolarized to "draw in" further Ca^{2+}. In FLS, Ca^{2+}-activated potassium channels appear to drive invasiveness of synoviocytes and progression of arthritis in both human and rodent RA models (Petho et al., 2016; Tanner et al., 2019), by increasing production of both inflammatory mediators and catabolic enzymes (Hu et al., 2012; Friebel et al., 2014; Tanner et al., 2015). This is a paradoxical effect for a potassium conductance, that would be predicted to hyperpolarize cells and reduce migration, proliferation and activity in general.

The synovium is an obvious target for the development of novel interventions in both RA and OA. The role of synovitis, the low-grade inflammation of the synovial lining of the joint, in OA progression is gradually emerging. Therefore, in this work we investigate the pathophysiology of cytokine induced synovitis in cultured synovial cells.

We investigate whether the TNFα and IL1β cytokine *in vitro* model of inflammation leads to a significant change of the BK ion channel and quantify the mechanism of this change. We use a combination of next generation RNA sequencing (NGS), qPCR, and patch-clamp electrophysiology to uncover several changes in potassium channel gene expression together with changes in cellular phenotype which involves a phenotypic switch in response to inflammation.

MATERIALS AND METHODS

Further methodological details are included in the **Supplementary Methods** section (see **Supplementary File S2**).

Animals

Synovial cells were prepared from tissue from rats euthanized by Home Office Approved methods for unassociated reasons in line with the ARRIVE Guidelines. All rats were untreated/wild-type male adult Wistar.

Preparation of FLS Cells

Synovial fibroblasts were isolated from rat knee joints as described previously. Briefly, patella and menisci with attached synovial membranes were isolated and placed in 12-well plates in low glucose DMEM (Thermo Fischer, United Kingdom) with 20% fetal bovine serum (FBS), 100 U/ml penicillin, 100 μg/ml streptomycin and 2.5 μg/ml amphotericin B (Thermo Fischer, United Kingdom) at 37°C in a 5% CO_2 incubator. For the first 7 days medium was replaced daily whilst out-growing FLS emerged from the tissues. At 7 days residual tissue was discarded and cells cultured as normal; when confluent, cells were detached from the flask surface by 1% Trypsin-EDTA solution. The suspension was centrifuged (340 × *g*, 5 min) and the resulting pellet was resuspended in culture medium (as above).

Immunohistochemistry

In brief, cell suspension at a density of 2.5×10^4 cell/ml was transferred to multiwall plates and fixed with 2% paraformaldehyde in PBS at room temperature. CD248 (an FLS marker) immunohistochemistry was performed using rabbit anti-CD248 primary antibody (Ab, 1:100 dilution; Abcam, Cambridge) and FITC-conjugated donkey Anti-rabbit IgG secondary antibody (Ab, 1:500 dilution; Jackson ImmunoResearch Laboratories). Non-specific binding was blocked as previously described (Mobasheri et al., 2005). After 24 h at 4°C, cells were washed three times for 5 min with 0.05% SSC-20 and 0.005% Triton-X100. Slides were finally dipped into distilled water, air dried, and mounted with mounting media (Vectashield with DAPI). Cells were visualized with confocal microscopy.

Real−Time PCR

RNA extraction was carried out using the RNeasy Plus Micro kit, together with gDNA eliminator and MinElute spin columns (Qiagen, United Kingdom). cDNA synthesis (mRNA) was performed using the RT2 First Strand kit (Qiagen, Netherlands) according to the manufacturer's protocol. qPCR analysis was performed using the Stratagene MX3000P RT-PCR System (Stratagene, La Jolla, CA, United States) in a 25−μL reaction mixture. Expression relative to housekeeper Rplp1 was calculated as ΔCt.

RNA "Next Generation Sequencing" (NGS)

Figure 1 summarizes our NGS workflow. In brief, cells were treated with 10 ng/ml of both TNF-α + IL1β (TNF-α from Thermo Fischer, United Kingdom and IL1β from R&D systems) for 72 h. RNA extraction was carried out using the RNeasy Plus Micro kit (Qiagen, United Kingdom) according to the manufacturers protocol. Any RNA samples with concentrations of less than 5 μg/ml and/or purity (260/280 and 260/230) less than 1.8 were excluded. RNA samples were sent to GATC-Biotech, Germany for sequencing. Samples were read as paired-end with a sequencing depth of 30 M and a read length of 50 bp. Further details are included in **Supplementary Methods** (see **Supplementary File S2**). Further bioinformatics were performed with R, for example the DAPCA package or our local installation of the Galaxy server suite (Afgan et al., 2018). Specific packages are mentioned in the text, **Supplementary Methods** (see **Supplementary File S2**) and **Figure 1**. *Full data are available on the EBI array express database with accession number: E-MTAB-7798.*

Electrophysiology

Electrophysiology was performed as described previously (Lewis et al., 2013) but using isolated FLS. Intracellular solution was 115 mM gluconic acid/potassium salt, 26 mM KCl, 1 mM $MgCl_2$ (BDH, VWR International Ltd.), 5 mM Ethylene glycol tetraacetic acid (EGTA), 10 mM HEPES, pH 7.2. Extracellular (bath) solution was 140 mM NaCl, 5 mM KCl, 2 mM $CaCl_2$ (Fluka Analytical cat#: 21114), 1 mM $MgCl_2$, 10 mM HEPES, and 5 mM Glucose, osmolality approximately 300 mOsm, pH 7.4. Junction potential −14.4 mV (Lewis et al., 2013). Thick-walled patch-pipettes were pulled from borosilicate glass capillary tubes (outer diameter 1.5 mm, inner diameter 0.86 mm; Intracel, United Kingdom) and gave a resistance of ∼8 MΩ when filled. Whole cell patch-clamp electrophysiology was performed on FLS cells using a Cairn Optopatch amplifier (Cairn Research, United Kingdom). To compare voltage-gated currents, we performed whole-cell patch clamp experiments with voltage steps starting from a holding potential of −80 mV for 2 s. Recordings were filtered at 1 kHz, digitized at 3 kHz and recorded on a computer using WinWCP 5.3.4 software (John Dempster, Strathclyde University, United Kingdom). All experiments were performed at room temperature (18–22°C), and the results are expressed as the mean ± SEM.

Analysis was performed using WinWCP 5.3.4 software (John Dempster, Strathclyde University, United Kingdom). Boltzmann curve fits were computed in MATLAB through non-linear least squares optimization.

RESULTS

Enriched Pathways in FLS Cells After Cytokine Treatment

RNA-seq detected 33251 transcripts and the *full data are available on the EBI array express database with accession number: E-MTAB-7798.* The top (highest FPKM) expressed 10 genes were similar between control and cytokine treated cells (**Supplementary Tables S1, S2**). Our first bioinformatic analysis tested the reproducibility of the 72 h, 10 ng/ml TNFα + IL1β treatment. We used discriminant analyses of

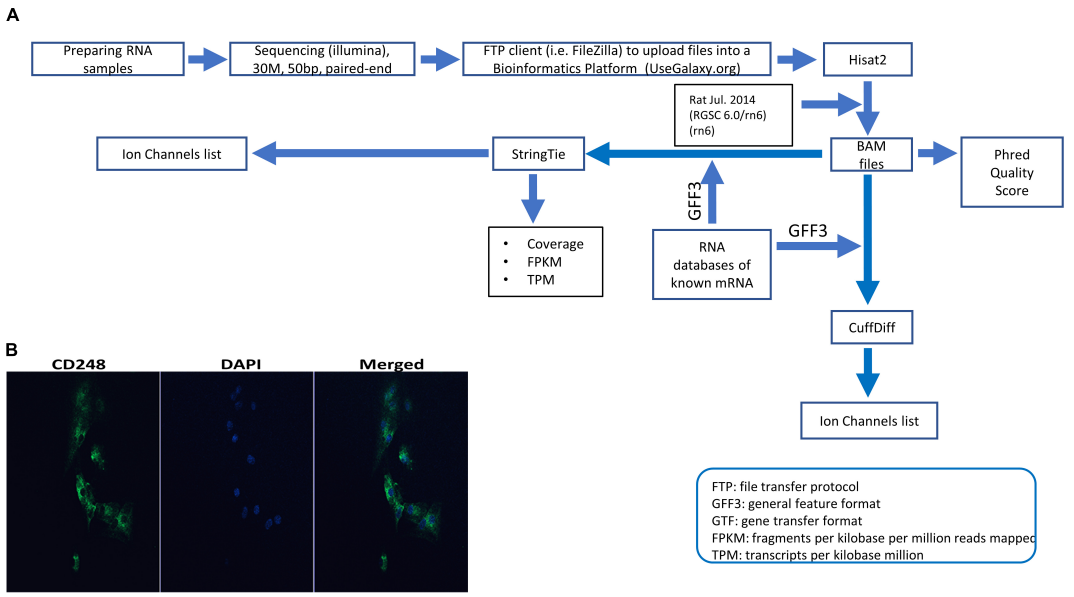

FIGURE 1 | Experimental pipeline and verification. **(A)** Schematic of the next generation sequencing (NGS) pipeline. RNA was extracted from synovial tissue from eight animals, were split into control and test groups and the test samples were treated with 10 ng IL1β and TNFα as described in the section "Materials and Methods." These eight samples sequenced with Illumina and raw data files were uploaded using a FTP client to a bioinformatics platform for analysis. Within the bioinformatics platform, reads were aligned/mapped with Hisat2 program using the reference genome Rat Jul. 2014 (RGSC 6.0/rn6) (rn6). The resulting BAM files were used to measure phred quality score for all samples. Also, BAM files along with an annotation file (Rat GFF3) to assemble mapped reads and quantify gene expression. Such assembly and quantification took place with StringTie and CuffDiff package/tool that generated gene abundance estimates and differentially expressed genes, respectively. After that, using several servers and a local custom-script in MATLAB software allowed us to filter the transcriptome for all known ion channel genes for further analysis (for example, see **Tables 1**, **2**). **(B)** Expression of CD248 in FLS cells. Immunofluorescence FLS cells showing the FLS marker CD248. DAPI was used for nuclear counterstaining (see **Supplementary Methods** in **Supplementary File S2** for details).

principal components (DAPC) with in the DAPC package to show good separation of the two populations (**Figure 2**); the genes primarily discriminating the treatment and control populations are largely those well established to be important for joint function, including several collagens and a matrix metallopeptidase (MMP2). Ingenuity pathway (IPA) analysis (Qiagen, United Kingdom) was then used to identify the upstream regulators of the global differential expression pattern. This analysis predicted the top two regulators to be TNFα and IL1β (p-values 3e-17 and 6e-13, respectively), this is unsurprising since this was indeed the treatment regimen.

Figure 3 shows the canonical calcium signally pathway ($p < 0.5e-7$), which was enriched following cytokine treatment. In addition, the rheumatoid ($p < 5e-13$) and OA ($p < 1e-9$) pathways and cellular movement and proliferation canonical pathways (predicted *activation*, $p < 1e-13$ in both cases) were also enriched following cytokine treatment (data not shown). In all cases, TNFα was determined to be the top *causal* agent, but four ion channels were also significant causal regulators (adjusted $p < 0.05$) of the transcript-wide treatment changes; Clcn5, Trpv4, Trpv1, Kcnn4.

Next Generation RNA Sequencing Analysis of Ion Channel Gene Expression

Initial RNA-seq experiments were intended to give a transcriptome wide, unbiased, assessment of ion channel changes in cytokine treated FLS. We identified 190 channel genes, including porins, connexins and ion-channel isoform genes (including α- to ε-subunits), but excluded interacting proteins, other regulatory proteins and the so-called potassium tetramerization domain proteins. The top 50 genes, in terms of FPKM are given for control and cytokine treated datasets in **Supplementary Tables S3, S4**, respectively.

Next Generation RNA Sequencing Ion Channel Differential Expression

One of the key ion channels involved with regulation of FLS is the large calcium activated potassium channel (BK, Kcnmx) and it is notable that there was a reduction in expression of β-subunit Kcnmb1/2 and appearance of Kcnmb3 after cytokine treatment. We further analyzed this family transcript by transcript for the 13 known (already annotated) splice variants of these channels; Kcnma1, Kcnmb1, Kcnmb2, Kcnmb3, Kcnmb4 (**Figure 4C**). The most abundantly expressed of all these transcripts is Kcnma1 (ENSRNOT00000077671) with rather lower expression of any of the β-subunits and no detection of the one annotated Kcnmb4 variant. Following cytokine treatment expression of all of the detectable Kcnma1 splice variants was higher, but there was a lower abundance of Kcnmb4.

In total, 20 ion channel genes, undetectable in control conditions became detectable or 'appeared' after cytokine treatment (**Supplementary Table S5**), of which, the top expressed

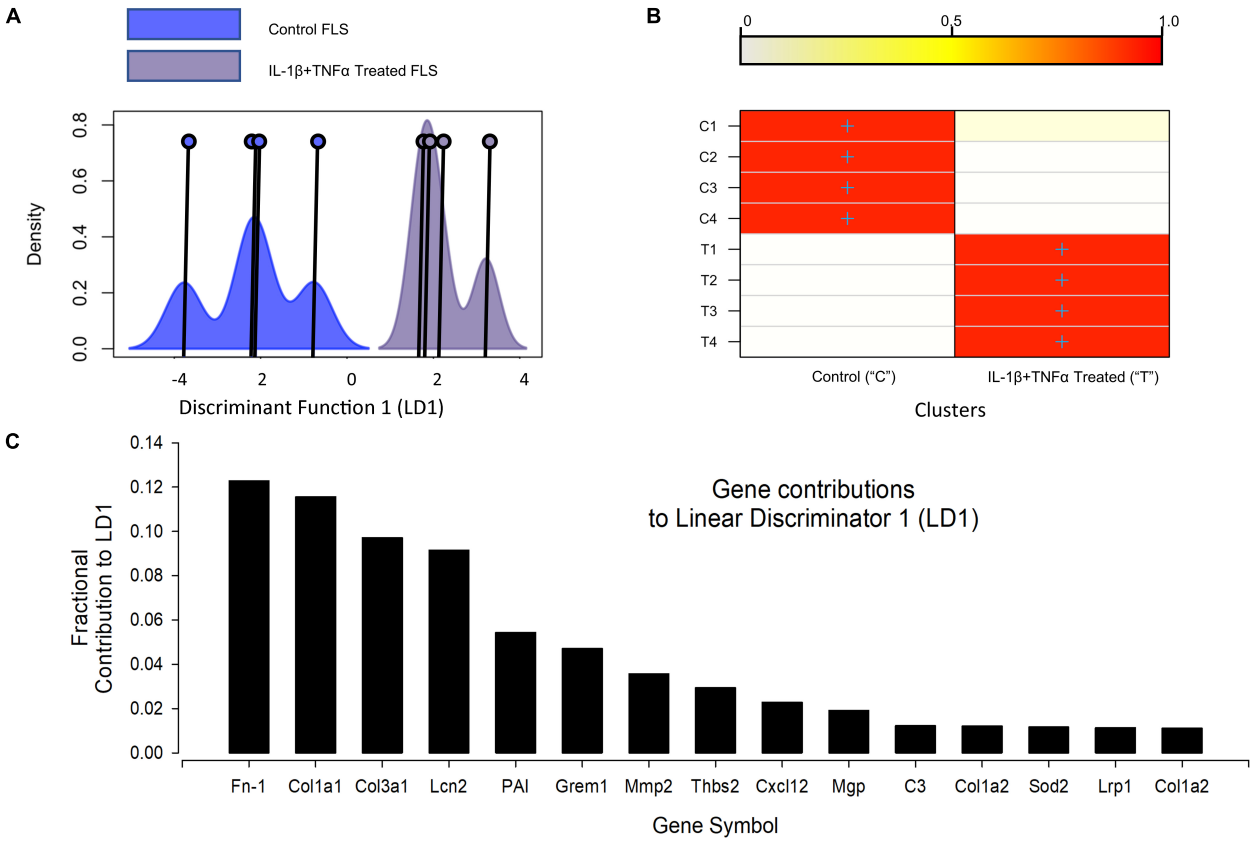

FIGURE 2 | Discriminant analyses of global IL-1β TNFα treatment effects. **(A)** Shows the kernel density plots of the discriminant component co-ordinates for the control and IL-1β/TNFα treatment groups; co-ordinates on the *x*-axis and density on the *y*-axis; Individual co-ordinate center points are illustrated by the vertical line and circle. There is clear separation between control and cytokine treated FLS samples. **(B)** A graphical confusion matrix showing the actual group membership (*y*-axis) and predicted cluster membership (on the *y*-axis). All groups are correctly clustered with greater than 0.9 probability. **(C)** The top 15 contributors to the linear discriminator function: Fn-1, fibronectin 1; Col1a1, collagen type I alpha 1 chain; Col3a1, collagen type III alpha 1 chain; Lcn2, lipocalin 2; PAI, serpine1; Grem1, gremlin 1; Mmp2, matrix metallopeptidase 2; Thbs2, thrombospondin 2; Cxcl12, C-X-C motif chemokine ligand 12; Mgp, matrix Gla protein; C3, complement C3; Col1a2, collagen type I alpha 2 chain; Sod2, superoxide dismutase 2; Lrp1, LDL receptor related protein 1; Col1a2, collagen type I alpha 2.

of these was Trpc3. Conversely, seven ion channel genes became undetectable or "disappeared" following cytokine treatment (**Supplementary Table S6**). Following cytokine treatment, we found an additional 15 genes to be down by −1.5 ($\log_2$) or more and 21 genes 1.5 ($\log_2$) greater than control (**Tables 1**, **2**, respectively). We used tissue from four animals for the NGS study each animal tissue split into test and control groups; the "*n*" presented in the legends refers to the number of biological replicates (= animals).

qPCR Verification of RNA Changes

To add further support to the unbiased RNA-seq ion channel analysis we performed qPCR on sets of control and IL1β/TNFα treated FLS with panels of Ca^{2+}-potassium channels (Kcnma1, Kcnn1, Kcnn2, Kcnn3) and other ion channel genes (**Figure 4B**). We did not have primers for all the potassium channel genes identified by next generation sequencing. Three potassium genes were differentially expressed; two voltage-gated potassium channels Kcna6 and Kcnc2-significantly decreased ($p < 0.05$, $n = 4,4$), whereas the large calcium potassium channel Kcnma1 was upregulated ($p < 0.05$, $n = 4,4$).

Electrophysiology

Neither RNA nor protein expression studies can confirm changes in functional ion channel expression or, functional changes resulting from post-translational changes, Furthermore, several different potassium channel isoforms were identified, of which some upregulated and some downregulated. Therefore, to investigate the effect of cytokine treatment on the electrophysiological fingerprint, we conducted functional assays of ion channel expression with patch-clamp electrophysiology. The primary changes observed in the more limited qRT-PCR data would predict over all *loss of* voltage-gated potassium ion channel activity and increase in the less voltage-dependent calcium activated potassium channels.

Resting Membrane Potential

Following cytokine treatment, the resting membrane potential of FLS decreased (depolarized) from −48.6 ± 1.7

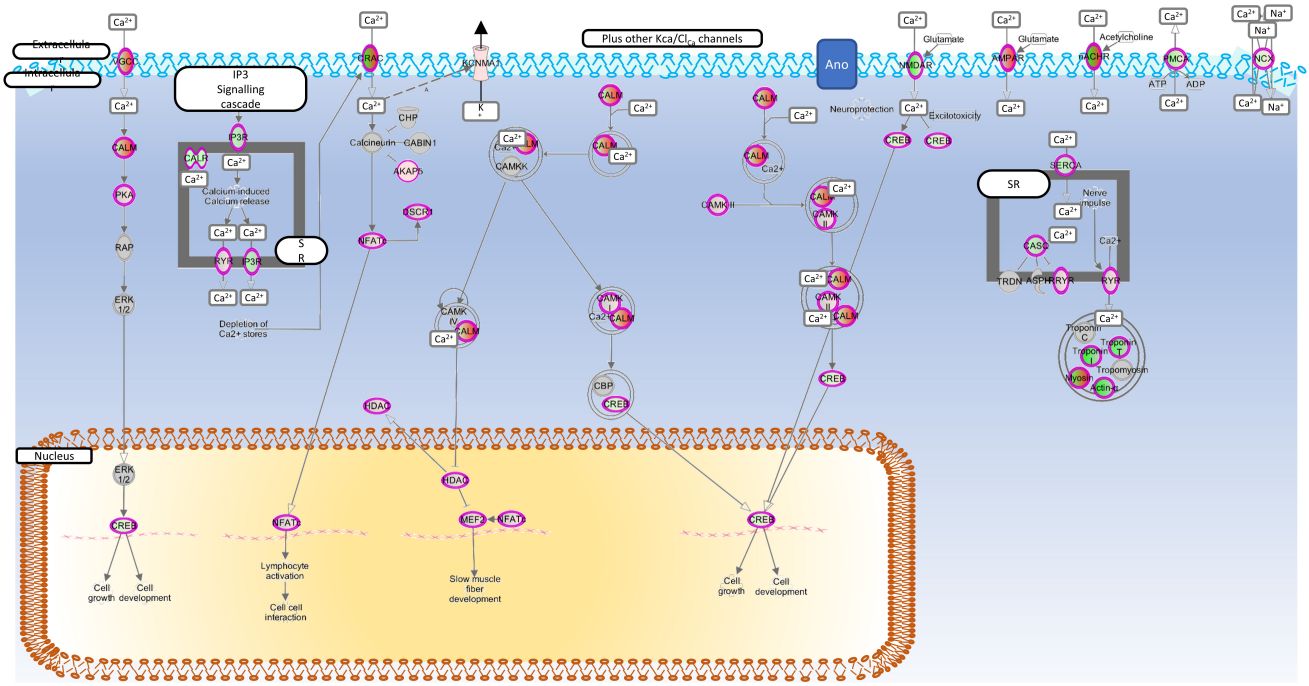

FIGURE 3 | Enriched calcium regulation pathway. Genes mapped to the calcium signaling canonical pathway by IPA. Red, increased expression; green, decreased expression (for interpretation of the references to color in the figure legend, please refer to the online version of this article).

to −38.6 ± 2.8 mV, junction potential corrected (data not shown, $p \leq 0.05$, unpaired *t*-test).

Current Voltage Currents

As seen in **Figure 5A**, some cells exhibited clear transient and sustained components whereas others exhibited only the sustained component of the current. We therefore analyzed the transient and sustained components of the current separately in all cases.

We found no overall change in the maximum amplitude of the transient current (**Figure 5B**), but the sustained current (**Figure 5C**) density, measured at +20 mV was decreased (12.5 ± 2.3 pA/pF to 3.8 ± 0.8 pA/pF, n = 24,20, $p < 0.05$). There was no change in chord conductance measured at this potential (271 ± 45 pS/pF to 120 ± 20 pS/pF, n = 24,20). To characterize the nature of the conductance apparently *inhibited* by cytokine treatment we calculated the difference current for cytokine treatment (i.e., cytokine-treated current; **Figure 5D**). This revealed a strongly voltage-gated current with mid-point for activation 40 ± 1.2 mV and slope 17.6 ± 1.2 mV, n = 25.

Pharmacological Modulation of Currents

Despite the *increase* of KCNMA1 RNA in both qPCR and RNA-Seq our electrophysiological data show a reduced current density. To investigate if the maximum possible BK current is altered in cytokine treatment, we repeated our standard voltage protocol (above) in the presence of 1 μM of the BK channel opener NS1619 and found a significant increase in current density in the presence of NS1619 in control cells (**Figures 6A,C**, $p \leq 0.05$, n = 9,6), we did not see an equivalent increase in the cytokine treated cells (**Figures 6B,D**). We then repeated this experiment with 1 μM of the BK channel inhibitor paxilline. Untreated cell current density was significantly smaller in the presence of paxilline, but not significantly reduced in treated cells (**Figures 6E,F**).

DISCUSSION

In this study, we used an *in vitro* model of synovial cell inflammation to investigate the pathophysiology of cytokine induced synovitis. We have demonstrated that IL1β and TNFα treatment of FLS cells resulted in profound changes in arthritic, inflammatory, and Ca^{2+} regulatory pathways similar to that reported in RA models. We found differential expression of several ion channels with transcriptomics and our electrophysiological experiments show a reduction of whole-cell current density.

The Pathophysiological Validity of the 72 h IL1β and TNFα Model

Treatment of joint tissue with TNFα and IL1β cytokines is an established *in vitro* model of inflammatory arthritis with tissue typically exposed to between 10 ng/ml of TNFα and IL1β for between 2 and 7 days. In the present study, we use the lower end of the concentration range, 10 ng and treat for 72 h (De Ceuninck et al., 2004; Stevens et al., 2008, 2009; Pretzel et al., 2009; Williams et al., 2011;

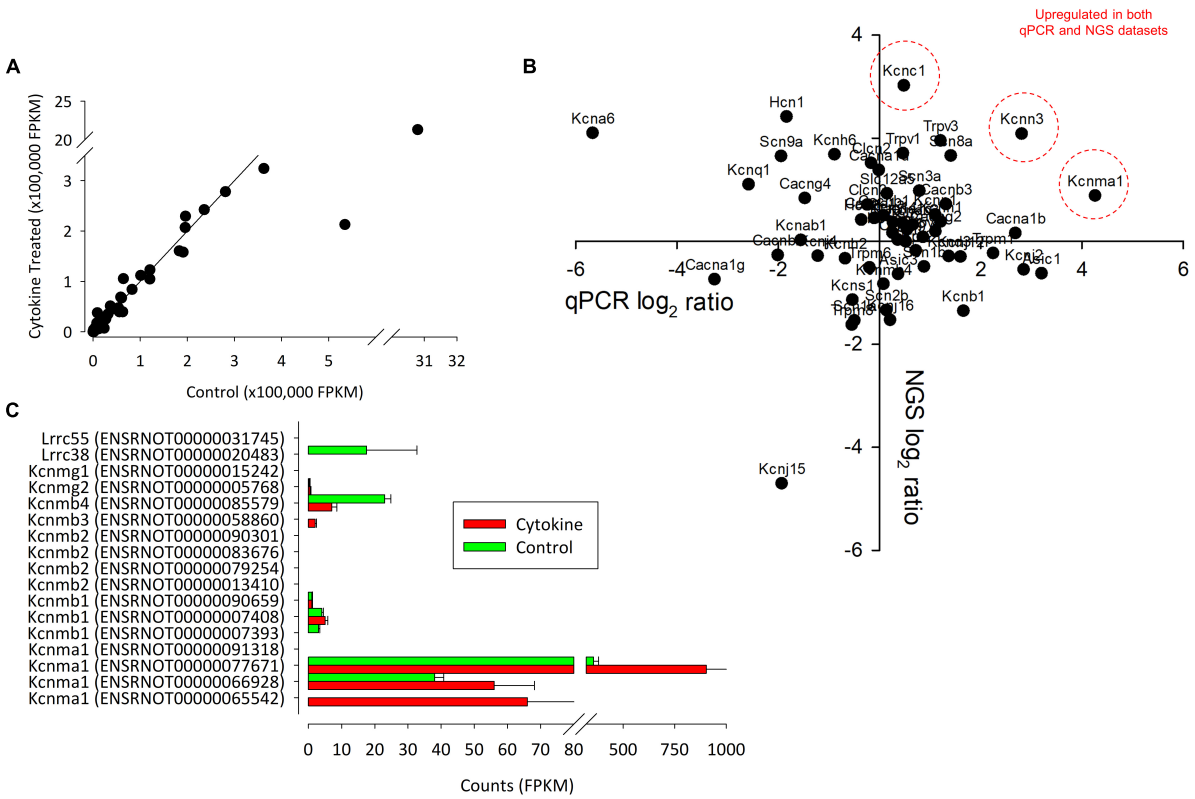

FIGURE 4 | The correlation between control and NGS expression data. **(A)** We found a strong correlation between control and treated (72 h of IL1β + TNFα) channel expression data. Each point represents the intersection of four control and four test values. In **(B)**, the correlation between qPCR ($\Delta\Delta$Cts) and NGS ratio (FPKM values) are shown. Data suggest that there only a weak linear correlation between qPCR and NGS. *P*-value = 0.3. $R = 0.29$. $n = 14$ (eight animals for NGS and six animals for PCR). Genes that were upregulated in both datasets are indicated in red. **(C)** Summary of NGS expression of all known (rat) splice variants of Kcnma1 and associated Kcnmb subunits.

Williams, 2014). This regime is hypothesized to activate inflammatory pathways, but there will be no cytokine remaining by the time of the electrophysiological experiments that could cause confounding direct effects. We treated FLS cells with the pro-inflammatory cytokines IL1β and TNFα in order to understand the cellular changes that occur when these FLS are subjected to higher-than-normal levels of these cytokines *in vivo*, for example, in arthritis. This model has distinct advantages of 3Rs, consistency, reproducibility and allowing the investigation of distinct pathways in isolation but since it is an acute model it may lack some chronic features of *in vivo* models. Our transcriptome analysis demonstrated that pathways were activated in common with arthritis movement of cells, proliferation and both RA and OA. In an *in vitro* model of RA, Tanner et al. (2019) also showed up regulation of Kcnma1 (message and protein) analogous to that observed with our 72 h cytokine treatment. Furthermore, more recent data suggests a correlation between FLS invasiveness and expression of the β-subunit (KCNMB3) in human samples of FLS from RA patients (Petho et al., 2016). *Taken together with the changes in Ca^{2+} signaling, we show that our in vitro model captures several features of the inflammatory joint phenotype and that FLS have been "activated" as observed in animal models of arthritis.*

Causal analysis is a relatively new mathematical technique that allows one to move from probability of agreement or simple correlation toward probability of causation in networks. The IPA implementation of this identified both IL1β and TNFα as master-regulators of the changes we observe and considering our experimental design included time matched controls, this strongly supports a suitable dosage and incubation time. Whilst both IL1β and TNFα were identified by IPA as "master regulators," TNFα transcriptome-wide causation was stronger than that of IL1β. Interestingly, FLS cells harvested from RA patients exhibit a marked transient elevation of intracellular Ca^{2+} on exposure to TNFα (Yoo et al., 2006) raising the possibility that this could be the initial trigger for the resulting pathway changes. However, it should be noted that such a transient lasts less than a minute and in our study cells were challenged with cytokines 72 h prior to experiments. Furthermore, cells were replaced in cytokine-free medium for electrophysiology, so there would be no cytokine physically present at that time. Also, the previously reported TNFα induced Ca^{2+} signal was only clear in FLS from RA; it was largely absent in FLS from OA patients and not investigated in FLS from healthy controls (Yoo et al., 2006).

TABLE 1 | FLS channel gene RNA expression lower after cytokine (10 ng/ml TNFα and IL1β) treatment.

Gene	Official name	Log_2 (95% CI)
Kcnj15	Potassium inward rectified channel subfamily j member 15	−5.51 (−9.57 to −2.48)
Ano2	Anoctamin 2	−2.59 (−5.5 to 0)
Kcnb1	Potassium voltage-gated channel subfamily b member 1	−2.44 (−1.85 to −1)
Kcnv2	Potassium voltage-gated channel modifier subfamily v member 2	−2.4 (−4.85 to 0)
Kcnip1	Potassium voltage-gated channel interacting protein 1	−2.36 (−3.88 to −0.88)
Kcnmb1	Potassium calcium-activated channel subfamily m regulatory beta subunit 1	−1.98 (−3.28 to 0.69)
Kcns1	Potassium voltage-gated channel modifier subfamily s member 1	−1.88 (−6.84 to −0.42)
Kcnj8	Potassium inward rectifier j member 8 (Kir6.1)	−1.79 (−4.71 to 2.17)
Kcnd3	Potassium voltage-gated channel subfamily d member 3	−1.78 (−2.63 to 0.29)
Nalcn	Sodium leak channel, non-selective	−1.77 (−3.43 to −0.85)
Clca2	Chloride channel accessory 2	−1.76 (−6.72 to 0.65)
Kcne3	Potassium voltage-gated channel subfamily e regulatory subunit 3	−1.67 (−1.84 to −0.15)
Asic1	Acid sensing ion channel subunit 1	−1.64 (−6.44 to 0)
Clcn4	Chloride voltage-gated channel 4	−1.61 (−2.61 to −0.95)
Trpm8	Trpm8 channel associated factor 1	−1.61 (−2.09 to −0.99)

Qualification cytokine log_2 (geometric mean) < −1.5 of control (= approximately 33%), n = 4 control and 4 cytokine treated samples (from four animals).

TABLE 2 | FLS channel gene RNA expression increased after cytokine (10 ng/ml TNFα and IL1β) treatment.

Gene ID	Official name	Log_2 (95% CI)
Kcnc1	Potassium voltage-gated channel subfamily c member 1	4.32 (0.68 to 5.93)
Kcnc3	Potassium voltage-gated channel subfamily c member 3	3.46 (0.76 to 5.94)
Trpc3	Transient receptor potential cation channel subfamily c member 3	3.06 (3.73 to 6.5)
Catsper3	Cation channel sperm associated 3	2.83 (0.14 to 5.75)
Kcng3	Potassium voltage-gated channel modifier subfamily g member 3	2.81 (2.77 to 6.65)
Tmc7	Transmembrane channel like 7	2.77 (1.99 to 5.53)
Gjc3	Gap junction protein gamma 3	2.75 (0.03 to 4.35)
Scnn1g	Sodium channel epithelial 1 gamma subunit	2.56 (2.77 to 5.45)
Asic2	Acid sensing ion channel subunit 2	2.52 (0.66 to 4.65)
Kcnmb3	Potassium calcium-activated channel subfamily m regulatory beta subunit 3	2.34 (0 to 4.73)
Cracr2a	Calcium release activated channel regulator 2a	2.32 (0.01 to 1.96)
Kcnn3	Potassium calcium-activated channel subfamily n member 3	2.07 (0.57 to 4.09)
Tmc4	Transmembrane channel like 4	1.94 (0.27 to 2.47)
Asic4	Acid sensing ion channel subunit family member 4	1.75 (0.52 to 2.76)
Kcnj11	Potassium inward rectifier j member 11 (Kir6.2)	1.74 (0 to 6.56)
Trpv6	Transient receptor potential cation channel subfamily v member 6	1.7 (0.01 to 5.43)
Hvcn1	Hydrogen voltage gated channel 1	1.69 (0.98 to 2.84)
Trpv1	Transient receptor potential cation channel subfamily v member 1	1.61 (0.98 to 2.07)
Kcnk7	Potassium two pore domain channel subfamily k member 7	1.6 (−1.85 to 1.03)
Cacna1d	Calcium voltage-gated channel subunit alpha1 d	1.57 (0.32 to 2.09)
Asic5	Acid sensing ion channel subunit family member 5	1.55 (0 to 5.78)

Qualification cytokine log_2 (geometric mean) > 1.5 of control (= approximately 300%), n = 4 control and 4 cytokine treated samples (from four animals).

Previous Studies of Differential Expression of Membrane Ion Channels in Synovium

Until very recently, little was known of the FLS ion channel compliment (the "channelome") compared to that of the another central joint cell, the chondrocyte (Barrett-Jolley et al., 2010). One of the best-studied families of ion channels in FLS, however, is the Ca^{2+}-activated potassium channel family. The high conductance member of this family, termed BK ($K_{Ca}1.1$ or KCNMA1) and the "intermediate" conductance member ("IK," or $K_{Ca}3.1$) are both expressed and have roles in invasive migration, proliferation, cytokine, and MMP release (Hu et al., 2012; Friebel et al., 2014). Interestingly, inhibitors of BK decrease the signs of joint degeneration in the pristane-induced arthritis model. These channels are therefore potential drug targets to protect against joint degeneration as well as being putative biomarkers. Whilst the BK channel β- subunit (KCNMB1) was slightly increased in transcript abundance in the Lambert et al., 2014 data (similar seen by Huber et al., 2008), both of the two BK α-subunit (KNMA1) probes on the chip exhibit small decreases in expression. It should be noted that the expression of BK channel β- subunits confers modulation of ion channel activity, in many cases decreasing its sensitivity to, for example, Ca^{2+} ions (Lippiat et al., 2003; Mobasheri et al., 2012).

A recent study by Kondo et al. (2018) demonstrated that human FLS express high levels of both intermediate ($K_{Ca}3.1$) and large (BK/$K_{Ca}1.1$/KCNMA1) Ca^{2+}-activated potassium channels. The other most highly expressed ion channels identified by Kondo et al. (2018) were KCNK2, ANO6, ANO10, and KCNK6. KCNK2/6 are members of the two-pore-domain potassium channel family and are particularly thought of as molecular sensors, whereas the ANO (anoctamin) channels are members of the large chloride channel family. This family is relatively understudied compared to potassium channels, but ANO6 (TMEM16F) is, interestingly, thought to be a Ca^{2+}-activated chloride channel as well as a lipid "scramblase" (Scudieri et al., 2015), therefore, likely to be activated in parallel to Ca^{2+}-activated potassium channels.

Changes in Ion Channel Currents in the Present Study

The phenotype of FLS current recorded by whole-cell patch clamp was quite variable in terms of the presence of transient and sustained components of current, as seen in **Figure 5**. We found no significant changes in the transient phase of current and therefore, we focused on the sustained component of voltage

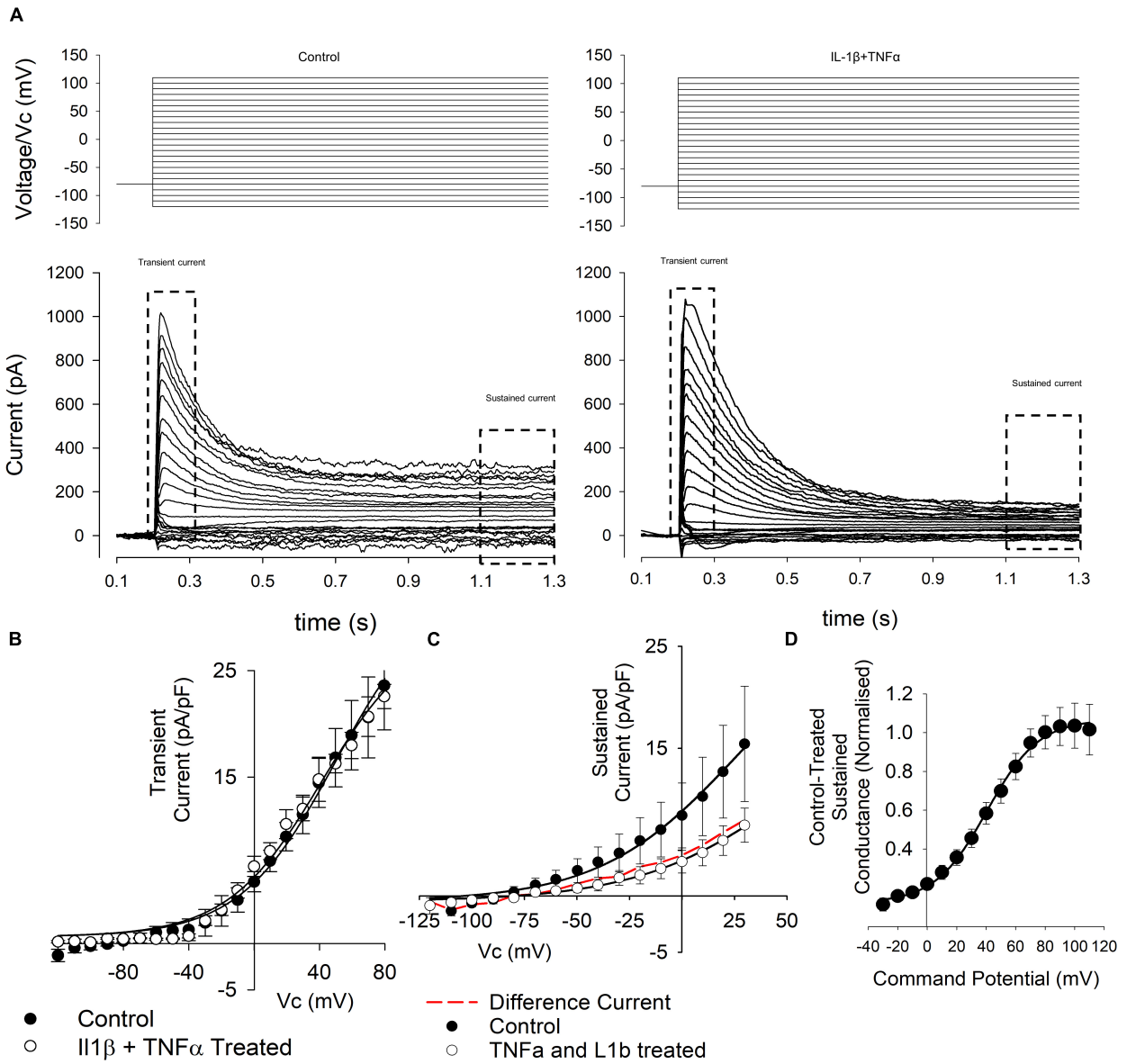

FIGURE 5 | Whole-cell voltage-gated currents from control and cytokine treated FLS. **(A)** Top panels show the voltage step protocols and the evoked currents are shown below for control (left) and IL1β + TNFα (right) conditions. Note that FLS exhibit both transient and sustained currents. These phases of current were then analyzed separately as indicated. **(B)** Current–voltage curves (left) from the *transient* currents recorded in a number or experiments such as that illustrated in **(A)**. There was no significant difference between control and treated *transient* current density. Data points are shown as mean ± SEM (n = 18 for control and n = 11 for IL1β + TNFα). **(C)** Current–voltage curves from the *sustained* currents recorded in a number or experiments such as that illustrated in **(A)**. The red line in the current–voltage curve is the difference current for control-cytokine treated. **(D)** Difference conductance–voltage curve for the cytokine difference current shown in **(C)**. The line is fit with a Boltzmann, *see text*.

activated currents that would be expected to include BK activity if it was present. Although we found a significant increase in RNA expression of the BK α-subunit gene, Kcnma1, following cytokine treatment (by qPCR), there was a decrease in over-all current density of the sustained current. To characterize the voltage-gated characteristics of the current *lost* after cytokine treatment we subtracted IV curves following cytokine treatment from the control IV curves and transformed this to a conductance-voltage curve. Since this curve fully saturated, we were able to fit it with a Boltzmann curve and derive the midpoint for activation; +40 mV. This is rather positive to most voltage-gated potassium channels, the most "positive" of which (Kcnbx/Kcncx) have activation mid-points in the +10 to +20 mV range (Coetzee et al., 1999). This cytokine sensitive conductance could be an ensemble average of a number of different ion channel changes, including increase of some and decrease of others. It could also be a BK current under conditions of low intracellular Ca^{2+} (Cui et al., 1997, 2009; Coetzee et al., 1999; Contreras et al., 2012),

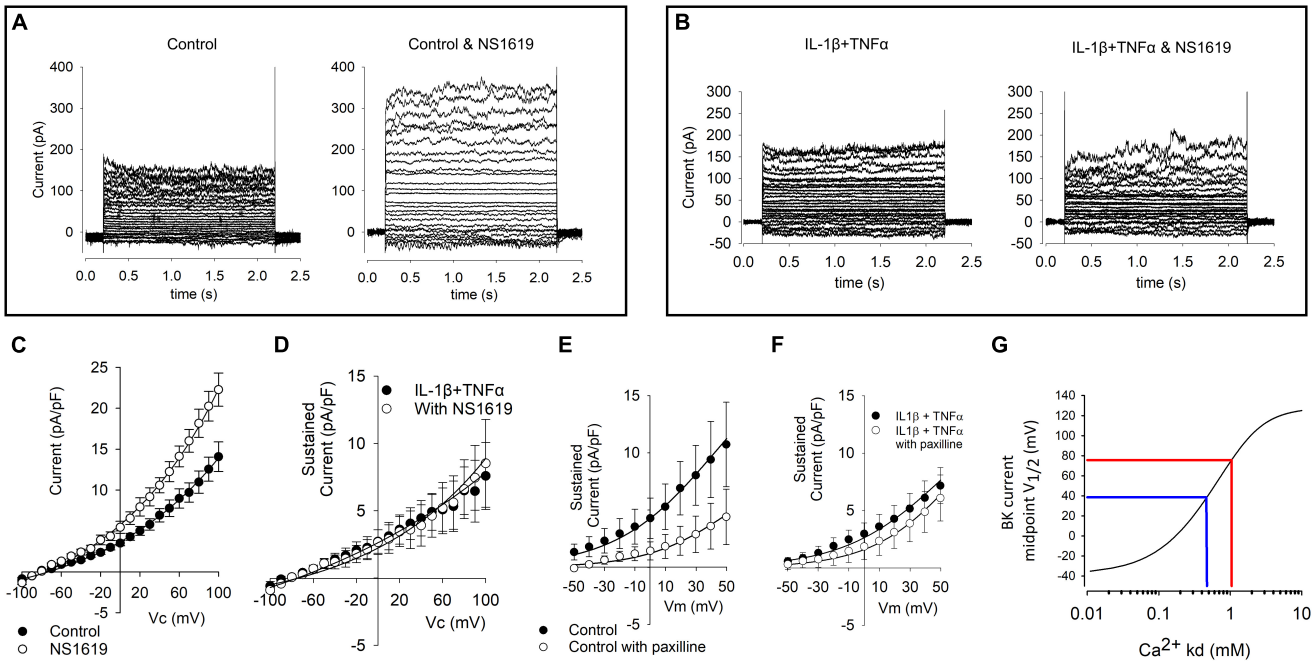

FIGURE 6 | Effects of BK channel drugs on FLS whole-cell currents. **(A)** Representative examples of untreated (control) cells before (left) and in the presence of 1 μM of the BK channel opener NS1619 (left). Voltage protocols as shown in Figure 5. **(B)** Representative raw example current families of cytokine (10 ng/ml IL1β + TNFα) treated cells in the absence (left) and presence (right) of 1 μM NS1619. **(C)** Current–voltage curves from a number of control FLS cells such as that shown in **(A)**. Current is significantly greater in the presence of NS1619, $p < 0.05$, $n = 9$ and 6. **(D)** Current–voltage curves for a number of treated FLS cells such as that shown in **(B)**. These two curves are not significantly different from each other $n = 6$ and 6. **(E)** Current–voltage curves from a number of control FLS cells treated with and without paxilline; there is a significant decrease in paxilline current $p < 0.05$ $n = 13,5$), but **(F)** there was no significant different of current density in the presence of the BK inhibitor paxilline following cytokine treatment ($n = 6, 12$). **(G)** *Numerical simulation of data from Clark et al. (2017) model*. To quantify the degree of change of BK channel modulation apparently taking place with this treatment we used the model of verbatim with the exception that we varied the inherent BK channel Ca^{2+} sensitivity parameter *Kd*. In this simulation, the independent variable *Kd* is plotted on the *x*-axis and the predicted BK current midpoint ($V_{1/2}$) is plotted on the *y*-axis. In blue, we have added hypothetical midpoints of 40 mV and 80 mV representing a hypothetical shift in 40 mV by cytokine treatment. The complete MATLAB code for this simulation is included in the **Supplementary File S1**.

but, since the true local concentration of intracellular Ca^{2+} is unknown, this is difficult to assess. $V_{1/2}$ for the BK channel in the virtual absence of Ca^{2+} can be much higher, for example 200–300 mV (Bao and Cox, 2005; Orio and Latorre, 2005; Wang and Brenner, 2006). The value of this parameter also depends on the nature of the co-expressed β-subunit (Coetzee et al., 1999; Contreras et al., 2012). $V_{1/2}$ is typically shifted to the left in the presence of beta subunits (Brenner, 2014). In our transcript data (**Figure 4C**), we show a range of BK transcripts including the Lrrcx subunits, but none, on their own, show significant alteration by treatment. Note that with experimentally elevated intracellular Ca^{2+} concentration these would likely lie well to the left of where they lay in our experiments. In our experiments we included 5 mM EGTA, which allows for the Ca^{2+}-activation of BK channels so long as they are physically close to the Ca^{2+} source (Fakler and Adelman, 2008). Functional coupling between BK and the Ca^{2+} source appears a common phenomenon (Fakler and Adelman, 2008); we also showed this with a coupling between TRPV4 channels and K_{Ca} channels previously in neurones (Feetham et al., 2015) and it has also been shown in smooth muscle cells too (Nilius and Droogmans, 2001). Increasing, or attempting to "clamp" intracellular Ca^{2+} before investigating BK channels would be tempting, but this could cause greater constitutive activation of BK and mask a physiological coupling.

Our electrophysiological experiments also demonstrated significantly more depolarized resting membrane potentials in cytokine treated cells. This could result from loss of constitutive potassium or chloride conductances, but equally it could result from the elevation of the non-specific or Na^{+} selective or ion channels such as Trpc3 or Asic2, etc. (**Table 2**).

The BK pharmacological activator (NS1619) and inhibitor (paxilline) both had the expected effects (increase and decrease of current density, respectively) in the untreated FLS but neither had a significant effect. This is surprising in the light of the Tanner et al. (2015) data showing that paxilline ameliorate development joint degeneration in a model of RA and the continued effectiveness of paxilline in FLS from RA patients (Petho et al., 2016). One possible explanation could be differences in transcript expression between strains as has been observed with ion channels previously (Kunert-Keil et al., 2006). Our RNA data showed a clear shift from RNA-expression of β1 (and β2) subunits to β3 and sensitivity to voltage, calcium and some drugs is well-known to be conveyed by co-expression of the β subunits (McManus et al., 1995; Uebele et al., 2000; Yang

et al., 2009). However, neither paxilline nor NS1619 themselves are thought to be influenced by the β-subunit; paxilline acts as a closed channel blocker (Zhou and Lingle, 2014) whereas NS1619 opens the BK channel by binding to the KCNMA1 S6/RCK linker and is effective in some splice variants, but not others (Soom et al., 2008; Gessner et al., 2012). In humans there are 93 known s[lice variants of KCNMA1, but there are only four in rats listed on ENSEMBL (Zerbino et al., 2018). **Figure 4** shows the relative transcript expression for Kcnma1. The most abundant transcript (ENSRNOT00000077671 Kcnma1-203) is present in both conditions. None of the Kcnma1 transcripts decrease with cytokine so it seems unlikely (but not impossible) that pharmacological changes result directly from splice variant switching. Note that the one known transcript that was not detected is the truncated transcript Kcnma1-204 (ENSRNOT00000091318). The lack of effect of NS1619 and paxilline after cytokine treatment could be also be secondary to changes in β-subunits or intracellular Ca^{2+} in microdomains or some unknown reason leaving insufficient residual functional BK activity to be noticeably modulated. The simple (K^+ channel focused) FLS electrophysiological model of Clark allows us to use numerical simulation to estimate the change in BK channel Ca^{2+} that would be required to shift a BK conductance voltage curve by about +40 mV and largely leave the cells virtually free of measurable BK current (**Figure 6G**). We find that retaining all the parameters of Clark et al. (2017) except the Ca^{2+} *Kd* itself, such data would be the equivalent to increasing *Kd* from 0.46 μM to approximately 1.05 μM. The upstream pathway (beyond the activation of the cytokine pathway including NFκB, etc.) for these changes is difficult to identify from our data, especially since there are relatively few ion channel interaction data in the IPA databases. It is notable, however, that there were significant changes in the calcium signaling pathway (**Figure 3**) and so it is possible that change in calcium activated potassium channel expression follows this, by way of compensatory expression. The lack of apparent effect of paxilline could also be technical. For example, there was considerable variability between cells and we compared population means rather than pairing each cell with and without paxilline increasing the risk of a type II error.

Role of Ion Channels in Pro-inflammatory Cytokine Production and Secretion

Ion channels are involved not just in the response to cytokines, but can also contribute to their production. For example, ionotropic NMDA and kainite glutamate receptors contribute to synovial inflammation by increasing expression of the inflammatory cytokine IL-6 (Flood et al., 2007) and nicotinic acetylcholine receptor activation reduces the synovial production of IL-6, IL-8, TNFα, and several other cytokines (Waldburger et al., 2008; van Maanen et al., 2009). P2X7 is an established conduit for release of mediators such as IL1β (Mortaz et al., 2012). We saw little P2X7 RNA, but there is evidence that in chondrocytes P2X1, may sub serve the same function (Varani et al., 2008) and we detected RNA for this channel only after cytokine treatment. In a previous report, inhibition of the small Ca^{2+} activated potassium ion channel decreased the production of cytokines IL-6, IL-8, and MCP1 in response to TGF-1β, but they did not examine secretion of IL1β or TNFα (Friebel et al., 2014). In other-words activation of Ca^{2+} potassium ion channels is essentially a secretion trigger. This result is somewhat counter intuitive since one would expect activation of a potassium channel to hyperpolarize and decrease secretion. One possible explanation is that activation of Ca^{2+} potassium ion channels draws in additional Ca^{2+} by increasing the driving force for Ca^{2+} entry.

$$Ca^{2+}\ entry\ \alpha\ (Vm - Eq_{\mathrm{Ca2+}})$$

Where negative values are equivalent to inward driving force for Ca^{2+}, *Vm* is the membrane potential and $Eq_{\mathrm{Ca2+}}$ is the equilibrium potential for Ca^{2+}.

CONCLUSION

To our knowledge, this is the first report using a combined NGS and patch-clamp electrophysiological approach to understanding the control of potassium channels in inflammation in joint tissues. We found an increased RNA expression of the BK potassium gene Kcnma1, but the constitutive activity of the channel was not increased. The decreased sensitivity to voltage activation and to drugs could be explained by a switch the RNA expression of β-subunits KcnmB1, 2, and 3.

DATA AVAILABILITY STATEMENT

The datasets generated for this study can be found in the https://www.ebi.ac.uk/arrayexpress/experiments/E-MTAB-7798/.

ETHICS STATEMENT

The animal study was reviewed and approved by the University of Liverpool Veterinary Ethics Committee.

AUTHOR CONTRIBUTIONS

All authors have conceptualized and designed the study, and analyzed and interpreted the data. RB-J, FO, and KK drafted the manuscript. All authors have critically revised the manuscript for important intellectual content. All authors have finally approved the manuscript. RB-J, AM, and OH obtained the funding.

FUNDING

This study was funded by the European Union's Seventh Framework Programme (EU FP7; grant agreement No. 305815),

BBSRC (BB/N003020/1), The University of Liverpool, and King Abdulaziz University, Jeddah, Saudi Arabia.

ACKNOWLEDGMENTS

For funding, the authors would like to thank the European Union's Seventh Framework Programme for research, technological development, and demonstration (Grant agreement no. 305815) and King Abdulaziz University, Jeddah, Saudi Arabia.

SUPPLEMENTARY MATERIAL

The Supplementary Material for this article can be found online at: https://www.frontiersin.org/articles/10.3389/fphys.2020.00226/full#supplementary-material

REFERENCES

Afgan, E., Baker, D., Batut, B., van den Beek, M., Bouvier, D., Cech, M., et al. (2018). The Galaxy platform for accessible, reproducible and collaborative biomedical analyses: 2018 update. *Nucleic Acids Res.* 46, W537–W544. doi: 10.1093/nar/gky379

Bao, L., and Cox, D. H. (2005). Gating and ionic currents reveal how the BKCa channel's Ca2+ sensitivity is enhanced by its beta1 subunit. *J. Gen. Physiol.* 126, 393–412. doi: 10.1085/jgp.200509346

Barrett-Jolley, R., Lewis, R., Fallman, R., and Mobasheri, A. (2010). The emerging chondrocyte channelome. *Front. Physiol.* 1:135. doi: 10.3389/fphys.2010.00135

Bartok, B., and Firestein, G. S. (2010). Fibroblast-like synoviocytes: key effector cells in rheumatoid arthritis. *Immunol. Rev.* 233, 233–255. doi: 10.1111/j.0105-2896.2009.00859.x

Berenbaum, F. (2013). Osteoarthritis as an inflammatory disease (osteoarthritis is not osteoarthrosis!). *Osteoarthr. Cartil.* 21, 16–21. doi: 10.1016/j.joca.2012.11.012

Brenner, R. (2014). Knockout of the BK β2 subunit reveals the importance of accessorizing your channel. *J. Gen. Physiol.* 144, 351–356. doi: 10.1085/jgp.201411291

Clark, R. B., Schmidt, T. A., Sachse, F. B., Boyle, D., Firestein, G. S., and Giles, W. R. (2017). Cellular electrophysiological principles that modulate secretion from synovial fibroblasts. *J. Physiol.* 595, 635–645. doi: 10.1113/JP270209

Coetzee, W. A., Amarillo, Y., Chiu, J., Chow, A., Lau, D., McCormack, T., et al. (1999). Molecular diversity of K+ channels. *Ann. N. Y. Acad. Sci.* 868, 233–285.

Contreras, G. F., Neely, A., Alvarez, O., Gonzalez, C., and Latorre, R. (2012). Modulation of BK channel voltage gating by different auxiliary beta subunits. *Proc. Natl.Acad. Sci. U.S.A.* 109, 18991–18996. doi: 10.1073/pnas.1216953109

Cui, J., Cox, D. H., and Aldrich, R. W. (1997). Intrinsic voltage dependence and Ca2+ regulation of mslo large conductance Ca-activated K+ channels. *J. Gen. Physiol.* 109, 647–673. doi: 10.1085/jgp.109.5.647

Cui, J., Yang, H., and Lee, U. S. (2009). Molecular mechanisms of BK channel activation. *Cell Mol. Life Sci.* 66, 852–875. doi: 10.1007/s00018-008-8609-x

De Ceuninck, F., Dassencourt, L., and Anract, P. (2004). The inflammatory side of human chondrocytes unveiled by antibody microarrays. *Biochem. Biophys. Res. Commun.* 323, 960–969. doi: 10.1016/j.bbrc.2004.08.184

Fakler, B., and Adelman, J. P. (2008). Control of K(Ca) channels by calcium nano/microdomains. *Neuron* 59, 873–881. doi: 10.1016/j.neuron.2008.09.001

Feetham, C. H., Nunn, N., Lewis, R., Dart, C., and Barrett-Jolley, R. (2015). TRPV4 and KCa ion channels functionally couple as osmosensors in the paraventricular nucleus. *Br. J. Pharmacol.* 172, 1753–1768. doi: 10.1111/bph.13023

Fernandez-Madrid, F., Karvonen, R. L., Teitge, R. A., Miller, P. R., An, T., and Negendank, W. G. (1995). Synovial thickening detected by MR imaging in osteoarthritis of the knee confirmed by biopsy as synovitis. *Magn. Reson. Imaging* 13, 177–183. doi: 10.1016/0730-725X(94)00119-N

Flood, S., Parri, R., Williams, A., Duance, V., and Mason, D. (2007). Modulation of interleukin-6 and matrix metalloproteinase 2 expression in human fibroblast-like synoviocytes by functional ionotropic glutamate receptors. *Arthritis Rheum* 56, 2523–2534. doi: 10.1002/art.22829

Friebel, K., Schonherr, R., Kinne, R. W., and Kunisch, E. (2014). Functional role of the KCa3.1 potassium channel in synovial fibroblasts from rheumatoid arthritis patients. *J. Cell Physiol.* 230, 1677–1688. doi: 10.1002/jcp.24924

Gessner, G., Cui, Y. M., Otani, Y., Ohwada, T., Soom, M., Hoshi, T., et al. (2012). Molecular mechanism of pharmacological activation of BK channels. *Proc. Natl. Acad. Sci. U.S.A.* 109, 3552–3557. doi: 10.1073/pnas.1114321109

Grubb, B. D. (2004). Activation of sensory neurons in the arthritic joint. *Novartis Found Symp.* 260, 28–36discussion 36- 48, 277–279.

Hu, X., Laragione, T., Sun, L., Koshy, S., Jones, K. R., Ismailov, I. I., et al. (2012). KCa1.1 potassium channels regulate key proinflammatory and invasive properties of fibroblast-like synoviocytes in rheumatoid arthritis. *J. Biol. Chem.* 287, 4014–4022. doi: 10.1074/jbc.M111.312264

Huber, R., Hummert, C., Gausmann, U., Pohlers, D., Koczan, D., Guthke, R., et al. (2008). Identification of intra-group, inter-individual, and gene-specific variances in mrna expression profiles in the rheumatoid arthritis synovial membrane. *Arthritis Res. Ther.* 10:R98. doi: 10.1186/ar2485

Kahlenberg, J. M., and Fox, D. A. (2011). Advances in the medical treatment of rheumatoid arthritis. *Hand Clin.* 27, 11–20. doi: 10.1016/j.hcl.2010.09.002

Kondo, C., Clark, R. B., Kim, T. Y., Belke, D., Banderali, U., Szerencsei, R. T., et al. (2018). Atp triggers a robust intracellular [ca^{2+}]-mediated signalling pathway in human synovial fibroblasts. *Exp. Physiol.* 103, 1101–1122. doi: 10.1113/EP086851

Kumahashi, N., Naitou, K., Nishi, H., Oae, K., Watanabe, Y., Kuwata, S., et al. (2011). Correlation of changes in pain intensity with synovial fluid adenosine triphosphate levels after treatment of patients with osteoarthritis of the knee with high-molecular-weight hyaluronic acid. *Knee* 18, 160–164. doi: 10.1016/j.knee.2010.04.013

Kunert-Keil, C., Bisping, F., Kruger, J., and Brinkmeier, H. (2006). Tissue-specific expression of TRP channel genes in the mouse and its variation in three different mouse strains. *Bmc Genomics* 7:159. doi: 10.1186/1471-2164-7-159

Lambert, C., Dubuc, J.-E., Montell, E., Vergés, J., Munaut, C., Noël, A., et al. (2014). Gene expression pattern of cells from inflamed and normal areas of osteoarthritis synovial membrane. *Arthritis Rheumatol.* 66, 960–968. doi: 10.1002/art.38315

Large, R. J., Hollywood, M. A., Sergeant, G. P., Thornbury, K. D., Bourke, S., Levick, J. R., et al. (2010). Ionic currents in intimal cultured synoviocytes from the rabbit. *Am. J. Physiol. Cell Physiol.* 299, C1180–C1194. doi: 10.1152/ajpcell.00028.2010

Lewis, R., Feetham, C. H., Gentles, L., Penny, J., Tregilgas, L., Tohami, W., et al. (2013). Benzamil sensitive ion channels contribute to volume regulation in canine chondrocytes. *Br. J. Pharmacol.* 168, 1584–1596. doi: 10.1111/j.1476-5381.2012.02185.x

Lippiat, J. D., Standen, N. B., Harrow, I. D., Phillips, S. C., and Davies, N. W. (2003). Properties of BK(Ca) channels formed by bicistronic expression of hSloalpha and beta1-4 subunits in HEK293 cells. *J Membr. Biol.* 192, 141–148. doi: 10.1007/s00232-002-1070-0

Martel-Pelletier, J., Alaaeddine, N., and Pelletier, J. P. (1999). Cytokines and their role in the pathophysiology of osteoarthritis. *Front. Biosci.* 4:D694–D703.

Mathiessen, A., and Conaghan, P. G. (2017). Synovitis in osteoarthritis: current understanding with therapeutic implications. *Arthritis Res. Ther.* 19:18. doi: 10.1186/s13075-017-1229-9

McManus, O. B., Helms, L. M., Pallanck, L., Ganetzky, B., Swanson, R., and Leonard, R. J. (1995). Functional role of the beta subunit of high conductance calcium-activated potassium channels. *Neuron* 14, 645–650. doi: 10.1016/0896-6273(95)90321-6

Mobasheri, A., Gent, T. C., Womack, M. D., Carter, S. D., Clegg, P. D., and Barrett-Jolley, R. (2005). Quantitative analysis of voltage-gated potassium currents from primary equine (Equus caballus) and elephant (*Loxodonta africana*) articular chondrocytes. *Am. J. Physiol. Regul. Integr. Comp. Physiol.* 289, R172–R180. doi: 10.1152/ajpregu.00710.2004

Mobasheri, A., Lewis, R., Ferreira-Mendes, A., Rufino, A., Dart, C., and Barrett-Jolley, R. (2012). Potassium channels in articular chondrocytes. *Channels* 6, 416–425. doi: 10.4161/chan.22340

Mortaz, E., Adcock, I. M., Shafei, H., Masjedi, M. R., and Folkerts, G. (2012). Role of P2X7 receptors in release of IL-1β: a possible mediator of pulmonary inflammation. *Tanaffos* 11, 6–11.

Nilius, B., and Droogmans, G. (2001). Ion channels and their functional role in vascular endothelium. *Physiol. Rev.* 81, 1415–1459. doi: 10.1152/physrev.2001.81.4.1415

Noss, E. H., and Brenner, M. B. (2008). The role and therapeutic implications of fibroblast-like synoviocytes in inflammation and cartilage erosion in rheumatoid arthritis. *Immunol. Rev.* 223, 252–270. doi: 10.1111/j.1600-065X.2008.00648.x

Orio, P., and Latorre, R. (2005). Differential effects of beta 1 and beta 2 subunits on BK channel activity. *J. Gen. Physiol.* 125, 395–411. doi: 10.1085/jgp.200409236

Petho, Z., Tanner, M. R., Tajhya, R. B., Huq, R., Laragione, T., Panyi, G., et al. (2016). Different expression of beta subunits of the KCa1.1 channel by invasive and non-invasive human fibroblast-like synoviocytes. *Arthritis Res. Ther.* 18, 103. doi: 10.1186/s13075-016-1003-4

Pretzel, D., Pohlers, D., Weinert, S., and Kinne, R. W. (2009). In vitro model for the analysis of synovial fibroblast-mediated degradation of intact cartilage. *Arthritis Res. Ther.* 11:R25. doi: 10.1186/ar2618

Roemer, F. W., Felson, D. T., Yang, T., Niu, J., Crema, M. D., Englund, M., et al. (2013). The association between meniscal damage of the posterior horns and localized posterior synovitis detected on T1-weighted contrast-enhanced MRI—The MOST study. *Semin. Arthritis Rheum* 42, 573–581. doi: 10.1016/j.semarthrit.2012.10.005

Scudieri, P., Caci, E., Venturini, A., Sondo, E., Pianigiani, G., Marchetti, C., et al. (2015). Ion channel and lipid scramblase activity associated with expression of TMEM16F/ANO6 isoforms. *J. Physiol. Lon.* 593, 3829–3848. doi: 10.1113/Jp270691

Sellam, J., and Berenbaum, F. (2010). The role of synovitis in pathophysiology and clinical symptoms of osteoarthritis. *Nat. Rev. Rheumatol.* 6, 625–635. doi: 10.1038/nrrheum.2010.159

Soom, M., Gessner, G., Heuer, H., Hoshi, T., and Heinemann, S. H. (2008). A mutually exclusive alternative exon of slo1 codes for a neuronal BK channel with altered function. *Channels* 2, 278–282. doi: 10.4161/chan.2.4.6571

Stevens, A. L., Wishnok, J. S., Chai, D. H., Grodzinsky, A. J., and Tannenbaum, S. R. (2008). A sodium dodecyl sulfate-polyacrylamide gel electrophoresis-liquid chromatography tandem mass spectrometry analysis of bovine cartilage tissue response to mechanical compression injury and the inflammatory cytokines tumor necrosis factor alpha and interleukin-1beta. *Arthritis Rheum* 58, 489–500. doi: 10.1002/art.23120

Stevens, A. L., Wishnok, J. S., White, F. M., Grodzinsky, A. J., and Tannenbaum, S. R. (2009). Mechanical injury and cytokines cause loss of cartilage integrity and upregulate proteins associated with catabolism, immunity, inflammation, and repair. *Mol. Cell Proteomics* 8, 1475–1489. doi: 10.1074/mcp.M800181-MCP200

Sutton, S., Clutterbuck, A., Harris, P., Gent, T., Freeman, S., Foster, N., et al. (2009). The contribution of the synovium, synovial derived inflammatory cytokines and neuropeptides to the pathogenesis of osteoarthritis. *Vet. J.* 179, 10–24. doi: 10.1016/j.tvjl.2007.08.013

Tanner, M. R., Hu, X., Huq, R., Tajhya, R. B., Sun, L., Khan, F. S., et al. (2015). KCa1.1 Inhibition Attenuates Fibroblast-like Synoviocyte Invasiveness and Ameliorates Disease in Rat Models of Rheumatoid Arthritis. *Arthritis Rheumatol* 67, 96–106. doi: 10.1002/art.38883

Tanner, M. R., Pennington, M. W., Chauhan, S. S., Laragione, T., Gulko, P. S., and Beeton, C. (2019). KCa1.1 and Kv1.3 channels regulate the interactions between fibroblast-like synoviocytes and T lymphocytes during rheumatoid arthritis. *Arthritis Res. Ther.* 21:6. doi: 10.1186/s13075-018-1783-9

Uebele, V. N., Lagrutta, A., Wade, T., Figueroa, D. J., Liu, Y., McKenna, E., et al. (2000). Cloning and functional expression of two families of beta-subunits of the large conductance calcium-activated K+ channel. *J. Biol. Chem.* 275, 23211–23218. doi: 10.1074/jbc.M910187199

van Maanen, M. A., Stoof, S. P., van der Zanden, E. P., de Jonge, W. J., Janssen, R. A., Fischer, D. F., et al. (2009). The alpha7 nicotinic acetylcholine receptor on fibroblast-like synoviocytes and in synovial tissue from rheumatoid arthritis patients: a possible role for a key neurotransmitter in synovial inflammation. *Arthritis Rheum* 60, 1272–1281. doi: 10.1002/art.24470

Varani, K., De Mattei, M., Vincenzi, F., Tosi, A., Gessi, S., Merighi, S., et al. (2008). Pharmacological characterization of P2X1 and P2X3 purinergic receptors in bovine chondrocytes. *Osteoarthr. Cartil.* 16, 1421–1429. doi: 10.1016/j.joca.2008.03.016

Waldburger, J. M., Boyle, D. L., Pavlov, V. A., Tracey, K. J., and Firestein, G. S. (2008). Acetylcholine regulation of synoviocyte cytokine expression by the alpha7 nicotinic receptor. *Arthritis Rheum* 58, 3439–3449. doi: 10.1002/art.23987

Wang, B., and Brenner, R. (2006). An S6 mutation in BK channels reveals beta1 subunit effects on intrinsic and voltage-dependent gating. *J. Gen. Physiol.* 128, 731–744. doi: 10.1085/jgp.200609596

Williams, A. (2014). *Proteomic Studies of an Explant Model of Equine Articular Cartilage in Response to Proinflammatory and Anti-Inflammatory Stimuli*. PhD Thesis, University of Nottingham, Nottingham.

Williams, A., Smith, J. R., Allaway, D., Harris, P., Liddell, S., and Mobasheri, A. (2011). Strategies for optimising proteomic studies of the cartilage secretome: establishing the time course for protein release and evaluating responses of explant cultures to il-1 beta, tnf-alpha and carprofen. *Osteoarthr.Cartil.* 19, S209–S209.

Yang, C. T., Zeng, X. H., Xia, X. M., and Lingle, C. J. (2009). Interactions between beta subunits of the KCNMB family and Slo3: beta4 selectively modulates Slo3 expression and function. *PLoS One* 4:e6135. doi: 10.1371/journal.pone.0006135

Yoo, S. A., Park, B. H., Park, G. S., Koh, H. S., Lee, M. S., Ryu, S. H., et al. (2006). Calcineurin is expressed and plays a critical role in inflammatory arthritis. *J. Immunol.* 177, 2681–2690. doi: 10.4049/jimmunol.177.4.2681

Zerbino, D. R., Achuthan, P., Akanni, W., Amode, M. R., Barrell, D., and Bhai, J. (2018). Ensembl 2018. *Nucleic Acids Res.* 46, D754–D761. doi: 10.1093/nar/gkx1098

Zhou, Y., and Lingle, C. J. (2014). Paxilline inhibits BK channels by an almost exclusively closed-channel block mechanism. *J. Gen. Physiol.* 144, 415–440. doi: 10.1085/jgp.201411259

Conflict of Interest: The authors declare that the research was conducted in the absence of any commercial or financial relationships that could be construed as a potential conflict of interest.